OCS Study
MMS 94-0047

A Physical Oceanographic Field Program Offshore North Carolina

Final Synthesis Report

MMS U.S. Department of the Interior
Minerals Management Service
Gulf of Mexico OCS Region

OCS Study
MMS 94-0047

A Physical Oceanographic Field Program Offshore North Carolina

Final Synthesis Report

Authors

Thomas J. Berger
Peter Hamilton
Robert J. Wayland
Science Applications International Corporation

Jackson O. Blanton
Skidaway Institute of Oceanography

William C. Boicourt
University of Maryland

James H. Churchill
Woods Hole Oceanographic Institution

D. Randolph Watts
University of Rhode Island

Prepared under MMS Contract
14-35-0001-30599
by
Science Applications International Corporation
615 Oberlin Road, Suite 300
Raleigh, North Carolina 27605

Published by

U.S. Department of the Interior
Minerals Management Service
Gulf of Mexico OCS Region

New Orleans
October 1995

DISCLAIMER

This report was prepared under contract between the Minerals Management Service (MMS) and Science Applications International Corporation (SAIC). This report has been technically reviewed by the MMS and approved for publication. Approval does not signify that the contents necessarily reflect the views and policies of the Service, nor does mention of trade names or commercial products constitute endorsement or recommendation for use. It is, however, exempt from review and compliance with MMS editorial standards.

REPORT AVAILABILITY

Extra copies of the report may be obtained from the Public Information Unit (Mail Stop 5034) at the following address:

U.S. Department of the Interior
Minerals Management Service
Gulf of Mexico OCS Region
Public Information Unit (MS 5034)
1201 Elmwood Park Boulevard
New Orleans, Louisiana 70123-2394

Telephone Number: 1-504-736-2519
1-800-200-GULF

CITATION

Suggested citation:

T. J. Berger, P. Hamilton, R. J. Wayland, J. O. Blanton, W. C. Boicourt, J. H. Churchill, and D. R. Watts. 1995. A Physical Oceanographic Field Program Offshore North Carolina, Final Synthesis Report. OCS Study MMS 94-0047. U.S. Department of the Interior, Minerals Management Service, Gulf of Mexico OCS Region, New Orleans, La. 345 pp.

EXECUTIVE SUMMARY

This report documents an initial analysis of data from a physical oceanographic field program conducted off North Carolina between February 1992 and February 1994. The focus of the analysis, because of time constraints, has been on the first 18 to 20 months of data. The data represent the most extensive measurements made to date in the complex oceanographic regime around Cape Hatteras, and also present opportunities for new insights into the dynamics of the region and for additional detailed analyses. Data sources for this study included moored current meters in water depths from 20 m to 3000 m over the continental shelf and slope just north and south of Cape Hatteras, North Carolina, hydrographic surveys in the same areas, meteorological and water level measurements, satellite SST measurements, and Lagrangian drifters on the mid to outer shelf and in the near shore zone.

The study region covered an area in which the continental shelf narrows, from 70 km at Cape Lookout to approximately 35 km across Diamond Shoals at Cape Hatteras, and then broadens again to 125 km off Chesapeake Bay in the Middle Atlantic Bight. In the same span the continental slope steepens as it approaches Diamond Shoals. The shore line in the study area consists primarily of low lying barrier islands - the North Carolina Outer Banks - behind which lie Currituck, Albemarle and Pamlico Sounds. Fresh water input along the North Carolina coast is primarily from Chesapeake Bay (at the northern edge of the study area) with smaller amounts through various inlets between the North Carolina Sounds and the continental shelf.

The dominant oceanographic feature of the study region is the Gulf Stream and its associated meanders and frontal eddies; while Slope Sea influences appear to be limited in the study area. Gulf Stream rings also appear to have little affect on regional circulation patterns except indirectly during interactions near Cape Hatteras between cold core rings and the Gulf Stream. Warm core rings were not observed during the study and are thought to be rare in the region. Cold core ring interactions were observed in April, June and December 1992 but not through at least August 1993. Cold core ring interactions reduced Gulf Stream currents to practically zero at the slope moorings: C4, during all three events; B4, in April and December and A5, only in December. There were few current reversals above 300 m at the three moorings; the strongest reversal was at B4 during the December cold core ring interaction.

The Gulf Stream path has its least variability, after leaving the confines of the Straits of Florida, in the area just southeast of Cape Hatteras. The Gulf Stream was apparently in a 'small meander' mode upstream from Cape Hatteras during most of the study period except possibly during March and June 1992. During 1992 the Gulf Stream was relatively closer to the shelf, straighter and with stronger currents than in 1993. No seasonal patterns in the Gulf Stream path were discernible but there were clear one- to four-month trends and a possible 10 km annual shift in position. The current records at deep water moorings C4, B4, and A5 (means at 100 m ≈110-125 $cm \cdot s^{-1}$ to the northeast) and C3 and B3 on the shelf edge all suggest that these moorings were in or near the edge of the Gulf Stream most of the time. In contrast, mooring A4 was in the Slope Sea all the time with weak mean (3-5 $cm \cdot s^{-1}$) currents directed to the south and southeast.

Gulf Stream currents were observable on the shelf consistently at moorings C3 and B3. Currents at these two moorings were highly coherent with currents at C4 and B4 offshore. Even during the March 1993 storm when flows on the shelf were generally southward, flow at C3 and B3 was coherent with the Gulf Stream. During Hurricane Emily in August 1993 the current at B3 reversed briefly while C3 had low or no current but no reversal.

Gulf Stream water was identifiable at mooring A3, the northernmost shelf edge mooring, about 10% of the time (12 incidents during the first 18 months), but no comparable velocity signal was detected. These incidents varied in duration from less than a day (2 incidents) to more than five days (5 incidents). Four of the incidents penetrated to mooring A2 at mid-shelf.

While the study was not designed to provide details on the south-southwestward flowing Deep Western Boundary Current (DWBC) which crosses under the Gulf Stream, data from the deep water moorings were analyzed to detect this current. The DWBC was detectable at levels below 800 m on moorings A4, B4 and C4; but at A5 the currents above 1900 m were more consistent with flow of the Slope Sea gyre curving eastward to flow along the Gulf Stream. Typical speeds were 20-30 $cm \cdot s^{-1}$ with peaks of 40-60 $cm \cdot s^{-1}$ due to TRWs superimposed on the mean flow. Variability in the deep levels was due to TRWs and coupling between upper and lower level eddies. Coupling of upper level Gulf Stream meanders with lower level eddies was most prevalent at C4 and B4. There was evidence at these moorings of growing and decaying baroclinic instabilities.

Meteorology of the region is characterized by relatively weak, northeastward winds, approximately parallel to the coast in summer and strong south-southwestward flow in winter with the synoptic wind period of 2.5 to 12 days overlapping the energetic Gulf Stream meander period of 3 to 10 days. The winter patterns are punctuated by complex cyclogenesis and cold air outbreaks which can result in severe storms with heavy snowfall along the East Coast. The summer patterns are occasionally punctuated by tropical cyclones and hurricanes. During the study period there were three major meteorological events which had varying, but generally short-lived, effects on regional circulation. A major winter storm occurred in December 1992 that forced large southward flows over the whole width of the shelf to Diamond Shoals; another storm in March 1993 ("storm of the century") caused extensive snowfall in the northeast and heavy property damage in the northern part of the Outer Banks; while Hurricane Emily in late August 1993 passed near Cape Hatteras and caused damage to the southern portion of the Outer Banks primarily through storm surge in Pamlico Sound.

Wind forced currents on the shelf in winter present a classic Ekman response. Currents at all levels north of Diamond Shoals and at C1 and C2 surface were highly coherent with winds and sea level. Large wind-forced current fluctuations on the inner shelf north and south of Cape Hatteras had important contributions from pressure gradients caused by sea level differences around Cape Hatteras. Currents at lower levels in Raleigh Bay were less coherent with the winds and more coherent with the Gulf Stream. Gulf Stream forcing on the shelf is almost absent in winter because of the insulating affect of a strong shelf break front and stratification and stronger wind forcing. During summer the wind stress and sea level fluctuations are about half the magnitude of those in winter. Winds in summer 1993 were weaker than in 1992. In the summers of 1992 and 1993 there was evidence that Gulf Stream fluctuations were observed as far as the coast in northern Raleigh Bay (Line C).

Hydrographic surveys provided information on the various circulation processes on the North Carolina continental shelf, through brief glimpses of processes caught in the midst of their evolution, and through tracer distributions which are the integral result of processes acting over a span of time. The Gulf Stream is a source of heat, salt, and momentum to the North Carolina continental shelf. Its warm, salty waters create marked contrasts in the temperature-salinity characteristics of the shelf region. Furthermore, the combination of strong forcing (with low-frequency

variability) and strong water-mass contrasts creates a situation prone to large interannual swings in the structure and circulation of these shelf waters. Two years of survey data illustrate possible interannual variability resulting from changes in Gulf Stream position, spring runoff, and changes in wind.

The seasonal progression of stratification in the Middle Atlantic Bight, primarily through vernal warming, was observed; this process was augmented in 1993 by higher and earlier than normal buoyancy flux from Chesapeake Bay. Stratification decreased spatially from north to south, not in a smooth gradient, but rather as punctuated changes at two locations. The first location is the sharp transition occurring where the cold water in the lower layers of the Middle Atlantic Bight turn offshore, 40-70 km north of Cape Hatteras. The second location is the cross shelf front separating Middle Atlantic Bight and South Atlantic Bight waters which represents what was thought to be the "oceanographic barrier" of the offshore extension of Diamond Shoals. While this front generally crossed the shelf at an angle (southwest to northeast) in the vicinity of Diamond Shoals, occasionally it was distorted along the coast by intrusions of Middle Atlantic Bight water past Diamond Shoals into Raleigh Bay. These "Virginia Coastal Water" intrusions appeared to be driven by strong and relatively long-duration southwestward wind events and occurred during all seasons of the year. Cessation of the wind events was followed closely by retreat of the front, and the advected Middle Atlantic Bight water, back to the normal position near Cape Hatteras. Stratification in Raleigh Bay is, in general, weak and may be driven by either temperature or salinity fluctuations. Gulf Stream intrusion events, augmented by wind-driven Ekman flow, can provide transient intervals of stratification as high-salinity water moves from offshore and penetrates shoreward along the bottom.

As spring transitions into summer, the cold band water over the outer shelf in the Middle Atlantic Bight narrows, and may even decrease in temperature, reflecting the cold temperatures of the source region in the Gulf of Maine and the amount of insulation and mixing during its southward travel. The transition from spring to summer did not occur until June in 1992 but in May in 1993. Wind patterns during both summers were similar.

With the fall season comes cooling and wind mixing, and the decrease of stratification. By winter, shelf stratification on both sides of Cape Hatteras is usually transient, with intrusion

and extrusion events stratifying the water column over the outer shelf. Subsequently, winter storms can quickly destratify the shelf as was observed during and following the December 1992 and March 1993 storms, in particular.

The Slope Sea portion of the study area was found to be hydrographically complex with Middle Atlantic Bight shelf water, slope water and Gulf Stream water in varying proportions. Rotary motions, coherent to at least 300 m depth, dominate near surface Slope Sea currents in the study area. The strongest of these appear to be due to the circulating flow of discharged Gulf Stream water parcels. As observed further to the north, these motions do not extend onto the continental shelf. Slope water was detected at the shelf break only once, at A3 in August 1993.

Export of water from the Middle Atlantic Bight Shelf occurs in the region just north of Diamond Shoals, generally between moorings B3 and D2 when the Gulf Stream was away from the shelf but between D2 and D1 when the Gulf Stream was closer. This shifting region is where direct export to the Gulf Stream takes place. Some Middle Atlantic Bight water may also be exported to the Gulf Stream from Raleigh Bay after first intruding into Raleigh Bay over Diamond Shoals. Another path for shelf water export is along the northern boundary of Gulf Stream water extrusions in the southern end of the Slope Sea rather than along the Gulf Stream itself. Volume transport off the shelf along the Gulf Stream north of Diamond Shoals is estimated to be about the same magnitude as the volume transport along the continental shelf north of Cape Hatteras. Raleigh Bay shelf water also appears to be exported by entrainment along the Gulf Stream front just south of Diamond Shoals. There often are converging shelf flows in the region of Diamond Shoals from the southward flowing Middle Atlantic Bight and northward flowing Raleigh Bay water.

A series of drogued drifter deployments tracked the progression of near surface layers from the shelf to the Gulf Stream. None of the drogued drifters released outside the nearshore region were recovered ashore in the Cape Hatteras region; while seven were found beached in England (1), France (3), the Canary Islands (1), and the Bahamas (2) 14 to 35 months after deployment. Estimates of residence time on the shelf ranged from less than eight to more than 27 days. In general the drifters deployed in Raleigh Bay had the shortest residence time.

Drifter tracks during the Near Shore Experiments revealed vigorous and highly variable coastal currents near the sea surface. Although these were clearly influenced by the wind to a large degree, comparison of the drifter velocities with the wind record from the Corps of Engineers facility at Duck, North Carolina showed occasional departures from a classical nearshore wind response. Other possible contributors to the drifter motion include buoyancy-driven and surface wave-induced currents. Buoyancy-driven cross-shore motion of the drifters appeared often to have been influenced by the near-shore front common to the study area. Drifter convergence to the front was observed in two drifter deployments. On two other occasions, the front appeared to have been the outer boundary of a zone of surface transport onto the beach, i.e. drifters deployed inside the front came ashore while those deployed outside the front did not. This transport is attributed to driving by the onshore wind component with likely assistance from surface wave-induced currents. On two occasions during these experiments when ARGOS tracked drifters were left in the water rather than being redeployed, they were eventually entrained along the Gulf Stream.

Analysis of data from this program confirmed many notions about the nature of the complex circulation of the Cape Hatteras region, including the dominant role of the Gulf Stream and its meanders on Raleigh Bay and the shelf break just north of Diamond Shoals. Export of water from the Middle Atlantic Bight shelf occurs just north of Diamond Shoals in a band whose location can shift depending on the location of the Gulf Stream.

Occasional advection of Middle Atlantic Bight water past the "oceanographic barrier" at Diamond Shoals, so-called Virginia Coastal Water instrusions, was observed. Material released on the shelf outside a near shore frontal zone, approximately 2-4 km from the beach, appears likely to be eventually entrained along the Gulf Stream. Residence times for such material ranged from eight to 27 days with generally shorter residence times being observed in Raleigh Bay. Material advected southwestward past Cape Hatteras in "Virginia Coastal Water" intrusions is advected back to the Middle Atlantic Bight when the wind forcing relaxes. It seems unlikely that materials discharged into the ocean past the mid-shelf region would find their way onto the North Carolina beaches.

TABLE OF CONTENTS

TABLE OF CONTENTS

TABLE OF CONTENTS

TABLE OF CONTENTS

LIST OF FIGURES

LIST OF FIGURES

LIST OF FIGURES

LIST OF FIGURES

LIST OF FIGURES

LIST OF FIGURES

LIST OF FIGURES

LIST OF FIGURES

LIST OF FIGURES

LIST OF FIGURES

LIST OF FIGURES

LIST OF FIGURES

LIST OF FIGURES

LIST OF FIGURES

LIST OF FIGURES

LIST OF FIGURES

LIST OF FIGURES

LIST OF FIGURES

LIST OF FIGURES

LIST OF FIGURES

LIST OF FIGURES

LIST OF FIGURES

LIST OF TABLES

ACKNOWLEDGEMENTS

The Program Manager expresses particular thanks to Mr. James Singer of SAIC who really kept the data collection effort going through thick and thin. The office staff in Raleigh, Ms. Elaine Jones, Ms. Susan Root, Ms. Stephanie Bowens, Ms. Wendi Jackson, and Ms. Sharon Goodhart all contributed in untold ways throughout the course of the study including production of this report.

The continued support of the University of Miami in image processing matters is gratefully acknowledged. The superior efforts of the Masters and Crews of R/V Cape Henlopen, M/V Seaward Explorer and F/V Sea Dragon, Mr. Paul Higley and Mr. Scott Sharpe, of Specialty Devices, Inc., Mr. Craig Boyd and Mr. Paul Blankinship were absolutely essential to the success of this Program.

The continued support and encouragement of Dr. Walter R. Johnson and Dr. Robert Miller, the Contracting Officer's Technical Representative during the bulk of the Program, and the assistance of his successors, Mr. Alvin Jones and Dr. Murray Brown, are most gratefully acknowledged.

PHYSICAL OCEANOGRAPHIC FIELD PROGRAM
OFFSHORE NORTH CAROLINA

I. INTRODUCTION

1.1 Objectives

The main objective of this study, as delineated by the Minerals Management Service (MMS) in Request for Proposals 3599 and Contract 14-35-0001-30599, was to "develop an adequate understanding of the physical oceanography of the Cape Hatteras region" in a study area which extended from 34°30'N to 37°00'N and from the coast eastward to 73°00'W (but excluding Chesapeake Bay). The study area is shown in Figure 1.1-1 in relation to major U.S. East Coast topographic features and Gulf Stream axis. The major issue ultimately to be addressed was "the extent to which contaminants released over the continental slope can penetrate onto the shelf and thus shoreward."

Thus the field program was designed to address "processes associated with flow between the slope area and the shelf break, flow across the shelf break, alongshore flow on the shelf, and cross-isobath flow towards the beach in the inner shelf zone".

1.2 Scope of Study

The study encompassed two years of field work from February 15, 1992 through February 22, 1994. Nine cruises aboard either M/V Seaward Explorer or R/V Cape Henlopen were completed to perform mooring placement, servicing and recovery, and hydrographic measurements. Two Near Shore Experiments were conducted from a shore base and day trips aboard the F/V Sea Dragon during June and September 1993. The overall study design was specified by the North Carolina Peer Review Panel which convened at MMS headquarters on September 24-26, 1990.

Field measurement techniques used to complete this study included

- fifteen current meter moorings on the shelf and in deep water as shown in Figure 1.2-1;
- quarterly hydrographic surveys concurrent with current meter servicing cruises (Figure 1.2-2 through Figure 1.2-5), with the exception that no hydrographic measurements were made during the initial cruise in February 1992, 16 stations were

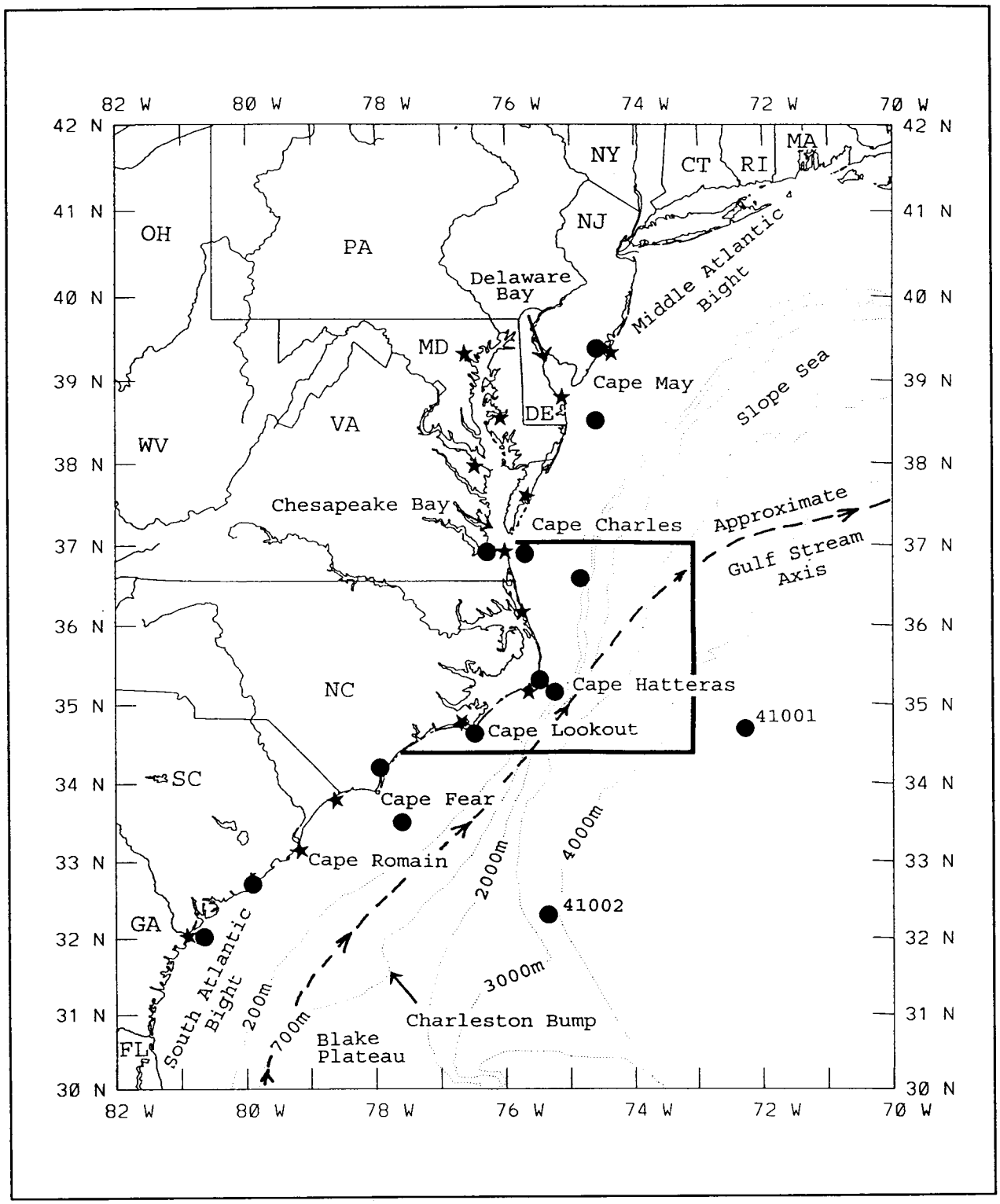

Figure 1.1-1. U.S. Eastcoast oceanographic features. Study area is indicated by heavy lines. Meteorological stations (●) and water level stations (★) are marked.

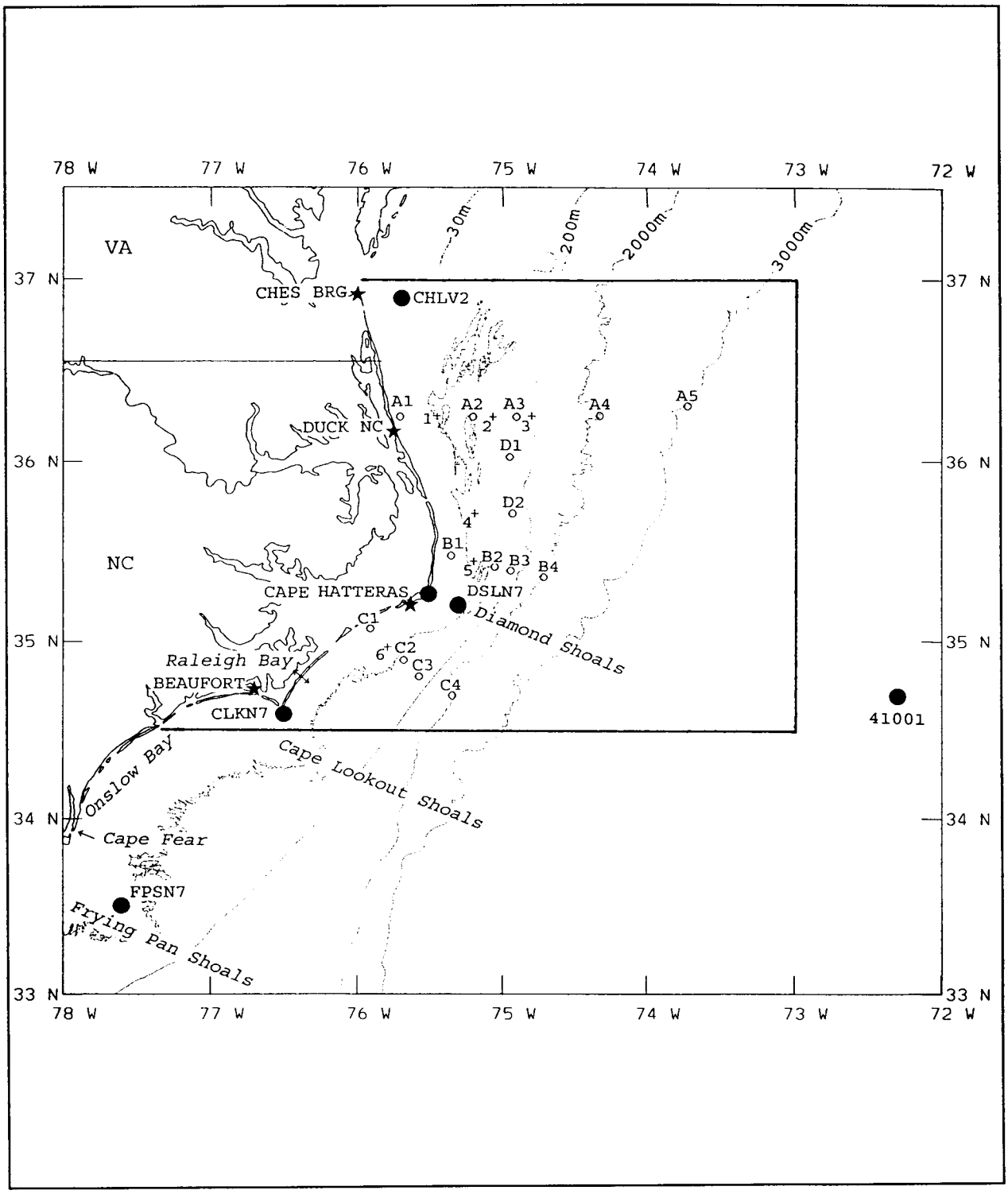

Figure 1.2-1. Region around Cape Hatteras. Study area is indicated by heavy lines. Only the meteorological stations (●) and water level stations (★) actually used in the analysis are indicated. Current meter moorings (∘) and drifter deployment sites (+) are also shown.

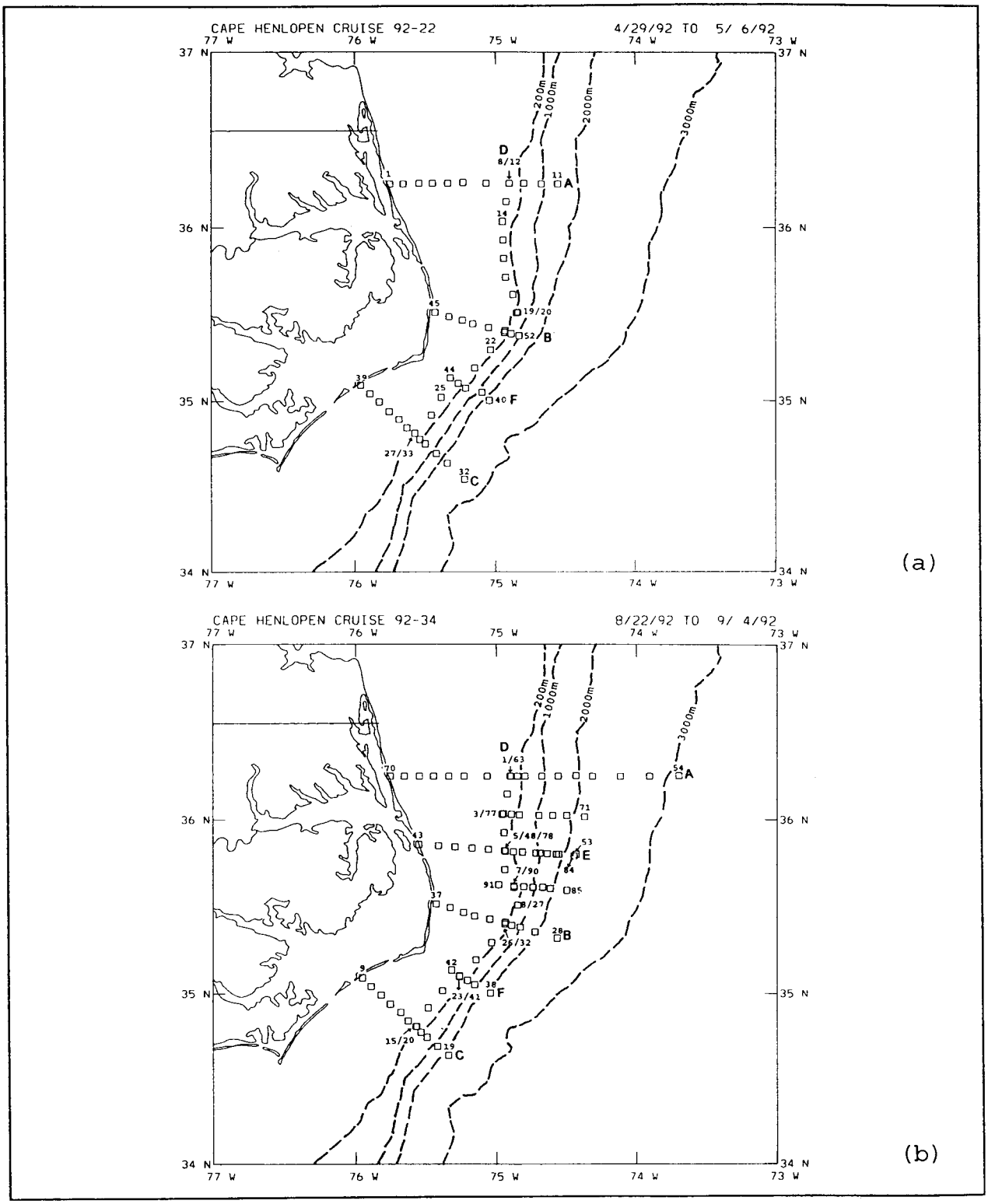

Figure 1.2-2. Hydrographic station locations during cruises (a) CH9222 April 29-May 6, 1992 and (b) CH9234 August 22-September 4, 1992. Unlabeled lines are part of special event surveys.

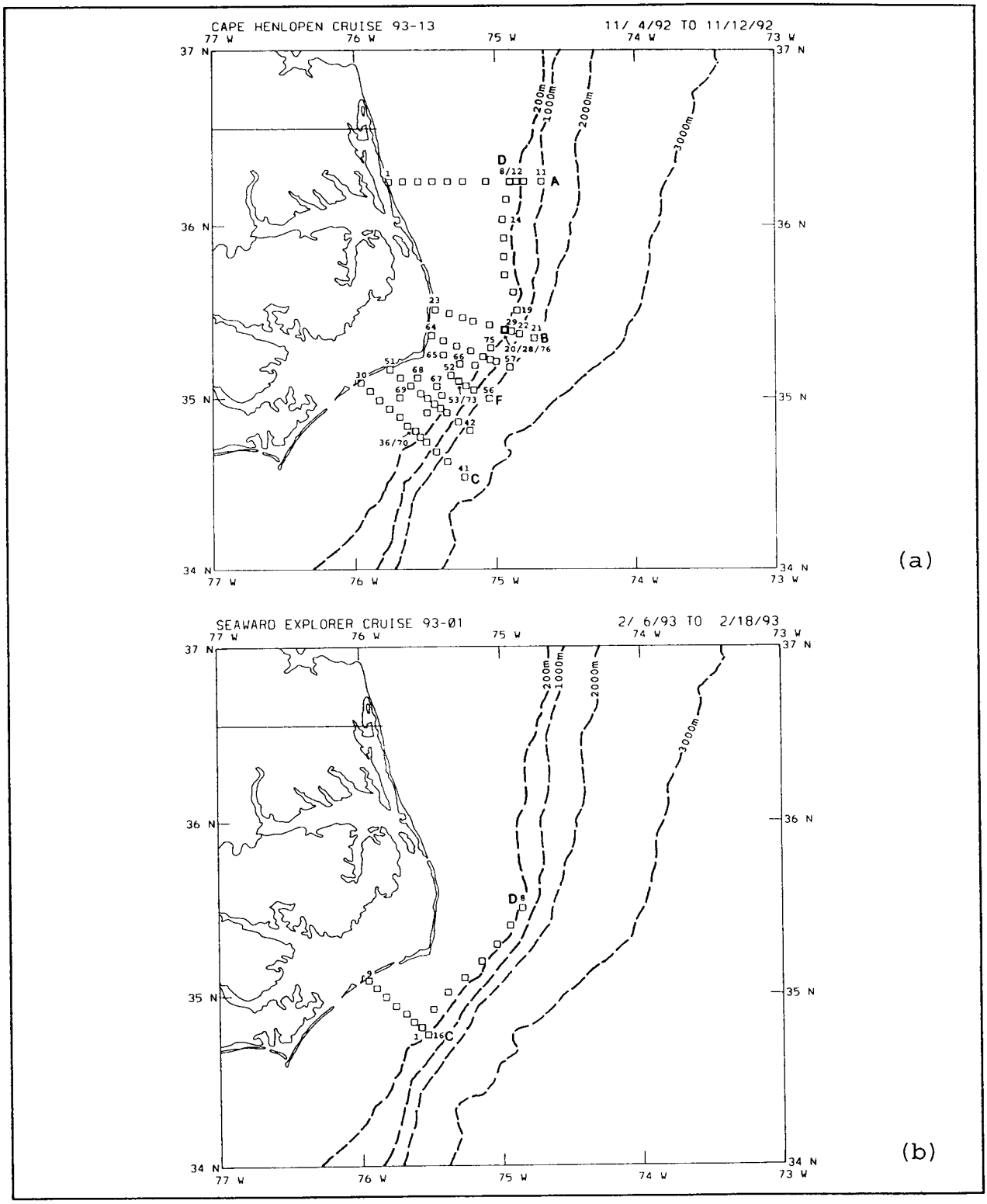

Figure 1.2-3. Hydrographic station locations during cruises (a) CH9313 November 4-12, 1992 and (b) SE9301 February 6-18, 1993. Unlabeled lines are part of special event surveys.

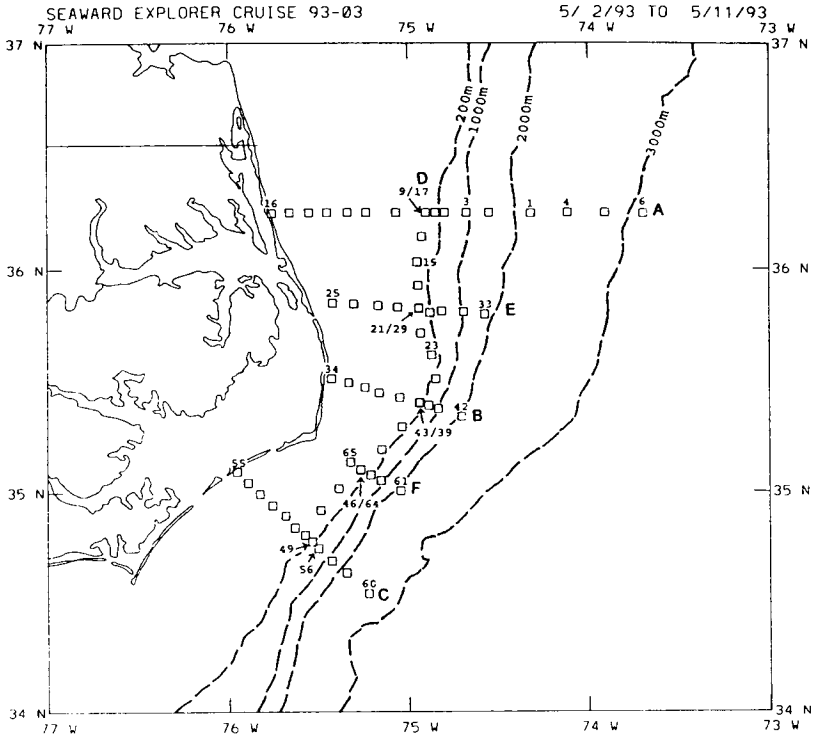

Figure 1.2-4. Hydrographic station locations during cruises (a) SE9303 May 2-11, 1993 and (b) SE9309 August 19-28, 1993.

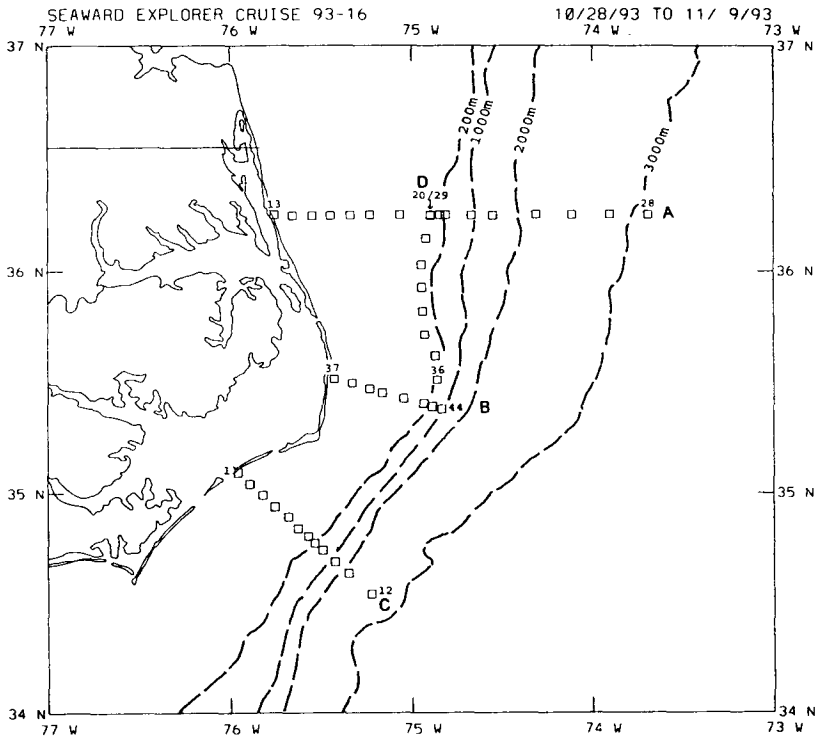

Figure 1.2-5. Hydrographic station locations during cruise SE9316 October 28-November 9, 1993.

completed in February 1993 and only four shallow stations were completed during the final cruise in February 1994, all because of bad weather;

- three special event surveys, which consisted of detailed hydrographic and shipboard acoustic Doppler current profiler (ADCP) surveys of offshore flow or Virginia Coastal Water intrusions into Raleigh Bay, and two Near Shore Experiments with Global Positioning System (GPS) drifters;

- seven sets of Lagrangian drifter deployments, at sites shown in Figure 1.2-1, which were designed to evaluate the potential for materials discharged near the shelf break to reach the near shore region; and

- collection of collateral data, i.e., satellite infrared imagery of sea surface temperature (SST), and meteorological and water level data along the coast within 500 km of Cape Hatteras, to support analysis and synthesis of the primary data.

The field activities have been documented in nine Cruise Reports, two Near Shore Experiment Reports, and two Annual Progress Reports. These reports cover the details of how the data were collected and the volume of data collected. Such details are not repeated here. Table 1.2-1 lists the various hydrographic cruises, the number of stations occupied and significant events during a cruise. The hydrographic stations are shown graphically in Figures 1.2-2 through 1.2-5. The main hydrographic stations were located along five fixed lines approximately normal to the coast and a sixth line along the 60 m isobath (Line D). Three lines (A, B and C) passed through the current meter locations. Two additional, shorter, lines were located between the current meter positions, namely Line E between Lines A and B, and Line F between Lines B and C. The lines were often abbreviated (or omitted) if the weather was unfavorable. Reference to hydrographic sections in the text uses line designations, however the figures refer to cruise ID and station number during that cruise. Additional short CTD lines were occupied in June and September 1993 during the Near Shore Experiments (Figure 1.2-6). Figures 1.2-7 and 1.2-8 provide timelines for the moorings shown in Figure 1.2-1.

Figure 1.2-9 provides a timeline of meteorological and water level stations actually used in the analyses. The station locations are

Table 1.2-1. Cruise Summary

Cruise ID	Dates	CTD Stats.	Remarks
SE9208	February 15-28, 1992	0	Mooring Deployment only because of weather.
CH9222	April 28 - May 10, 1992	52	No CTDs on Line E, Lines A and B shortened.
CH9234	August 19 - September 5, 1992	91	
CH9313	November 3-13, 1992	76	No CTDs on Line E. 22 CTDs in Special Event Survey bracketing Diamond Shoals.
SE9301	February 2-18, 1993	16	Bad Weather
SE9303	May 1-12, 1993	65	
SE9309	August 18-29, 1993	65	Cruise terminated to avoid Hurricane Emily. Line A shortened.
SE9316	October 28 - November 10, 1993	44	Lines E, F and Line D South of Diamond Shoals not occupied.
SE9401	February 7-22, 1994	4	Inshore end of Line C.
SD9301	June 8-18, 1993	86	Nearshore Survey 1.
SD9302	September 10-23, 1993	88	Nearshore Survey 2.

Table 1.2-2. Inventory of Clear Sky AVHRR Images

	J	F	M	A	M	J	J	A	S	O	N	D
1992	-	45	29	39	38	36	44	48	35	24	32	14
1993	15	27	33	57	78	66	69	56	61	39	28	32
1994	31	-	-	-	-	-	-	-	-	-	-	-

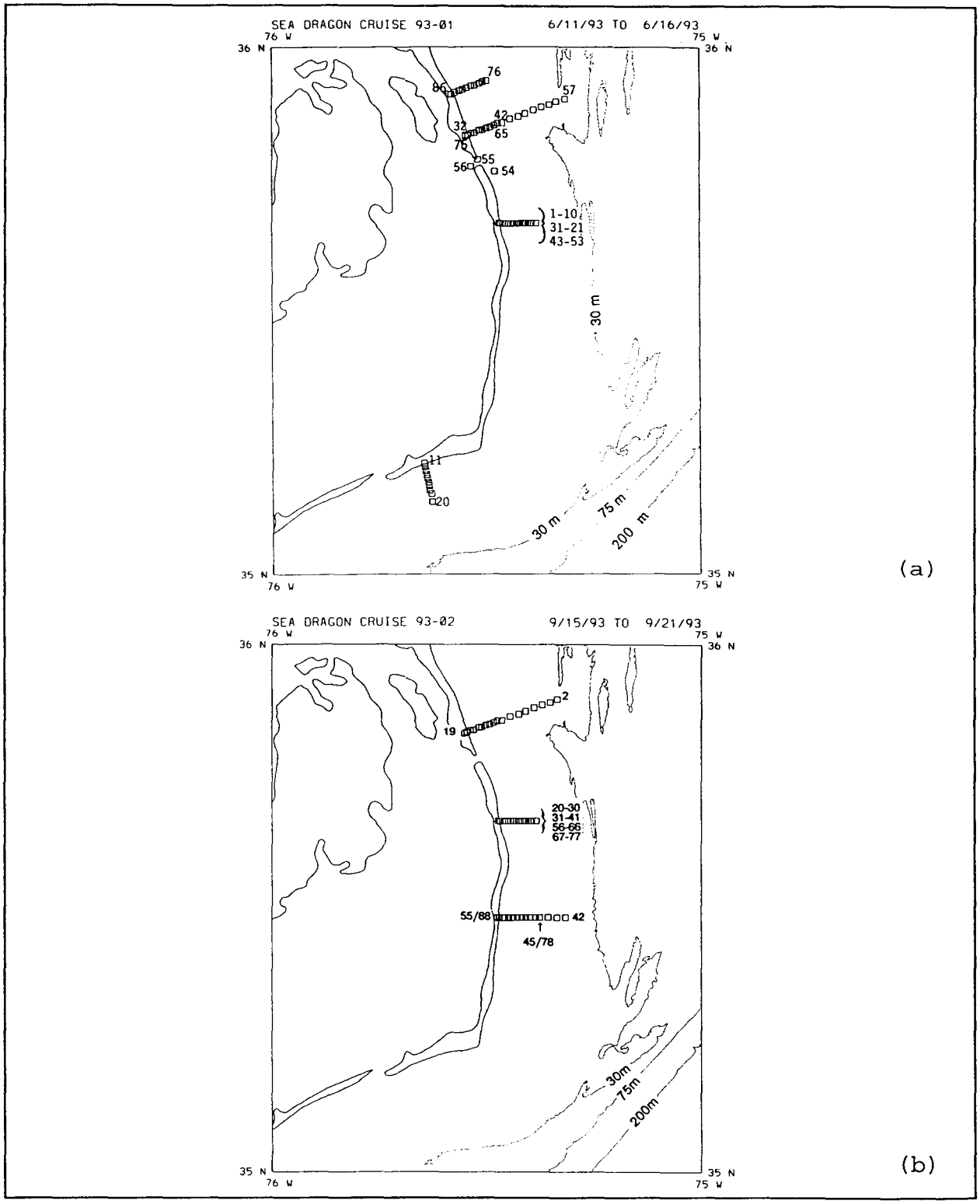

Figure 1.2-6. Hydrographic station locations during Near Shore Experiment cruises (a) SD9301 June 11-16, 1993 and (b) September 15-21, 1993.

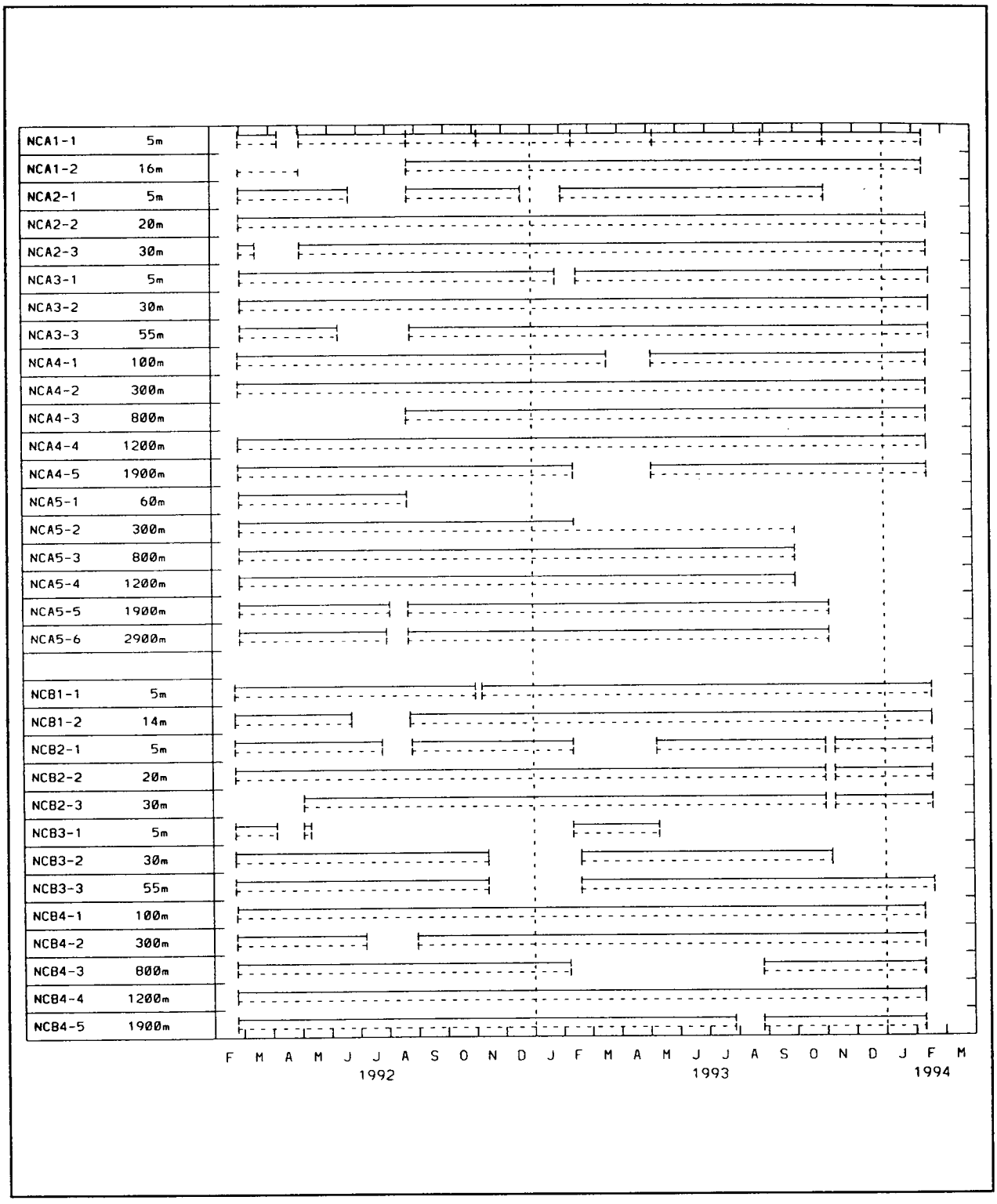

Figure 1.2-7. Timelines for Moorings A1, A2, A3, A4, A5, B1, B2, B3 and B4.

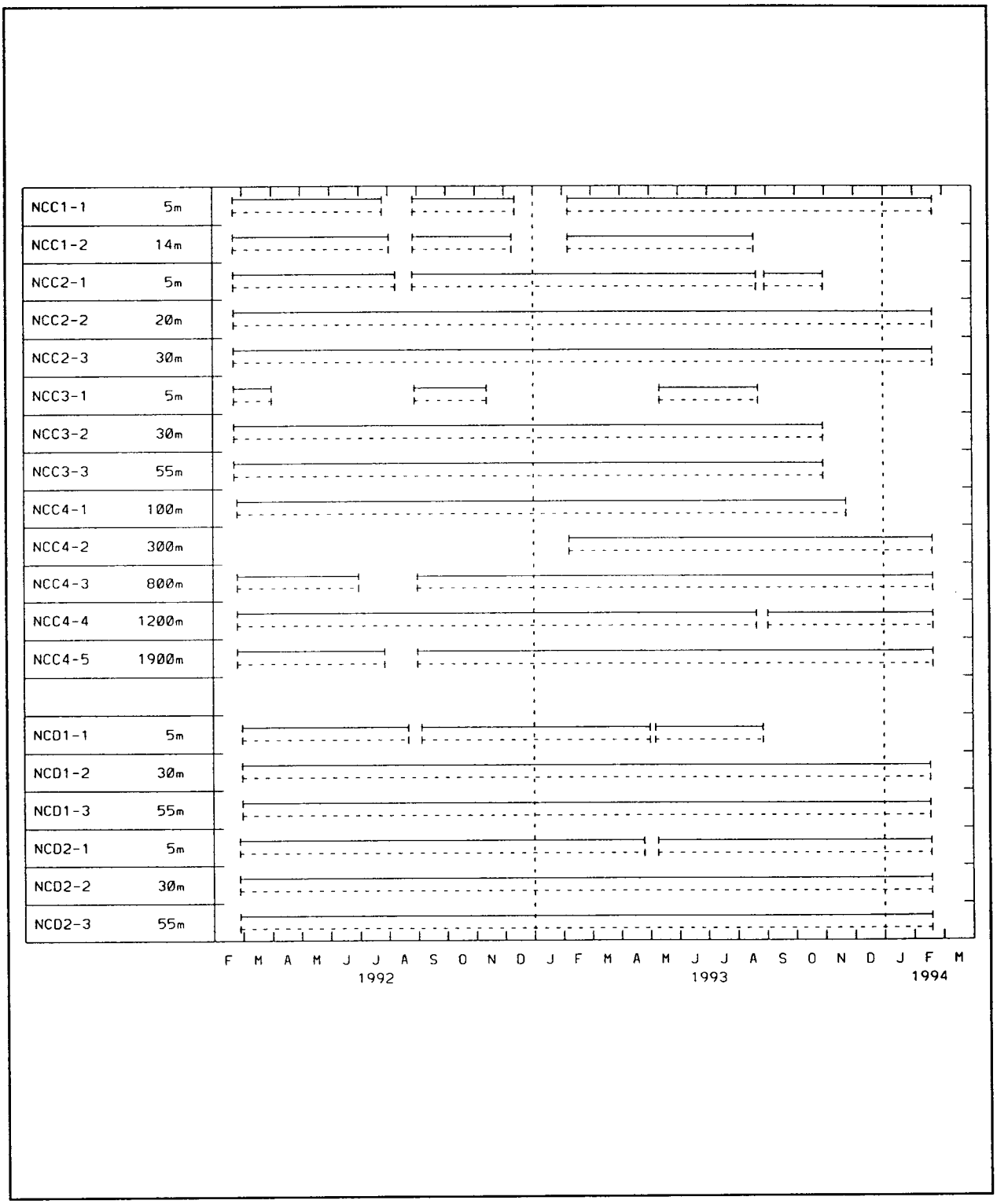

Figure 1.2-8. Timelines for Moorings C1, C2, C3, C4, D1 and D2.

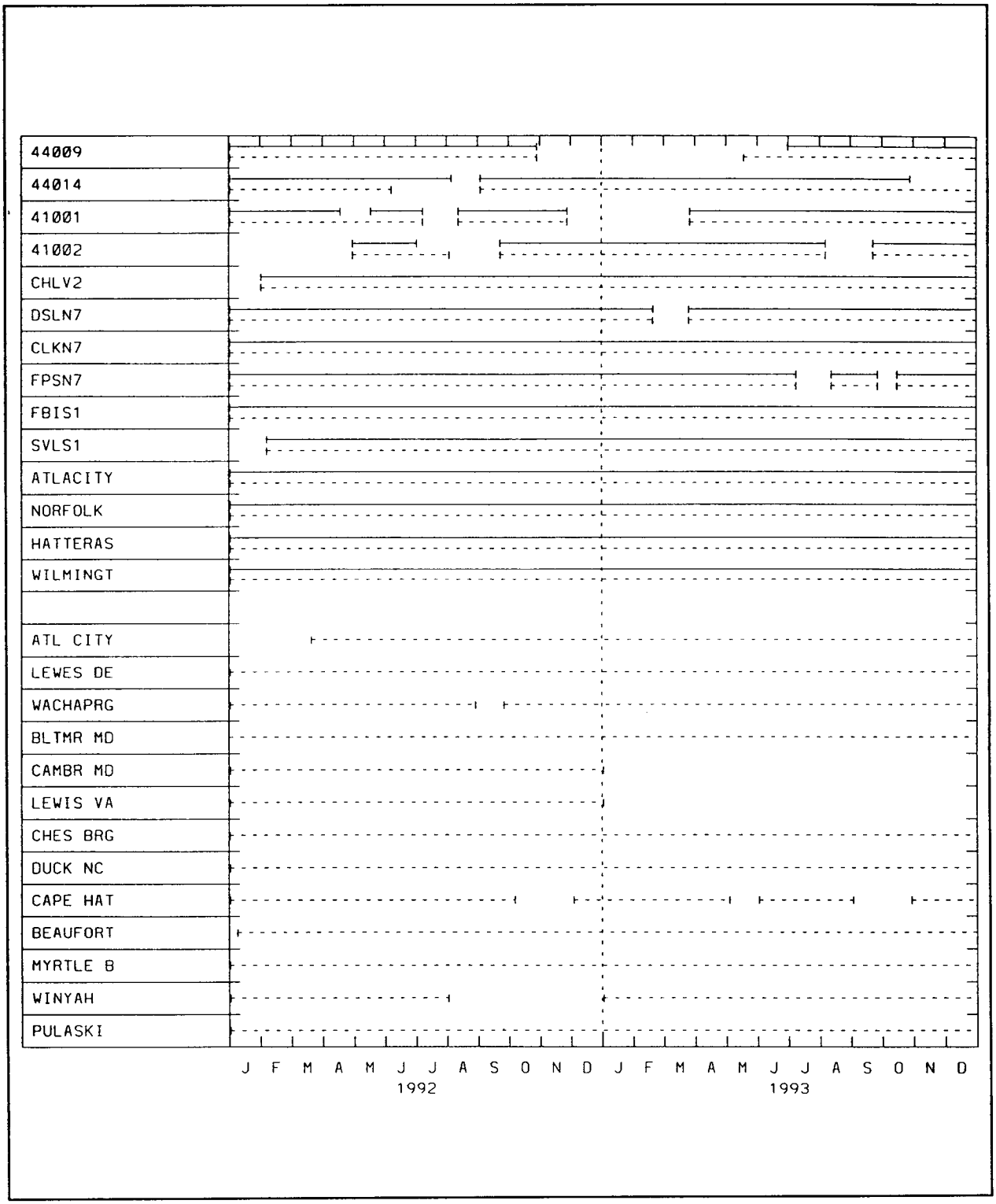

Figure 1.2-9. Timelines for meteorological data (upper set) from NDBC Buoys and C-MAN Stations and NWS Stations and water level stations (lower set) from Atlantic City, NJ to Fort Pulaski (Savannah), GA.

shown in Figures 1.1-1 and 1.2-1. Table 1.2-2 enumerates the number of clear sky AVHRR images available during each month of the study. Current meter data, hydrographic station data, and ARGOS tracked drifter data have been archived at the National Oceanographic Data Center under Project Number 0208.

Three major meteorological events occurred during the study period - a major winter storm in December 1992; the 'storm of the century' in March 1993, which originated in the Gulf of Mexico; and Hurricane Emily which passed just east of Cape Hatteras at the end of August 1993 and caused substantial damage to parts of the North Carolina Outer Banks which had not been hit during the March 1993 storm.

1.3 Methods and Approach

This section describes data processing procedures and the quality assurance (QA) plan aimed at obtaining the highest quality data possible and maximizing data return.

1.3.1 Moored Instrumentation Operational Checkout and Calibration

Each moored instrument (Aanderaa RCM 7/8, General Oceanics MkI and MkII and InterOcean S4 Current Meters, and Benthos acoustic releases) had a deployment/recovery log, and as appropriate, a data processing log and detailed check off list completed at each step of its preparation and handling prior to deployment and following recovery. These log sheets were used throughout the process to verify that start and stop times of time series data were correct. Prior to initial deployment and following final recovery, all current meters were checked out and calibrated by their respective manufacturers (Aanderaa, General Oceanics and InterOcean).

Data were recovered from each instrument using software provided by the various manufacturers. Multiple downloads of data were routinely made to assure full data recovery and copies were stored on 3½" IBM compatible diskettes. Data were evaluated in the field for completeness, i.e., start and stop times consistent with those recorded in the log sheets, and for reasonableness. If no problems were detected the instruments were serviced according to the manufacturer's instructions and redeployed. If problems were encountered, the instrument was replaced by a backup unit of the same type, if available.

Current meter data were transferred into the SAIC Physical Oceanographic Data Base Management System (PODBMS) and a unique identifier (ID) was assigned. Plots of the raw data components were made and current values were evaluated for consistency with nearby instruments and among deployments at the same site. Temperature and salinity data, taken primarily at shelf mooring sites, were compared with nearby conductivity temperature depth (CTD) casts made at the beginning and end of the deployments, to detect either offsets or drift in the data.

Following completion of QA procedures, the current meter data were filtered with a three-hour-low-pass (3-HLP) filter to remove spurious noise, and decimated to one-hour intervals. At most locations the data were also rotated into a coordinate frame determined from the local bathymetry and the principal axis of the data. The degree of rotation is shown as part of the label in all current meter record plots. Data from each deployment period were concatenated to provide continuous records for as long a period as possible. Data files were also passed through a 40-HLP (Lanczos Squared) filter to remove tidal and inertial signals.

1.3.2 Hydrographic Data Calibration, Sample Analysis and Quality Assurance

Salinity, temperature, and depth measurements were made using the Neil Brown Mark IIIB (during the major hydrographic surveys) or Sea-Bird SBE-19 (during the Nearshore Experiments) conductivity, temperature and depth sensor (CTD). Data were collected using software provided by each manufacturer and were stored on 3½" IBM compatible diskettes.

CTD data were transferred into the PODBMS and a unique ID assigned. The data were then checked for spikes, large data gaps and total number of points through an interactive digital processing routine. Initial data inspection was accomplished through temperature versus salinity (T-S) plots of all data from a particular cruise. Vertical temperature profiles were then checked individually as required, using an interactive graphics editor, for accuracy and smoothness. The routine allowed the user to clip bad/noisy casts and to apply a spline to noisy or gappy data in an attempt to smooth the data or supply missing data. The smoothing could be applied to an entire cast or to only a portion of the cast. Bad casts were deleted from the PODBMS.

The data were calibrated in several ways. The near bottom and near surface Niskin bottles were fitted with National Institute of Standards and Technology trackable reversing thermometers (two protected and one unprotected) for primary temperature calibration. Water samples collected in mixed layers provided primary salinity calibration. A Guildline conductive salinometer was used for this determination at Texas A&M University. Periodically during each cruise duplicate salinity samples were collected for a calibration intercomparison with a second institution. The depth sensors were checked by a comparison to wire out, and the depth calculated from the unprotected and protected reversing thermometer readings. The final CTD data were then corrected for any constant, depth, or time-dependent errors. The corrected data were archived to tape (nine-track, EXABYTE, or ¼" cassette) and stored for later use.

One-meter increment data were used to produce vertical sections along and across isobaths and horizontal contour maps of selected temperature surfaces or temperature at a selected depth. Surface tracks were also generated for each survey.

1.3.3 Lagrangian Data

1.3.3.1 ARGOS Tracked Drifters

Both drogued and undrogued drifters (provided separately by MMS and tracked by them) were released during the mooring rotation cruises. Undrogued drifters were either 28 cm diameter spheres manufactured by Metocean Inc., or 37 cm by 18 cm ellipsoids ('pills') made by Aanderaa to a design developed at Charles Stark Draper Laboratories. The drogued drifters consisted of an Aanderaa surface ellipsoid, a 1.0 m long tether and a 0.8 m diameter by 2.5 m long holey sock drogue suspended beneath the tether (mean drogue depth of 2.25 m). This configuration gave a drag/area ratio of 60.6:1. All drifters were tracked via Service ARGOS which provided on the order of six positions per day with an accuracy of roughly ± 500 m. Aanderaa drifters had an on/off operational check using a hand-held test receiver at the time the unit was first turned ON. Access to the Service ARGOS U.S. Global Processing Center (USGPC), through TYMNET, provided an operational end to end check of each drifter at this time. Ship deployed drifting buoys were turned ON before the deployment vessel left port and then monitored to verify correct system operation (location and temperature). In this way, each drifter was monitored for approximately two days prior to the

actual deployment. A backup buoy was carried for each deployment and tested in the same manner.

Drifter data were received daily from Service ARGOS over the Internet. The drifter data were also available through a dialup service, essentially in real time, for use in the field to verify correct operation. These data included all transmissions received from each drifter and each position of the drifter determined by Service ARGOS. The files were edited to separate the position data for processing in the PODBMS, while the transmissions from the drifters were reviewed to evaluate qualitatively battery condition, drogue presence, and sea water temperature.

Interactive procedures removed duplicate positions, verified the validity of each position fix, sorted the data into a time-ordered sequence and archived the data into the PODBMS. Once loaded into the system, a final visual check was made on the data by plotting the individual buoy trajectories on a high-resolution map of the study area, which contained detailed bathymetry and coastline, and looking for spurious changes in the buoy's movement. The ARGOS tracked drifters were initially set to transmit for 50 days. This setting was subsequently reduced to 40 days and finally 30 days. An idiosyncracy of the drifter software resulted in some of the drifters having an ambiguous OFF position in that they came back ON after approximately three months for another 30 to 50 days. One drifter deployed on September 2, 1992 was eventually recovered in early January 1994 aground on Cape Cornwall in England. Two drifters deployed on November 8, 1992 and February 14, 1993 were recovered on the beach near the mouth of the Gironde estuary in France in mid-April 1994. A fourth drifter deployed on August 29, 1992 was recovered on northern Tenerife, Canary Islands in June 1994.

1.3.3.2 Davis-type GPS Drifters

Surface drifters in a configuration designed by Russ Davis (Davis *et al.* 1982) at Scripps Institute of Oceanography were provided by Brightwater Instruments, Inc. The Brightwaters Model 104V drifters were equipped with five channel global positioning system (GPS) receivers (Rockwell NAVCOR V) and VHF packet communications telemetry transceivers. The drifter comprised a central vertical tube containing the VHF transmitter and central memory unit, batteries and antenna support masts for the GPS unit and VHF antenna; four drag producing vanes emanating at 90 degree angles

from the center tube; and four spherical floats attached by flexible lines at the upper outer extension of the vanes to provide flotation. This design was generally considered to be a good surface current following device with a buoy slip on the order of 1.5 to 3.0 $cm \cdot s^{-1}$ (Davis *et al.* 1982). GPS tracking permitted accurate geographic location to within tens of meters. An ARGOS tracked spherical drifter was loosely tethered to each of these drifters to aid in location if the drifter were out of VHF range. A total of seven drifter deployments were carried out, four in June 1993 and three in September 1993, with up to four days tracking duration.

Data were recovered from these instruments over VHF radio links in real time and by copying the same data from an internal memory unit when the units were recovered. The first step in processing drifter positions was to eliminate occasional spurious fixes. This was accomplished by taking advantage of the tendency for drifter velocity to change slowly relative to the positioning frequency. The procedure was to divide the position time series into segments of six positions each. Linear regressions of position component vs. time were carried out within each segment. If any position component within a segment deviated from the regression line by more than 150 m, the most deviant point of the segment was eliminated. It was replaced with a position which fell on a position component vs. time regression line computed with all the segment's other points.

Linear regression was also used in determining drifter velocity from the position time series with spurious fixes eliminated. The north or east velocity component at the mid-point of a data segment was taken as the slope of the position component vs. time linear regression over the segment (i.e., north velocity was set to the slope of the north position vs. time regression line, and east velocity was set to the slope of the east position vs. time regression line). A velocity component time series was determined in this manner by stepping a "regression window" of 17 points (4.25 hours) long through a position component times series. Results of these experiments were used primarily in the discussion in Chapter 8.

1.4 Report Organization

The remainder of this report consists of analysis of the data collected during the first eighteen months of the study and

synthesis with existing knowledge. The report is organized in the following Chapters:

- II. THE GULF STREAM - a discussion of Gulf Stream mean path, meanders and frontal eddies, and cross stream structures;

- III. DEEP SLOPE CURRENTS - a discussion of the Deep Western Boundary Current (DWBC) and Topographic Rossby Waves (TRW);

- IV. SHELF CLIMATOLOGY - a discussion of means, standard deviation and standard error of currents, winds, hydrography, tides, and Middle Atlantic Bight/South Atlantic Bight front convergence;

- V. SHELF SLOPE PROCESSES - a discussion of Gulf Stream current influence, Gulf Stream Water intrusions, Shelf Water export, and Slope Water influences;

- VI. WIND FORCING - a discussion of statistics of major meteorological events (December 1992 storm, March 1993 'storm of the century', and Hurricane 'Emily' in August 1993) which occurred during the study period;

- VII. SHELF TRANSPORT PROCESSES - a discussion of upwelling/downwelling, freshwater influences from Chesapeake Bay and the Carolina Sounds, and VCW intrusions; and

- VIII.NEARSHORE CIRCULATION - a discussion of nearshore hydrography and onshore/offshore flow.

II. THE GULF STREAM NEAR CAPE HATTERAS

2.1 Background

The Gulf Stream flows just offshore of the edge of the continental shelf in the Cape Hatteras region. Because the continental shelf is only 20-30 km wide here, compared to as much as 200 km wide to the north and south, off New Jersey and Georgia, the current approaches relatively near to the Cape Hatteras shore. Offshore of the shelf break, the continental slope is also particularly narrow and steep in the Cape Hatteras region, dropping from 200 m to 2000 m (or 3000 m) in an additional distance of only 15 km (or respectively 45 km). In this steep bottom-slope region the Gulf Stream exhibits a minimum in meandering: for example the width of the envelope of root-mean-square (rms) lateral shifting of its path is only 10 km (Watts 1983).

The Gulf Stream may be said to follow a time-varying "path" which meanders, because the cross-sectional structures of the current and of the water temperature are remarkably similar from one time to another, when viewed in a frame that shifts laterally with the path. (This statement excludes times of interactions with Gulf Stream rings.) Consequently, various easily-identified features encountered in any section across the Gulf Stream, such as the northern edge, at which the SST changes rapidly, or the high-speed core, may be taken as indicators of its "position," and linked together alongstream to define its "path". A representative example of a transect of the temperature and velocity structure spanning the whole Gulf Stream just offshore Cape Hatteras will be shown in Figure 3.1-1, from Pickart and Lindstrom (1994). Other, earlier transects taken within a few hundred kilometers up and downstream of Cape Hatteras were shown in the SAIC (1993) summary of scientific literature in the study region.

Meandering motions of the Gulf Stream front with periods ranging from a few days to several months are often called frontal eddies. The crests (shoreward deflections of the front) often have steep trailing edges and strong cyclonic circulations in the troughs, which upwell colder deeper water to the surface layers. The vigorous circulations can expel warm Gulf Stream waters from the crest to generate characteristic trailing filaments. Bane *et al.* (1981) describe meander and frontal eddy circulations along the Carolina Bays. The amplitude of the meanders varies up to 50 km, and alongslope wavelengths range from 60 to 250 km. Meander phase

speeds in this region range from about 10 to 60 km•d^{-1} (Tracey and Watts 1986; Bane and Dewar 1988), with shorter periods propagating faster and longer periods slower.

A more detailed summary of the current and temperature structure and of the variability of the Gulf Stream near Cape Hatteras may be found in SAIC (1993).

2.2 Gulf Stream Path and Shoreward Edge Currents

This section summarizes the climatology and variability during the North Carolina field program regarding currents and temperatures measured at the two uppermost levels (100 m and 300 m) on the moorings on the continental slope, A4, A5, B4, and C4. Means, variances, time-series characteristics, and events are discussed and interpreted in this section.

The three offshore-most moorings (A5, B4, and C4) were located within the shoreward edge of the Gulf Stream, and mooring A4 was in the southernmost wedge of the Slope Sea water, whose upper waters flow into the Gulf Stream. (The measurement records at 800 m and deeper on these same moorings are treated in Chapter III.)

2.2.1 Mean Currents and Variances

Figures 2.2-1 and 2.2-2 summarize the means and variance ellipses on moorings A4, A5, B4, and C4 at 100 m and respectively 300 m depths. The first three six-month mooring periods are included in this summary, February 1992 to August 1993. Moorings A4, B4, and C4 were located along the 2000 m isobath and mooring A5 was on the 3000 m isobath.

In the mean, very similar currents were experienced at the three offshore-most moorings (A5, B4, C4): about 110-125 cm•s^{-1} to the northeast at 100 m depth and about 35-50 cm•s^{-1} at 300 m depth. The direction at 300 m depth was approximately parallel to that of the 100 m mean current; small backing or veering of the direction with height will be discussed shortly.

On mooring A4 the mean currents were, by contrast, weak (3-5 cm•s^{-1}) and to the southeast and south at 100 m and 300 m depths. This mooring was located in the mean near the southern limit of the Slope Sea waters, offshore of the continental shelf and inshore of the Gulf Stream. The upper Slope Sea waters flow generally

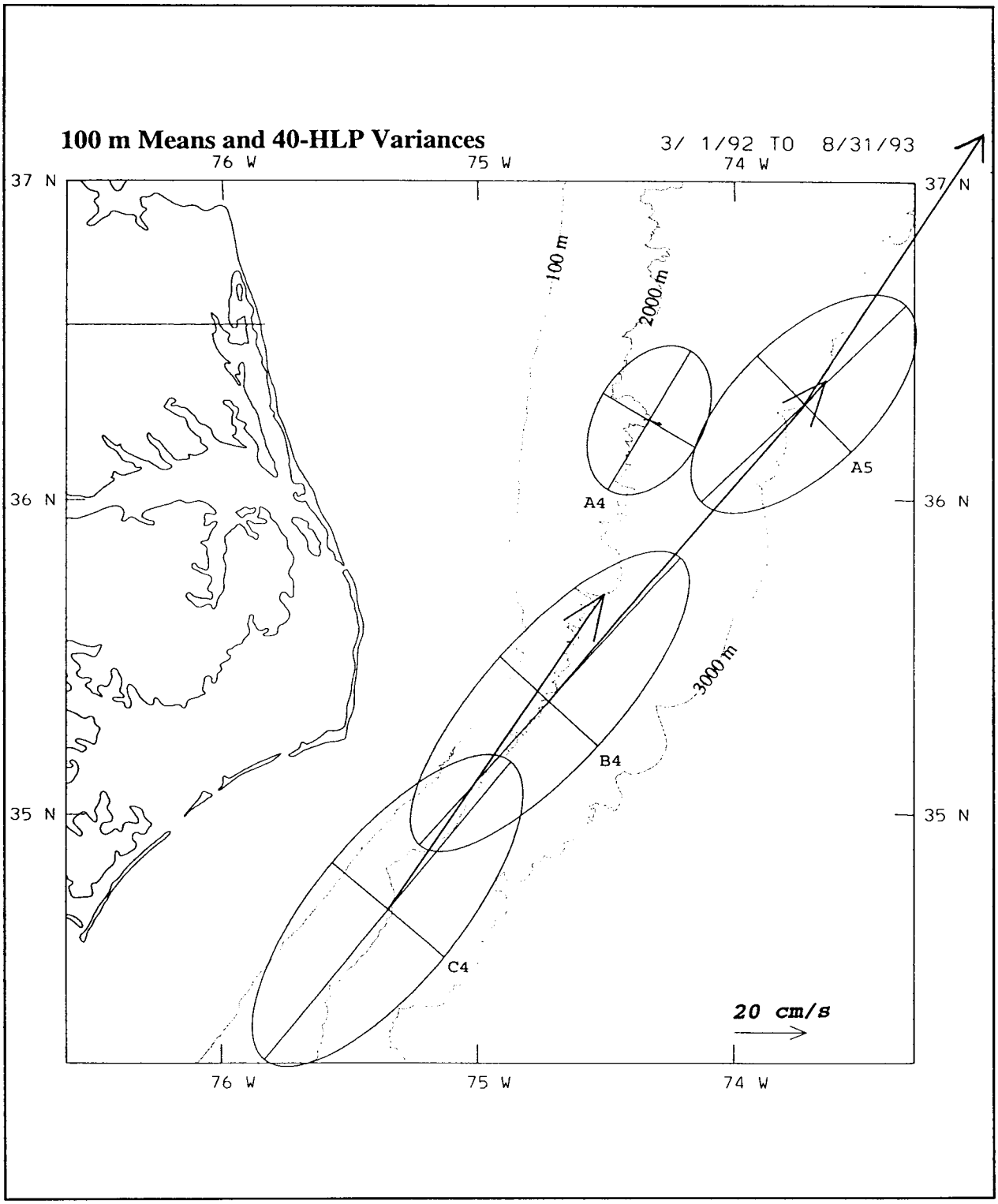

Figure 2.2-1. Mean current vectors and variance ellipses for Moorings A4, A5, B4 and C4 at 100 m. Time period is March 1992 through August 1993.

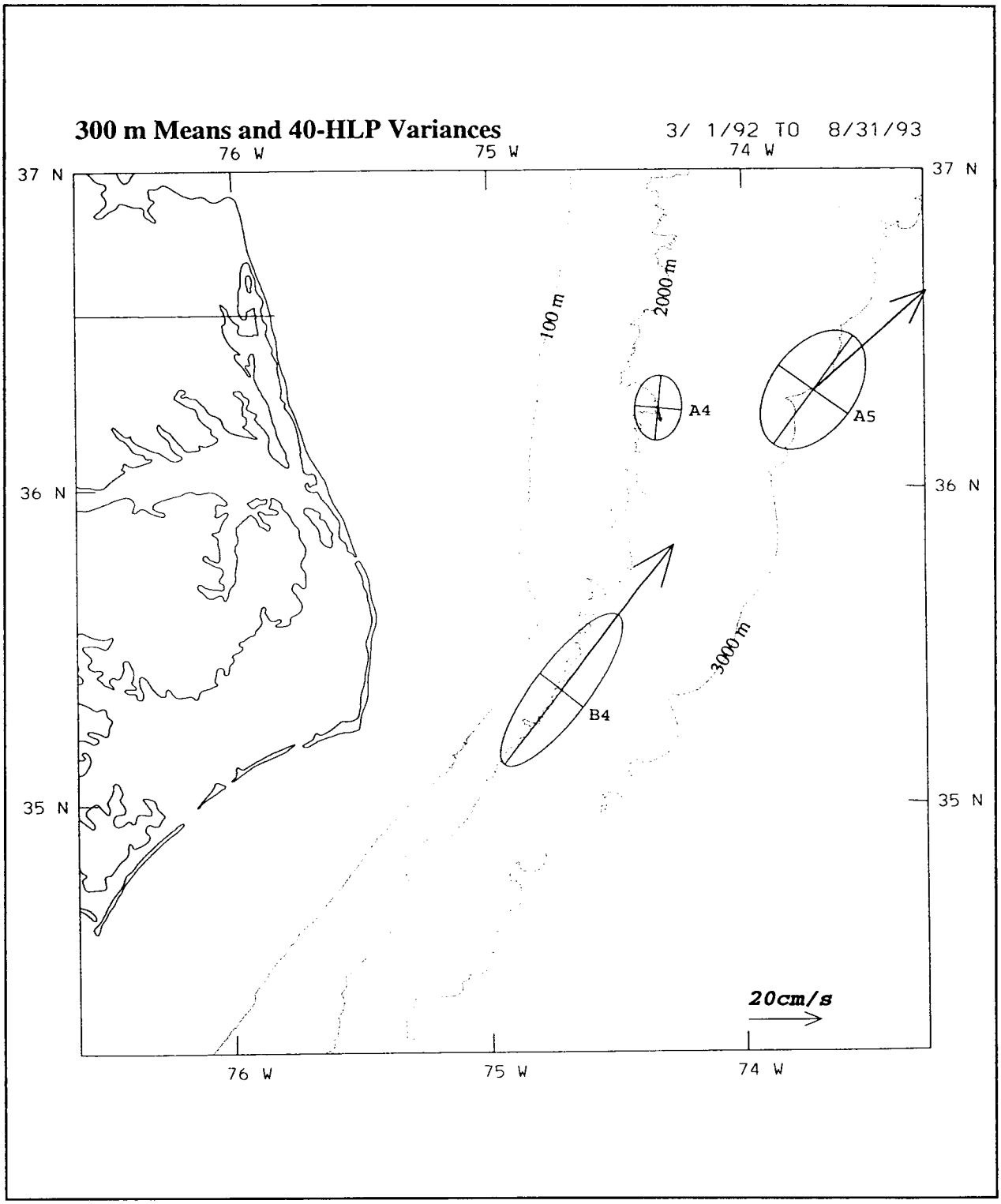

Figure 2.2-2. Mean current vectors and variance ellipses for Moorings A4, A5 and B4 at 300 m. Time period is March 1992 through August 1993.

southwestward and then turn to the east to join the Gulf Stream. (Portions of the deeper, colder Slope Sea waters can cross southward under the Gulf Stream as part of the DWBC, as will be discussed in the next chapter.)

Before discussing the variability at these sites, it is helpful to view these mean currents in relationship to the mean cross-sectional current profile of the Gulf Stream on the 100 m and 300 m levels, as illustrated in Figure 2.2-3. These profiles are taken from measurements by Halkin and Rossby (1985) on a transect just 60 km northeast of mooring A5. The profiles represent the mean current structure on fixed horizons directly measured during 18 Pegasus surveys spanning three years. The mean currents in this figure were calculated in "stream coordinates", in which the current position for each survey was shifted and rotated (as described in Halkin and Rossby 1985) so that the position of the current was consistent for each section and the angle was always normal. Comparison with this stream coordinates section seems most appropriate for the new data on the Cape Hatteras sections, where the current only shifts laterally by a small fraction of its width, as shown in Figure 2.2-4, and as will be quantified later.

The geostrophic current section (absolutely referenced) shown later in Figure 3.1-1 was measured on a transect between sites A5 and B4; these measurements show an upper current structure above about 500 m that is very similar to the Pegasus mean section in Figure 2.2-3, although it is important to note that deeper levels in this region may exhibit different structure for two reasons: (1) Energetic topographic Rossby waves affect the instantaneous section of the deep currents; and (2) The nearness of the steep continental slope and the DWBC crossing under the Gulf Stream may alter the deep current structure (both discussed in the following chapter).

It is informative to discuss the currents along the Gulf Stream inshore edge in relationship to the full jet structure, as revealed in the Pegasus section (Figure 2.2-3). The mean currents on this section at x=-20 to -30 km are consistent with the mean currents at 100 m of 110-125 $cm \cdot s^{-1}$ and at 300 m of 35-50 $cm \cdot s^{-1}$, such as observed on moorings A5, B4, and C4. The variability of the currents at 100 m and 300 m is strong at sites A4, A5, B4, and C4, in association with lateral shifting of the Gulf Stream and with inshore frontal eddies. Plotted in Figures 2.2-1 and 2.2-2 are also the standard deviation ellipses (square root of the variance about the mean on semi-major and semi-minor axes) at respectively 100 m and 300 m

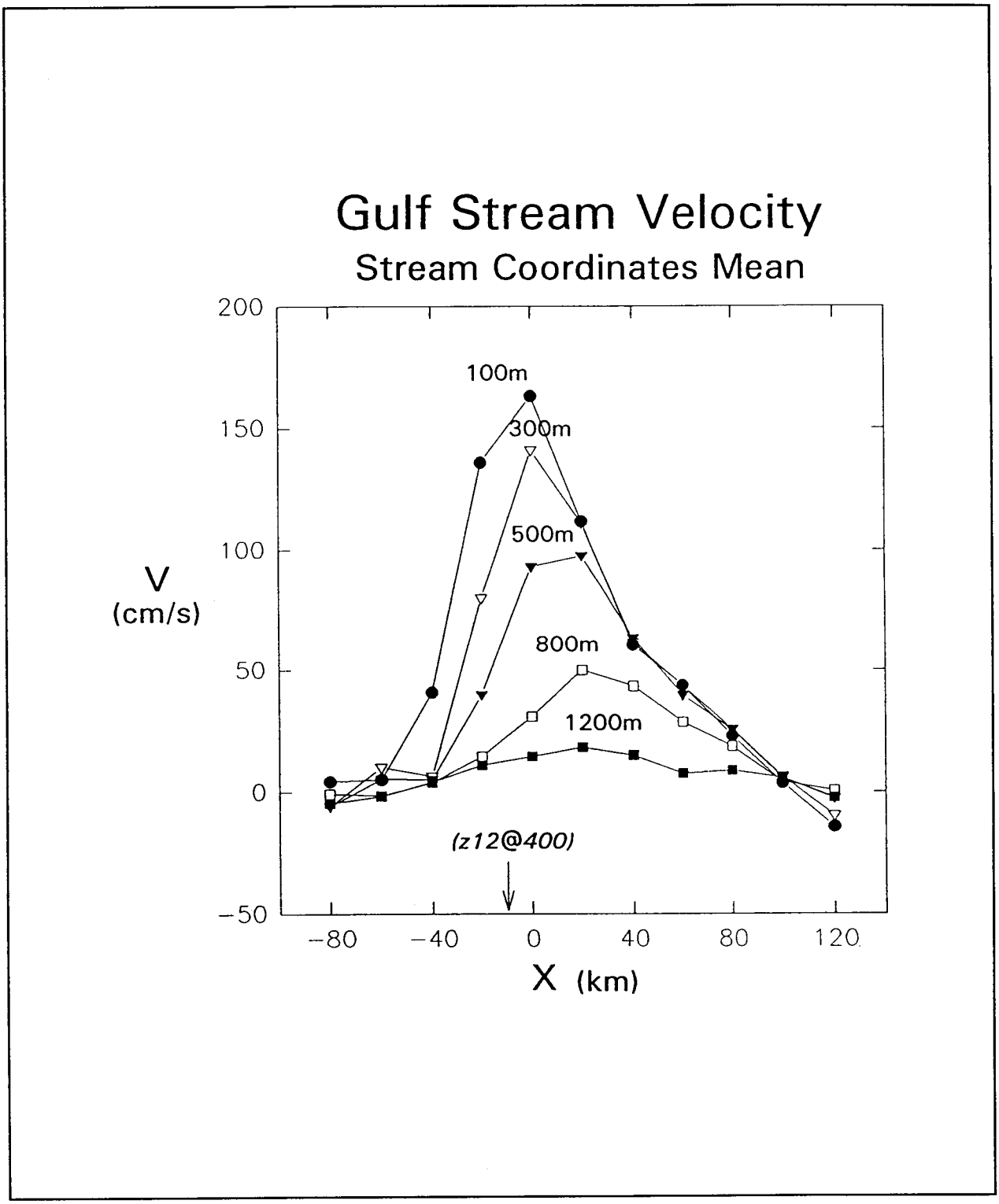

Figure 2.2-3. Cross stream velocity profiles of the Gulf Stream on horizons (data extracted from Halkin and Rossby 1985).

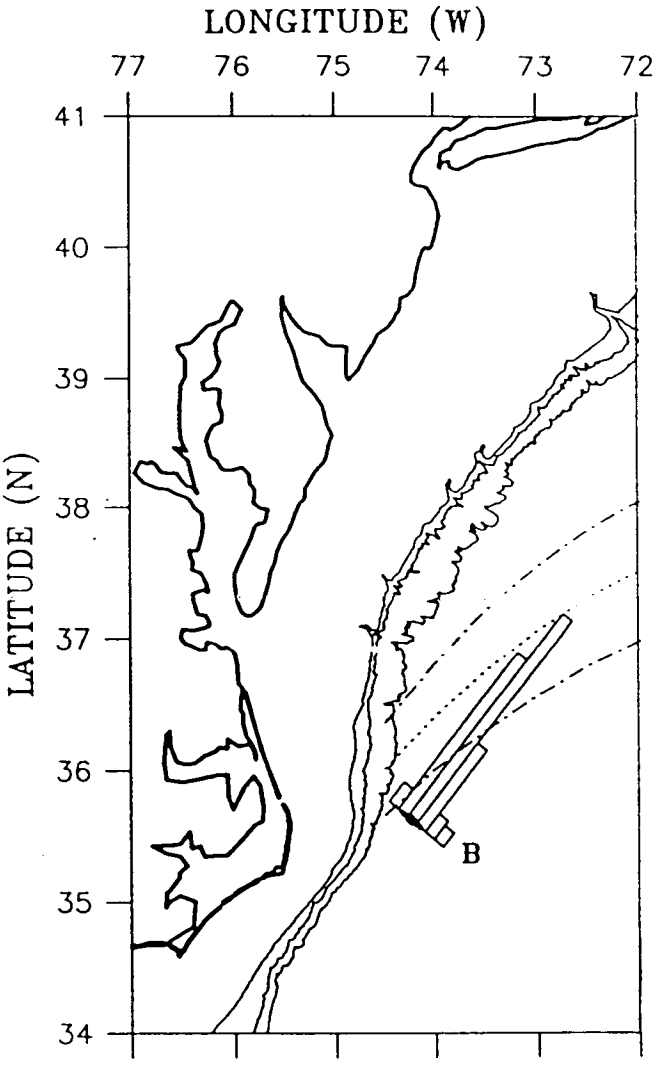

Figure 2.2-4. Histogram of Gulf Stream positions offshore Cape Hatteras (from Watts *et al.* 1995). Dotted and dash-dot lines indicate the Gulf Stream mean path and standard deviation, respectively, of the surface front during 1982-1989 supplied by Lee (1994).

depths. The ellipses are relatively elongated (longitudinally polarized) at the southern two sites B4 and C4, with semi-major axes around 50-60 $cm \cdot s^{-1}$ at the 100 m depth and nearly parallel to the mean currents; the semi-minor axes are about 20 $cm \cdot s^{-1}$. The corresponding values at 300 m depth are about 25 $cm \cdot s^{-1}$ on the semi-major axes and 8 $cm \cdot s^{-1}$ on the semi-minor axes at sites B4 and C4.

The standard deviation ellipses may be interpreted simply and consistently with the small observed amount of lateral shifting and angle change of the basic Gulf Stream profiles (*e.g.*, Figure 3.1-1) as follows: The rms amount of lateral and angular shifting of the Gulf Stream offshore of Cape Hatteras is reported in Watts *et al.* (1994) from IES measurements that resolved the Gulf Stream position with 5 km accuracy. Figure 2.2-4 shows those results on a line that extended offshore from Line B of this program for about three years, in 1987-1990, preceding this experiment. Shown is the probability histogram of the position where the 12°C isotherm crosses 400 m depth, which, relative to the current velocity structure of Figure 2.2-3 corresponds to about -10 km, under the left side of the current core. Figure 2.2-4 also shows that the rms lateral shifting of this position is only about 10 km. They also report that the rms angle change is about 10° at this location. By combining this variability with the information on the mean current structure in Figure 2.2-3, convolving as if it were a rigid structure, one may obtain the following estimates of the standard deviation (ellipses) of alongstream and lateral components of current. A lateral shift of ±10 km about x=-30 km would produce an alongstream component change of ±50-60 $cm \cdot s^{-1}$ at 100 m and ±20 $cm \cdot s^{-1}$ at 300 m. Similarly a ±10° turn in current path would produce a cross-stream sine-projection of the alongstream current components at 100 m and 300 m (120 $cm \cdot s^{-1}$ and 50 $cm \cdot s^{-1}$ at x=-30 km) of respectively 20 $cm \cdot s^{-1}$ and 9 $cm \cdot s^{-1}$. These values are in excellent agreement with the standard deviation ellipses observed at sites C4 and B4. Altogether, this evidence supports the concept that the Gulf Stream current and temperature structure shifts like a remarkably rigid structure.

The standard deviation ellipses at site A5, although its mean position and currents are similarly located to sites B4 and C4, are somewhat smaller than the above corresponding values. They are also more nearly circular (unpolarized) with both axes about 30 $cm \cdot s^{-1}$ at 100 m depth and about 15 $cm \cdot s^{-1}$ at 300 m depth. The preceding simplified arguments, based on an increased amount of meandering at site A5 over B4 or C4, would have predicted a

slightly greater alongstream-component of variability. The values for site A5 at 100 m were only from the first six-months deployment, for which the current variability at sites B4 and C4 was somewhat lower than the second and third deployment periods, and thus may slightly under-represent the 18-month standard deviations. However, on mooring A4 the first six-month variances were roughly typical of the other two periods. The differences between the standard deviation ellipses at site A5 are not statistically distinct from those at sites B4 and C4.

The standard deviation ellipses at site A4 are somewhat smaller yet than the above at the corresponding 100 m and 300 m depths. They are also more nearly circular. This corresponds to weaker, unpolarized eddy variability in the Slope Sea adjacent to the Gulf Stream. At 100 m depth the semi-major and semi-minor axes are about 20 $cm \cdot s^{-1}$ and 15 $cm \cdot s^{-1}$; at 300 m depth the corresponding values are 9 $cm \cdot s^{-1}$ and 7 $cm \cdot s^{-1}$.

2.2.2 Stability of the Statistics

In most cases, from a tabulation of all the moored current results summarized separately by mooring period, the mean currents and variances at 100 m and 300 m observed at all the Cape Hatteras slope sites (A4, A5, B4, and C4) produced remarkably stable statistical estimates. The different averages taken over individual six-month periods agreed well in most cases. The degree of consistency among all these measurements is presumably a result of the steep bathymetry constraining the Gulf Stream to meander very little off Cape Hatteras.

The variability of these six-month means around the values plotted and discussed above was particularly small at the three sites C4, B4, and A5, which were located along the Gulf Stream shoreward edge. Six-month means and directions varied by less than 25% and 5°. Moreover, the standard deviation along the principal (downstream) component varied by less than 20%. Of course there is some variability between mooring periods; for instance at site B4 (100 m) the first six months had about 35% lower standard deviation than the other two mooring periods, as the Gulf Stream remained closer to shore and meandered somewhat less during this period. Site A4 also had fairly consistent six-month averages at 300 m, with speed and direction varying around those shown in Figure 2.2-2 by only 35% and 21°. However, at 100 m on A4 during the third six-month deployment the mean speed was about 75% higher than the other

two, and the mean angle shifted nearly 60° to south-southeast. All of these may still be taken as remarkable stability between averages of only six-month records of currents, suggesting that the 18-month averages are quite reliable.

2.2.3 Time Series and Events.

The time series measurements of currents at C4 and B4 (Figure 2.2-5) and A4 and A5 (Figure 2.2-6) are treated in this subsection. At all four sites the currents on the 100 m and 300 m levels are very similar, (*i.e.*, with high visual coherence and differing mainly by a scale factor of approximately two from 300 m to 100 m). By contrast, the currents at 800 m and deeper also show a high degree of vertical coherence on each given mooring (as will be discussed in Chapter III), but they bear little resemblance to the current records at the two upper levels. The reasons behind this change in character above and below 800 m are associated with the facts that upstream of Cape Hatteras the Gulf Stream flows on the Blake Plateau in mean depths of 800 m or less, whereas in greater depths near Cape Hatteras the Deep Western Boundary Current crosses under the Gulf Stream.

Because fluctuations tend to translate downstream, the discussion begins with records C4 and B4 at 100 m and 300 m. These two records also exhibit a great deal of downstream coherence (Figure 2.2-5). At both levels the currents almost always flow in a direction parallel to the Gulf Stream and almost never reverse. The speeds do oscillate rapidly in strength with characteristic period 7 days. At 100 m depth they range often from 200 $cm \cdot s^{-1}$ to near zero; at 300 m depth they range from about 100 $cm \cdot s^{-1}$ to near zero. Peak speeds at 100 m exceeded 250 $cm \cdot s^{-1}$, and at 300 m exceeded 125 $cm \cdot s^{-1}$. The strongest current reversal at 100 m occurred at site B4 near December 15, 1992, with 140 $cm \cdot s^{-1}$ flow offshore and slightly southward. A satellite SST image from December 18, 1992 (Figure 2.2-7) is suggestive of a Gulf Stream ring interaction at this time.

Preceding that event for several days around November 29, 1992, the upper currents at both sites B4 and C4 exhibited the strongest case of reversal that also had a shoreward component of flow (50 $cm \cdot s^{-1}$). To the south in Raleigh Bay, Gulf Stream water had intruded well onto the shelf, and just downstream of that, the currents at mooring sites C4 and B4 exhibit large eddy fluctuations.

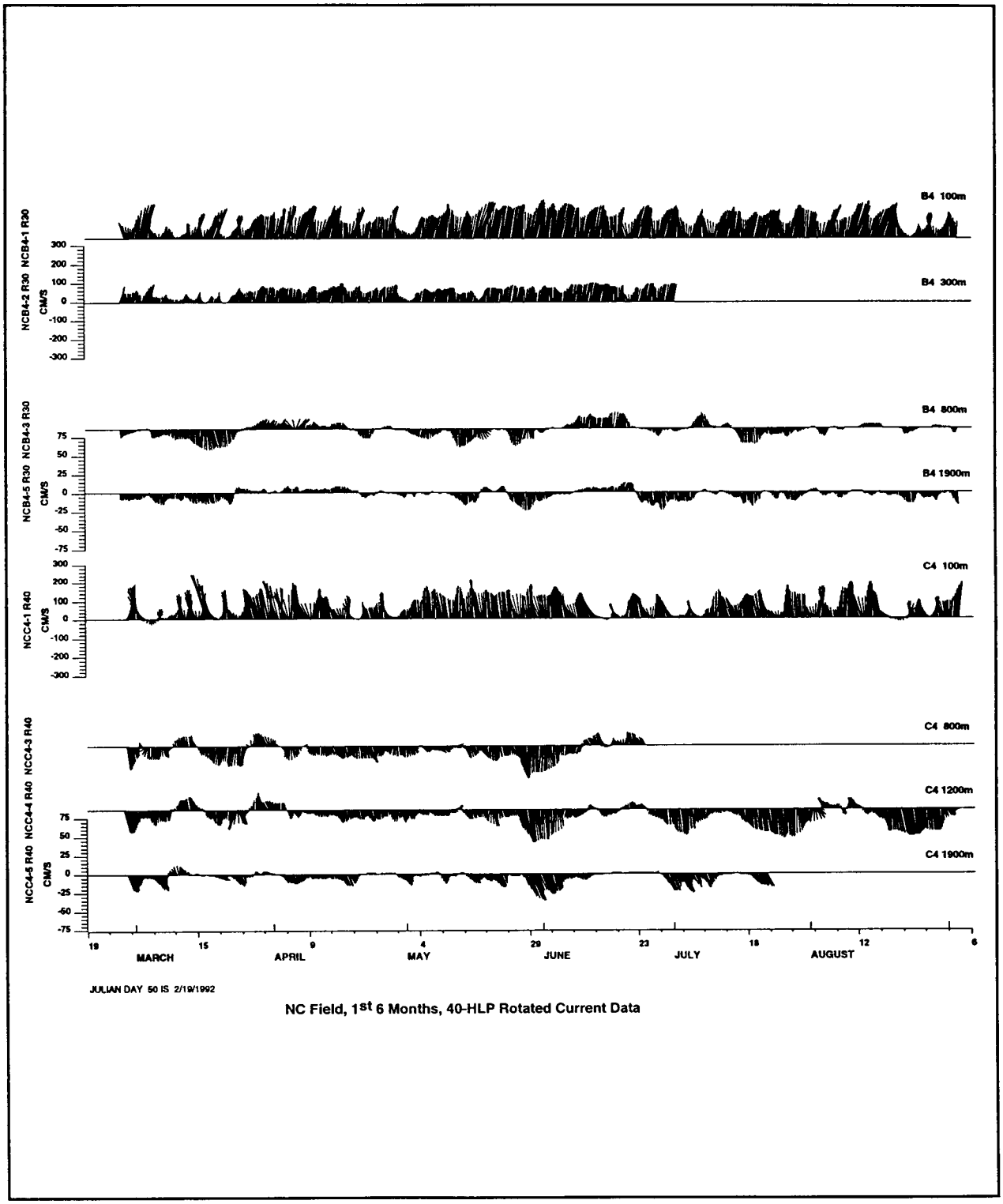

Figure 2.2-5(a). Stick vector plots of 40-HLP currents at Moorings C4 and B4 for the period February 19, 1992 through September 6, 1992.

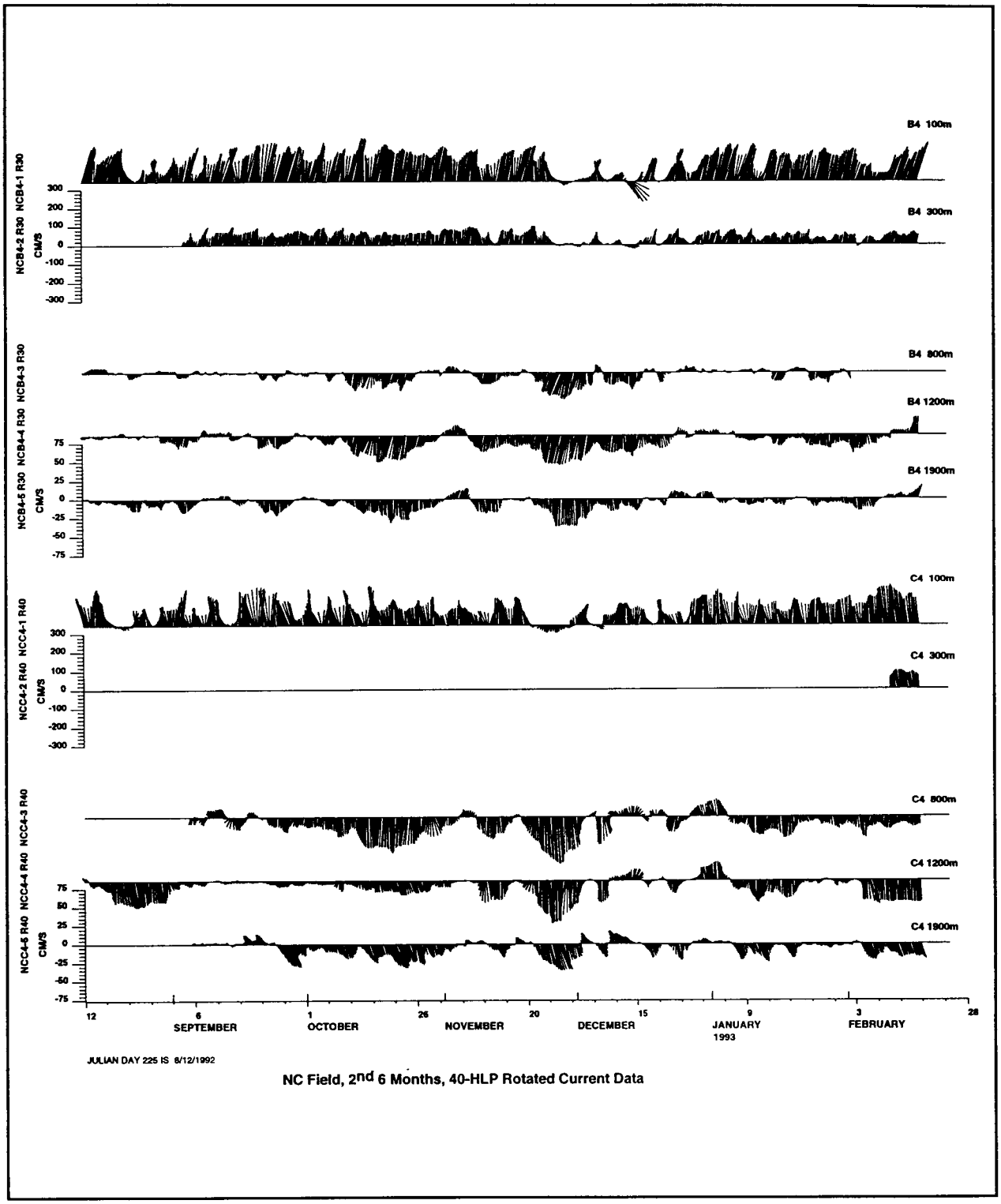

Figure 2.2-5(b). Stick vector plots of 40-HLP currents at Moorings C4 and B4 for the period August 12, 1992 through February 28, 1993.

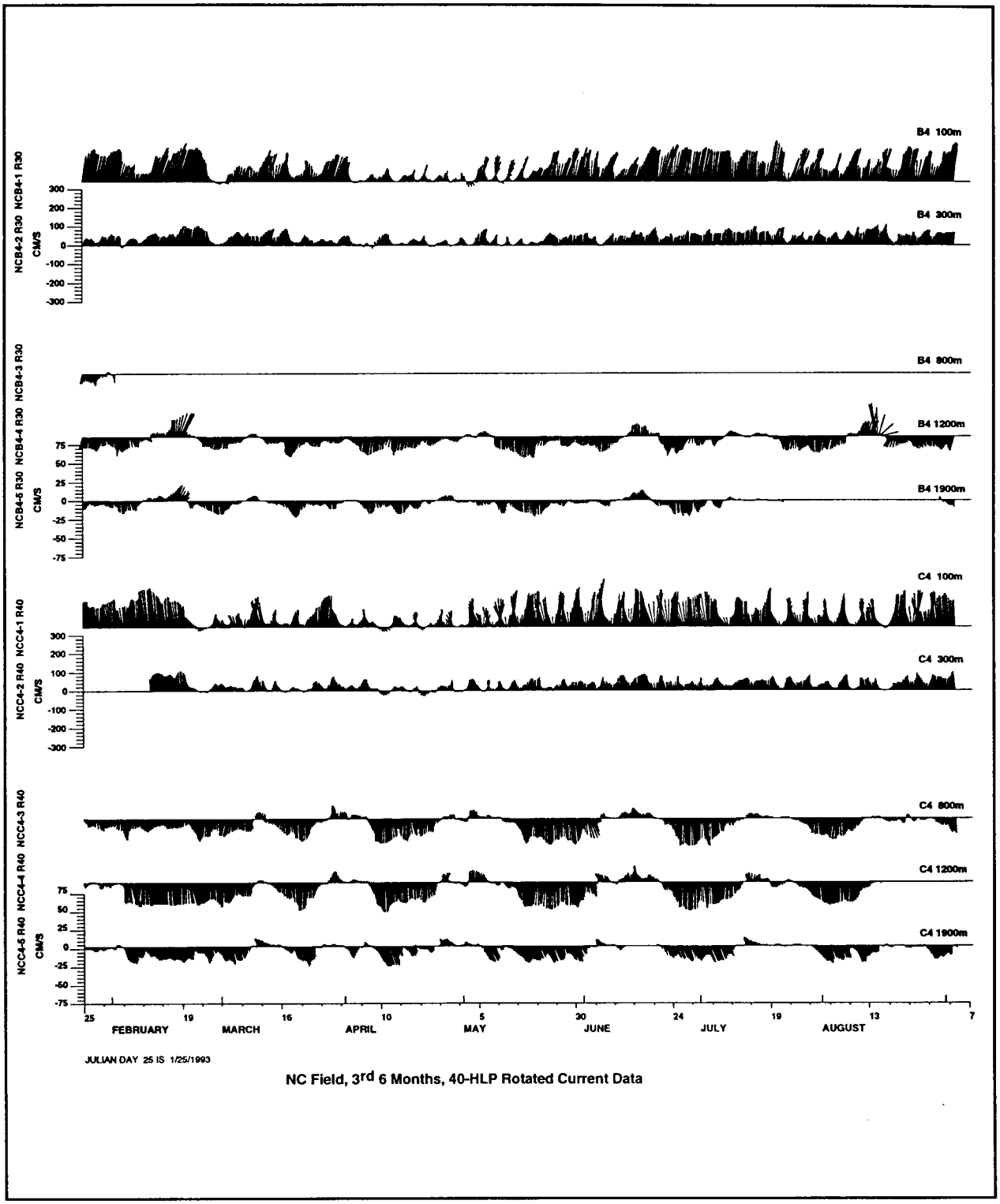

Figure 2.2-5(c). Stick vector plots of 40-HLP currents at Moorings C4 and B4 for the period January 25, 1993 through September 7, 1993.

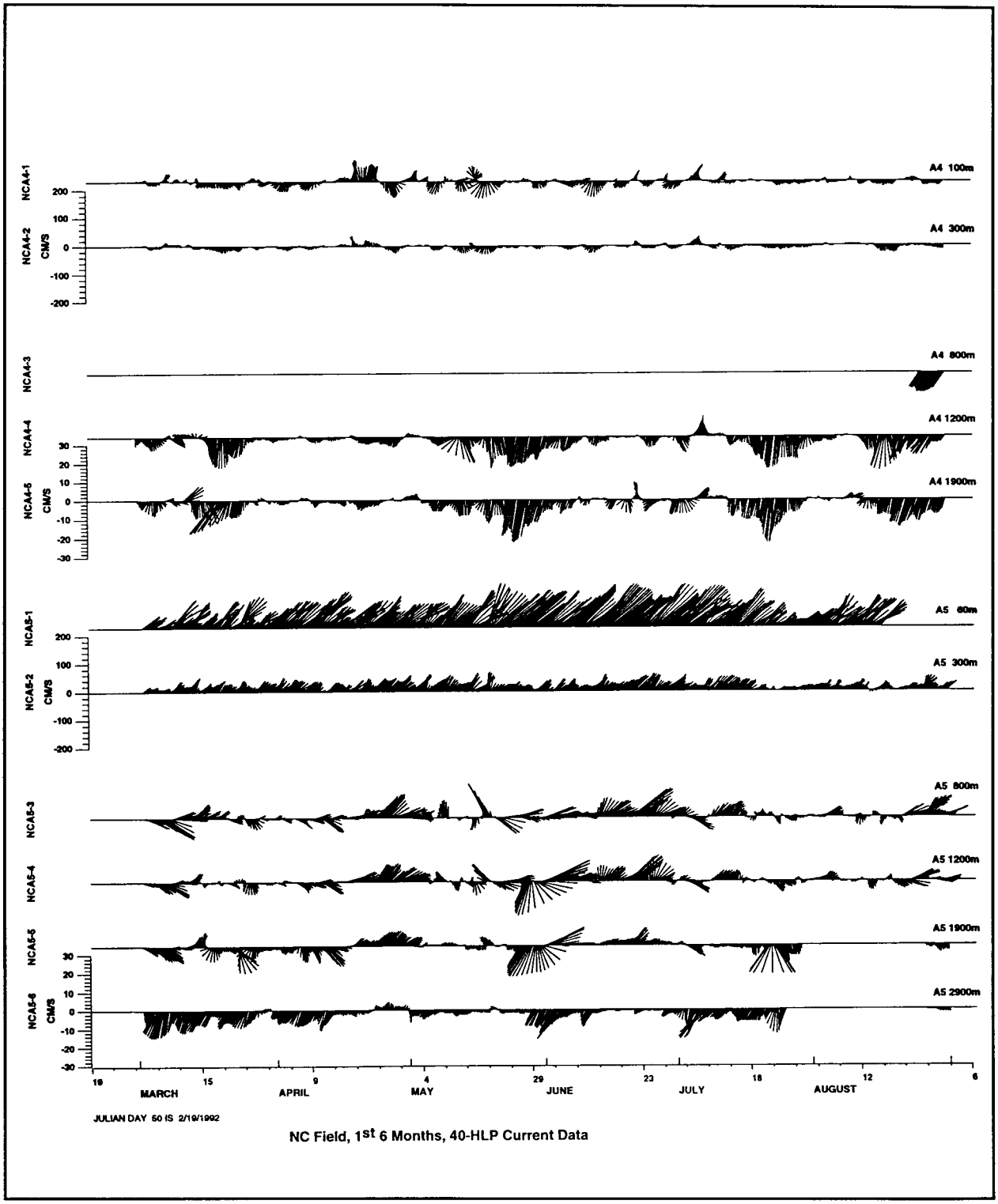

Figure 2.2-6(a). Stick vector plots of 40-HLP currents at Moorings A4 and A5 for the period February 19, 1992 through September 6, 1992.

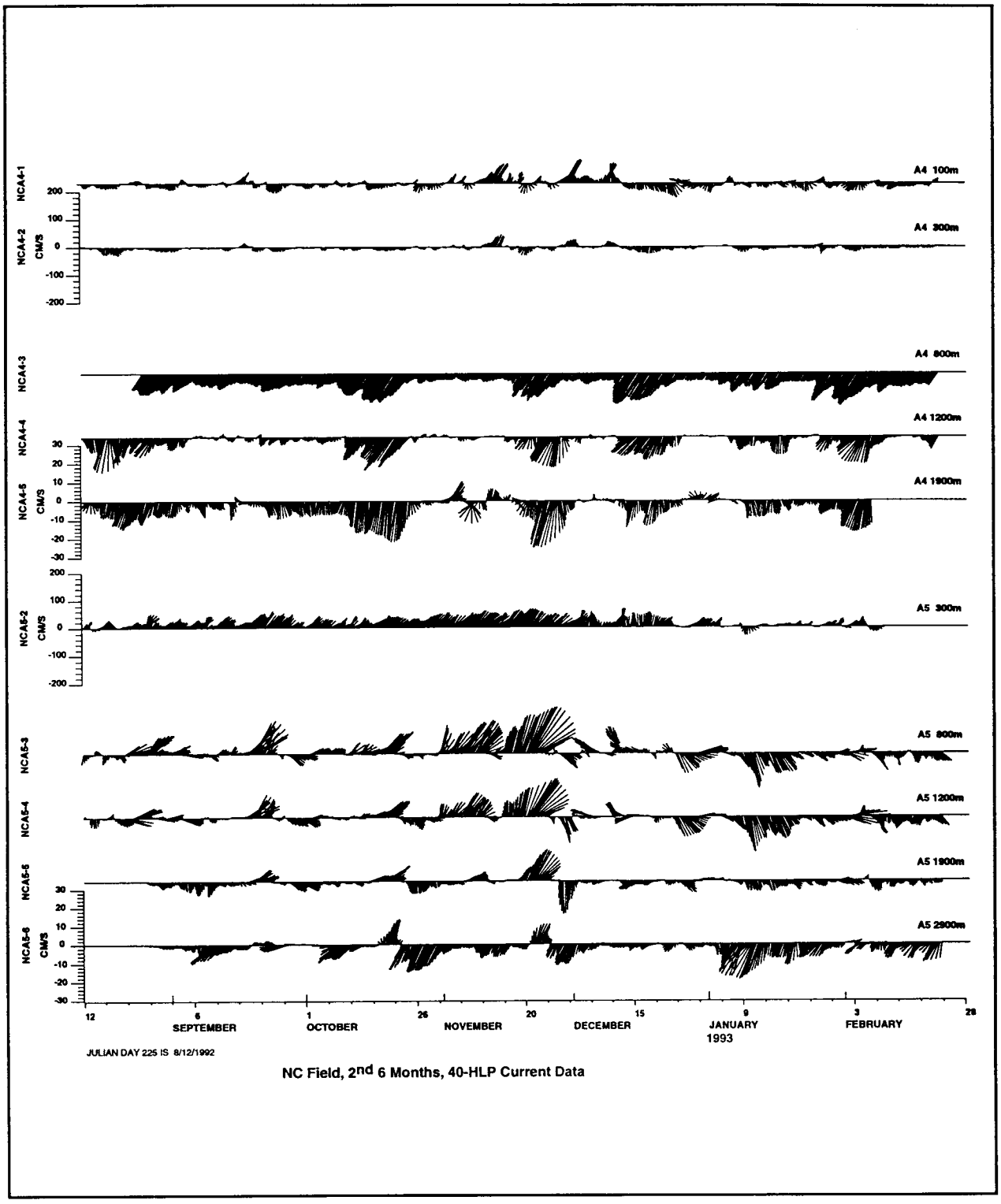

Figure 2.2-6(b) Stick vector plots of 40-HLP currents at Moorings A4 and A5 for the period August 12, 1992 through February 28, 1993.

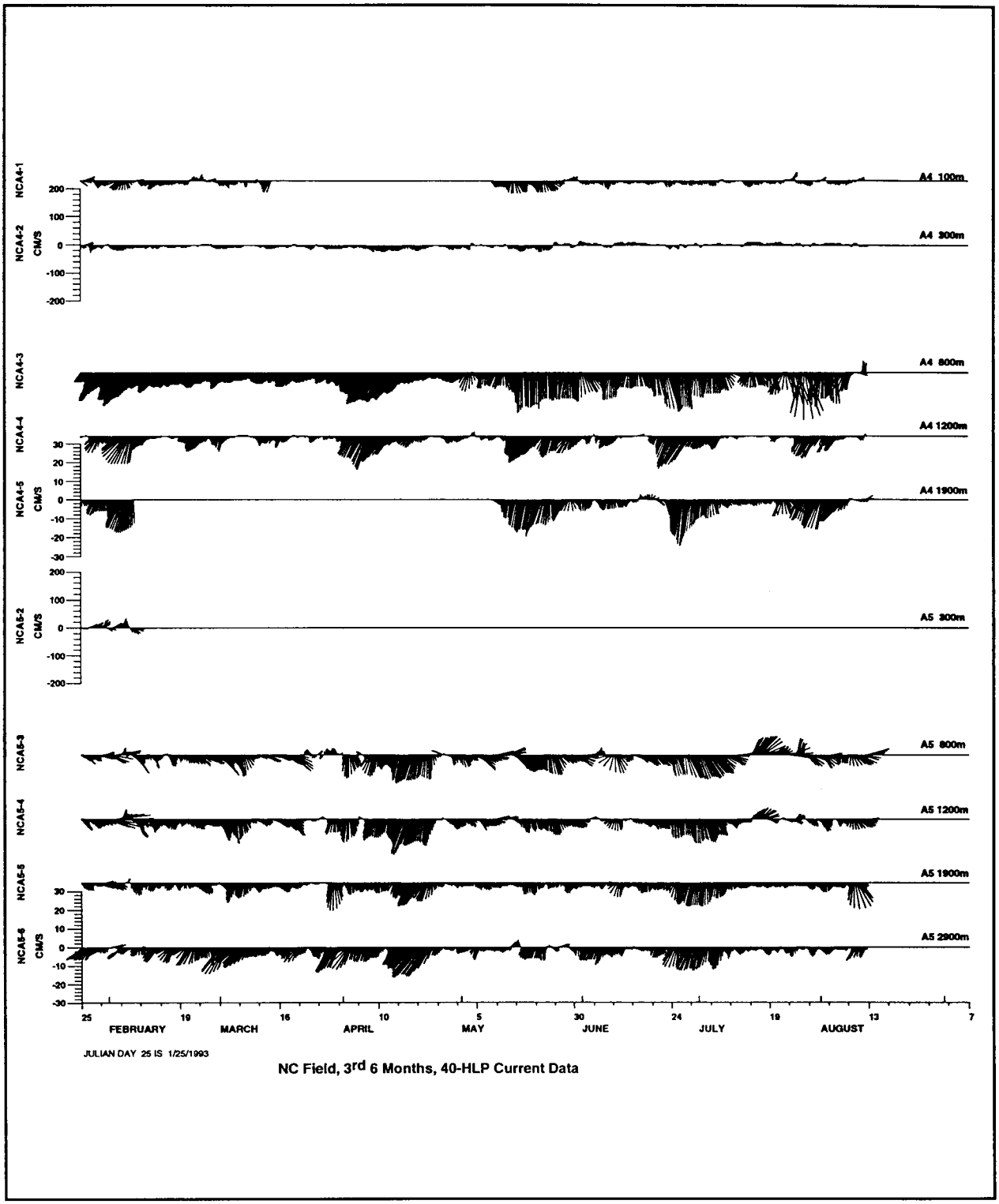

Figure 2.2-6(c). Stick vector plots of 40-HLP currents at Moorings A4 and A5 for the period January 25, 1993 through September 7, 1993.

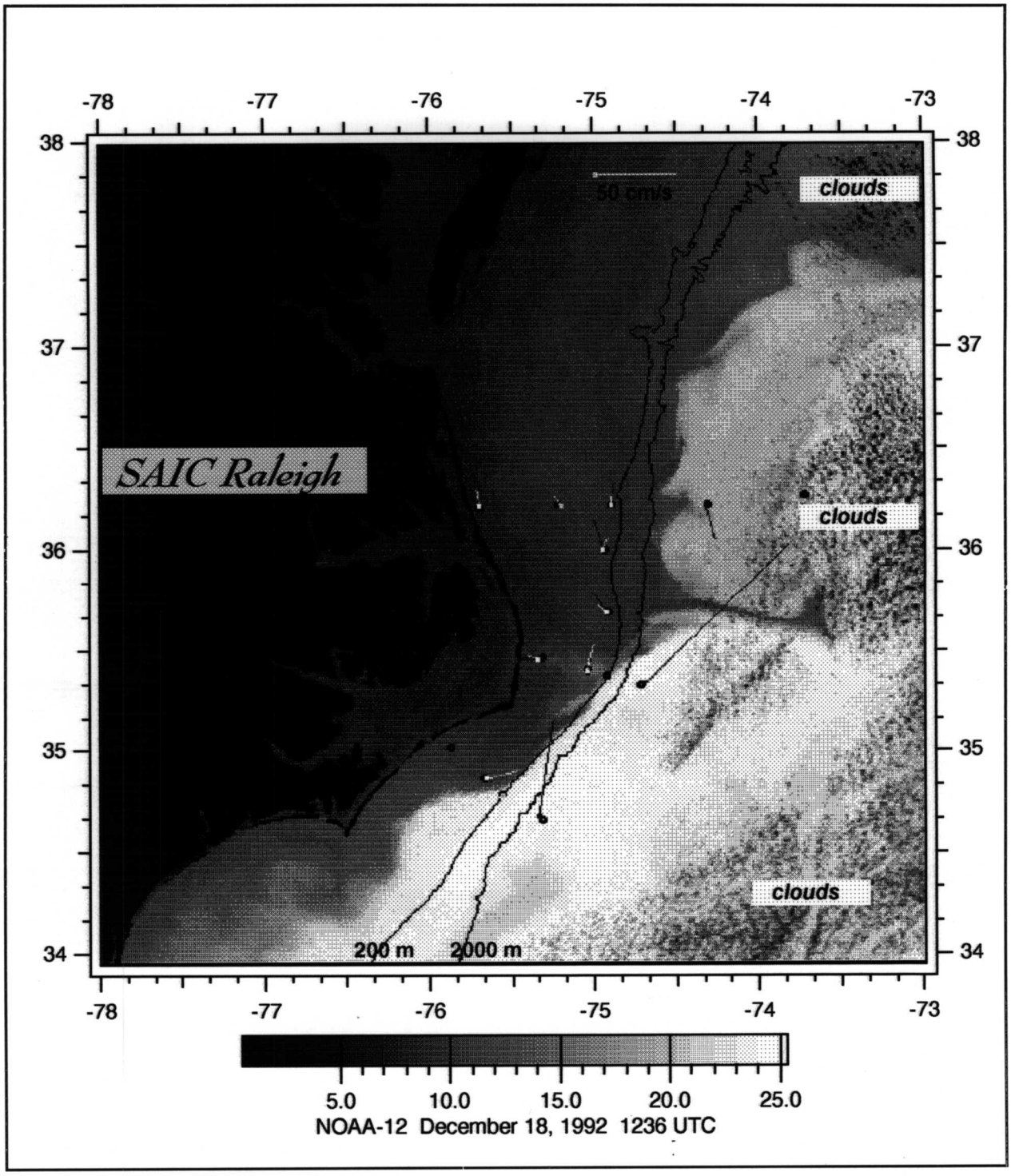

Figure 2.2-7. Satellite SST image and daily average current vectors on December 18, 1992. Vector scale is at top of figure. Surface vectors (dark) are at 5 m (shelf moorings) and 100 m (deep moorings). Bottom vectors (light) are 5 m above bottom on shelf.

The characteristic period of upper current pulsing and relaxing at sites B4 and C4 decreased from 7 days in the first deployment period to 5 days in the third.

There was no obvious seasonal migration of the current onshore/ offshore. However, there were clearly shorter one- to four- month trends in position, which resulted in stronger or weaker currents at sites C4 and B4. The most pronounced and persistent trend at sites C4 and B4 was an offshore shift in the Gulf Stream from about April 1, 1993 to May 15, 1993. During this time period satellite images show the flow on the shelf having persistent southward flow, rounding Cape Hatteras well into Raleigh Bay before turning to join the Gulf Stream. A series of relatively large or rapidly growing inshore frontal eddies was evident in these images.

By contrast, during the spring months of the preceding year (April through June 1992) the currents at sites C4 and B4 can be seen in Figure 2.2-5(a) to be the most persistently strong, rather than weak as in spring 1993. The currents flowed at about 200 $cm \cdot s^{-1}$ as the Gulf Stream was shifted onshore relative to its mean path. Satellite images confirm this shift, and indicate that shelf water does not flow southward round Cape Hatteras during this period.

The time series of upper level currents north of Cape Hatteras at mooring sites A4 and A5 are shown in Figure 2.2-6. Site A5, in the currents of the Gulf Stream shoreward edge, has a record for only the first six-month deployment period. However, similar to sites B4 and C4, the currents at A5 show rapid oscillations of the strength of the northeastward current but no current reversals. The characteristic periods of fluctuation are 5-10 days. Site A5 also shows a two month period of relatively strong currents (exceeding 200 $cm \cdot s^{-1}$) from mid-May to mid-July, 1992. The onshore shift of the Gulf Stream noted above for sites B4 and C4 is confirmed by satellite images to continue northeastward in nearly a straight path over site A5, rather than follow its mean path, which curves slightly offshore.

The currents at A5 (300 m) are fairly coherent with the upper currents, but in this case only about one third as strong. Associated with upper current oscillations at mooring A5 are also strong oscillations in temperature (Figure 2.2-8) from about 10°C to 20°C at the upper level. These fluctuations ride on a seasonal warming trend of about 5°C from March to August, 1992 (Figure 2.2-8(a)). They range between temperatures characteristic of Gulf

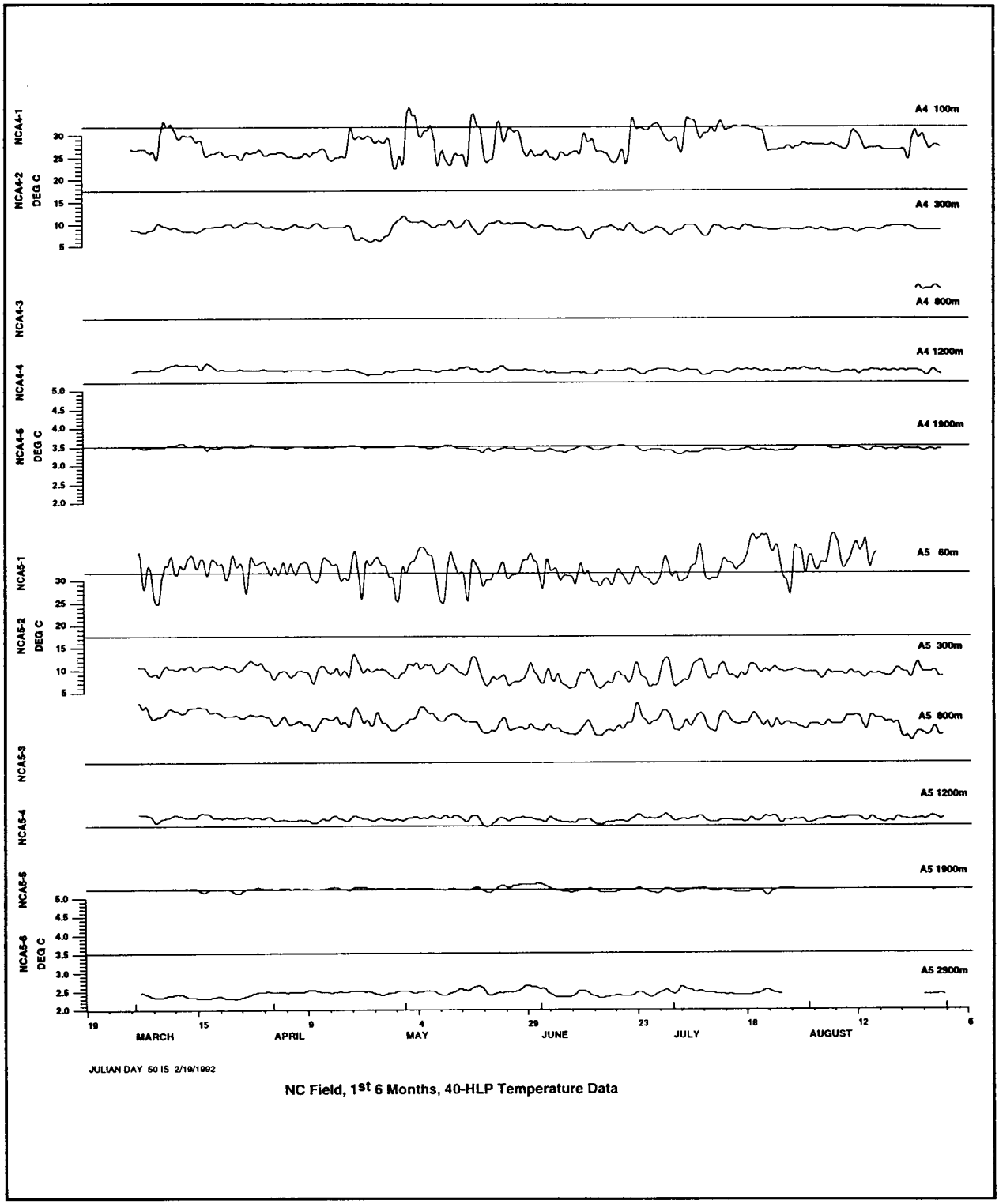

Figure 2.2-8(a). Time series plots of 40-HLP temperature at Moorings A4 and A5 for the period February 19, 1992 through September 6, 1992.

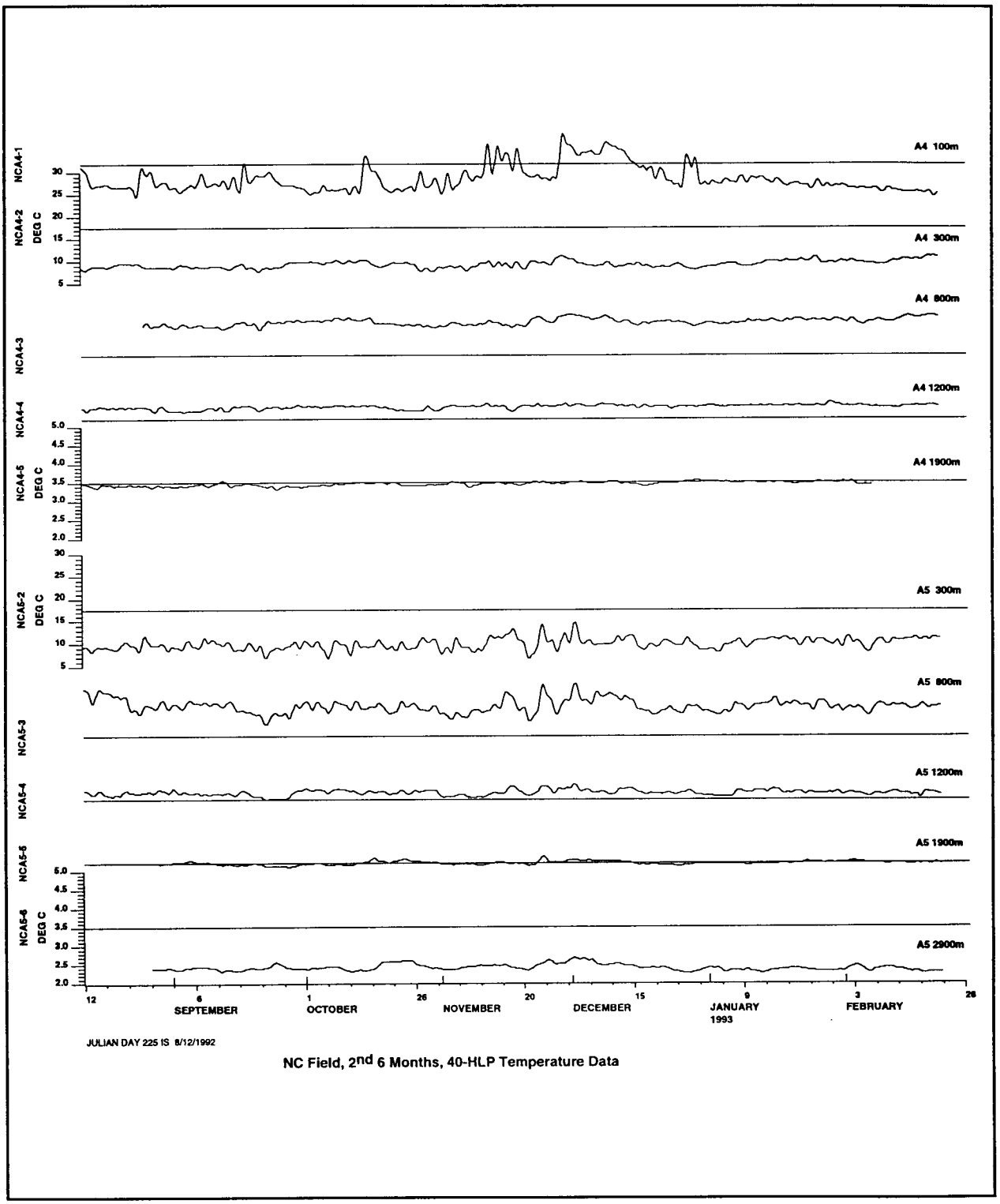

Figure 2.2-8(b). Time series plots of 40-HLP temperature at Moorings A4 and A5 for the period August 12, 1992 through February 28, 1993.

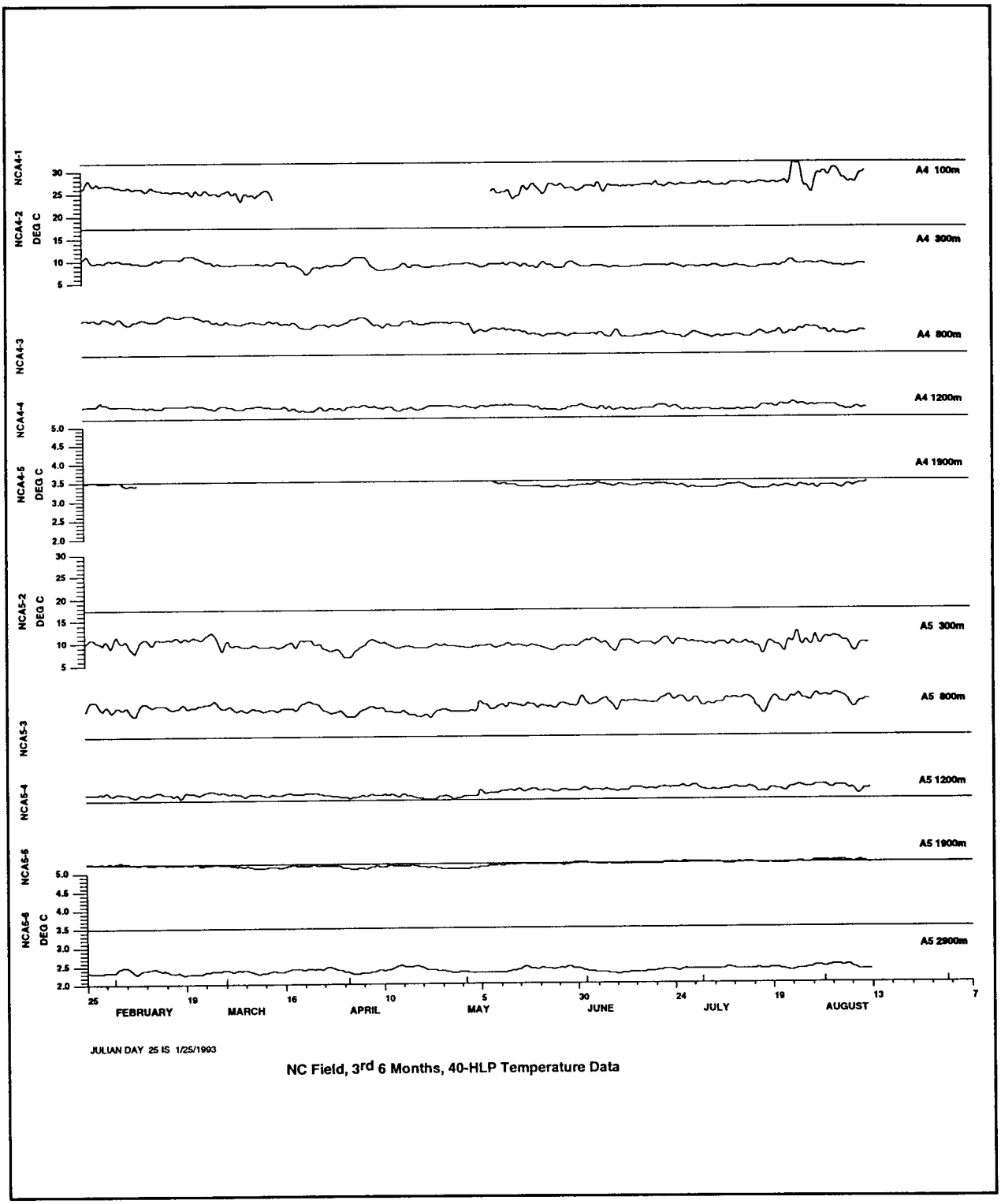

Figure 2.2-8(c). Time series plots of 40-HLP temperature at Moorings A4 and A5 for the period January 25, 1993 through September 7, 1993.

Stream water and shelf water from the "cold pool" (Ford, *et al.*, 1952; Fisher, 1972) flowing offshore to join the northern edge of the Gulf Stream. While the temperature fluctuations exhibit the same periodicities as the currents, the warmest and coolest temperatures do not clearly occur with respectively the strongest and weakest downstream currents. At site B4 on the other hand (Figure 2.2-9), the temperature record at 100 m fluctuates only about half as much (16° to 21°C) as at A5, but the warm peaks tend, interestingly, to occur in the current minima. (A more complete analysis of the phasing of temperatures and currents would first require compensation for mooring vertical motion.)

In contrast to the currents at moorings within the Gulf Stream shoreward edge, at site A4 the upper currents at 100 m and 300 m have strong eddy variability in all directions about the mean west-southwest current. The two levels have good visual coherence during most of the records, and the 300 m current strength is about half that at 100 m. Exceptional periods exist, however, when the 300 m current flows very differently from those on either the 100 m or the 800 m levels, such as during June through August, 1993 (Figure 2.2-6(c)). Characteristic time scales of these eddies are about 12 days, somewhat longer than the current-pulsing at the edge of the Gulf Stream.

Some of the largest southward deep maxima of currents at 800 m and below at site A4 (at periods of 30-40 days typically, as discussed in Chapter III) occur simultaneously with southward maxima in the 100 m and 300 m currents. Examples may be seen on March 20, 1992, December 20, 1992, and May 15, 1993 in Figure 2.2-6.

A final example of shelf water flowing offshore to join the Gulf stream is clearly depicted in the satellite image for May 21, 1992 (Figure 2.2-10). Site A4 has a strong eddy with currents exceeding 50 $cm \cdot s^{-1}$ at that time (Figure 2.2-6(a)). The temperature records on A4 have again a square-wave nature (Figure 2.2-8), shifting sharply between 11°C and 19°C as the different water types sweep past this site.

2.3. Dominant Modes of Variability in Upper Slope Currents

The variability that is coherent between measurement sites vertically and horizontally can be examined by EOF analysis within selected frequency bands. This dominant coherent variability is presented and discussed in this section. Much of the information

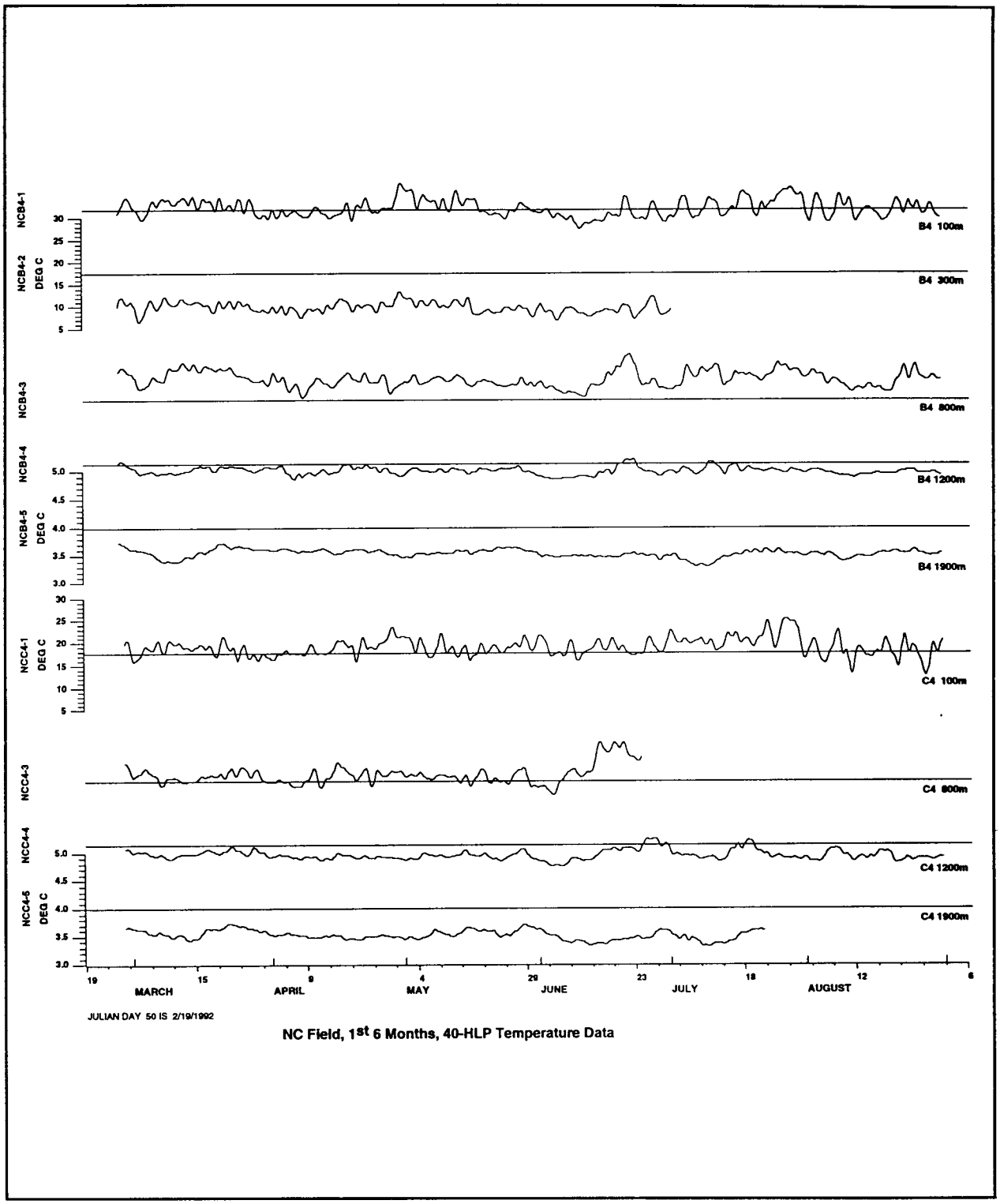

Figure 2.2-9(a). Time series plots of 40-HLP temperature at Moorings C4 and B4 for the period February 19, 1992 through September 6, 1992.

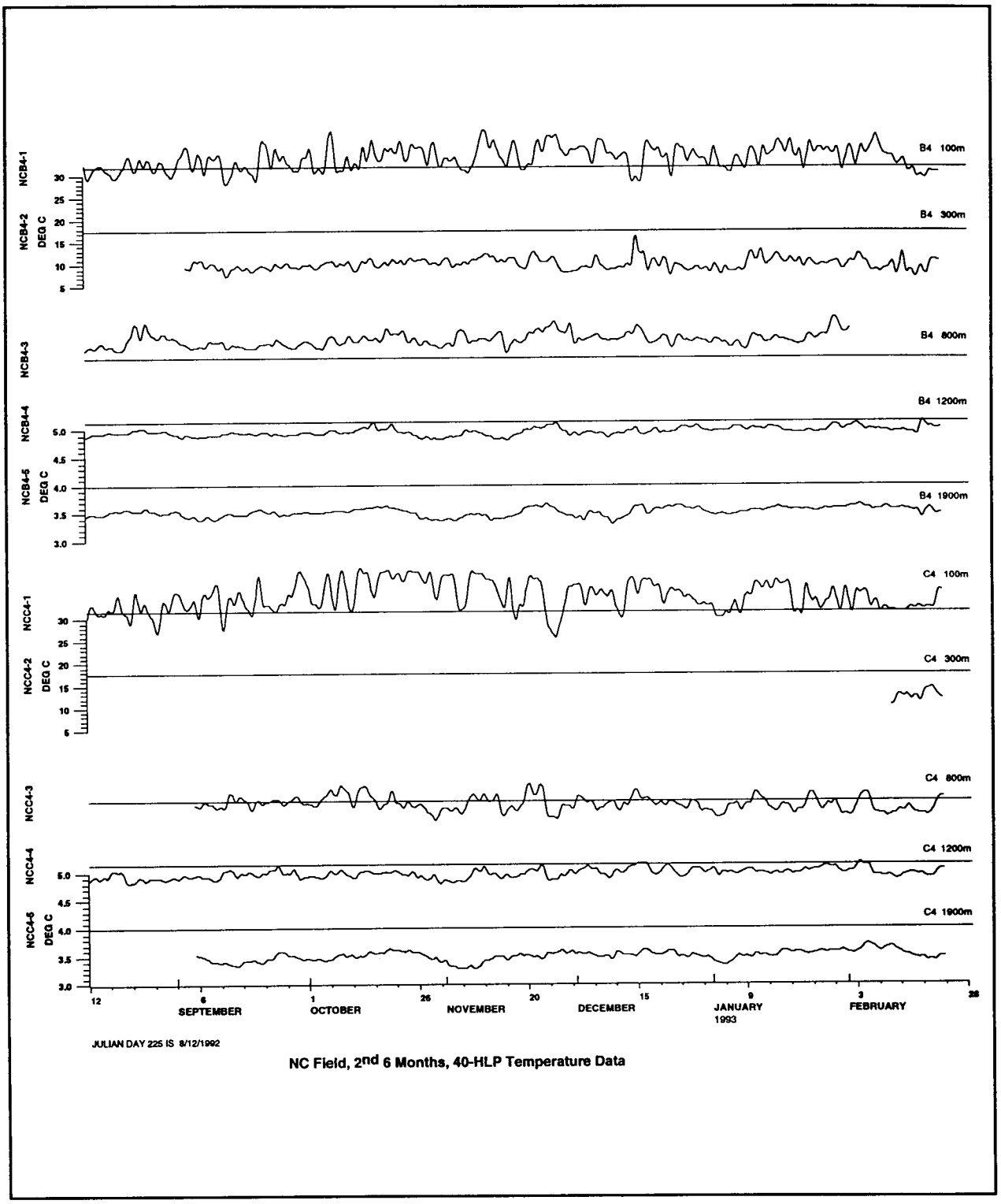

Figure 2.2-9(b). Time series plots of 40-HLP temperature at Moorings C4 and B4 for the period August 12, 1992 through February 28, 1993.

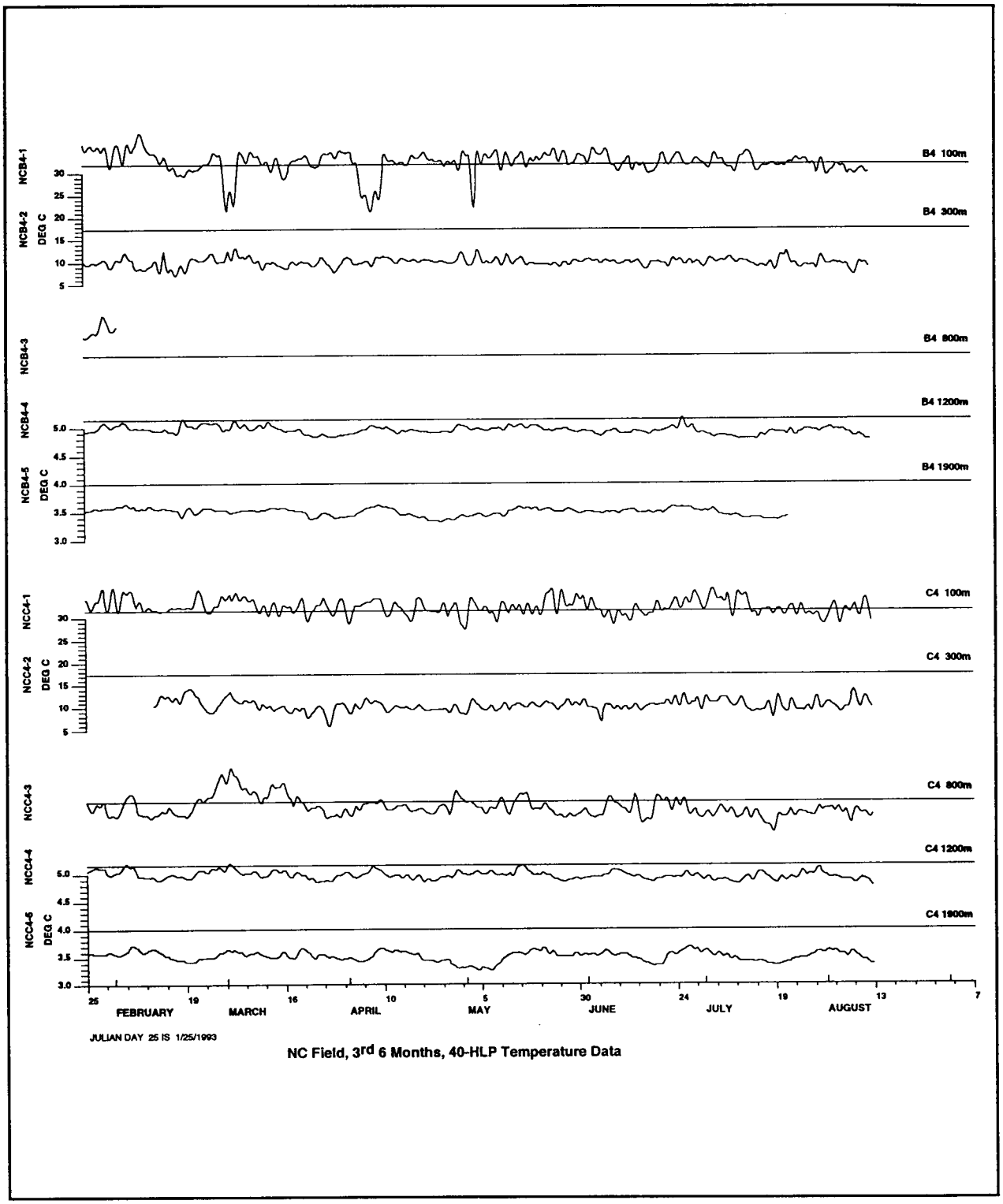

Figure 2.2-9(c). Time series plots of 40-HLP temperature at Moorings C4 and B4 for the period January 25, 1993 through September 7, 1993.

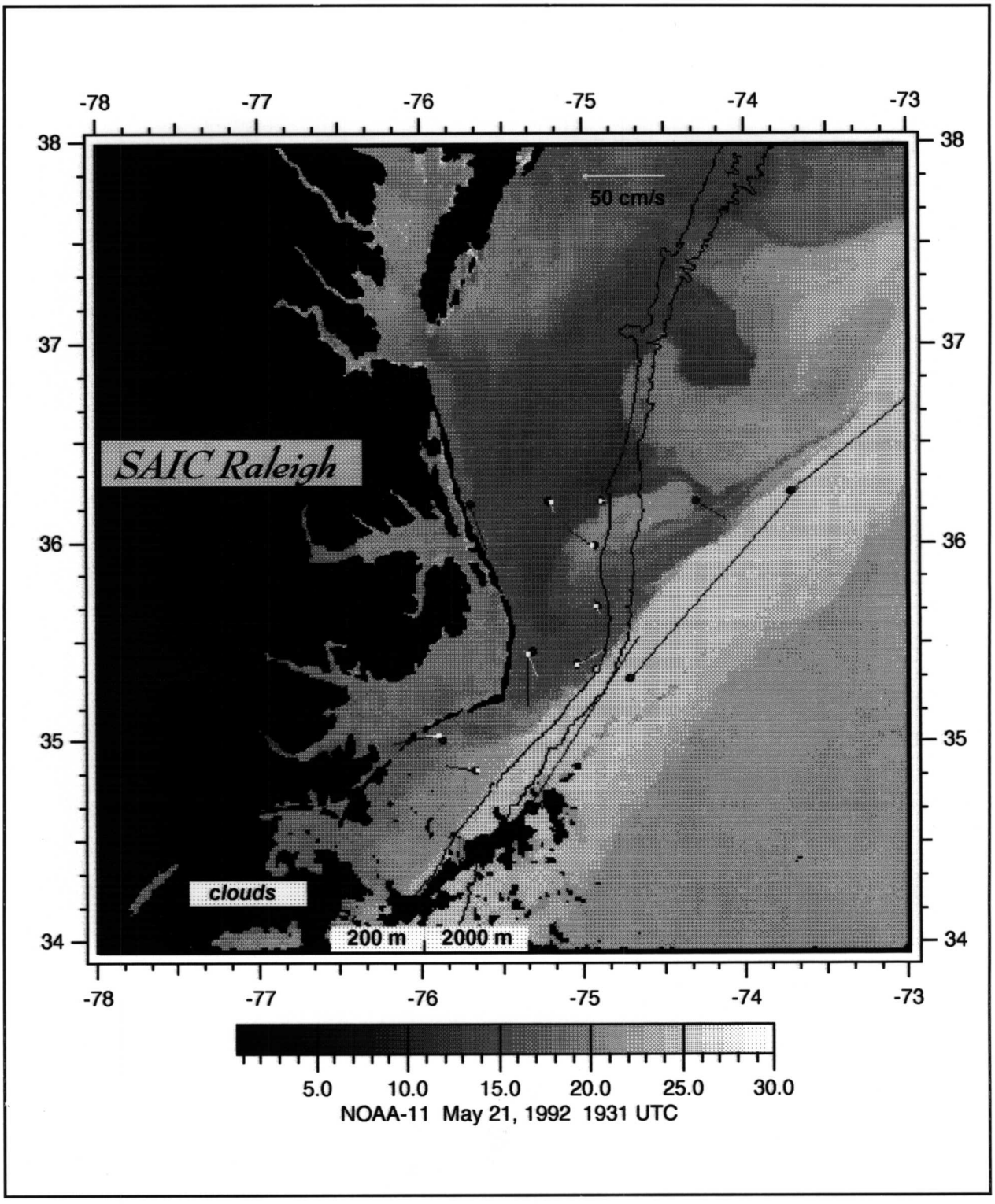

Figure 2.2-10. Satellite SST image and daily average current vectors on May 21, 1992. Annotated as in Figure 2.2-7.

that is revealed by this analysis has already been noted qualitatively in Section 2.2 by careful discussion of the time-series plots and the variance ellipses. However, the EOF analysis provides quantitative statistical information regarding the amplitude structure and phase relationships of the coherent variability, vertically and horizontally.

After examining the KE spectra, the frequency bands that contain high spectral variance were selected for further analysis. The KE spectra of the upper level currents (100 m and 300 m) are illustrated in Figure 2.3-1. The KE spectra confirm strong and relatively narrow peaks in spectral energy near 5-8 day periods, as noted in Subsection 2.2.3 while discussing the time series at sites C4, B4, and A4. They reveal additional lower frequency peaks near periods of 16-20 days, and through the longest periods resolved (to 500 days) peaked at 50-60 days. Moreover, consonant with the overall variance-ellipse plots shown in Figures 2.2-1 and 2.2-2, the spectral levels at 100 m are about five times greater than at 300 m (*i.e.*, the standard deviation ellipse axes are 2 to 2.5 times as large), and the 100 m levels at sites C4 and B4 have similar spectral variance, which is considerably higher than at sites A4 or A5.

Coherence analysis was conducted both vertically and horizontally between current measurement sites. As noted earlier, for these North Carolina slope current records, on each mooring the two upper level records at 100 m and 300 m were highly coherent with each other, and the lower level records at 800 m, 1200 m, 1900 m, and 2900 m were different but highly coherent with each other. Hence, this additional coherence analysis examines and quantifies the less-obvious (but significant) vertical coherence between the upper layer (100 m or 300 m) and lower layer (1200 m) currents. These particular depths were selected to represent the two layers because they had continuous current records on sites B4 and C4 for the first three deployment periods (18 months).

At sites B4 and C4, vertical coherence exceeding the 95% confidence level was observed between upper and lower layers in two relatively limited frequency bands, of periods 27-13 days, and near 7-8 days. Horizontal coherence was high in the upper layer between sites B4 and C4 (Figure 2.3-2) at essentially all periodicities longer than 4 days out to the longest periods observed (500 days).

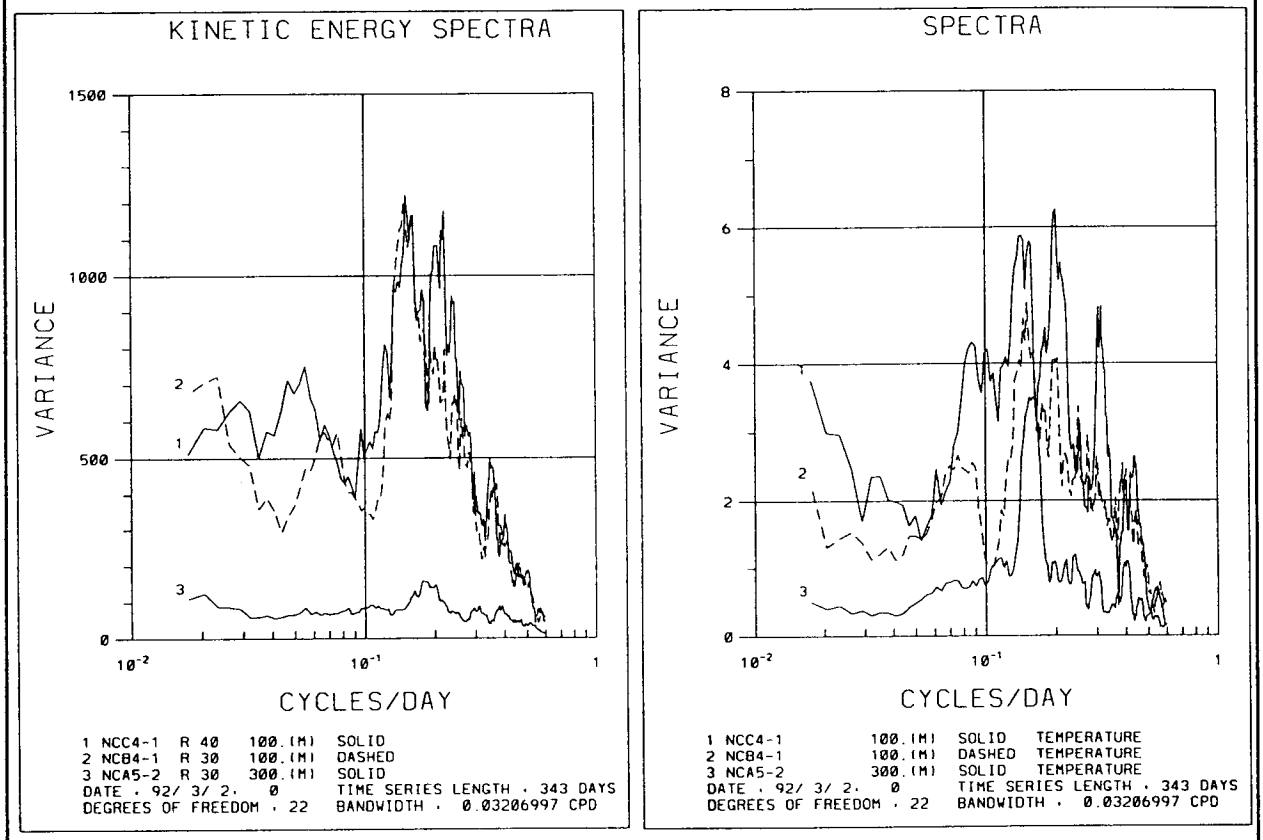

Figure 2.3-1. Spectra at Moorings C4(100 m), B4(100 m) and A5(300 m) of (a) KE and (b) temperature.

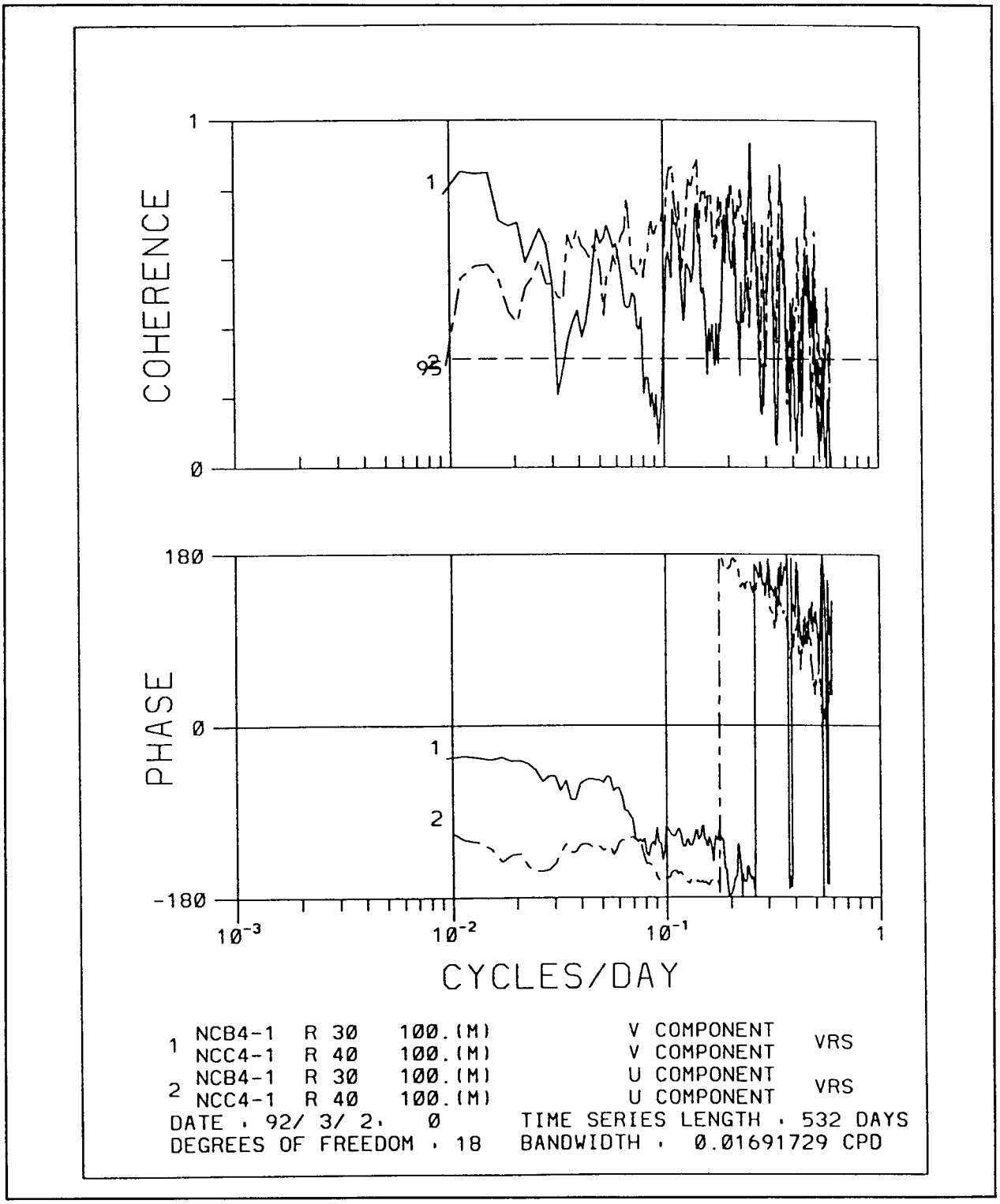

Figure 2.3-2. Coherence squared and phase difference of velocity components between Moorings C4 and B4. Time series length is 532 days.

From the phase lag in the rotated v components (*i.e.*, the most energetic northeastward components) between sites C4 and B4, one can estimate the corresponding meander propagation speed. This analysis includes the first, second and third six-month deployments. The sites are separated by 94 km. Table 2.3-1 summarizes the meander propagation characteristics.

Table 2.3-1. Meander Propagation Characteristics Between Moorings C4 and B4

Wave Period Range Center Period (days)	500-27 15	27-13 18	(20-16) 18	11-4 6	(6-5) 5.5
Distance (km)	94	94	94	94	94
Average Phase Lag (deg) (+/-)	45 (15)	80 (25)	60 (15)	140 (40)	150 (30)
Time Lag (days)	7.5 (2.5)	4 (1)	3 (1)	2 (0.5)	2.5 (0.5)
Wavelength (km) (+/-)	750 (250)	425 (125)	550 (150)	270 (50)	240 (45)
Phase Speed ($km \cdot d^{-1}$)	13 (4)	24 (6)	30 (9)	45 (9)	40 (8)
Average Phase Speed ($km \cdot d^{-1}$)	13	27		42	

For the energetic 16-20 day band a phase lag of about 3 days and a phase speed of about c= 30 $km \cdot d^{-1}$ were found. For the energetic 5-6 day band a phase lag of about 2.5 days and a phase speed of about c= 45 $km \cdot d^{-1}$ were found. Other horizontal coherences, in the upper layer currents from B4 to A4 or A5, were not statistically significant for this measurement interval.

The above meander-propagation information is confirmed, and more information is revealed by the combined horizontal and vertical EOF analysis shown in Figures 2.3-3(a,b,c). These figures show, for each of three frequency bands, the most-significant mode (mode-1) calculated for the upper (100 m or 300 m) and lower (1200 m) levels considered together. All are plotted with the same velocity scale, with the thicker ellipses representing the lower level. All analyses used 18-month continuous records from the first three deployment periods.

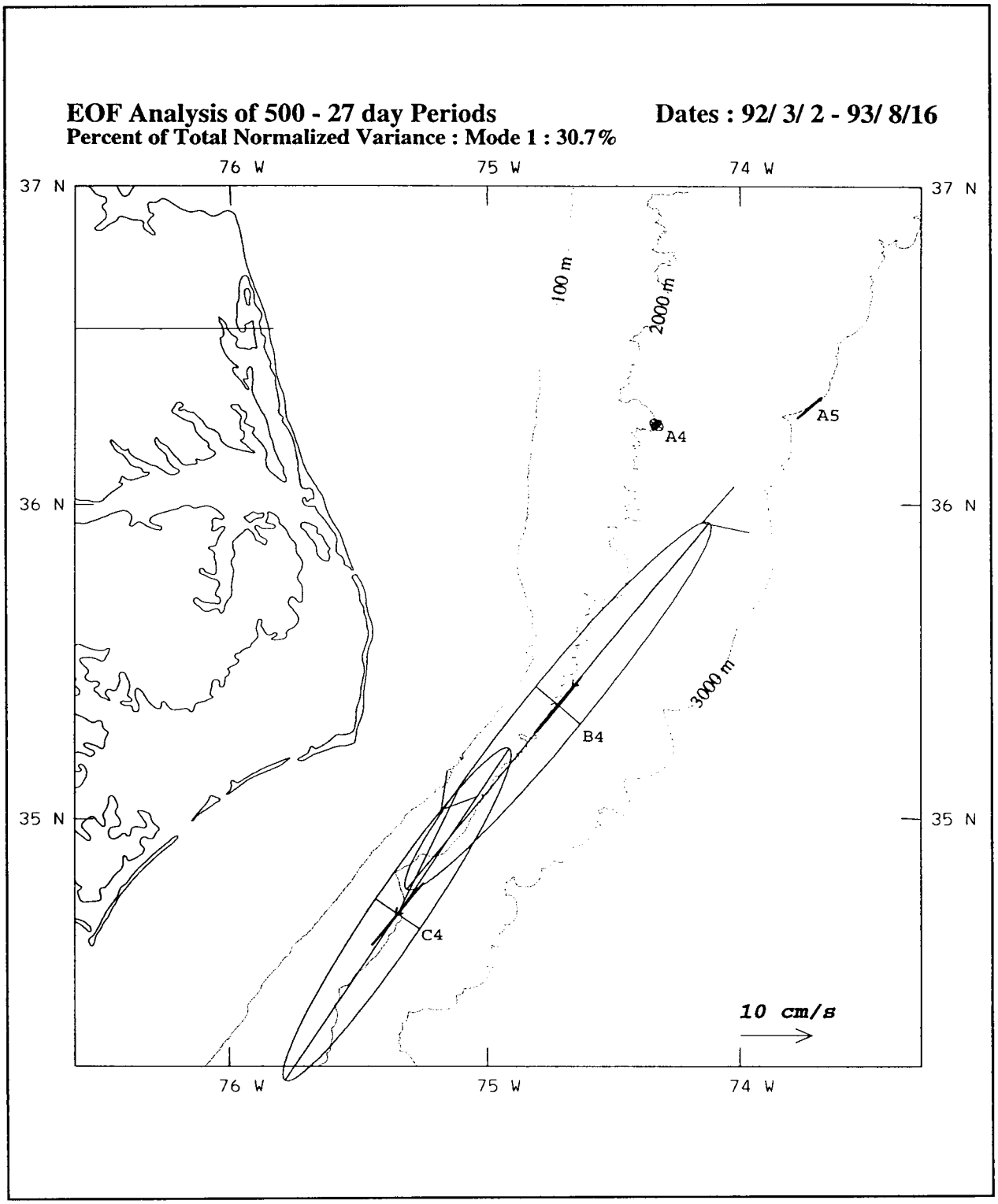

Figure 2.3-3(a). Combined horizontal and vertical EOFs (Mode-1) at Moorings A4, A5, B4 and C4 in 500-27 day band.

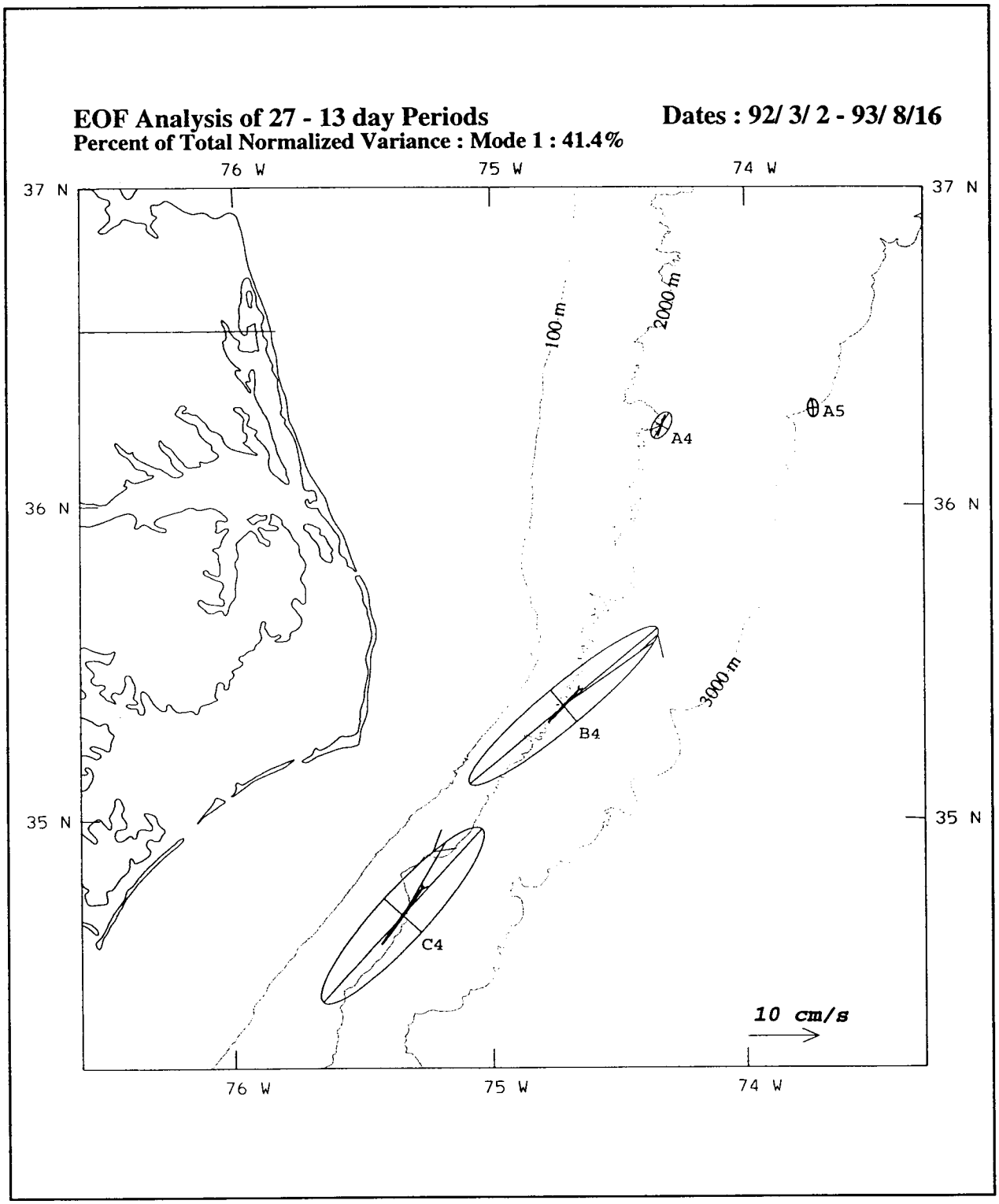

Figure 2.3-3(b). Combined horizontal and vertical EOFs (Mode-1) at Moorings A4, A5, B4 and C4 in 27-13 day band.

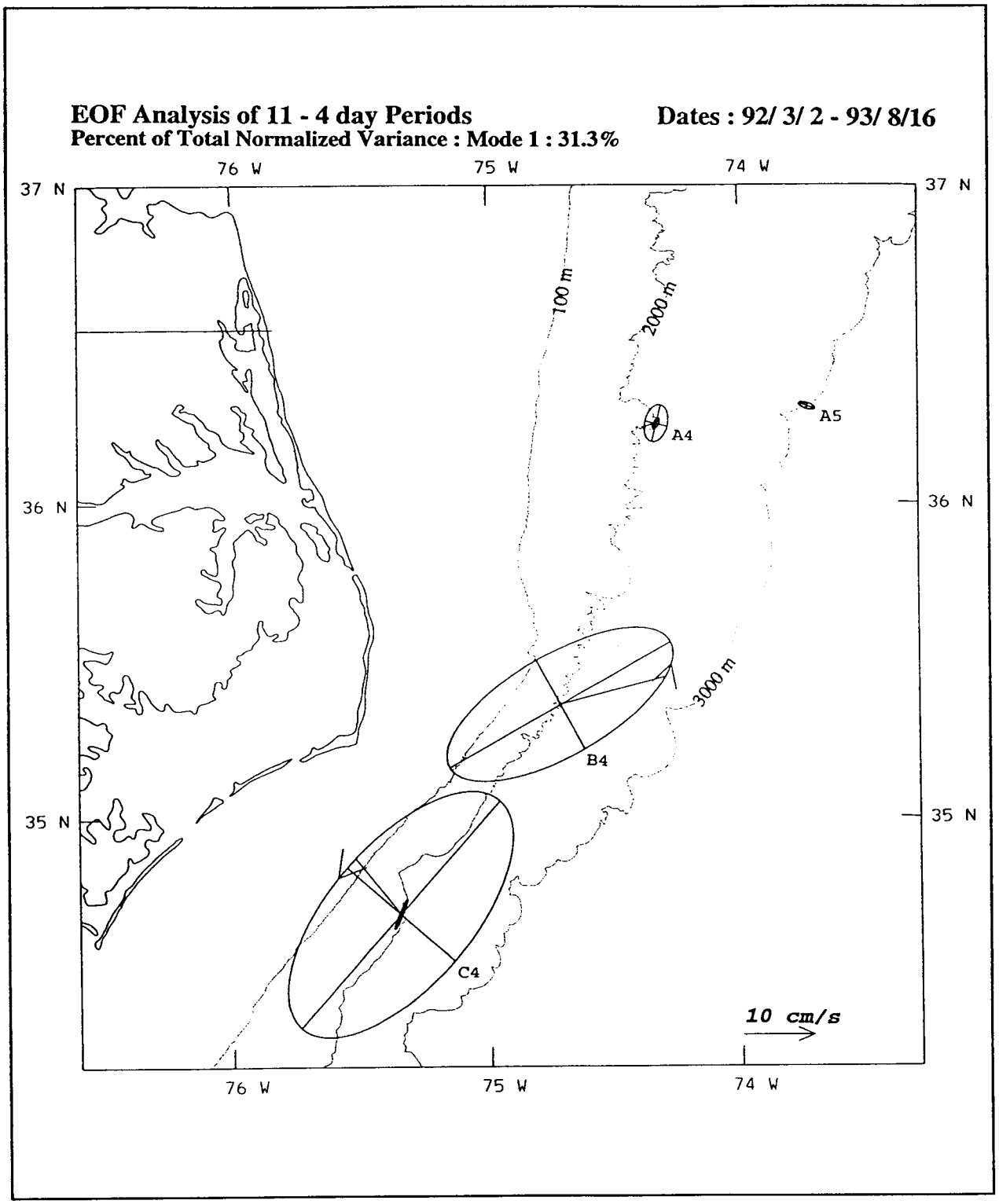

Figure 2.3-3(c). Combined horizontal and vertical EOFs (Mode-1) at Moorings A4, A5, B4 and C4 in 11-4 day band.

In the longest period band (500-27 days), shown in Figure 2.3-3(a), the normalized variance contained in mode-1 is 32%, representing mainly the high downstream coherence between the site C4 and B4 upper level downstream (v) components. The principal component axis length of about 30 $cm \cdot s^{-1}$ is in accord with calculating 32% of the previously summarized observation that the overall variance ellipse axis length along nearly the same direction was 56 $cm \cdot s^{-1}$ (shown in Figure 2.2-1), *i.e.*, in terms of rms quantities, 56 $cm \cdot s^{-1}$*sqrt(0.32) ~30 $cm \cdot s^{-1}$. The phase lag from C4 to B4 (30°) is within the error bars listed in Table 2.3-1. The vertical coherence on moorings B4 and C4 between 100 m and 1200 m is also reflected in this mode, containing about 7 $cm \cdot s^{-1}$ rms alongshore component of velocity at 1200 m. This accounts for about 25% of the total variance at 1200 m, represented by the total variance ellipse whose principal axis standard deviation is about 15 $cm \cdot s^{-1}$. However, the vertical phase lags on moorings B4 and C4 are not consistent, and because of the low overall vertical coherence in this frequency band, the vertical phases are probably not significant. Sites A4 and A5 also show no significant relationship to the mode-1 EOF in this low frequency band.

In the energetic 27-13 day band, (Figure 2.3-3(b)) the normalized variance contained in EOF mode-1 is 41%. This again mainly reflects the high coherence between the v (northeastward) components of upper level velocity on sites C4 and B4. The coherent rms upper level velocity along the principal axis is about 17 $cm \cdot s^{-1}$; the axis is rotated slightly offshore, tilted in a sense to enhance the mean cyclonic shear at the edge of the Gulf Stream and act in a barotropically stabilizing sense. The phase lag of about 60° from C4 to B4 (upper levels) agrees approximately with the preceding discussion of coherence and Table 2.3-1. As in the previous paragraph, the mode amplitude horizontally separated to sites A4 and A5 is insignificant. Vertically at sites B4 and C4, mode-1 accounts for about 5 $cm \cdot s^{-1}$ rms at 1200 m, or about 10% of the lower level variance, but the vertical phase information is probably uncertain.

In the 11-4 day band (Figure 2.3-3(c)), the normalized variance contained in mode-1 is 31%. It is again dominated by the high and coherent variance of the B4 and C4 upper level currents in the northeast principal axis direction. Site C4 leads B4 by about 100°, indicating a slightly shorter delay (2 days) and faster phase speed (45 $km \cdot d^{-1}$) for this coherent mode than for the overall variance in the 5-6 day band that was presented in Table 2.3-1, but

they agree within the error bars. Sites A4 and A5 are essentially unaffected by this mode. Vertically between layers at sites C4 and B4 the 1200 m currents have about 3 $cm \cdot s^{-1}$ rms amplitude coherent with the upper level fluctuations in this frequency band, but the vertical phase relationship is inconsistent between sites B4 and C4 and is probably not statistically significant (as with the other two frequency bands). These combined vertically and horizontally coherent modes represent Gulf Stream meanders, and quantitatively their downstream propagation speeds offshore Cape Hatteras have been summarized in Table 2.3-1.

Meanders of the Gulf Stream dominate these coherence calculations even more if only the upper currents are considered. Upper level A5 has good coherence with upper level B4 and C4 (not shown), but when the lower level currents are considered together with them, as was shown in Figures 2.3-3, the strong vertical coherence on B4 and C4 dominates Mode-1 and has little relationship to site A5. Nevertheless, in either case similar meander propagation speeds are estimated as a function of wave period.

Meander signals at most periods translate past Cape Hatteras into the Middle Atlantic Bight, where they begin to amplify. Altogether, the dominant coherent modes of slope current variability confirm the qualitative discussion of the time-series in Subsection 2.2.3. More discussion will be given in Section 3.3 regarding the vertical structure of EOFs, considering only individual moorings on the North Carolina Slope.

III. DEEP SLOPE CURRENTS NEAR CAPE HATTERAS

3.1 Background

Cape Hatteras is the location of an important crossover of currents along its steep continental slope. From the north, currents approach from the Slope Sea; this southward flow throughout the water column includes components of an intermediate and deep western boundary current (DWBC). From the south, the Gulf Stream currents approach, and near Cape Hatteras they leave the continental margin to flow northeastward as a free jet of current over the much deeper bathymetry of the open ocean. At Cape Hatteras, the upper portions of the Slope Sea circulation turn to join the Gulf Stream, and some portions of the deep flow cross under the Gulf Stream on its inshore edge, as the DWBC.

Chapter II summarized the strong flows in the upper water column associated with the Gulf Stream; there it was noted that the greatest influence of this current was above about 800 m, the characteristic depth over which the Gulf Stream had flowed in its path northward over the Blake Plateau. Within a span of a few hundred kilometers centered around Cape Hatteras, much additional water joins the flow of the Gulf Stream and increases its transport dramatically. Inflow to the Gulf Stream occurs throughout the water column, and apparently from both sides in the region northeast of Cape Hatteras. In particular, it is the relatively depth-independent (nearly barotropic) component of flow below about 800 m under the Gulf Stream that is responsible for most of the increase in transport. This barotropic component has been postulated (Worthington 1976) to feed principally from a barotropic recirculation gyre south and offshore of the Gulf Stream. However, more recent studies (Csanady and Hamilton 1988; Johns *et al.* 1994) have also indicated that a substantial fraction of the inflow is from a recirculation gyre to the north of the Gulf Stream (the Slope Sea gyre).

On transects extending offshore of Cape Hatteras, however, the deep flow under the Gulf Stream is not all in the same direction as the Gulf Stream. Instead, at depths of about 800 m and deeper at Cape Hatteras the DWBC crosses under and inshore of the Gulf Stream, hugging the continental margin closely. The dynamical processes by which the Slope Sea circulation collides with the Gulf Stream and the DWBC crosses under it have been the subject of recent studies (Pickart and Watts 1990; Pickart and Lindstrom 1994). More

observations and modeling are required to obtain a full understanding. However, a key aspect of the crossing process (by which dynamical constraints are satisfied to conserve potential vorticity) is that the DWBC descends and shifts slightly offshore as it encounters the baroclinic front of the Gulf Stream in the upper waters. Thus components of the southward flow in the Slope Sea, in order to continue southward as the DWBC, are described to shift offshore and to continue following bathymetric contours that are about 600-800 m deeper to the south of the Gulf Stream. Under this scenario, for example, components approaching southward in the depth range 800-3000 m would be expected to shift to depths around 1400-3600 m along the outer edge of the Blake Plateau.

The variability of the deep currents has been found to be energetic on the deep slope northeast of Cape Hatteras. Root-mean-square currents around 7-12 $cm \cdot s^{-1}$ have been observed in similar locations to this experiment, *i.e.*, exceeding the typical mean deep currents in the region (3-7 $cm \cdot s^{-1}$). The steep bathymetry and the water-density stratification combine to dynamically constrain the current to flow nearly parallel to bathymetric contours; current components that cross up- or downslope are much weaker and variable with time.

Much of the deep variability has been shown in earlier studies in the region (*e.g.*, Johns and Watts 1986; Hamilton 1984) to be due to topographic Rossby waves (TRWs), although variation in the strength of the DWBC and some coupling to meandering of the Gulf Stream has also been demonstrated. An overview of the DWBC and of TRWs in for the Cape Hatteras region was provided in SAIC (1993). Results of some newer studies in the literature are summarized here.

TRWs are a wave mode supported by the planetary dynamics of potential vorticity conservation in the presence of sloping bathymetry. There are several studies of TRWs in the Middle Atlantic Bight or Cape Hatteras region, for example by Thompson (1977), Hogg (1981), Hamilton (1984), Johns and Watts (1986), Shaw and Peng (1987), and Pickart and Watts (1990). In the Cape Hatteras region, in particular, the most energetic wavelengths and periods range around 70-200 km and 20-60 days, although higher frequencies with periods as short as 5-10 days are supported by the steep bathymetry. With their long spatial and temporal scales, the TRW current velocities are close to geostrophic, and their vertically sheared (baroclinic) components perturb the temperature and density structure across (normal to) the current.

Figure 3.1-1 shows cross-sections of Gulf Stream temperature (as a proxy for density) and velocity right at Cape Hatteras. Two realizations of the velocity field are shown in this figure, illustrating nicely for the following discussion both the TRW and DWBC field. The middle panel is the geostrophic velocity section obtained from the density measurements, with the velocity absolutely referenced by direct measurements of velocity (in this case, from Pogo transport floats dropped at each CTD; however, the Pickart and Lindstrom (1994) paper shows that this same velocity structure is also obtained using deep current meter records or shipboard ADCP profiles to reference the same geostrophic velocity calculations). The deep velocity field in this figure has a laterally banded, bottom-intensified nature, associated with a TRW of wavelength about 120 km (as determined from the phase lag between deep current meters that sampled coincident with this transect). The velocity maxima in this section, both positive and negative alongshore, are around 7-10 $cm \cdot s^{-1}$ near the bottom. Knowing the TRW's cross-transect wavelength, they applied a spatial notch-filter to remove the TRW, without affecting longer or shorter lateral scales or the mean transport in the section. The filtered velocity field is shown in the right panel of Figure 3.1-1, thus revealing the "TRW-free" structure of the DWBC, as it crosses southward under the Gulf Stream.

The fluctuating currents also tend to parallel the bathymetry, but at a small angle by which the stretching of the water column in the presence of stratification provides the restoring force for these waves; the lowest frequencies are very nearly parallel to the bathymetry, turning with increasing frequency to a high-frequency cutoff (period around 5 days off Cape Hatteras) at which the fluctuations flow directly up- and downslope. The currents are bottom-intensified. Long wavelength (200 km) components may be only 5% stronger near the ocean bottom than at 1000 m, but shorter waves decay proportionately faster in the vertical.

For the energetic low frequency TRWs the phase (*i.e.*, peaks of positive and negative velocity) propagates almost directly offshore, while the parcel- and group velocity and the energy propagation is nearly along the bathymetry. Ray-tracing theory by Pickart (1994) has suggested that TRWs should be generated by meanders of the Gulf Stream farther to the east, perhaps around 72°W to 68°W.

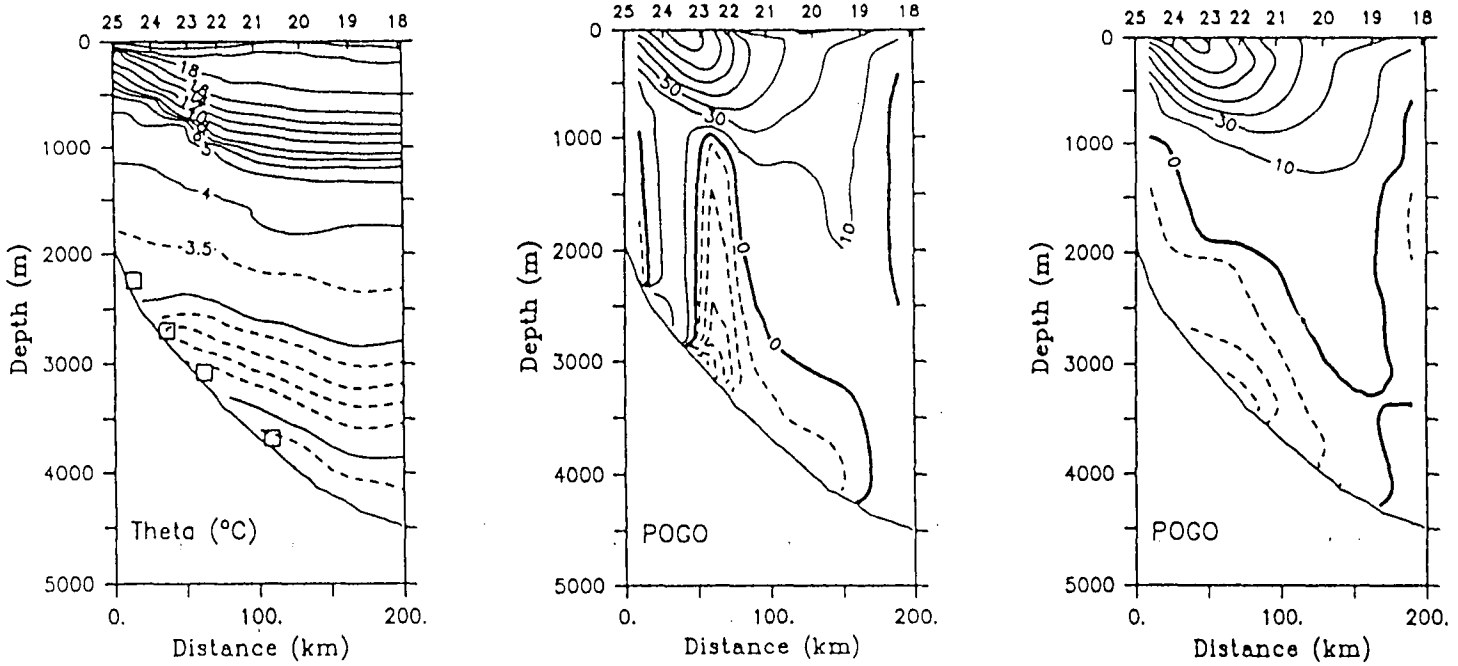

Figure 3.1-1. Cross-section of Gulf Stream temperature and current structure (from Pickart and Lindstrom 1994).

TRWs are generally treated as linear waves, although in fact their parcel speeds can be comparable to their group and phase speeds, and their transverse oscillatory nature does not generate a net flux of solutes. For settling particles, however, the currents associated with TRWs will disperse particle paths across isobaths.

The DWBC is formed mainly from northern convective sources that are traditionally envisioned to include North Atlantic Deep Water (NADW) from the Norwegian-Greenland Seas outflow, and Labrador Sea Water (LSW). The traditional picture indicates that the DWBC flows equatorward as a continuous band of water along the continental margin of the entire Western North Atlantic. More recent work (Pickart and Watts 1990; Watts 1991; Pickart and Smethie 1993) has shown that the DWBC consists of several components at different temperatures in a vertically-banded structure, each component flowing equatorward at different speeds (3-7 $cm \cdot s^{-1}$) and roughly following bathymetric contours.

The depiction in Figure 3.1-1 is representative of these other findings that the DWBC appears to occupy a ribbon of vertical thickness about 900-1500 m above the ocean bottom, in a sloping width more than 150 km and spanning isobaths from about 4000 m to shallower than 2000 m. The potential temperatures (θ) range from about 6°C to as cold as 1.8°C. More details regarding the temperature and velocity structure of the DWBC were summarized in the SAIC (1993).

This background information has defined the terminology and processes for interpreting the deep slope current measurements during this experiment. Although a more specific and complete array of current meter mooring sites along and across the slope would be required to determine new details about the TRWs and DWBC transport and structure, the climatology of the currents observed and their associated low frequency variability may be readily interpreted in this context.

3.2 Climatology and Variability During 1992-1993

This section summarizes the means, variances, and attributes of the observed deep slope currents. The time series and events will be discussed and interpreted. Current meter measurements at 800 m and deeper are discussed for moorings C4, B4, and A4, which lie along the 2000 m isobath, and for mooring A5, which is northeast of Cape Hatteras on the 3000 m isobath. Current meters were located at 800

m, 1200 m, and 1900 m (levels 3, 4, and 5) on all four moorings, plus at 2900 m (level 6) on mooring A5.

Figure 3.2-1 shows the mean and standard deviation ellipses of the currents respectively at 800 m, 1200 m, and 1900 m, with the A5 (2900 m) level included, offset, in the 1900 m plot.

In discussing these currents it is of interest also to note the approximate mean *in situ* temperature (T) or approximate potential temperature (θ) associated with each record. However, these temperature values are rough approximations (although quoted to 0.1°C) because of several factors: The current meter thermistors standardly have calibration uncertainty of at least 0.1°C; the adjustment from T to θ is simply to subtract a nominal adiabatic temperature gradient of $0.1°C \cdot km^{-1}$ in depth; only the nominal depth of each instrument has been considered without compensating for small differences between true depths on different mooring sites and times. Hence although the temperatures on each level give useful information regarding their location relative to the watermass structure, it is not appropriate to attempt to interpret small differences between temperatures on a fixed level at different sites or deployments.

The mean *in situ* temperatures at the 800 m level on the four slope moorings are about 4.0°C to 4.4°C, corresponding to θ about 3.9°C to 4.3°C. These records are thus in waters of Subarctic Intermediate Water (SAIW) characteristics (Watts 1991). The mean flow (Figure 3.2-1(a)) at the three sites along the 2000 m isobath is equatorward. Each six-month deployment produced remarkably consistent estimates of the mean current speed and direction. The 800 m means for 18 months and the range of different estimates obtained from the various six-month deployments are as follows:

site A4(800 m), 9 ± 2 $cm \cdot s^{-1}$ at T/θ = 4.2/4.1°C;
site B4(800 m), 4 ± 2 $cm \cdot s^{-1}$ at T/θ = 4.3/4.2°C;
site C4(800 m), 9 ± 3 $cm \cdot s^{-1}$ at T/θ = 4.0/3.9°C,

where in each case the direction is along the isobaths. Site A5(800 m) has mean current 5 ± 0.5 $cm \cdot s^{-1}$ nearly due east, at T/θ = 4.4/4.3°C, showing that the Slope Sea southwestward transport turns to join the Gulf Stream. The instantaneous flow at site A5 will be seen later to be highly variable, but the time scales are short, and the mean vector estimates are consistent within $\pm$ 0.5 $cm \cdot s^{-1}$ between the three six-month records.

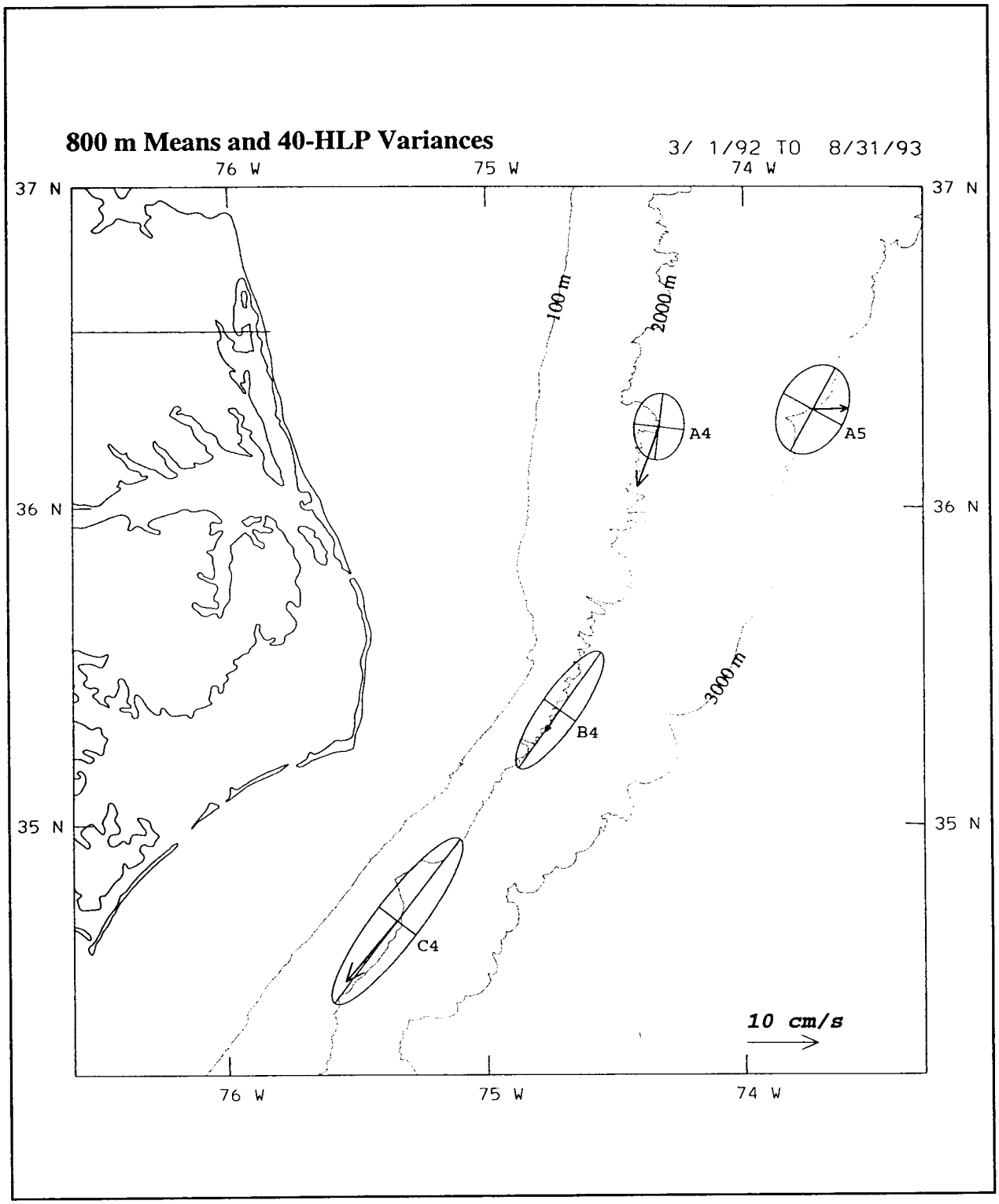

Figure 3.2-1(a). Mean current vectors and variance ellipses for Moorings A4, A5, B4 and C4 at 800 m. Time period in March 1992 through August 1993.

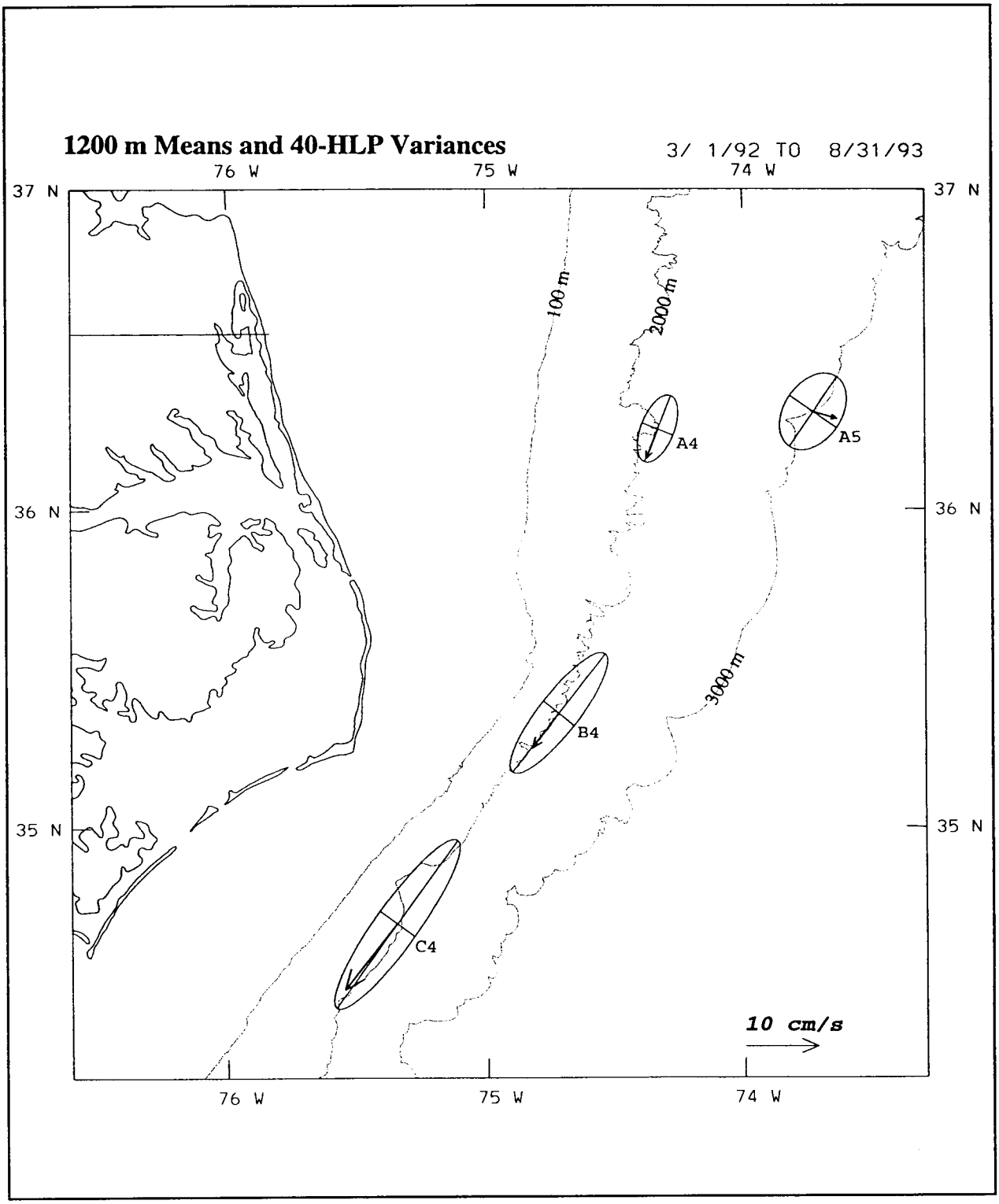

Figure 3.2-1(b). Mean current vectors and variance ellipses for Moorings A4, A5, B4 and C4 at 1200 m. Time period is March 1992 through August 1993.

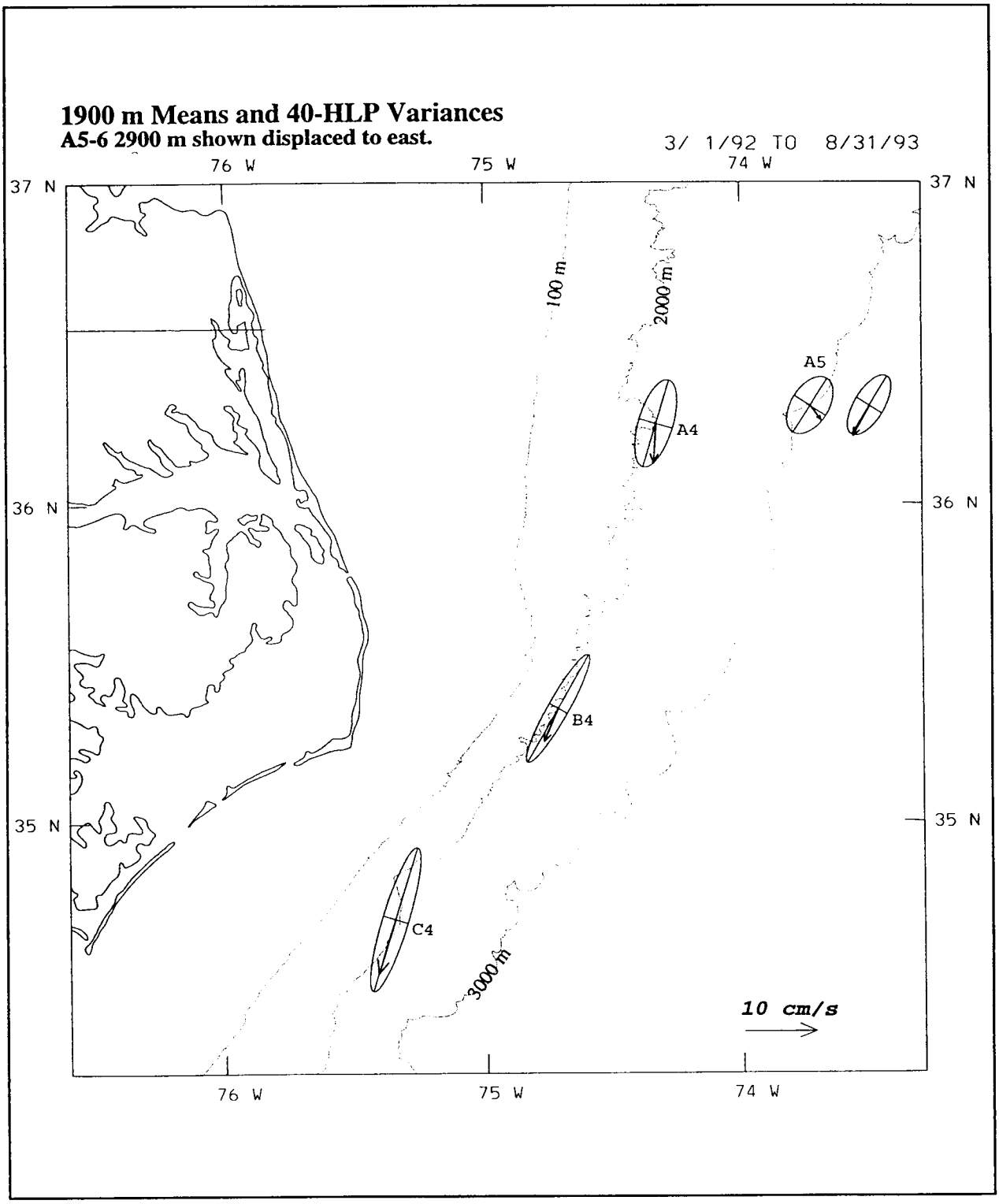

Figure 3.2-1(c). Mean current vectors and variance ellipses for Moorings A4, A5, B4 and C4 at 1900 m. Mooring A5 2900 m level is also shown and is offset for clarity. Time period is March 1992 through August 1993.

At the 1200 m level (Figure 3.2-1(b)) the mean *in situ* temperatures are about 3.7-3.8°C, with corresponding θ about 3.6-3.7°C. These records are thus in waters of LSW and upper NADW characteristics. The mean flow at the three sites along the 2000 m isobath is equatorward, for the total records and for each six-month deployment; again there was remarkable consistency of the mean flow estimates. The 1200 m means and range of six-months estimates are as follows:

site A4(1200 m), 4±0.4 $cm \cdot s^{-1}$ at T/θ = 3.8/3.7°C;
site B4(1200 m), 9±2 $cm \cdot s^{-1}$ at T/θ = 3.8/3.7°C;
site C4(1200 m), 13±2 $cm \cdot s^{-1}$ at T/θ = 3.8/3.7°C.

Site A5(1200 m) has mean current to the east (3.3±0.7 $cm \cdot s^{-1}$ at T/θ = 3.7/3.6°C), with a somewhat smaller north-south component that varies in sign between six-months mean estimates.

The current means at 800 m and 1200 m are very similar at each of the four mooring sites. The entire time-series measurements to be discussed later also show a high degree of vertical coherence between the 800 m and 1200 m levels.

At the 1900 m level (Figure 3.2-1(c)) the mean *in situ* temperatures on the four slope moorings are about 3.4-3.5°C, with corresponding θ about 3.2-3.3°C. These temperatures characterize deeper LSW and upper NADW. The mean flow 100 m off the bottom (i.e above the benthic boundary layer) on the three sites along the 2000 m isobath is again consistently equatorward and parallel to the bathymetry. As at the 800 m and 1200 m levels, the 18-month mean and the small range of six-month mean estimates show remarkable consistency:

site A4(1900 m), 6±0.3 $cm \cdot s^{-1}$ at T/θ= 3.4/3.2°C;
site B4(1900 m), 5±2 $cm \cdot s^{-1}$ at T/θ= 3.5/3.3°C;
site C4(1900 m), 8±1 $cm \cdot s^{-1}$ at T/θ= 3.5/3.3°C.

Site A5(1900 m) has mean current 3±1.5 $cm \cdot s^{-1}$ (at T/θ = 3.5/3.3°C) slightly south of east and in the SE quadrant for each six-month deployment.

Site A5 in 3000 m water also had a current measurement 100 m off the bottom at 2900 m. Its mean T/θ was about 2.4/2.1°C, which is characteristic of lower NADW. The 18-month mean and range of six-month mean estimates were 4.5±0.7 $cm \cdot s^{-1}$, turned nearly parallel to the isobaths and in each case in the southwest quadrant.

Much can be deduced about the vertical and lateral structure of the DWBC from the above means. A common factor at all four slope sites is that the mean current 100 m off the bottom is equatorward and

parallel to the bathymetry. However, the vertical structure of the mean currents differs at the 3000 m site from that at the three sites along the 2000 m isobath. At the latter, the equatorward mean flow extends up through the 1200 m and 800 m levels, but at the 3000 m site the mean flow at the 1900 m level and shallower turns progressively more to the east with height (i.e, turns counterclockwise with height or "backs", in the mean) to flow into and join the Gulf Stream. The instantaneous spatially-filtered representation of DWBC flow that was shown in Figure 3.1-1 (right panel) is similar to and helpful in understanding the above mean structures. The DWBC may be viewed as a thin ribbon of equatorward flow hugging the continental slope. Towards its shallow side (near the 2000 m isobath) its vertical thickness extends through 1900 m, 1200 m, and 800 m, *i.e.*, is at least 1200 m thick. Near its middle (near the 3000 m isobath) it appears not to extend up to the 1900 m level, *i.e.*, the ribbon is less than 1100 m thick in the mean.

The variance ellipses (or standard deviation ellipses as shown in Figure 3.2-1) at 800 m and deeper are elongated with principal axes nearly parallel to the bathymetry, particularly at sites B4 and C4, in accord with the background discussion of TRW variability in section 3.1. There is a southward increase in variance from site A4 to B4 to C4 at all levels 800 m and deeper.

The standard deviation along the principal axis (SDP) is somewhat greater than the mean vector at all the 800 m and deeper levels on the slope moorings, except at A4 (800 m), whereon the mean (9 $cm \cdot s^{-1}$) exceeds the SDP (5 $cm \cdot s^{-1}$). The SDP at the southern two sites (B4 and C4) is roughly twice that at A4 and A5: For the southern sites SDP at 800, 1200, and 1900 m is about 10-13 $cm \cdot s^{-1}$, 10-15 $cm \cdot s^{-1}$, and 9-12 $cm \cdot s^{-1}$, respectively. For sites A4 and A5, SDP at 800, 1200, and 1900 m is about 5-7 $cm \cdot s^{-1}$, 3-4 $cm \cdot s^{-1}$, and 5-7 $cm \cdot s^{-1}$, respectively. At sites A4 and A5 100 m off the sea floor, the current ellipses are similarly elongated; however, higher in the water column they show a progressively more circular nature. Thus the eddy variability higher in the water column at A4 and A5 appears to result from a mixture of at least two types of processes, TRWs, that are somewhat bottom-intensified and polarized relative to isobaths, plus nearly isotropic and weakly depth dependent or slightly surface-intensified eddies on the inshore side of the Gulf Stream.

Examining the time series stick-plots of currents shown in Figures 2.2-5 and 2.2-6, the deep currents tend to vary from weakly

equatorward to more strongly equatorward, *i.e.*, seldom is the current poleward, although some cases of current reversal are observed.

Northward (or poleward, for records that have been rotated) peaks of flow tend to be somewhat surface-intensified, and southward (equatorward) peaks tend to be bottom-intensified. Examples may be seen in Figure 2.2-6(a). Southward peaks occurring at site A4 around March 20, 1992, May 25, 1992, and July 23, 1992 are obviously bottom-intensified. At the same site, northward peaks occurring around April 24, 1992 and July 5, 1992 are surface-intensified. Similarly for site A5, a southward pulse is bottom-intensified around March 20, 1992, and surface-intensified northward pulses may be identified around April 29, 1992 and June 23, 1992. Similar examples may be identified on records from sites A4 and A5 for the second and third six-month deployment periods (Figure 2.2-6(b) and (c)), *e.g.*, northward at A5 on September 21, 1992 and November 25, 1992, and at A4 on November 15, 1992 and December 5-10, 1992. Many examples of southward, bottom-intensified peaks exist at regular intervals throughout the records. The above pattern can be explained very simply as a barotropic eddy perturbation of a mean baroclinic current shear profile that increases to the north at the surface and towards the south at the bottom.

A striking aspect of all the sub-thermocline current records on the North Carolina slope sites is the regularity with which equatorward peaks of flow are observed having typical speeds 20-30 $cm \cdot s^{-1}$ (although we will note some peak examples of 40-60 $cm \cdot s^{-1}$). These are TRWs superposed on a mean southward current. Spectral analysis of these currents, while very useful, tends to lump together different observed periodicities into single-frequency bands, so it is useful to examine each of the time-series directly.

Starting with site A4, in the first six months Figure 2.2-6(a) shows the first three southward peaks separated by 65 days and 56 days; following this and continuing into the second six months (Figure 2.2-6(b)) more peaks continue to arrive at about 56 days interval, but additional peaks begin to arrive intermediate between them, creating a roughly 28-32 day period also. In the third six months at A4, vestiges of the 56 day waves may continue to contribute to the variability, but a new dominant wave train of period 41 days begins, exhibiting five regularly spaced peaks.

At site A5 the deep TRW signal is not so dominant, but nevertheless it is clearly present. The turning of the currents with height that was noted earlier on mooring A5, such that the deeper fluctuations are more parallel to the bathymetry, may also be identified directly in the time series. Thus, we examine particularly the deepest record, A5 (2900 m) to characterize its TRW variability: During the first six months (Figure 2.2-6(a)) there is some cross-slope coherence visually with site A4, and the largest southward peaks are again separated by about 65 days and 55 days. During the second six months on A5 (Figure 2.2-6(b)) the peaks are regularly spaced at 41 day intervals, *i.e.*, the same period as was observed at A4 in the subsequent six months. During the third six-month period at A5 (2900 m) (Figure 2.2-6(c)) the periodicities are not so clearly defined, but there is again some visual coherence with the 41 day peaks at A4, but lagging by roughly six days.

At site A5 the intermediate level current records at 800 m, 1200 m, and 1900 m, have a high degree of visual coherence, with relatively isotropic fluctuations of 15-25 $cm \cdot s^{-1}$. They appear to be a mixture involving TRWs and shear in the direction of the Gulf Stream.

The time series stick plots of currents at slope sites B4 and C4 were shown in Figure 2.2-5 for the three six-month deployment periods. In the intermediate and deep current records at 800 m, 1200 m, and 1900 m some of the major events (equatorward current peaks) that occurred at sites A4 and A5 were also observed at sites B4 and C4. The peaks exhibit a southward intensification from A4 to B4 to C4, in agreement with the earlier-remarked observation that the variance ellipse axes increase to the south. This intensification probably arises from the southward steepening of the continental slope and the narrowing of distances between isobaths from line A to B to C, thus refracting and focussing the flow somewhat as it proceeds southward. Examples of along-slope coherent events may be seen in all three six-month deployments, *e.g.*, near March 20, 1992, June 1, 1992, October 20, 1992, November 26, 1992, April 12, 1993, May 20, 1993 and June 27, 1993. The time delay from a peak at A4 to B4 to C4 is about three days in each distance of approximately 90 km, suggesting an along-slope group speed around 30 $km \cdot d^{-1}$ for these waves of period approximately 30 to 40 days.

Some southward (more generally, equatorward) flow events are extraordinarily large, for deep current levels, and coherent

throughout the water column at site B4, and particularly at site C4. Site B4 has peak currents exceeding 20 $cm \cdot s^{-1}$ in almost every cycle of 30-40 days, and it has peaks lasting several days as high as 30 $cm \cdot s^{-1}$ and 40 $cm \cdot s^{-1}$ during the first and second deployment periods, respectively. Most major southward current events at C4 are near 40 $cm \cdot s^{-1}$, lasting several days, in all three six-month deployment periods.

The largest southward current event at B4 and C4, near November 25, 1992, occurs during the time that a cold core ring appears in satellite images just offshore Cape Hatteras, approaching and coalescing with the Gulf Stream. Images from November 17, 1992 (Figure 3.2-2) and November 29, 1992 (not shown) illustrate the ring approaching and the Gulf Stream path greatly perturbed (for this region) throughout the experiment area, from Line A to C.

Regularly spaced southward peaks of current appear in the B4 and C4 records for all three deployment periods. As observed in the site A4 and A5 records, the period of the TRWs changes as different wave trains pass through. In the first six-month deployment, for the first four months there are only two southward pulses separated by about 68 days; then during the later three months a series of peaks at about 28 day interval passes through. In the second deployment on B4 and C4 the dominant TRW period is 47 days. In the third six months the period shortens to about 37 days, as five regularly spaced current pulses pass through, as seen best on site C4. It is possible that differences in TRW wave period of around 20% observed during the same deployment time, but at different sites (A4, B4, and C4), could arise because of different Doppler shifting of the same train of TRWs by the mean currents; the mean current speeds are around 20% or more of the wave group speeds along the slope, and thus capable of creating substantial Doppler shifts.

3.3. Dominant Modes of Variability in Deep Slope Currents

The variability that is coherent vertically and/or horizontally among the slope moorings and current measurements at different levels in the lower layer (800 m and deeper) is examined in this section by EOF analysis within selected frequency bands. This EOF analysis quantifies statistically the amplitude and phase relationships of the coherent variability that has been observed and discussed in the preceding section on the time series of deep current measurements.

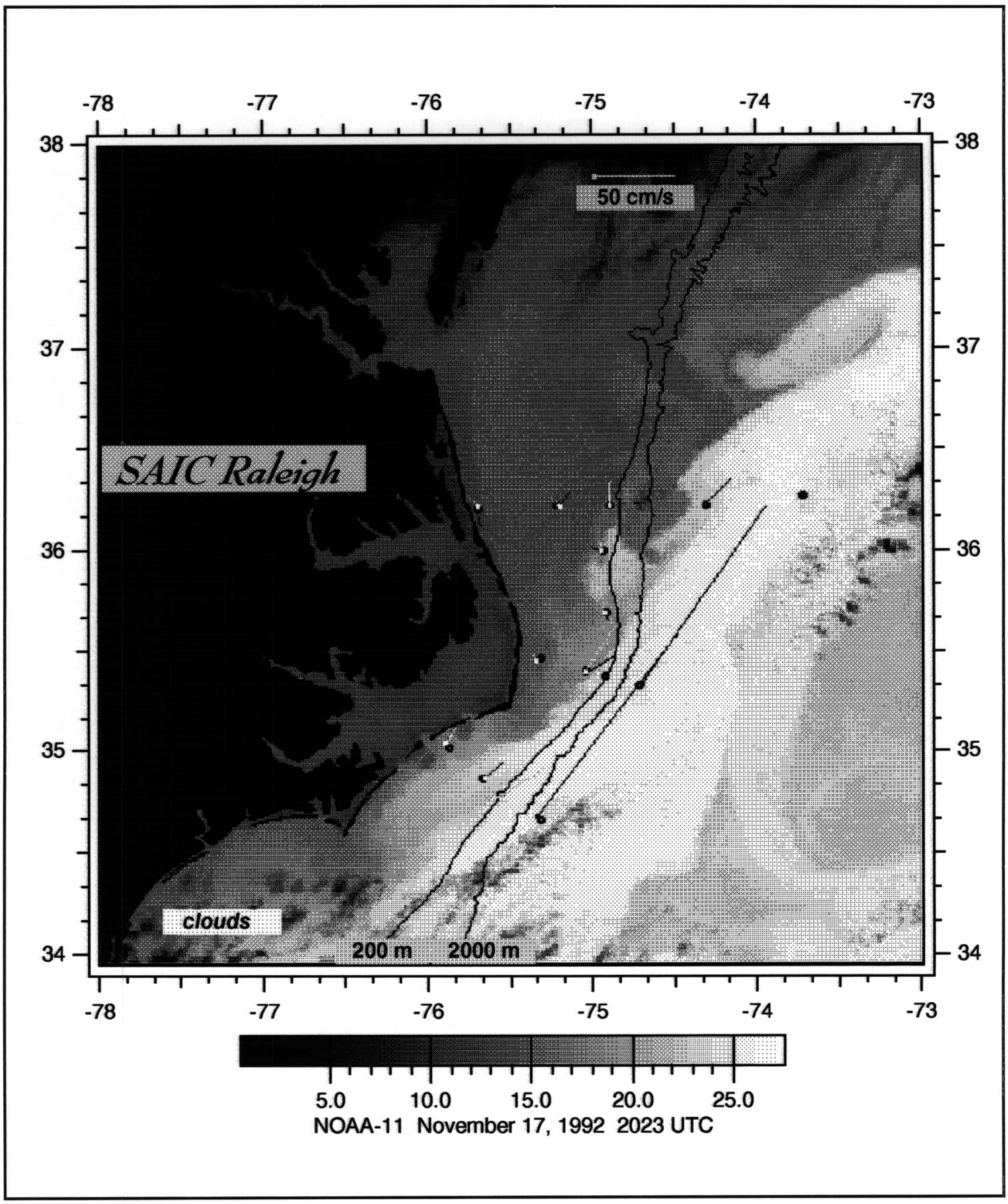

Figure 3.2-2. Satellite SST Image and Daily Average Current Vectors on November 17, 1992. Annotated as in Figure 2.2-7. Cold core ring is indicated east of the Gulf Stream.

For the following analyses, continuous and contemporaneous measurement records are required. This section therefore focuses on all the complete current meter records on the slope moorings from the second and third six-month deployments.

3.3.1. Kinetic Energy Spectra

The KE spectra for the lower level records are represented in Figure 3.3-1. These three sets of KE spectra are at sites A4, A5, and C4, respectively, for data from the second and third six-month deployments. The first thing to notice is that the information that one gets from the spectra vs. from the time series is somewhat different but complementary: The lower level time series revealed strong equatorward pulses of current that repeated at regular intervals, which, however, changed period (within the range 25 to 60 days) in different portions of the first three six-month records; these "pulses" were of course modulated by higher and lower frequency variability. The KE spectra, calculated by Fourier-transform of the full record, group all the spectral variability under one curve having generally a broad low-frequency peak and a distribution of higher-frequency peaks; a better estimate of the record-long average spectral variance is thereby obtained, but information is lost regarding non-stationarity of the frequency/ periodicity content. (The same comment applies regarding cross-spectral variance and phase information between pairs of records.)

Figure 3.3-1(a) shows the KE spectra for site A4, 300 m, 800 m and 1200 m. The lower two levels are very similar, having a broad peak around periods of 16 to 50 days, with maximum near 25 days, and a shoulder of relatively high spectral variance out to periods as short as 7 to 8 days. At shorter periods yet, the spectrum drops off quickly. The 300 m spectrum at A4 is of course higher and has substantial variance extending to higher frequencies, with local maxima at periods near 6 d, 2.5 d, and 2 d.

Figure 3.3.1(b) shows the KE spectra for site A5 lower levels (800 m, 1200 m, and 2900 m). The largest peak, of similar height in all three KE spectra, is near periods 12 to 18 days. Other spectral peaks around 20 days, 10 days, 5 to 7 days, 3 days, and 2.5 days are common to all deep levels, but in contrast, their variance decreases with increasing depth.

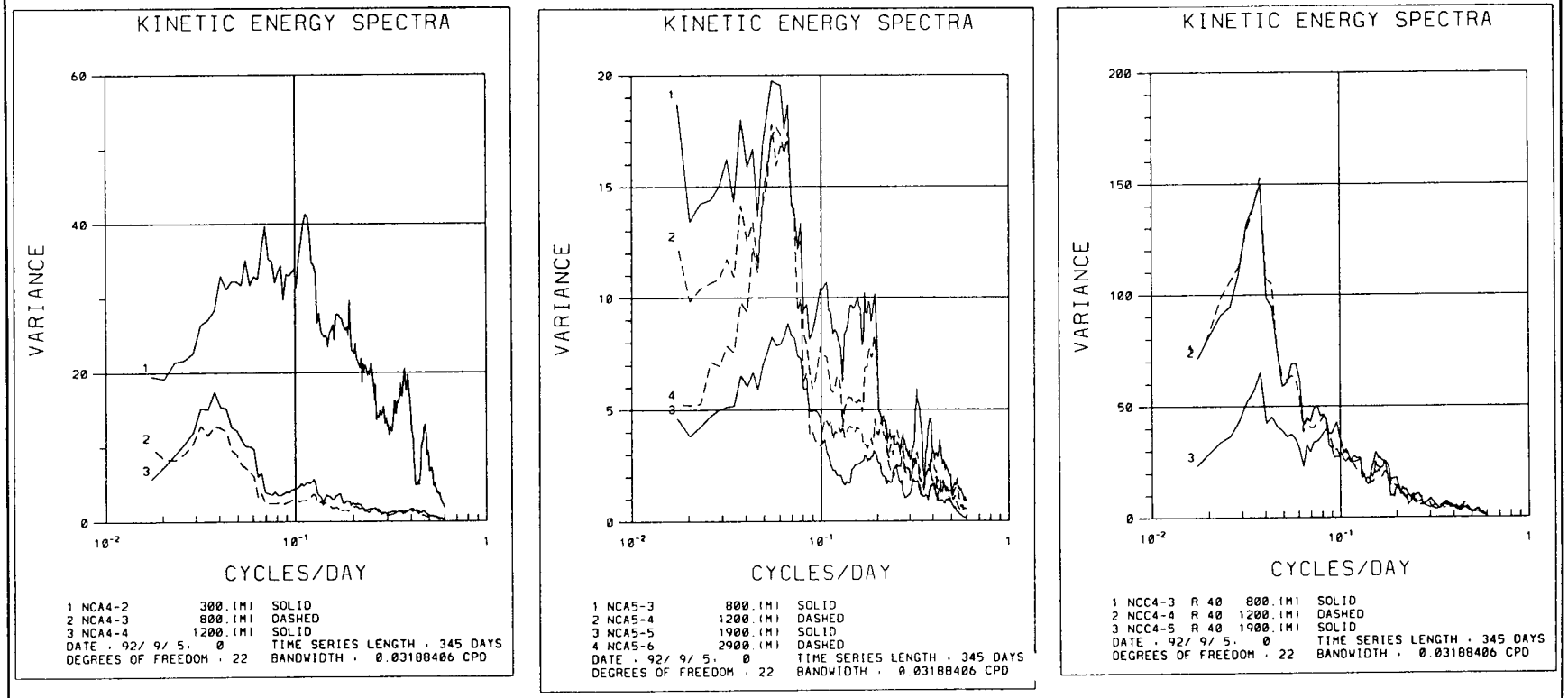

Figure 3.3-1. KE spectra for deep current meters at (a) A4, (b) A5 and (c) C4. Record lengths are 345 days.

Figure 3.3-1(c) shows the KE spectra for site C4 lower levels (800 m, 1200 m, and 1900 m). The largest spectral peaks are in frequency bands common to all three levels, but with different heights. All have a low frequency peak around periods of 20 to 40 days, centered near 25 days, with additional small peaks around 12 days and 6 to 7 days. The spectral heights suggest that the deep fluctuating currents are nearly barotropic from 800 m to 1200 m, with somewhat weaker flow at 1900 m (100 m off the bottom).

3.3.2. Vertical EOFs

Vertical EOF analyses for the most significant mode (mode-1), considering one mooring at a time, are presented in Figure 3.3-2 for four frequency bands of respective periods, 345 to 27 days, 27 to 13 days, 50 to 20 days, and 11 to 4 days. (Note that the third band overlaps the first two.) These bands encompass essentially all the spectral variance under the low and high frequency peaks discussed above. All records on each mooring were included that were continuous through the second and third six-month deployments; thus different sets of currents meter levels were included in the analysis for different moorings. Each serves to illustrate aspects of closely related phenomena. Processes north and south of Cape Hatteras will be seen to define a consistent, complementary pattern.

For site A4, in the southernmost wedge of the Slope Sea, levels 300 m, 800 m, and 1200 m are included in Figure 3.3-2(a). Thus in this covariance analysis, the weaker of the two upper level records (and hence less dominant in variance) is included, plus two of the lower level records.

Mode-1 contains 53% to 75% of the variance, as labeled, for the different bands. To first order we note that within bands the mode is essentially identical for the two lower levels, *i.e.*, the direction of the principal axes, their size, and the phase are essentially the same for the two lower ellipses. The mode is linearly polarized and nearly parallel to the slope isobaths for the three longest period bands; the mode for the shorter period band is rotated 15° to 20° clockwise. These kinematics correspond well to TRW variability, with phase propagating offshore, transverse to the polarization (principal axis), and with the energy propagating equatorward and slightly onshore but nearly parallel to the isobaths.

Vertical EOF's for Mooring A4. Analysis Period 92/ 9/ 5 - 93/ 8/ 6.

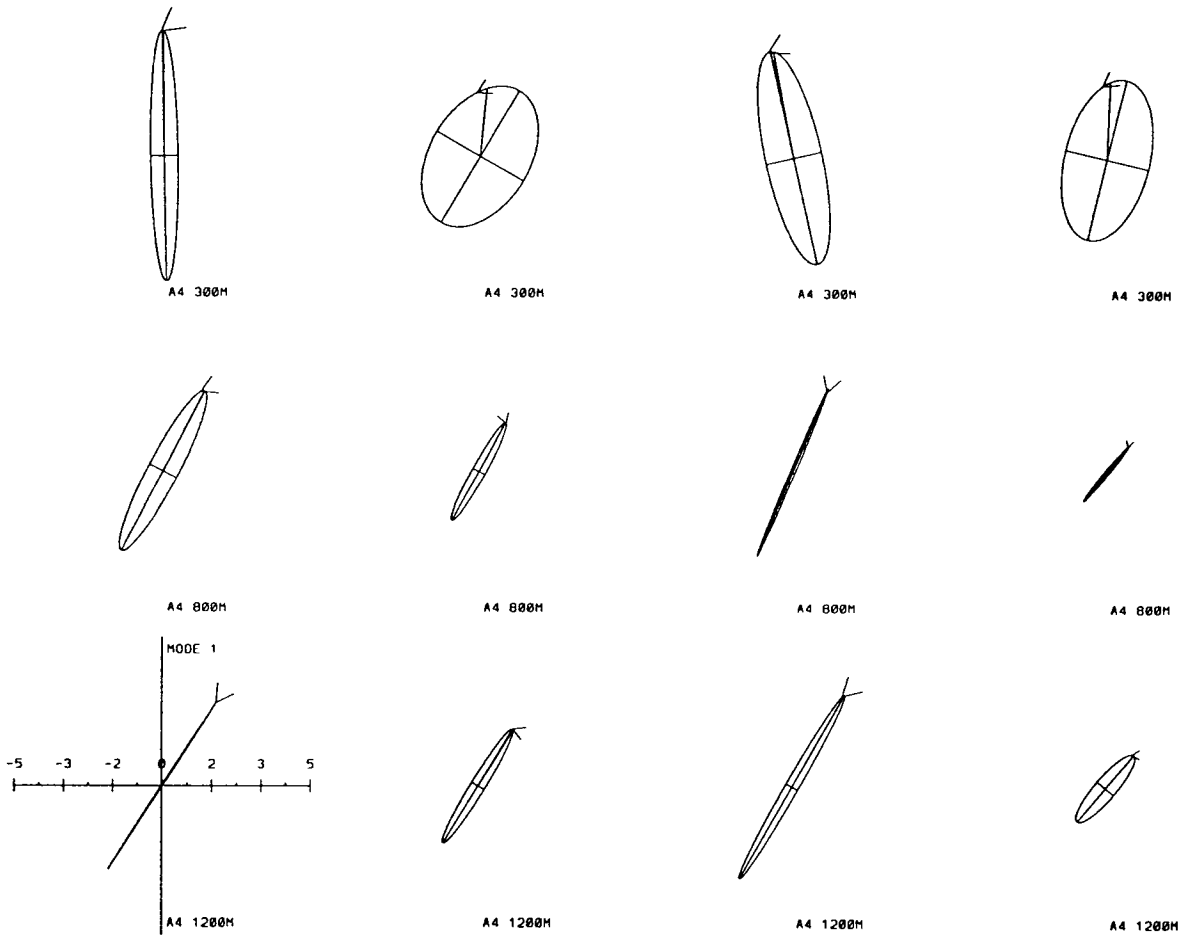

Frequency Bands			
345 - 27 days	27 - 13 days	50 - 20 days	11 - 4 days
Percent of Total Normalized Variance : Mode 1.			
53.8	68.0	74.6	53.4

Figure 3.3-2(a). Vertical EOFs (Mode-1) at Mooring A4, 300 m, 800 m, and 1200 m levels. Analysis period is September 5, 1992 through August 6, 1993 in four frequency bands as labeled.

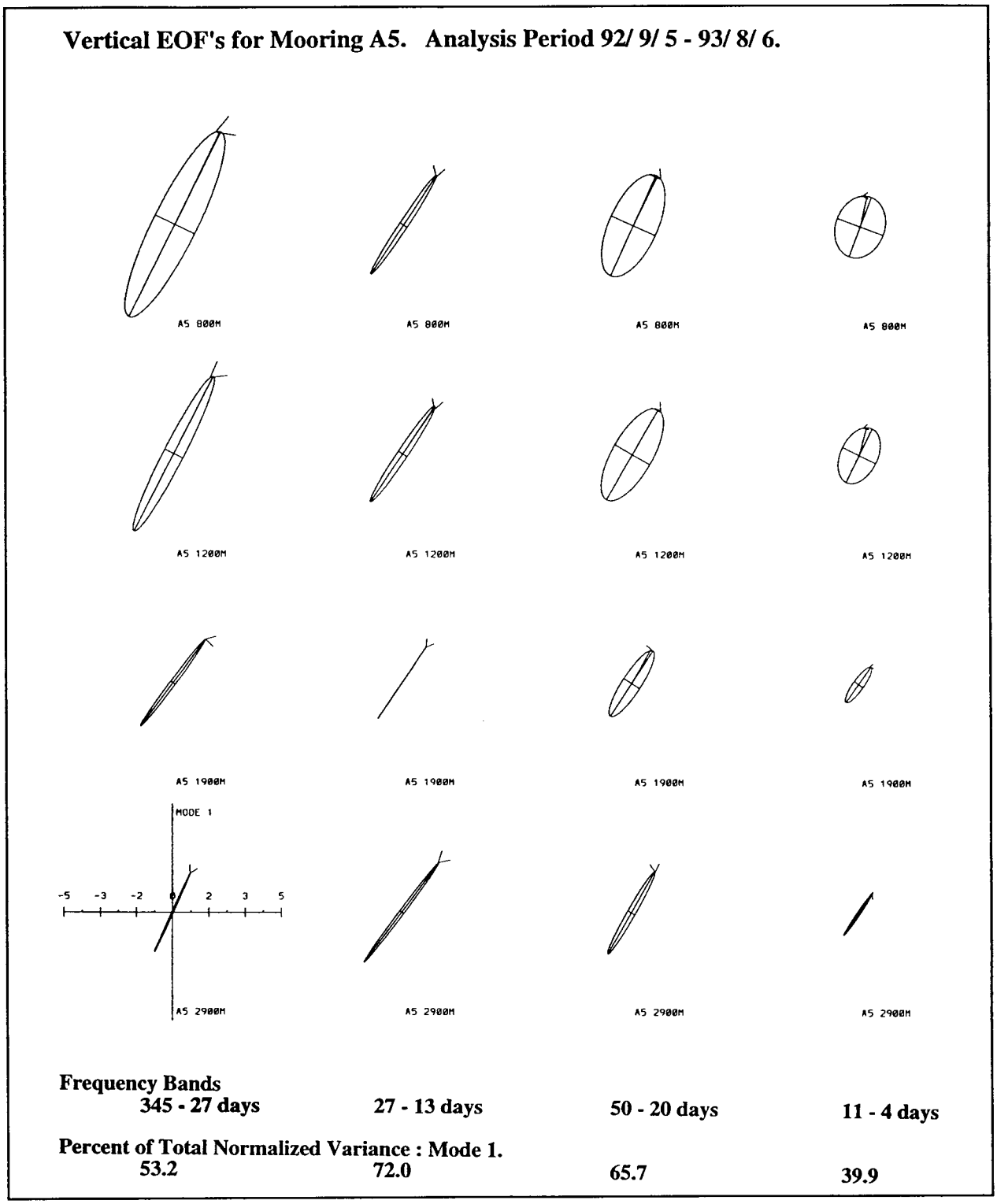

Figure 3.3-2(b). Vertical EOFs (Mode-1) at Mooring A5, 800 m, 1200 m, 1900 m, and 2900 m levels. Analysis period and frequency bands as in (a).

Vertical EOF's for Mooring B4. Analysis Period 92/ 9/ 5 - 93/ 8/ 6.

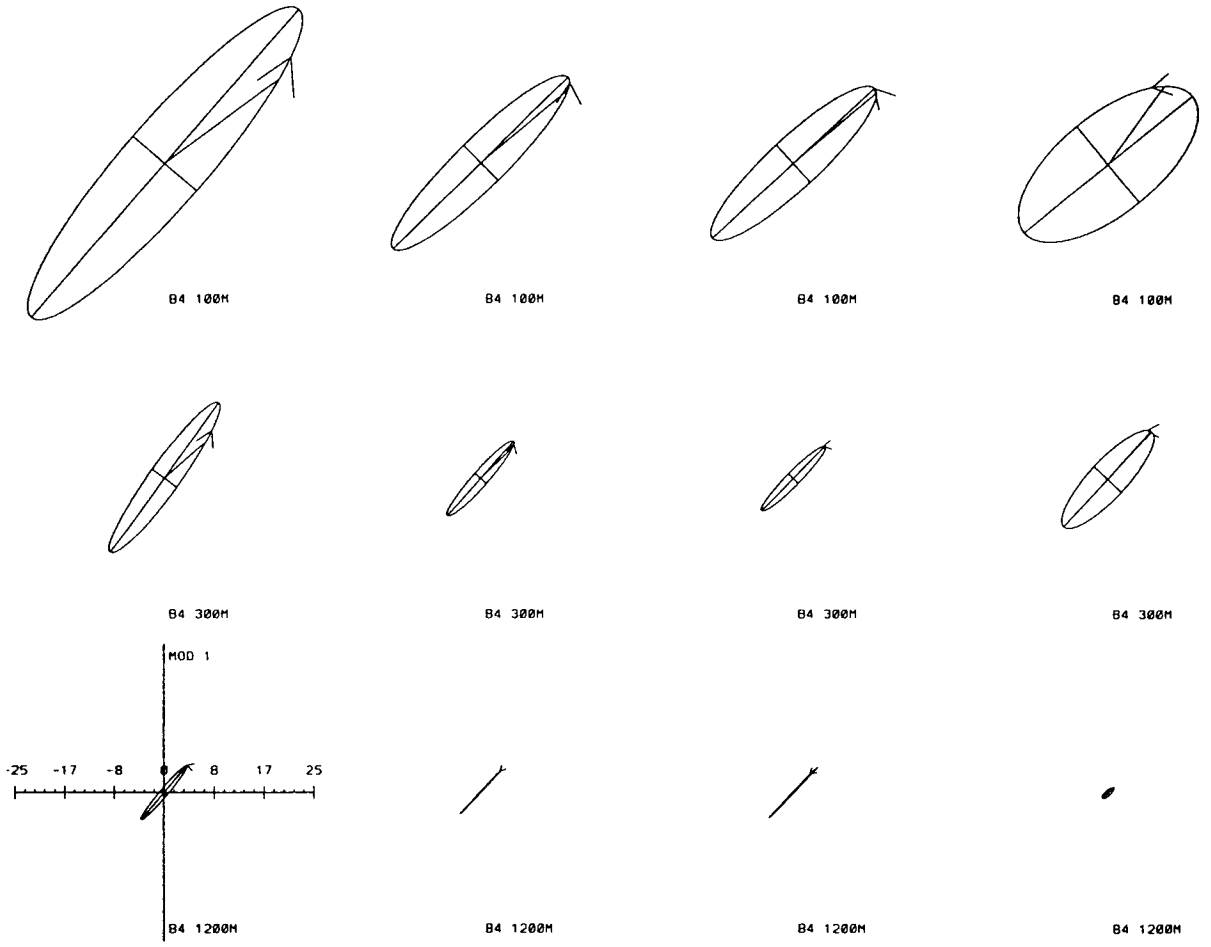

Frequency Bands			
345 - 27 days	27 - 13 days	50 - 20 days	11 - 4 days
Percent of Total Normalized Variance : Mode 1.			
63.8	75.6	67.9	50.7

Figure 3.3-2(c). Vertical EOFs (Mode-1) at Mooring B4, 100 m, 300 m, and 1200 m levels. Analysis period and frequency bands as in (a).

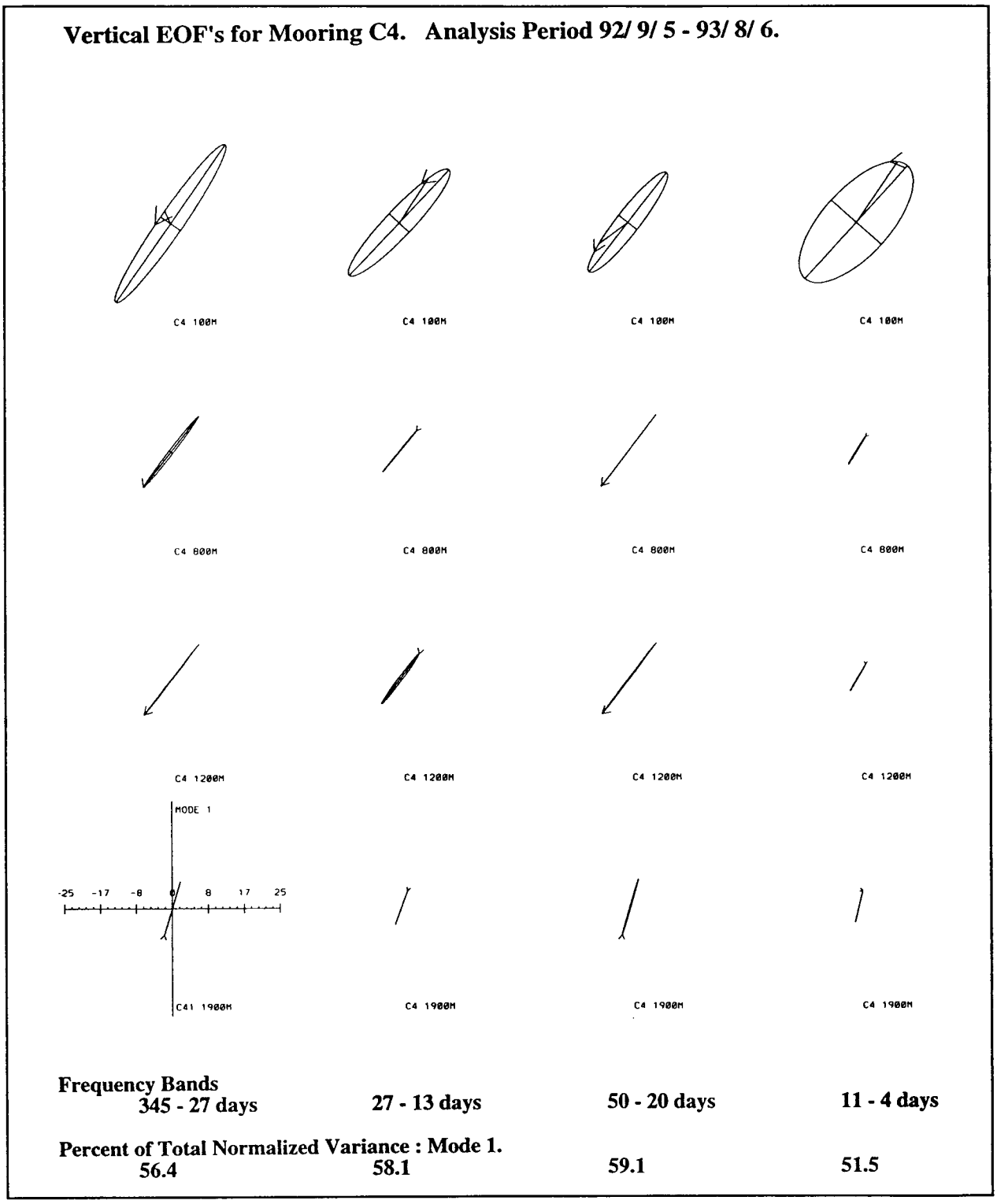

Figure 3.3-2(d). Vertical EOFs (Mode-1) at Mooring C4, 100 m, 800 m, 1200 m and 1900 m levels. Analysis period and frequency bands as in (a).

The upper layer principal axes at A4 (Figure 3.3-2(a)) are rotated about 30° anticlockwise from the lower level, and the phase is also shifted about 30°, such that the component of velocity along the principal axis remains in phase between the upper and lower levels. (Returning for more careful inspection of this mode in the two lower layers shows that the 800 m ellipse is also rotated 5° to 10° from that at 1200 m, with the same "in phase" interpretation.) The kinematics of this dominant vertical EOF mode correspond to a systematic "backing" (*i.e.*, anticlockwise turning with height) of the fluctuating slopewater currents. Backing indicates cold advection and suggests (since the temperature tendency is small at these low frequencies) systematic vertical motion of water parcels, downwelling when approaching the Gulf Stream baroclinic front (*i.e.*, tending to flow along the inclined density surfaces). The backing can also be noted clearly in the time series plots for site A4 (Figure 2.2-6).

For site A5, on the shoreward edge of the Gulf Stream and the seaward edge of the Slope Sea, levels 800 m, 1200 m, 1900 m, and 2900 m are considered together for the vertical EOFs shown in Figure 3.3-2(b). Thus the records contributing to these EOFs are all from the lower layer. Mode-1 contains between 40% and 66% of the total variance, as listed, for the different frequency bands. The features of this EOF mode are very similar to what has just been discussed for site A4, but even more clearly displayed. The currents are all linearly polarized and phased such that the velocity component along the principal axis (even though it is turned in the vertical) is in phase throughout the lower water column. The fluctuating currents of this mode systematically back with height for each frequency band. The backing is only 5° to 10° between each neighboring pair of levels, but again this indicates cold advection and downwelling as the fluctuating equatorward currents cross at a small angle obliquely under the baroclinic Gulf Stream front.

Mimicking site A4 in another aspect, the EOFs at site A5 (Figure 3.3-2(b))turn the principal axes systematically with frequency. In accord with TRW kinematics (with a slightly onshore component of energy propagation), higher frequencies have a polarization rotated anticlockwise and cross isobaths relatively more. The rotation may be seen most clearly between pairs on each level of the two left columns (lowest frequency columns). The highest frequency analysis-band includes periods shorter than the TRW-cutoff for site A5, which has a gentler bottom slope that only supports TRWs down

to periods of 6 to 8 days. Consequently, the 11-4 day band vertical EOF at A5 shows evidence of some admixture of TRWs and vertical coupling to variance from upper layer meanders; being less uniquely organized in the vertical, this EOF accounts for the least percent variance (40%) among all the lowest modes discussed here, and the upper ellipses (800 m and 1200 m) are more nearly circular than linearly polarized, unlike any of the others that are dominated purely by TRWs.

For site B4, right at Cape Hatteras in the shoreward edge of the Gulf Stream, levels 100 m, 300 m, and 1200 m are considered together for calculating vertical EOFs (Figure 3.3-2(c)). Thus these EOFs examine coupling between the highly energetic and coherent two upper levels and variability in the lower level. Mode-1 accounts for 51% to 76% of the variance, as listed, for the four frequency bands. The principal axes are nearly parallel at all three levels. The 100 m and 300 m phases are essentially the same within each band (as the stick plots confirm), and phase differences are also small to the 1200 m level. This pattern is suggestive, as was also noted in the time series discussion, of relatively depth-independent shifting and turning of the basic vertical shear profile. For the three low frequency bands, the deep phase leads by about 15°, and for the high frequency band the deep phase lags by about 15°. This phase pattern is respectively against and with the mean shear, and is thus suggestive of growth at low frequency and decay at high frequency by baroclinic instability processes.

For mooring C4, south of Cape Hatteras in the shoreward edge of the Gulf Stream, current records at 100 m, 800 m, 1200 m, and 1900 m are considered together to calculate EOFs (Figure 3.3-2(d)). Thus these vertical EOFs examine coupling between the highly coherent lower level currents and the highly energetic 100 m level. Mode-1 accounts for 52% to 59% of the overall variance. This is a larger fraction of variability that is found to be coherent between the upper and lower levels than might be judged "by eye" from the stick plots. The EOFs on this mooring provide an illuminating contrast to those from the two sites north of Cape Hatteras: Whereas the deep levels all have their components essentially linearly polarized and in phase relative to the principal axes, the sense of turning on C4 is consistently clockwise with height ("veering"). Veering is associated with warm advection and is again suggestive of vertical motion, as the fluctuations cause water parcels to obliquely cross the front. The 100 m ellipses are veered more yet,

and the phase of the deep fluctuations in the two longest period bands (345-27 days and 50-20 days) leads the upper level by about 30°. This tendency would be consistent with low frequency growth by baroclinic instability.

A large fraction of the deep level variability observed in the KE spectra has thus been explained as a mixture of TRWs and coupling between eddies in the upper and lower levels. Altogether, these vertical EOFs explain a large fraction of the overall variance in mode-1 and are very informative regarding processes that are active (TRWs, upper-lower coupling, and indications of growth or decay in different frequency bands).

3.3.3. Horizontal EOFs

Horizontal EOFs have also been calculated for the lower level, as represented in Figures 3.3-3(a) and (b). Records are complete at the 1200 m level for all four Slope moorings throughout the second and third six-month deployments, and the variability at 1200 m may be taken as representative of the lower level (as the vertical modes discussion has just indicated). Two frequency bands (periods 60-25 days and 25-13 days) are illustrated in this figure, and mode-1 accounts for respectively 51% and 50% of the spectral variance. The horizontally coherent variability is again essentially linearly polarized along isobaths at all four sites, and the phases are such that the component along the principal axis is very nearly in phase between sites. The phase lags (relative to the principal axis) by roughly 10° from A4 to B4 to C4, in both bands, indicating rapid equatorward propagation (group speed roughly 40 $km \cdot d^{-1}$). In the 25-13 day band, site A4 also leads A5 by around 20°-30° (*i.e.*, about 1 day), consistent with offshore phase propagation of TRWs. While the angle from A4 to A5 is not approximately normal to the isobaths or to the variance ellipse principal axes, and hence is not along the wave number vector for TRWs, rough (cosine-corrected) estimates of the phase speed and wavelength are 40 $km \cdot d^{-1}$ and 450 km. Altogether, the horizontal EOFs tend to confirm the dominance of topographic Rossby waves governing the deep slope variability.

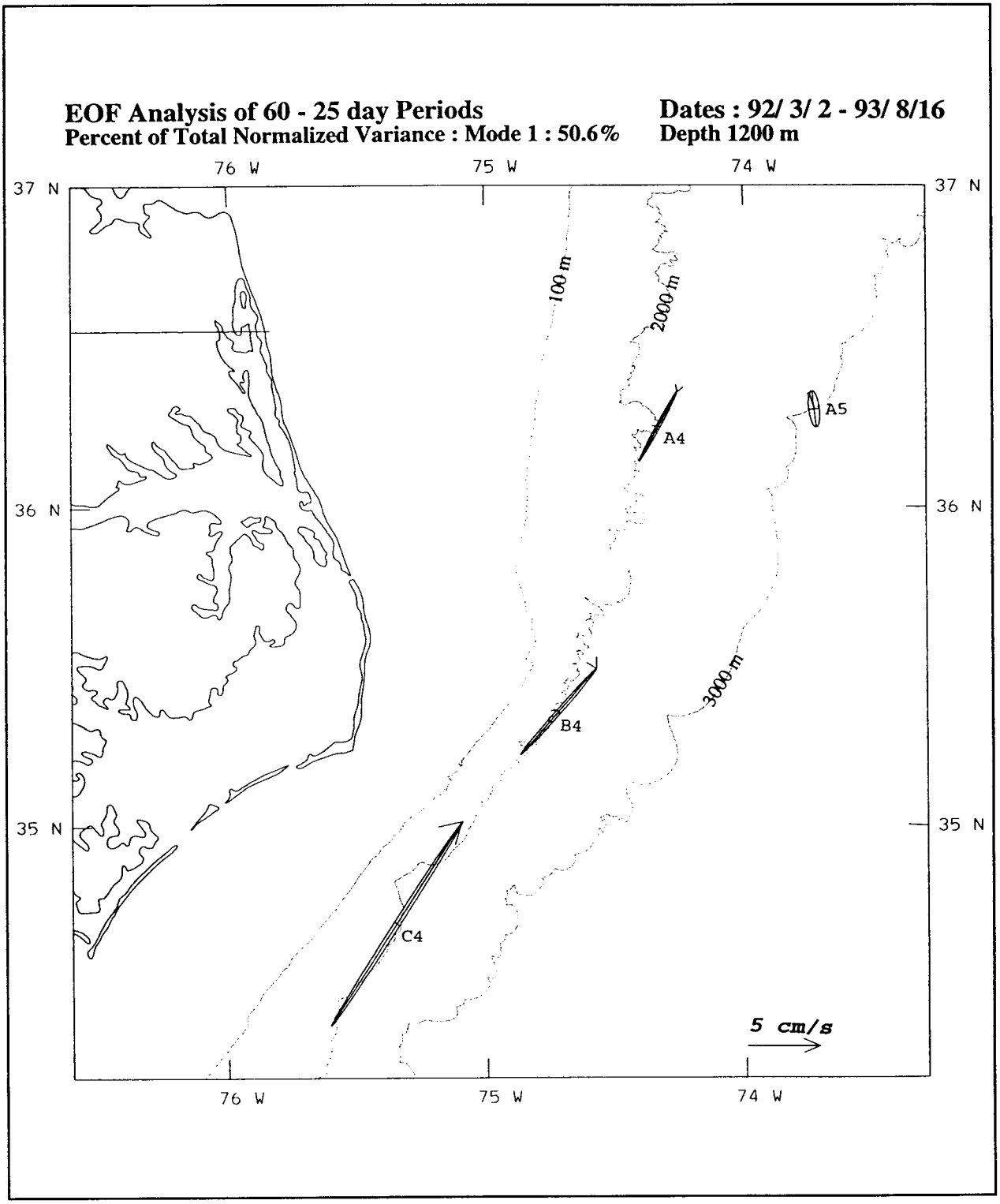

Figure 3.3-3(a). Horizontal EOF analysis (Mode-1) at 1200 m at Moorings A4, A5, B4 and C4 in frequency band 60-25 d. Analysis period is March 2, 1992 through August 16, 1993.

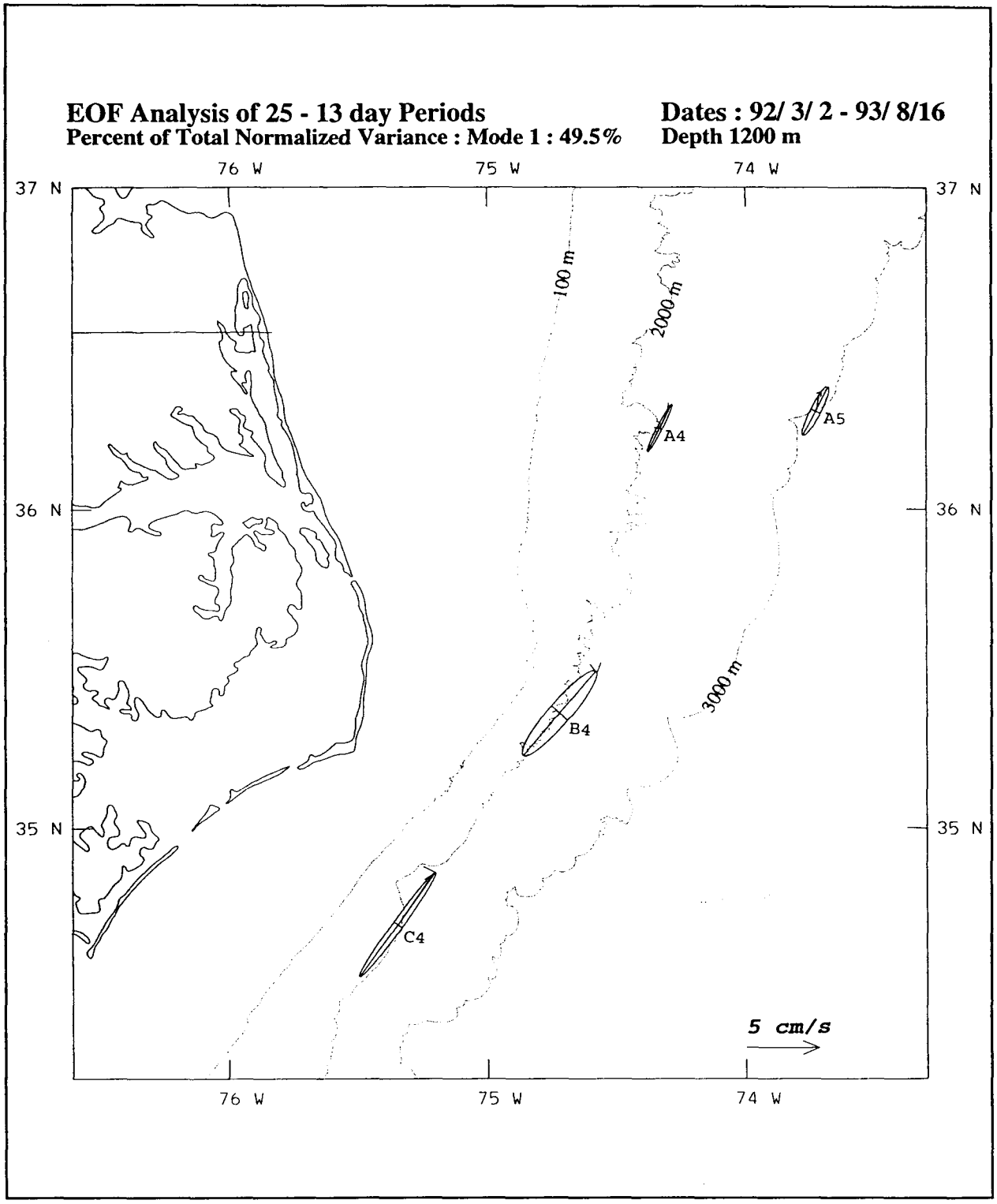

Figure 3.3-3(b). Horizontal EOF analysis (Mode-1) at 1200 m at Moorings A4, A5, B4 and C4 in frequency band 25-13 d. Analysis period is March 2, 1992 through August 16, 1993.

IV. SHELF CLIMATOLOGY

4.1 Currents

The basic statistics of the sub-tidal current records have been calculated for all available data between March 1982 and August 1993. To further illustrate significant seasonal differences, the records have been divided into two summer periods, June through September 1992 and May through August 1993 (avoiding Hurricane Emily on August 31), and one winter period December 1992 through April 1993. The shelf current meter records show a fairly abrupt transition from the energetic winter to the mild spring-summer regime around the end of April in both 1992 and 1993. The fall transition is more gradual with increasing numbers of storms and frontal passages as the fall progresses from about mid-September to the end of November.

Figures 4.1-1(a), (b) and (c) show the record means and variance ellipses of the 40-HLP current at the near surface, mid-depth and near bottom instruments, respectively. The records at each depth have a cumulative length of at least 12 months to be included (see the time lines for data recovery in Figures 1.2-7 and 1.2-8, for more detail). The means at all depths are southward on the southern Middle Atlantic Bight except near Cape Hatteras (B2 and B3 and surface D2) where the influence of the Gulf Stream is evident. Southward mean flows are stronger at depth on the outer shelf than at the surface (A2, D1 and D2) and also show small offshore components which is also observed at the 5 m level of D2. This turning offshore of the outer shelf water in the lower water column is a reflection of export of this water along the north wall of the Gulf Stream. There is also a southeastward mean at the 100 m level of A4 indicating that upper Slope Sea water is also turning towards the Gulf Stream on Line A.

In Raleigh Bay, mean flows are northeastward and converge towards the Gulf Stream at the 20 m level at C2 (Figure 4.1-1(b)) and towards the coast at C1. C3 is strongly influenced by the Gulf Stream and flows are aligned along the direction of the shelf-break isobath. The converging shelf mean flows north and south of Diamond Shoals implies an export of Middle Atlantic Bight and South Atlantic Bight water off the shelf, which appears to be concentrated in the region of Cape Hatteras. The strong Gulf Stream mean currents (~100 $cm \cdot s^{-1}$) at C4 and B4 are very similar, as

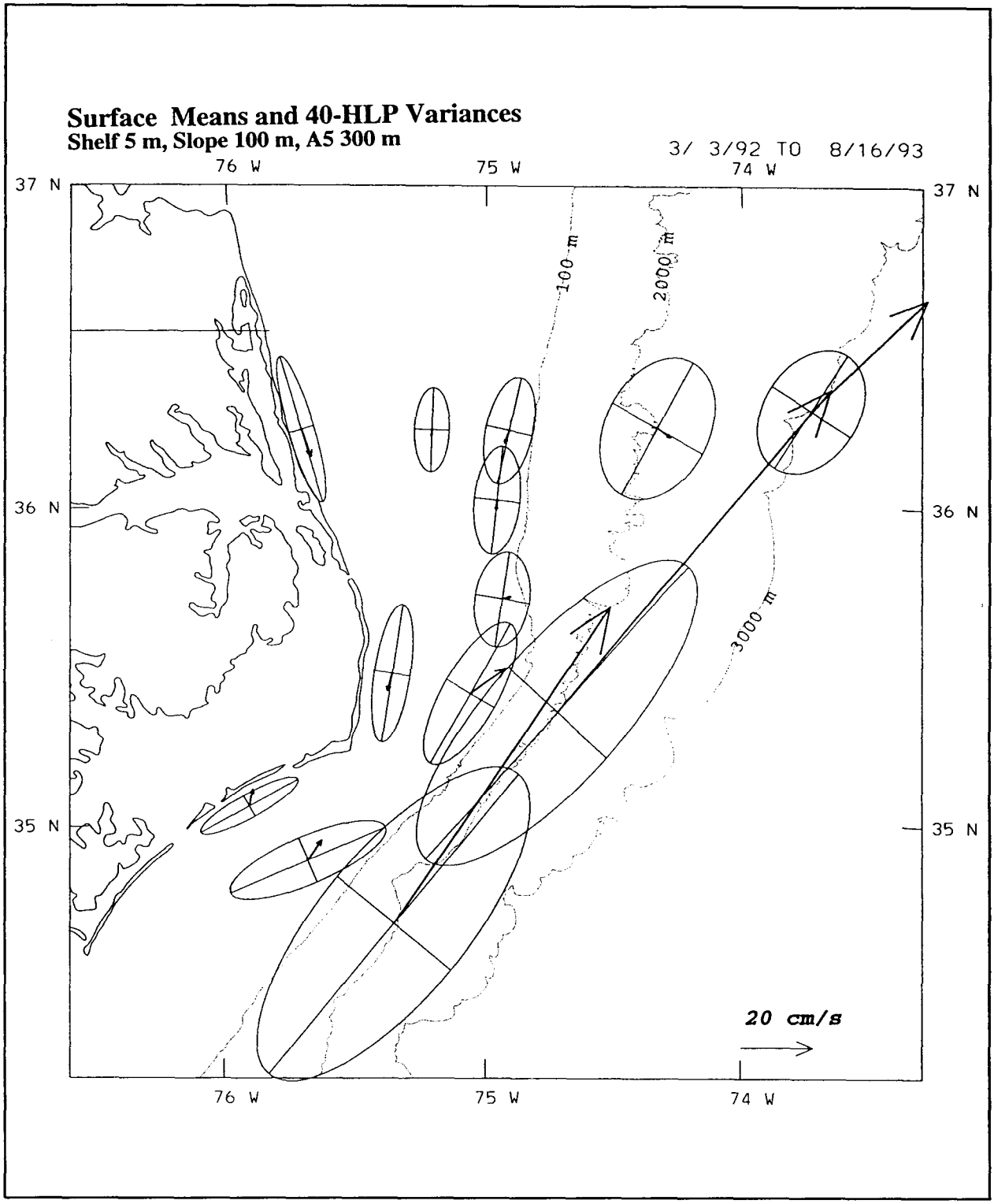

Figure 4.1-1(a). Means and Standard Deviation Ellipses for all available near surface current records.

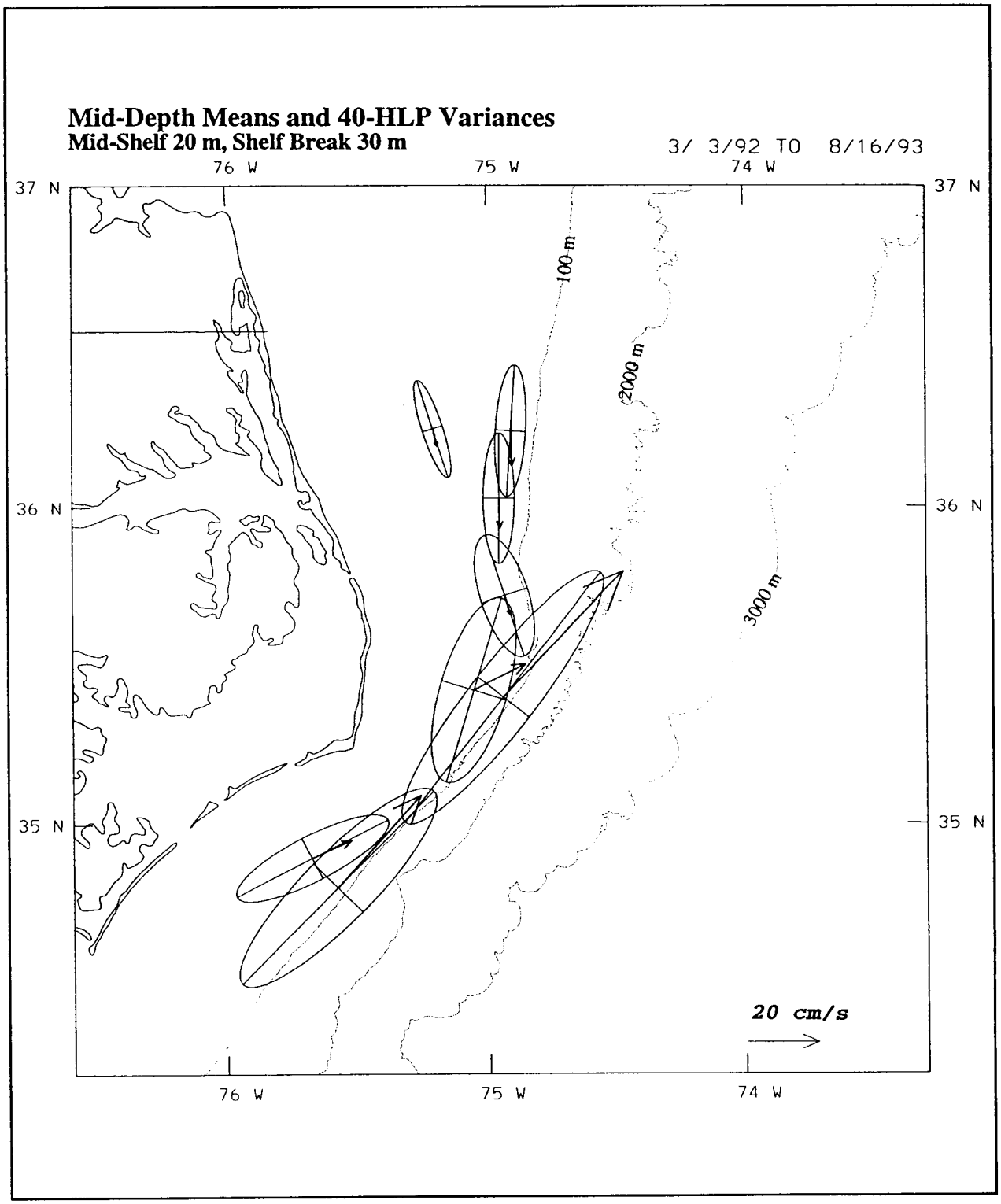

Figure 4.1-1(b). Means and Standard Deviation Ellipses for all available mid-depth current records.

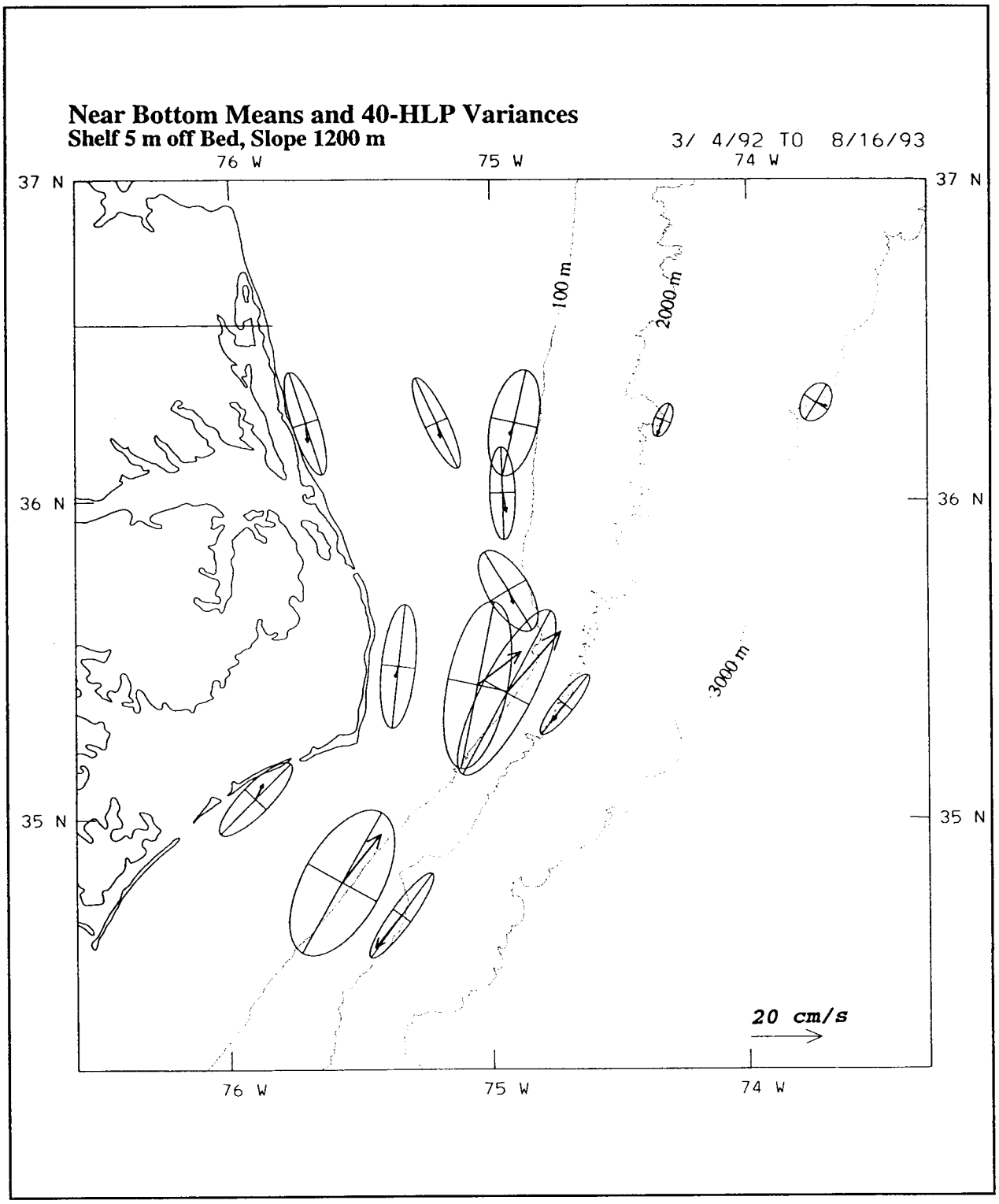

Figure 4.1-1(c). Means and Standard Deviation Ellipses for all available near-bottom current records.

is the rms variability, which is primarily the result of Gulf Stream meander motions.

Standard errors of the means range from about 0.5 to 1.3 $cm \cdot s^{-1}$ on the shelf and about 4 to 5 $cm \cdot s^{-1}$ in the Gulf Stream. Therefore, except for the very small mean flows calculated for some of the 5 m level records (e.g. A2, D2 and D1) the majority of the means exceed their standard error and therefore can be considered to be significant estimates of true long-term means. The standard errors of the means are small because of the length of the records and the relatively short decorrelation time scales of about one day for the shelf and two days for the slope currents.

On the shelf, the variance ellipses are quite uniform both horizontally and vertically. Line A shows an increase in amplitude at the coast and Lines B and C show increases at the shelf break caused by the influence of Gulf Stream meanders. The higher amplitude at the 5 m level of A1 is probably attributable to increased southward flows caused by coastal jet surges of Chesapeake Bay outflow. The principal axes are aligned with the general trend of the isobaths at each location except for the lower layers at D2 where shelf water export and Gulf Stream intrusions may cause the clockwise rotation of the axis from the isobath direction, and at A2 where the anticlockwise rotation is consistent with lower layer Ekman turning from wind forced upwelling and downwelling.

The 40-HLP means and variance ellipses for the available records for the summers of 1992 and 1993 are given in Figure 4.1-2 and 4.1-3, respectively. Mean wind stress (in mPa; 1 $dyne \cdot cm^{-2}$ = 100 mPa) is shown for Cape Hatteras and in both summers is small and directed towards the north or north-northeast. There is clearly a difference in the behavior of the Gulf Stream. In 1992, there is a definite anti-cyclonic curvature to the mean flow between C4 and B4. There is a similar rotation of the principal axes of the variance ellipses as well as a decrease in meander energy. This implies that the Gulf Stream is penetrating a little further onto the outer shelf between Line C and D2 in 1992 than 1993 when the Gulf Stream is more straight. The slightly larger fluctuations at B2 near-surface and D2 in 1992 compared with 1993 are also consistent with greater Gulf Stream influence on the outer shelf at Cape Hatteras (Figures 4.1-2 and 4.1-3). Examination of the summer imagery corroborates this supposition.

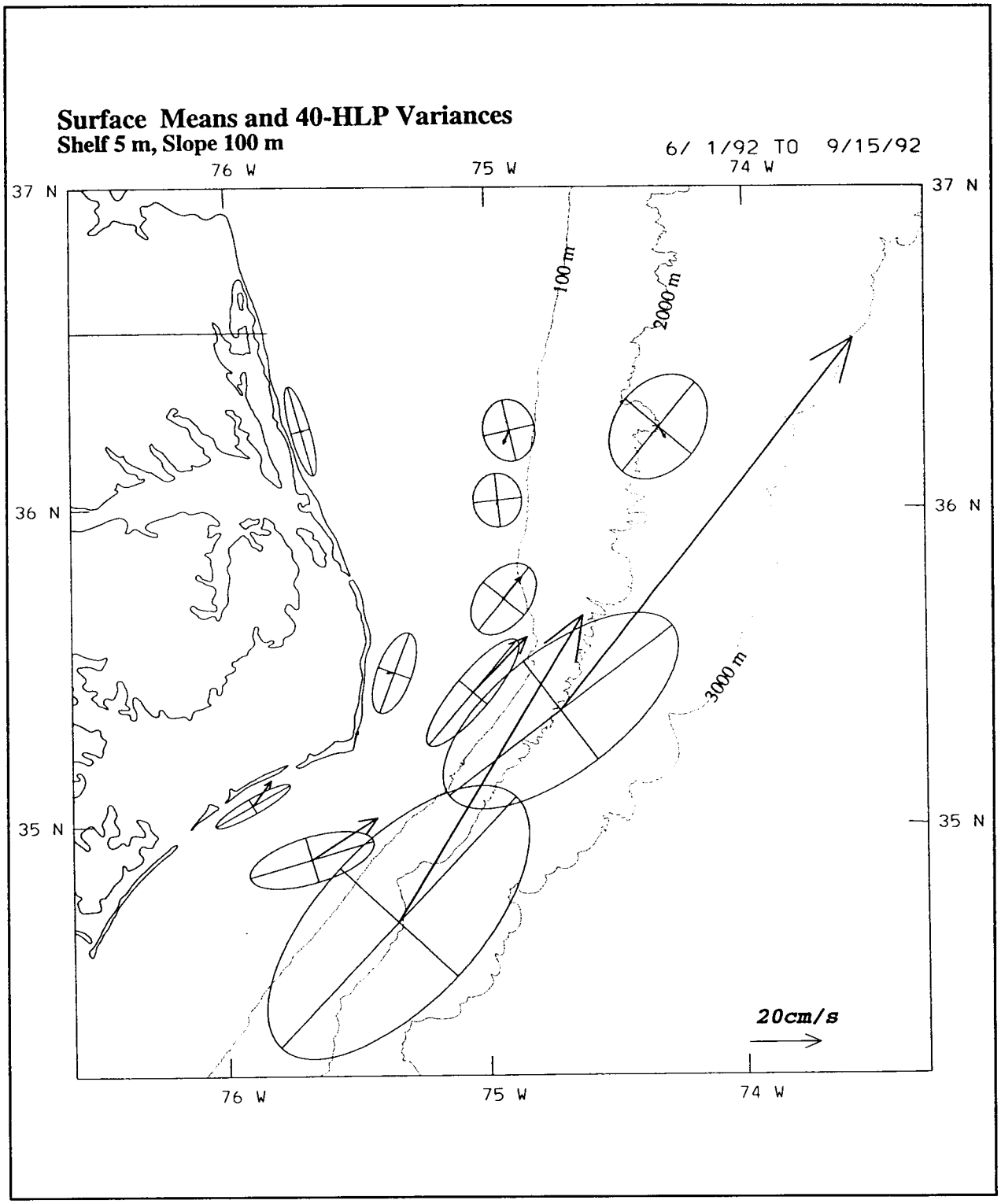

Figure 4.1-2(a). Summer 1992 Means and Standard Deviation Ellipses for all available near-surface current records. Wind stress vector is shown for Cape Hatteras in mPa (same scale as current vectors).

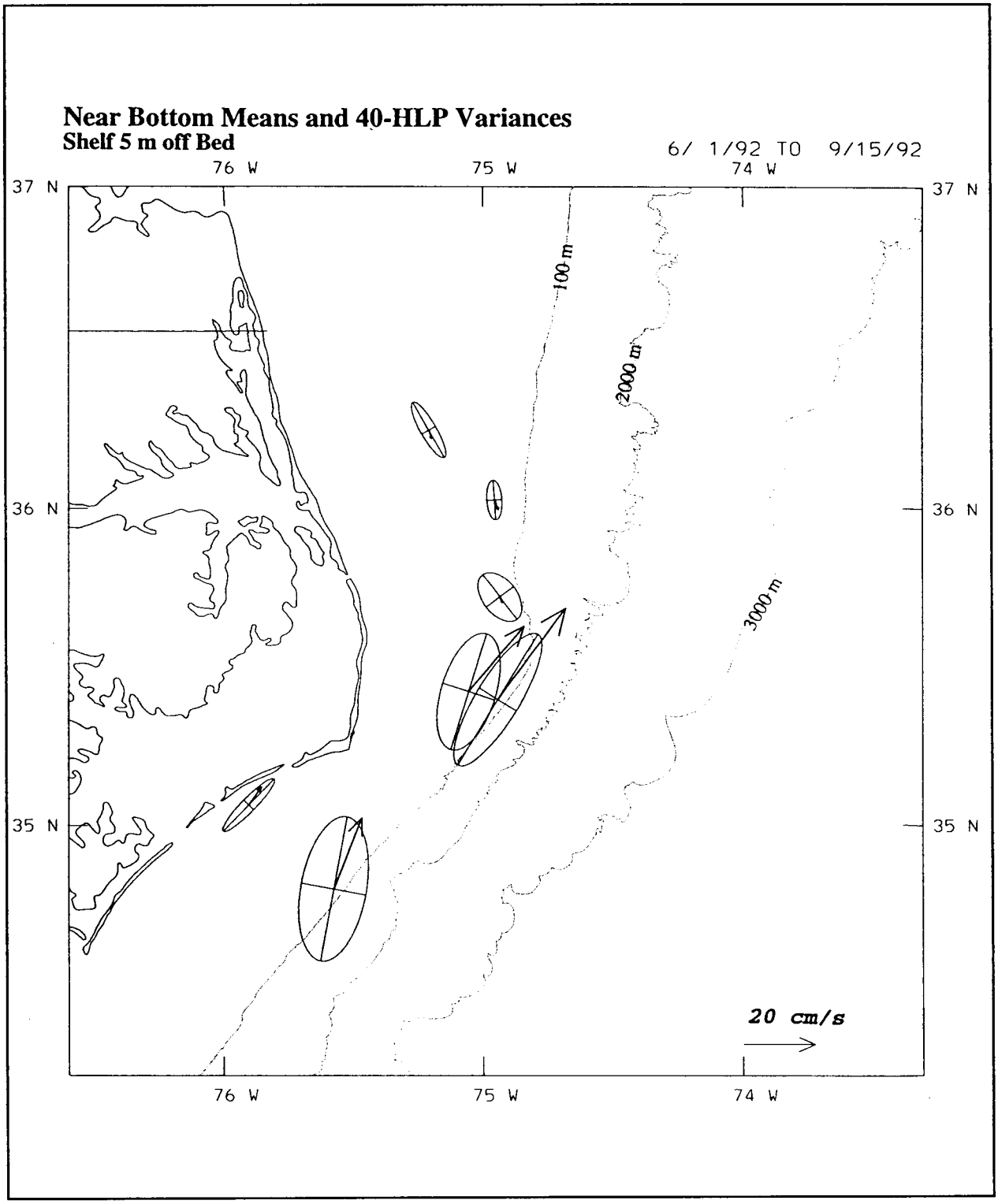

Figure 4.1-2(b). Summer 1992 Means and Standard Deviation Ellipses for all available near-bottom current records. Wind stress vector is shown for Cape Hatteras in mPa (same scale as current vectors).

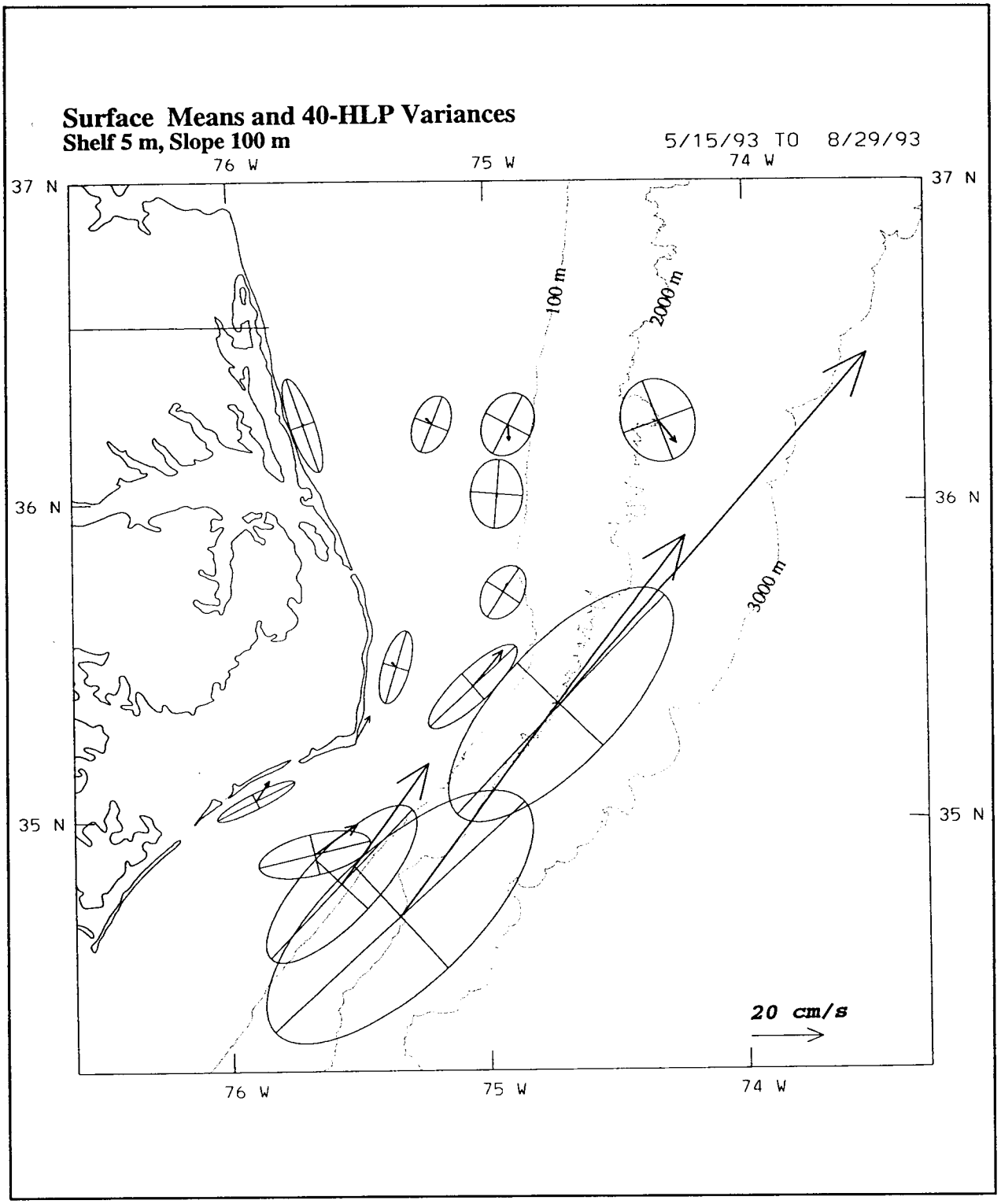

Figure 4.1-3(a). Summer 1993 Means and Standard Deviation Ellipses for all available near-surface current records. Wind stress vector is shown for Cape Hatteras in mPa (same scales as current vectors).

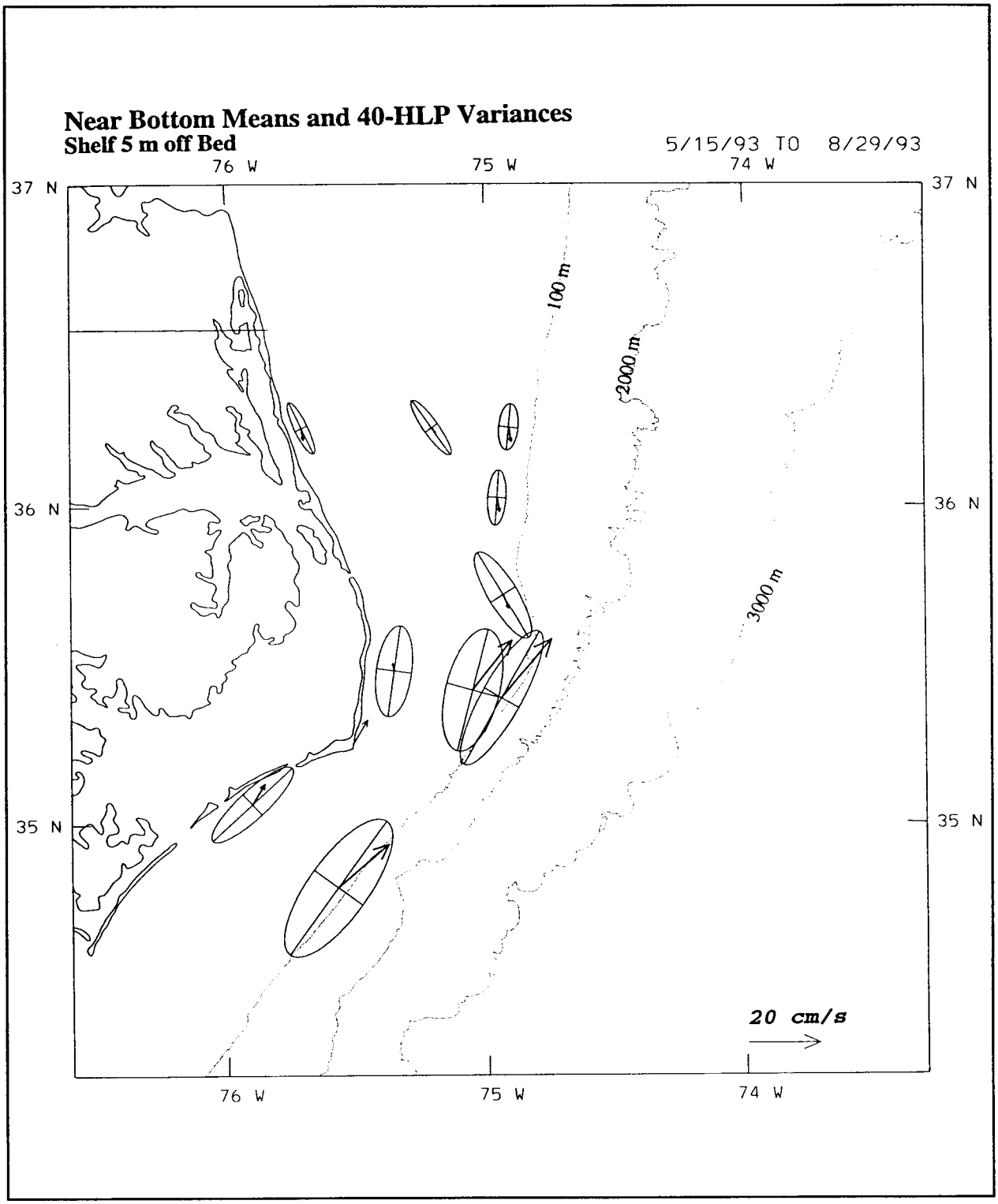

Figure 4.1-3(b). Summer 1993 Means and Standard Deviation Ellipses for all available near-bottom current records. Wind stress is shown for Cape Hatteras in mPa (same scale as current vectors).

There is substantial northeastward mean flow on the shelf at Line C in both years. There are however, interesting differences on the outer shelf. The near-surface layer C2 shows convergence towards the Gulf Stream in both years, but the near bottom mean flow, at C3 in 1992, and the orientation of the variance ellipses is similar to the 100 m level at C4 and presumably indicates meander penetration onto the outer shelf. In 1993, bottom mean flows at C3 are directed towards the Gulf Stream and the variance ellipse is orientated parallel to the 75 m isobath indicating a straighter Gulf Stream and convergence of bottom shelf flow into the Gulf Stream on the outer shelf as well as the middle shelf.

On the shelf north of Cape Hatteras, southward near-surface mean flows are small in both years (Figures 4.1-2(a) and 4.1-3(a)) and mainly confined to the outer shelf. Mean flows are close to zero or have a northward component at B1 and A1. Southward flows (Figures 4.1-2(b) and 4.1-3(b)) are a little more prevalent near-bottom, which is probably a reflection of lessening influence of northward surface wind stress against the prevailing southward mean flow of the Middle Atlantic Bight shelf (Beardsley and Boicourt 1981). The strongest difference between surface and bottom is at D2, in both years, where the near surface is part of Gulf Stream related flows and the near-bottom is showing the offshore export directed towards the Gulf Stream front. Shelf fluctuation amplitudes at positions not influenced by the Gulf Stream are relatively small (~10 $cm \cdot s^{-1}$) with outer shelf, near-surface, cross shelf fluctuations north of Cape Hatteras having almost as much energy as the along isobath component.

The 1992-93 winter means and variance ellipses are shown in Figure 4.1-4. Immediately apparent are the much larger amplitude of the fluctuations (~20 $cm \cdot s^{-1}$) and the prevailing southward and southwestward flows over both the Middle Atlantic Bight shelf and northern Raleigh Bay. There is a substantial, southward directed, mean wind stress of about 23 mPa at Cape Hatteras which is probably enhancing the Middle Atlantic Bight southward drift. The Gulf Stream also has larger along slope fluctuations than in the two summers. These amplify between C4 and B4 and Gulf Stream has little curvature, particularly in the principal axes of the variance ellipses (Figure 4.1-4(a)). A straight Gulf Stream is also observed in the imagery. On Line C, the near-surface is flowing southwestward with a component directed towards the coast whereas the lower layer currents (Figure 4.1-4(b)) are directed northeastward against the mean wind. The lower layer mean at C3 is

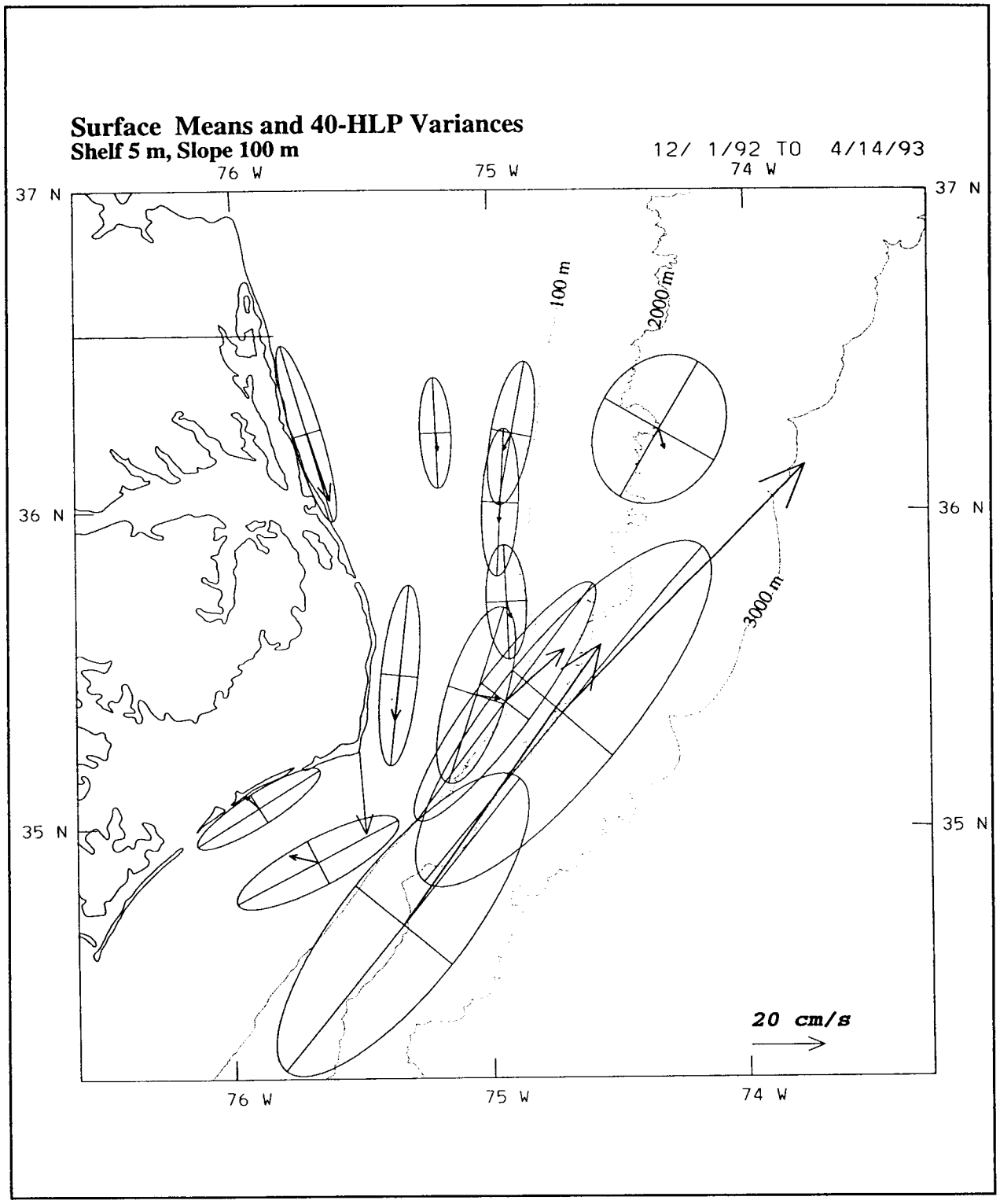

Figure 4.1-4(a). Winter 1992-1993 Means and Standard Deviation Ellipses for all available near-surface current records. Mean wind stress vector shown for Cape Hatteras in mPa (same scale as current vectors).

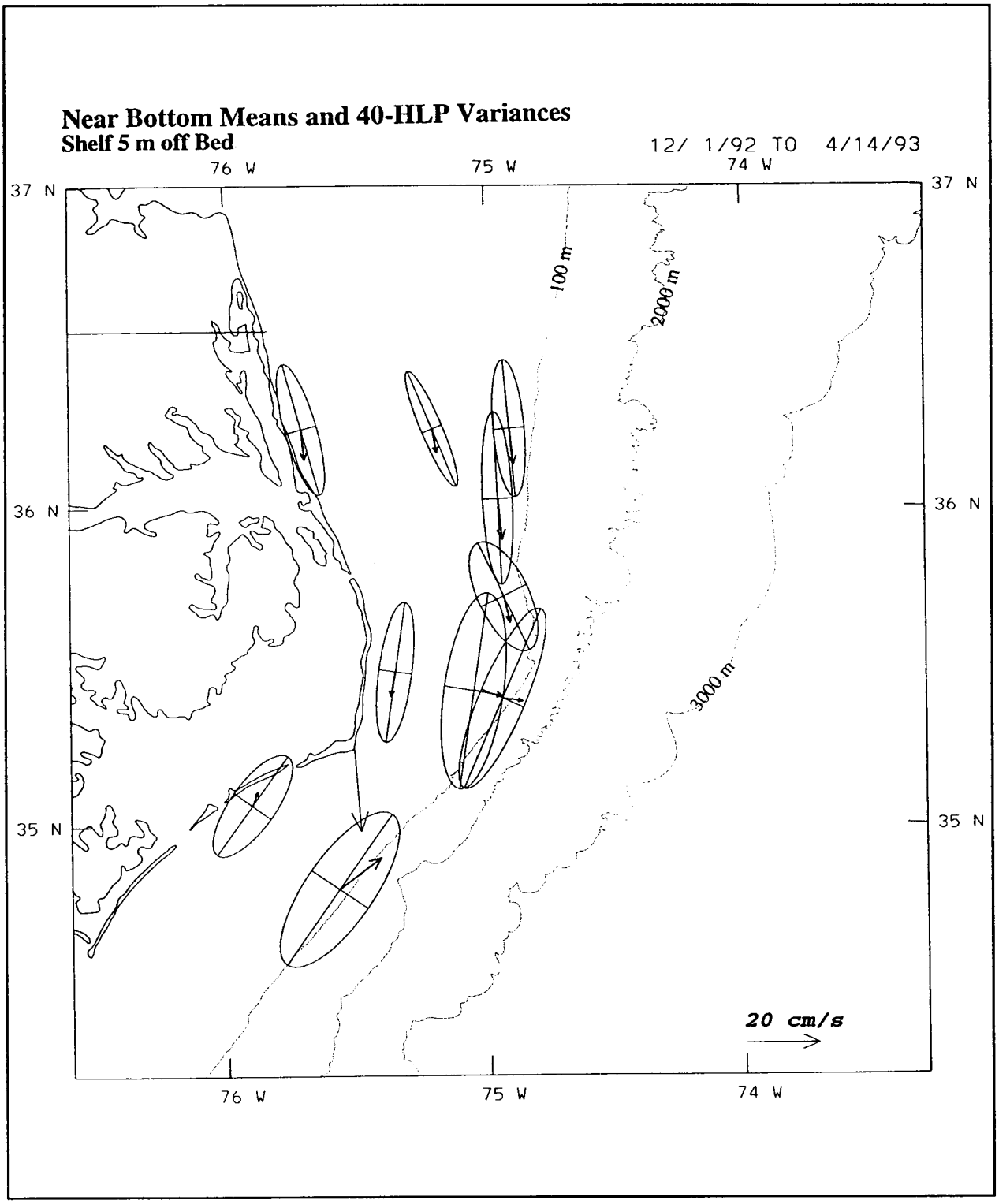

Figure 4.1-4(b). Winter 1992-1993 Means and Standard Deviation Ellipses for all available near-bottom current records. Mean winds stress vector shown for Cape Hatteras in mPa (same scale as current vectors).

directed into the Gulf Stream at an oblique angle similar to that found in the summer of 1993 (Figure 4.1-3(b)).

North of Diamond Shoals the mid and outer shelf moorings at B2 and D2, respectively, do not have the direct influence of Gulf Stream; unlike in the summers, because the orientation of the principal axes of the ellipses are more parallel to the isobaths than to the Gulf Stream front. This is even more apparent in the mean flows where the shelf flow is directed offshore across the isobaths at B2 and the near-bottom instrument at B3. Outer shelf mean flows at A2, D1 and D2 are southward with small offshore and onshore (except D2) components at the bottom and surface, respectively. The principal axes for the near-bottom at D2 are again directed into the Gulf Stream front as in the summers, though with larger variances. At A1, the near surface means are enhanced over the bottom and offshore at A2, showing a surface jet of the Chesapeake Bay outflow plume which is expected to be adjacent to the coast under northerly, downwelling favorable winds.

The major differences between winter and summer are the larger shelf variances and mean flows caused primarily by larger wind stress fluctuations with prevailing winter northerlies or northwesterlies. The Gulf Stream is much more confined to upper slope and outer shelf in winter because of the sharper surface density front between the shelf and Gulf Stream. In summer the development of the seasonal thermocline reduces the contrasts between surface Gulf Stream and shelf waters and Gulf Stream currents seem to penetrate towards mid-shelf at Lines B and C and northwards along the shelf break to encompass D2. Offshore export of shelf water, as indicated by the seasonal mean flows along the shelf break transect (A3, D1, D2 and B3), seems to occur closer to Diamond Shoals in winter than in summer. Middle Atlantic Bight shelf water also shows continuity of mean flow, in winter, north and south of Diamond Shoals which is not the case in the two summers examined.

4.2 Winds

The circulation processes offshore of North Carolina are influenced by the variation in water depth across the shelf, the unique geography of the region and the local and basin scale meteorological processes which affect the area. Variation of the meteorological processes in both space and time serves to provide distinctive circulation features for the waters offshore of North

Carolina. The climatology of events in this region varies from the synoptic scale which includes intense winter extratropical cyclones, severe summer tropical systems and mild, gentle breezes of the mid-summer period to the mesoscale systems such as sea breezes, thunderstorms and ocean-atmosphere exchanges along thermal discontinuities. Each such event can affect the circulation of the region.

The surface wind field is a major driving force of the currents over both the inner and outer continental shelf region. Hamilton (1987) has observed the periodicity of meteorological frontal passages in surface and near surface currents in response to atmospheric forcing by the wind stress field. This section presents the average seasonal surface wind field along the North Carolina coast as it pertains to the general oceanic circulation of this region. For the purposes of this discussion, the year has been divided into four three-month seasons as follows:

- Winter (December 1 - February 28)
- Spring (March 1 - May 31)
- Summer (June 1 - August 31), and
- Fall (September 1 - November 30).

The data used in this climatology were taken from the National Data Buoy Center (NDBC) Coastal-Marine Automated Network (C-MAN) stations located along the Virginia, North Carolina and South Carolina coastal area. Wind stress calculations were generated for the Chesapeake Light, Virginia (CHLV2), Diamond Shoals Light (DSLN7) and Frying Pan Shoals Light, North Carolina (FPSN7) stations because of their proximity to the open ocean. The data collected at Diamond Shoals Light are generally more energetic due the height of the instrumentation above sea level. Wind stress was calculated as follows:

$$\tau_s = \rho_a * CDN * U_{10} * U_{10},$$

where τ_s is the wind stress vector, ρ_a is the density of air, CDN is the drag coefficient at 10 m under neutral conditions and U_{10} is the vector wind speed recorded at 10 m. The drag coefficient (CDN) computation used the methodology formulated by Large and Pond (1981):

$$10^3\ CDN = 1.2 \qquad \text{for } 4\ m \cdot s^{-1} \le U_{10} < 11\ m \cdot s^{-1}$$

$$10^3\ CDN = 0.49 + 0.065 * U_{10} \qquad \text{for } 11\ m \cdot s^{-1} \le U_{10} < 25\ m \cdot s^{-1}$$

Due to the length of the current meter deployments, two seasonal periods were captured for each time period except the winter season, where only one realization was recorded.

4.2.1 Winter

The dominant atmospheric feature of the wintertime North Atlantic Ocean is the Icelandic Low, which is a strong, semi-permanent system with an average surface pressure of approximately 996 mb. This system provides a strong counterclockwise circulation for the entire basin, which enhances the flow of cold, continental arctic air masses into the region. Superimposed on this background circulation are smaller waves (cyclones) which develop and migrate along the polar front (or jet stream) approximately every five to seven days during winter. These systems provide intense pressure gradients which generate strong wind events, generally of short duration (two to three days). Often, these cyclogenesis events occur in conjunction with Cold Air Outbreaks (CAOs) (SAIC 1993).

Cold Air Outbreaks occur when a cold, dry air mass of continental polar or arctic origin migrates southeastward from the central Canadian region into the United States. These events occur along the mid-Atlantic United States coast approximately 15-20 times a year. Generally, one third of these events can be classified as severe where the air temperature is < 0°C and the Gulf Stream SST is > 20°C. Due to the close proximity of the Gulf Stream to the southeastern United States, air mass modification processes are very intense over the shallow coastal and shelf waters immediately offshore of this area. Large amounts of heat, mass and momentum can be exchanged between the ocean and atmosphere during these events. Total (sensible + latent) heat flux values offshore of North Carolina of 1045 $w \cdot m^{-2}$ have been observed during a strong CAO (Konrad and Colucci 1989; Grossman and Betts 1990; and Wayland and Raman 1989,1994).

The winter of 1992-1993 along the North Carolina coast was characterized by a general south and south-southwestward wind flow regime (in the oceanographic sense) with a strong southeastward wind stress component. North of Cape Hatteras the prevailing synoptic wind field was southerly, with a general clockwise rotation south of Cape Hatteras resulting in more south-southwesterly and west-southwesterly wind patterns in this region. Mean wind speeds are higher during the winter at all stations than the other seasonal periods: and, as expected increase in the

offshore direction, primarily in response to reduced surface friction and longer open fetch distances. There were nominally 12 CAOs and four major cyclogenesis events during this period. Additionally, there were four strong high pressure (anticyclones) events which caused wind stress reversals along the North Carolina shelf. Figure 4.2-1 is a 40-HLP time series of the wind stress at Chesapeake Light, Diamond Shoals Light and Frying Pan Shoals Light for the winter period. The frequency and magnitude of the individual synoptic events is clearly evident in this figure.

The wind stress values observed during this period were also the highest observed during the field program, with the alongshelf component (τ_y) of the stress averaging approximately three times the magnitude of the across shelf component (τ_x) at all three C-MAN locations. Lee *et al.* (1989) and Blanton *et al.* (1989) also recorded a similar wind stress pattern in the winter of 1986 for the region during the Genesis of Atlantic Lows Experiment (GALE). In general, wind stress increases with distance offshore and with latitude in the South Atlantic Bight region. However, north of Cape Hatteras (i.e. CHLV2) there is a slight reduction in wind stress approaching the Middle Atlantic Bight region.

4.2.2 Spring

Spring along the eastern United States coast is a period of transition marked with extreme temperature contrasts across the mid-latitude region. As the polar jet slowly migrates northward, warm, moist air masses of tropical origin collide with the front and create an unstable atmospheric environment. This transition period begins as early as March in some years, but is generally well established by April. The reduction in strength of the Icelandic Low coupled with the deepening and expanding subtropical Bermuda/Azores anticyclone creates a shift in the general synoptic wind field. Often these shifts in the global circulation will segment the North Carolina shelf into two regions: (1) north of Cape Hatteras; and, (2) south of Cape Hatteras. This occurs as the northern region remains under the synoptic influence of the Icelandic Low, while south of Cape Hatteras, the building subtropical anticyclone dominates the mean atmospheric circulation regime. Evidence of this segmentation is found in the differences in the spring of 1992 and 1993 (SAIC 1993).

In the spring of 1992, the stations located north of Cape Lookout, North Carolina remained under the influence of a "winter-type"

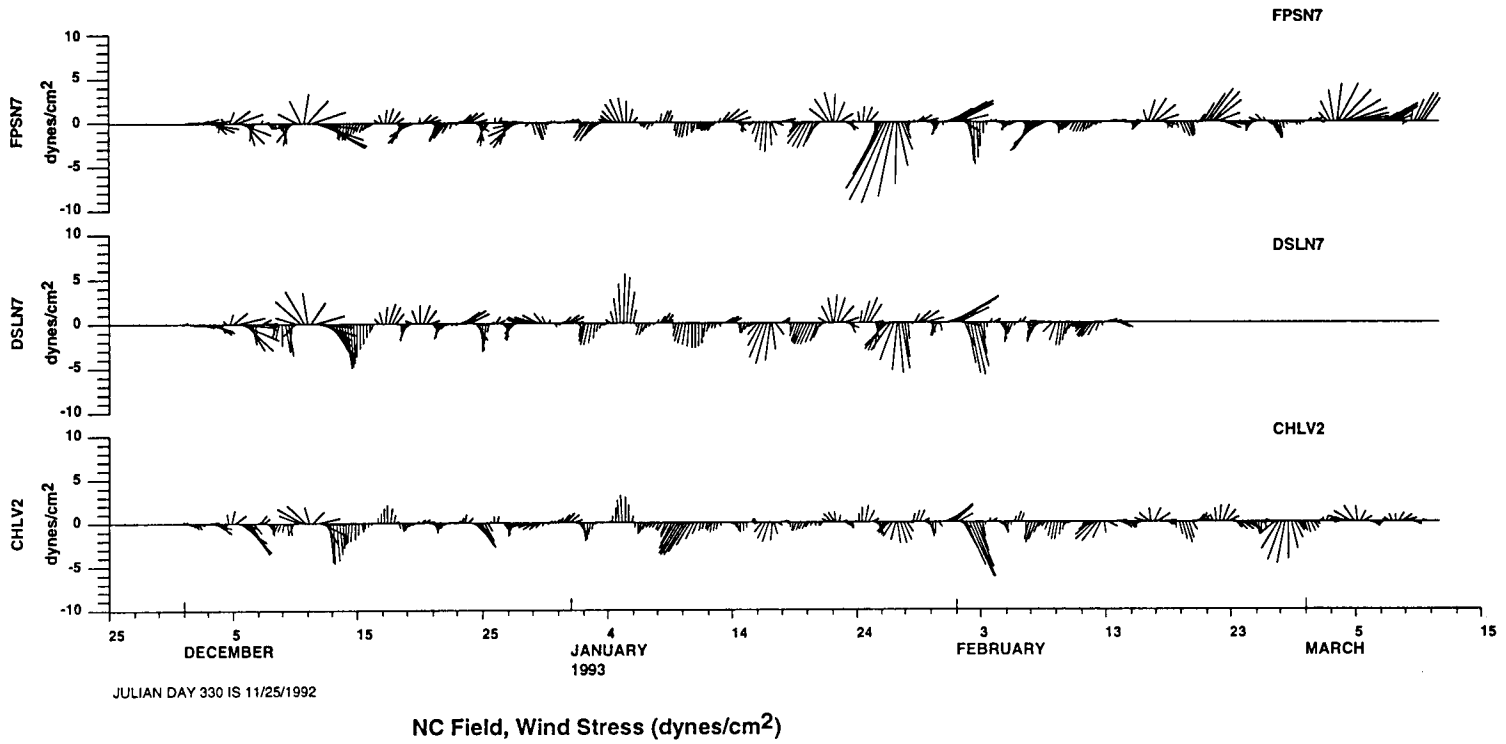

Figure 4.2-1. 40-HLP wind stress vectors for Chesapeake Light, (CHLV2), Diamond Shoals Light (DSLN7) and Frying Pan Shoals Light (FPSN7) for the 1992 - 1993 winter period (December - February).

(i.e. south, southwestward) synoptic flow, while the stations located south of this region transitioned over into the normal spring regime of more east and northeastward flow. Mean wind speeds averaged slightly less (~1-2 $m \cdot s^{-1}$) than those observed during the winter period. The resultant wind stresses at these locations were approximately 90° out-of-phase. The predominant wind stress in the northern area was towards the southwestern quadrant, while south of Cape Lookout, the wind stress was directed towards the southeast. Figure 4.2-2 summarizes the 40-HLP wind stress vectors for the spring 1992 period. South of Cape Lookout the alongshelf component (τ_y) of the stress was approximately one and a half times greater than the cross shelf component (τ_x). However, north of this area, the cross shelf component was approximately twice the magnitude of the alongshelf stress. The transition to the predominant summer northeastward stress did not occur during 1992 until the middle of June.

Spring 1993 showed the characteristic summer northeasterly synoptic and stress (Figure 4.2-3) fields arriving during the first week of May and remaining throughout the summer months. However, the mean synoptic wind speeds were not significantly different from spring 1992. The wind stress fields showed considerably more variation than the earlier spring season, as would be expected due to the mean directional differences in the wind field. At Chesapeake Light, a strong, predominantly north stress field was observed during the 1993 season as compared to the week southerly stress field of spring 1992. The Diamond Shoals Light data showed a relatively strong easterly, cross shelf wind stress component, while the Frying Pan Shoals Light station experienced roughly equal alongshelf and cross shelf forcing. These results agree well with earlier findings of Lee *et al.* (1989), where the dominant wind forcing comes from alongshore winds, which tend to drive cross-shore Ekman-type transports. Additionally, near Cape Hatteras (i.e. Diamond Shoals) wind stress events tend to have a strong cross-shelf component, whereas north and south of this region alongshelf stresses tend to be stronger.

The spring of 1993 will long be remembered for the "storm of the century" which occurred during March 12-14, 1993. This extratropical system broke several surface pressure, snowfall and wind speed records along the eastern seaboard, which had stood since the mid- to late-1800s. However, because of this storm's inland track and rapid movement through the southeastern United States, the resultant stress field offshore of North Carolina was

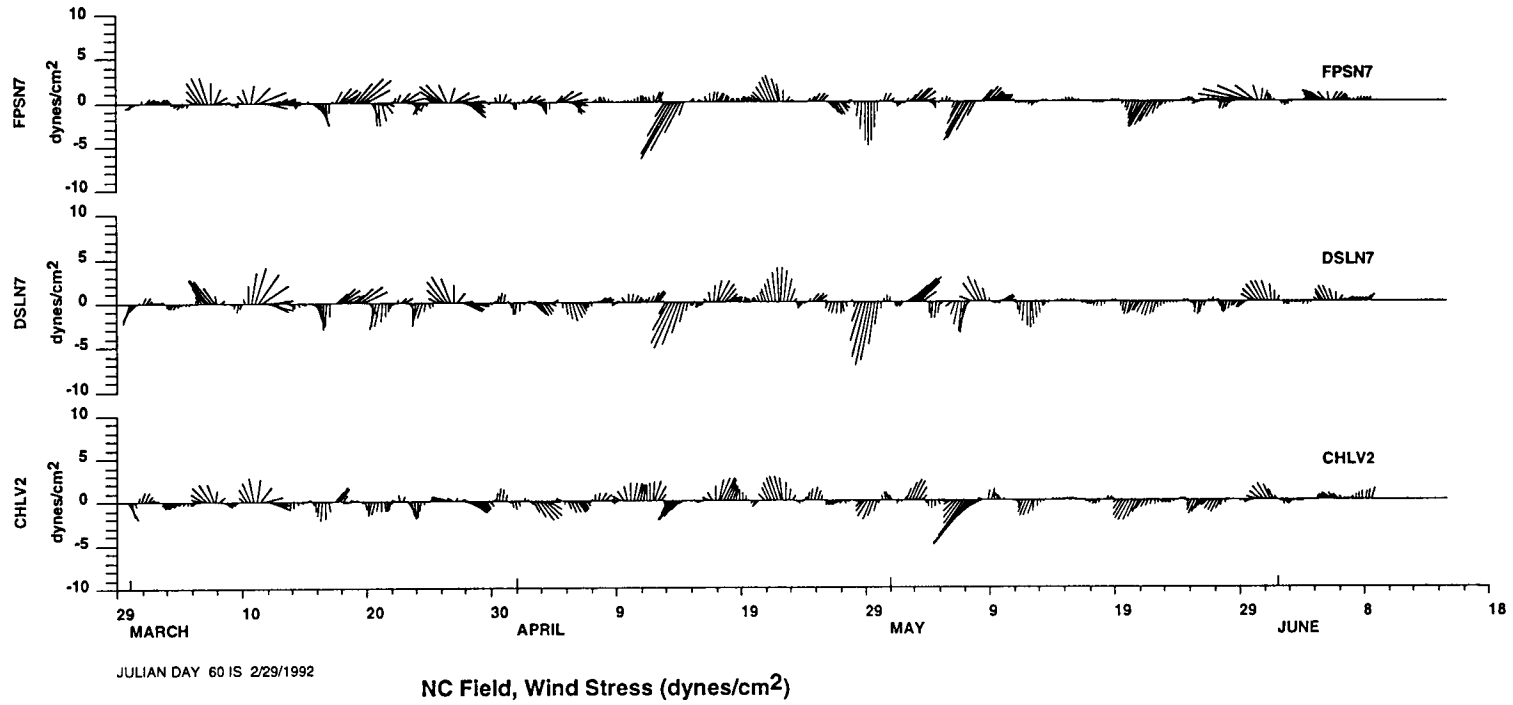

Figure 4.2-2. 40-HLP wind stress vectors for Chesapeake Light (CHLV2), Diamond Shoals Light (DSLN7) and Frying Pan Shoals Light (FPSN7) for the 1992 spring period (March - May).

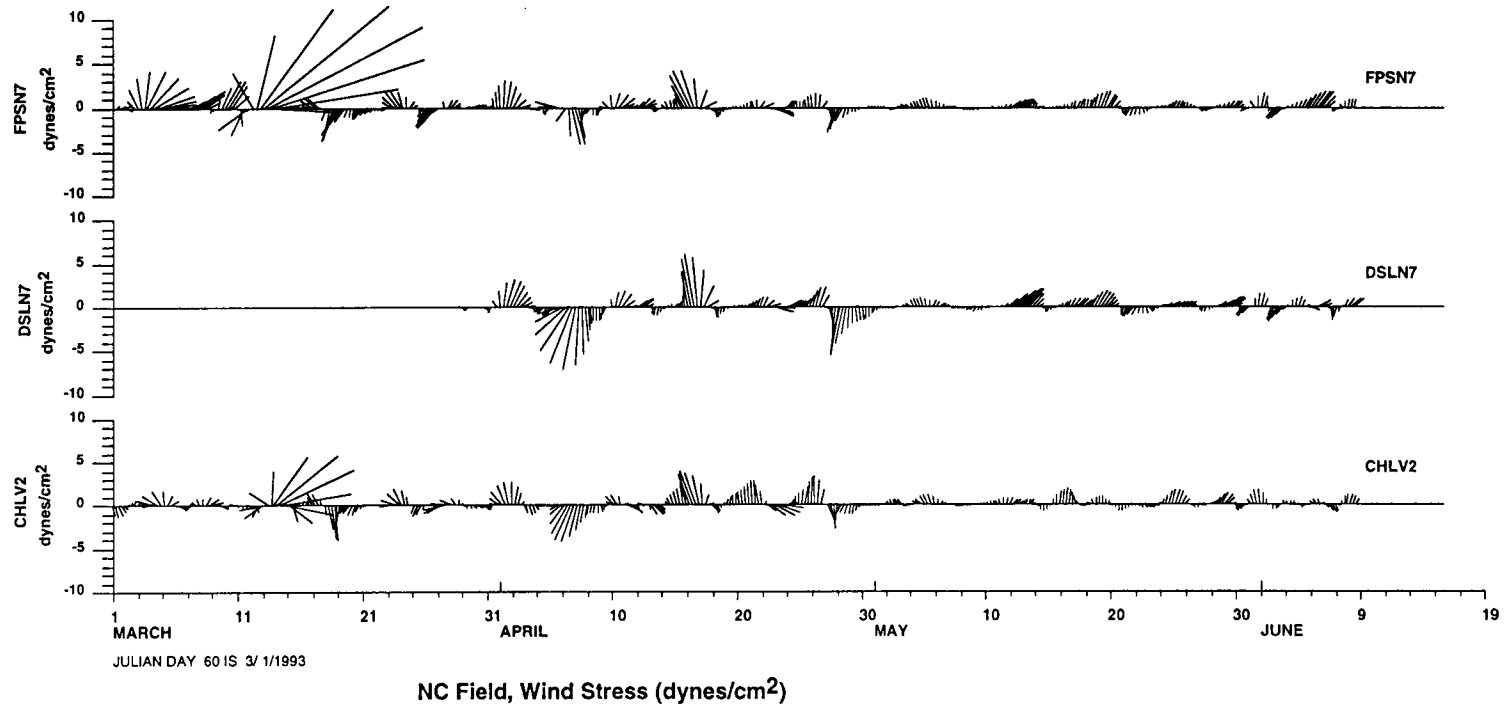

Figure 4.2-3. 40-HLP wind stress vectors for Chesapeake Light (CHLV2), Diamond Shoals Light (DSLN7) and Frying Pan Shoals Light (FPSN7) for the 1993 spring period (March - May).

very similar to those associated more commonly with a large anticyclone anchored offshore of the eastern United States. The specifics of this event are discussed in detail in Chapter 6.

4.2.3 Summer

Summers along the coast of the southeastern United States are characterized by very little contrast between surface air and ocean temperatures. The mean synoptic atmospheric circulation is dominated by the broad Bermuda anticyclone, which generally produces light north and northeastward winds averaging less than 6 $m \cdot s^{-1}$, which are the lowest observed for the four seasonal periods. Additionally, with the polar jet residing primarily north of the mid-latitudes, synoptic disturbances are at a minimum during this season, except for the occasional tropical system. The warm oceanic waters, in conjunction with the overlying moist, unstable atmosphere, are conducive for tropical system development during the early to mid-summer time period. However, in late summer and early fall, upper atmospheric steering currents make it more difficult for storms to make it to the mid-latitude eastern United States coastal areas. Thus, summers in this region are relatively free of disturbances and the synoptic wind regime, in conjunction with local mesoscale processes (i.e., sea breezes, etc.) drive the circulation of the oceans (SAIC 1993).

In general, the summer of 1992 had moderately larger mean winds (~0.5 $m \cdot s^{-1}$) than the 1993 period. The mean synoptic wind field was as expected during 1992, with north and northeastward winds prevailing. The wind stress field, which is shown in Figure 4.2-4, also was observed to be contained primarily within the northeast quadrant and did not vary significantly in magnitude between the 1992 and 1993 periods. Chesapeake Light, exhibited a strong northward, alongshelf stress component, while Diamond Shoals Light and Fry Pan Shoals Light both displayed a more northeastward wind stress vector. Again, the Cape Hatteras area (Diamond Shoals Light) showed the strongest cross-shelf stress component of the three stations. During June - August 1992 no tropical systems affected the North Carolina coast. Figure 4.2-5 shows the tracks for all named tropical cyclones for the 1992 Tropical Season.

Summer 1993 was not significantly different from its predecessor, except for a direct hit of a major hurricane (Emily, Category 3) on the Cape Hatteras area at the end of August. The synoptic winds, while slightly less in magnitude, were predominantly north and

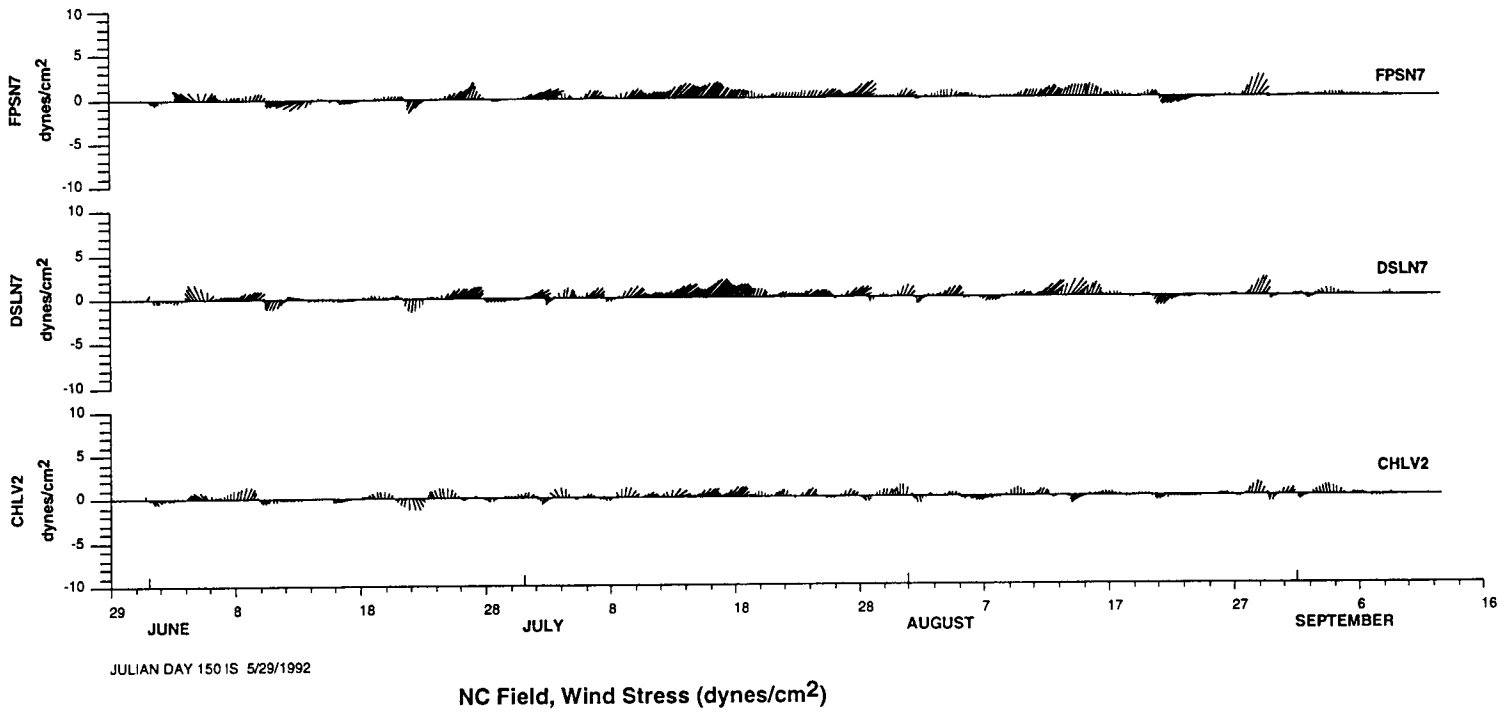

Figure 4.2-4. 40-HLP wind stress vectors for Chesapeake Light (CHLV2), Diamond Shoals Light (DSLN7) and Frying Pan Shoals Light (FPSN7) for the 1992 summer period (June - August).

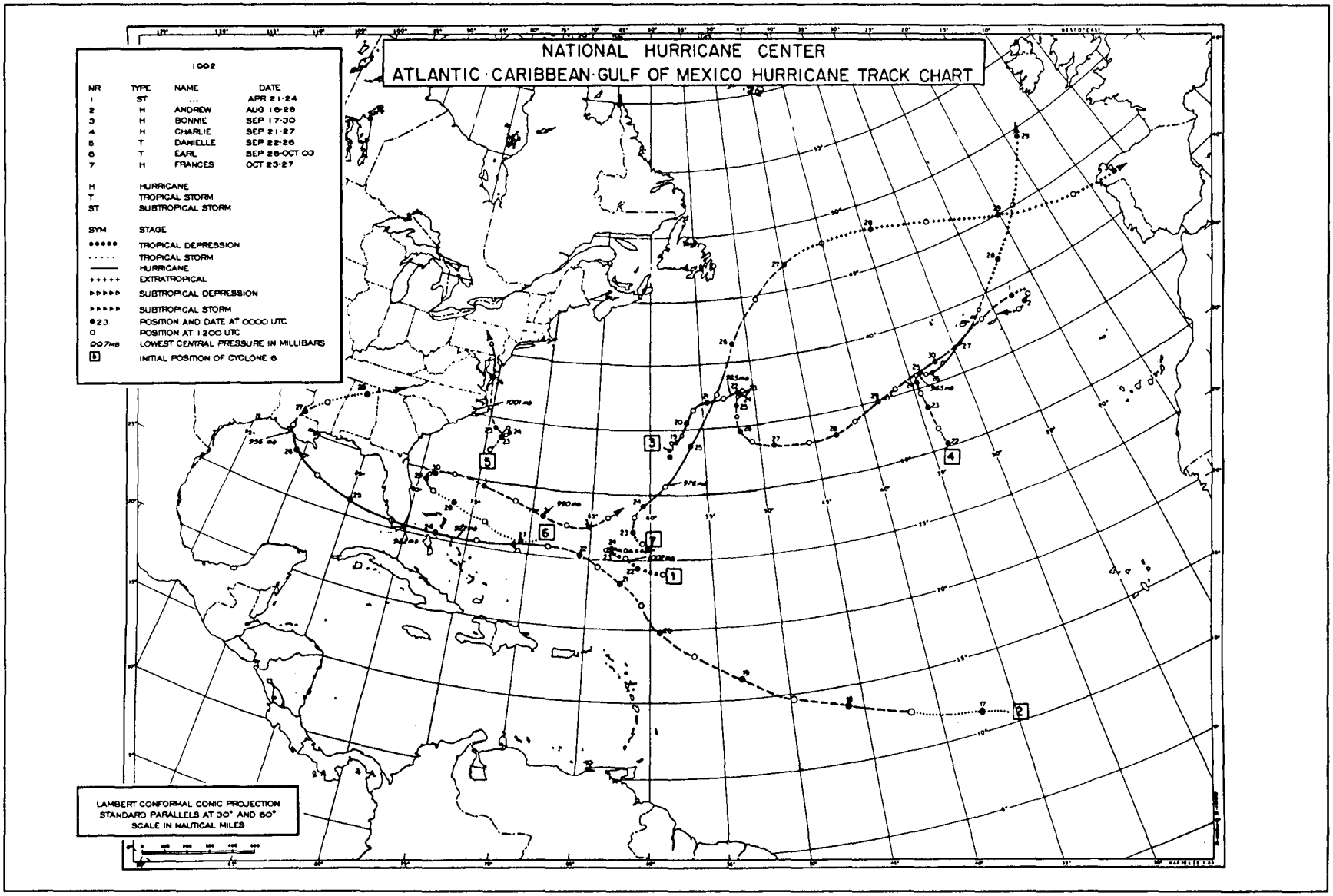

Figure 4.2-5. Tracks of 1992 tropical cyclones for the North Atlantic Basin (from NOAA 1992).

northeastward with a similar stress field (Figure 4.2-6). The Chesapeake Light and Frying Pan Shoals Light stations again exhibited strong alongshelf wind stress components, while the Diamond Shoals Light data showed a much stronger cross-shelf wind stress component than was observed during the summer of 1992. Hurricane Emily, the first major storm of the 1993 Tropical Season, formed roughly 1100 km east-northeast of the Leeward Islands on August 22, 1993. The preliminary track of this system is shown in Figure 4.2-7 (SRCC 1993). The specifics of this storm as related to the North Carolina coastal region are discussed in Chapter 6.

4.2.4 Fall

The fall season offshore of North Carolina is signaled by a weakening in the subtropical anticyclone and an increased presence of the Icelandic Low in the mean synoptic circulation patterns. As in spring, the fall season is a period of transition. The polar jet begins to migrate south into the mid-latitudes, bringing cold, dry continental air with it. However, the warm, moist maritime tropical air is also retreating at this time, creating less opportunities for frontal confrontation and atmospheric instability. The mean winds during this season are also generally comparable to or less energetic than those observed during the spring (~7-8 $m \cdot s^{-1}$). During the fall, with the reduction in air temperature, air-sea interactions again become an effective means of transferring heat between the ocean and atmosphere. Due to the increased baroclinicity of the atmosphere during the fall, which is caused by the increasing air-SST difference, an increase in cyclogenesis activity is observed along the coastal regions. Additionally, in early fall, it is not uncommon for tropical cyclones to effect the coastal areas of the southeastern United States.

The prevailing mean winds for the fall of 1992 were southwestward along the coast, with some northward winds observed offshore at the NDBC buoy (41001). The segmentation north and south of the Cape Hatteras region is again observed in the wind stress field (Figure 4.2-8). C-MAN stations located at Chesapeake Light and Frying Pan Shoals Light both showed a near equal component contribution to the wind stress field, which was oriented towards the northeast and southwest, respectively. On the other hand, Diamond Shoals Light exhibited a mean stress field oriented towards the southwest with a strong alongshore component. Two tropical systems, Hurricane Danielle and Tropical Storm Earl, affected the circulation offshore

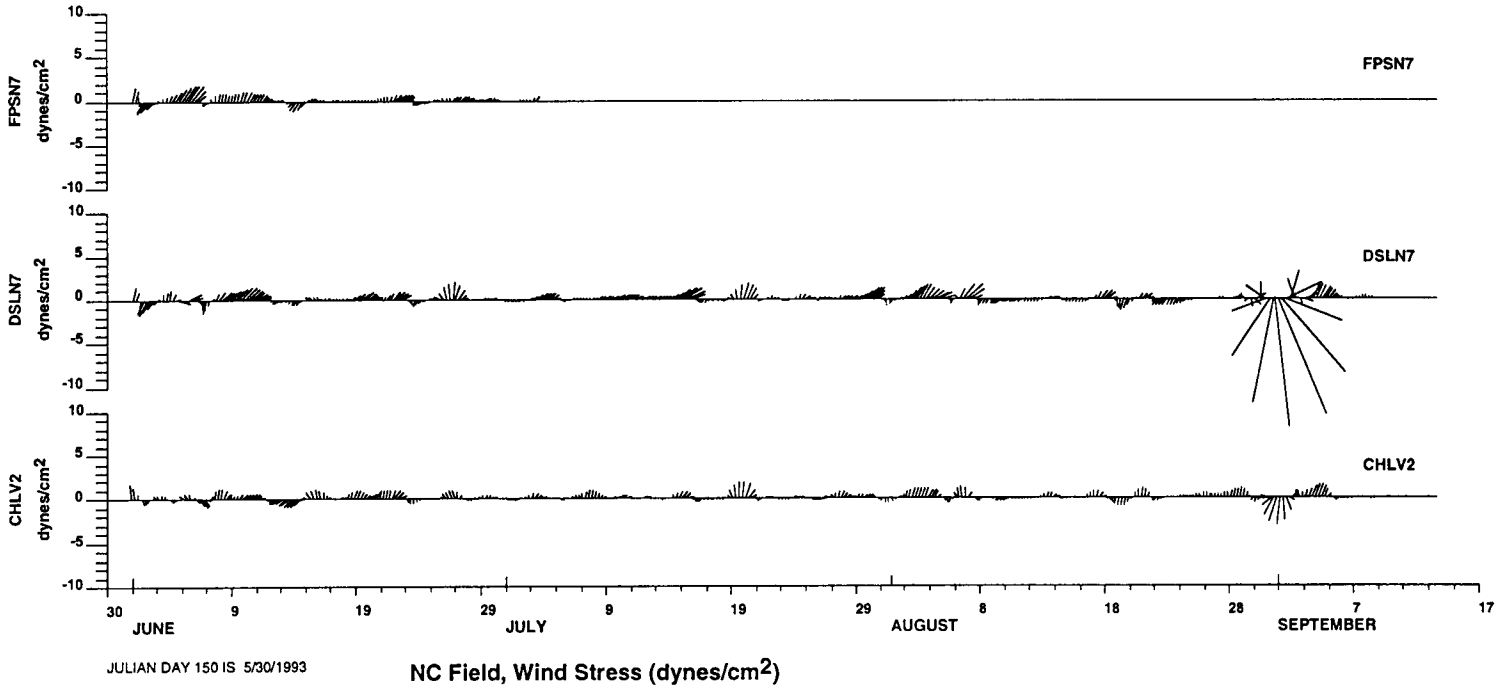

Figure 4.2-6. 40-HLP wind stress vectors for Chesapeake Light (CHLV2), Diamond Shoals Light (DSLN7) and Frying Pan Shoals Light (FPSN7) for the 1993 summer period (June - August).

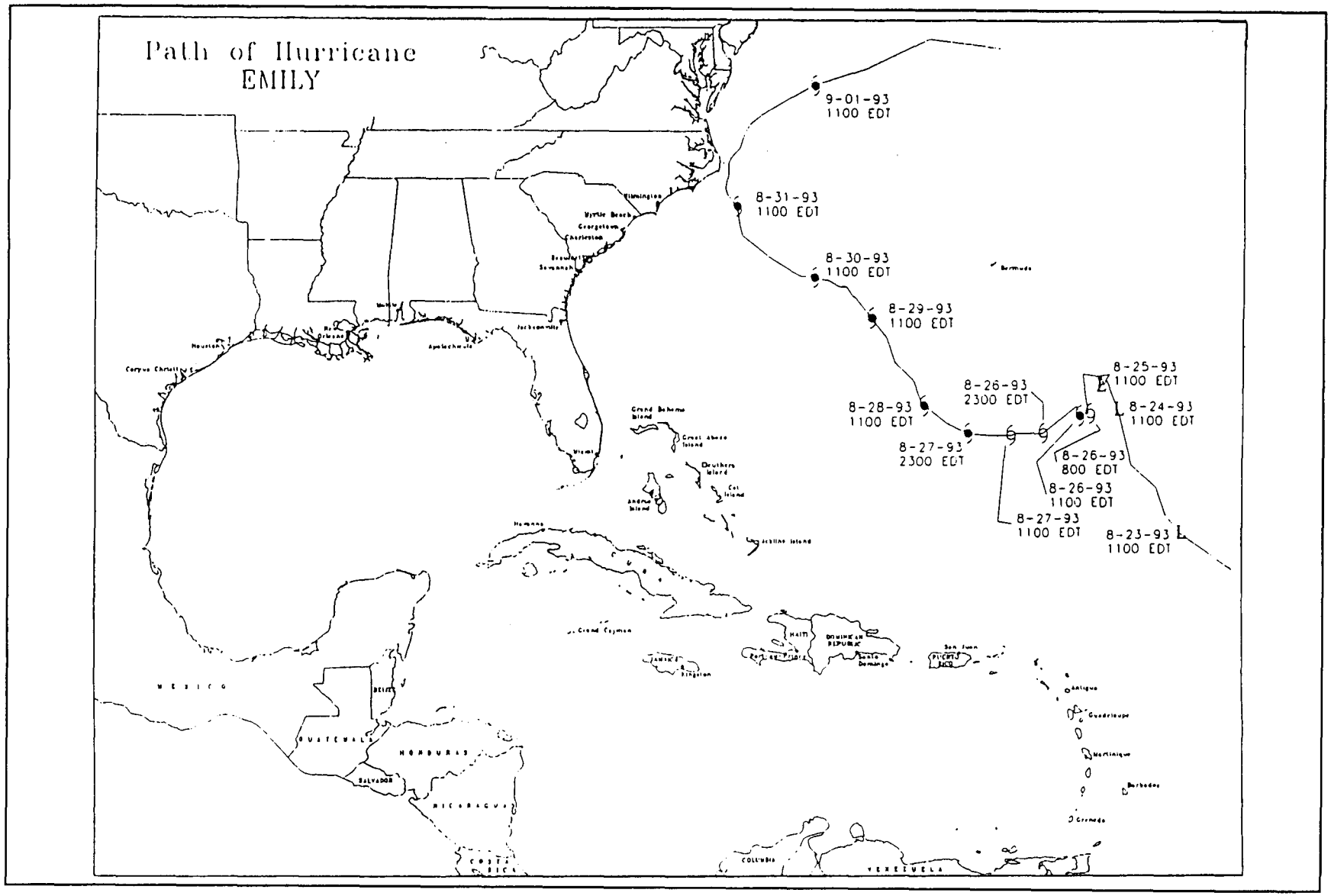

Figure 4.2-7. Preliminary track for Hurricane Emily (from SRCC, 1993).

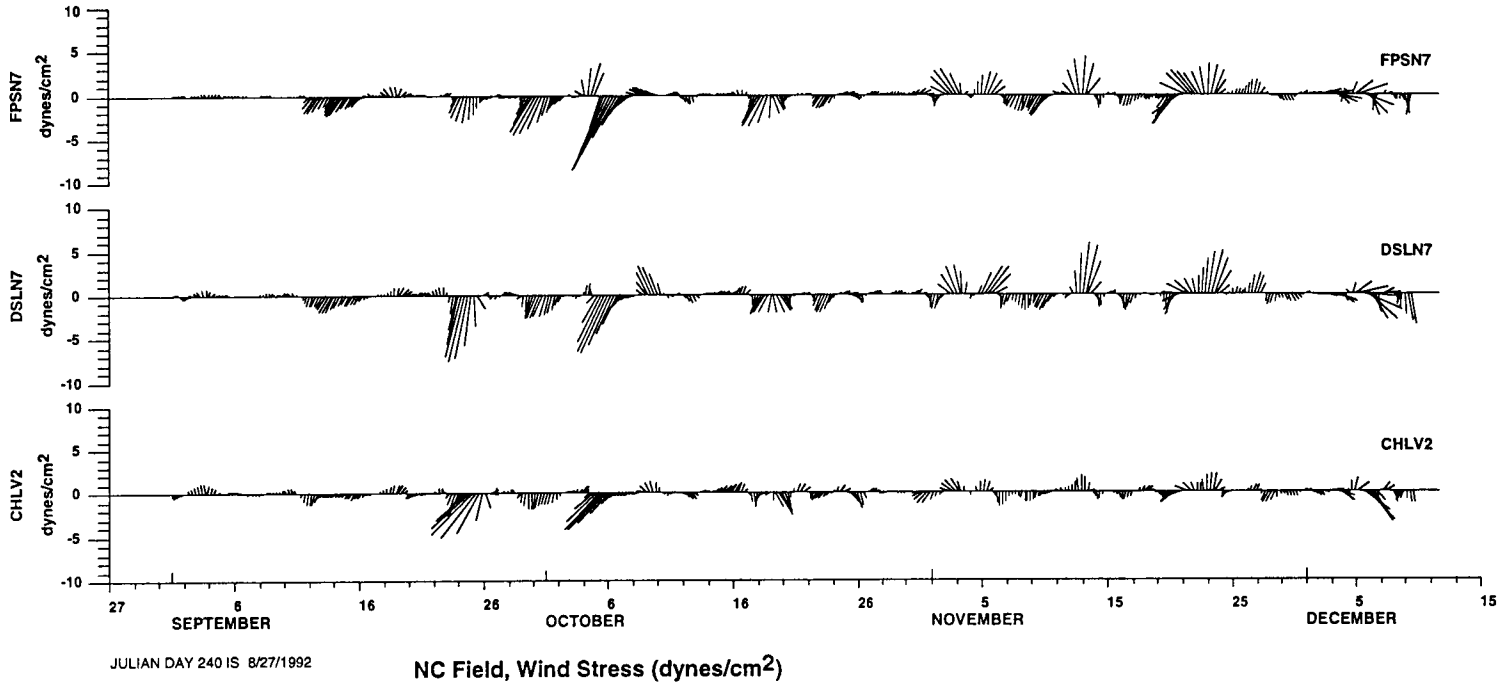

Figure 4.2-8. 40-HLP wind stress vectors for Chesapeake Light (CHLV2), Diamond Shoals Light (DSLN7) and Frying Pan Shoals Light (FPSN7) for the 1992 fall period (September - November).

of North Carolina during this period, with Danielle passing just west of Cape Hatteras and skirting up the coast of the northern Outer Banks. Danielle formed in proximity to a weak persistent area of low pressure near the southeast United States coast in conjunction with a weak tropical wave which passed through the area (NOAA 1992).

The mean circulation for the fall of 1993 was not markedly different from the previous fall period. However, all three stations observed strong alongshelf wind stress components (Figure 4.2-9). The northern- and southernmost stations exhibited some onshore (westward) transport, while the Diamond Shoals stations displayed primarily offshore (eastward) transport. The effects of Hurricane Emily, which originated during the latter days of the summer season of 1993, were still noticeable during the first week of the fall 1993 period.

4.3 Hydrography

The waters off Diamond Shoals were once thought to be an oceanographic "barrier," separating the Middle Atlantic Bight from the warmer, saltier waters of the South Atlantic Bight. Although this barrier has been found to be more permeable than once thought (Bumpus and Pierce 1955; Stefannson *et al*. 1971; see also section 7.3.2), it remains a distinct feature throughout most of the annual progression. In general, this feature consists of a strong frontal boundary sustained by convergent flow from the two shelf provinces and by marked differences in their water properties. The structure of the Middle Atlantic Bight-South Atlantic Bight front is modulated by the seasonal progression of the cold-water band ("cold pool") over the outer shelf in the Middle Atlantic Bight.

The marked seasonal and interannual variability in water-mass properties on the continental shelf in this region is enhanced by the episodic interaction with the warm, salty Gulf Stream. The seasonal cold band of water along the bottom of the Middle Atlantic Bight shelf can create the seemingly paradoxical situation where, for the outer shelf, both maxima and minima in annual temperatures occur in summer (Boicourt 1973). At the time when surface temperatures reach upward of 30°C in the Middle Atlantic Bight, the cold (<10°C) band of winter water penetrates southward along the outer shelf at 30-50-m depths.

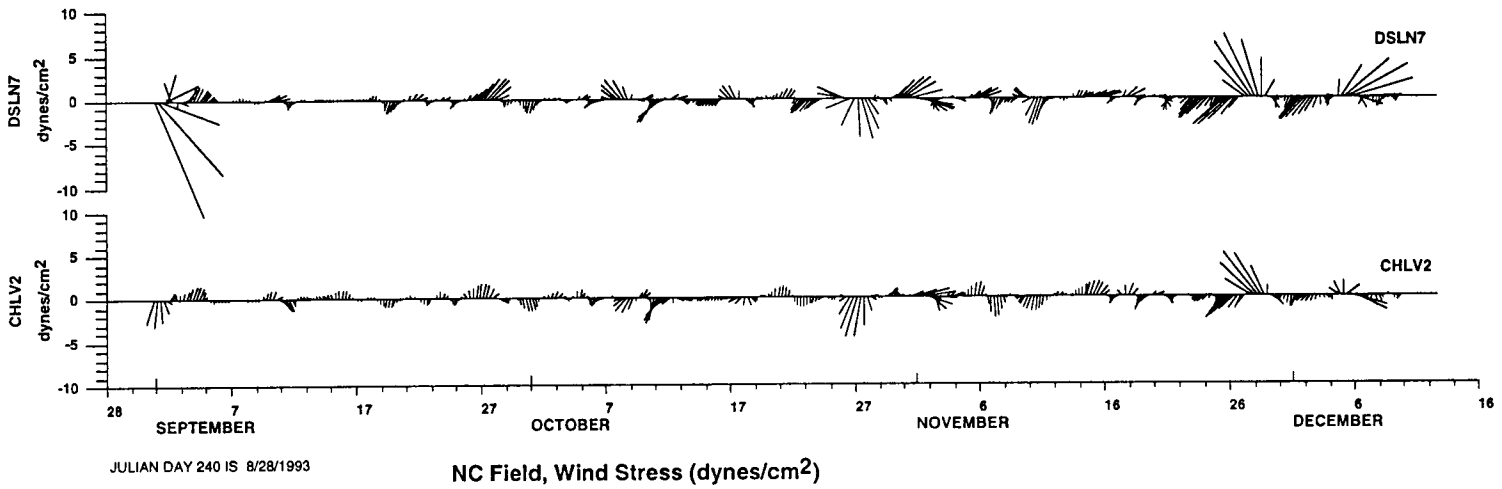

Figure 4.2-9. 40-HLP wind stress vectors for Chesapeake Light (CHLV2) and Diamond Shoals Light (DSLN7) for the 1993 fall period (September - November).

The 1992-93 hydrographic data, though not temporally intensive, reveal not only the seasonal progression of temperature and salinity structure on the North Carolina continental shelf, but also the possible modes of variability. Prior to this study, there were few surveys that provided a detailed look at the Middle Atlantic Bight-South Atlantic Bight front. In addition, while previous work indicated that the cold-water band of the Middle Atlantic Bight moved seaward south of Chesapeake Bay, there was uncertainty as to its fate. The question of local mixing versus offshore flow into the Slope Water and/or entrainment into the Gulf Stream remained unanswered. Previously documented intrusions of Middle Atlantic Bight water around Diamond Shoals and into Raleigh Bay have recently been observed through satellite thermal imagery, but they have seldom been supported with hydrographic measurements to produce a flux estimate.

4.3.1 Seasonal Progression of the Middle Atlantic Bight-South Atlantic Bight Front

The temperature and salinity structure of the frontal boundary between the Middle Atlantic Bight and the South Atlantic Bight, while prone to synoptic variability driven by winds, Gulf Stream fluctuations, and freshwater runoff events, is also modulated by seasonal changes in the water-mass structure in the two shelf provinces. Cape Hatteras and Diamond Shoals not only mark the north-south change in seasonal range on the continental shelf, they also can mark a change in stratification process. In the southern Middle Atlantic Bight, temperature is the dominant contributor to stratification, except over the inner 10-30 km, where the buoyant discharge from Chesapeake Bay can drive a coastal current extending southward, occasionally to Cape Hatteras. The proximity of the Gulf Stream to the northern South Atlantic Bight creates conditions where the shelf can be stratified by either temperature or salinity.

Surface temperature and salinity maps from spring 1992 (Figure 4.3-1) show the transition between the fresher, isothermal southern Middle Atlantic Bight to the warmer, saltier Raleigh Bay. At this time of the year, the coldest water is inshore (Figure 4.3-2(a)), a result of winter cooling over the Middle Atlantic Bight. In April-May 1992, vernal warming and runoff were not sufficiently developed to stratify the southern Middle Atlantic Bight shelf in the presence of the mixing energy from the spring winds. Cross-shelf temperature and salinity sections (Figure 4.3-2)

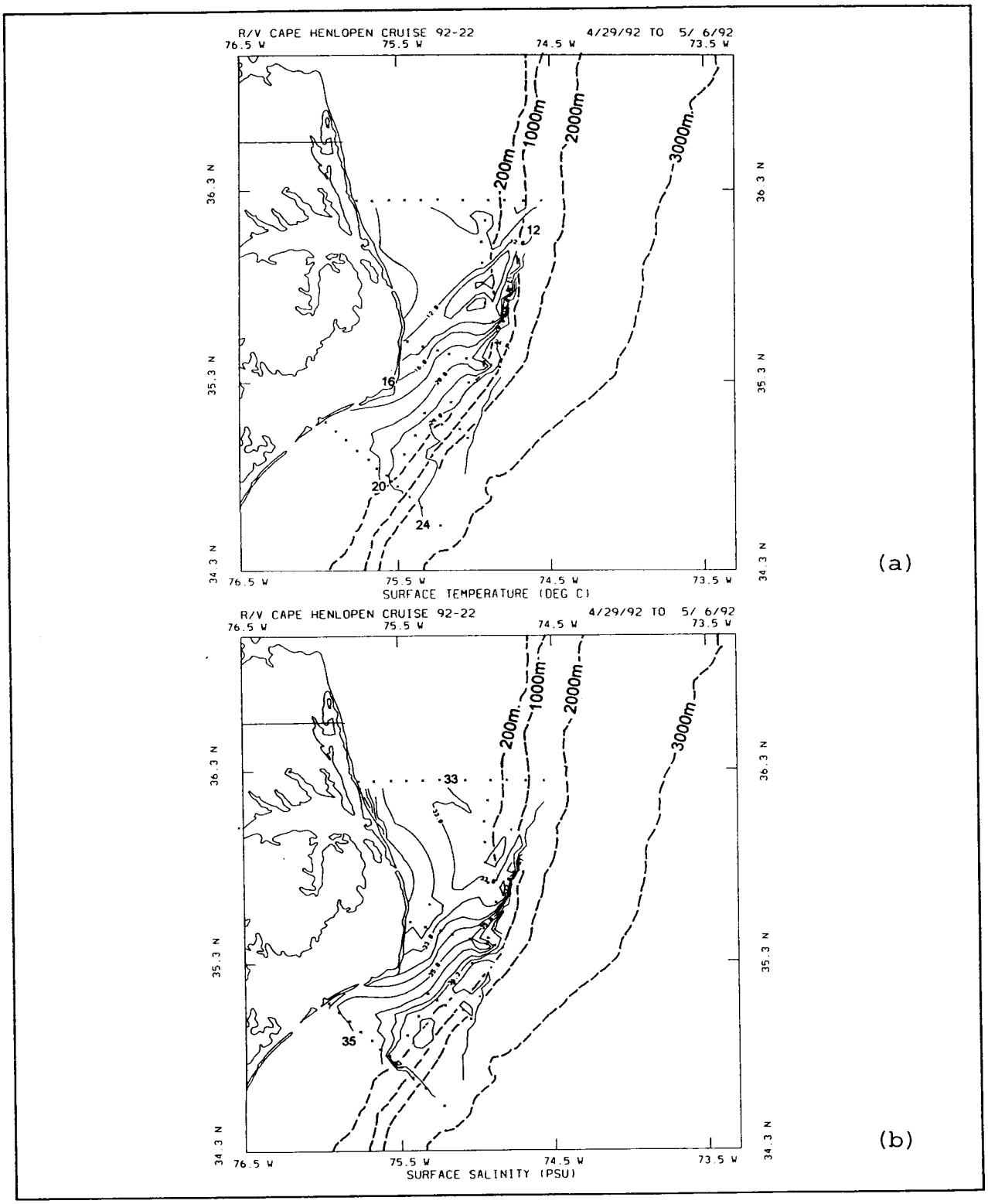

Figure 4.3-1. Surface contour map of (a) temperature and (b) salinity during cruise CH9222 April 29 - May 6, 1992.

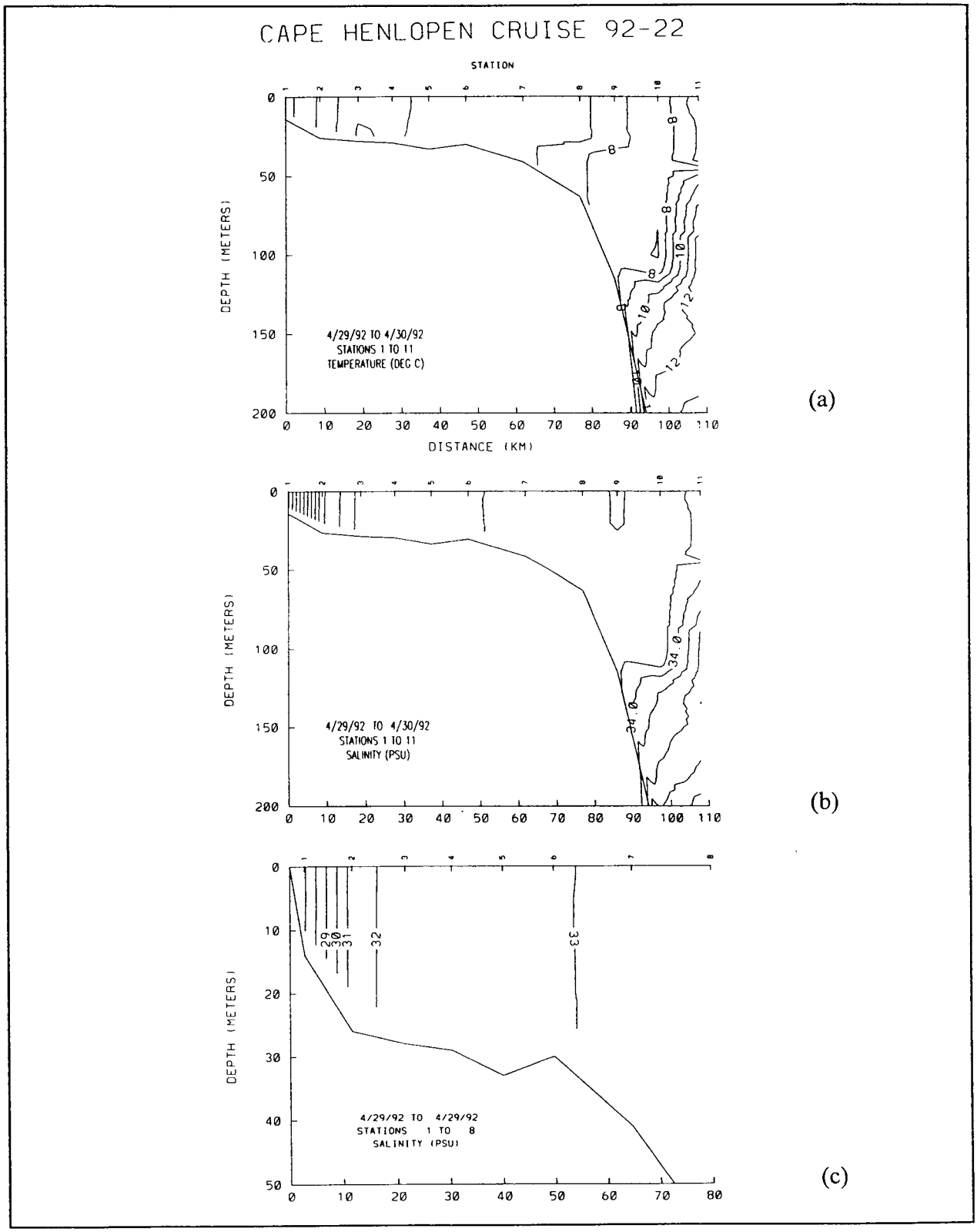

Figure 4.3-2. Cross-shelf sections along Line A of (a) temperature and (b) salinity and (c) salinity (shelf only) (stations 1-8) taken during cruise CH9222 on April 29, 1992-April 30, 1992.

reveal that even the cold, low-salinity coastal current is mixed vertically. In contrast, Raleigh Bay is (albeit weakly) stratified (Figure 4.3-3). Satellite imagery at this time (Figure 4.3-4) indicates that the Gulf Stream is in its large eddy mode (Glenn and Ebbesmeyer 1994a,b) in Raleigh Bay, which may influence the apparent intrusion of warm, high-salinity water onto the shelf in the deeper layers. The surface salinity distribution (Figure 4.3-1) indicates that the low-salinity water along the coast (Figure 4.3-3) is the result of a small amount of the Middle Atlantic Bight coastal current moving over Diamond Shoals, past Cape Hatteras.

The sharp front between the Middle Atlantic Bight and South Atlantic Bight is most dramatically shown by the outer-shelf distribution of temperature along the 60-m isobath (Figure 4.3-5(a)). The front appears nearly vertical, with cross-frontal differences of greater than 10°C and 3 psu. The strong thermal gradient is nearly compensated by the salinity distribution, such that only a 0.6 σ_t difference in density occurs across the front. The frontal gradients are strongest over the outer shelf north line B, and then the frontal boundary trends shoreward, crossing isobaths and appearing between station 46 and 47, approximately 40 km from the shelf break (Figure 4.3-6), and still north of Cape Hatteras and Diamond Shoals.

The summer structure of the Middle Atlantic Bight-South Atlantic Bight front is similar to the spring picture, in that the front is strongest over the shelf break north of line B, and then weakens and shoals as it crosses the shelf, apparently north of line B, although its position is not well resolved by the station grid pattern (Figure 4.3-7). The 60-m isobath transect (line D, Figure 4.3-8) reveals that the front is more complex than in spring, when the outer-shelf cold band is not present in the Middle Atlantic Bight. Above this summer cold band, the density increases across the front from north to south, from colder, fresher to warmer, saltier water. At the depths of the cold band, the density gradient is opposite to the gradient in the upper layers, with the cold band's temperature overcoming the effect of the salinity gradient.

The observed offshore progression of the cold band south of Chesapeake Bay led Boicourt (1973) to suggest an offshore turn and flow into the Slope Water or entrainment in the Gulf Stream. Such a progression is evident in Figure 4.3-9. At line A, the cold band is over the shelf break, but 40 km south at line E, the cold band

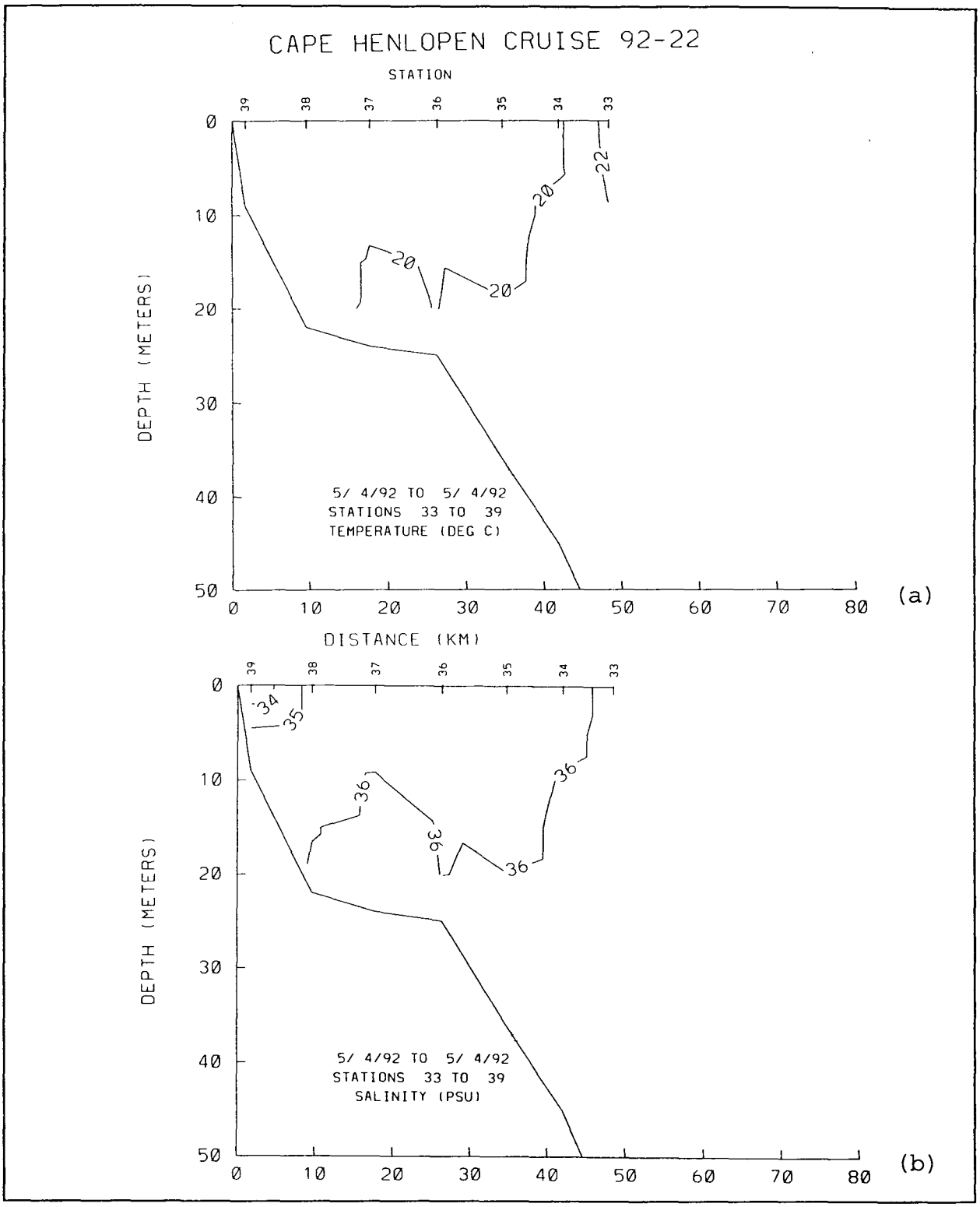

Figure 4.3-3. Cross-shelf sections along Line C of (a) temperature and (b) salinity taken during cruise CH9222 on May 4, 1992.

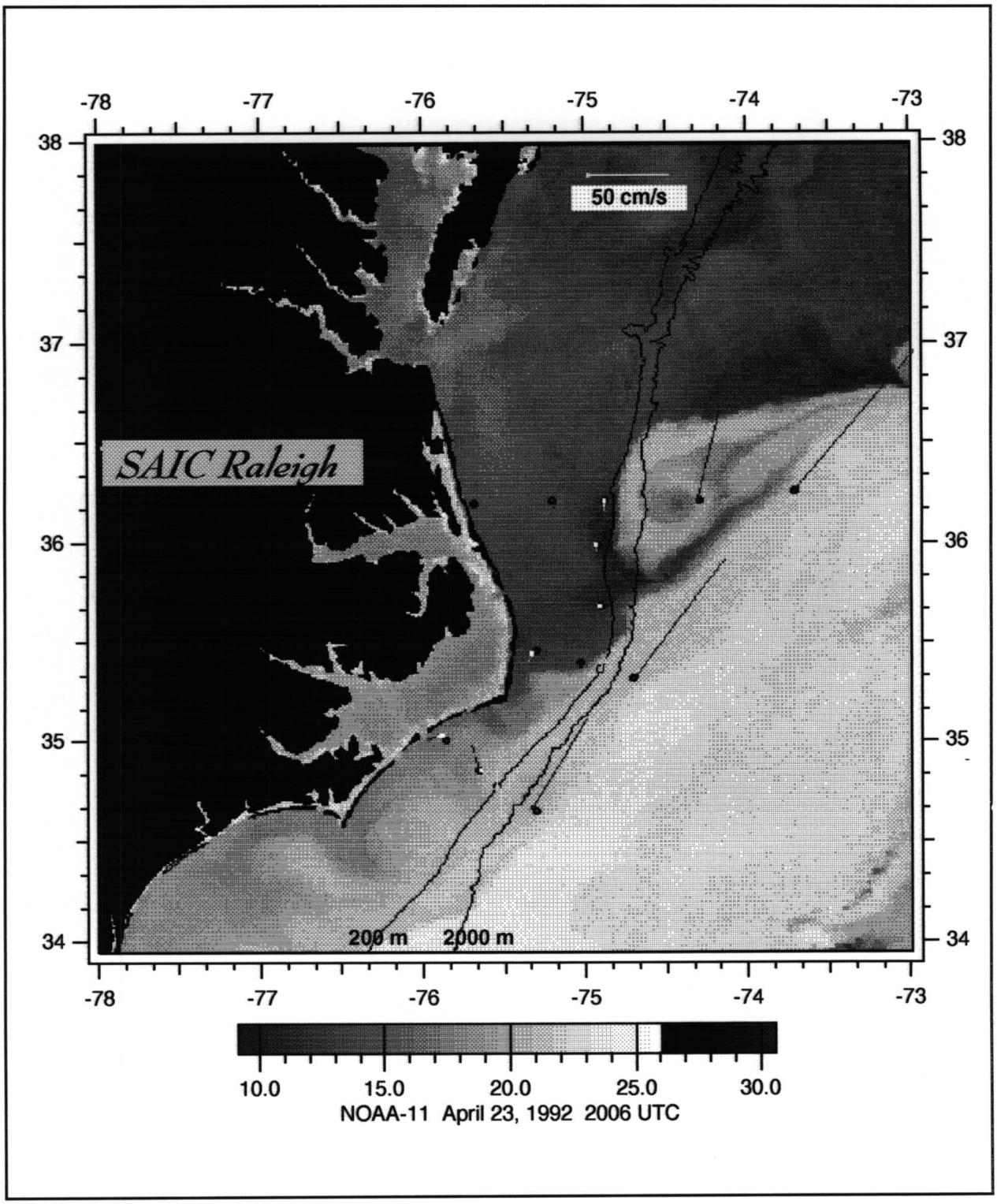

Figure 4.3-4. Satellite SST Image and Daily Average Current Vectors on April 23, 1992. Annotated as in Figure 2.2-7.

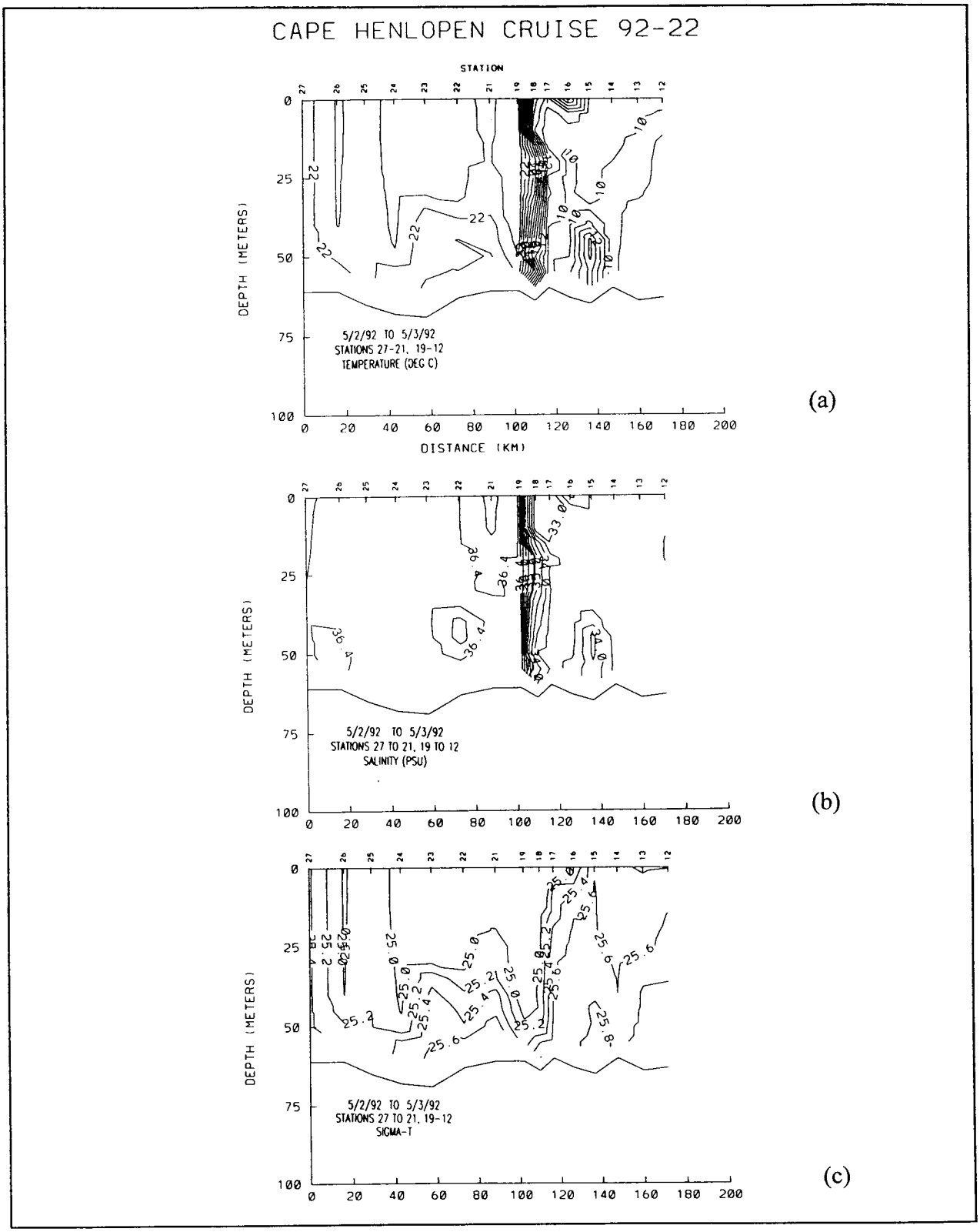

Figure 4.3-5. Along-shelf (60-m isobath) sections of (a) temperature, (b) salinity and (c) σ_t taken during cruise CH9222 on May 2-3, 1992.

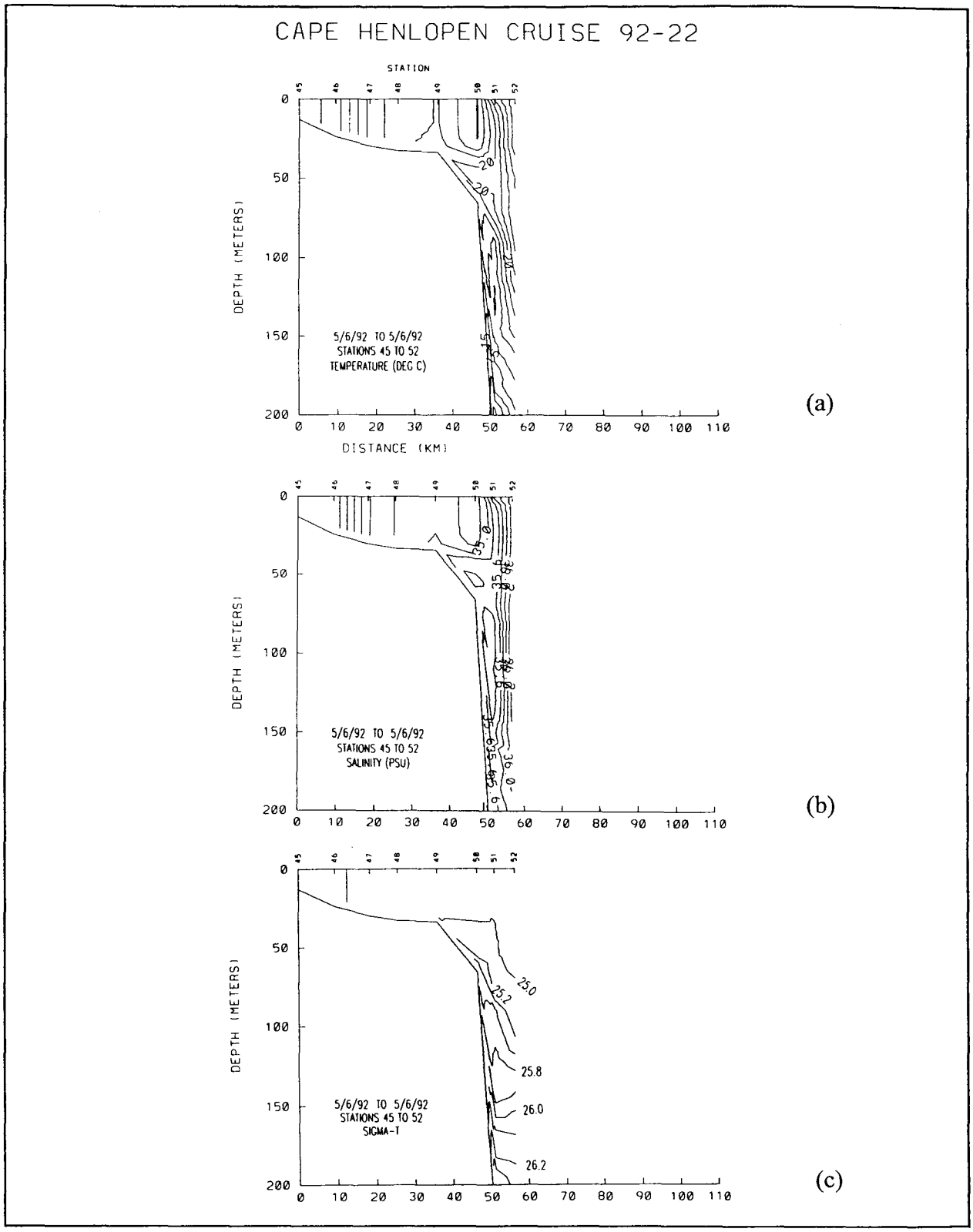

Figure 4.3-6. Cross-shelf sections along Line B of (a) temperature, (b) salinity, and (c) σ_t taken during cruise CH9222 on May 6, 1992.

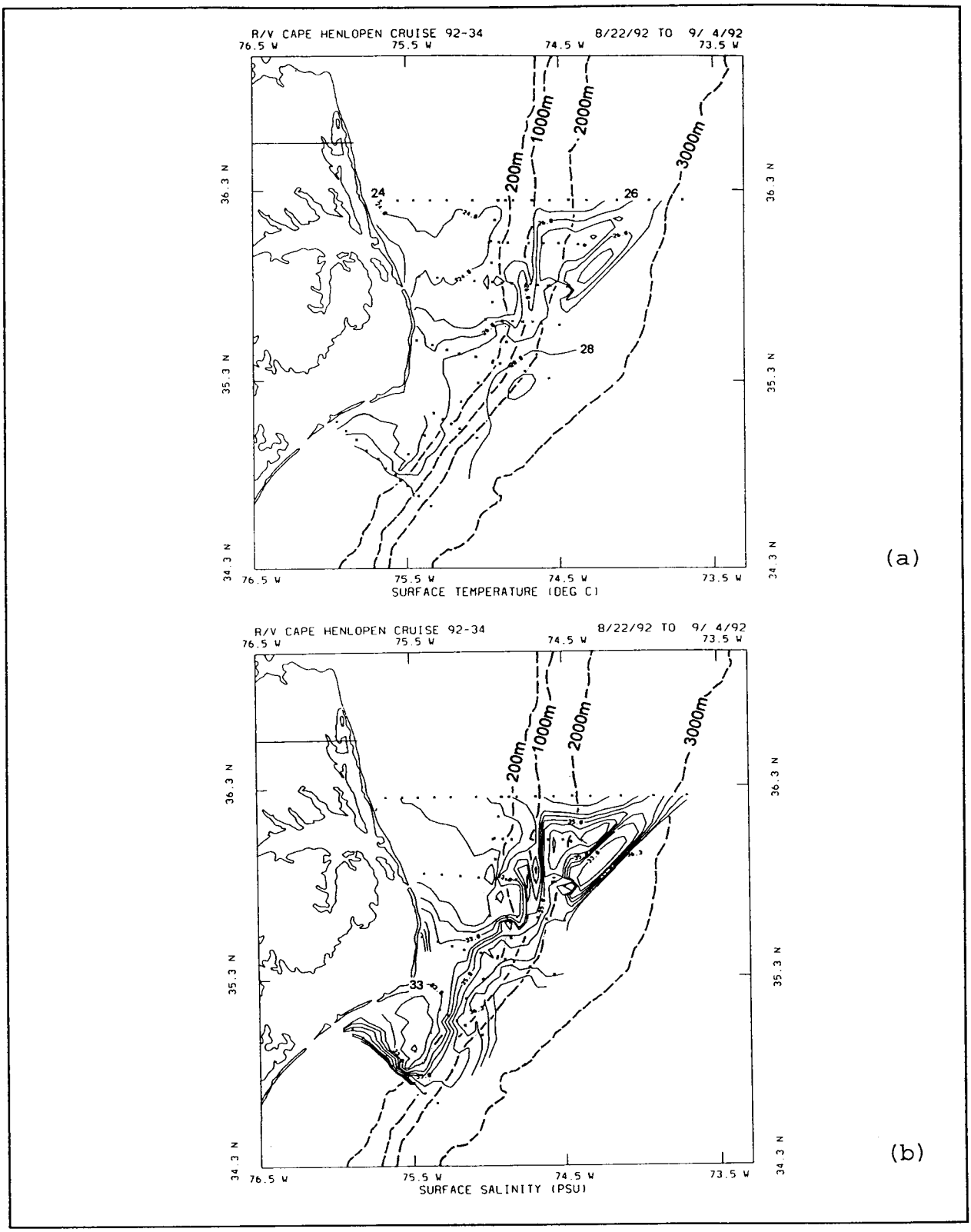

Figure 4.3-7. Surface contour map of (a) temperature and (b) salinity during cruise CH9234 August 8 - September 4, 1992.

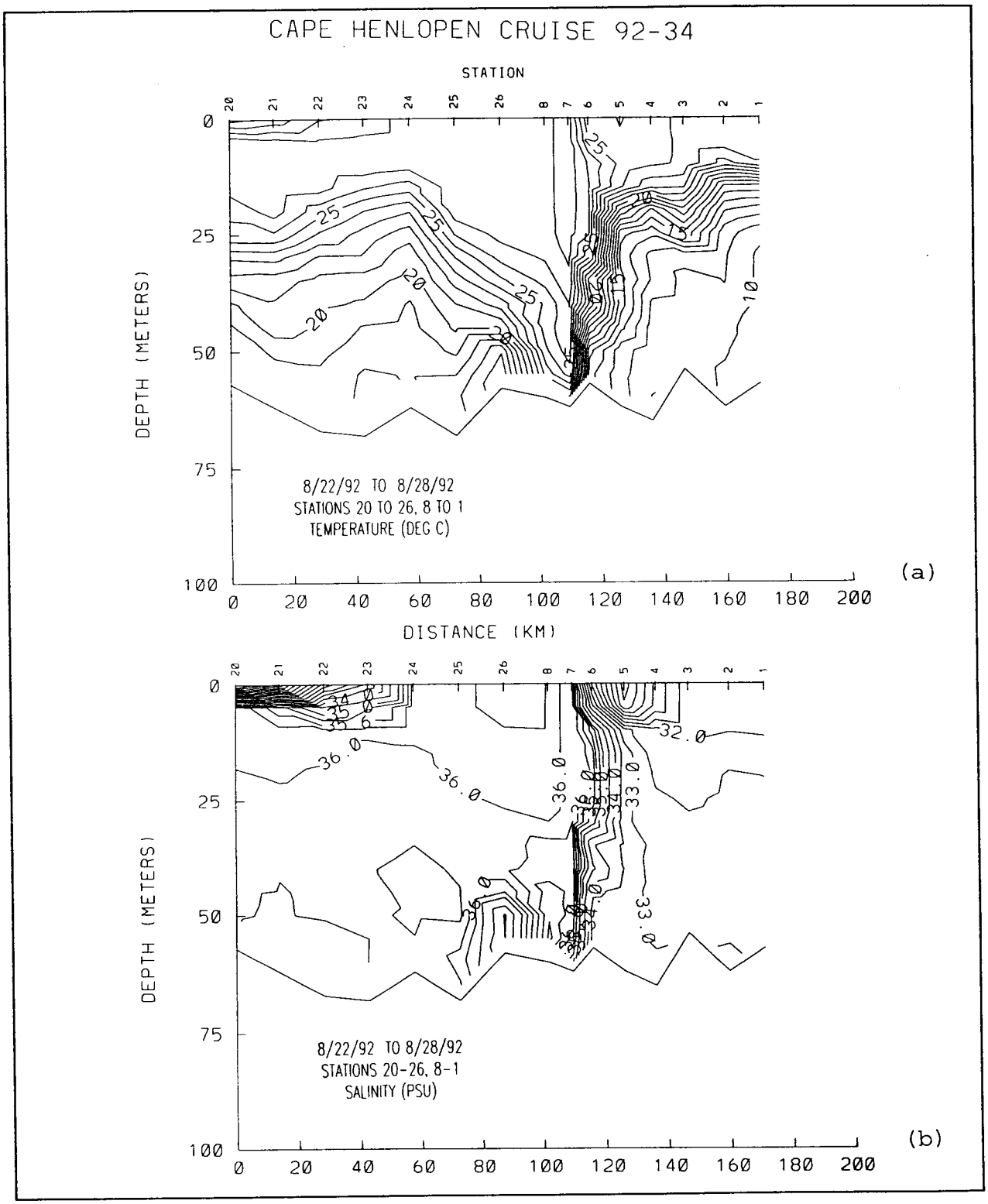

Figure 4.3-8. Alongshelf (60 m isobath) sections of (a) temperature and (b) salinity taken during cruise CH9234 on August 22-23 (northern half) and August 28 (southern half), 1992.

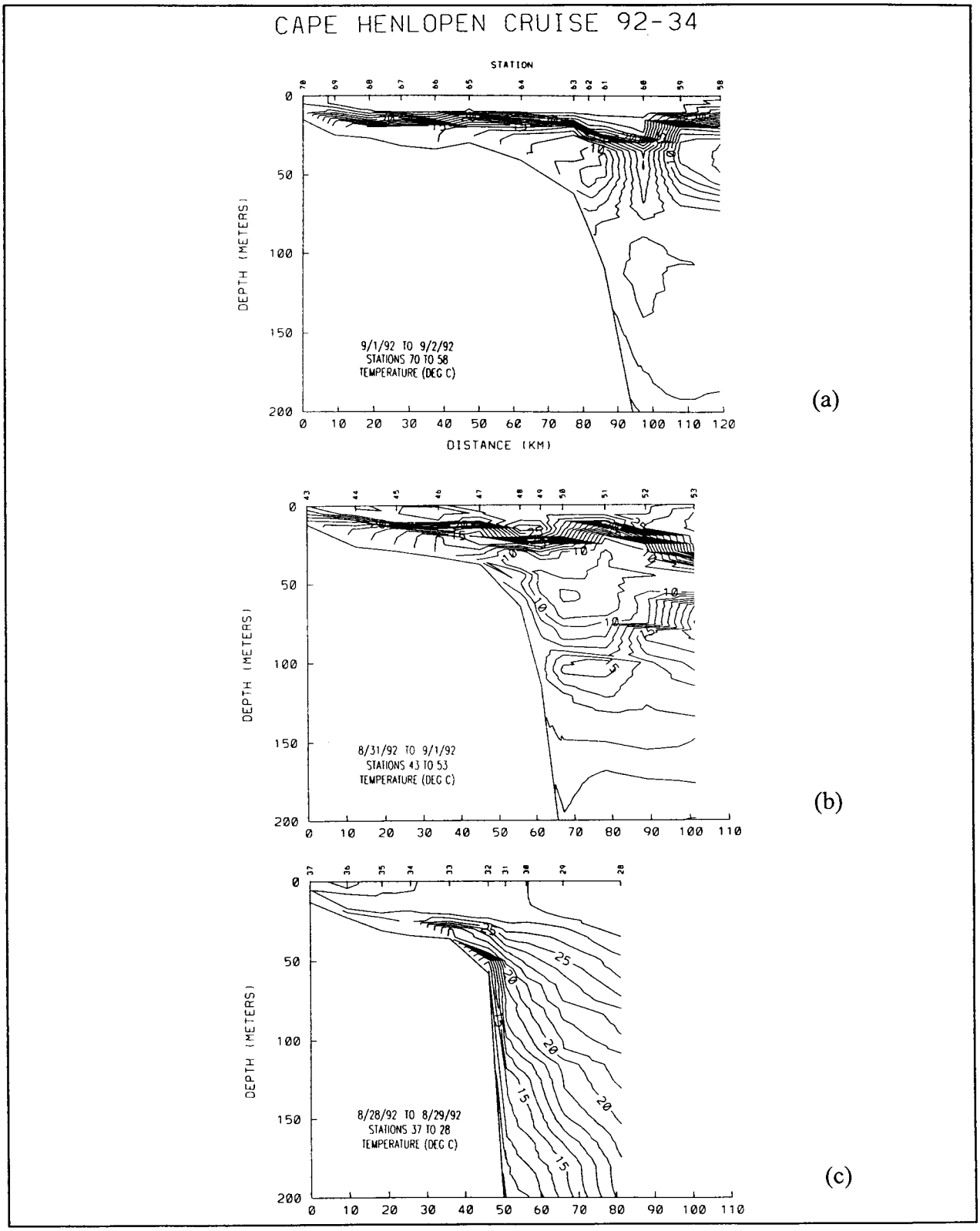

Figure 4.3-9. Cross-shelf sections of temperature taken during cruise CH9234 along (a) Line A on September 1-2, 1992, (b) Line E on August 31-September 1, 1992 and (c) Line B on August 28-29, 1992.

is seaward of the break. At line B, the cold band is not present. Although the broad region of cold water (with temperatures less than 10°C and reaching a minimum of less than 8°C) reaching offshore at line E might suggest wholesale movement of this water into the Slope region, such pictures by themselves do not offer sufficiently convincing evidence for this process. Such apparent calving of shelf water off into the Slope Water has been observed all along the Middle Atlantic Bight shelf break, from Nantucket Shoals southward. The strongest argument in favor of wholesale offshore movement of the cold band would seem to be continuity; with the cold band moving southward at 5-10 $cm \cdot s^{-1}$ this water must flow offshore between line E and line B. The pathway and time dependence of this flow, however, is not easily revealed by the hydrographic measurements.

Expanded sections over the shelf show the effects of the prevailing upwelling-favorable winds during the summer season. The northern section (Figure 4.3-10(a)-(c)) shows the typical summer section in the Middle Atlantic Bight, with upwelling-favorable winds tilting the pycnocline near shore. The Ekman divergence near the coast detaches the salinity minimum associated with the Chesapeake Bay plume from the coast, although this minimum is somewhat diffuse at line E as a result of wind mixing. The southern section (Figure 4.3-10(d)-(e)) is devoid of cold water and shows a strong intrusion at mid-depth of high-salinity Gulf Stream water far onto the shelf. A similar intrusion was seen by Boicourt (1973) and ascribed to upwelling favorable winds. Along with the subsurface intrusion, Ekman drift moves the surface salinity minimum offshore. Churchill *et al.* (1989) point out the role of Gulf Stream eddies and intrusions in similar processes. Satellite imagery from August 31 (Figure 4.3-11), two days after the hydrographic survey along line B, does not reveal any candidate feature, although later imagery suggests that some undetected (due to the weak thermal contrasts at this time of year) eddy activity might be present at this time . Even in the absence of wind driving or eddy activity, there is a salinity maximum layer over the outer shelf in the Middle Atlantic Bight (Boicourt and Hacker 1976; Gordon *et al.* 1976; see section 4.3.2).

Around Diamond Shoals, the waters of Raleigh Bay show little stratification in late summer (Figure 4.3-12). The only structure of note is the low-salinity water near the coast, the source of which is probably a combination of Middle Atlantic Bight water and

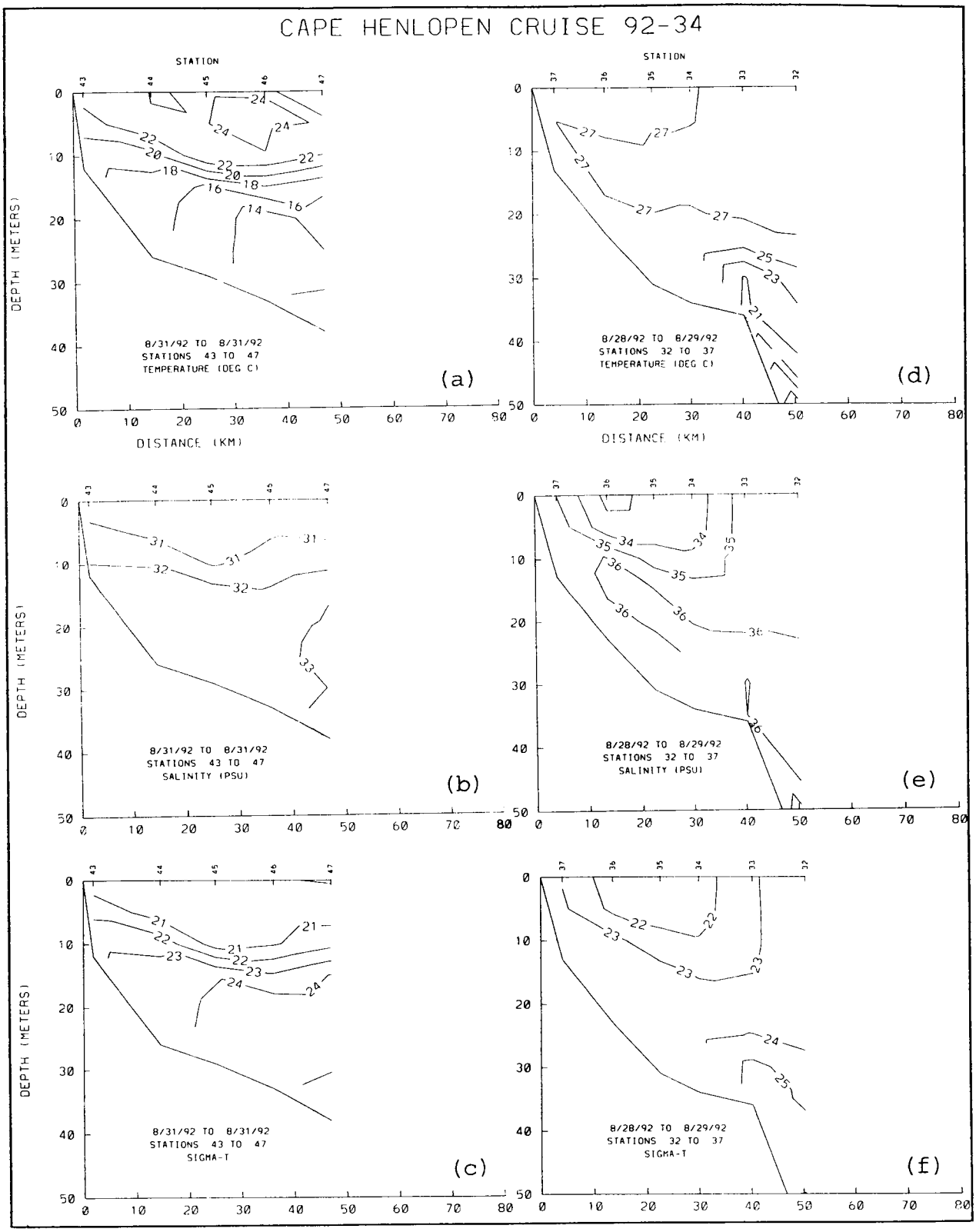

Figure 4.3-10. Cross-shelf sections of (a) temperature, (b) salinity and (c) σ_t along Line E; and of (d) temperature, (e) salinity and (f) σ_t along Line B taken during cruise CH9234 on August 28-31, 1992.

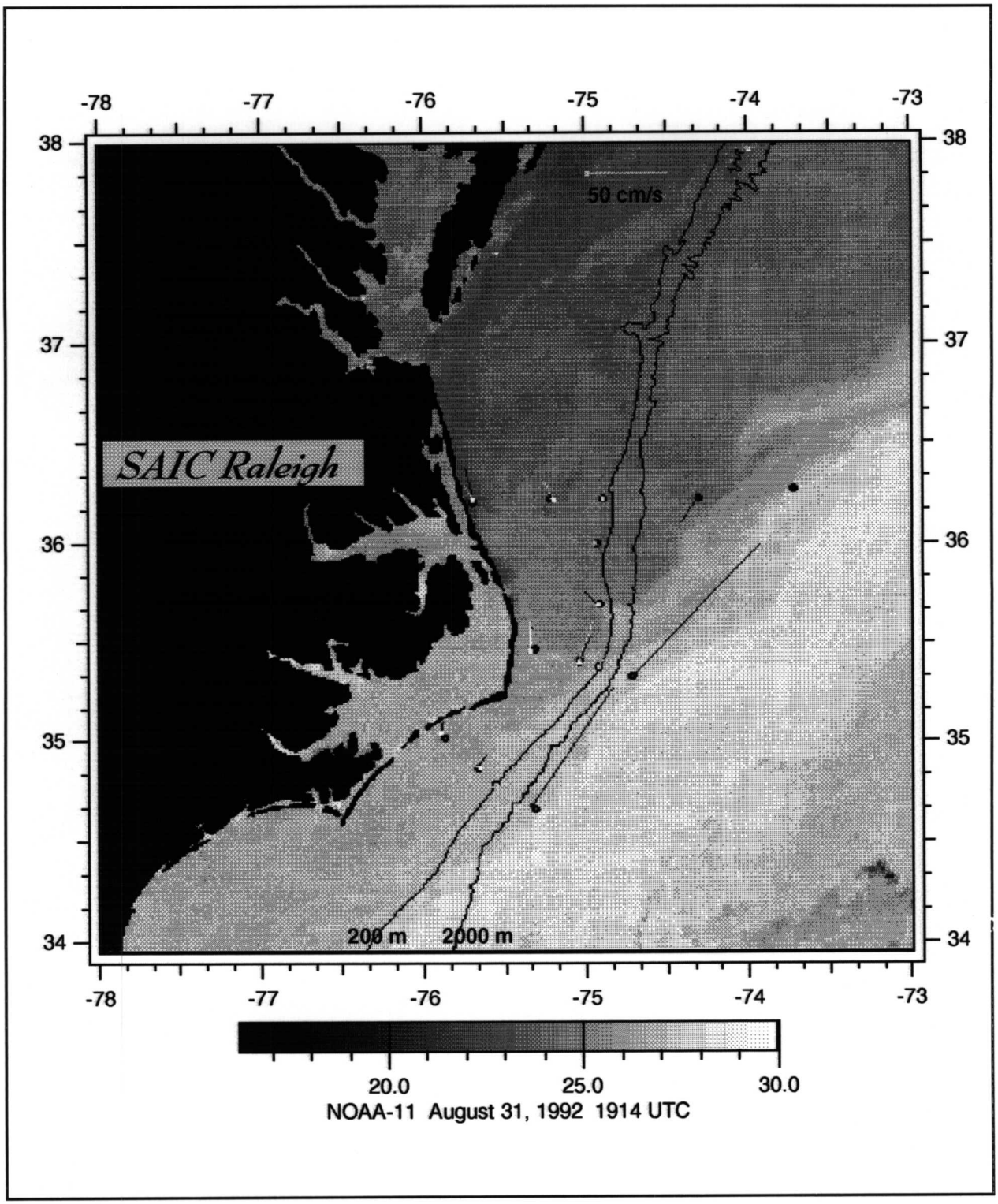

Figure 4.3-11. Satellite SST Image and Daily Average Current Vectors on August 31, 1992. Annotated as in Figure 2.2-7.

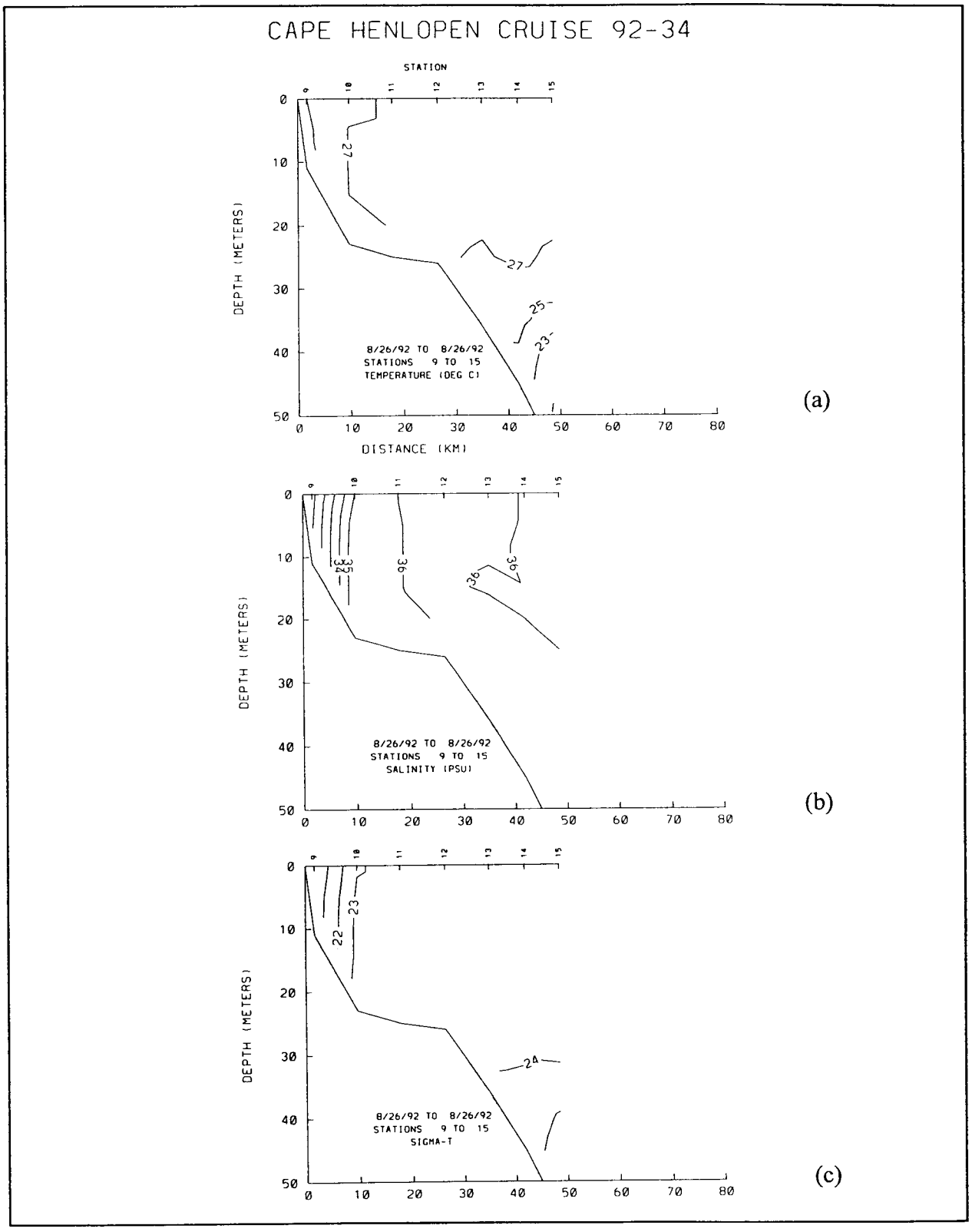

Figure 4.3-12. Cross-shelf sections along Line C of (a) temperature, (b) salinity and (c) σ_t taken during cruise CH9234 on August 26, 1992.

low-salinity water from Pamlico Sound mixing seaward into the coastal boundary layer.

By November, autumnal cooling and the mixing associated with cold-air outbreaks has greatly reduced the summer stratification in the Middle Atlantic Bight. The winds at this season are prevailing northwesterly, and drive Middle Atlantic Bight water around Cape Hatteras, over Diamond Shoals and into Raleigh Bay. Surface temperature and salinity maps show that these winds forced the Middle Atlantic Bight-South Atlantic Bight front southward from its spring and summer 1992 position north of Cape Hatteras, to well south of Cape Hatteras (Figure 4.3-13). The 60-m isobath sections (line D) still show a very strong front at the shelf break (Figure 4.3-14), but the front does not cross over the shelf until line F and line C, south of Hatteras (Figure 4.3-15).

The buoyancy input from Chesapeake Bay creates a two-layer structure at the latitude of Oregon Inlet (Figure 4.3-16), but it is nearly eliminated by line B (Figure 4.3-17). The Raleigh Bay water column is also well-mixed vertically (Figure 4.3-18), but the increased salinity creates a north-south density difference across Diamond Shoals. Satellite imagery (Figure 4.3-19) and surface salinity maps indicate southward transport across Diamond Shoals (which were well covered by hydrographic stations; Figure 4.3-13), although the frequency and magnitude of this buoyancy flux is not sufficient to maintain a stratified water column over inner Raleigh Bay in the presence of wind mixing. Some of this transport is evident in the cold water over inner Raleigh Bay in February (Figure 4.3-20).

4.3.2 Interannual Variability

Spring of 1993 was a season of record runoff from the largest buoyancy source to the Middle Atlantic Bight--the Susquehanna River debouching at the head of Chesapeake Bay. During large runoff years such as 1993, the contributions from the Delaware and Hudson estuaries to the lowering of salinities along the inner shelf are also noticeable (Boicourt 1973). This flow was greater than normal, but also peaked in March, slightly earlier than normal. The result of this elevated buoyancy flux was an augmentation of the vernal thermal stratification of the shelf in the southern Middle Atlantic Bight, perhaps earlier than usual. A secondary effect of this buoyancy contribution to stratification is the reduction in vertical mixing by increasing stability, thus

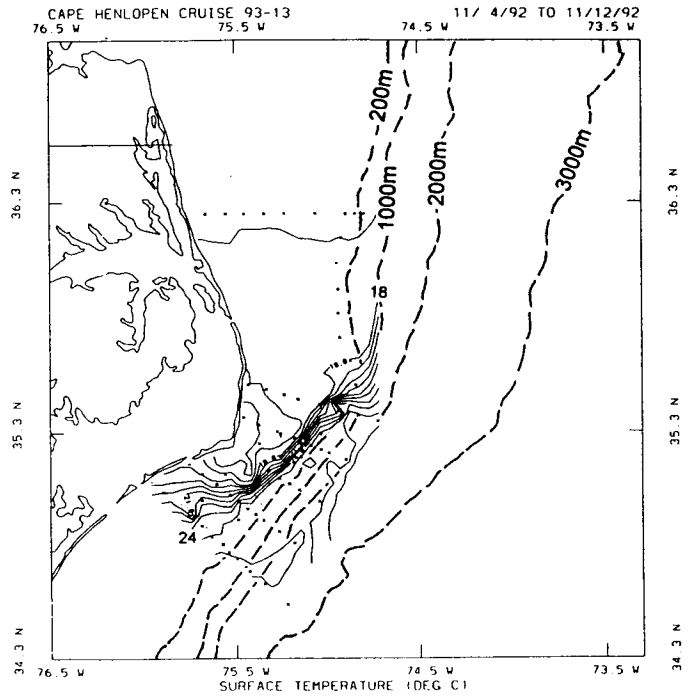

(a)

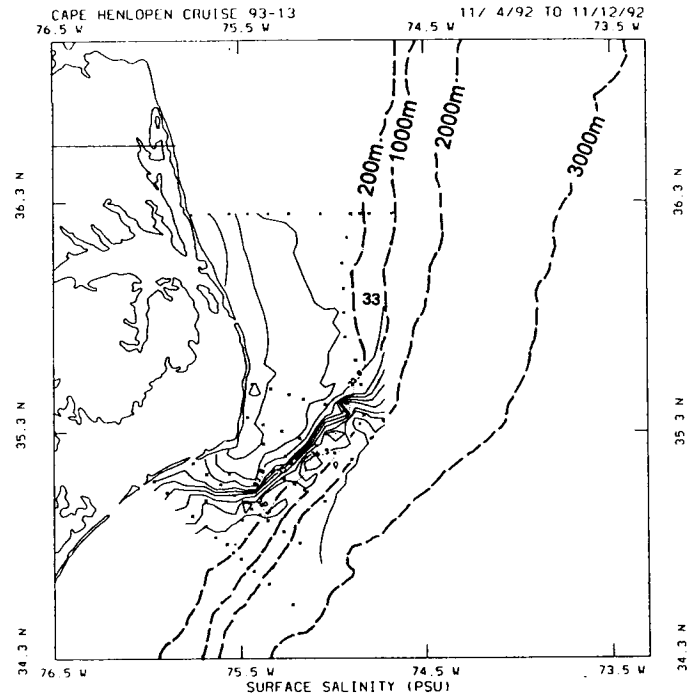

(b)

Figure 4.3-13. Surface contour map of (a) temperature and (b) salinity during cruise CH9313 November 4-12, 1992.

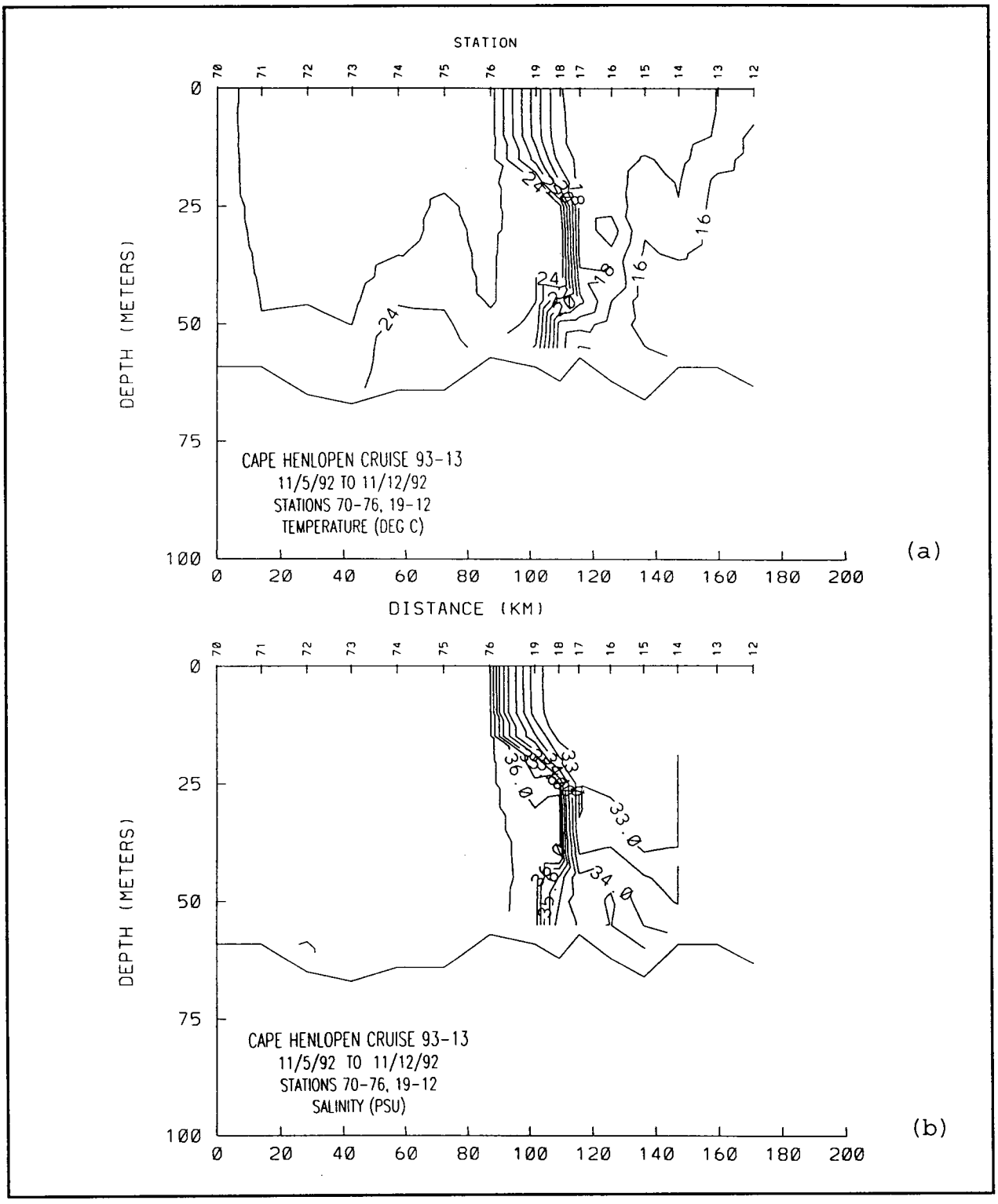

Figure 4.3-14. Along-shelf (60-m isobath) sections of (a) temperature and (b) salinity taken during cruise CH9313 on November 5-12, 1992.

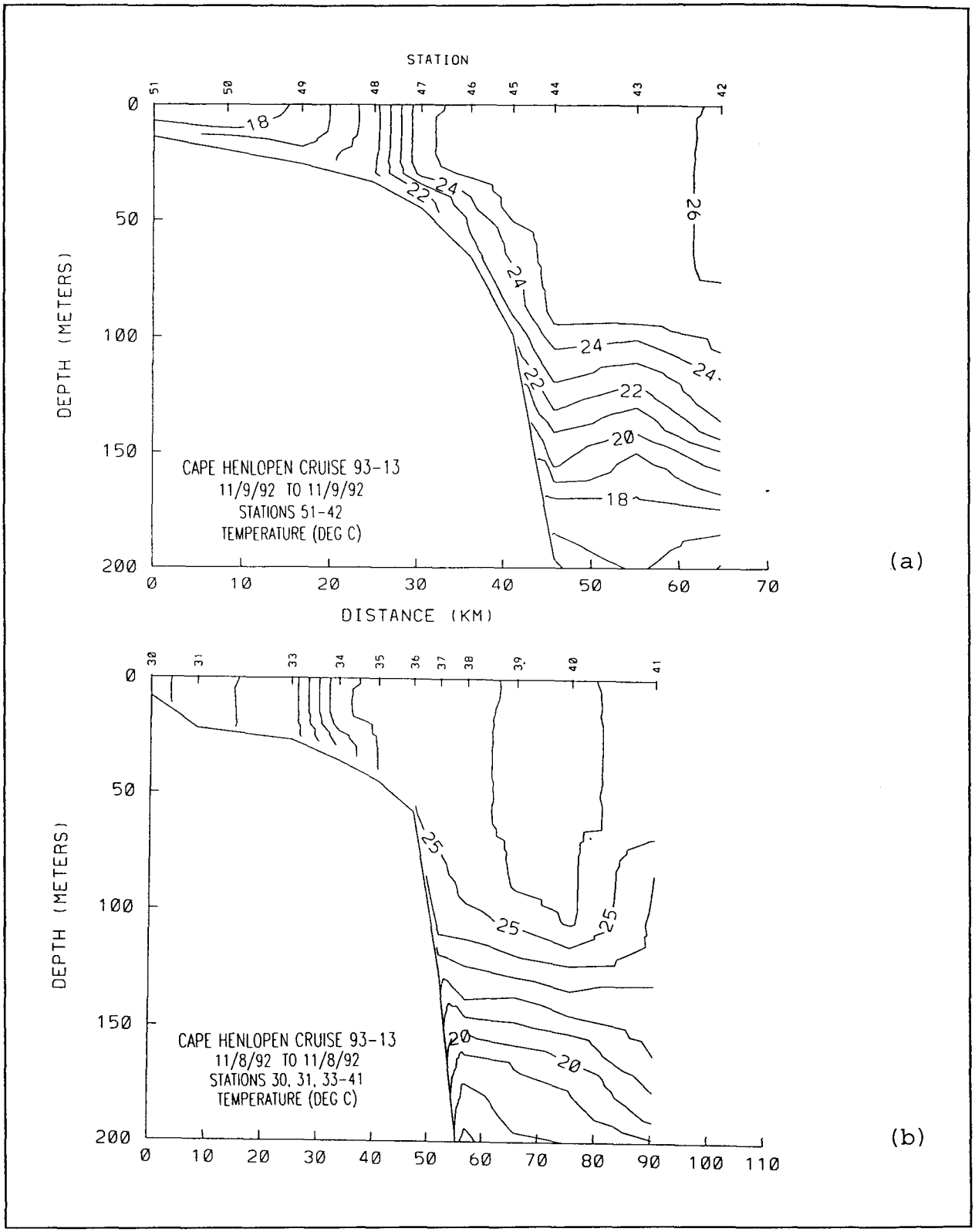

Figure 4.3-15. Cross-shelf sections of temperature taken during cruise CH9313 along (a) Line G on November 9, 1992 and (b) Line C on November 8, 1992.

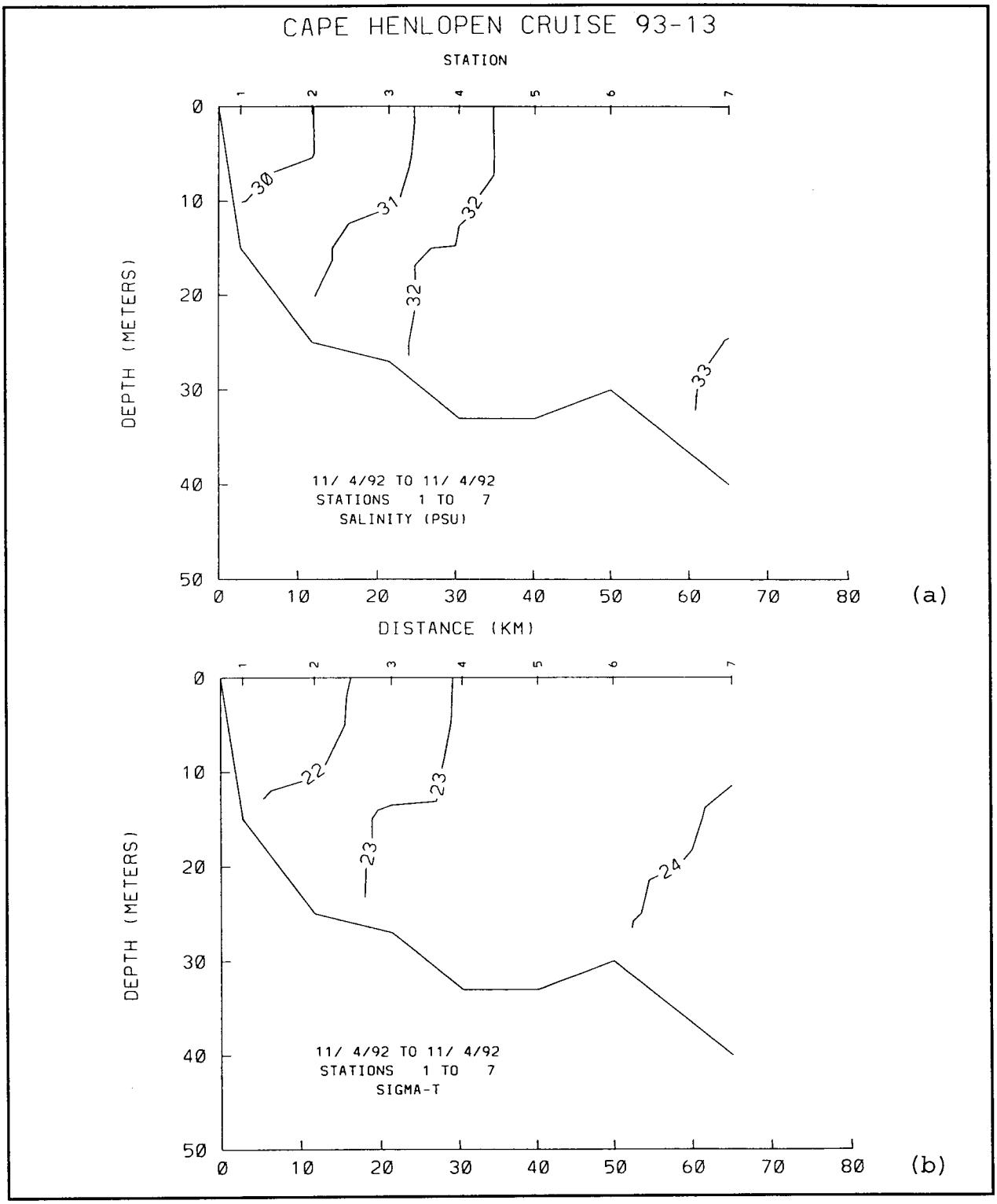

Figure 4.3-16. Cross-shelf sections along Line A of (a) salinity and (b) σ_t taken during cruise CH9313 on November 4, 1992.

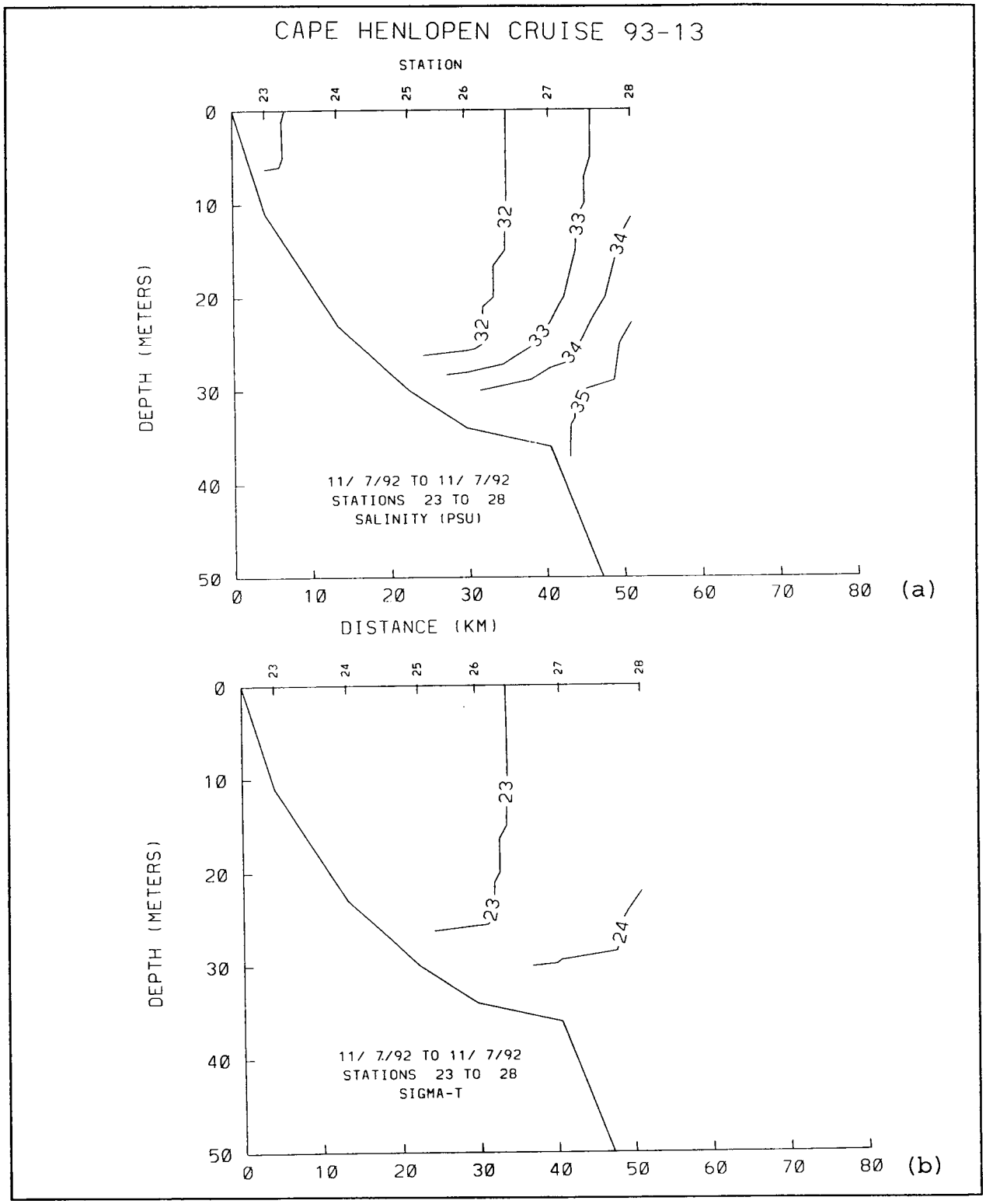

Figure 4.3-17. Cross-shelf sections along Line B of (a) salinity and (b) σ_t taken during cruise CH9313 on November 7, 1992.

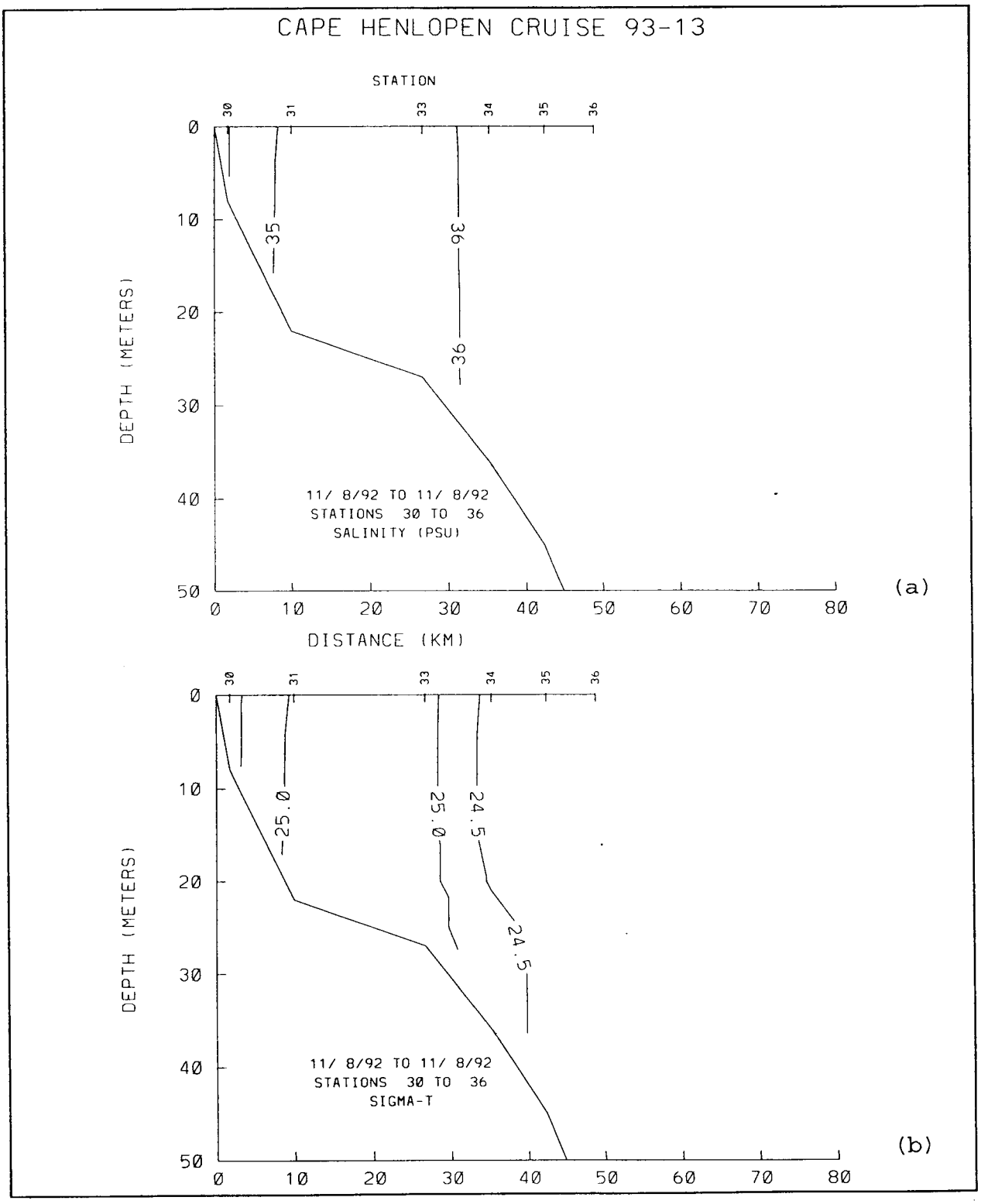

Figure 4.3-18. Cross-shelf sections along Line C of (a) salinity and (b) σ_t taken during cruise CH9313 on November 8, 1992.

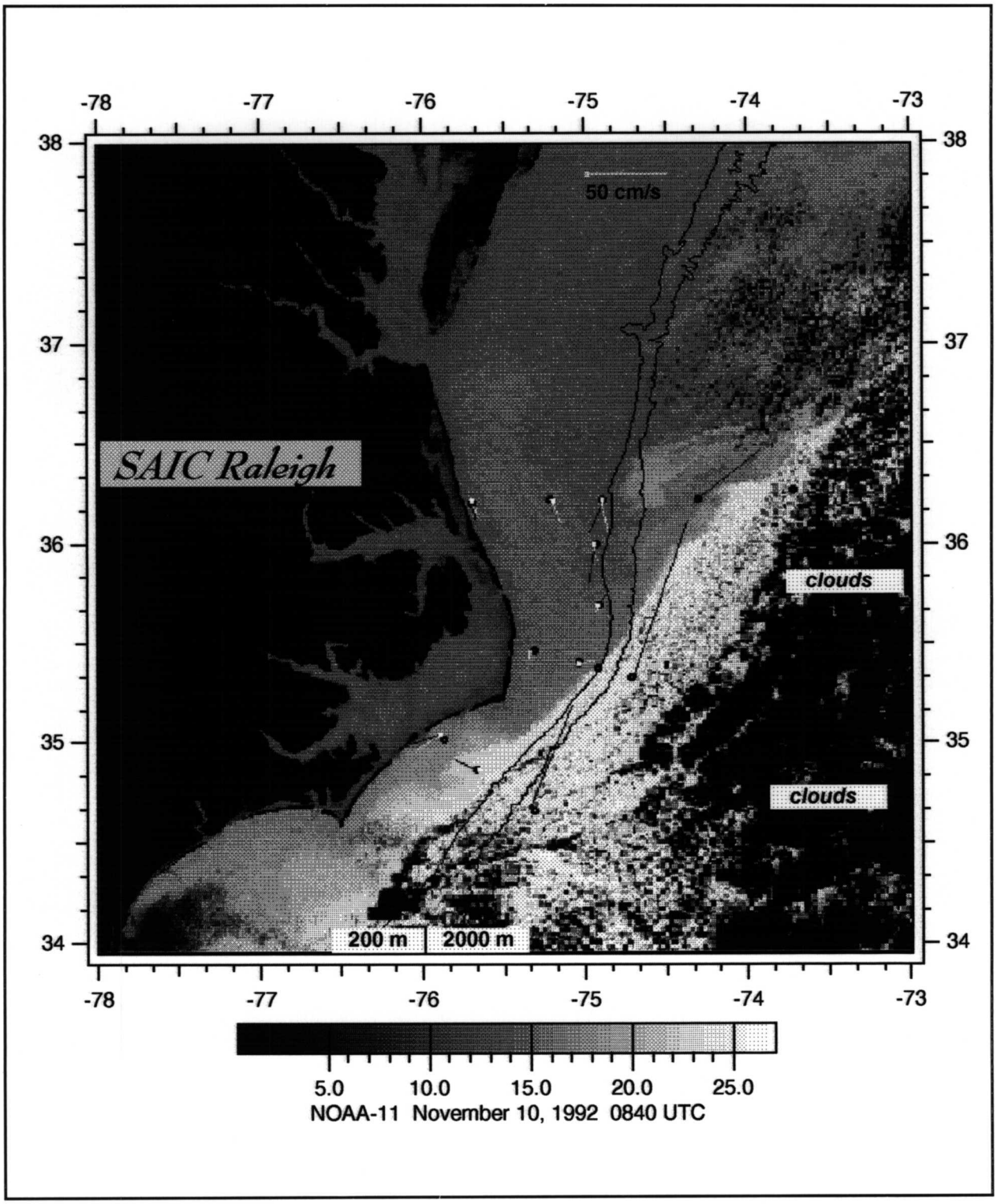

Figure 4.3-19. Satellite SST Image and Daily Average Current Vectors on November 10, 1992. Annotated as in Figure 2.2-7.

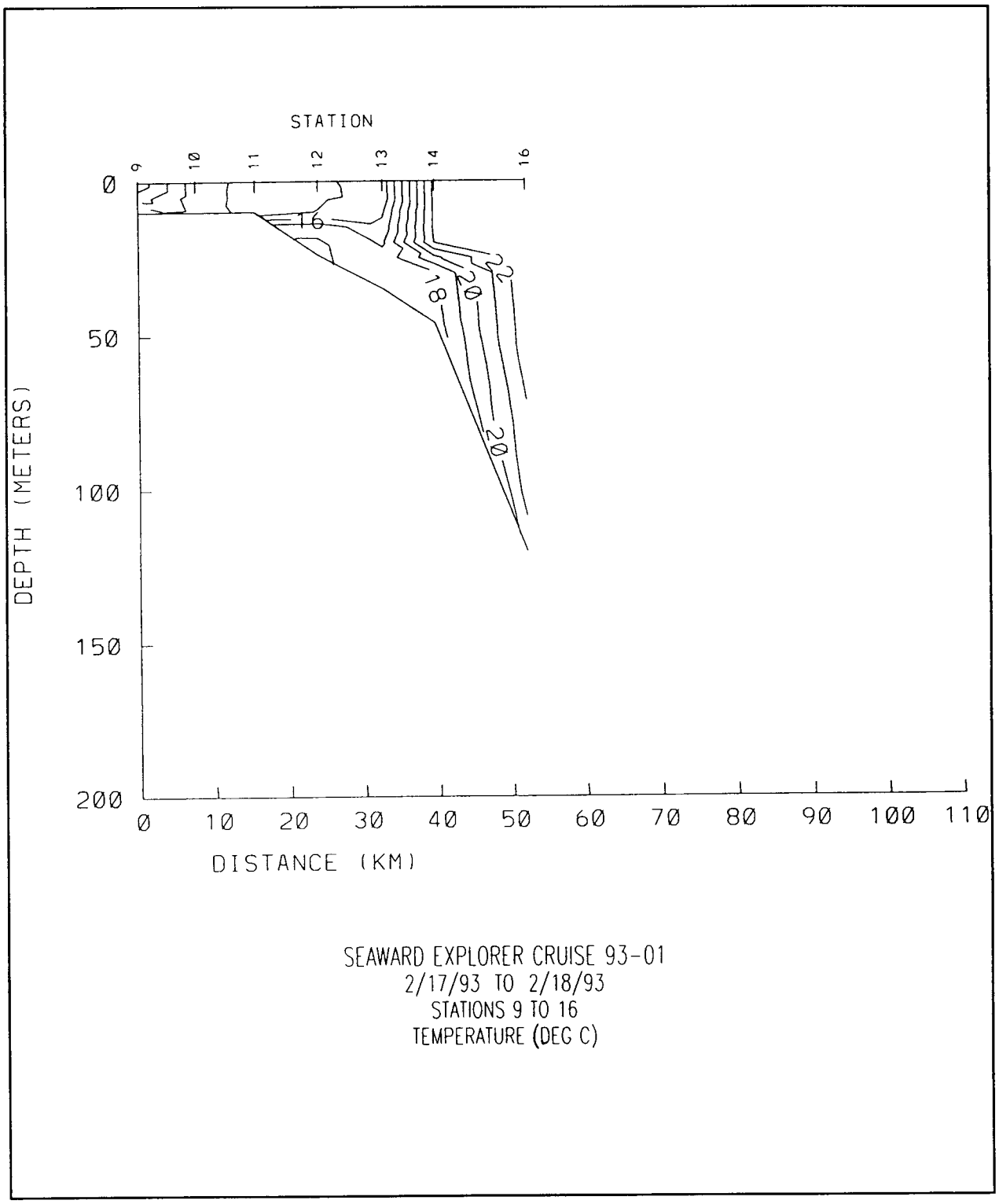

Figure 4.3-20. Cross-shelf section along Line C of temperature during cruise SE9301 February 17-18, 1993.

providing increased insulation to the cooler lower layers (see Houghton and Ou 1982). A larger buoyancy flux also increases the stability of the coastal current set up after the initial near-field turn of the Chesapeake Bay plume. The coastal current maintains its integrity in the face of upwelling favorable winds, which not only oppose the coastal jet but also act to decrease its density difference with the ambient waters via mixing. With the lag time between Susquehanna discharge and Chesapeake Bay outflow of the order one month, the effect of the March runoff should be evident on the shelf in the May cruise. The surface salinity map (Figure 4.3-21) shows both the unusually low salinities over the shelf and the salinity front bounding the offshore extent of the buoyancy-driven coastal current. Although some distortion of the salinity patterns is evident over Diamond Shoals as a result of the inability to occupy hydrographic stations in this hazardous region, there is clear evidence of transport of low-salinity water around Cape Hatteras and into Raleigh Bay. This intrusion is seen in the AVHRR imagery (and current vectors) in the week preceding the survey (Figure 4.3-22).

An interesting salinity maximum band extends northeastward from Cape Hatteras (Figure 4.3-21). The logical pathway for the arrival of this low-salinity water over the outer shelf is not via wind-driven transport and mixing across the shelf, but for transport south as a coastal current, then either offshore turning prior to Cape Hatteras or entrainment along the north wall of the Gulf Stream in Raleigh Bay after passing over Diamond Shoals. Cross-shelf sections of temperature and salinity on line A (Figure 4.3-23) reveal the early stratification brought on by both the buoyancy flux and insolation. The lower layers in the Middle Atlantic Bight remain cold, and the thermal gradient south to Raleigh Bay is particularly sharp (10°C in 10 km; Figure 4.3-24). The mid-shelf salinity maximum is not obvious in the surface salinity map on line C (Figure 4.3-21), but the cross-shelf transect (Figure 4.3-25) shows the maximum dividing the low-salinity water over the outer shelf. This section prompts the suggestion that the salinity maximum might be due to mid-shelf upwelling (seaward of the stable coastal current and its associated buoyancy flux).

Although the effect of the high spring runoff in 1993 extends into late summer, the strength of the coastal current driven by the Chesapeake Bay outflow is diminished. The surface salinity map from cruise SE9309 (Figure 4.3-26) shows the salinity minimum

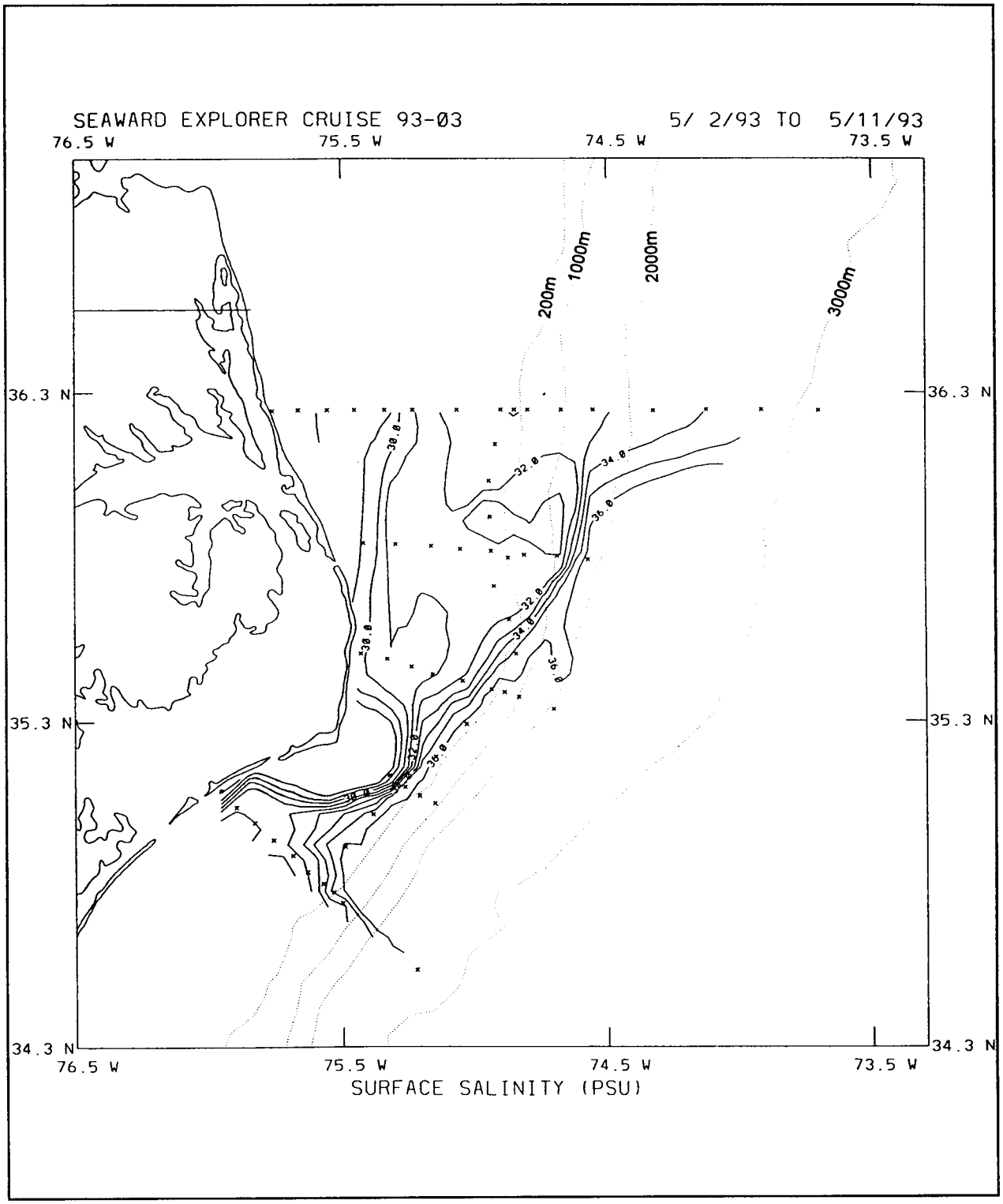

Figure 4.3-21. Surface salinity map during cruise SE9303 May 2-11, 1993.

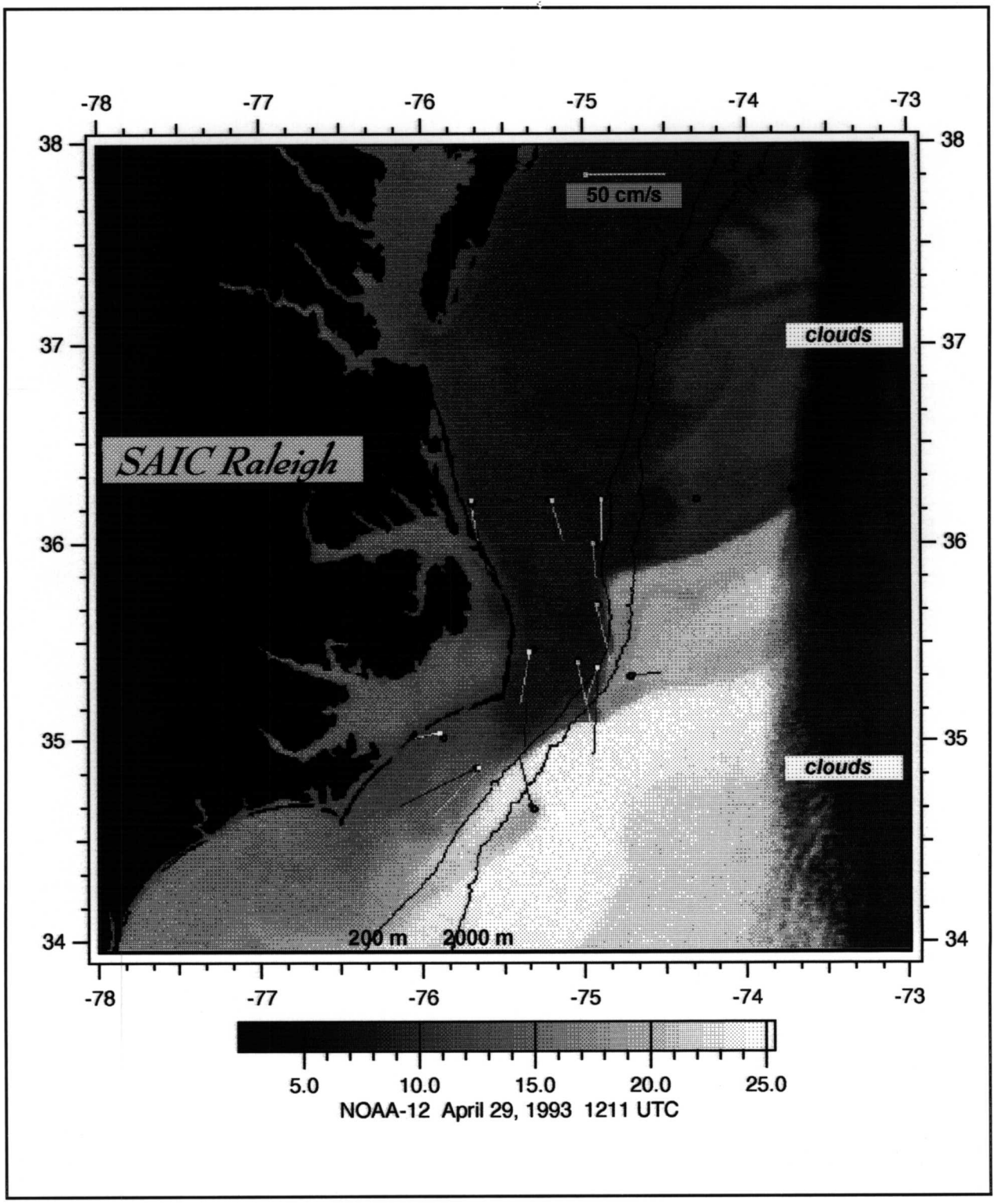

Figure 4.3-22. Satellite SST Image and Daily Average Current Vectors on April 29, 1993. Annotated as in Figure 2.2-7.

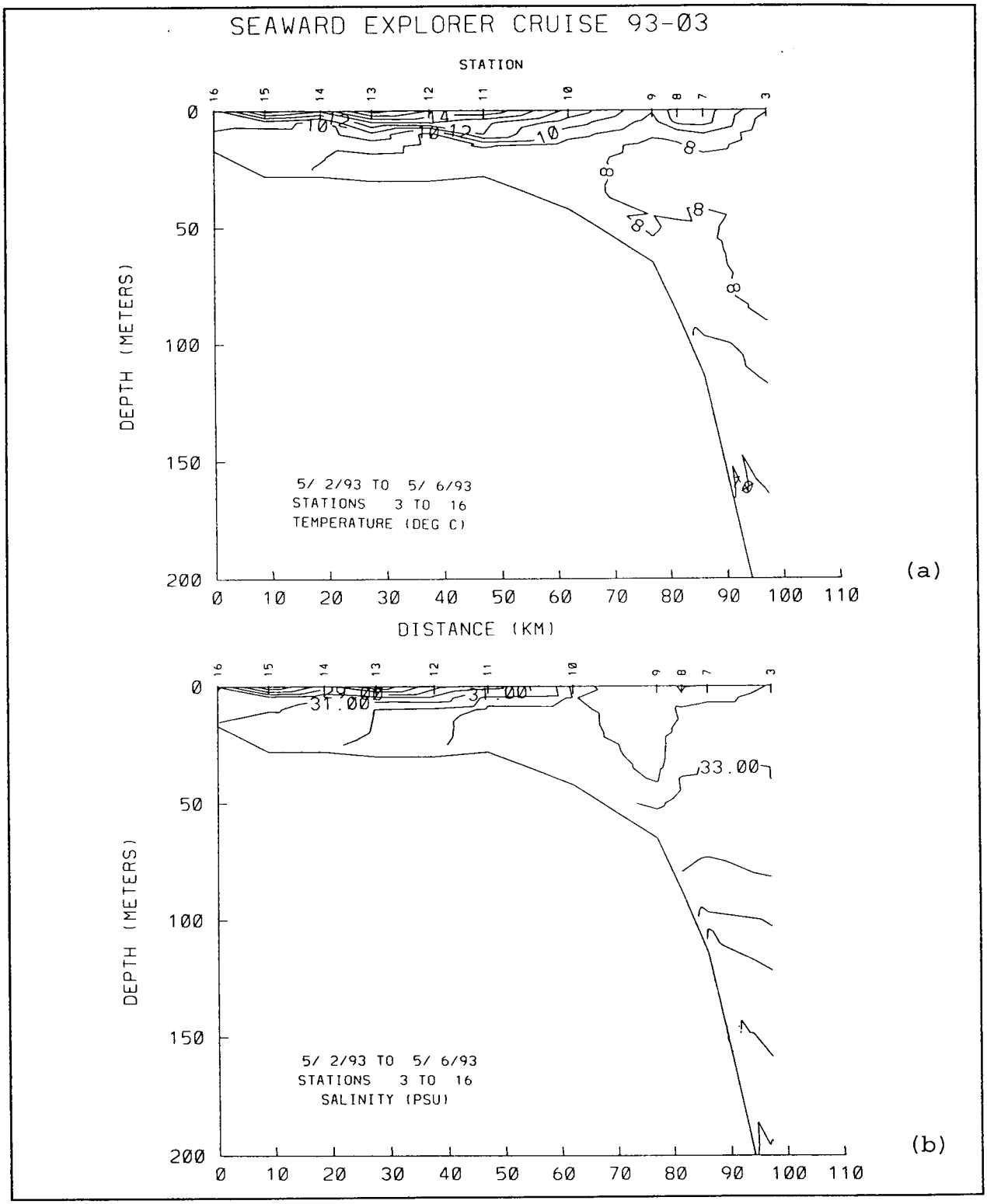

Figure 4.3-23. Cross-shelf sections along Line A of (a) temperature and (b) salinity taken during cruise SE9303 on May 3 and 16, 1993.

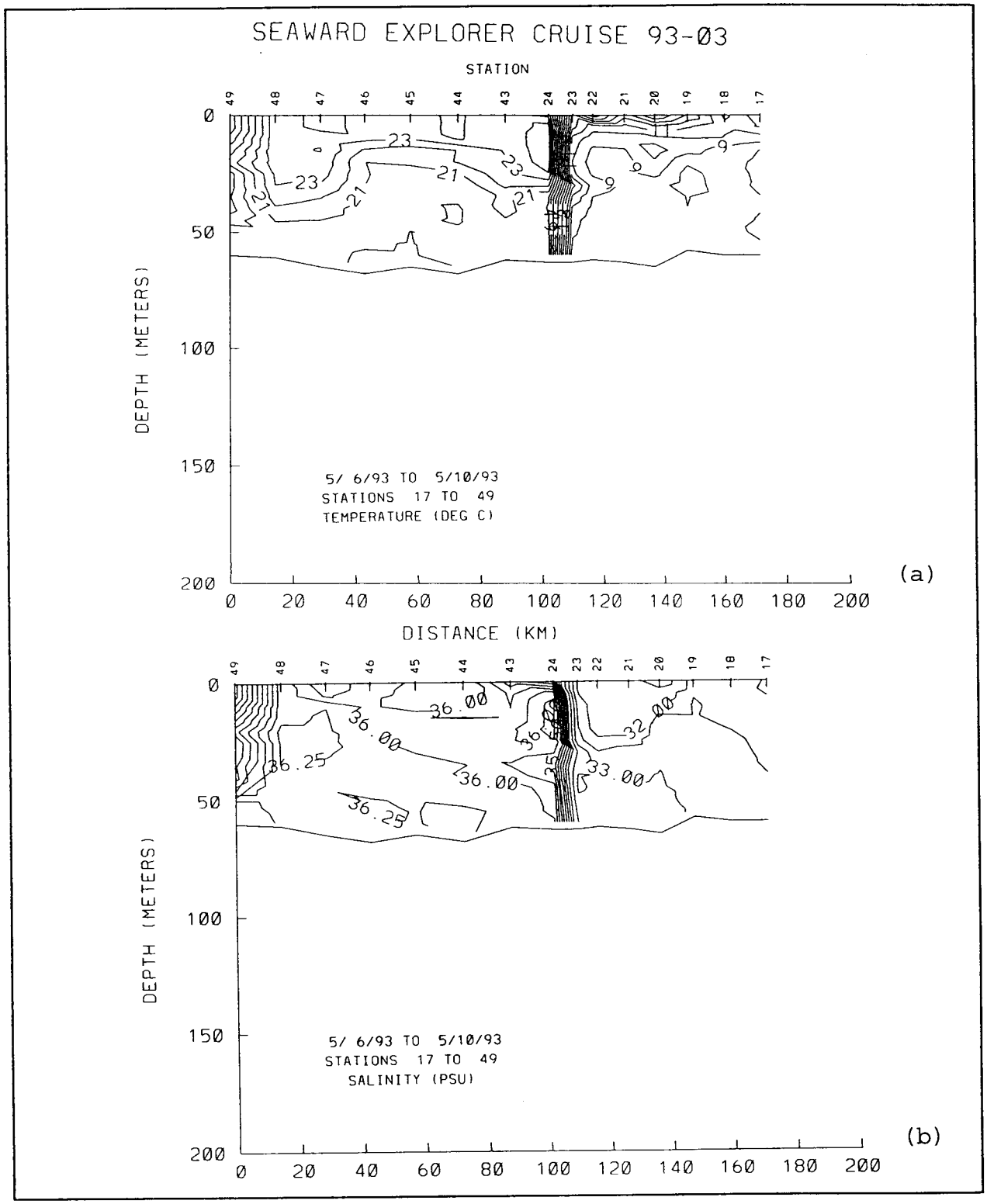

Figure 4.3-24. Alongshelf (60-m isobath) sections of (a) temperature and (b) salinity during cruise SE9303 on May 6-10, 1993.

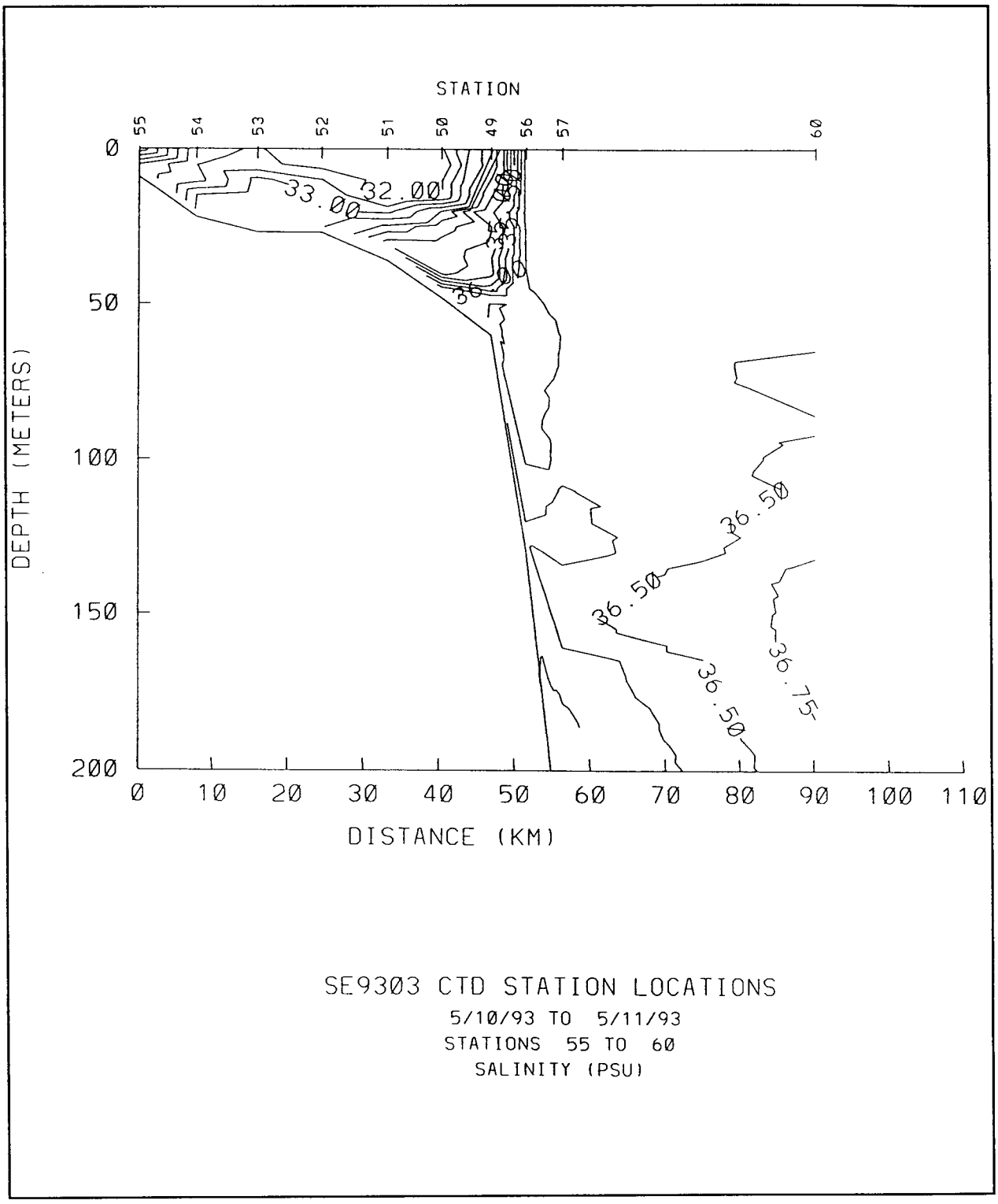

Figure 4.3-25. Cross-shelf sections along Line C of salinity taken during cruise SE9303 on May 10-11, 1993.

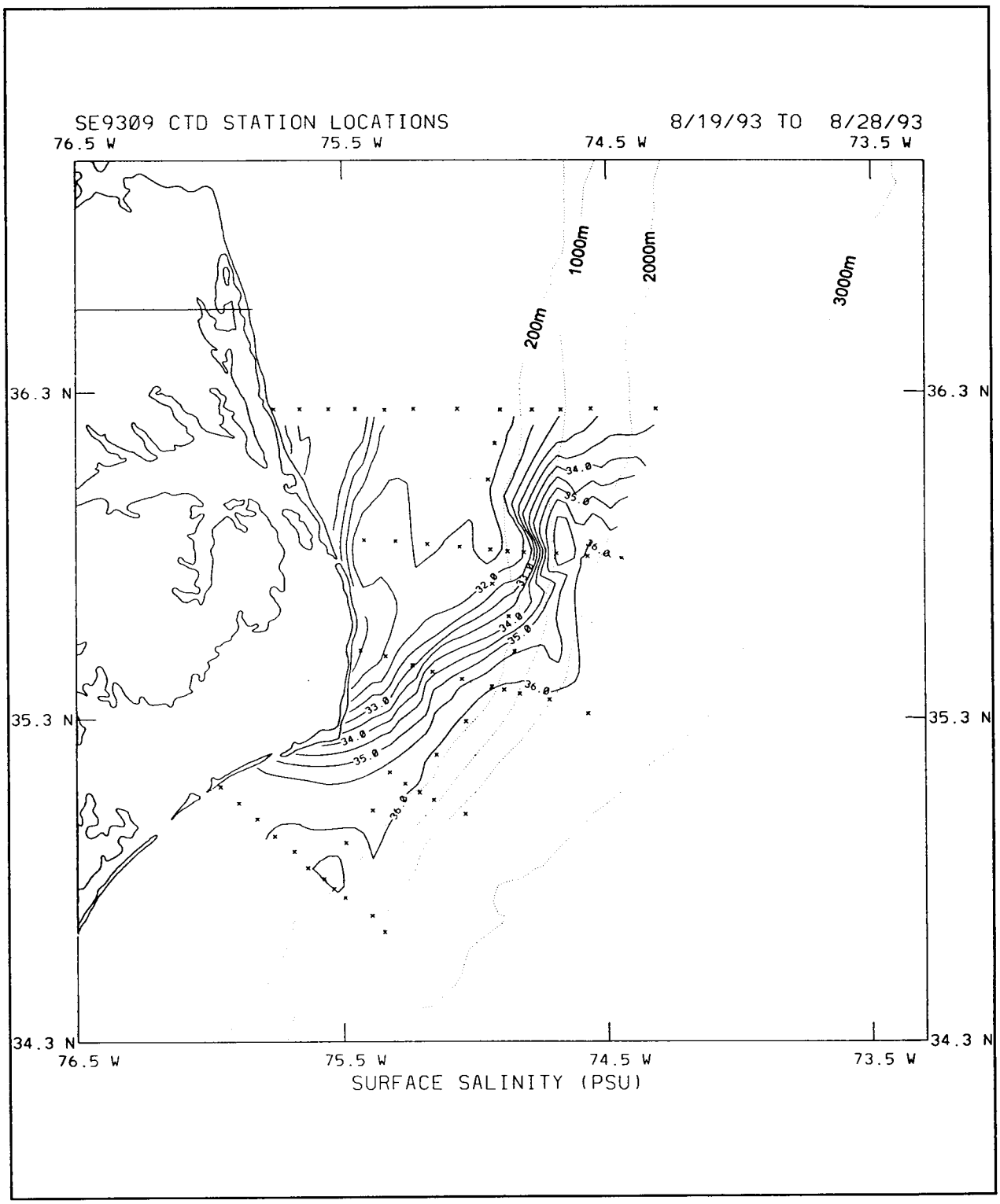

Figure 4.3-26. Surface salinity map for cruise SE9309 August 19-28, 1993.

(detached from the coast by upwelling-favorable winds) on line A, but it is significantly weaker than in late spring. Surface isohalines (again, contoured over Diamond Shoals where station coverage is sparse) suggest that this coastal current does not extend around Cape Hatteras. The prevailing southwesterly winds during this season prevent substantial transport in this direction. The Middle Atlantic Bight-South Atlantic Bight front is well-formed, and probably remains north of Cape Hatteras as it did in summer 1992, although the station coverage does not allow a definitive determination in this region. Temperature and salinity distributions on line A (Figure 4.3-27) show the offshore salinity minimum of the coastal current, and the upwelling inshore of this feature. In addition the salinity-maximum layer intruding above the cold band is clearly evident. Along line E (Figure 4.3-28), this intrusion structure is replaced by the north wall of the Gulf Stream, which is nearer to the shelf break than it was in 1992. The late summer 1993 hydrographic structure in Raleigh Bay is again nearly homogeneous (Figure 4.3-29).

Despite the high buoyancy flux of 1993, the influence of local spring runoff does not extend to November. The surface salinity map (Figure 4.3-30) stands in contrast to the November 1992 map (Figure 4.3-13) in that little transport of low-salinity water around Cape Hatteras is evident. In addition, the surface layers are considerably saltier than in 1992.

4.3.3 Virginia Coastal Water

Bumpus and Pierce (1955) introduced the term Virginian Coastal water in their study of the zooplankton distribution on the North Carolina shelf. In keeping with their names of the two faunal provinces identified north and south of Cape Hatteras (distinguished primarily on the basis of chaetognaths), they applied the term Virginian Coastal water to the entire shelf region between Cape Cod and Cape Hatteras. Later, Bumpus (1973) came to refer to this region as the Middle Atlantic Bight (citing Uchupi's 1965 bathymetric map of the east coast of the United States). Although Norcross and Harrison (1967) reminded oceanographers that historical records indicate that Captain John Smith called it the Virginian Sea, convention has settled on the Middle Atlantic Bight for the designation.

A primary aim of this study was to determine transport pathways in the waters off North Carolina and Virginia. Over the past two

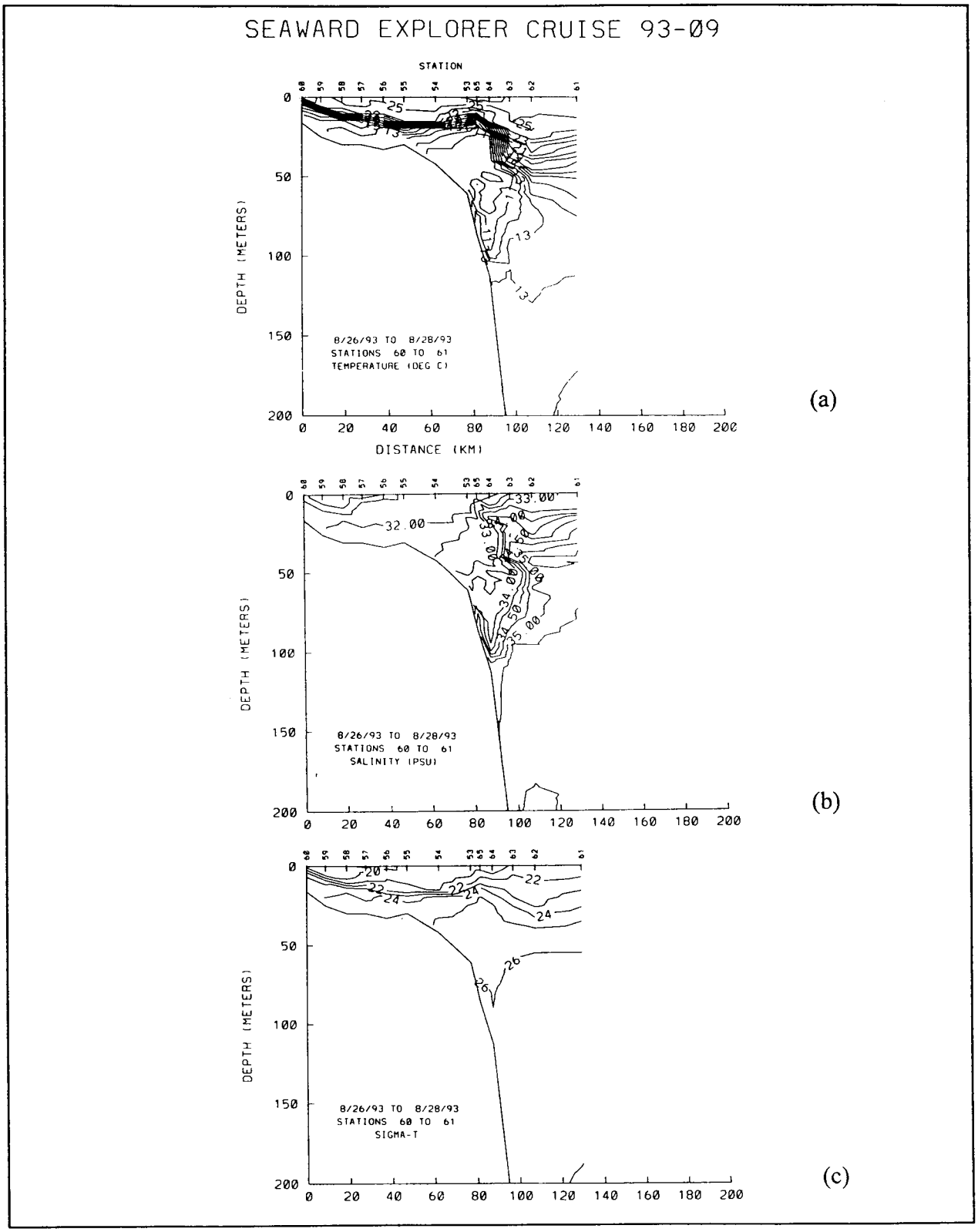

Figure 4.3-27. Cross-shelf sections along Line A of (a) temperature, (b) salinity, and (c) σ_t taken during cruise SE9309 on August 26-28, 1993.

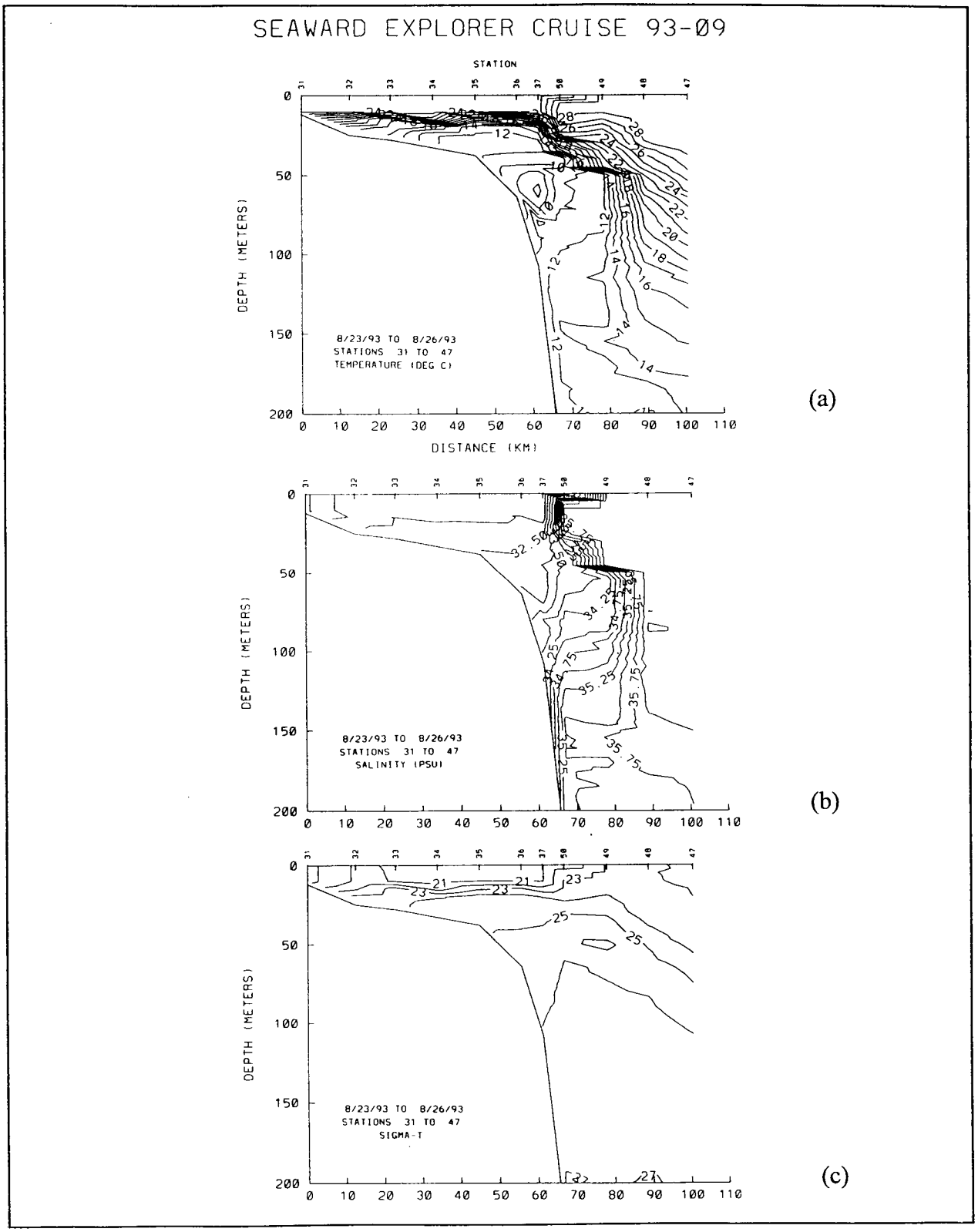

Figure 4.3-28. Cross-shelf sections along Line E of (a) temperature, (b) salinity, and (c) σ_t taken during cruise SE9309 on August 23-26, 1993.

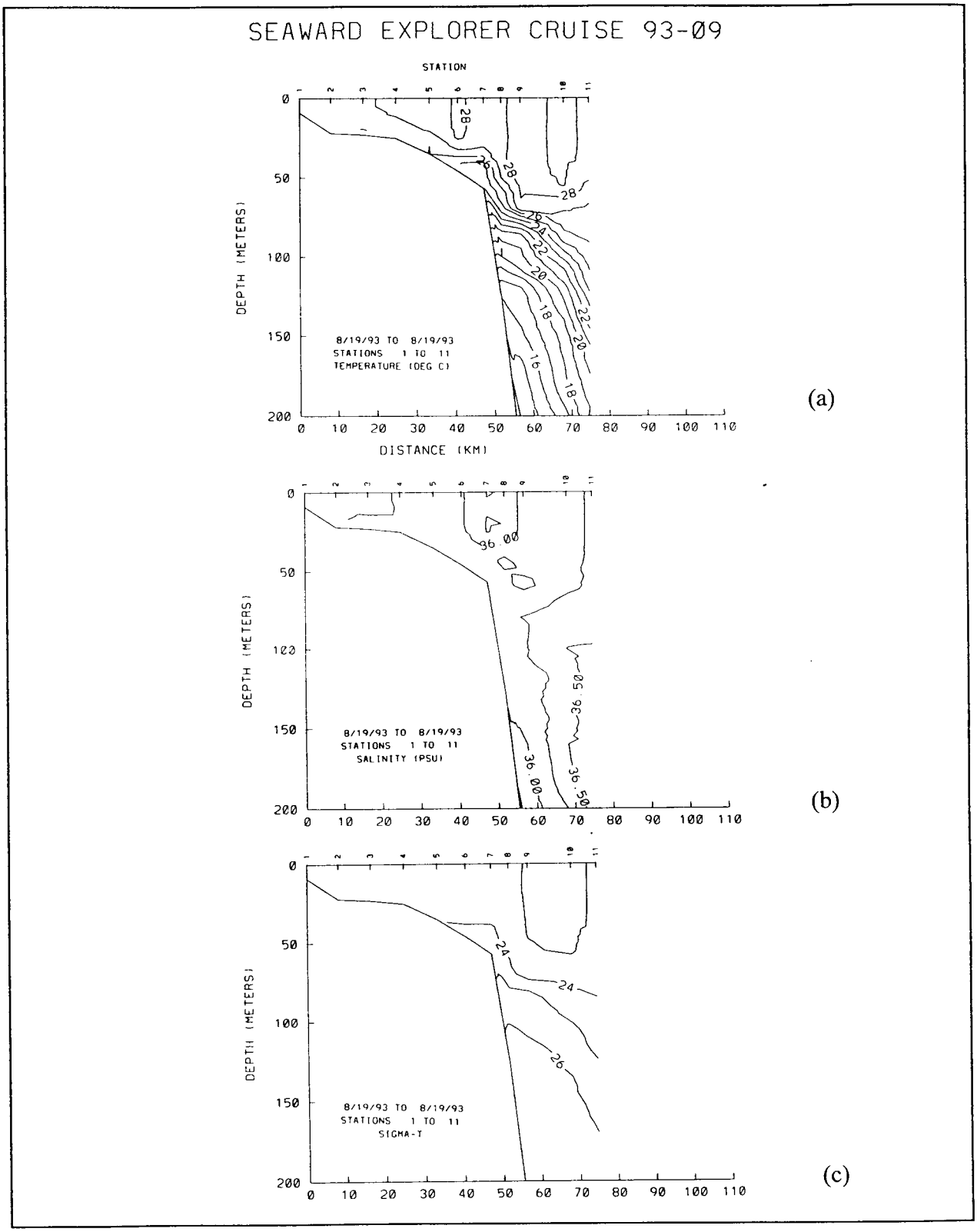

Figure 4.3-29. Cross-shelf sections along Line C of (a) temperature, (b) salinity, and (c) σ_t taken during cruise SE9309 on August 19, 1993.

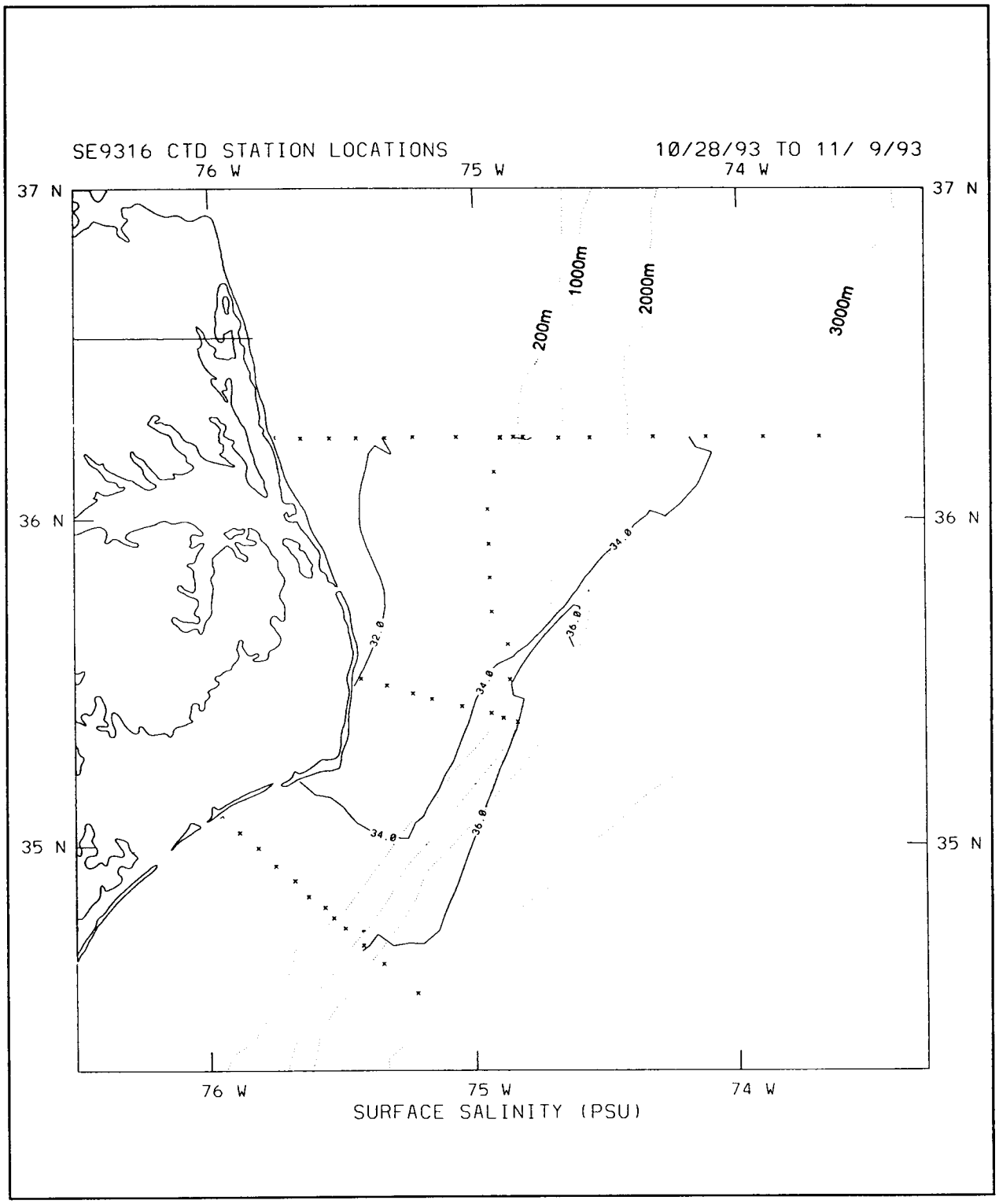

Figure 4.3-30. Surface salinity map for cruise SE9316 October 28 - November 9, 1993.

decades, the continental shelf water off Virginia has been considered part of an oceanographic continuum extending from Cape Cod to Cape Hatteras. Recently, the term Virginia Coastal water has been invoked by researchers in the Department of Energy's Ocean Margin Program (Flagg, personal communication) to describe a regional Water mass off Virginia and North Carolina deemed sufficiently distinct to warrant a separate designation. Presumably, this water mass is southern Middle Atlantic Bight water modified by the outflow from the Chesapeake Bay. Depending upon the season, the combined effect of the volume discharge, property differences and mixing on the shelf may create an identifiable water mass, although there is a question whether it constitutes a sufficiently large or stable body of water to be worthy of a label.

Transport processes on the Virginia and North Carolina shelves are discussed in Section VII. The presence of the Chesapeake Bay outflow creates conditions on the shelf where both buoyancy and wind forcing are active. Property distributions and temperature-salinity diagrams from this study not only reveal these influences on the transport and fate of southern Middle Atlantic Bight water, but also help settle the question of the Virginia Coastal water mass.

The temperature-salinity scatter diagram from the April-May 1992 cruise (Figure 4.3-31(a)) reflects a relatively simple picture of colder, fresh shelf water mixing with the warmer, saltier upper layers of the Slope Water and Gulf Stream. The only identifiable mixing end points within shelf waters are the cold band water at 7°C and 33 psu, and the Chesapeake Bay plume. Otherwise, the shelf water represents a broad range of temperature-salinity characteristics indicative of mixing with Slope Water. The volume and freshwater fraction of Chesapeake Bay discharge was low during spring 1992, so that the Bay plume water lost a significant amount of its salinity difference between the ambient shelf waters by the time it reached 36°15'N, Line A, the northernmost hydrographic and mooring transect. Salinities of the Chesapeake Bay plume at this location were 32.5 psu (Figure 4.3-31(a)). The temperature-salinity scatter diagrams from the August-September 1992 cruise (Figure 4.3-31(b)) appear structurally similar to the April-May diagram (Figure 4.3-31(a)). The primary changes are the warming of shelf waters, and the addition of low salinity water from rivers and estuaries. In 1992, this water is chiefly from the Chesapeake Bay. In contrast to these changes in the upper-layer

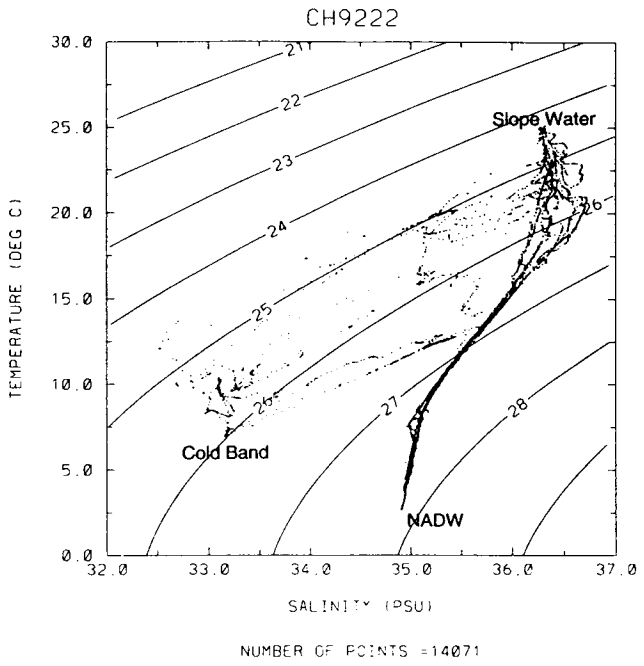

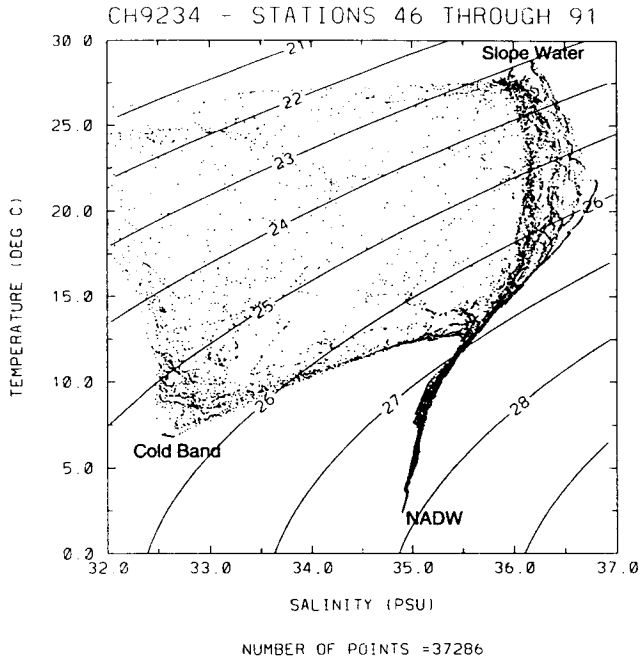

Figure 4.3-31. Temperature-salinity scatter diagrams from cruises in (a) Spring 1992 and (b) Summer 1992. Chesapeake Bay Plume is offscale to left. Cold Band Water, Slope Water, and North Atlantic Deep Water (NADW) are identified.

waters, the temperature-salinity characteristics of the cold-water band are nearly invariant between spring and summer cruises.

The stronger spring runoff in 1993 produced a pronounced Chesapeake Bay plume. The plume delivered a sufficient volume of low-salinity water to reduce inner-shelf surface salinities in the study region to less than 30 psu, as discussed in Section 4.3.2. Despite these marked interannual changes in the strength and distribution of Chesapeake plume waters, the remainder of the shelf showed relatively little interannual change in temperature-salinity characteristics. The temperature-salinity diagrams from May 1993 (Figure 4.3-32(a)) and August 1993 (Figure 4.3-32(b)) show the effect of the cold band water advecting southward over the outer shelf. In May, water colder than 8°C is distributed over a broad range of salinities, whereas in the summer, the cold band water had a comparatively narrow salinity range centered near 32.7 psu. The scatter diagram from summer 1992 (Figure 4.3-31(b)) indicates that, while the cold band of 1993 was colder, the salinity appears almost identical. The slightly colder temperatures in 1993 may reflect the stable upper-layer insulation that the spring buoyancy flux provided this year. The invariant salinity might suggest that the interannual variation in the production of winter water from the Gulf of Maine (where the cold band water originates) was small.

Lower coastal runoff, autumnal cooling, and stronger wind stress create more homogeneous water-mass conditions in the southern Middle Atlantic Bight in the fall and winter. The November 1992 temperature-salinity diagram (Figure 4.3-33(a)) indicates that the Chesapeake Bay plume end-point was probably not much fresher than 32 psu, and that the cold band over the outer shelf had lost much of its temperature difference, presumably by vertical mixing. The October-November 1993 cruise data show this cold-band erosion in progress (Figure 4.3-33(b)). Again, the low-salinity end point is produced by the Chesapeake Bay plume. The temperature-salinity scatter diagram and the surface salinity map (Figure 4.3-30) show that the plume's salinity was only slightly less than 32 psu. Both are indications that the plume's buoyancy flux at this time of year was not sufficient to produce a strong plume extending toward Cape Hatteras in the presence of the mixing.

Although the 1992-93 data covered only the Middle Atlantic Bight region south of 36°15'N, there is little evidence from the property distributions or the temperature-salinity structure for a separate water mass that is sufficiently large or stable to warrant

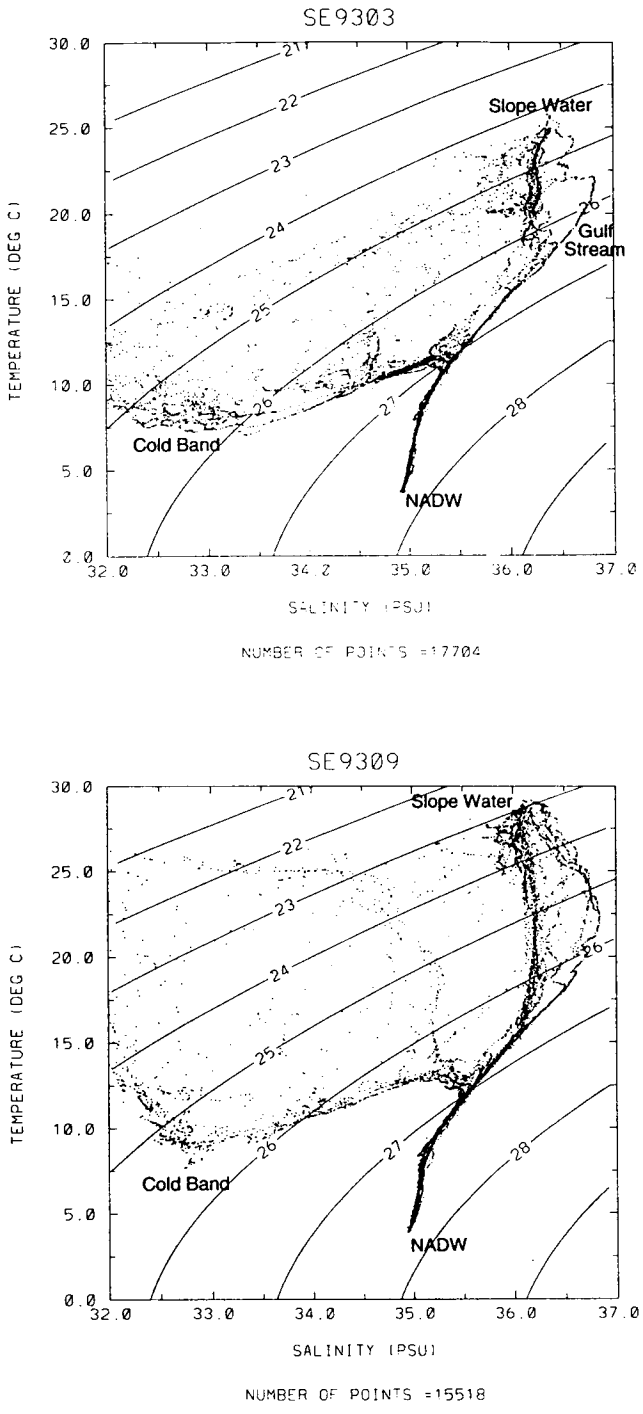

Figure 4.3-32. Temperature-salinity scatter diagrams from cruises in (a) Spring 1993 and (b) Summer 1993. Annotated as in Figure 4.3-31.

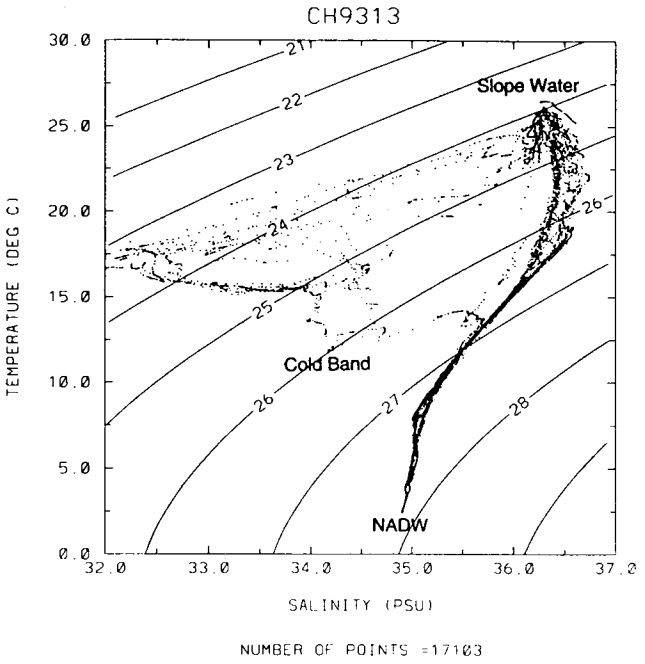

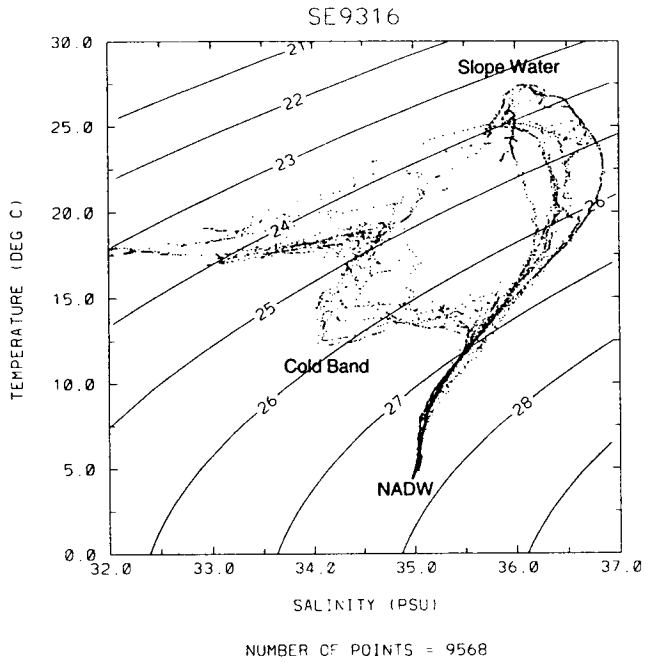

Figure 4.3-33. Temperature-salinity scatter diagrams from cruises in (a) Fall 1992 and (b) Fall 1993. Annotated as in Figure 4.3-31.

designation as Virginia Coastal Water. Both the present and previous studies indicate that the temperature-salinity characteristics of the deeper shelf waters represent a continuous southward flowing band of water from Georges Bank to Cape Hatteras, a band that is modified by mixing with Slope water and the fresher upper layers as it progresses. The upper layers of the southern Middle Atlantic Bight are freshened during both the stratified and unstratified seasons by introduction of fresh water from rivers and estuaries. Because the Chesapeake Bay outflow constitutes approximately half of all the freshwater introduced directly (rather than indirectly via the flow from the Scotian Shelf and the Gulf of Maine around Georges Bank) to the Middle Atlantic Bight, it can exert a strong influence in the makeup of the upper layers of the shelf waters south of the Bay entrance. Furthermore, the transport and mixing processes can filter the time-variable signal of the Bay discharge so that the middle and outer portions of the shelf show relatively slowly varying salinity compared with the inner shelf, where the plume typically resides. However, the buoyancy flux from the Chesapeake Bay and the wind-influenced behavior of the Bay plume on the continental shelf are still so variable that an attempt to establish even a seasonal water mass that exhibits sufficient distinction from the continuum of the upper layers of the Middle Atlantic Bight would seem to counterproductive. A detailed volumetric temperature-salinity census by season for the entire Middle Atlantic Bight might reveal a repeatable node in a bivariate distribution, but such a subdivision is not expected to be helpful in this highly variable shelf region.

4.4 Tides

Tides are mixed along the North Carolina coast with the semi-diurnal constituents dominant. Tidal currents were analyzed for surface and bottom meters using standard harmonic constituent methods (Foreman 1979). The results are shown in Figures 4.4-1 through 4.4-4 for the M_2 and K_1/P_1 constituents. These figures represent a northward continuation of the tidal analyses given in the FRED report (FRED Group 1989) for Raleigh and Onslow Bays and complements the earlier study of Pietrafesa *et al.* (1985) for Onslow and Long Bays.

The M_2 tide is approximately in phase along the coast. The mouth of the Chesapeake Bay lags Duck and Cape Hatteras by about 20° (about 40 minutes), because of the effects on the tidal wave of the

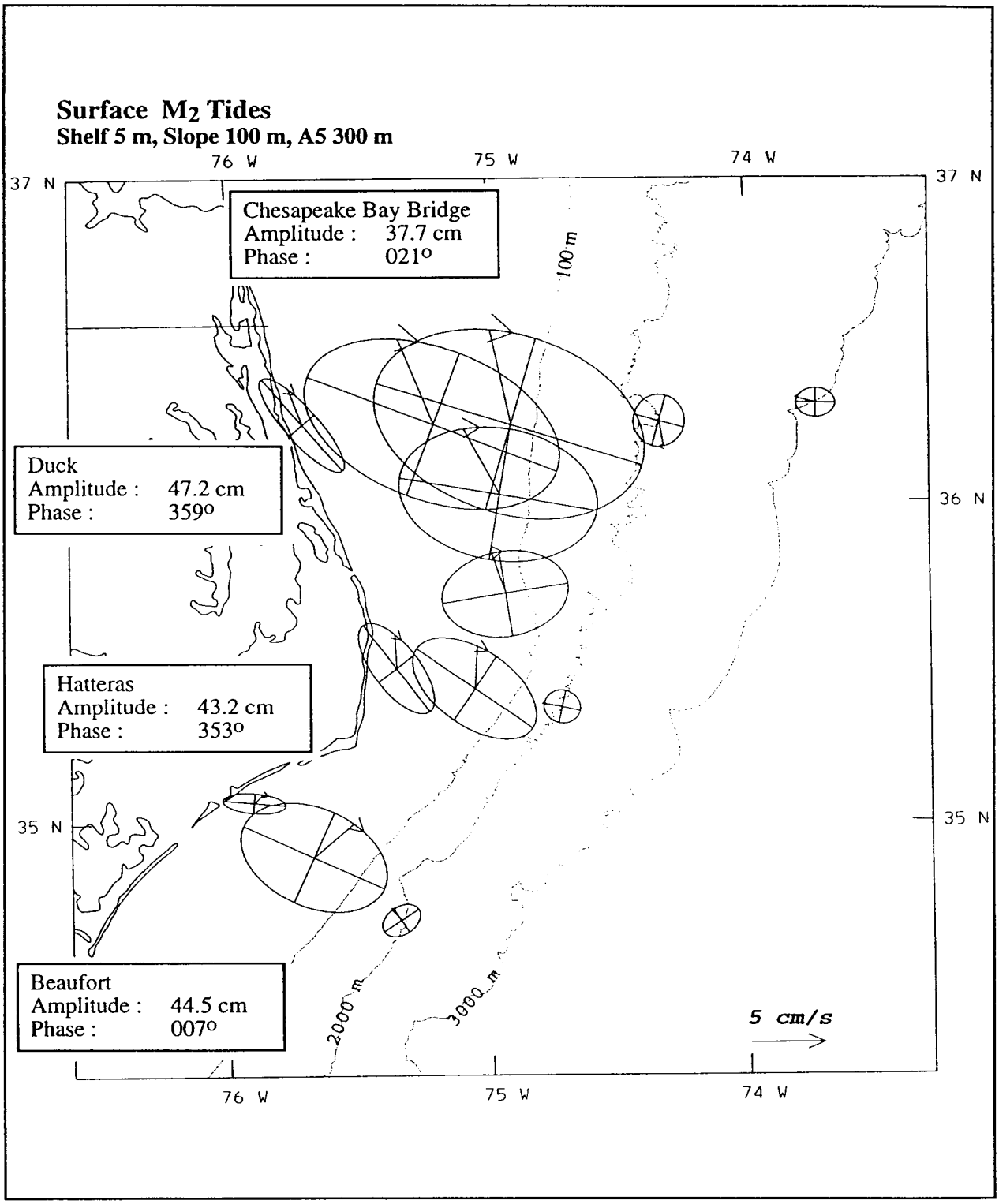

Figure 4.4-1. M_2 near surface tidal current ellipses. The arrow shows the direction of rotation and the Greenwich phase angle. Surface M_2 tidal amplitudes and phases are given for the coastal stations.

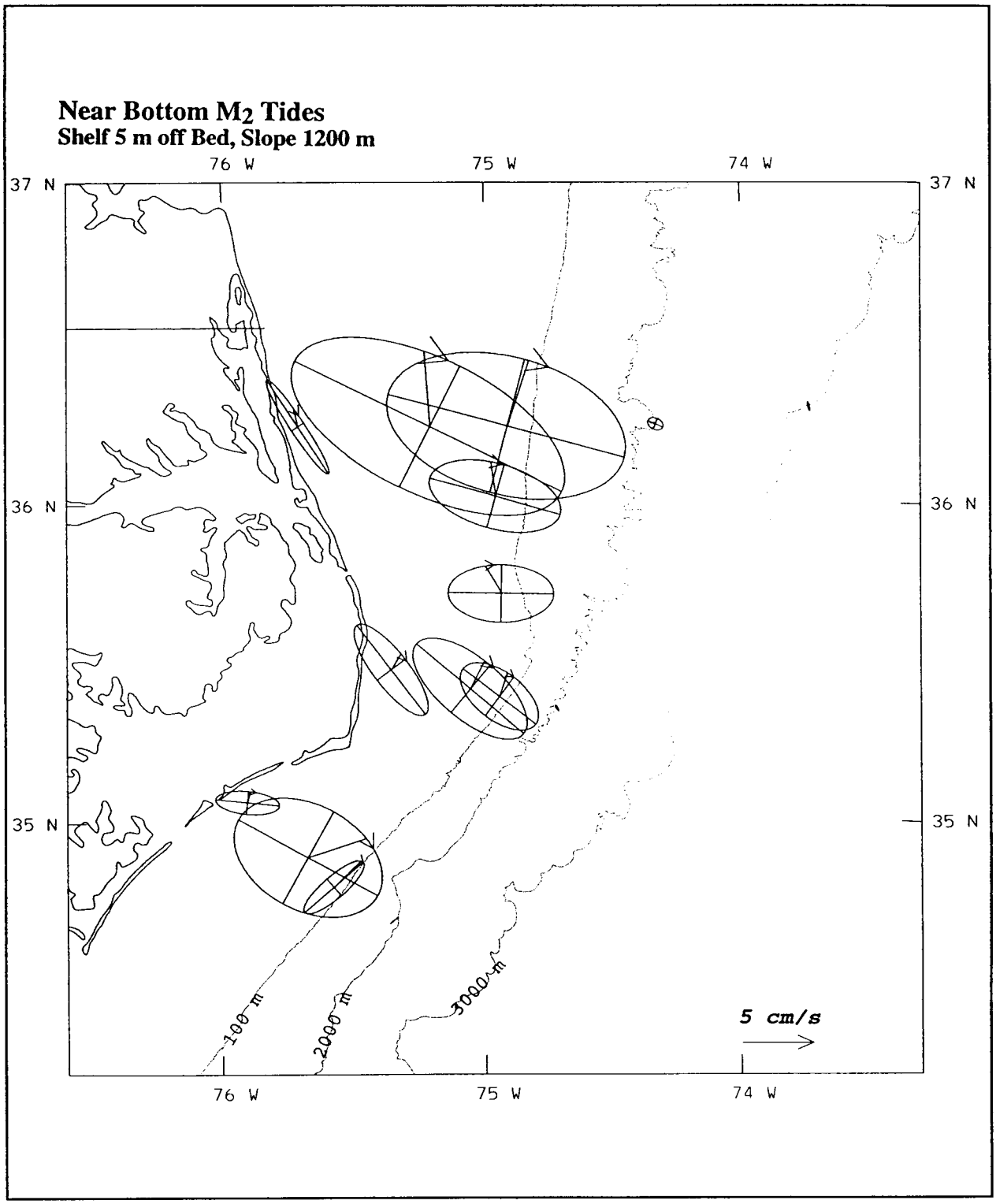

Figure 4.4-2. M_2 near bottom tidal current ellipses. The arrow shows the direction of rotation and the Greenwich phase angle.

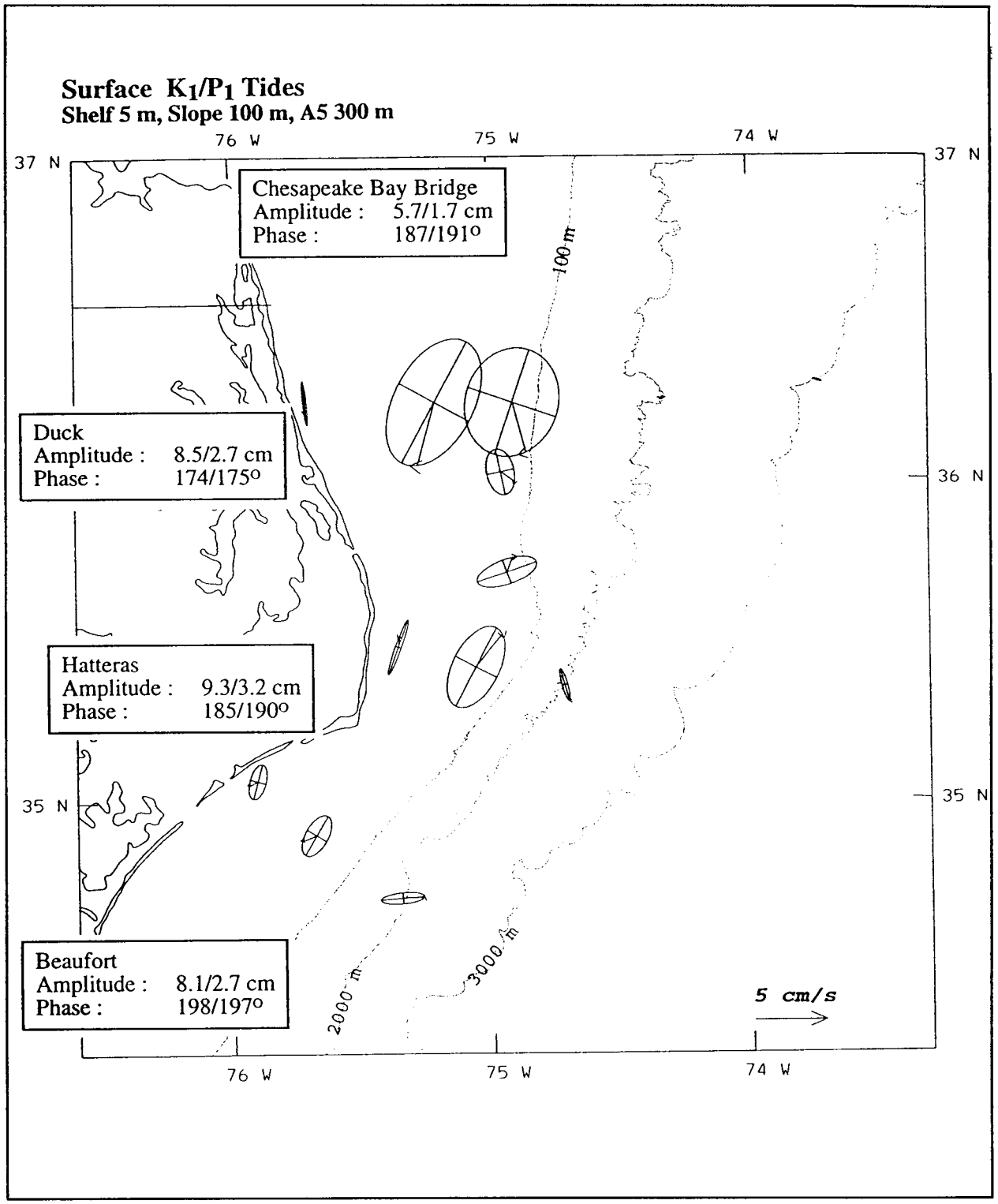

Figure 4.4-3. K_1/P_1 near surface tidal ellipses. The arrow shows the direction of rotation and the Greenwich phase angle. Surface K_1/P_1 tidal amplitudes and phases are given for the coastal stations.

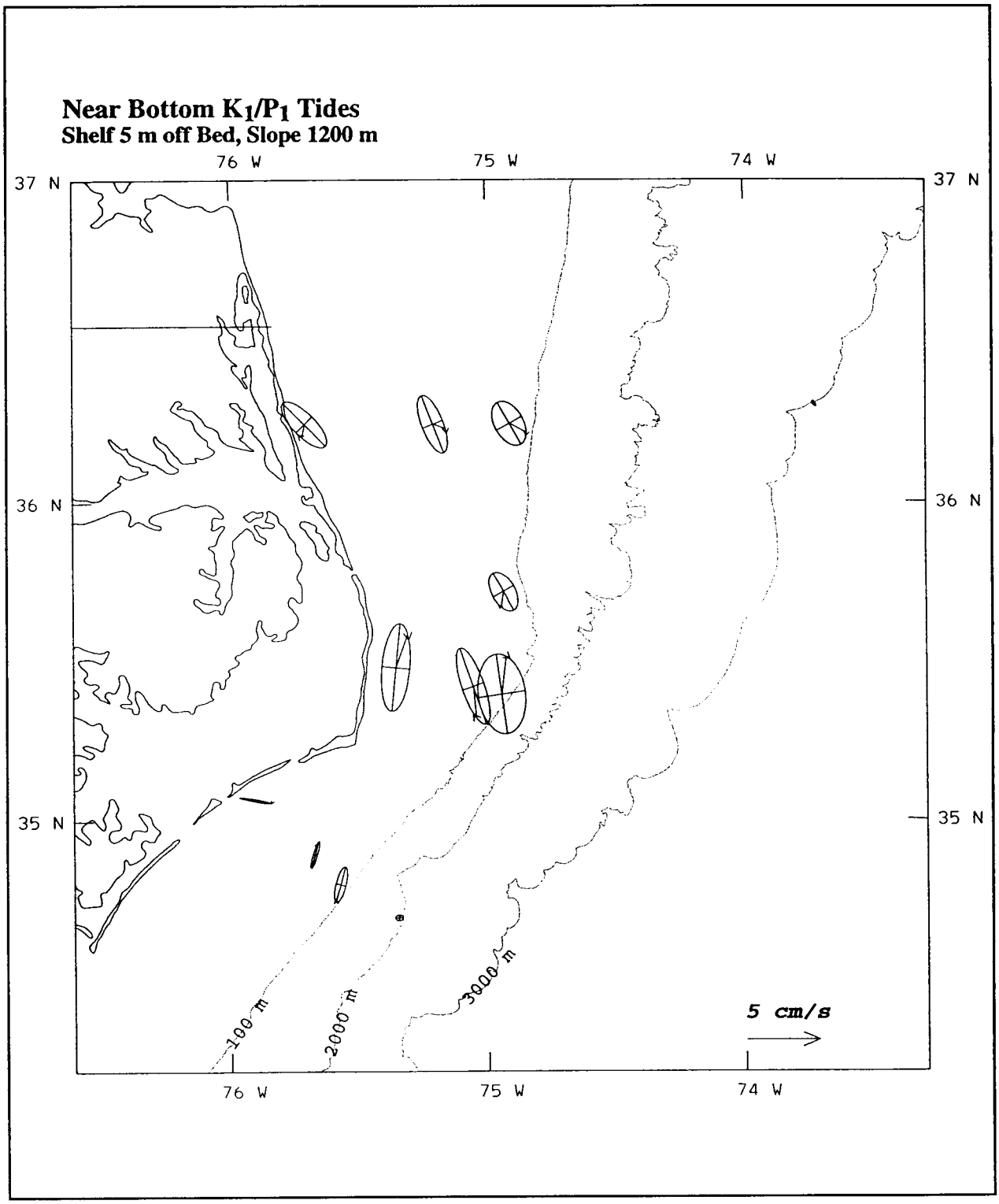

Figure 4.4-4. K_1/P_1 near bottom tidal ellipses. The arrow shows the direction of rotation and the Greenwich phase angle.

Chesapeake Bay. The M_2 tidal currents are also in phase across the shelf (Figures 4.4-1 and 4.4-2) lagging the surface tide by about 90°. Thus, a standing wave is generated by the M_2 tide across the width of the shelf with generally weaker currents near shore and nearer the shelf break and stronger currents at mid-shelf. The major axes of the tidal ellipses are approximately perpendicular to the isobaths. There is a marked effect of shelf width on the M_2 tidal current amplitudes with larger currents occurring as the shelf width increases to the north (compare bottom tidal amplitudes at B3, D2, D1 and A3; Figure 4.4-2). The FRED Group (1989) showed an increase of M_2 tidal current amplitudes with increasing shelf width to the southwest in Raleigh and Onslow Bays. The general characteristics of the M_2 tidal currents are explained by application of the theory of Battisti and Clark (1982) and Clarke (1991), where the coast is relatively straight and the deep sea tide has low variability along the shelf break. The M_2 tidal currents over the slope are weak in the upper water column and non-existent below about 800 m and show inconsistent phase relations. Unlike over the shelf, major and minor axes are approximately equal. There is no evidence of internal tide generation at the shelf break in these current data, unlike the bottom amplification found off Frying Pan Shoals, where the upper slope is less steep (FRED Group 1989).

The diurnal constituents of the surface tide are about 20 to 25% of the semi-diurnal. Excluding the distortions of the Chesapeake Bay, the diurnal tide appears to propagate southwards around Cape Hatteras. In general the K_1/P_i tidal current ellipses (Figures 4.4-3 and 4.4-4) are fairly uniform both along and across the shelf. The currents south of Cape Hatteras are a little weaker, particularly near the bottom, than further north on Line A. The bottom ellipses tend to be rotated anticlockwise relative to isobaths and the surface ellipses, which is consistent with frictional damping for tidal frequencies > f. The cross shelf phase structure on Lines A, B and C seems complex with evidence of a 180° shift between outer and inner shelf. Apart from this, the diurnal constituents are generally consistent with a southward propagating shelf wave (Clarke 1991). The presence of the Gulf Stream at the shelf break south of Cape Hatteras may distort the wave characteristics and may be responsible for the complex cross-shelf structure observed in the diurnal currents. Even more so than with the M_2 currents, the diurnal current amplitudes in deep water are very small, except at the 100 m level at C4 where they are comparable to the shelf currents (~1.5 $cm \cdot s^{-1}$).

4.5 Dynamics of the Cross-shelf Cape Hatteras Front

One of the most remarkable features of the study region is the front separating the Middle Atlantic Bight and South Atlantic Bight shelf water masses. Situated shoreward of a western boundary current and cutting across isobaths, the dynamics of this type of front have rarely, if ever, been subject to scientific investigation.

Some general characteristics of the front are seen in the surface salinity fields of the six hydrographic surveys (Figure 4.5-1). The front is seen to be tightly spaced, order 10 km wide, in all but one field, that of the August 1993 survey. All fields show the front extending southward and onshore over the outer shelf. Frontal orientation seen in this region is typically only slightly (5-15°) clockwise of the shelf-edge. Frontal widths observed over the outer shelf vary considerably: from 5 to 35 km. In all fields, the front veers sharply to the coast over the middle and inner shelf in Raleigh Bay.

Considerable insight into the workings of the front is gained by examining the temperature and velocity records from the mid-shelf mooring B2. This mooring was frequently traversed by the front as indicated by the large and abrupt changes in the mooring's temperature and salinity records. Shown here are sample wintertime records of temperature and velocity measured at the mooring (Figures 4.5-2,3). To give a sense of the character of the currents directed along and across the front, the velocity records in these illustrations are separated into approximate along- and across- front components. In computing these velocities, a frontal orientation of 40°T was chosen. Based on the surface salinity fields of the hydrographic surveys, this was judged to be the "typical" frontal orientation at the mid-shelf. In examining the records from mooring B, it is useful to consider the direction of frontal movement past the mooring. Because higher temperature water is always situated seaward of the front, a significant increase in temperature at the mooring signals a shoreward advance of the front, while a large temperature decline indicates a seaward retreat of the front.

Significant differences between the structure of the retreating versus the advancing front are revealed by a disparity in the character the temperature increases and decreases seen in at mooring B2. Most of the large temperature increases recorded at

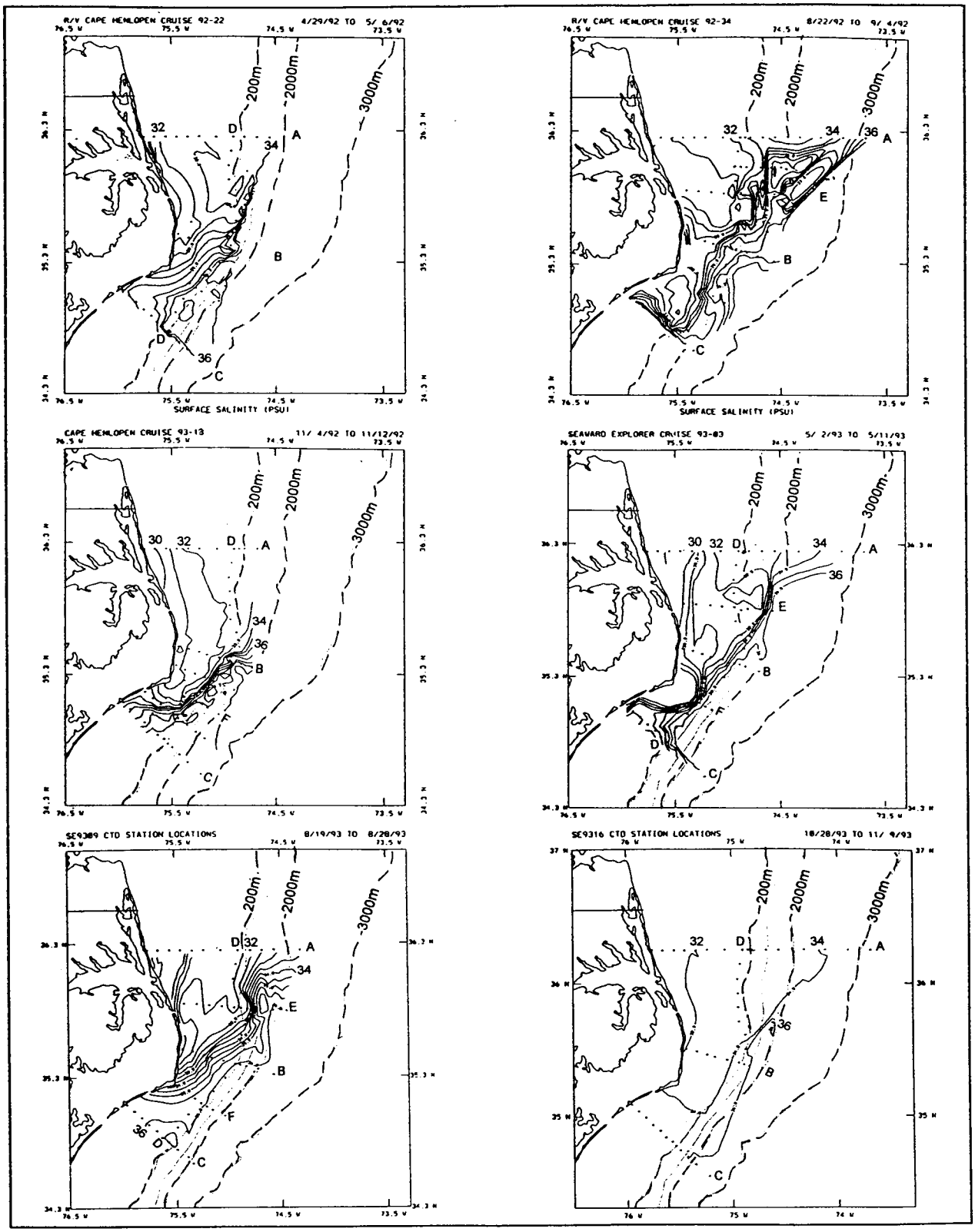

Figure 4.5-1. Surface salinity contours from hydrographic cruises CH9222, CH9234, CH9313, SE9303, SE9309, and SE9316.

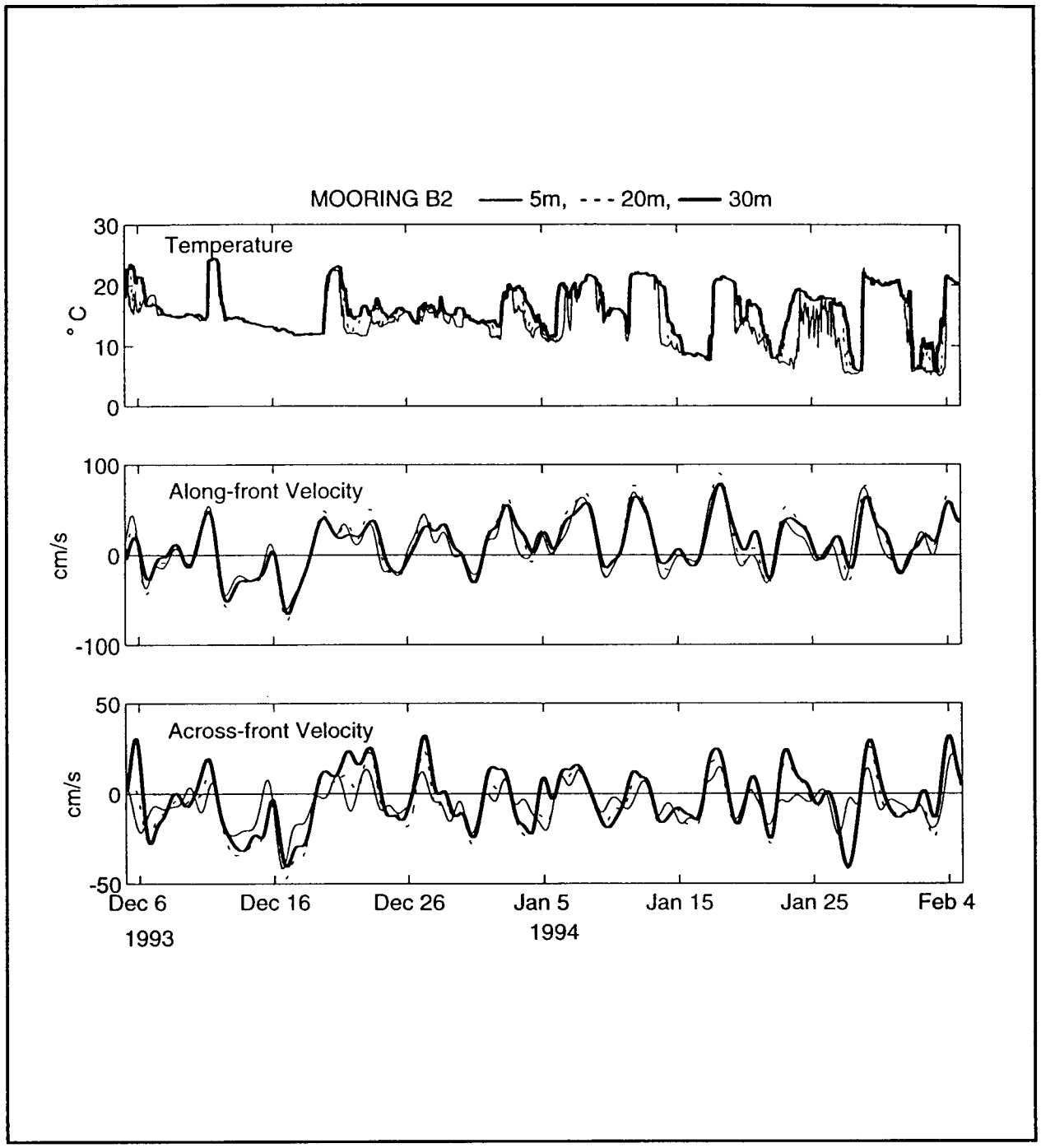

Figure 4.5-2. Time series of temperature and velocity measured at mooring B2 during December 6, 1993 through February 4, 1994. As detailed in the text, the velocity components are directed roughly along and across the front at the southern boundary of Middle Atlantic Bight shelf water. Along-front velocity is positive to the northeast (offshore). Across-front velocity is positive to the northwest (onshore).

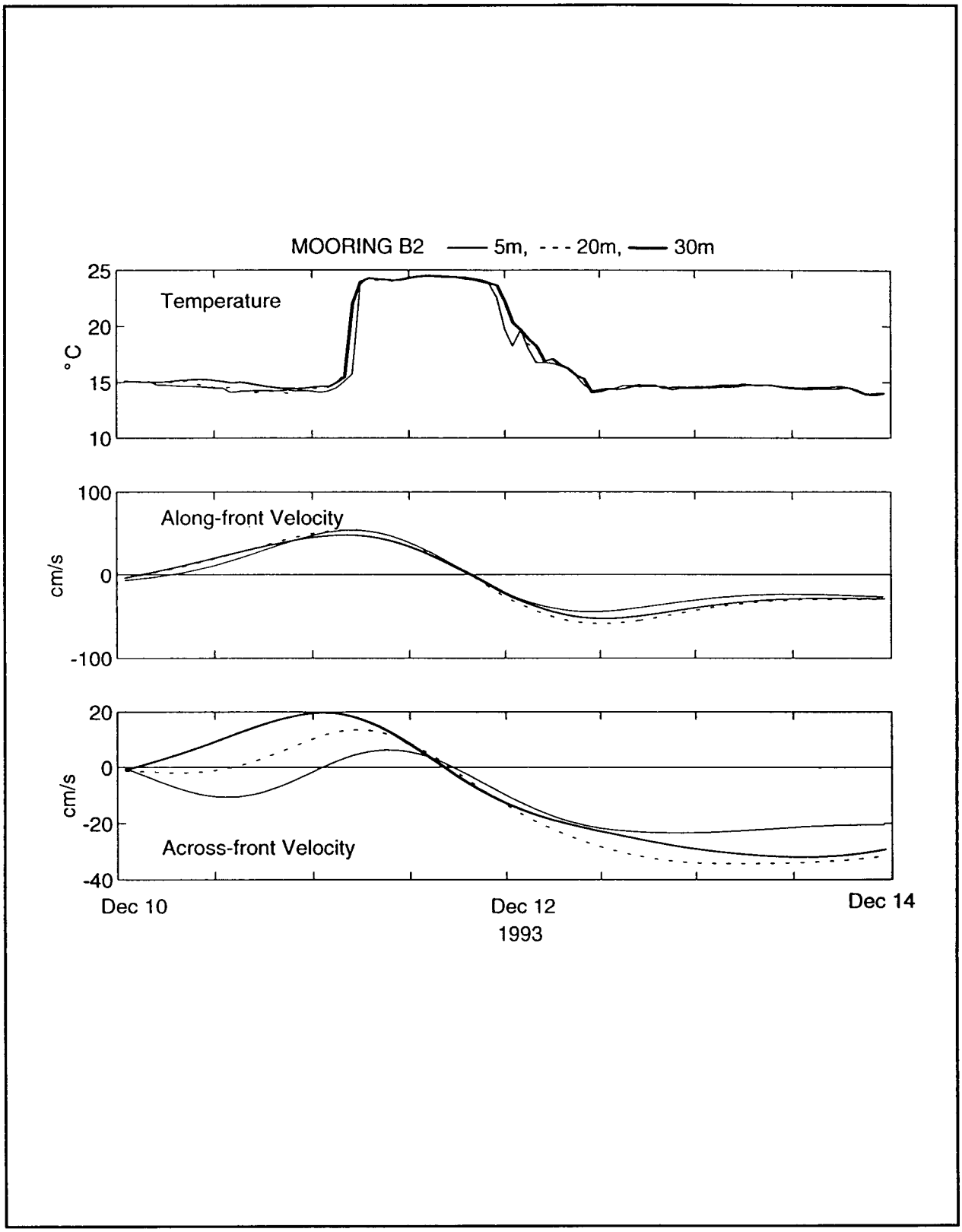

Figure 4.5-3. Time series of temperature and velocity measured at mooring B2 during December 10-14, 1993. Annotations same as Figure 4.5-2.

the mooring occur over a short period and are nearly simultaneous at the mooring's three measurement levels (Figures 4.5-2,3). It is not uncommon for the temperature at these levels to rise by 8°C or more over a period of six hours or less. This is seen six times in the two-month long segment of records shown in Figure 4.5-2. Such an occurrence can only be due to the passage of narrow and steeply inclined front (as illustrated in Figure 4.3-24). By contrast, the large temperature decreases seen at mooring B2 are relatively gradual and are not matched at all measurement levels; an indication that the retreating front tends to be broader and more gently inclined than the advancing front.

The measurements from mooring B2 also reveal significant differences in currents at the front which are associated with its direction of motion. In general, the estimated across-frontal velocity is related to frontal movement as deduced from the temperature records in the sense expected: directed onshore during a significant temperature increase at the mooring (advancing front) and offshore when temperatures at the mooring significantly decline (retreating front). In almost every case, a strong northeastward (offshore) along-front flow is seen during a large rise in temperature at the mooring. Typically, the rise in temperature nearly coincides with a peak in the northeastward current (Figures 4.5-2,3). By contrast, the estimated along- front velocity tends to be relatively weak, and is sometimes directed onshore (southwestward), when the temperature at mooring B2 declines by a significant amount.

Taken together, the observations at mooring B2 suggest that the cross-shelf front at the southern boundary of Middle Atlantic Bight shelf water has two basic states, each of which is associated with the direction of frontal motion. An advancing front tends to be narrow and steeply inclined, and contain a strong northeastward convergent flow. In comparison with the advancing front, a typical retreating front is relatively broad and gently inclined. Its along-front flow is comparatively weak and sometimes directed to the southwest. These differences are clearly seen in the four-day long record segment of Figure 4.5-3, which shows a single rise and fall in temperature at mooring B2.

V. SHELF SLOPE PROCESSES

Considered in this section is the interaction of coastal and deep sea water masses within the study region. In the most general of classification schemes, the study region contains two coastal water masses: Middle Atlantic Bight and South Atlantic Bight shelf water, and two deep sea water masses: the Gulf Stream and the Slope Sea. Although constantly in motion and often breached, the boundaries of these water masses are reasonably well defined. As detailed in Section 4, the Middle Atlantic Bight and South Atlantic Bight shelf water masses are separated by a salinity front running across the shelf in the region of Diamond Shoals and in Raleigh Bay (Figure 4.5-1). The Gulf Stream flows along continental margin of the South Atlantic Bight, bordering South Atlantic Bight shelf water, before veering seaward in the vicinity of Cape Hatteras. Within the deep ocean northeast of Cape Hatteras, the Gulf Stream is bordered to the north by the Slope Sea, which also forms the seaward boundary of Middle Atlantic Bight shelf water.

The influence of the Gulf Stream on the study region's coastal water masses is dealt with in Sections 5.1 and 5.2. Topics to be considered are the effects of Gulf Stream motions on shelf currents and coastal sea level, intrusions of Gulf Stream frontal eddies onto the shelf south of Cape Hatteras and the migration of displaced Gulf Stream water to the Middle Atlantic Bight shelf. A detailed treatment of Middle Atlantic Bight shelf water export to the Gulf Stream is given in Section 5.3. Finally, the effects of Slope Sea currents and intrusions on Middle Atlantic Bight shelf water are dealt with in Section 5.4.

5.1 Gulf Stream Influence

Because of its proximity to the shelf-edge, the Gulf Stream has a considerable impact on the shelf environment over the southern portion of the study region. In this area, which includes Raleigh Bay and Diamond Shoals, Gulf Stream meanders and displaced filaments from Gulf Stream frontal eddies regularly intrude onto the shelf. Their influence on the shelf motions and water properties is dealt with in this section.

Sections 2 and 4 pointed out that the Gulf Stream path undergoes a number of shifts with changes in meander amplitudes. Meander activity is almost always present at outer shelf moorings B3 and C3 even when the Gulf Stream moves offshore between February and May

1993. Analysis of the seasonal statistics in Section 4.1 showed greater penetration of Gulf Stream currents into Raleigh Bay and along Line B and at D2 during the summers of 1992 and 1993 than in the intervening winter period. There are also subtle differences between the two summers which generally correspond to the Gulf Stream being a little further offshore in 1993 than in 1992. Thus, the analyses which follow will concentrate on the same three seasons and attempt to quantify the degree to which the Gulf Stream currents are observed on the outer to mid-shelf. Less influence on the shelf in winter is expected because of the lack of shelf stratification and stronger density contrast across a sharper Gulf Stream front seem to inhibit meander fluctuations from penetrating onto the mid-shelf in Raleigh Bay. This may be the case even if there is no offshore shift in the Gulf Stream path such as occurred after the cold core ring interaction at the beginning of December 1992.

5.1.1 Gulf Stream Influence on Coastal Sea-Level

The Gulf Stream has its closest approach to the coast since leaving the Straits of Florida at Cape Hatteras. Meander or cross-stream fluctuations could be communicated across shelf and induce sea-level variability that is separate from that caused by local wind-forcing and southward propagating shelf waves from the Middle Atlantic Bight shelf (Wang 1979). Sea-level forcing by the Gulf Stream could induce a shelf wave component propagating south into the South Atlantic Bight and affect the development of sea-level differences between Duck and Cape Hatteras, which are a forcing mechanism for Virginia Coastal Water intrusions into Raleigh Bay (FRED Group 1989).

The meander periods of interest are 3 to 10 days which are similar to the wind-forced response of shelf currents and coastal sea-level. If the Gulf Stream front is modeled as a meandering wall intruding over the shelf break then sea-level will be changed by volume conservation such that a shoreward moving front, represented by onshore cross isobath velocities in the upper layers of the Gulf Stream, will cause an increase in sea-level. This effect will be most marked when the volume of shelf water or alternatively the shelf width is small. Meander induced sea-level fluctuations at the coast do not necessarily mean that the Gulf Stream directly influences along shelf currents over the mid to inner shelf. The cross and along isobath velocity components measured during the passage of a meander crest are very similar and are in quadrature

(Bane *et al.* 1981). Therefore, in testing for the presence of this effect, the coherence of the u or v component with sea-level could be used. In this section the u component is used because it is more closely related to the rate of change in the position of the front.

At subweekly frequencies, the Gulf Stream can also affect sea-level by changes in transport. An increase in transport, and hence, upper layer Gulf Stream velocities, will cause a decrease in sea-level at the shelf break and the signal can be propagated across quite wide shelves (Noble and Geflenbaum 1992). This is approximately opposite to the meander continuity effect on sea-level where an increase in upper layer currents is accompanied by shoreward movement of the meander crest. The subweekly transport effect does not require that the Gulf Stream change its position on a transect. Noble and Geflenbaum (1992) verified that sea-level changes at the shelf break off Charleston are related to transport and are communicated to the coast with a reduction in amplitude of less than 21%. They also found that changes in Gulf Stream transport on subweekly to seasonal time scales were not significantly related to changes in its cross-slope position.

Figure 5.1-1 shows coherence squared between the cross-slope velocity component at the 100 m level of the slope mooring C4 and sea-level at Cape Hatteras, Duck and Beaufort for three periods. The cross slope component of the current is used as a surrogate for the onshore-offshore movements for the Gulf Stream front directly offshore of the Cape Hatteras tide gauge. In the summer of 1992 (Figure 5.1-1(a)), there is moderate coherence for periods longer than about 7 days and a 180° phase difference for Cape Hatteras sea-level versus Gulf Stream meander currents. The 180° phase difference is consistent with offshore directed currents generating a decrease in sea-level. The Gulf Stream currents are not coherent with Duck sea-level to the north of Cape Hatteras and only moderately coherent with Beaufort (to the south) at periods longer than about 14 days. Examination of the longshore coherence squared between Duck, Cape Hatteras and Beaufort (Figure 5.1-2(a)), shows there is a lack of coherence between Duck and Cape Hatteras in the energetic 3-11 day band. Coherence between Cape Hatteras and Beaufort is high to moderate at all frequencies with Cape Hatteras leading Beaufort. Thus, it appears that the Gulf Stream is influencing sea-level at Hatteras for periods of 7 to 11 days and some of that signal is propagating southwards. No Gulf Stream influence is discernable at Duck.

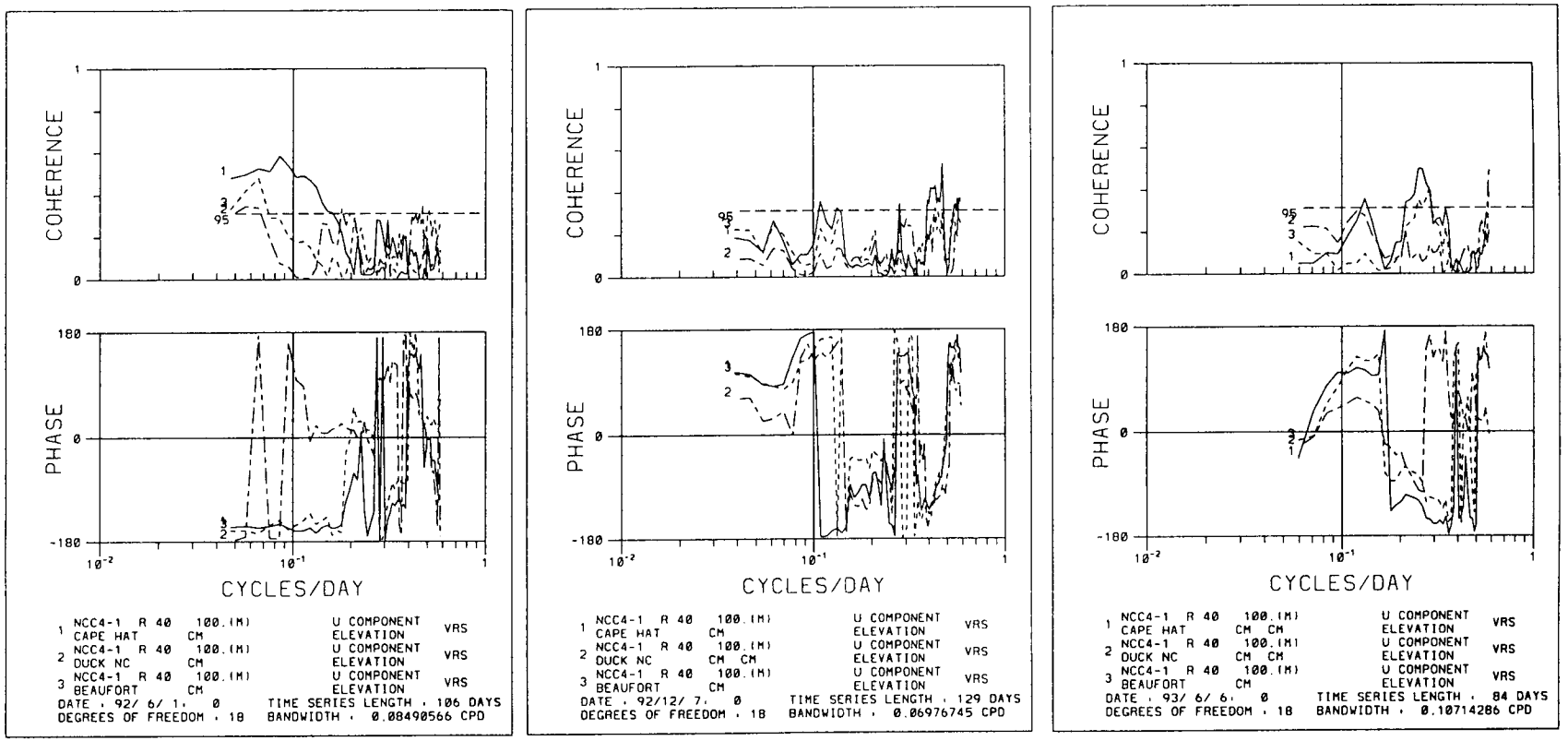

Figure 5.1-1. Coherence squared and phase differences between cross-slope currents at C4 and indicated sea-level for (a) summer 1992, (b) winter 1992-1993, and (c) summer 1993.

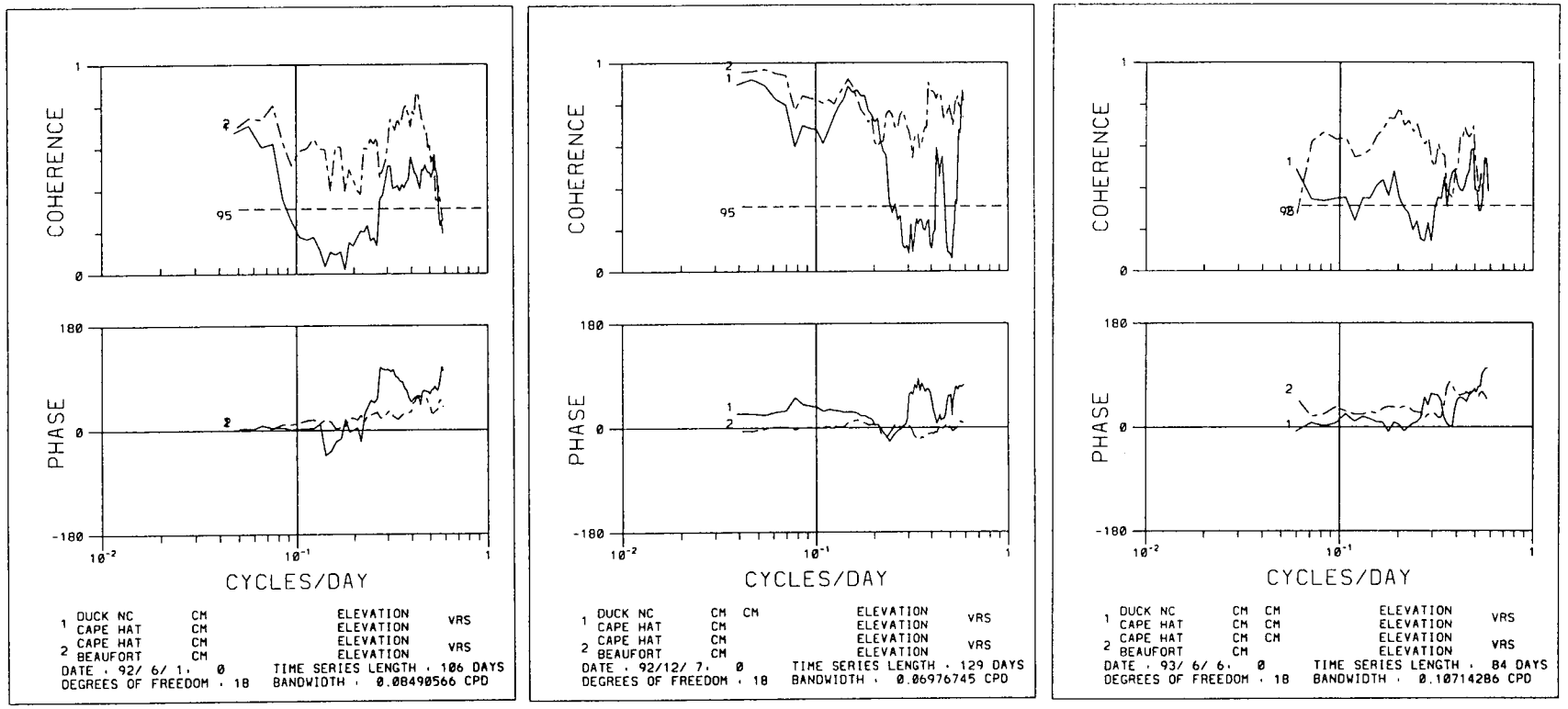

Figure 5.1-2. Coherence squared and phase differences between the indicated sea-levels for (a) summer 1992, (b) winter 1992-1993, and (c) summer 1993.

In the winter of 1992-93, the Gulf Stream moved offshore and there appears to be less penetration onto the outer shelf in Raleigh Bay. There is no significant connection of Gulf Stream currents to the sea-level at all three stations (Figure 5.1-1(b)) and, in contrast to the summer, longshore coherence is high (Figure 5.1-2(b)), particularly in the energetic 4-10 day band of the meanders. Duck leads Cape Hatteras by about 20° but Cape Hatteras and Beaufort are very nearly in phase indicating more local wind forcing south of Hatteras.

In the summer of 1993, the Gulf Stream was a little more offshore than 1992 and in this case, the 3-5 day band Gulf Stream currents are weakly coherent with Cape Hatteras and Beaufort sea-level (Figure 5.1-1(c)). There is no coherence with Duck sea-level and, in contrast to the other two seasons, there is only weak coherence at all frequencies between Duck and Cape Hatteras. There are similar coherences to the summer of 1992 of Cape Hatteras with Beaufort with Cape Hatteras leading Beaufort as before (Figure 5.1-2(c)).

Therefore, there is evidence from the coherence analysis that the Gulf Stream influences sea-level at Cape Hatteras, and by implication, the shelf circulation in the summers of 1992 and 1993, though in different meander frequency bands (7 days and longer in 1992 and 3-5 days in 1993). This may be caused by slightly different Gulf Stream paths and meander characteristics in these two periods. In the intervening winter the inner shelf is isolated from Gulf Stream influence. Whether this is due to the Gulf Stream being displaced offshore or the presence of a stronger surface front is uncertain at present.

5.1.2 Summer 1992 Currents

The influence of the Gulf Stream on shelf currents is examined by calculating the coherence squared and phase differences between the alongshelf (v) component levels and the alongslope currents for upper levels at the slope moorings which are always in the Gulf Stream. For the summer 1992 period, these are given in Figure 5.1-3. On Line C there is a very high coherence between the shelf break C3 (30 m)) and the slope C4 (100 m) at frequencies lower than 0.3 cpd. There is however, no significant coherence between C4 (100 m) and the mid-shelf C2 (20 m). Therefore, on Line C, the Gulf Stream direct influence on the currents is restricted to the outer shelf. On Line B, there are moderate coherences between both

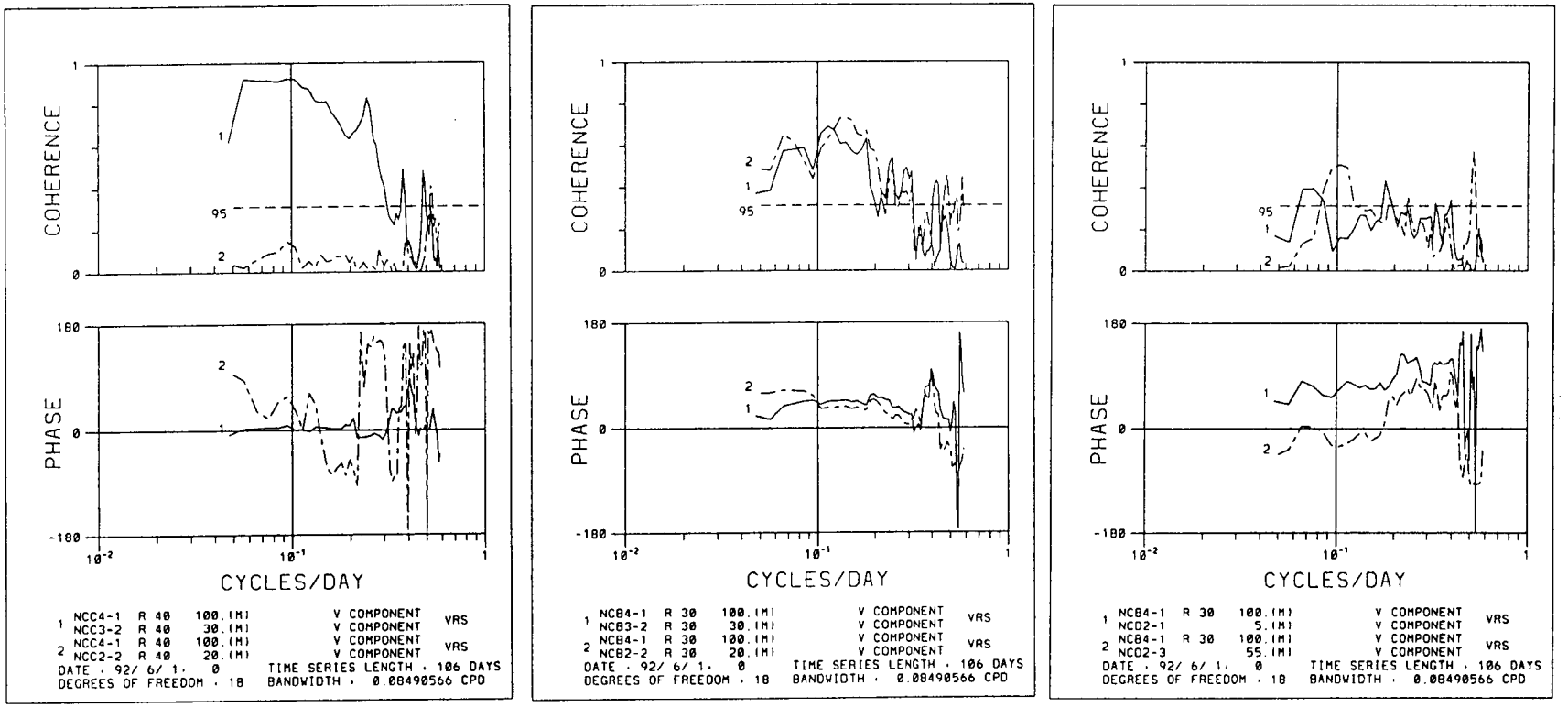

Figure 5.1-3. Coherence squared and phase differences between indicated alongshore (v) current components for the summer 1992, (a) Line C, (b) Line B, and (c) D2 and B4.

B2 (20 m) and B3 (30 m) v-components with the slope currents B4 (100 m). Note that in Figure 5.1-3(b) the currents are rotated 30° clockwise from north so that they are all in the same Gulf Stream frame of reference. The mean current statistics given in section 4 indicated that there may have been some slight curvature to the mean Gulf Stream (though this is not apparent in the imagery) which brings the Gulf Stream closer to Cape Hatteras than in Raleigh Bay. Therefore, Gulf Stream current fluctuations are reaching the 30 m isobath on Line B. Figure 5.1-3(c) shows coherences of B4 currents with the upper and lower levels at D2. It shows that both levels are slightly influenced by the Gulf Stream at periods longer than about 7 days. The structure of the relationship between B4 and D2 currents has been investigated using EOFs. It is quite complicated with different modes connecting the upper and lower layers at D2 to B4. Subsurface currents are more directed normal to the Gulf Stream while surface currents are directed parallel.

5.1.3 Winter 1992-1993 Currents

Similar coherences between Gulf Stream and shelf currents for winter 1992-1993 are given in Figure 5.1-4. On Line C, even the shelf break currents at C3 have little coherence with Gulf Stream currents except at very low frequencies. Middle shelf currents have similarly low coherences with C4 current. There are no data at the shelf break mooring B3 for this winter period, but the coherences between B4 and B2 alongshelf components show much weaker coherences than for the summer of 1992, except for periods centered around 14 days (Figure 5.1-4(b)). This seems to indicate that energetic short period meanders of 3 to 10 days remain off the shelf on Line C and probably only influence the shelf break on Line B. Longer period meanders of 10-20 days seem to have some moderate effects at mid-shelf on both transects. Very similar coherence patterns are observed between the Gulf Stream at B4 and currents at D2 (Figure 5.1-4(c)) which offers further evidence of the divorce of the shelf motions from the energetic 3-10 day period meanders.

5.1.4 Summer 1993 Currents

The cross-shelf coherence squared and phase differences for the summer of 1993 are given in Figure 5.1-5 for the same pairs of velocity components used in the above analyses. On Line C the 3-10 day period motions are coherent at the shelf break but not quite at the same level as in the summer of 1992. The mid-shelf, as before, is not significantly coherent with the C4 currents. The coherence

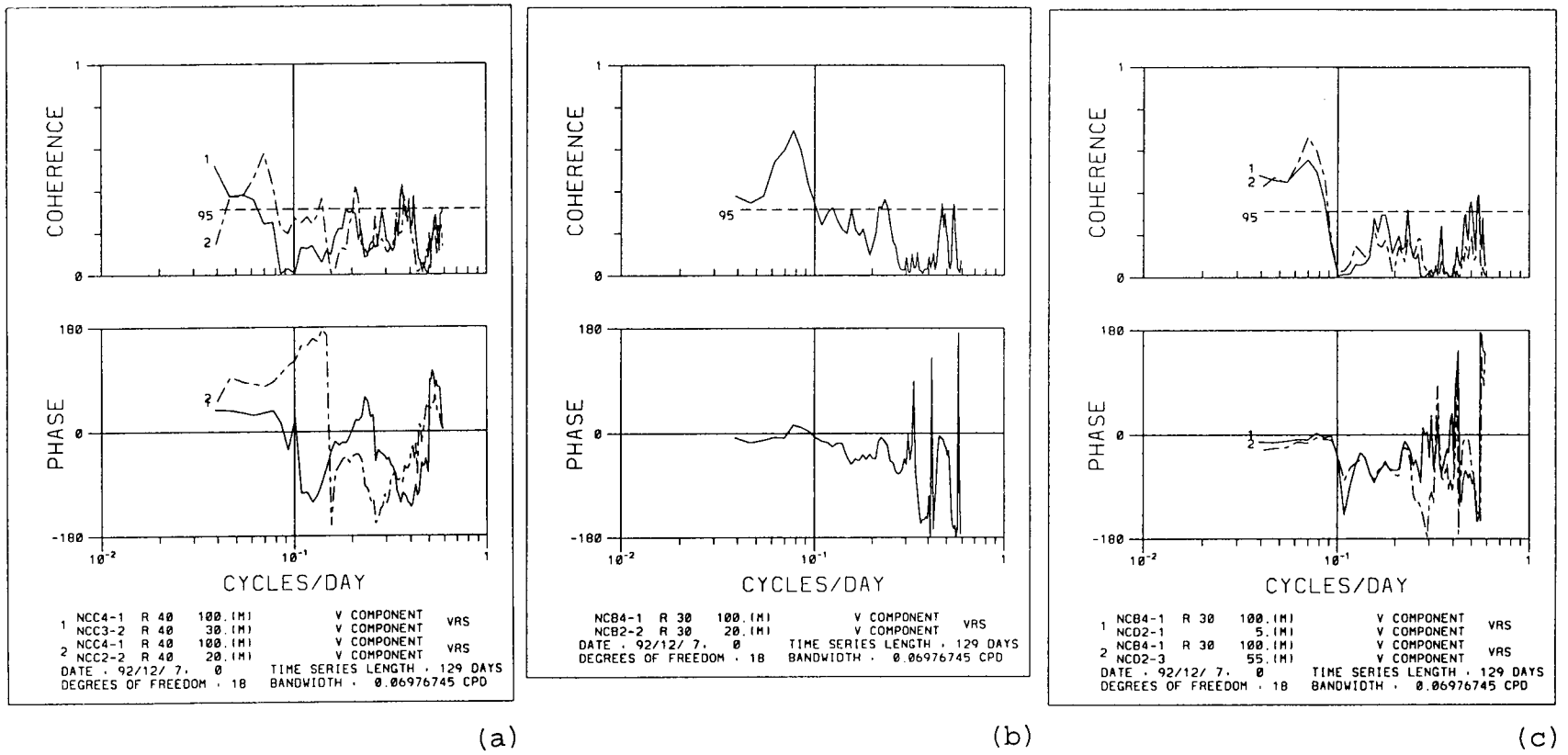

Figure 5.1-4. Coherence squared and phase differences between alongshore (v) current components for the winter 1992-1993 (a) Line C, (b) Line B, and (c) D2 and B4.

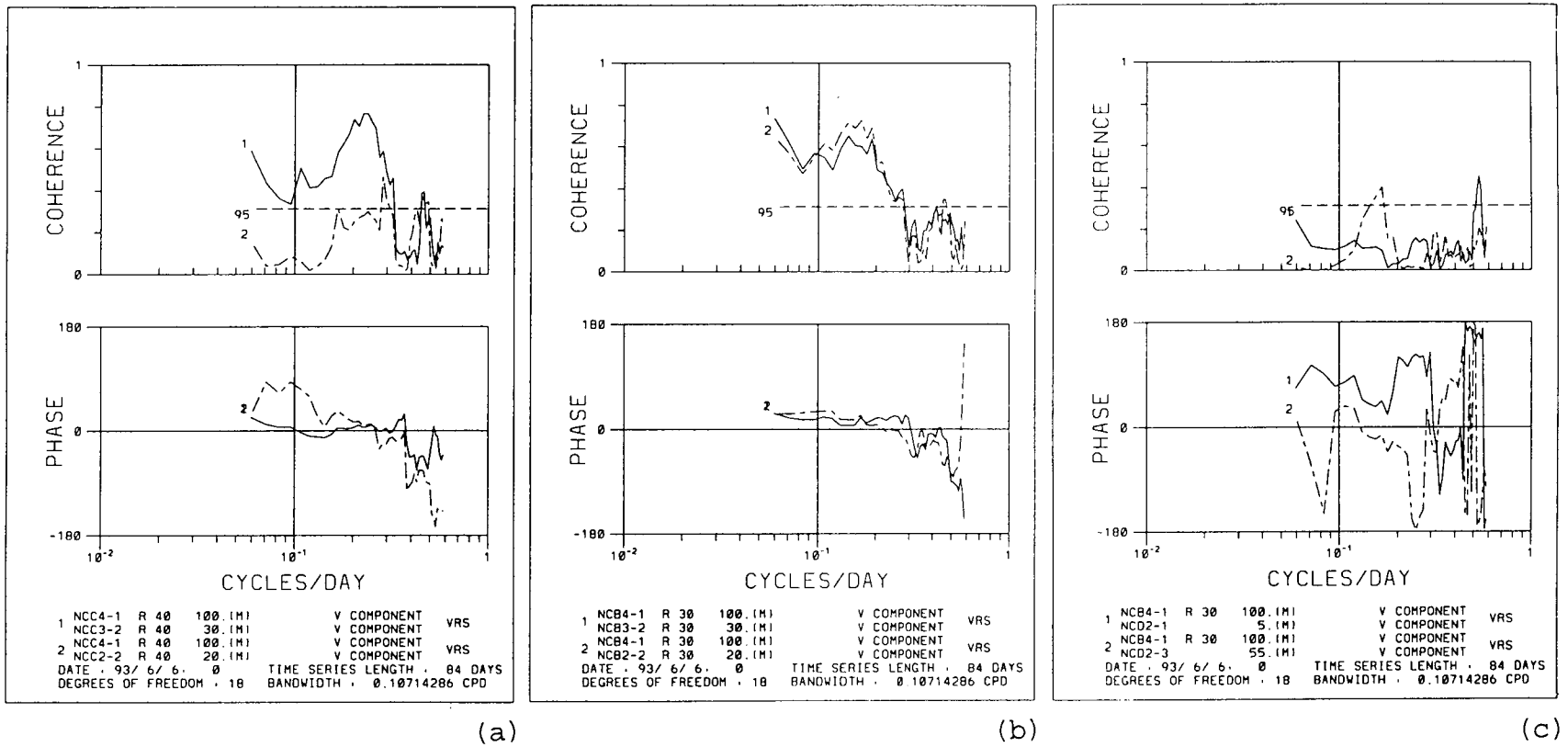

Figure 5.1-5. Coherence squared and phase differences between alongshore (v) current components for the summer 1993 (a) Line C, (b) Line B, and (c) D2 and B4.

squared between current components on Line B are very similar to these of the previous summer and again shows Gulf Stream meander motions penetrating to the 30 m isobath.

Between B4 and D2 there is almost no relationship, whereas in the summer of 1992 there were some marginal significance to the coherences. This is consistent with the Gulf Stream being slightly further offshore and curved slightly more southwards off the Middle Atlantic Bight than in the previous summer.

5.1.5 Evidence from Time Series

The Gulf Stream's influence on shelf-edge currents, explored statistically above, is clearly illustrated by the velocity records from the moorings along the 60 m isobath (Figures 5.1-6 and 5.1-7). These show frequent pulses of strong northeastward flow, marking the Gulf Stream's presence, at the Raleigh Bay and Diamond Shoals moorings (C3 and B3). At 30 m depth, these pulses occasionally attained magnitudes greater than 150 $cm \cdot s^{-1}$ and were typically in excess of 100 $cm \cdot s^{-1}$. In quantitative terms, the northeastward flow measured by the 30 m deep current meter on B3 exceeded 100[150] $cm \cdot s^{-1}$ 12[3]% of the time. Gulf Stream flows expectedly weakened going toward the bottom, but were still often in excess of 50 $cm \cdot s^{-1}$ at the shelf-edge current meters 5 m off the sea floor (20% of the time at B3). The Gulf Stream's penetration onto the shelf appears to have abruptly ceased just to the north of the Diamond Shoals section. The pulses of strong northeastward flow, frequent at the B3 mooring, were exceptionally rare at the D2 mooring just 35 km to the north, and were entirely absent 35 km further north at the D1 mooring.

The seasonal variation of Gulf Stream influence over Diamond Shoals, indicated by the above statistical analysis, is easily seen in the velocity records from the B3 mooring (Figures 5.1-6 and 5.1-7). Apparent in the first six months of these records (March through August 1992) are two distinct flow regimes. The latter, beginning in early June 1992, is characterized by stronger and more persistent northeastward flows, indicative of a greater Gulf Stream influence at B3. A similar and coincident change in flow characteristics is apparent in the first six month velocity record from mooring B2 (Figure 5.1-8), suggesting that the Gulf Stream's influence extended to the mid-shelf of Diamond Shoals. This pattern of increased and more persistent northeastward flows in summer is repeated in the B2 and B3 records of 1993 (Figures 5.1-7

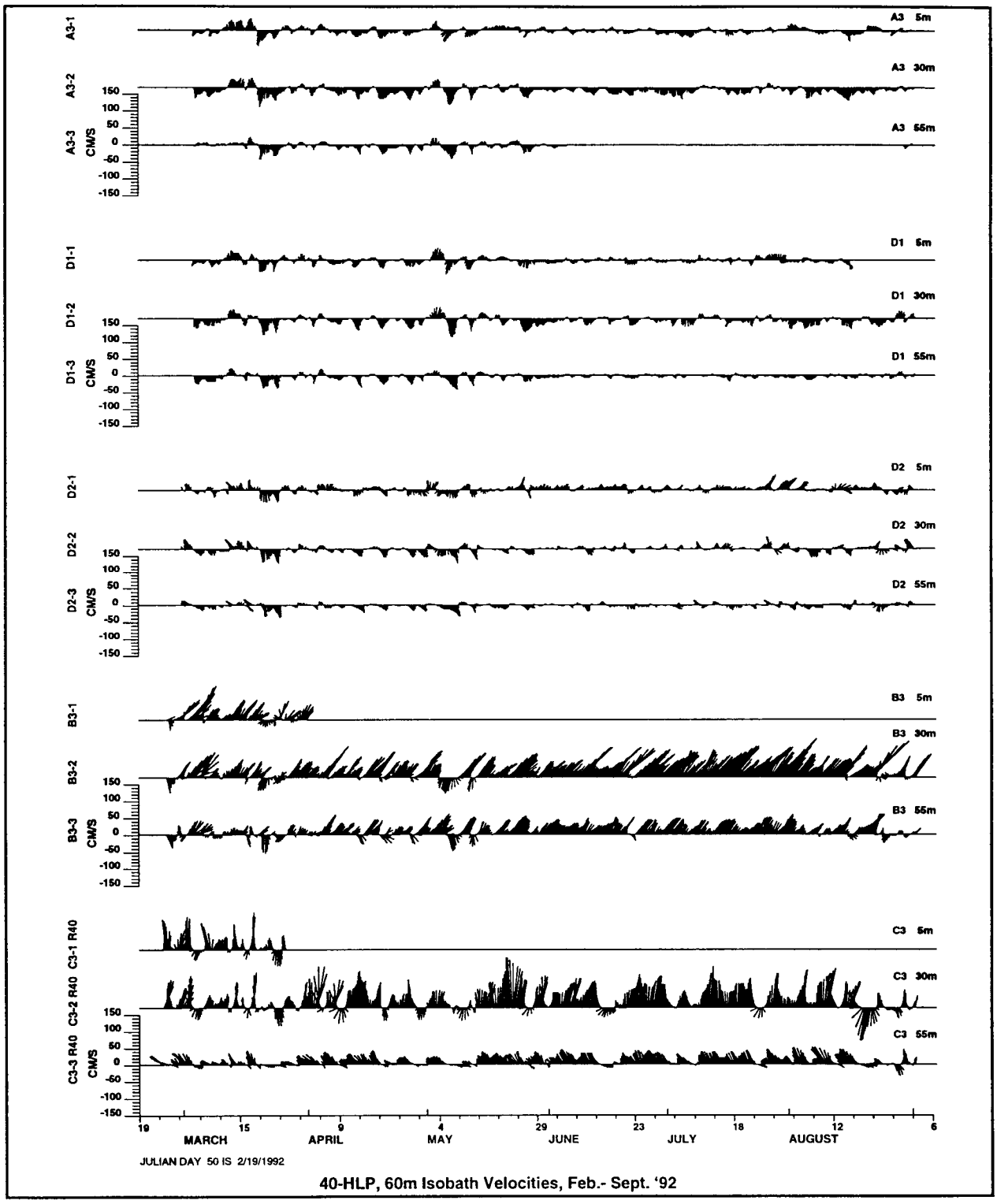

Figure 5.1-6. Velocities measured at the 60 m isobath for the period February 19-September 6, 1992.

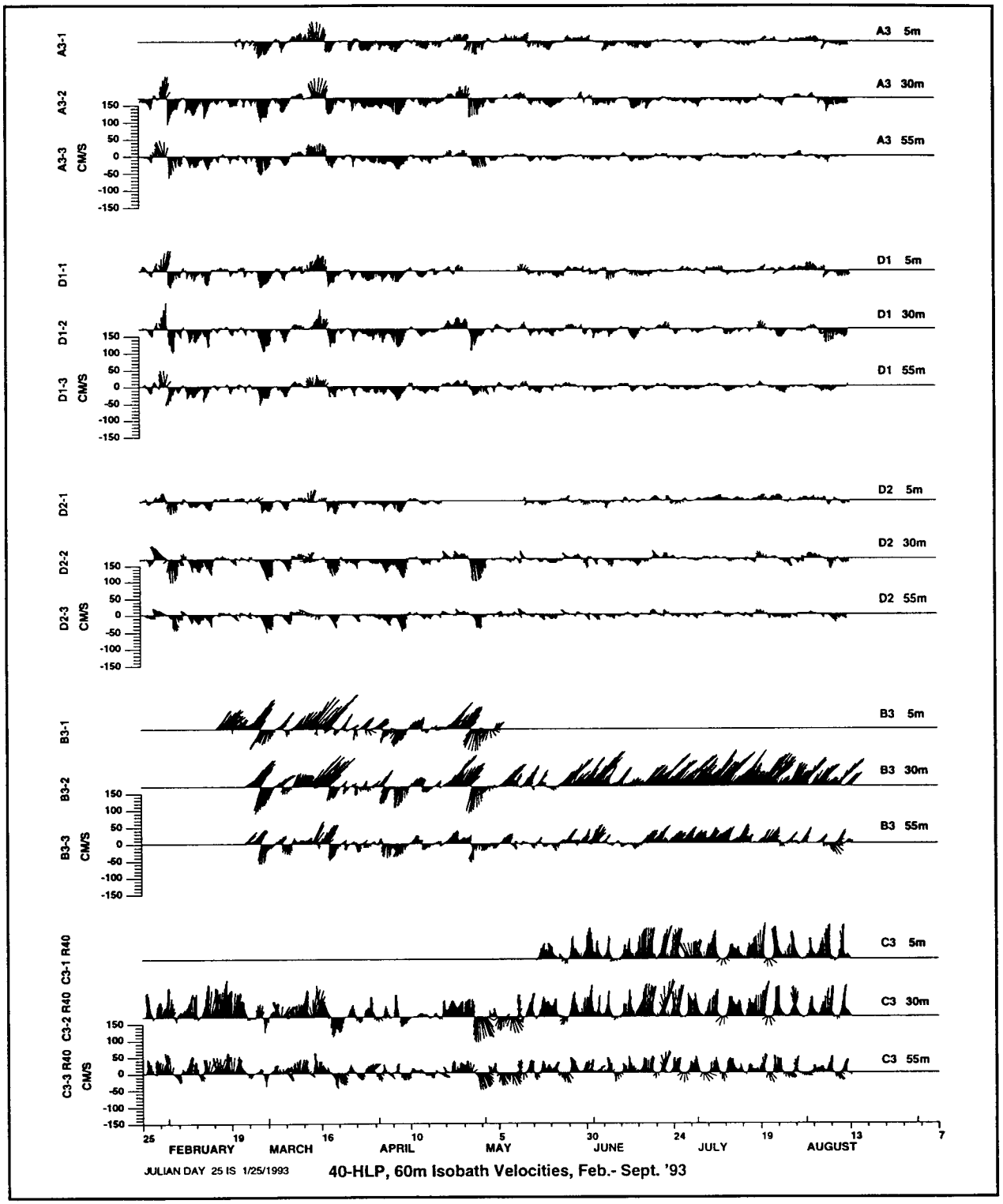

Figure 5.1-7. Velocities measured at the 60 m isobath for the period January 25-September 7, 1993.

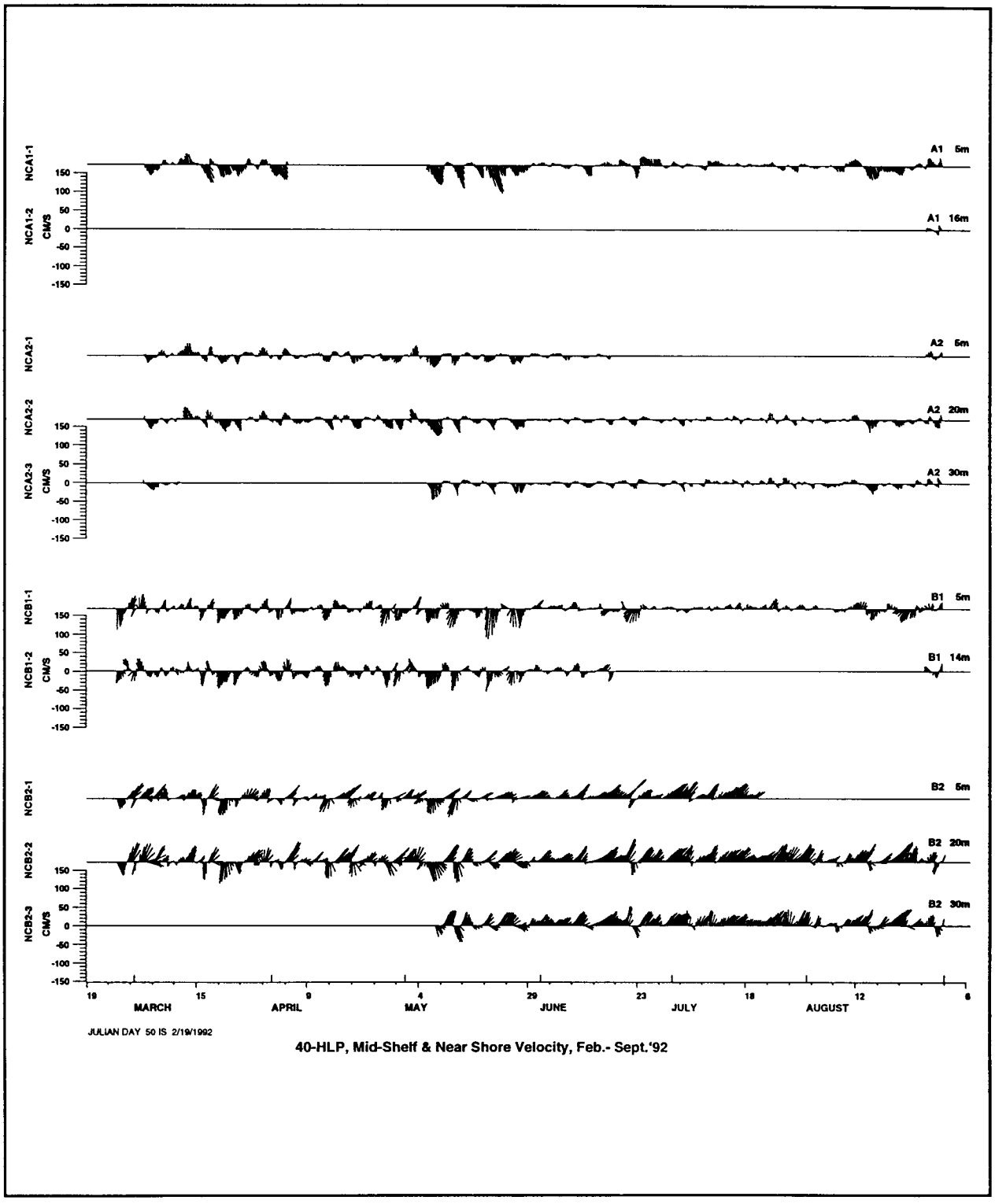

Figure 5.1-8. Mid-shelf and near-shore velocities for the period February 19-September 6, 1992.

and 5.1-9), with the change in flow regime again occurring in June. An obvious implication of these observations is that deep and persistent penetration of the Gulf Stream onto the Hatteras shelf may be a summertime phenomenon.

5.1.6 Observations of Frontal Eddies

As it flows along the continental margin south of Cape Hatteras, the Gulf Stream spawns energetic frontal eddies. These cyclonically rotating features form roughly once per week and propagate northward at a rate of up to 70 $km \cdot d^{-1}$ (Lee and Mayer 1977; Lee *et al.* 1981; McClain *et al.* 1984). Frontal eddies that have received the most scientific scrutiny have the distinctive features of a cold core of upwelled water and trailing warm water filament extending from the shoreward crest of the eddy (Lee and Atkinson 1983; McClain *et al.* 1984; Glenn and Ebbesmeyer 1994a,b). They significantly impact biological productivity at the shelf-edge due to the high concentration of nutrients carried towards the ocean surface within the cold core (Yoder *et al.* 1985; Lee *et al.* 1991; Yoder 1991). The warm filament of Gulf Stream water seen at the shoreward side of the eddy is typically of order 20 m deep and can extend southward from the eddy crest over distances of 100-200 km. Filaments of this type frequent Raleigh and Onslow Bays, and have been observed at the Carolina Coast (Glenn and Ebbesmeyer 1994a).

SST images of the study period (1992-1993) reveal numerous Gulf Stream frontal eddies over the southern portion of the study region (from Cape Hatteras to Cape Lookout). Some of these display the "classical form" of the frontal eddies described above: an elongated trailing warm filament and central cold core. An example of this type of eddy is shown here by the SST image of May 10, 1993 (Figure 5.1-10). A cross-sectional view of the eddy in this image is offered by the property distributions measured across the shelf and slope near Diamond Shoals on May 8-9, 1993 (Figure 5.1-11). These show isopycnal doming in the region of the shelf and upper slope as well as an intrusion of Gulf Stream water extending to the middle shelf.

Many SST images show Gulf Stream water intrusions extending well onto the shelf of Raleigh Bay which lack, at least in the surface temperature field, the "classical" form of the examples above. For example, the image of March 9, 1992 (Figure 5.1-12) shows an intrusion of this type which reached to within 10 km of the coast.

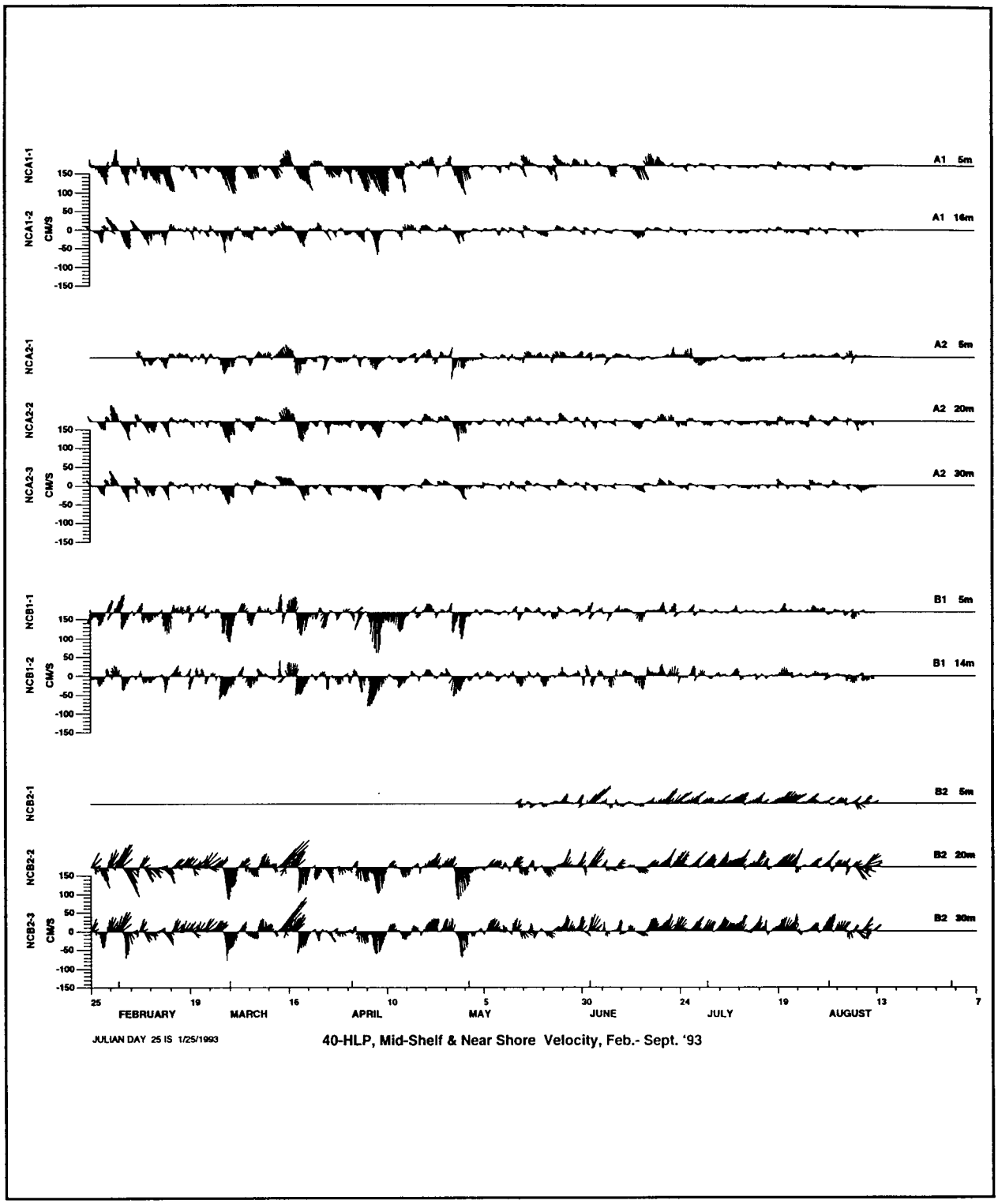

Figure 5.1-9. Mid-shelf and near-shore velocities for the period January 25-September 7, 1993.

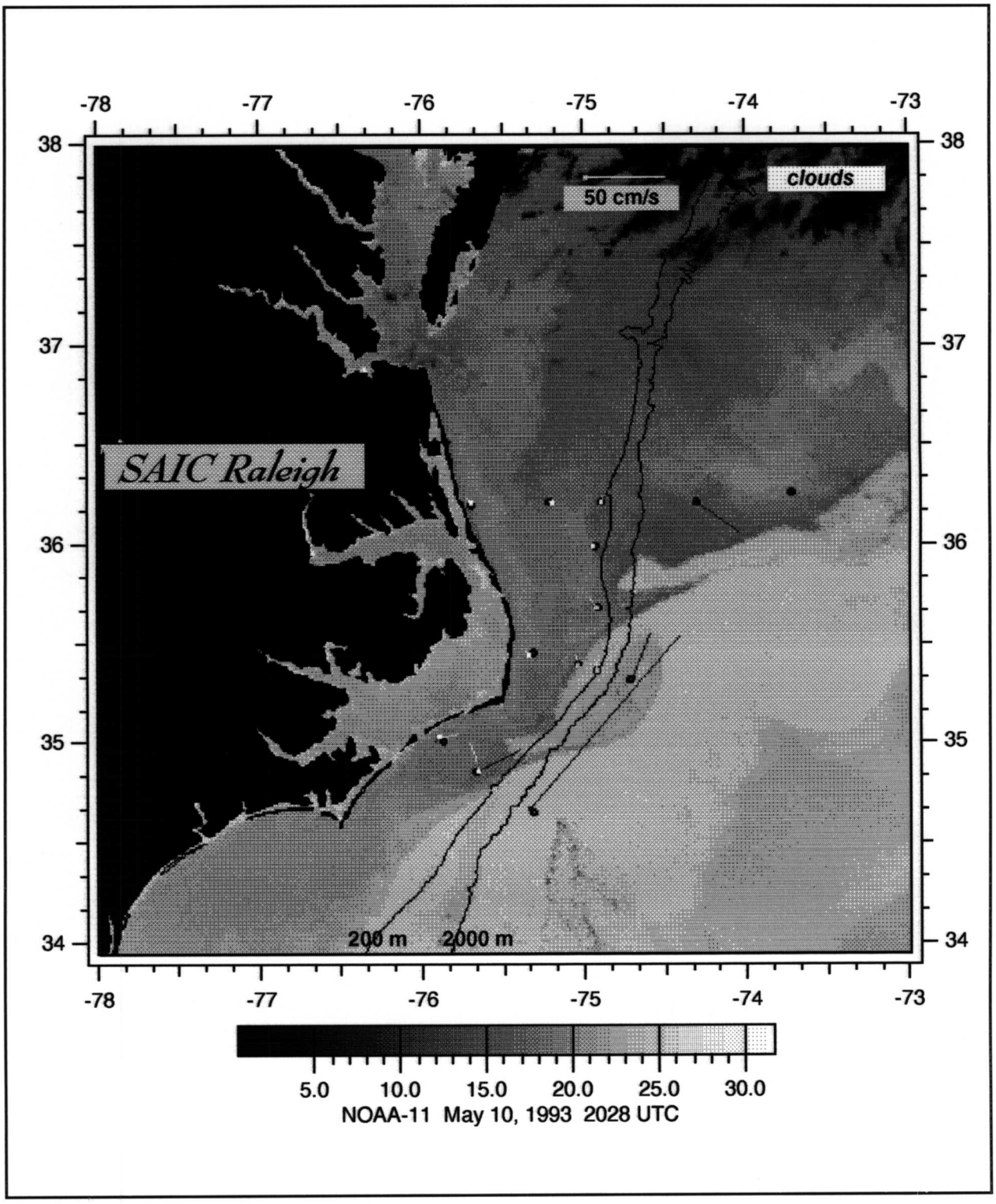

Figure 5.1-10. Satellite SST Image and Daily Average Current Vectors on May 10, 1993. Annotated as in Figure 2.2-7.

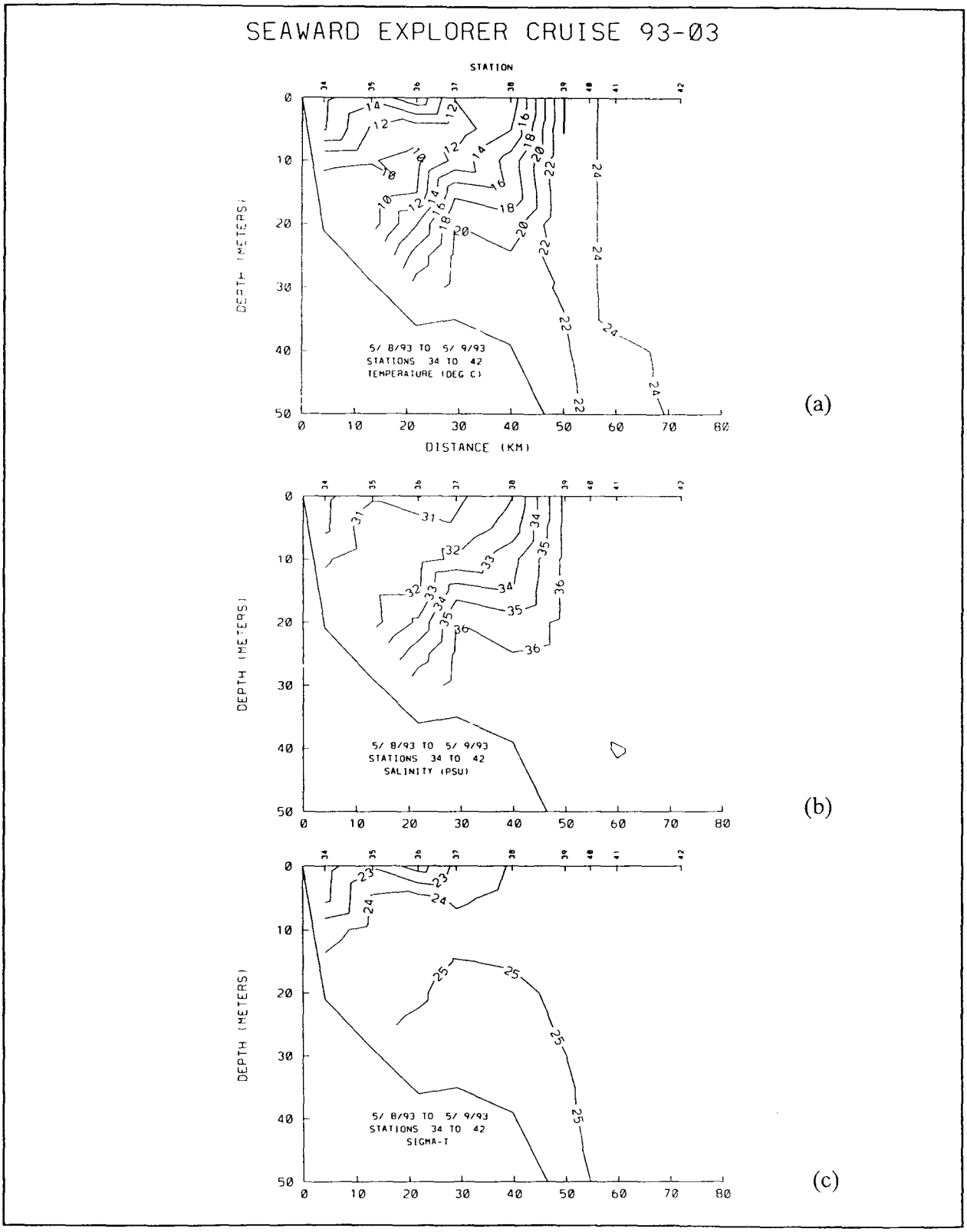

Figure 5.1-11. Cross-shelf sections along Line B of (a) temperature, (b) salinity, and (c) σ_t taken during cruise SE9303 on May 8-9, 1993.

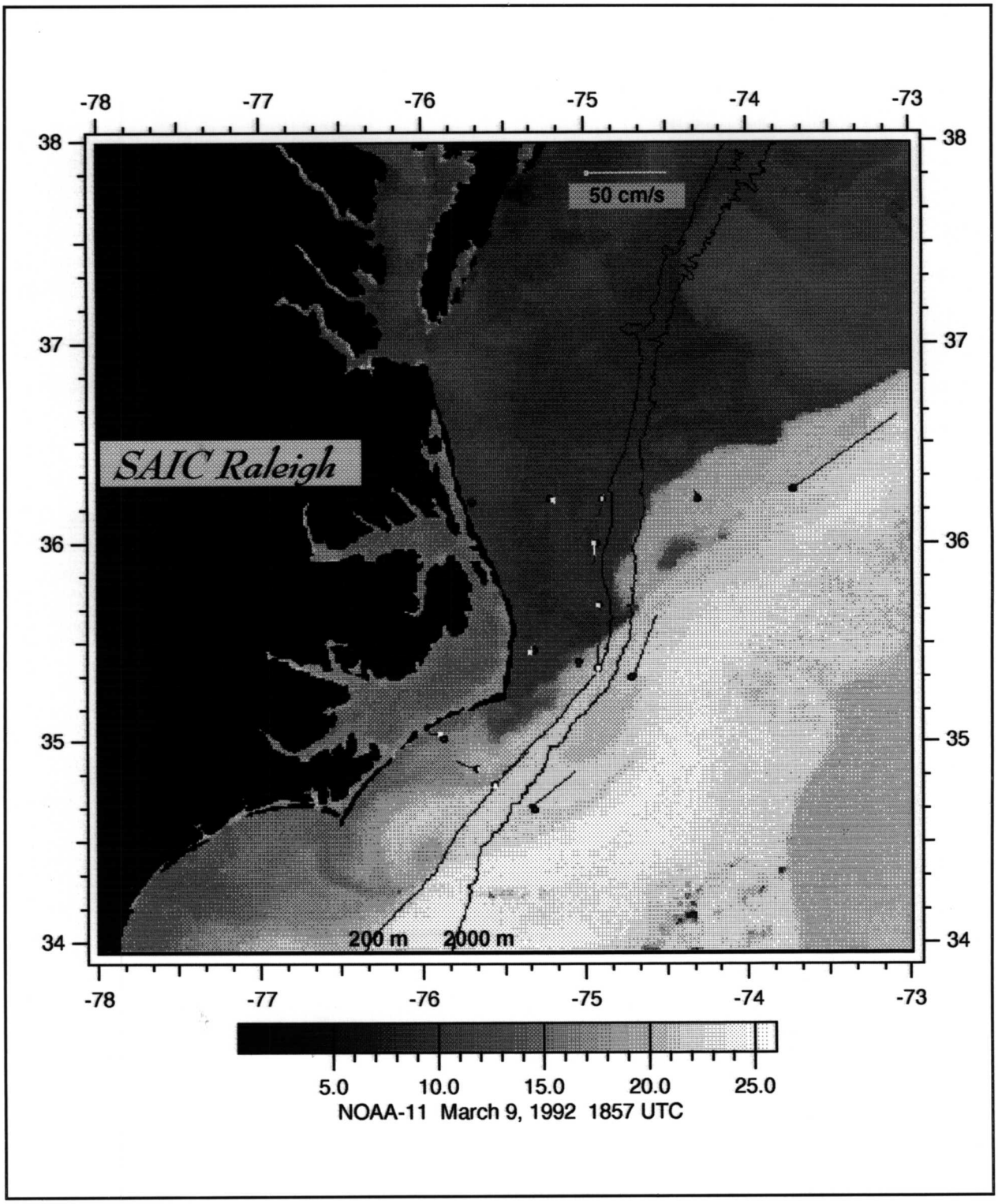

Figure 5.1-12. Satellite SST Image and Daily Average Current Vectors on March 9, 1992. Annotated as in Figure 2.2-7.

SST images also reveal a number of small-scale (order 10 km) eddies in Gulf Stream water at the shelf edge. The structure of one such eddy, seen in the SST fields of early May 1992, was partially resolved by coincident along-shelf ADCP and hydrographic sections taken on 1 and 2-3 May 1992, respectively (Figure 5.1-13). This eddy appeared within Gulf Stream water intruding onto the shelf near Diamond Shoals. As revealed by the ADCP sampling, it contained remarkably large horizontal and vertical velocity gradients. A surface intensified southeastward flow in excess of 60 $cm \cdot s^{-1}$ was measured at the eddy's northern margin (at ADCP station 13), while a bottom intensified northeastward flow peaking above 50 $cm \cdot s^{-1}$ was encountered less than 10 km to the south (at ADCP station 14).

5.2 Intrusions of Gulf Stream Water North of Diamond Shoals

Although frontal eddies form at the Gulf Stream's edge downstream of Cape Hatteras, they are seldom seen on the shelf very far north of Diamond Shoals due to their limited cross-stream scale (Churchill and Cornillon 1991a). Nevertheless, water displaced from the Gulf Stream, containing relatively weak currents and distinct from frontal eddies, often appears over the shelf and upper slope between Diamond Shoals and Baltimore Canyon (Gawarkiewicz *et al.* 1990; Churchill and Cornillon 1991a,b; Churchill *et al.* 1993). On the basis of hydrographic and nutrient measurements, Churchill and Cornillon (1991a) concluded that this type of water originates within nutrient rich layers of the Gulf Stream and tends to enhance near-surface nutrient concentrations over the Middle Atlantic Bight slope. It also tends to influence currents over the slope and affect shelf water export. Hydrographic and moored current meter data have revealed that an alongslope density gradient and an associated eastward current often occur at the northern margin of displaced Gulf Stream water over the Middle Atlantic Bight slope (Churchill and Cornillon 1991a; Churchill *et al.* 1993). This current frequently carries shelf water seaward of the shelf-edge front as evidenced by numerous SST distributions showing a band of surface shelf water extending eastward along the northern edge of a displaced Gulf Stream water mass (e.g. Plate 1 of Churchill *et al.* 1989 and Figures 1 and 6 of Churchill and Cornillon 1991b). The seaward transport of shelf water in one such band was estimated to be 0.1 Sv (Churchill and Cornillon 1991b; Churchill *et al.* 1993), comparable with the rate at which warm-core rings entrain shelf water (Morgan and Bishop 1977; Bisagni 1983; Churchill *et al.* 1986;

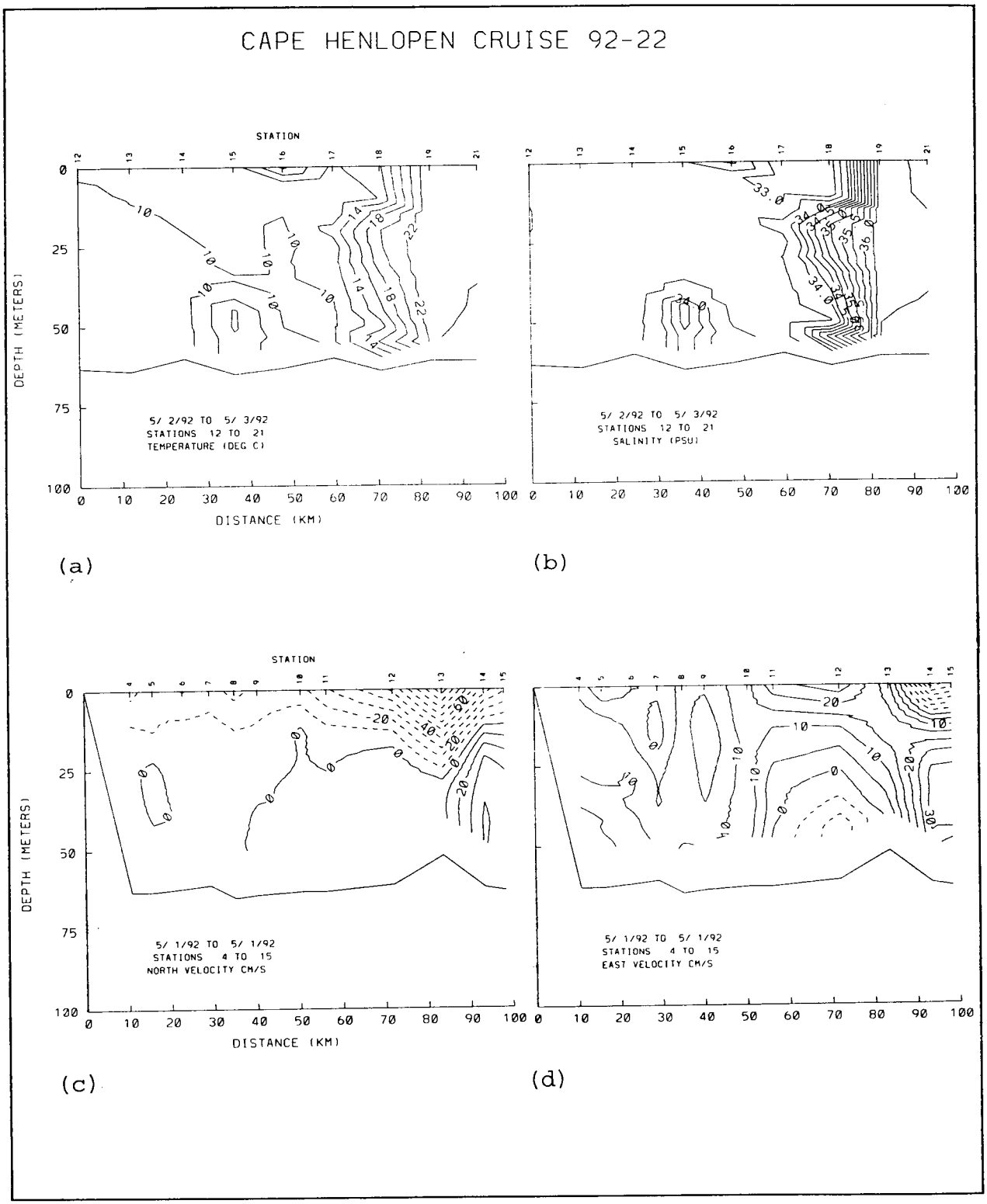

Figure 5.1-13. Temperature, salinity and velocity measured along the outer shelf north of Diamond Shoals in early May 1992.

Garfield and Evans 1987; Joyce and McDougall 1992). However, current meter and hydrographic data indicate that the influence of displaced Gulf Stream water on local circulation of the Middle Atlantic Bight effectively ceases going shoreward of the shelf-edge (Churchill and Cornillon 1991b).

SST images of the study period frequently show water over the southern Middle Atlantic Bight slope which appears to have been separated from the Gulf Stream. In the SST fields, this water is generally cooler than adjacent water within the Gulf Stream, consistent with the notion that it is upwelled Gulf Stream water. Apparent in many SST images is a band of shelf water extending seaward along northern margin of a displaced Gulf Stream water mass (e.g. the image of June 22, 1992 in Figure 5.2-1).

Water which has been displaced from the Gulf Stream is identified in hydrographic sections by the presence of high salinities (>36 psu) in an region of gently sloping isopycnals. Water properties meeting these criteria appear at the shelf-edge in all three of the hydrographic sections along line E (east of Oregon Inlet). In all cases, SST images confirm the presence of displaced Gulf Stream water at the transect. The hydrographic data show this water intruding onto the shelf in a subsurface layer coincident with the seasonal pycnocline. In the example offered here, from the August-September 1992 cruise, an isolated lens of Gulf Stream water appears at the outer shelf along the Oregon Inlet transect (Figure 5.2-2). It is surrounded by shelf water and confined to a depth band of 10-25 m.

Frequent penetration of Gulf Stream water onto the shelf at the northern extreme of the study area is indicated by the data from the A mooring line. The large salinity difference between Gulf Stream and shelf water allows for easy identification of Gulf Stream water in the salinity records from this line. Examination of these records indicates that Gulf Stream water encountered the outer shelf A3 mooring, causing a salinity increase in excess of 2 psu, on 12 occasions during the first 18 months of the mooring's operation. As illustrated by the sample records of Figure 5.2-3, various forms of Gulf Stream intrusions appeared at the mooring. Of the 10 intrusions present when all the mooring's salinity sensors (at 5, 30 and 55 m) were functional, two appeared at the top two sensors only, one was present at only the bottom two sensors and seven appeared at all sensors. The tenure of the intrusions at the mooring also varied significantly. Two were

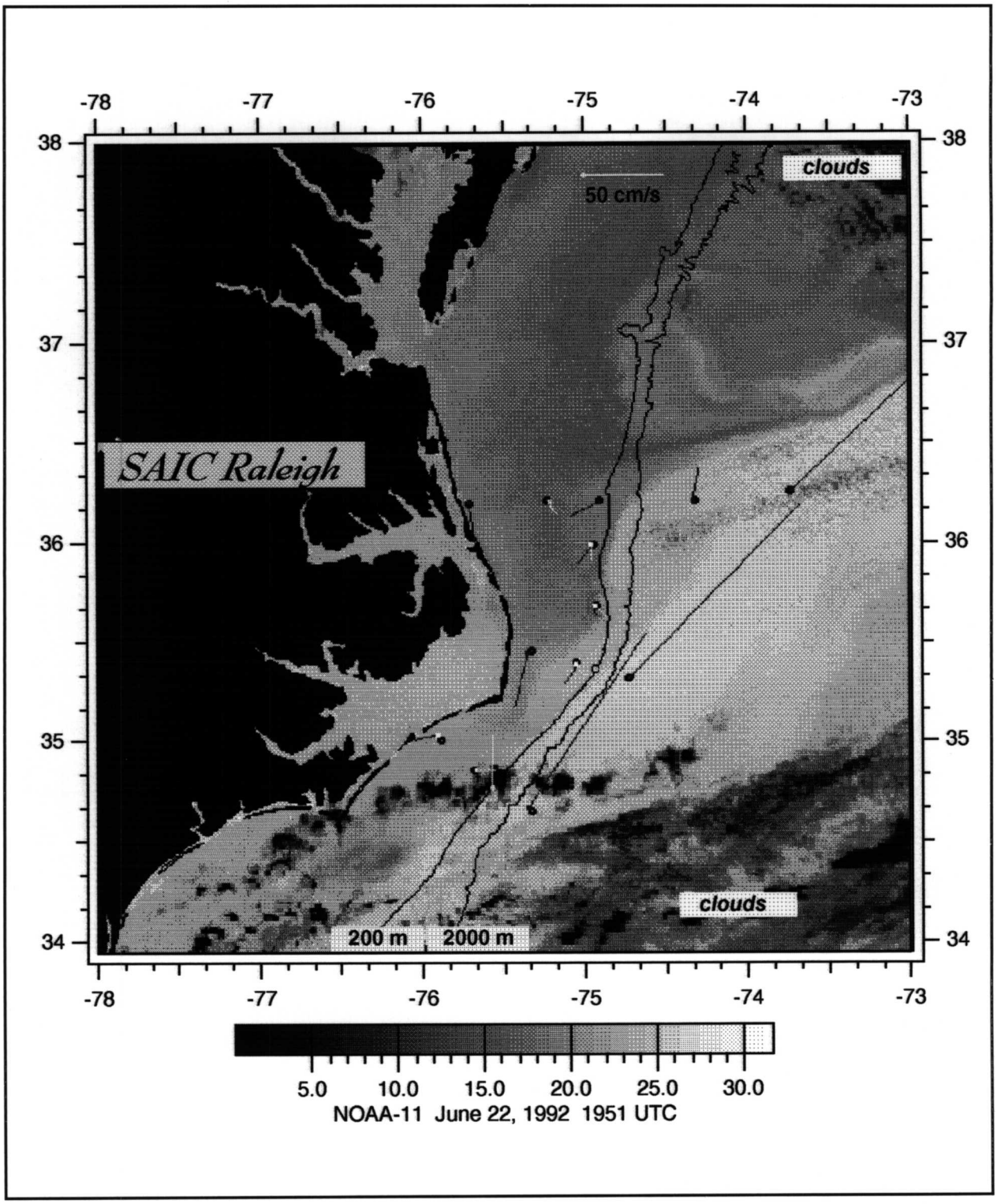

Figure 5.2-1. Satellite SST Image and Daily Average Current Vectors on June 22, 1992. Annotated as in Figure 2.2-7.

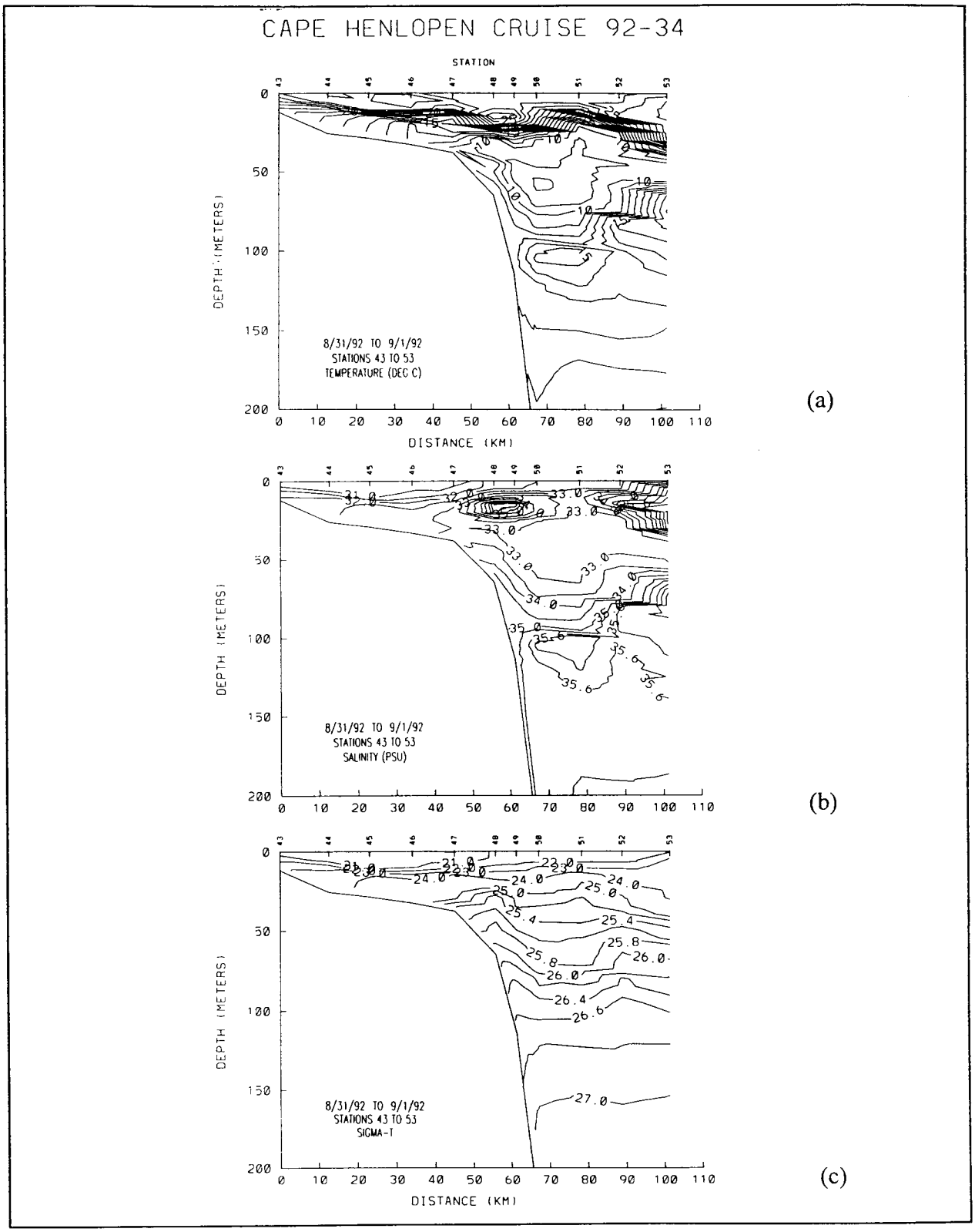

Figure 5.2-2. Cross-shelf sections along Line E of (a) temperature, (b) salinity, and (c) σ_t taken during cruise CH9234 on August 31-September 1, 1992.

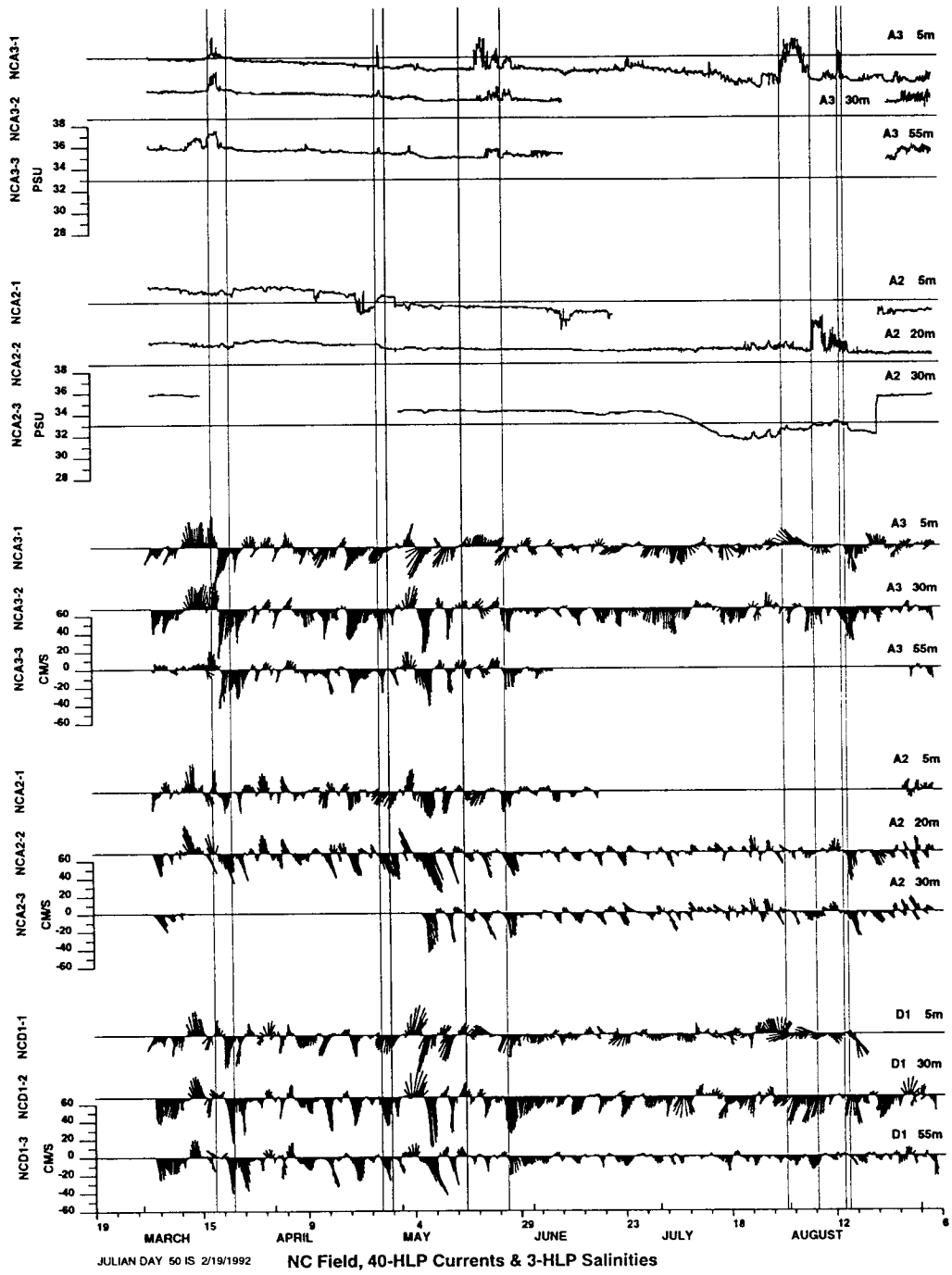

Figure 5.2-3. Salinity and velocity records from Lines A and D. The vertical lines bracket five Gulf Stream water intrusions at the A3 mooring.

present for less than a day. The remaining for three resided at the mooring for three or more days, and five lingered for at least five days. Overall, Gulf Stream water was present at mooring A3 roughly 10% of the time.

Most of the intrusions seen at the mooring appear to have been confined to the outer shelf, only four extended to the mid-shelf A2 mooring. It is noteworthy that three of these occurred in the month of August (the other appeared in March). It is possible that these intrusions may have penetrated the shelf as a result of wind-driven circulation. All occurred during a time of relatively strong (peaking at 8 $m \cdot s^{-1}$ or greater) winds directed to the north (upwelling favorable).

Unlike the frontal eddy described in Section 5.1, the Gulf Stream water seen at mooring A3 did not exhibit an anomalous velocity signal. The currents measured in this water were generally of similar magnitude and correlated (by visual inspection) with the currents measured at nearby moorings A2, D1 and D2 (Figure 5.2-3). This is consistent with the finding of Churchill and Cornillon (1991b) that Gulf Stream water seen on the shelf north of Cape Hatteras did not appreciably influence local circulation.

5.3 Shelf Water Export

In addition to influencing currents over the Hatteras Shelf, the Gulf Stream also plays a dominant role in removing shelf water from this region. Gulf Stream entrainment of Middle Atlantic Bight shelf water (hereafter referred to simply as shelf water) from the Hatteras region was first brought to light in the scientific literature by Ford *et al.* (1952) who reported on filaments of Middle Atlantic Bight shelf water stretching more than 2000 km along the northern edge of the Gulf Stream. Later investigators were able to estimate instantaneous transport of Middle Atlantic Bight shelf water at the edge of the Gulf Stream (Kupferman and Garfield 1977; Churchill *et al.* 1989; Lillibridge *et al.* 1990). That these estimates span a range of 0.01-0.5 Sv demonstrates the importance of Gulf Stream entrainment to the removal of the Middle Atlantic Bight shelf water and suggests that this entrainment may be a highly variable phenomenon. However, current knowledge of this process has largely come from measurements taken over the continental slope and rise within shelf water which has already fallen victim to entrainment. Data from the present study offer a opportunity to examine shelf water loss using measurements from the

Cape Hatteras shelf region. Considered below are: SST evidence regarding shelf water export near Cape Hatteras, the effect of export on the cross-section and transport of shelf water over the Carolina Shelf, observations of seaward shelf water movement, the effect of motions of the across-shelf front on shelf water entrainment, and the residence time of water over the Carolina Shelf.

5.3.1 Evidence from SST

Two mechanisms have been identified as important in conveying shelf water to the Gulf Stream near Cape Hatteras. One is direct injection of water into the Gulf Stream current at the continental margin (Fisher 1972). The other involves parcels of water ejected from the Gulf Stream. As noted in Section 5.2, these often extend from the Gulf Stream to the shelf-edge and are bounded to the north by an eastward current carrying shelf water to the Gulf Stream (Churchill *et al.* 1989, 1993; Churchill and Cornillon 1991a,b). Evidence of both entrainment processes is provided by the available satellite radiometer-derived SST images of the study period (February 1992-February 1994).

Examples of direct Gulf Stream entrainment of shelf water near, and considerably to the north of, Cape Hatteras are provided here by the SST images October 26, 1992 (Figure 5.3-1) and December 18, 1992, (Figure 2.2-7). The image of December 18 gives evidence of another possible mechanism of shelf water export. Apparent from this image's temperature field and superimposed velocity vectors is a strong velocity shear at the A mooring line between northward flowing shelf water and southward moving slope water. Convolution of the shelf/slope water frontal boundary in the region of this shear suggests that it may have given rise to frontal instabilities. As observed by Garvine *et al.* (1988), such instabilities can induce cross-shelf flow and shelf water export.

An example of shelf water export along the northern edge of displaced Gulf Stream water abutting the continental margin appears here in the image of June 22, 1992 (Figure 5.2-1). Other images indicate that this form of entrainment occurs over a broad region. It is seen in the east of the Chesapeake Bay mouth in the images of early December 1992.

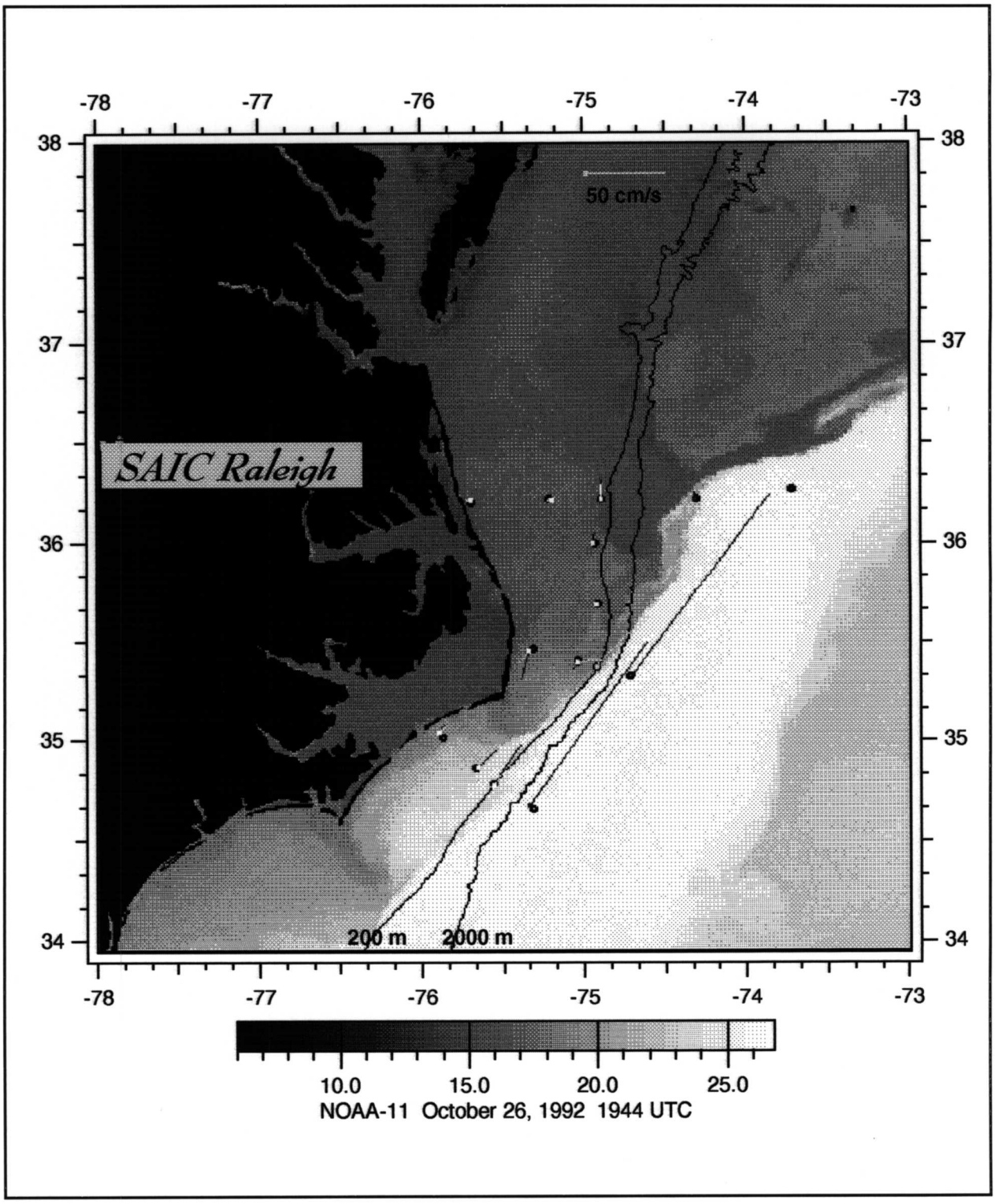

Figure 5.3-1. Satellite SST Image and Daily Average Current Vectors on October 26, 1992. Annotated as in Figure 2.2-7.

5.3.2 Effect on Shelf Water Area and Transport

As illustrated here by the cross-shelf salinity sections of the May 1993 survey (Figure 5.3-2), data from the hydrographic surveys reveal a significant change in shelf water distribution proceeding southward over the northern Carolina Shelf. All salinity fields measured along the A mooring line show a distribution of shelf water (S<34 psu) typically seen in the Middle Atlantic Bight north of the Carolina Shelf. It is one in which shelf water extends across the shelf and is bounded by a surface to bottom salinity front intersecting the bottom at the shelf-edge (Figure 5.3-2(a)). This distribution appears in only one section along the B mooring line, from November 1992. Other salinity sections from this line show a significant quantity of Gulf Stream or South Atlantic Bight shelf water (S>35 psu) extending onto the shelf (Figure 5.3-2(b)). In none of these does the base of the shelf water boundary reach beyond the middle shelf. When present, shelf water is even more confined in sections from the C mooring line. In only one section from this line is shelf water seen beyond the inner shelf.

To quantify the change in shelf water cross-section sampled by the hydrographic surveys, the area of shelf water encountered by each of the mooring line transects was estimated from the transects' contoured salinity fields. The results (Table 5.3-1) reveal a persistent and significant loss of Middle Atlantic Bight shelf water going southward over the study region. When averaged over all surveys, Middle Atlantic Bight shelf water cross-section declines from 5.2×10^6 m^2 across the A mooring line to 0.7×10^6 m^2 over the B mooring line to 0.2×10^6 m^2 across mooring line C. Reduction of shelf water cross-section from line A to line B in all individual surveys is large, no less than a factor of three. The scale of shelf water loss is particularly well defined in the three surveys which included hydrographic measurements over a cross-shelf line located roughly mid-way between the A and B mooring lines, the E line. In all sections from these surveys, shelf water cross-section declines by about a factor of two going from the A to the E line and lessens further by at least a factor of four from the E to the B line (Table 5.3-1). It thus appears that a sizeable loss of shelf water often occurs over a relatively small region, extending roughly 40 km north of Diamond Shoals.

To examine the variation of Middle Atlantic Bight shelf water flux in the Cape Hatteras region, the hydrographic observations and the moored current meter data were used to estimate the alongshore

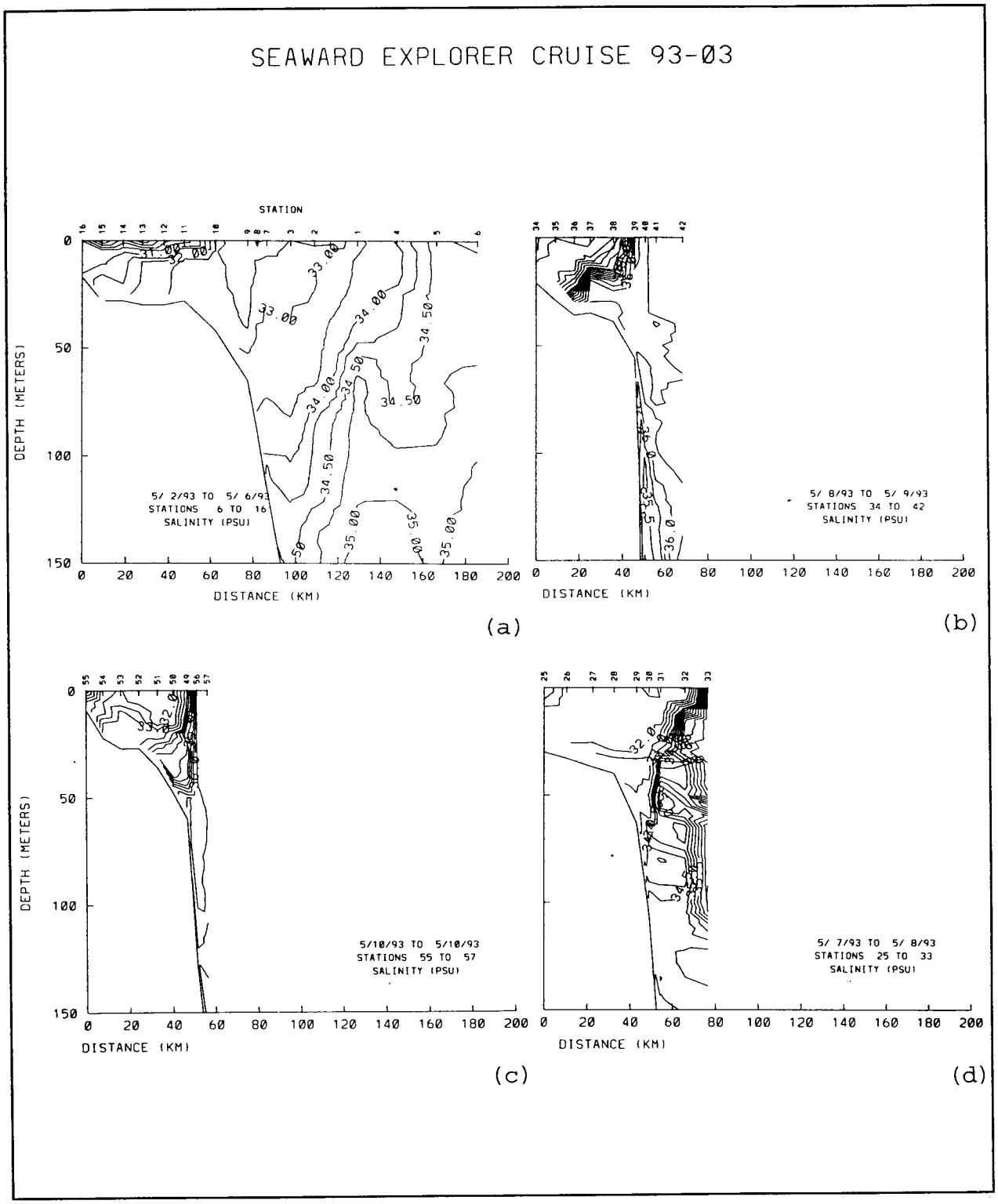

Figure 5.3-2. Cross-shelf sections to 150 m of salinity along Lines (a) A, (b) B, (c) C, and (d) E during cruise SE9303 in May 1993.

transport of Middle Atlantic Bight shelf water sampled by selected hydrographic surveys. The procedure involved dividing the shelf water cross-section along a given mooring line transect into a number of segments, each encompassing a moored current meter. A representative alongshelf velocity for a segment was determined by averaging the alongshelf current measured by the segment's current meter over a 24 hour period which included the time of the hydrographic survey along the transect. The alongshelf transport of the segment was taken as the product of this velocity and the segment area. Summing these transports gave an estimate of the alongshelf flux of Middle Atlantic Bight shelf water sampled along

Table 5.3-1 Estimated cross-section and along-isobath flux of Middle Atlantic Bight Shelf water (S < 34 psu).

	LINE A		LINE E		LINE B		LINE C	
Time Period	Area $m^2(x10^6)$	Flux Sv	Area $m^2(x10^6)$	Flux Sv	Area $m^2(x10^6)$	Flux Sv	Area $m^2(x10^6)$	Flux Sv
04/29-05/06/92	6.1+	-0.81+	----		0.6	-0.25	0	0
08/26-09/02/92	6.0	----	4.3+		0.2	----	0.1	----
11/04-08/92	3.3+	-0.38+	----		1.3	-0.11	0	0
05/02-11/93	7.3	-0.16	3.2		0.8	-0.04	1.1	-0.01
08/19-28/93	4.4	----	2.6		0.5	----	0	----
10/28-11/09/93	4.4	----	----		0.9	----	0	----

Note: Determined from hydrographic transect and moored current meter data. Flux is positive to the north (lines A and B) and northeast (line C). A plus sign following an area or flux indicates shelf water extended beyond the hydrographic transect.

the mooring line. This procedure was carried out to give flux estimates for three of the hydrographic surveys. The others were excluded because their property distributions along the A mooring line included a large quantity of shelf water over the slope and rise. It was deemed that the available velocity data could not adequately represent the flow of this water. Even for those surveys with relatively little shelf water over the slope, our procedure clearly gives only rough approximations of shelf water transport. Nevertheless, these offer an interesting view as to how this transport varies over the study region.

The computed transports (Table 5.3-1) change in a manner similar to the Middle Atlantic Bight shelf water cross-sections: they consistently decline proceeding southward from mooring line A. In two of the surveys, however, the southward lessening of shelf water transport is significantly less than that of its cross-section. For example, going from line A to line B, the Middle Atlantic Bight shelf water area sampled by the April-May 1992 survey declines by an order of magnitude but the estimated shelf water transport is reduced by less than a factor of four. This is due to the relatively large alongshelf velocities measured in the shelf water sampled along the B mooring line. These were order 40 $cm \cdot s^{-1}$, as compared with the order 10 $cm \cdot s^{-1}$ velocities measured in the shelf water sampled along the A mooring line. A reasonable conclusion is that Middle Atlantic Bight shelf water which escapes export north of Diamond Shoals may tend to concentrate into a relatively high velocity coastal current.

5.3.3 Observations of Export

The surveys of April-May 1992 and August-September 1992 included "special event" components featuring vertical and horizontal sampling of currents using an ADCP. ADCP sections of both surveys intercepted shelf water moving seaward. Details of shelf water transport deduced from the ADCP measurements are presented below.

May 1992

As part of the special event survey of May 1992, ADCP sampling was carried out over the portion of line D coincident with the 60 m isobath between lines A and B. This was immediately followed by a hydrographic survey along the same line. As indicated by the hydrographic data (Figure 5.1-13), most of the line was occupied by shelf water bounded to the south by a warm and saline water mass. The ADCP measurements indicate that this southern water mass was part of the Gulf Stream and was flowing to the northeast at a speed of roughly 50 $cm \cdot s^{-1}$ (Figure 5.1-13). Also revealed by the ADCP measurements is that most of the shelf water found along the survey line was moving seaward (to the east) at a rate of up to 14 $cm \cdot s^{-1}$. The mean offshelf velocity of the shelf water sampled by the ADCP was found to be 8.1 $cm \cdot s^{-1}$. Its offshelf transport was determined by integrating the ADCP eastward velocity component over the shelf water cross-section. However, because the ADCP measurements did not include the upper and lower 10 m of the water column, the result of 0.15 Sv falls shy of the total shelf water transport

along the line. To adjust this to a full water column transport, it is reasonable to assume that the mean velocity of the upper 10 m of shelf water was equal to that sampled by the ADCP and that the mean velocity of the lower 10 m was half this value. This puts the total seaward transport of shelf water found along the line at 1.4 times the value determined from the ADCP data about 0.21 Sv. This is comparable with the along-isobath shelf water transport estimate of Beardsley *et al.* (1976) and those of Table 5.3-1. Clearly, the shelf water export across the ADCP section constituted a significant loss of total shelf water flow.

September 1992

The special event survey of September 1992 offered a view of shelf water which had exited the shelf. It was sampled by a hydrographic cast at the 1000 m isobath (station 74 in Figure 5.3-3). Situated beneath a thin layer of Gulf Stream water, it occupied a depth range of 20-90 m. The flow of this and surrounding water was detailed by ADCP stations. These were aligned with the 1000 m isobath and were occupied over a three hour period ending four hours before the hydrographic observations of the shelf water mass were acquired. The ADCP-derived velocities indicate that the shelf water was located to the north of the Gulf Stream and in an area of significant along-isobath shear of the eastward (offslope) velocity component (Figure 5.3-3). The large station spacing of the special event hydrographic survey prevents resolution of the alongslope extent of the exported shelf water mass and therefore its transport. Nevertheless, the ADCP data indicate it was moving offslope at a significant rate. In the depth 20-90 m depth range, mean velocities of 22 and 52 $cm \cdot s^{-1}$ were measured by the ADCP stations bracketing the hydrographic station at which the shelf water was sampled.

5.3.4 Residence Time of Near-surface Water over the Carolina Shelf

The analysis above indicates that water entering the Carolina shelf from the north tends to be diverted offshore to the Gulf Stream. This would support the view that most of the material introduced onto the Carolina shelf (e.g. accidental oil discharge or recently spawned fish larvae) will eventually be swept off the shelf. However an assessment of the possible impact of such material must take into account its likely residence time over the shelf the probability that it be carried to shore. These issues were addressed in part by the drifter tracking component of this

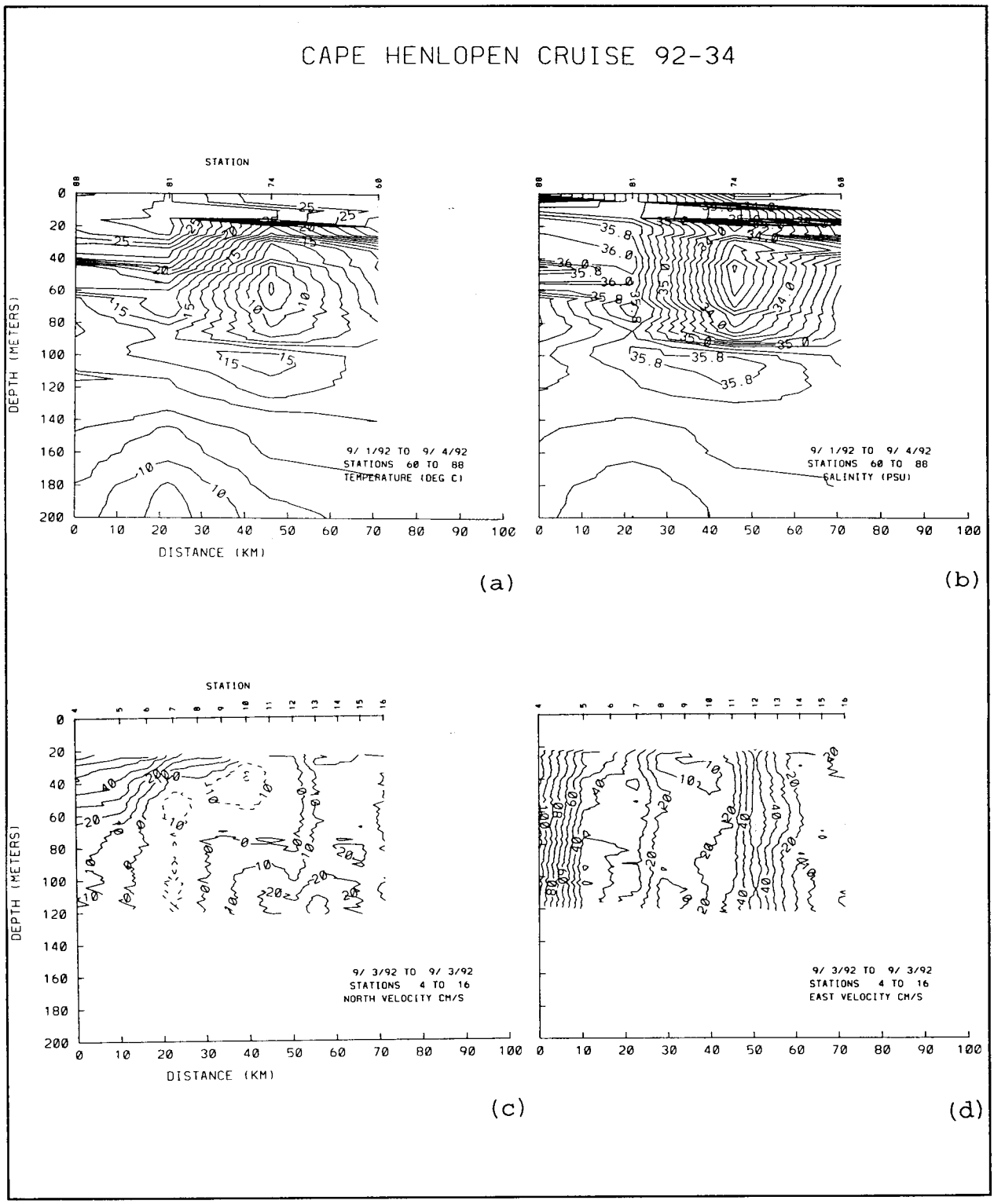

Figure 5.3-3. Distributions of temperature, salinity and velocity measured over the 1000 m isobath in early September 1992.

program. Drifters were released as part of a concentrated study of near-shore circulation, and were routinely set out at fixed locations over the middle and outer shelf during the mooring rotation cruises. The drifter tracks of the near-shore circulation study are dealt with in Section 8. Considered here are the tracks of drifters released over the middle and outer shelf. Because the surface drifter tracks were influenced by direct wind forcing to a large but unknown degree, attention here is given only to the drogued drifter tracks as indicators of near-surface water movement.

Drogued drifters were deployed repeatedly at five sites over the North Carolina shelf (Figure 5.3-4). Two were along the Line A mooring, one at the outer shelf and the other at the shoreward edge of the middle shelf. The other sites were at the mid-shelf: one in Raleigh Bay, another on the B mooring line and the third 30 km north of the B line. During seven mooring rotation cruises between April 1992 and November 1993 a total of 30 drogued drifters were deployed at these sites. A simple, but significant, result is that none of the drogued drifters were carried to the coast. All were either observed exiting the shelf or remained over the shelf throughout their operational lifetime. The time of observed residence inside the 200 m isobath of each drifter has been determined (Table 5.3-2). The residence times spanned a large range: from less than a day to more than 27 days. As would be anticipated, they tended to be greatest for drifters deployed at site 1 (Figure 5.3-4) on Line A. Three drifters deployed at this site remained on the shelf during their entire time of operation: of 6.5, 18.3 and 20.1 days (Note however that this last drifter was eventually recovered in early January 1994 on the beach at Cape Cornwall in southwest England. This unit minus drogue, was returned). Only one crossed the 200 m isobath within a week after its deployment. Shelf residence times of drifters deployed at the seaward site on Line A were considerably shorter. Three of the six were less than 8 days, and the longest was 14 days. Surprisingly, relatively long shelf residence times, of greater than 10 days, were logged by three of the drifters set out at site 4: 30 km north of Line B. These included the longest residence time of 27.8 days. The drifters deployed at sites on Line B and Site 6 in Raleigh Bay had either very short, less than 6 days, or relatively long, more than 11 days, shelf residence. Overall, the results indicate that material introduced into and confined within near-surface waters over the middle and outer Carolina Shelf will tend to be carried

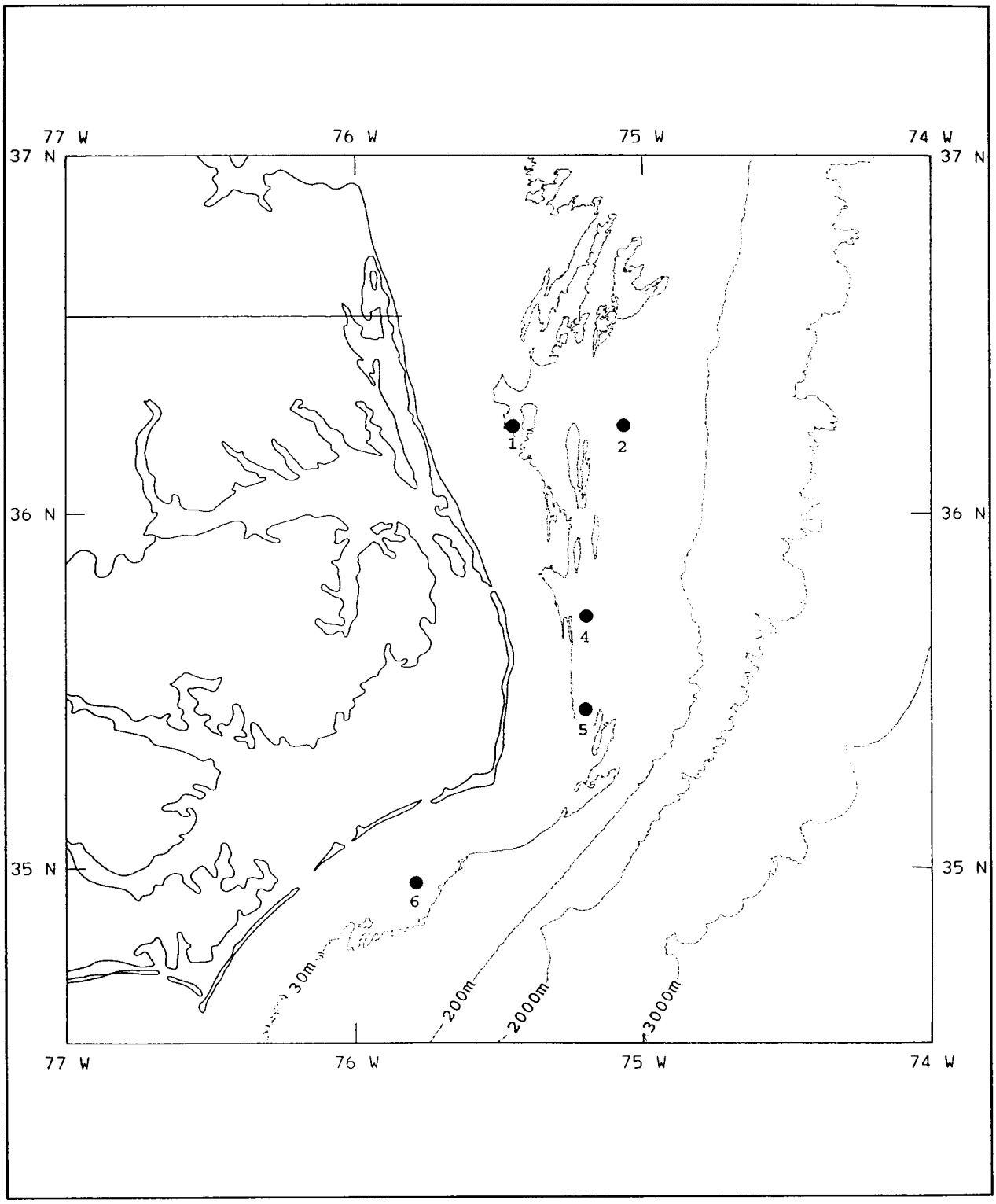

Figure 5.3-4. Drifter deployment sites during the mooring rotation cruises.

Table 5.3-2. Shelf residence times of ARGOS-tracked drogued drifters released over the Carolina Shelf. Deployment sites shown in Figure 5.3-5.

Deployment		Time to 200 m isobath or operational life on shelf (days)	Recovered
Site	Date		
1	September 2, 1992	20.2	UK, January 1994
	November 4, 1992	18.3 (NLS)	
	February 14, 1993	11.4	
	May 6, 1993	6.4	France, March 1995
	August 27, 1993	10.6	
	October 31, 1993	6.5 (NLS)	
2	May 1, 1992	7.5	
	September 2, 1992	9.1	
	November 5, 1992	1.1	Bahamas, May 1995
	February 14, 1993	14.0	France, April 1994
	May 6, 1993	10.1	
	October 31, 1993	4.9	
4	May 9, 1992	28.8	Bahamas, April 1995
	August 31, 1992	7.4	
	November 7, 1992	6.0	
	February 16, 1993	5.9	
	May 8, 1993	10.9	
	August 23, 1993	10.2	
5	May 6, 1992	19.2	Canary Islands, June 1994
	August 29, 1992	12.8	
	November 6, 1992	2.2	
	February 11, 1993	3.4	
	May 9, 1993	5.0	
	August 23, 1993	5.2 (NLS)	
6	May 5, 1992	11.7	
	August 26, 1992	14.2	
	November 8, 1992	5.8	France, April 1994
	February 5, 1993	10.7	
	May 12, 1993	0.9	
	October 29, 1993	1.6	

(NLS) indicates the drifter never left the shelf during its operational lifetime.

offshore, but that its residence time over the shelf will vary considerably: from a few days or less to a number of weeks.

As would be expected from the range of shelf residence times, the ensemble of drifter tracks (Figure 5.3-5) shows a significant variation of near-surface flow over the Hatteras Shelf. Nevertheless, some general flow patterns are apparent. Of most interest to this discussion are the tracks of the drifters released at four northern sites (1, 2, 4, and 5). Judging from the surface salinity fields of the hydrographic surveys (Figure 4.5-1), these were within the region usually occupied by Middle Atlantic Bight shelf water. The drifters set out at these sites tended to migrate south. Roughly one quarter of this group entered Raleigh Bay. However, all but two of these eventually turned north and returned to the Middle Atlantic Bight shelf. All of the drifters which exited the shelf (including those released at site 6) did so over a fairly narrow range, extending from 35° to 36°30'N.

5.3.5 Shelf Water Entrainment and the Hatteras Cross-Shelf Front

Much of the Middle Atlantic Bight shelf water seen south of line E was bordered by the Hatteras cross-shelf salinity front (Figure 4.5-1). As noted in Section 4.5, the character of this front varies, in a binary sense, with its direction of motion across the shelf. While advancing shoreward, the front tends to be steeply inclined and encompass a strong northeastward (offshore) flow. By comparison, it contains weak flows and is gently inclined while retreating seaward. The data from mooring B2 offer strong evidence that Middle Atlantic Bight shelf water is entrained along the front, and that this process also varies with the direction of the front's motion across the shelf.

An example of the difference in shelf water flow seen at the edge of the retreating versus the advancing front is given by the four-day long sample of temperature and velocity records in Figure 4.5-3. Through an abrupt temperature increase and subsequent decline, this shows a shoreward and seaward movement of the front past the B2 mooring. The alongfront velocity record indicates that shelf water (T~15°C) at the edge of the advancing front was flowing to the northeast (offshore). This shelf water was apparently part of a circulation pattern of convergence at the front, as its alongfront velocity steadily increased as the front approached the mooring. It attained a maximum northeastward velocity of 55 $cm \cdot s^{-1}$

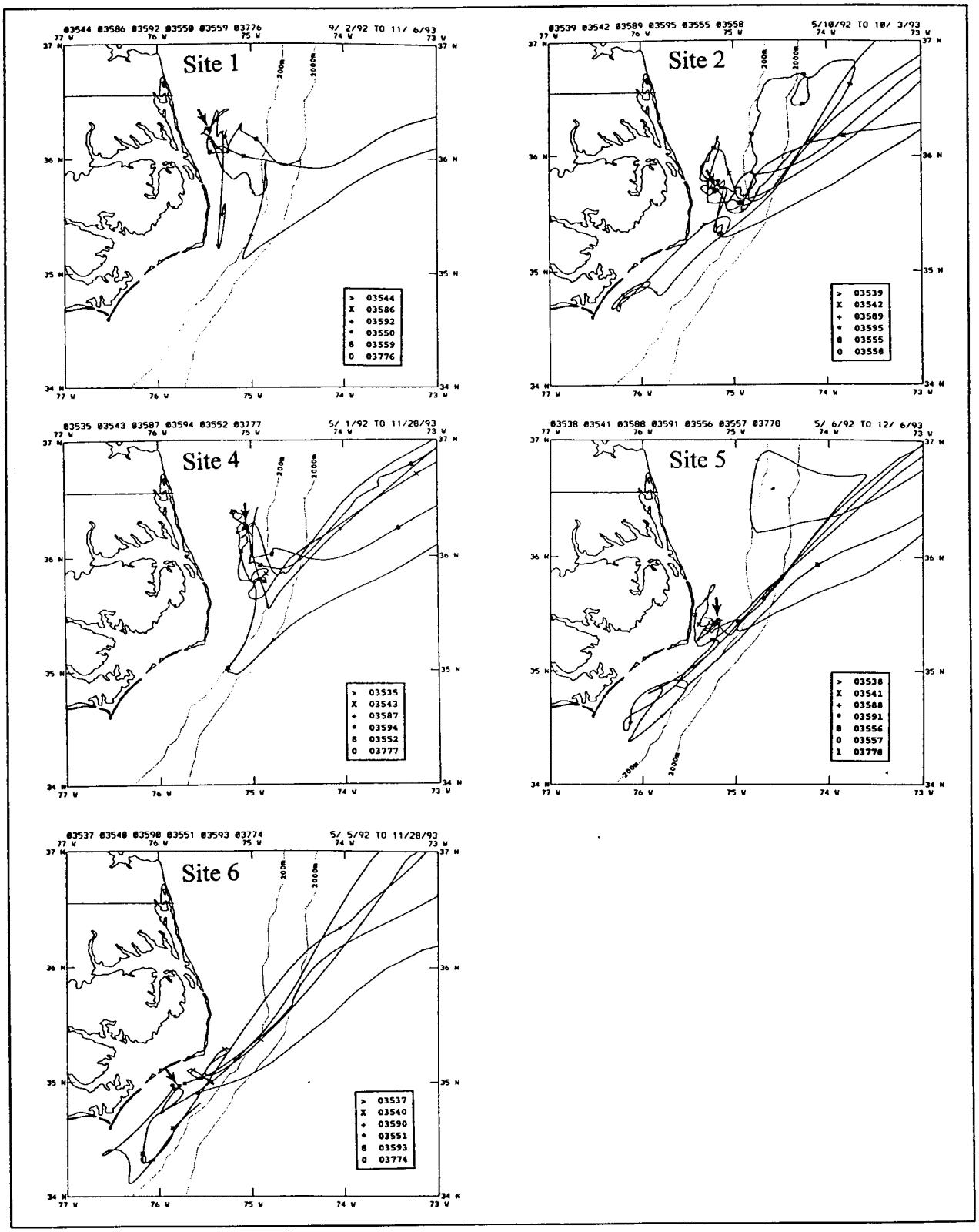

Figure 5.3-5. Smoothed drifter tracks from deployment sites 1, 2, 4, 5, and 6.

at the edge of the front. By contrast, shelf water at the edge of the retreating front was moving southwestward (onshore).

To quantify the difference in shelf water flow at the edge of the retreating and advancing front, averages of alongfront velocity measured in shelf water 24 hours before the arrival of an advancing front and 24 hours after the departure of a retreating front were computed using the records from mooring B2. As noted in Section 4.5, an along-front orientation of 40°T was chosen, based on the surface salinity fields of the hydrographic surveys. Shelf water as taken as fluid with T<15°C. Passage of an advancing front was assumed to be marked by a monotonic, or nearly monotonic rise, in temperature from less than 15°C to more than 20°C, while indication of a retreating front passage was taken as a corresponding decline in temperature. Averages were computed over the two-month long segment of records shown in Figure 4.5-2. This contained evidence of nine frontal passages in either direction as defined above. The averaged velocities for each measurement level and each direction of frontal motion were also averaged (Table 5.3-3). The means of the averaged of along-front shelf water flow seen in advance of the shoreward frontal passages (Table 5.3-3) are directed offshore at all three measurements levels and are roughly 30 $cm \cdot s^{-1}$ in magnitude: a clear indication that shelf water is entrained and rapidly carried seaward at the edge of an advancing front. In contrast, means of the averaged shelf water flows seen after afront's seaward passage are all relatively small (order 5 $cm \cdot s^{-1}$) and directed seaward: indicating that, on average, shelf water is not entrained at the edge of a retreating front. The disparate magnitude of these mean shelf water flows reveals that a sizeable net seaward transport of shelf water occurs at the edge of the front as it migrates shoreward and seaward across the shelf. The intermittency of this transport, associated with the front's motion, may explain variability of shelf water presence and transport seen at the edge of the Gulf Stream downstream of Cape Hatteras (Ford *et al.* 1952; Kupferman and Garfield 1977; Churchill *et al.* 1989; Lillibridge *et al.* 1990). Further evidence of shelf water entrainment at the edge of the cross-shelf Hatteras front is seen in the paths of the ARGOS-tracked drifters released during the mooring servicing cruises (Figure 5.3-5). Paths of many of the drifters released in Middle Atlantic Bight shelf water (at sites 1, 2, 4 and 5) are seen to exit the shelf at a rapid velocity in the region of the front and at an orientation matching that of the front as seen in the surface salinity fields of the hydrographic surveys.

Table 5.3-3 Means and standard deviations of along-front flow measured at mooring B2 over 24 hour periods before and after the Hatteras cross-shelf front passed the mooring. Nine onshore and offshore frontal passages are considered from the period of December 5, 1993 through February 5, 1994. Positive (negative) along-front velocity is directed northeastward (southwestward).

Measurement Level	Velocity before onshore frontal passage ($cm \cdot s^{-1}$)		Velocity after offshore frontal passage ($cm \cdot s^{-1}$)	
	Mean	Std. Dev.	Mean	Std. Dev.
5 m	30.8	9.0	-6.7	17.7
20 m	30.5	12.1	-4.8	18.2
30 m	25.8	8.1	-2.6	19.4

Taken together the drifter and current meter observations clearly show that the shelf water is actively entrained at the cross- shelf Hatteras front. The front appears to act something like a peristaltic pump, entraining shelf water only as it moves shoreward. It is reasonable to speculate that this entrainment results from an adjustment process occurring as the front advances into shallower water. Based on the analysis of Section 5.1, it is also reasonable to conclude that the migrations of the Hatteras front and the attendant shelf water entrainment are driven by Gulf Stream meanders at the shelf-edge.

5.4 Slope Sea Influences

As detailed by Csanady and Hamilton (1988), the upper few hundred meters of the Slope Sea is mostly occupied by a distinct "slopewater" mass with salinities falling between those of the Gulf Stream and Middle Atlantic Bight shelf water, roughly in the range of 35-35.6 psu. The portion of the Slope Sea within the study region is also frequented by water ejected from the Gulf Stream and displaced Middle Atlantic Bight shelf water (Gawarkiewicz *et al.* 1990; Churchill and Cornillon 1991a,b; Churchill *et al.* 1993).

A view of the Slope Sea and its interactions with Middle Atlantic Bight shelf water is provided by the data from the A mooring line. In agreement with previous findings (Csanady and Hamilton, 1988; Gawarkiewicz *et al.* 1990; Churchill and Cornillon 1991a; Churchill *et al.* 1993), hydrographic data from this line reveal a complex and

varying water mass distribution in the Slope Sea off the southern Middle Atlantic Bight. A different combination of water masses appears in each of the four Line A hydrographic sections which extended into the Slope Sea. Three sections, from the September 1992, May 1993 and November 1993 surveys, show shelf water extending more than 60 km seaward of the shelf-edge. In all of these, the shelf water is situated above slopewater. In one section (from the November 1993), the shelf water abuts the Gulf Stream, identified by high salinities and steeply sloping isopycnals (Figure 5.4-1). In another section (from the September 1992 survey), water ejected from the Gulf Stream appears at the seaward margin of shelf water (Figure 5.4-2). In only one Line A section (from the August 1993 survey) does slopewater abut the continental margin and shelf-edge front (Figure 5.4-3), a condition commonly seen in the northern Middle Atlantic Bight (Gordon and Aikman 1981; Houghton and Marra 1983; Aikman 1984; Lyne and Csanady 1984). Appearing in this section is an intrusion of slopewater onto the outer shelf which is confined to the seasonal pycnocline. This type of intrusion is a common summertime feature of the Middle Atlantic Bight (Boicourt and Hacker 1976; Gordon and Aikman 1981; Houghton and Marra 1983; Churchill *et al.* 1986).

Currents within the Slope Sea were consistently sampled at mooring A4 (and not at the more seaward mooring A5 which was frequently occupied by the Gulf Stream). 40-HLP velocity records from the 100 and 300 m current meters on the A4 mooring show frequent rotary currents of varying strength (Figure 5.4-4). Results of spectral analysis (Figure 5.4-5) indicate that these rotary motions are coherent and nearly in phase over the 100-300 m depth band. The strongest currents in this band tend to coincide with pulses of high temperature in the record of the 100 m thermistor on the A4 mooring (Figure 5.4-4). Examination of SST images reveal that these pulses of high temperature and the associated currents are usually due to the appearance of water ejected from the Gulf Stream current(this type of water is considered in detail in Section 5.2). A particularly clear example of a Gulf Stream water eddy at mooring A4 is provided by an SST image on April 23, 1992 (Figure 4.3-4). This image displays a circular band of displaced Gulf Stream water and an enclosed core of relatively cool water which are intersected by the A mooring line. The low-pass filtered current vectors superimposed on this image show the velocity measured at the A4 mooring to be in agreement with the cyclonic circulation inferred by surface thermal signature of the displaced Gulf Stream water band.

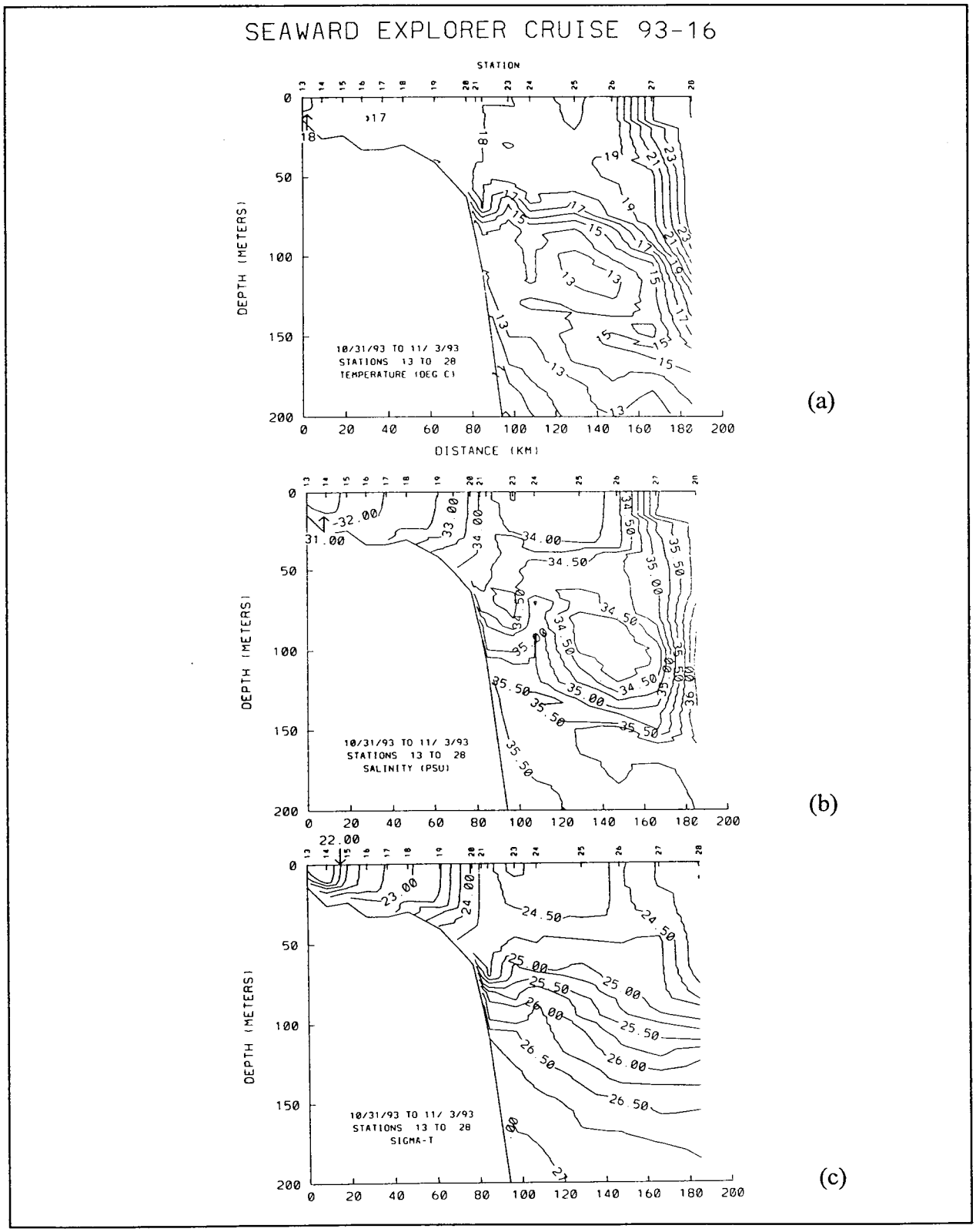

Figure 5.4-1. Cross-shelf sections along Line A of (a) temperature, (b) salinity, and (c) σ_t taken during cruise SE9316 on October 31-November 3, 1993.

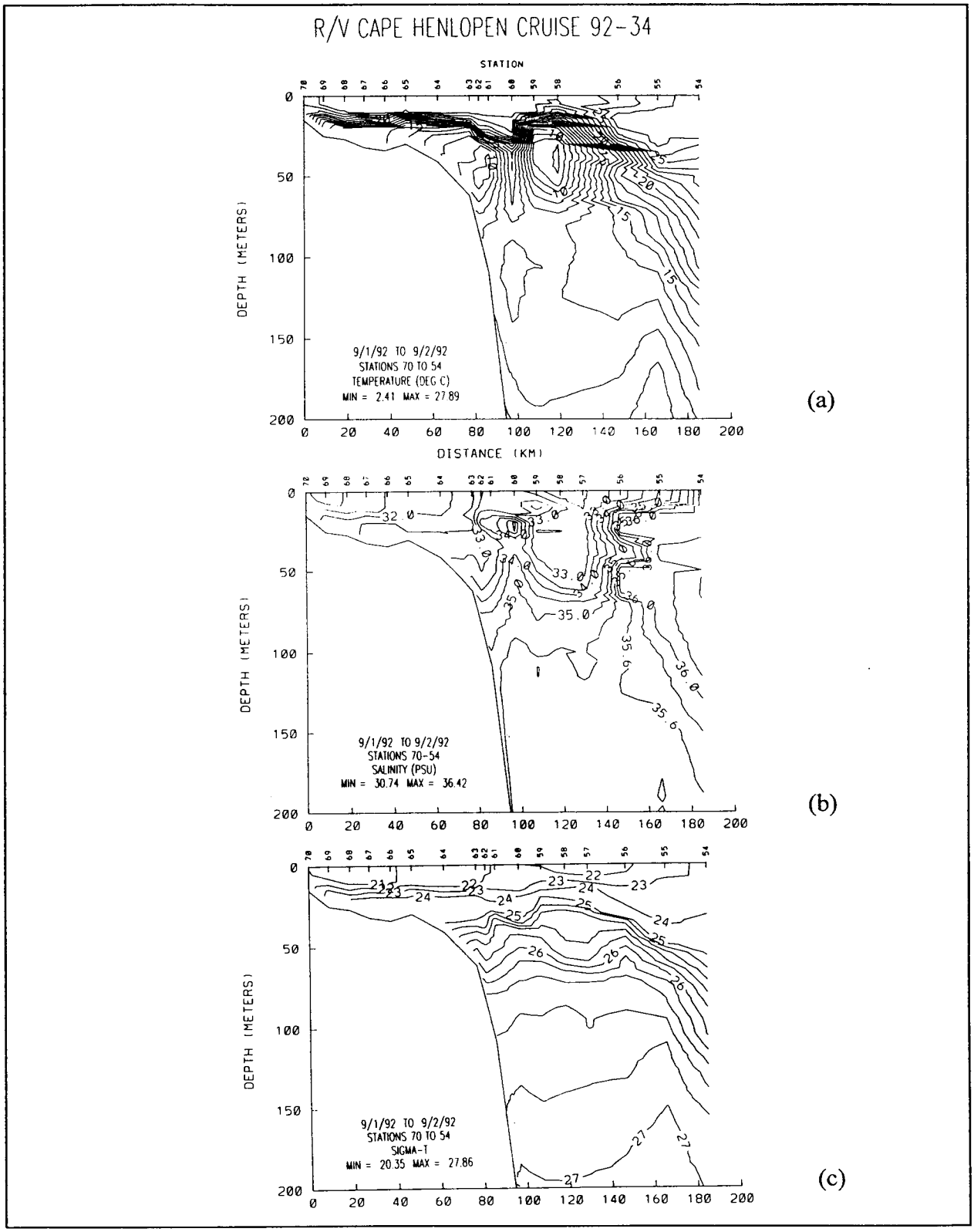

Figure 5.4-2. Cross-shelf distributions along Line A of (a) temperature, (b) salinity, and (c) sigma-t measured during cruise CH9234 on September 1-2, 1992.

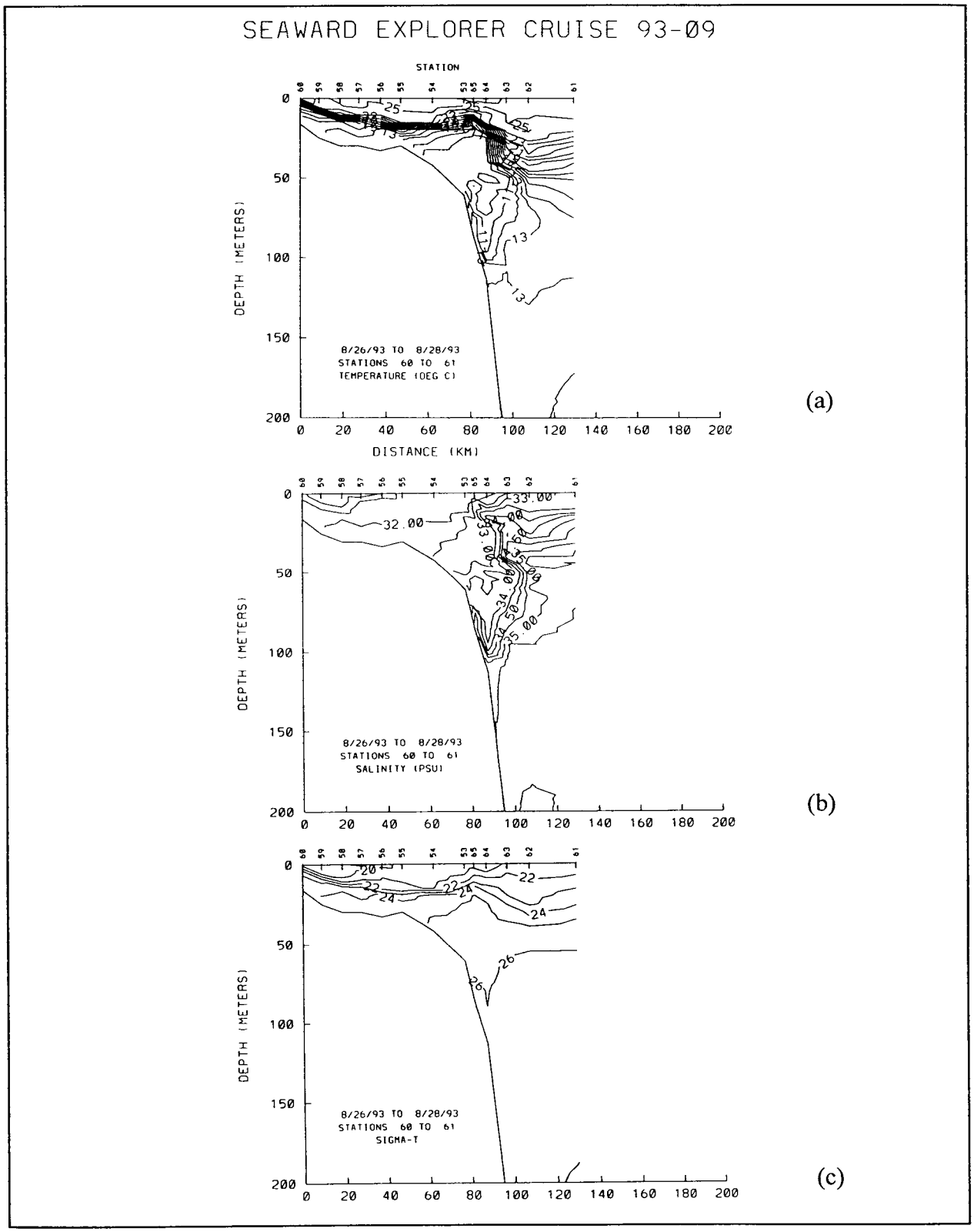

Figure 5.4-3. Cross-shelf sections along Line A of (a) temperature, (b) salinity, and (c) σ_t taken during cruise SE9309 on August 26-28, 1993.

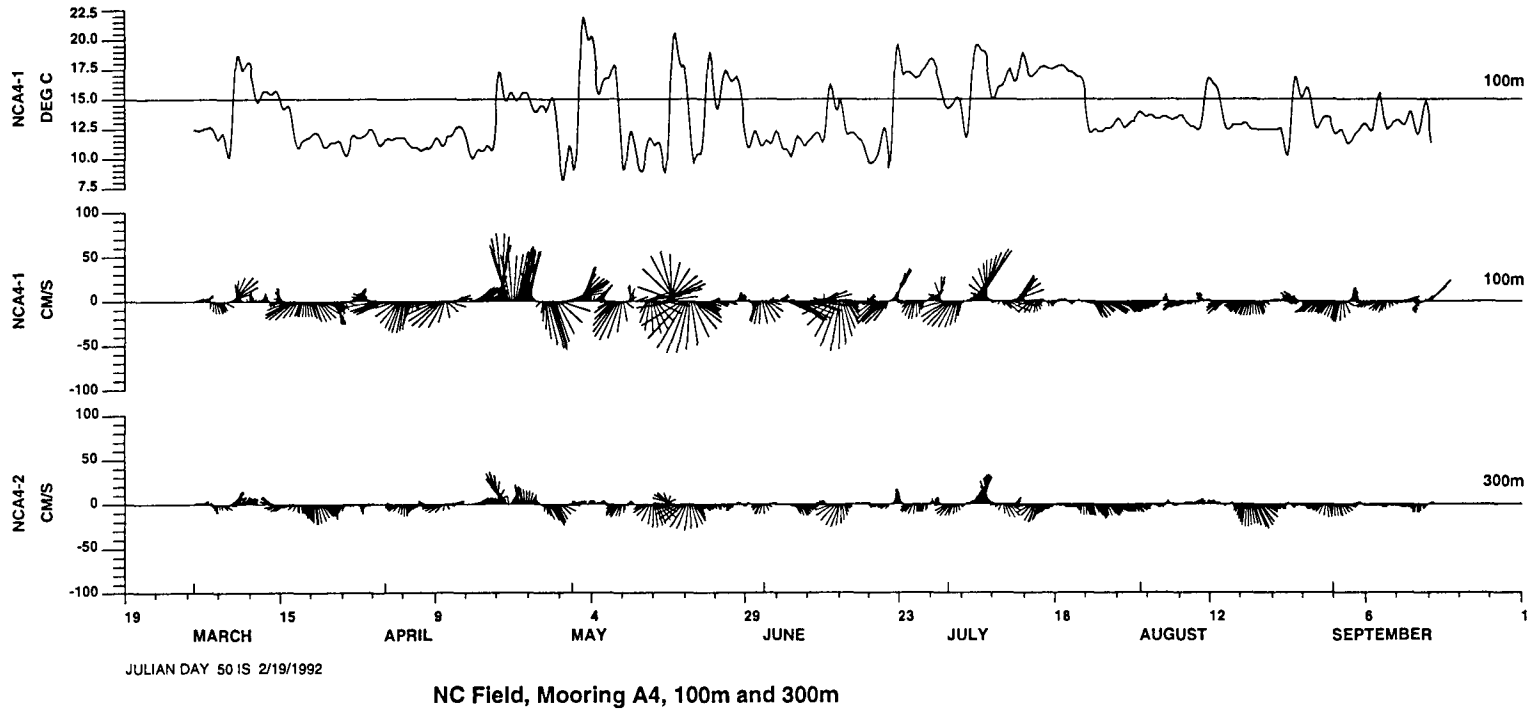

Figure 5.4-4. Stick vector plots of 40-HLP currents and temperatures at A4. The annotated depths give the nominal instrument level.

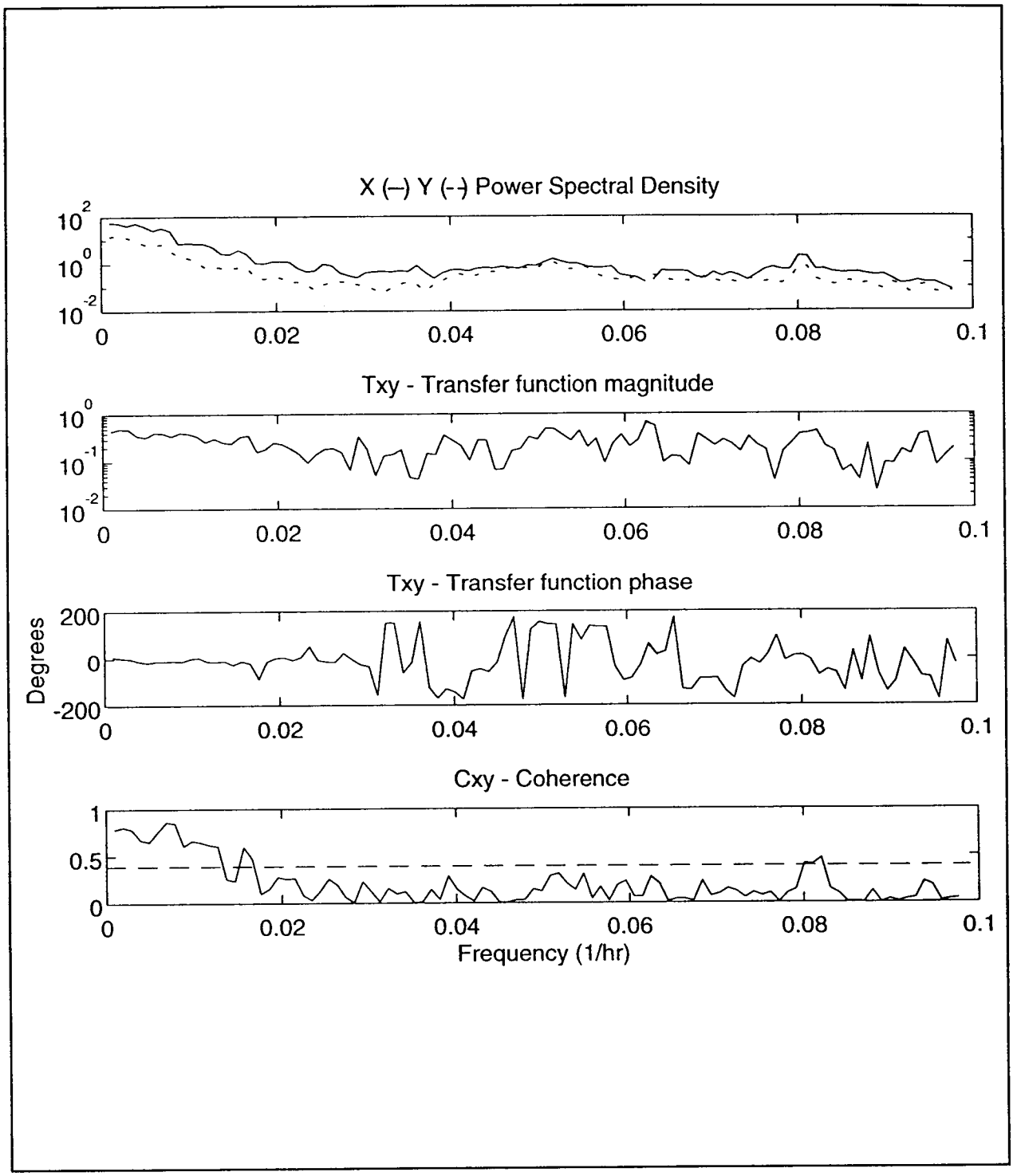

Figure 5.4-5. Power spectra of the north component of velocity measured by current meters at 100 (solid line) and 300 m (dashed line) on mooring A4 (top panel) together with the coherence and magnitude and phase of the transfer function relating the 100 and 300 m north velocity component (lower three panels).

In contrast to Gulf Stream currents which significantly influence shelf motions near Diamond Shoals (Section 5.1), Slope Sea currents do not appear to appreciably affect flow at the Middle Atlantic Bight shelf edge. In the 2-20 day frequency band, 100 and 300 m depth velocities at the A4 mooring are not coherent (at the 95% confidence level) with current measured at any level at the A3 mooring (e.g. Figure 5.4-6). This is consistent with the findings of Shaw and Csanady (1988). Based on analysis of moored current meter data, they concluded that low-frequency motions propagating shoreward from the deep sea tend to be deflected, turning to the along-isobath direction, before reaching the continental shelf. Earlier theoretical work by Csanady and Shaw (1983) and Shaw and Peng (1987) indicated that this phenomenon is due to the "insulating" effect of the steep continental slope.

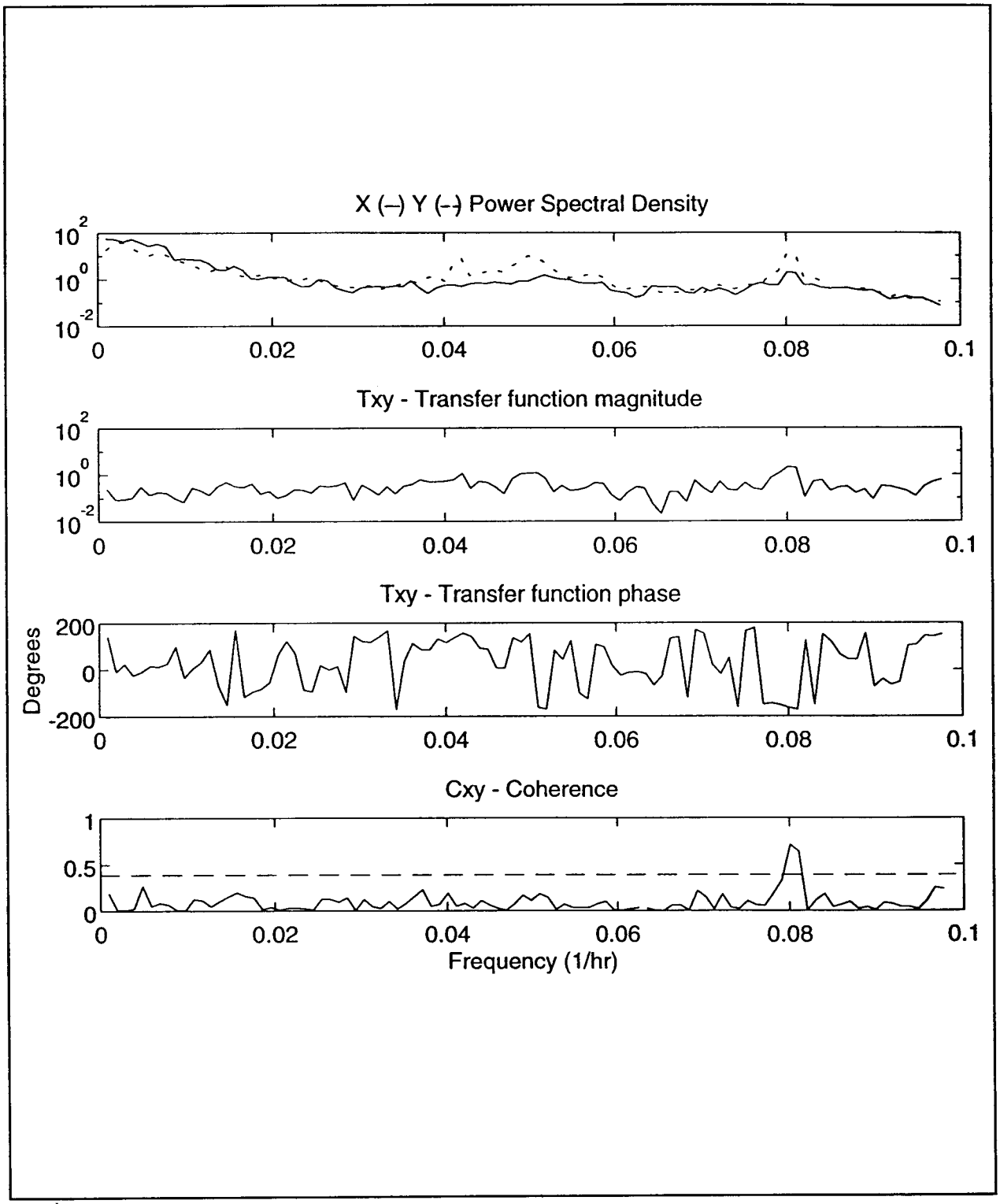

Figure 5.4-6. Same as Figure 5.4-5 except showing the results of spectral analysis relating to the north velocity component measured by the 100 m deep current meter on mooring A4 and the 5 m deep current meter on mooring A3.

VI. WIND FORCING

6.1 Background

Longshore winds are a primary forcing mechanism for continental shelf circulations. Wind forcing can be both local and indirect through propagation of coastal trapped waves. Previous studies have shown that south of Cape Hatteras in the Carolina Capes, local longshore wind fluctuations account for most of the subtidal fluctuations in sea-level and longshore currents (Chao and Pietrafesa 1980). On the other hand, Wang (1979) showed that remotely forced, southward propagating, coastal trapped shelf waves were an important influence on sub-tidal sea-level variability in the southern Middle Atlantic Bight. The continental shelf in the study region is characterized by a sharp change in the direction of the coastline at Cape Hatteras. The shelf at this position is at its narrowest and large shoals (Diamond Shoals) extend offshore. Therefore, the changes in shelf geometry and wind forcing characteristics and mechanisms between the Hatteras shelf and the Carolina Bays indicates that there may be substantial changes in the wind-driven circulations between the two shelves. In addition, there is the possibility that substantial sea-level differences could be generated around Cape Hatteras. Indeed, the FRED Group (1989) showed that large sea-level differences are generated between the Duck and Hatteras tide stations and are associated with Virginia Coastal Water intrusions into Raleigh Bay as well as with strong northerly or northwesterly winds.

On the two southern transects, B and C, Gulf Stream currents dominate the outer shelf in all seasons and influence the mid-shelf in summer. There is also a large seasonal component to the wind fields; frequent storms with northerly or northwesterly winds often forcing the shelf in winter as against much lighter winds that are often upwelling favorable in summer. The seasonal change is accompanied by a seasonal change on the shelf from well mixed conditions in winter to strongly stratified in summer. The degree of stratification in summer is much greater over the Hatteras shelf than in Raleigh Bay.

Therefore, wind forced response of the shelf is likely to differ by season and between the Hatteras shelf, which has little direct influence from the Gulf Stream, and the northern Raleigh Bay-Diamond Shoals region. The investigation has concentrated on detailed descriptions of three major storms that occurred during

the study. They are the December 10-16, 1992 wind event which generated very high sea-level anomalies all along the southern Middle Atlantic Bight; the March 12-14, 1993 "Storm of the Century"; and Hurricane Emily (August 30-September 1, 1993). This is followed by a statistical analysis of the sub-tidal shelf currents, winds and sea level for the winter-spring of 1992-1993 and the summers of 1992 and 1993. The latter sections attempts to quantify some of the relationships quantitatively described for the individual storms.

6.2 Major Wind-Forced Events

6.2.1 December 10-16, 1992 Wind Event

The first major wind-forced event during the study occurred during the second week of December 1992 and persisted for approximately one week. The event was characterized as a moderately strong Nor'easter (extratropical cyclone, 988 mb central pressure) which was sandwiched between two high pressure systems. The storm system generated high seas of 4.3-5.5 m near shore, which caused moderate beach erosion and ocean overwash along the Outer Banks coastal highway (NC 12). Figure 6.2-1 is an enlargement of the 40-HLP wind stress vectors for this wind event (NOAA 1992).

On December 8, 1992, the remnants of an intense low pressure system (968 mb) over the Canadian Maritime Provinces was moving rapidly towards the northeast; simultaneously, a broad ridge of high pressure (1027 mb) centered over the central United States plains was influencing the synoptic circulation of the eastern United States coastal region. The clockwise circulation around this expansive pressure system created southeastward wind flow at Cape Hatteras; further offshore at NDBC buoy 41001 the wind flow regime was more southward in response to the reduced surface friction over the water. By December 9, the high (1033 mb) was centered over Quebec and extended south-southeastward into the mid-section of Florida. The wind flow regime remained southward offshore of Cape Hatteras and southeastward along the coastal region. However, offshore wind speeds had increased during this time interval.

The extratropical cyclone system (1011 mb) formed along an occluded frontal system over central Louisiana and rapidly migrated eastward towards the southern Georgia coast by 0000 GMT on December 10. The Canadian high pressure remained strong (1033 mb) and began to migrate northeastward, causing the North Carolina coastal region to

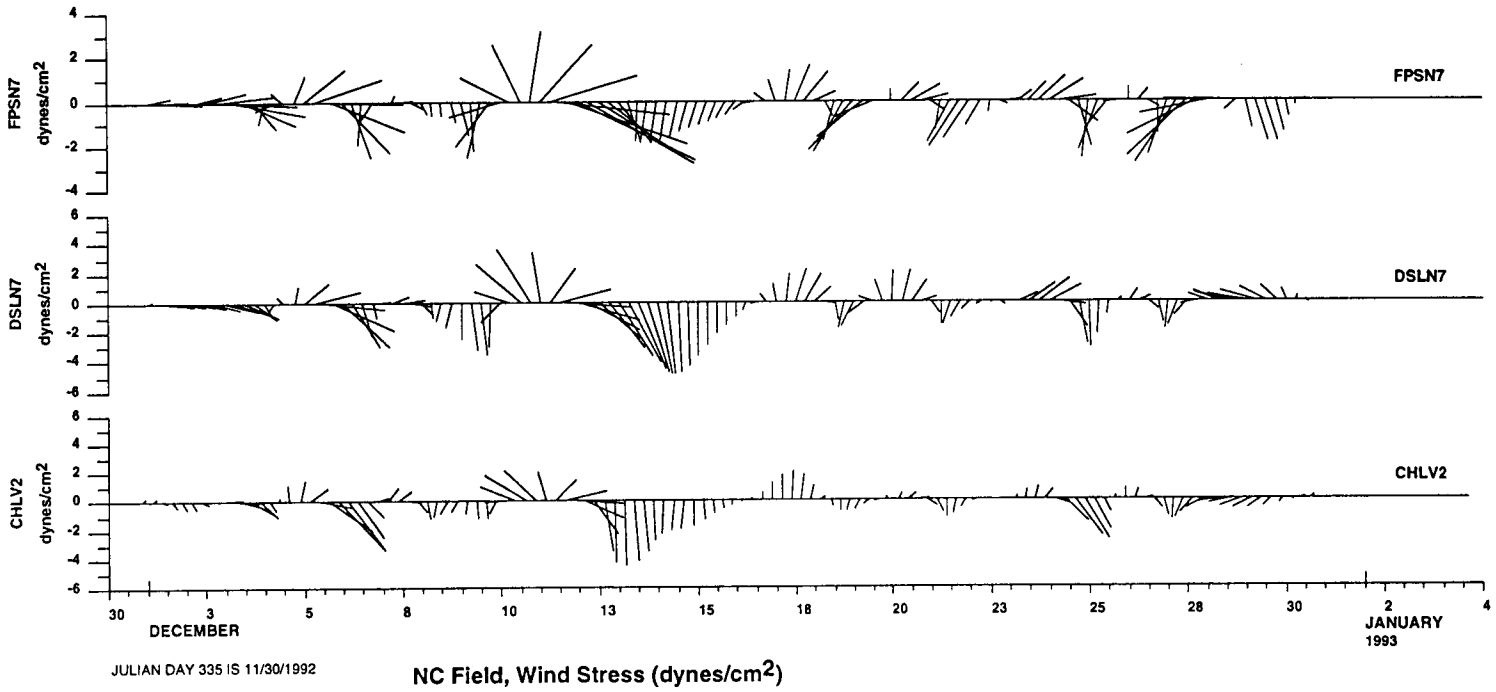

Figure 6.2-1.. 40 HLP wind stress vectors (dynes•cm^{-2}) for the 10-16 December 1992 Wind Event offshore of North Carolina.

be influenced primarily by the backside of the high. Winds now increased at both the offshore and coastal sites and became more westward. December 11 saw the cyclonic storm deepen rapidly (to 988 mb) and move quickly off to the northeast to near Baltimore, Maryland. However, because of the system's inland trajectory, the Cape Hatteras region received primarily eastward winds. Winds increased substantially in the offshore direction under this regime in part due to the reduction in surface friction and baroclinic effects. Recent studies have shown the tendency of the low-level wind field to accelerate in the vicinity of the Gulf Stream under baroclinic conditions (Wayland and Raman 1989, 1994). The rapid movement of the storm is easily detected in Figure 6.2-1, with the clockwise turning of the stress vectors as the cyclone tracked northeast along the mid-Atlantic United States.

By December 12, the storm system had weakened (996 mb) and stalled offshore in the New York Bight area, and the Cape Hatteras region was under the influence of a strong southeastward flow. During the next 24-hour period, the cyclone continued to weaken (1004 mb) and drift slowly east as a strong anticyclone (1034 mb) centered over Labrador began to influence the eastern seaboard. These two systems combined to create a strong pressure gradient parallel to the mid-Atlantic Bight area, which generated strong southward wind flow in the Cape Hatteras region. For the next two days (December 15-16) the anticyclone dominated the synoptic conditions along the eastern United States coast, creating primarily a south and southward wind flow regime along the North Carolina coast.

The overall response along the study area was well correlated. The greatest variation in the wind stress field was at the Frying Pan Shoals Light station and decreased with increasing latitude. The Chesapeake Light data showed a more abrupt transition between events than the data records at Cape Hatteras and further south. This cyclone-anticyclone system provided the first prolonged southerly flow regime along Lines A and B since late September 1992 (Hurricane Danielle).

6.2.2 Shelf Currents in December 1992

The shelf currents for December 1992 are given for Lines A, B, C and D in Figure 6.2-2. For each mooring, the 40-HLP stick vectors are shown for each instrument that returned data along with the near surface and near bottom temperatures. Also shown are sea-level and alongshore sea-level differences, and wind-stress vectors

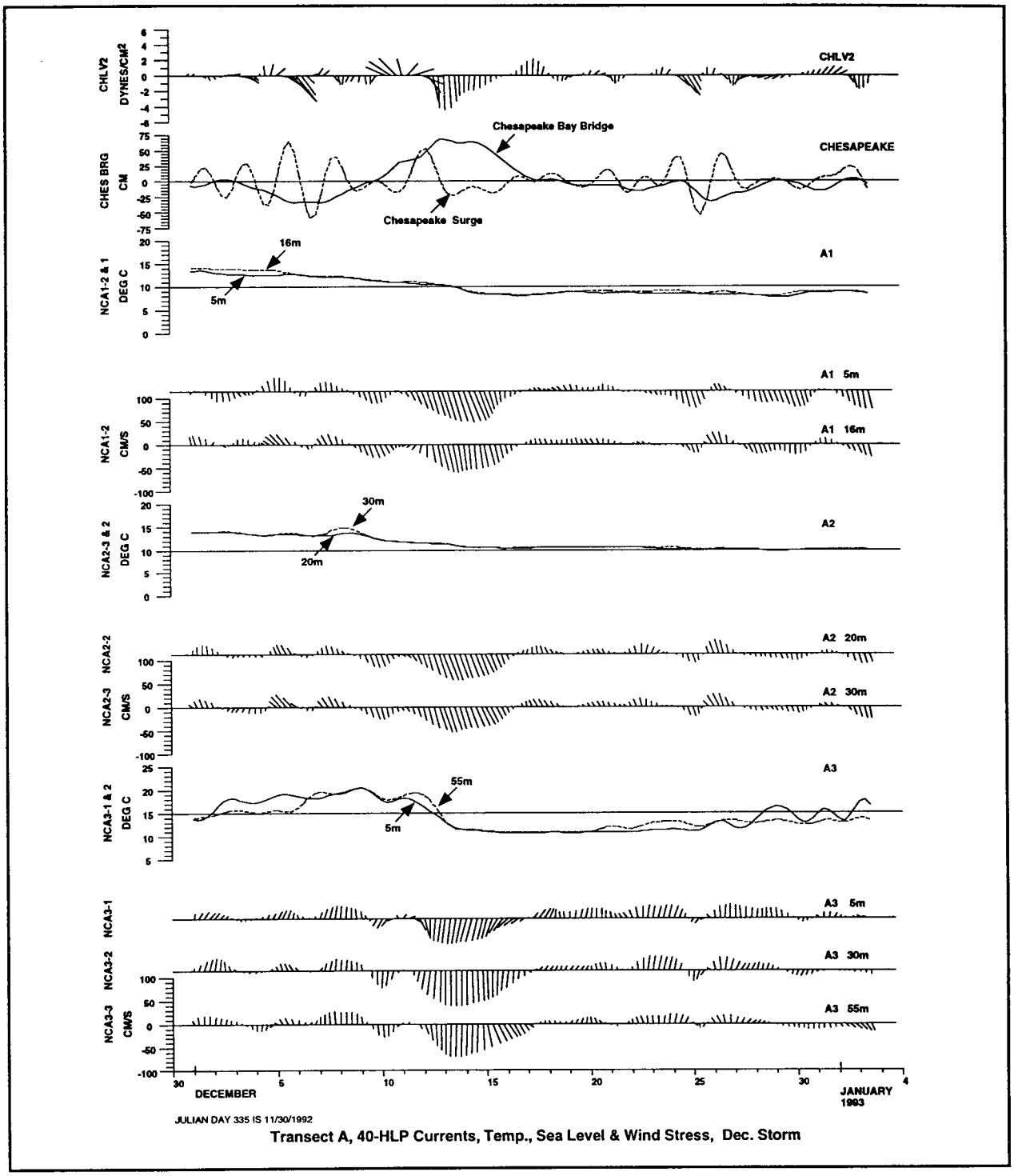

Figure 6.2-2(a). 40-HLP currents, temperatures, sea-level and windstress on Line A for December 1992. Temperatures from the deepest instrument on mooring are dashed. The Chesapeake surge analogue (see text) is dashed on the Chesapeake Bay Bridge sea-level plot (units $cm \cdot d^{-1}$).

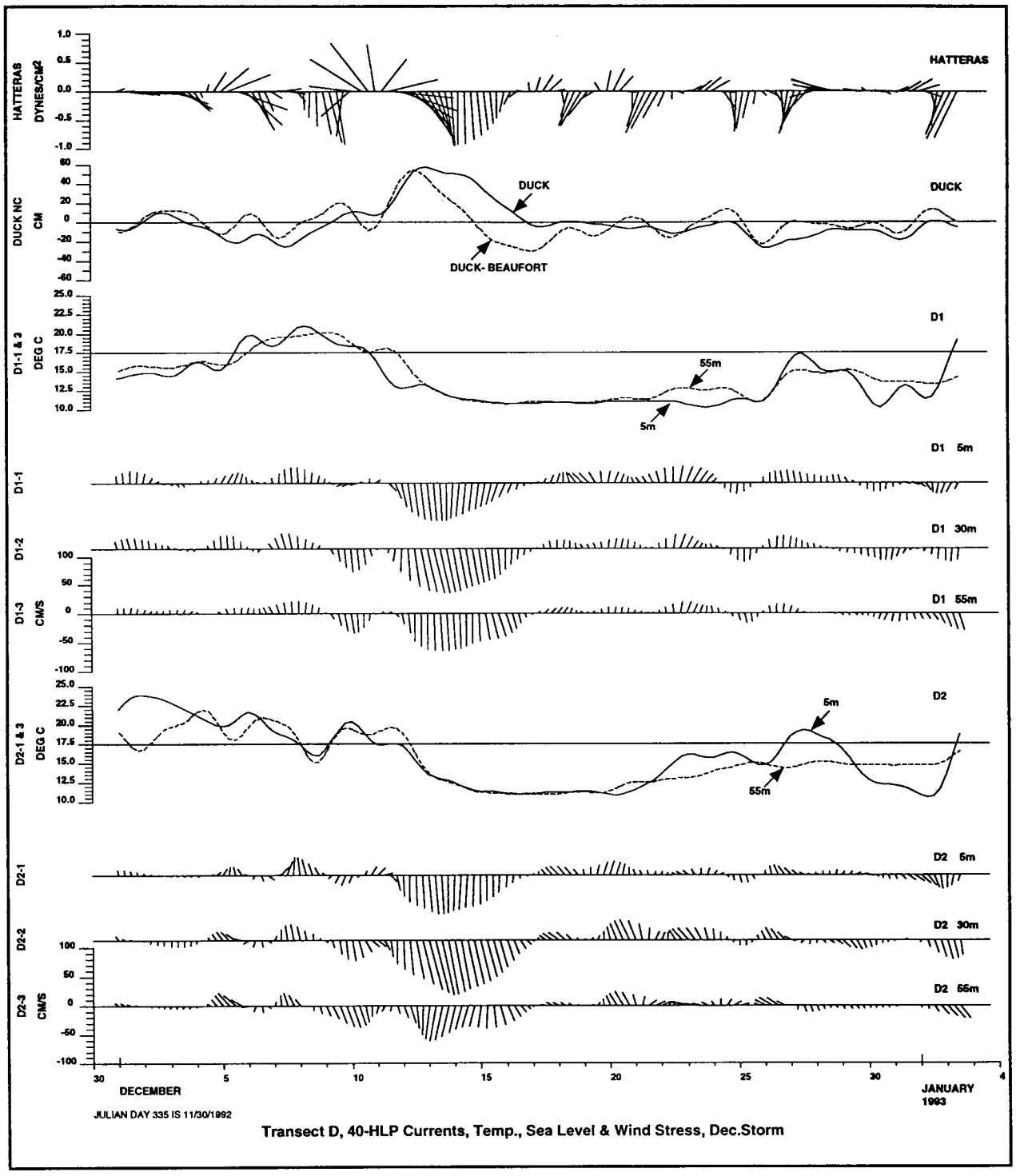

Figure 6.2-2(b). 40-HLP currents, temperatures, sea-level and windstress on Line D for December 1992. Temperatures from the deepest instrument on mooring are dashed. Sea-level difference between Duck and Beaufort is dashed on the Duck sea-level plot.

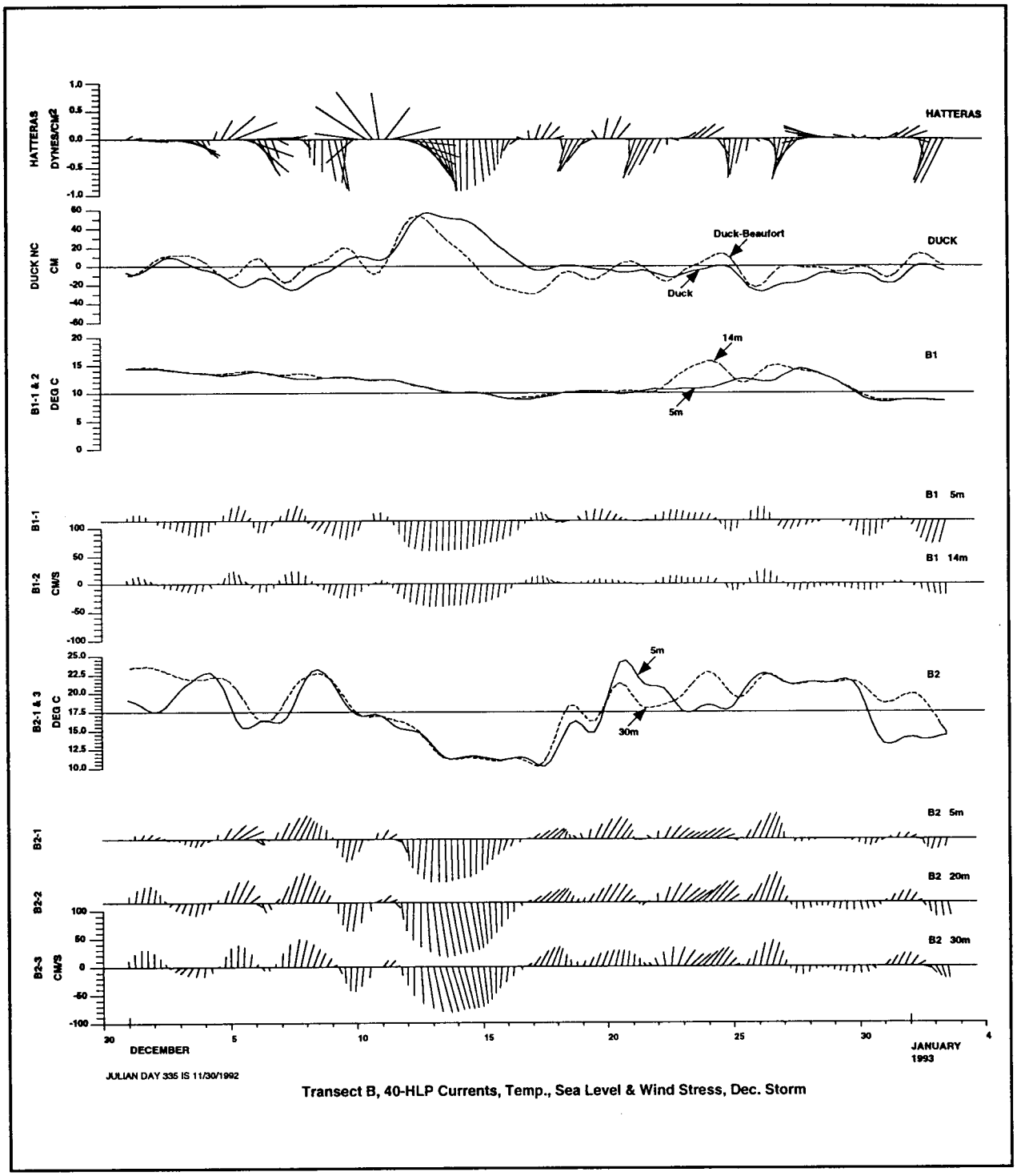

Figure 6.2-2(c). 40-HLP currents, temperatures, sea-level and windstress on Line B for December 1992. Temperatures from the deepest instrument on mooring are dashed. Sea-level difference between Duck and Beaufort is dashed on the Duck sea-level plot.

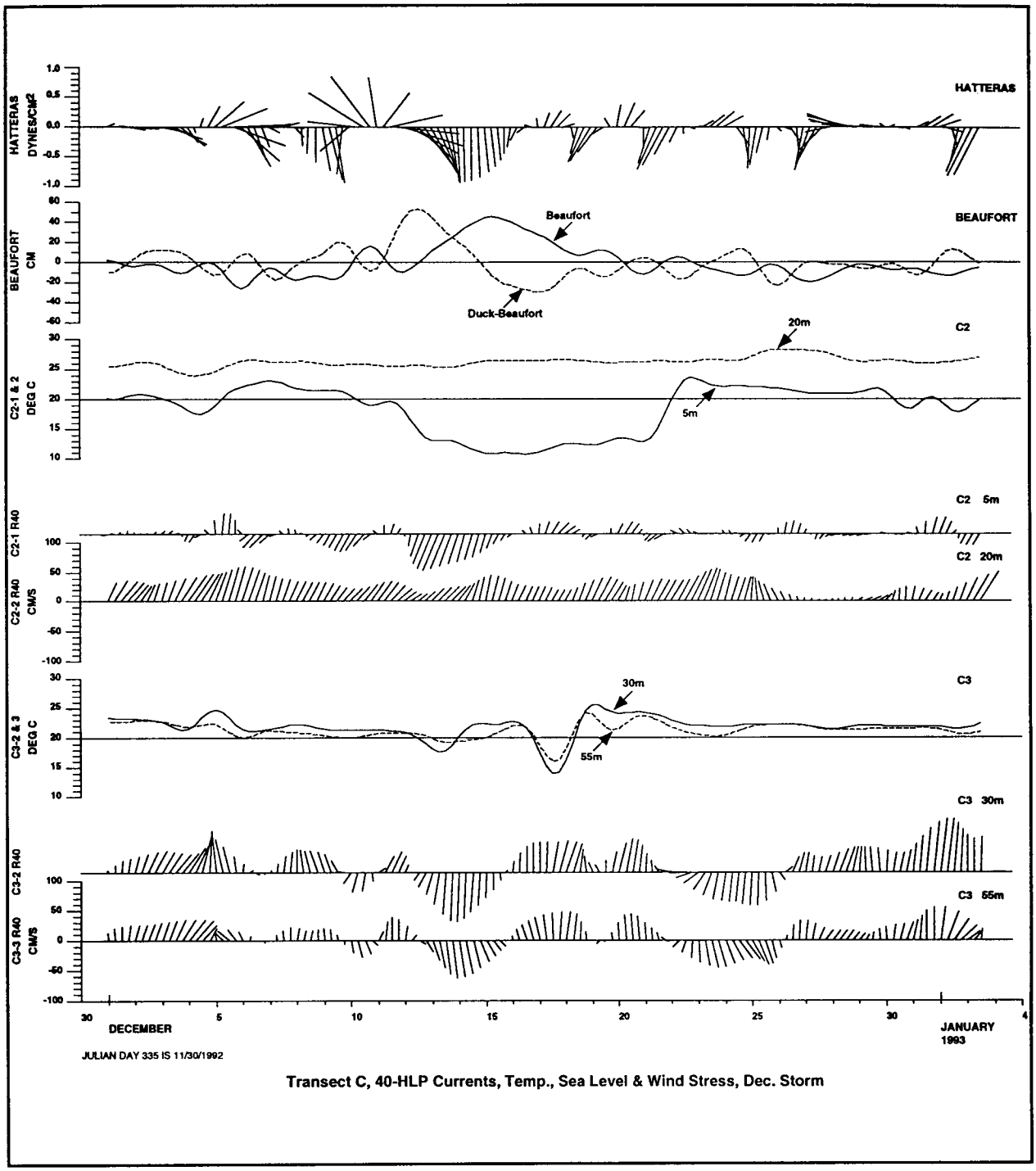

Figure 6.2-2(d). 40-HLP currents, temperatures, sea-level and windstress on Line C for December 1992. Temperatures from the deepest instrument on mooring are dashed. Sea-level difference between Duck and Beaufort is dashed on the Beaufort sea-level plot. Isobath coordinates are used (Up is 040°T).

from nearby wind stations. On Line A (Figure 6.2-2(a)), strong southward flows are observed across the shelf between December 12 and 17. Strong cooling of the water column is observed at the shelf break (A3) between December 10 and 12 but the shelf is basically well mixed across the transect. Current fluctuations are highly coherent across the transect and the response is quite uniform through the water column. Flows before and after the storm are a little more northward at the shelf edge (A3) than in the middle and inner shelf. The December 12-17 event is clearly related to both the large sea-level rise at the Chesapeake Bay Bridge and the sustained southward wind stress. Also shown in the sea level panel is the analogue of Chesapeake Bay outflow that is discussed in more detail in chapter 7. The analogue is constructed from the time derivative of the difference in 40-HLP sea-level between the Chesapeake Bay and Baltimore (e.g. d/dt (CBT-BLT)) with units of $cm \cdot d^{-1}$. It can be seen that this analogue is quite closely related to the alongshore (north-south) windstress fluctuations. Thus, it is not clear if the outflow pulses from the Chesapeake Bay contribute to shelf flows during December because of the similarities to the direct wind-forcing.

Currents and stratification along the shelf edge (Line D-Figure 6.2-2(b)) are essentially similar to A3. Maximum southward currents occur at mid-depth as at A3. No data are available at B3 for this time period, but again the mid and inner shelf on Line B show the southward event occurs at both B1 and B2, with similar magnitudes at B1 to A1, but markedly stronger flows (approaching 100 $cm \cdot s^{-1}$ at mid-depth) at B2 (Figure 6.2-2(c)) than A2. There is also much greater cooling at B2 than A2 which then warms much more rapidly when the currents reverse to the north on December 17. The warm water can be seen to progress along the outer shelf, returning on about December 22 at D2, December 26 at D1 and December 29 at A3 (Figures 6.2-2(b) and (a), respectively). No warm water is observed at A2 and A3 which continue to cool in response to cooling atmospheric temperatures throughout December.

Line C in Raleigh Bay (Figure 6.2-2(d)) shows markedly different response to the southwestward event which occupies the whole of the Hatteras shelf north of Diamond Shoals. A strong southward flow event is observed at C2 and C3 between December 12 and 16. At C2, however, only the surface layer is affected with the mid-depth instrument showing strong northeastward flow and warm temperatures. Surface temperatures are generally lower but rapidly cool on the 12th and remain cool until the 22nd despite weak reversals in

upper-layer current at C2. This surface cool water must also be less saline than lower layer so that Middle Atlantic Bight shelf water does not mix with the underlying warm salty water typical of Raleigh Bay. The fluctuations of C2, at 5 m, are clearly closely correlated to the longshore pressure gradient represented by the sea-level difference between Duck and Beaufort. (The Hatteras record is not complete for this period, but generally correlates highly with Beaufort-see Section 5.1). The sea-level difference has amplitude of ~50 cm during this event and this would account for the strong ~100 $cm \cdot s^{-1}$ flows at B2. Individual Duck and Beaufort sea-level fluctuations are given in Figures 6.2-2(c) and (d), respectively. A satellite image for December 18, 1992 (Figure 2.2-7) shows cold surface water extending throughout most of Raleigh Bay into Onslow Bay. This same image shows cold surface water extending offshore of the shelf break to about 1500 m isobath north of Cape Hatteras with a narrow tongue extending west-east along the Gulf Stream front at about 35°50'N. In contrast, the southwestward flow event in the lower half of the water column at C3 shows almost no cooling; but, when the currents reverse between December 16 and 19, cool water is advected past the mooring with the coldest water at mid-depth. The December 18 image indicates that a Gulf Stream meander crest is present at the shelf break on Line C. Therefore, the implications are that some of the cold, less saline water that flows south of Diamond Shoals between December 12 and 16 returns along the Gulf Stream front a few days later. During its journey, this cold, saline surface water has became more vertically mixed. The northward flowing return flow at C3 is not as cold as the southward flowing surface water at C2. The speculation is that much of the water that moves south, during this December event on the Hatteras shelf, moves offshore just north of Diamond Shoals, or is entrained into the Gulf Stream front in northern Raleigh Bay. No substantial offshore flows are observed at A3, D2 or D1. Unfortunately, the crucial mooring, B3, where much of the outflow may have taken place was lost in this winter period.

6.2.3 March 12-14, 1993 Wind Event ("Storm of the Century")

The wind, rain and snow event of March 12-14, 1993 has been dubbed by many who study extratropical cyclones as the "Storm of the Century". The system began to form over the southern United States plains and western Gulf of Mexico on approximately March 10. The storm system began to rapidly intensify on March 12 as it tracked northeast through the Gulf of Mexico and into the southeastern

United States. By 0000 GMT on March 13, a 976 mb low pressure center was located just to the south of Atlanta, Georgia, with an extremely tight pressure gradient extending from the Florida Keys to Long Island, New, York. As the storm system (966 mb) rapidly moved across the area on March 13 and into the northeastern United States on March 14, a strong (1036 mb), cold high pressure system was migrating southeastward from central Canada. The resultant circulations of the low pressure system moving away from the region and the oncoming anticyclone caused a strong east, southeasterly wind flow into the region. In addition to the record-breaking winds, sea level pressures and precipitation totals, this system brought record-breaking cold air into the mid-Atlantic states on the morning of March 15. This surge of cold, dry Arctic air created very intense Cold Air Outbreak conditions offshore of the eastern United States.

Figure 6.2-3 shows the 40-HLP wind stress vectors for this event at Chesapeake Light and Frying Pan Shoals Light. Initially, on March 12 the region is under the influence of a weak high pressure system (1024 mb) located over central Virginia. The air flow regime is predominantly from the northeast throughout the study area. However, by 0000 GMT on March 13, the extratropical system is well developed and deepening at rates exceeding the conventional "bomb" classification; and, in front of the approaching system, winds are approximately 18 $m \cdot s^{-1}$ towards the northwest at buoy 41001. By 0000 GMT on March 14, the center of the storm system is over Massachusetts Bay and has reached a central pressure of approximately 966 mb. The North Carolina coast is now on the back side of the storm and is being influenced by both the extratropical cyclone and the developing anticyclone in the central United States. Wind flow at 41001 remains strong (15 $m \cdot s^{-1}$), but has now shifted into the east. The conventional clockwise rotation of the winds and wind stress field for east coast extratropical cyclone passages is again evident in this event. By 0000 GMT on March 15, the high pressure system is almost directly over the region, resulting in light and variable winds across the region. However, because of the prevailing south, southeastward flow regime, the winds at Chesapeake Light are more energetic than those recorded at Frying Pan Shoals Light which is located in the wind shadow of Cape Hatteras. Wayland and Raman (1989,1994) have observed similar wind patterns during Cold Air Outbreaks in this general region.

The response of the shelf region during this wind event was affected by the storm's trajectory. The wind stress field at

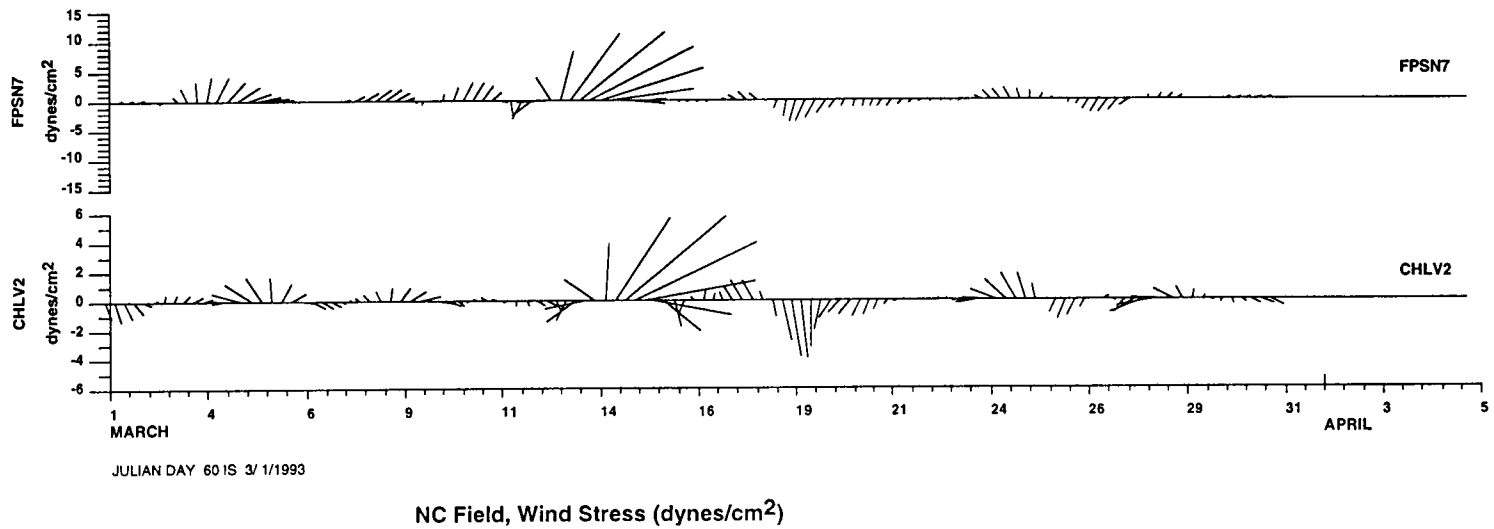

Figure 6.2-3. 40-HLP wind stress vectors (dynes•cm^{-2}) for the March 12-14, 1993 Wind Event offshore of North Carolina.

Chesapeake Light lagged the observations at Frying Pan Shoals by approximately one day and showed a much smoother transition into and out of the storm event. However, both records displayed the classical clockwise turning of the wind stress field as the storm passed through the region. The wind stress field was mirrored in the shelf current meter records from Lines A and B. The strongest shallow mooring currents, however, were recorded during the high pressure system following the cyclone event. Thus, as was observed during the earlier wind event (December 1992), the conjunction of an extratropical storm with a strong anticyclone ridging in behind the storm system generates a significant change in the overall shelf circulation.

6.2.4 Shelf Currents in March 1993

The sub-tidal currents and temperatures from the four transects for March 1993 are given in Figure 6.2-4. The arrangement of the data is similar to that of December 1992 in Figure 6.2-2. Flows are generally southwards except for C3 and B3 and the period of the March "storm of the century." There are two large Virginia coastal water intrusions into Raleigh Bay, during the period of the plots (February 24-April 11), with similar characteristics to those described for the December 1992 southward flow event in Section 6.2.2. They are from February 28-March 8 (satellite images for March 1, 8 and 12, 1993; Figure 6.2-5), and from March 25 to April 10. Differences with the earlier December event are that the flows and temperatures at C1 and C2 in Raleigh Bay are southwestward and cold through the water column rather than just at the surface (Figure 6.2-4(a)). There is some evidence of return flows along the Gulf Stream front at B3 and C3 as the events relax and retreat. There is strong offshore flow at B3, after the March 25 - April 10 event has relaxed. These Virginia Coastal water intrusions are again accompanied by strong, longshore surface pressure gradients (Duck higher than Beaufort). The impression from the current data and imagery is that slugs of Middle Atlantic Bight shelf water advance and retreat into Raleigh Bay forced by northerly winds and longshore pressure gradients and South Atlantic Bight shelf water is forced into a narrow band adjacent to the Gulf Stream front (see images for March 12, Figure 6.2-5(c). Therefore, except for the storm, the majority of the March and April, 1993 is dominated by shelf wide Virginia Coastal Water intrusions.

Because the March 12-14 storm moved northwards and the shelf responded to clockwise rotating northward windstress vectors, the

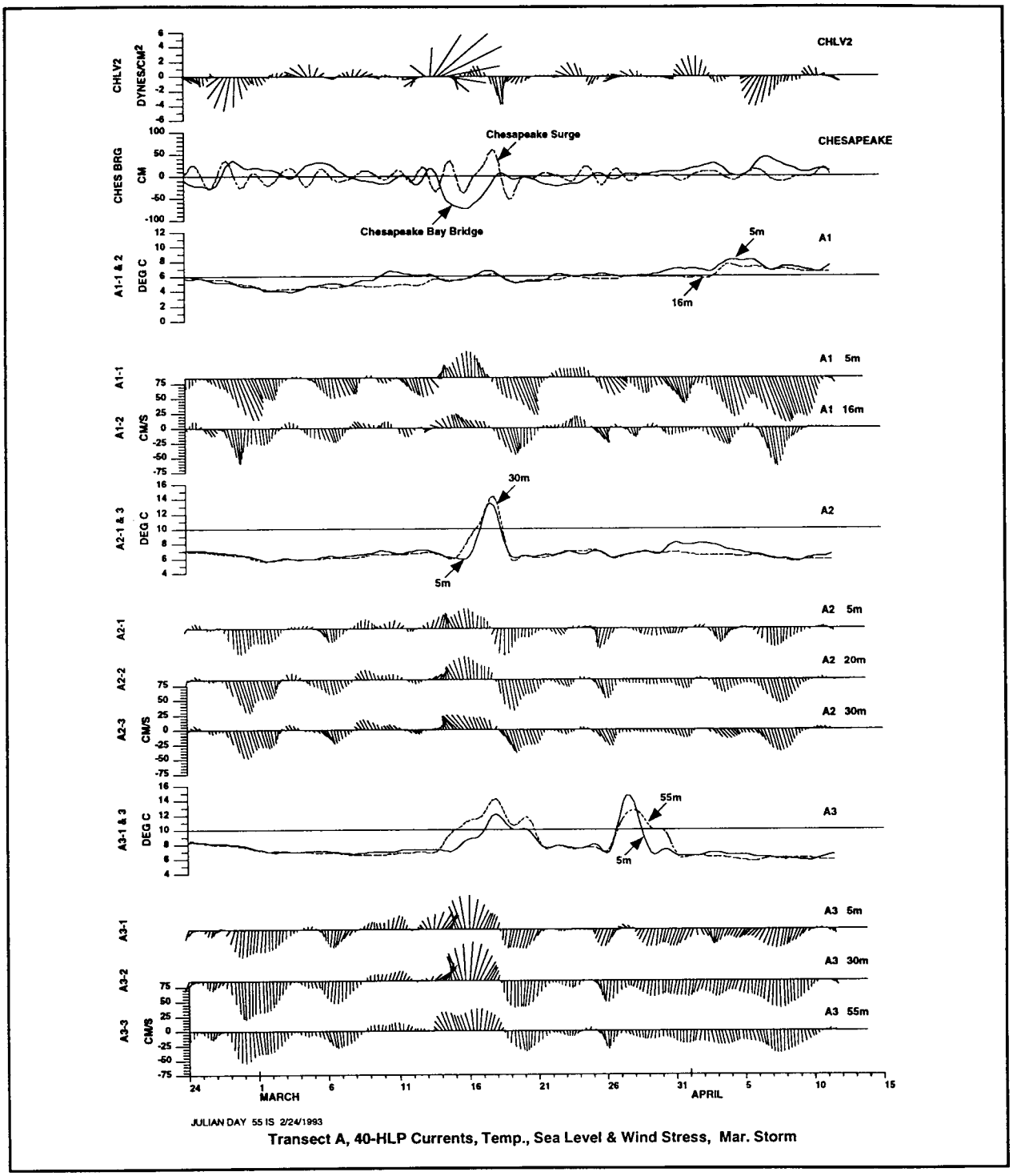

Figure 6.2-4(a). 40-HLP currents, temperatures, sea-level and windstress on Line A for March and April 1993. Temperatures from the deepest instrument on mooring are dashed. The Chesapeake surge analogue (see text) is dashed on the Chesapeake Bay Bridge sea-level plot (units $cm \bullet d^{-1}$).

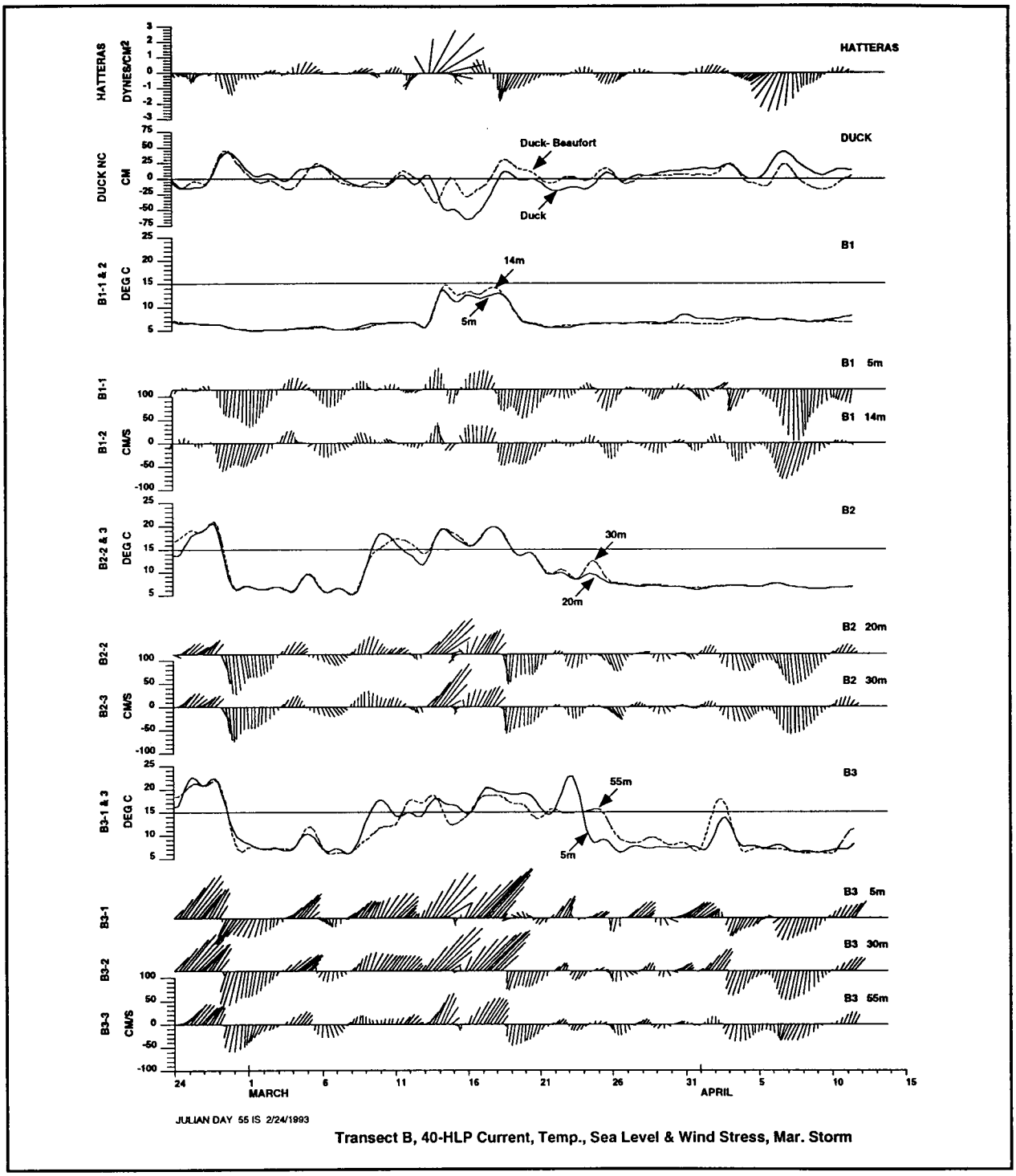

Figure 6.2-4(b). 40-HLP currents, temperatures, sea-level and windstress on Line B for March and April 1993. Temperatures from the deepest instrument on mooring are dashed. Sea-level difference between Duck and Beaufort is dashed on the Duck sea-level plot.

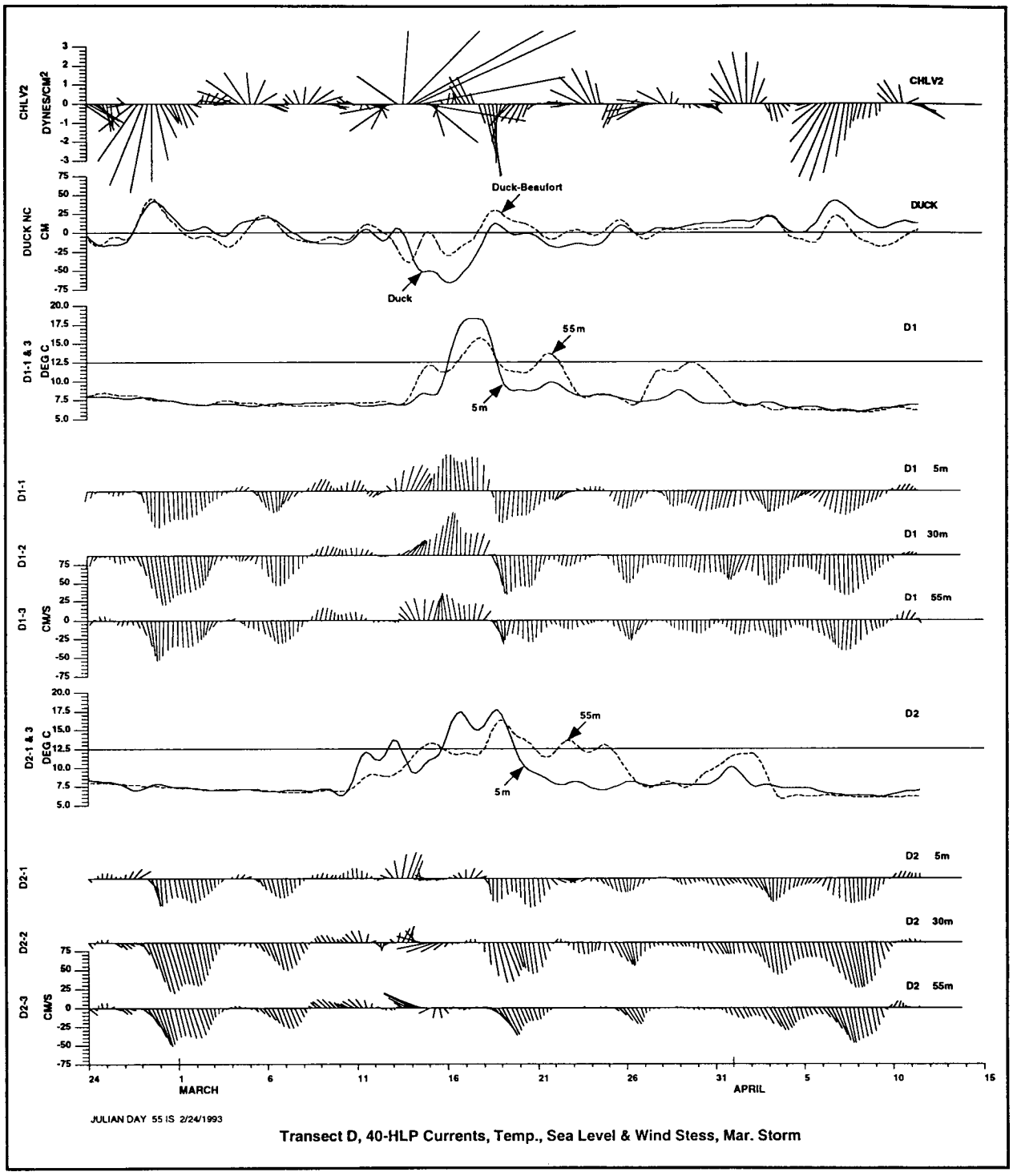

Figure 6.2-4(c). 40-HLP currents, temperatures, sea-level and windstress on Line D for March and April 1993. Temperatures from the deepest instrument on mooring are dashed. Sea-level difference between Duck and Beaufort is dashed on the Duck sea-level plot.

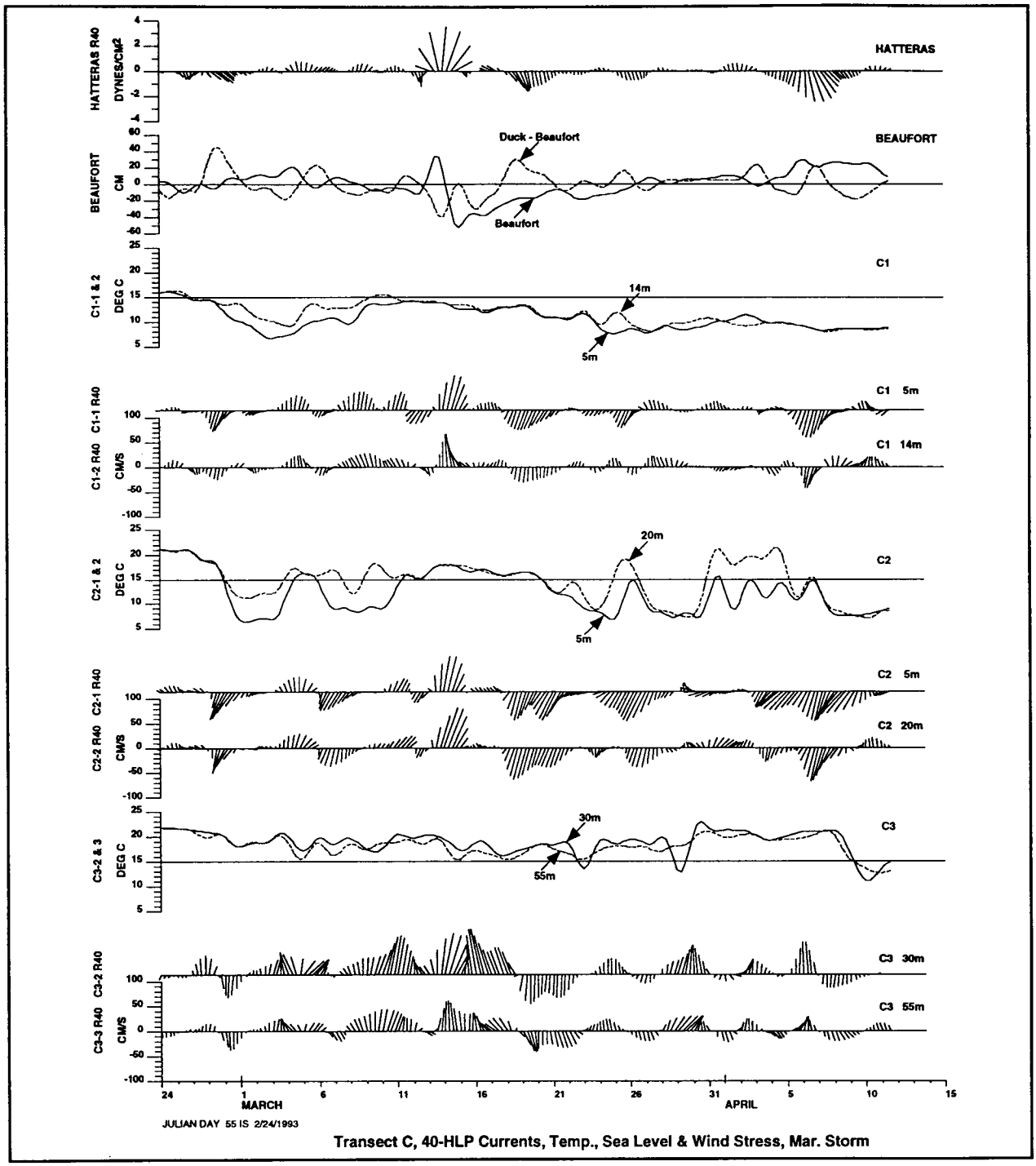

Figure 6.2-4(d). 40-HLP currents, temperatures, sea-level and windstress on Line C for March and April 1993. Temperatures from the deepest instrument on mooring are dashed. Sea-level difference between Duck and Beaufort is dashed on the Beaufort sea-level plot. Isobath coordinates are used (Up to 040°T).

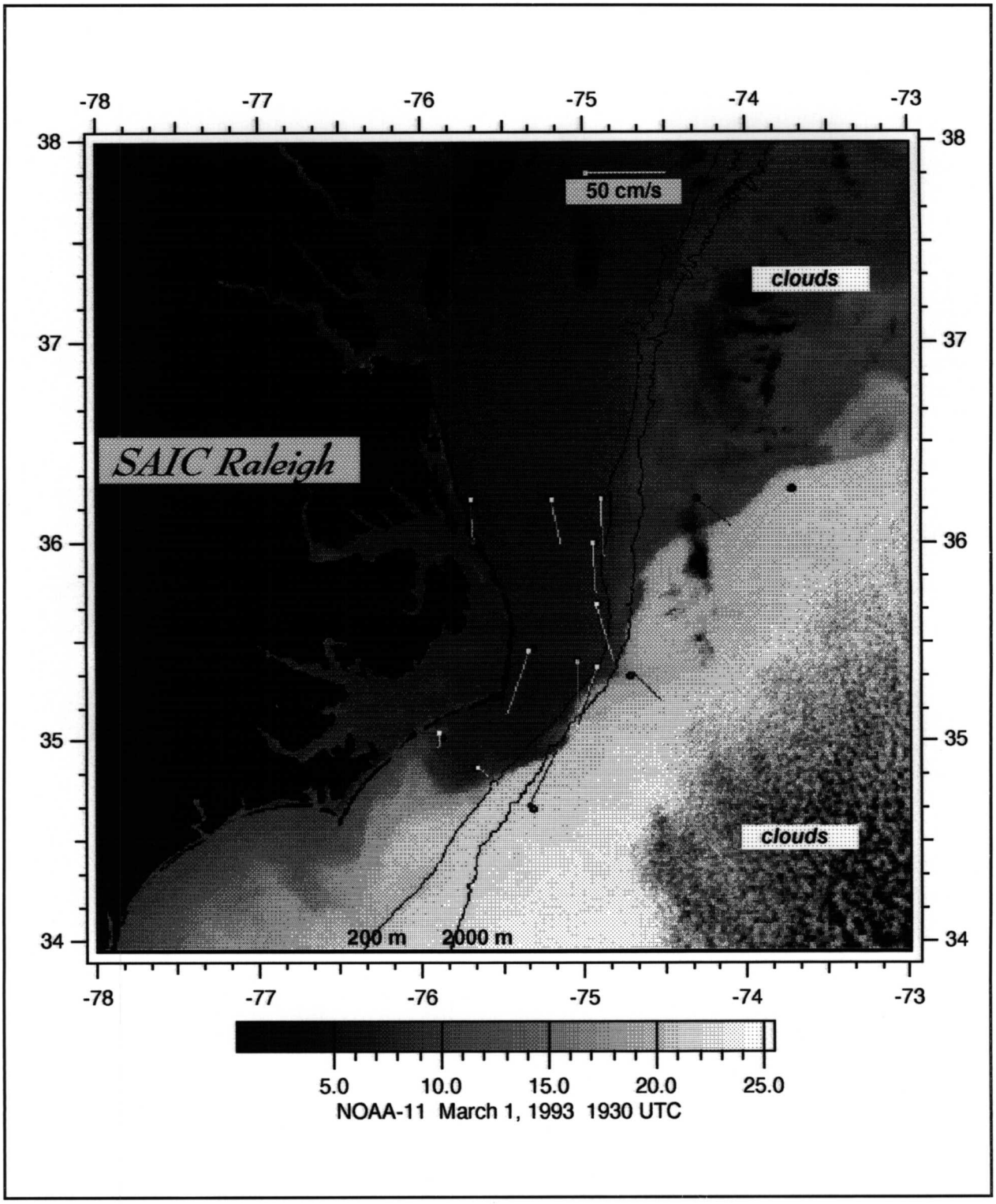

Figure 6.2-5(a). Satellite SST Image and Daily Average Current Vectors on March 1, 1993. Annotated as in Figure 2.2-7.

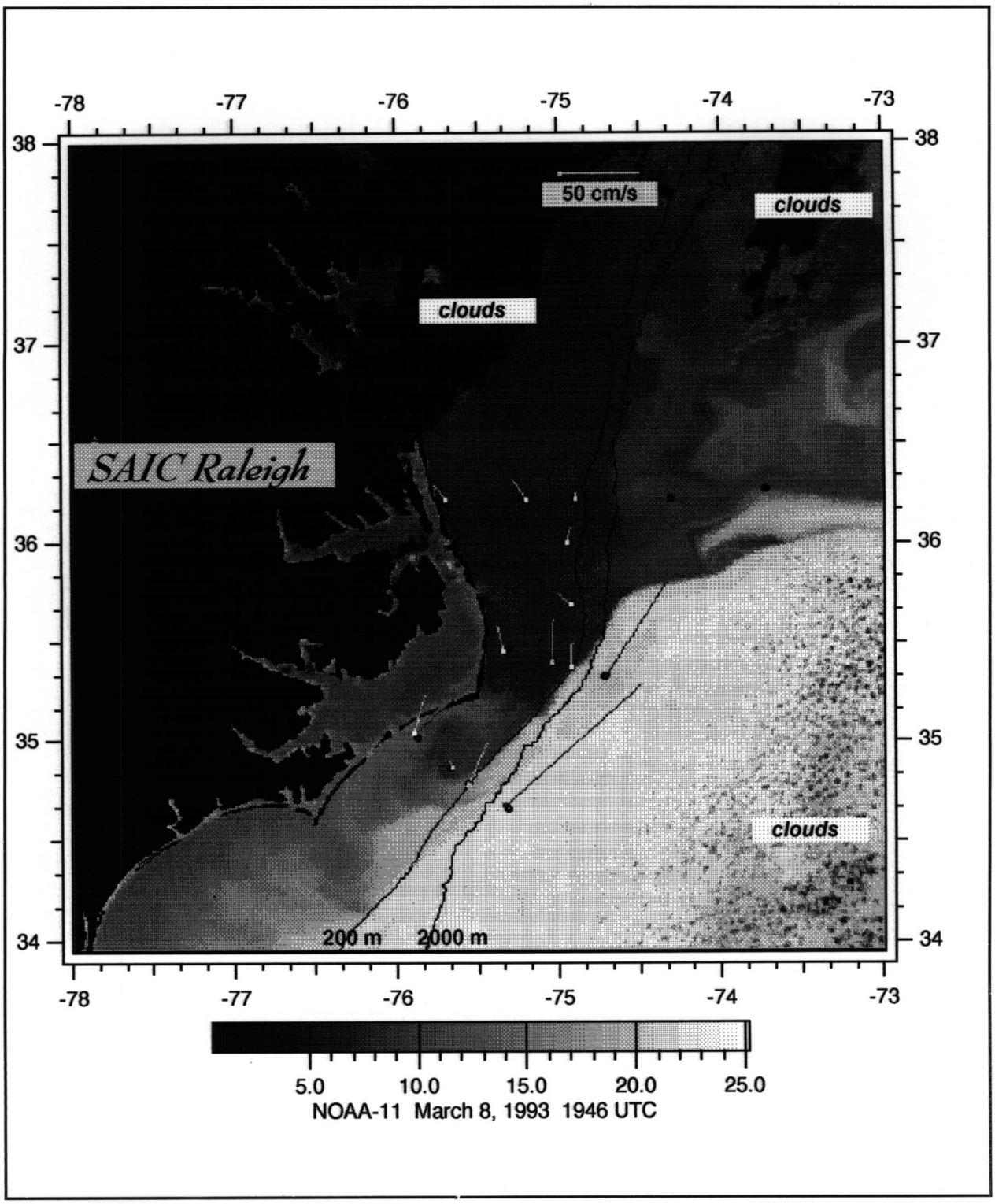

Figure 6.2-5(b). Satellite SST Image and Daily Average Current Vectors on March 8, 1993. Annotated as in Figure 2.2-7.

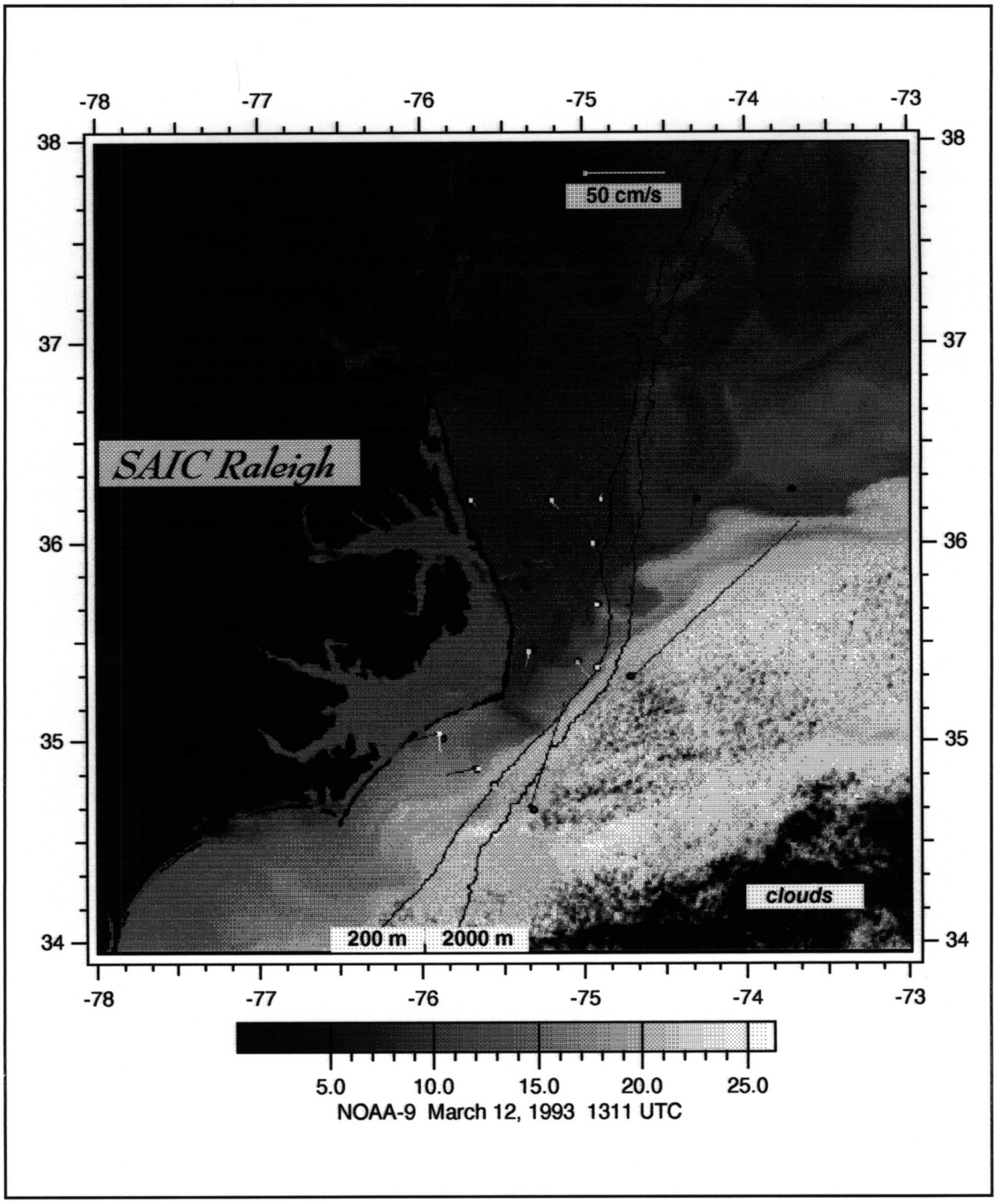

Figure 6.2-5(c). Satellite SST Image and Daily Average Current Vectors on March 12, 1993. Annotated as in Figure 2.2-7.

shelf current and temperature responses will be discussed from south to north. Figure 6.2-4(a) shows Line C currents and temperatures. The northward currents, with a clockwise rotating component, between March 12 and 15 are present at all upper-layer instruments. At C1 near-bottom, there is strong onshore shore flow during the second half of the event consistent with a bottom Ekman layer generated by local wind-forced upwelling. No bottom onshore flow is observed at C3 until the 16th and 17th of December. Immediately following the storm event a Gulf Stream meander crest produces a strongly sheared current at C3 (March 15 to 18). Temperatures show almost no stratification and remain relatively high at all the C moorings during the period of the storm.

A very similar sequence is observed on Line B with clockwise rotating northward currents observed during the storm and equally strongly during the following meander crest event which occurs at B3 about 12-18 hours later than at C3. It is uncertain, since there is no clear imagery, whether the northward flows at B1 and B2, between March 16 and 19, are wind forced or Gulf Stream forced. At B2, it seems likely that they are Gulf Stream forced because temperatures reach 20°C which is about 2° higher than temperatures at C2 on the same isobath and the same as at B3. The strength of storm currents at B1 is less than at C1 presumably because of the change in orientation of the coastline relative to the strongest winds. However, the March 16-19 event has current velocities, at B1, similar to that of the storm period but windstress is much less (~1 dyne•cm^{-2}). It is noted that the longshore pressure gradients have similar magnitudes (Beaufort higher than Duck) for both the storm and the following northward events. Thus, it is possible that longshore pressure gradient is a component of the forcing for the relatively strong northward flows at B1 between March 16 and 18.

The storm currents, as distinct from the following Gulf Stream event (March 14-18) on the shelf break north of Cape Hatteras (A3 (Figure 6.2-4(a)) D1 and D2 (Figure 6.2-4(b)),are relatively weak, ~20-30 cm•s^{-1}, compared to further south. There is, however, more depth structure. Strong onshore flow (~25 cm•s^{-1}) is observed at the 30 and 50 m levels of D2 between March 13 and 15. There seem compensating offshore flow at the 30 m level of D1 and the 5 and 30 m level of A3. This may be a response to the strong eastward component of the windstress at this time which may be directly forcing surface water off the shelf and resulting in compensating onshore flow at depth. The storm event merges into the following

Gulf Stream event which misses D2, but is observed at D1 and A3 on the 60 m isobath. Only this latter event causes substantial warming at D1 and A3 with maximum temperatures of 18°C at D1 and 14°C at A3 on March 18. This indicates substantial mixing of Gulf Stream derived water with surrounding shelf water. Since the meander crest is not, or only weakly, observed at D2 after March 16 and the water is warm but not as warm as at B3, it is possible that event at D1 and B3 are not directly the result of Gulf Stream currents but the result of extended Gulf Stream water advecting northwards along the outer shelf. Forcing for this flow could come from the wind and the longshore pressure gradient. Sea-level at Duck and the Chesapeake Bay Bridge are substantially depressed (~60-70 cm) from the middle of the storm on March 14 to the end of the Gulf Stream event in March 18 when temperatures reach their maximum values (Figures 6.2-4(a) and b)).

On the inner and middle shelf on A, the northward flows are from March 14 to 18 which corresponds exactly with the large depression of sea-level at the Chesapeake Bay Bridge and Duck. The initial part of the storm does not override the southward flow at the 5 m level at A1. Flows at A2 and A3 are fairly uniform with depth. Substantial warming is observed at A2 (from 6°C to 14°C) indicating that warm water at the shelf break, derived from the Gulf Stream, penetrates to mid-shelf. It is also possible that the warm water on Transect B, which has both a shelf and Gulf Stream origin is advected nortwards by the shelf currents. Bottom currents at A2 and A1 have onshore components and slightly warmer temperatures are observed at bottom than at the surface for A2 and A3. There is no warming at A1. Therefore, the strong northward winds and a Gulf Stream meander/overwash event at Cape Hatteras combine to flood most of the shelf, north of Diamond Shoals, with warm Gulf Stream derived water. Warm water on the inner shelf at B1 probably derives from the northward flux of warm water, forced by the wind, from the inner shelf in Raleigh Bay. This water may also contribute to the warm event at mid-shelf on transect A. Thus, the event is quite complex and it is difficult to distinguish the relative importance of the wind and the Gulf Stream forcings.

6.2.5 30-31 August - 1 September 1993 Wind Event (Hurricane Emily)

The first major Atlantic Hurricane of the 1993 season (June-November) approached the Outer Banks of North Carolina on August 30, 1993. The storm system originated about 1100 km east-northeast of the Leeward Islands on August 22. For the next four days Emily

remained a weak tropical depression (winds ≤ 15.6 $m \cdot s^{-1}$) drifting slowly towards the northwest. On August 27 Emily became a minimal hurricane and was located approximately 750 km south of Bermuda. By August 30, Emily had deepened to a Category 3 hurricane with sustained winds of 44 $m \cdot s^{-1}$. By August 31, the storm center (or eye) remained roughly 46 km offshore with the destructive western eyewall passing over Hatteras Island. To the northeast of Emily's eyewall, Air Force reconnaissance reported maximum sustained one-minute winds of 51.4 $m \cdot s^{-1}$. Additionally, the Diamond Shoals Light (C-MAN Station) reported a peak wind gust of 59.0 $m \cdot s^{-1}$. By late in the day on August 31, the system passed just offshore of Cape Hatteras and began a slow turn to the northeast, away from the United States mainland and the study area. By September 2, the storm system was approximately 740 km north of Bermuda and was effectively no longer influencing the current and wind regimes of the study area (SRCC 1993).

Figure 6.2-6 shows the 40-HLP wind stress vectors for Hurricane Emily for the Chesapeake Light and Diamond Shoals Light Station was C-MAN stations. The Frying Pan Shoals Light Station was not operational during this wind event. Prior to the hurricane, the eastern United States was under the influence of a broad ridge of high pressure (1024 mb), which was providing a general wind stress field towards the north. In conjunction with the hurricane a weak frontal system passed through the area, setting-up a general southwestward wind stress field. As the storm approached the North Carolina coastal region, the wind stress field turned counterclockwise as the storm initially approached, skirted and moved away from the region. Following Emily, a high pressure system (1024 mb) developed offshore of the region and provided a strong reversal in the stress field. This reversal was most notable at the Chesapeake Light C-MAN station.

6.2.6 Shelf Currents During Hurricane Emily

The strong southward windstress during the passage of Hurricane Emily drives a classical Ekman circulation on Line A (Figure 6.2-7(a)). This is most clearly observed at A2 between August 31 and September 3, where the near surface has an onshore component, the mid-depth the flow southward, parallel to the isobaths, and the near-bottom has a strong offshore component and is clearly in the bottom boundary layer. The water column is highly stratified but hurricane causes some reduction of surface temperature and corresponding increase in bottom temperature implying vertical

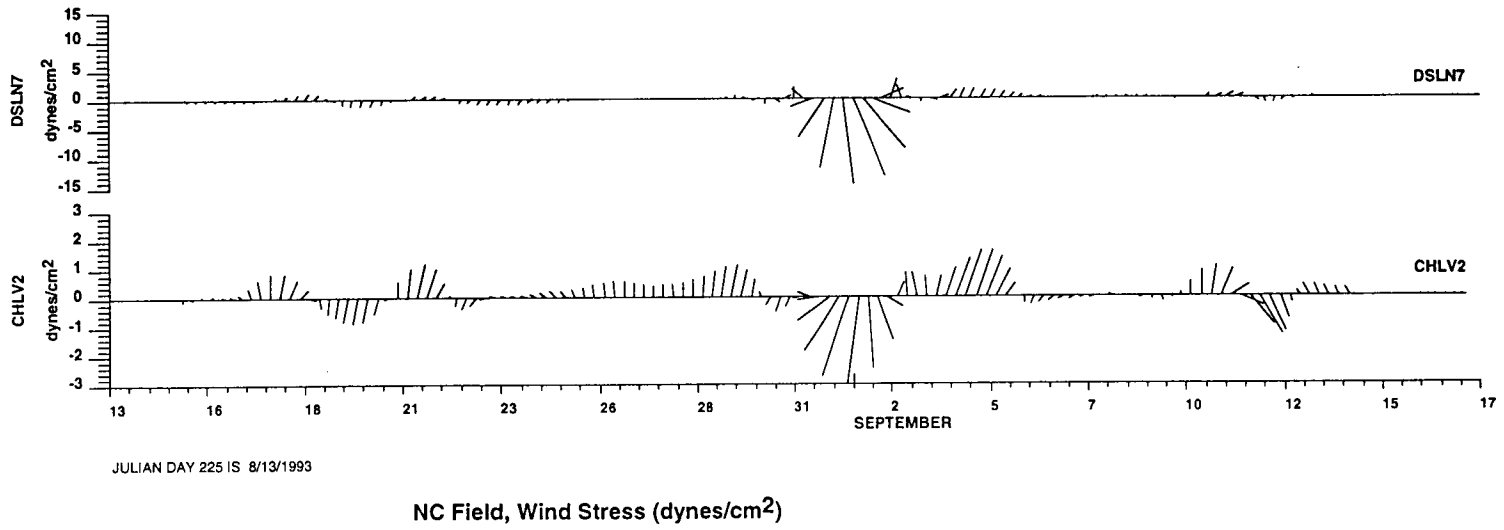

Figure 6.2-6. 40-HLP wind stress vectors (dynes•cm^{-2}) for the August 30-September 1, 1993 Wind Event offshore of North Carolina.

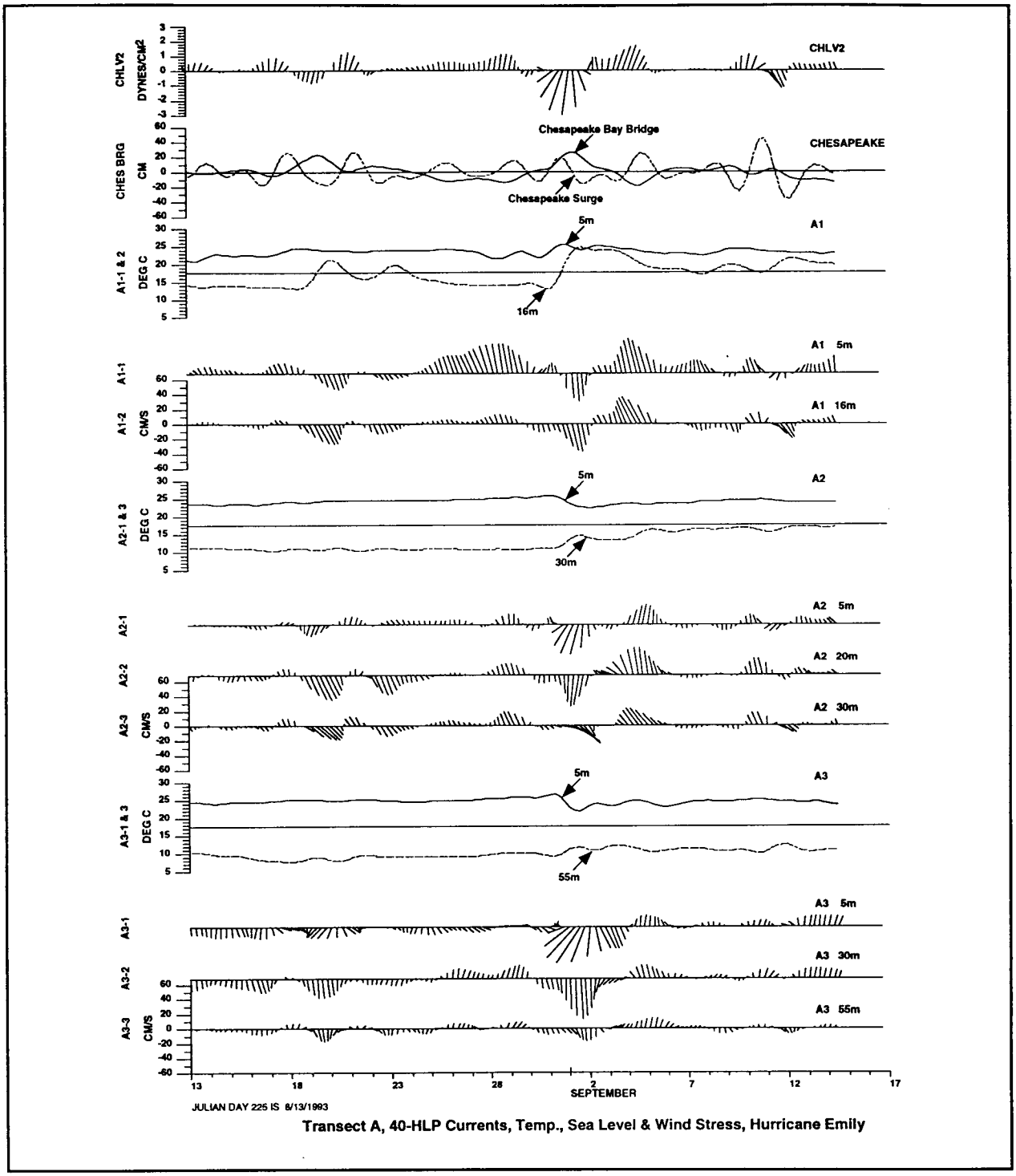

Figure 6.2-7(a). 40-HLP currents, temperatures, sea-level and windstress on Line A for August 1993. Temperatures from the deepest instrument on mooring are dashed. The Chesapeake surge analogue (see text) is dashed on the Chesapeake Bay Bridge sea-level plot (units $cm \bullet d^{-1}$).

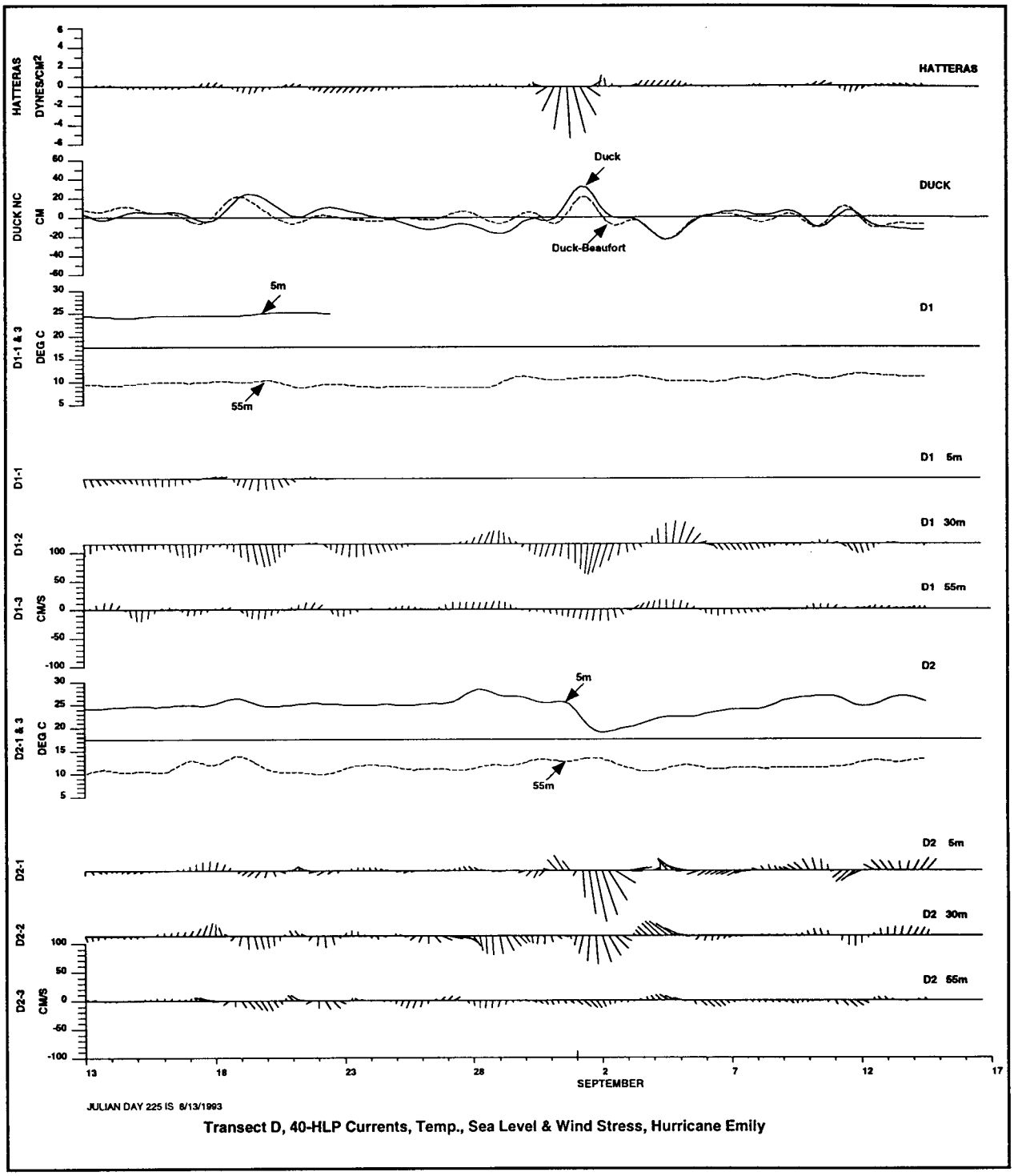

Figure 6.2-7(b). 40-HLP currents, temperatures, sea-level and windstress on Line D for August 1993. Temperatures from the deepest instrument on mooring are dashed. Sea-level difference between Duck and Beaufort is dashed on the Duck sea-level plot.

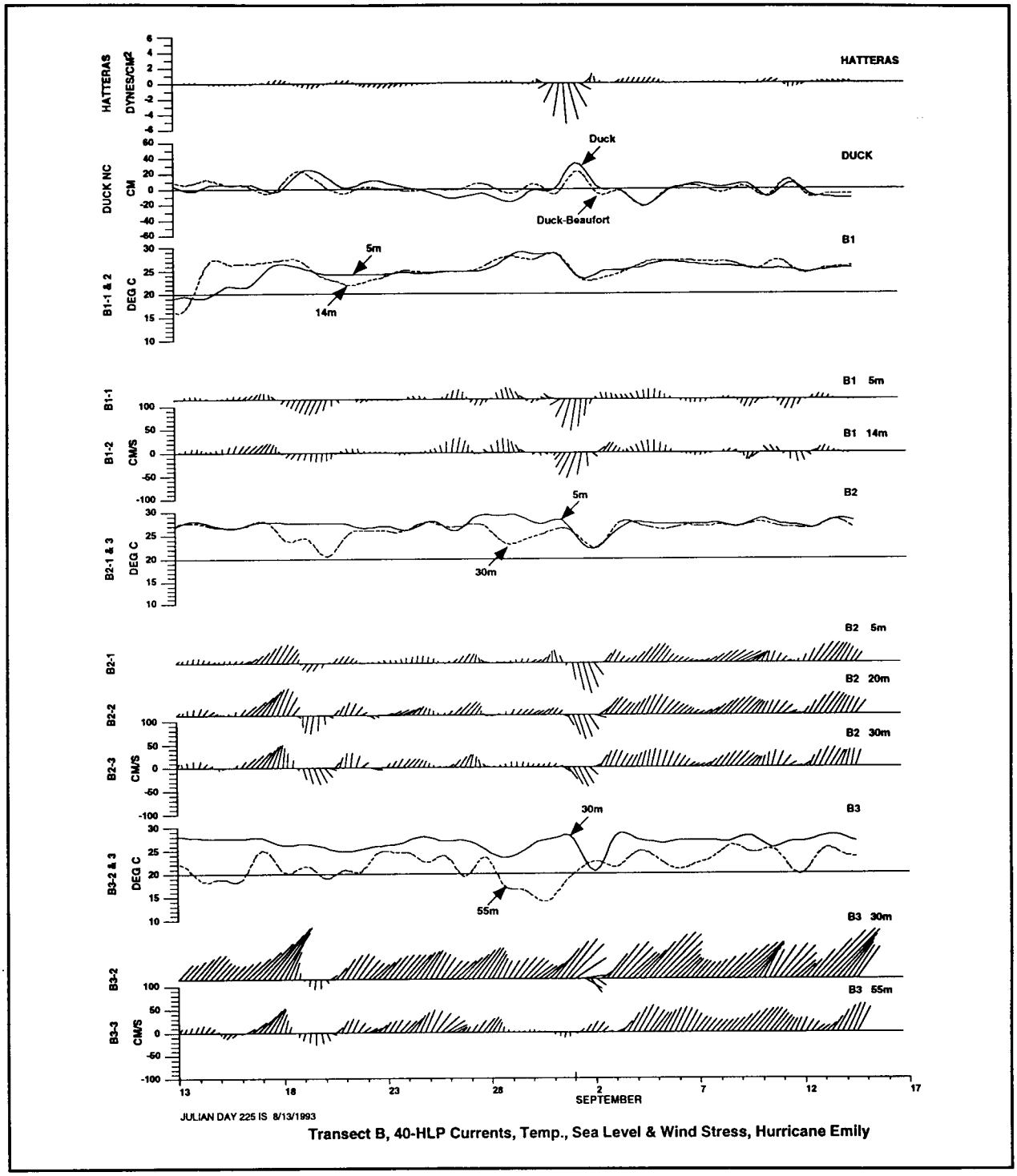

Figure 6.2-7(c). 40-HLP currents, temperatures, sea-level and windstress on Line B for August 1993. Temperatures from the deepest instrument on mooring are dashed. Sea-level difference between Duck and Beaufort is dashed on the Duck sea-level plot.

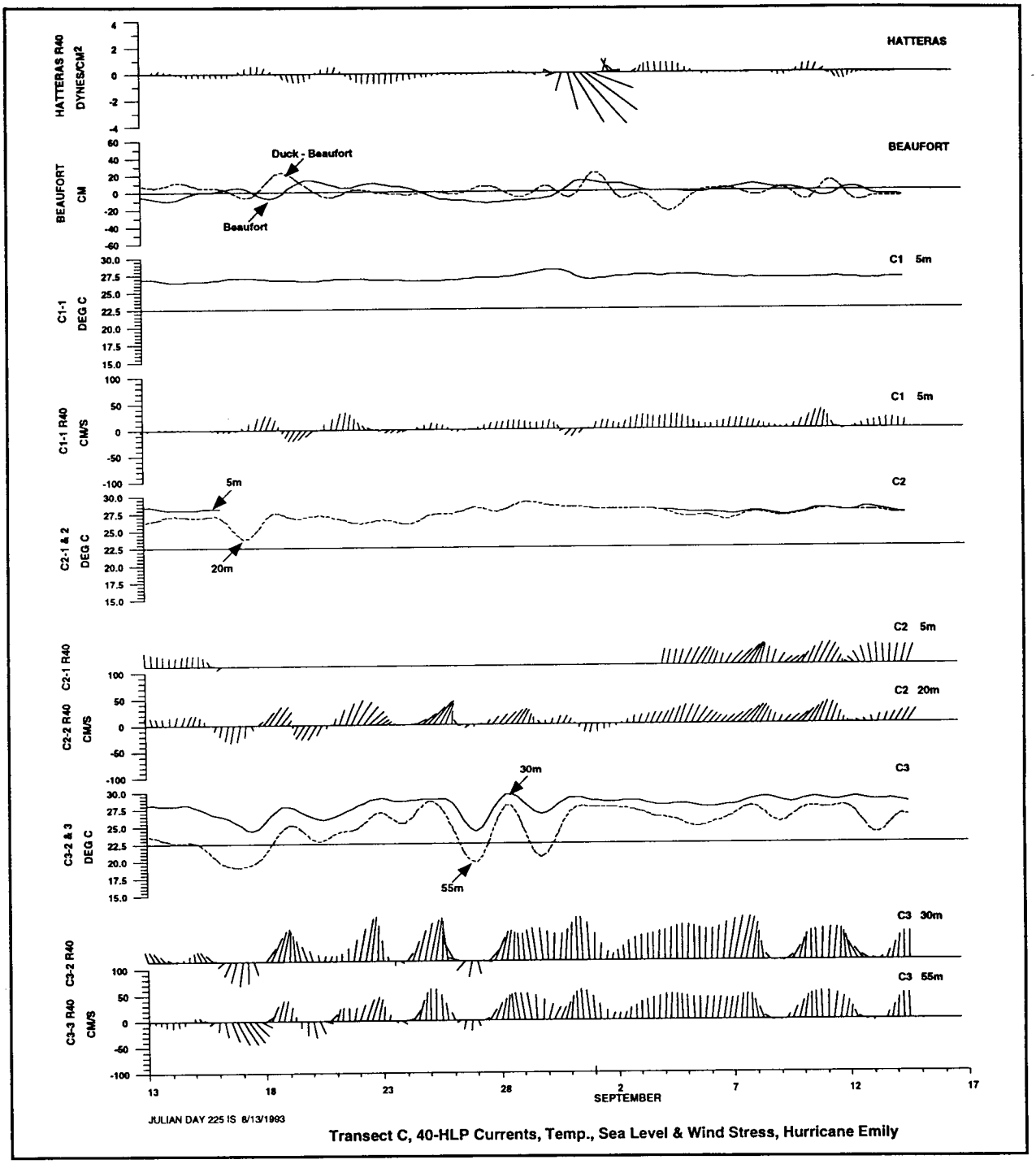

Figure 6.2-7(d). 40-HLP currents, temperatures, sea-level and windstress on Line C for August 1993. Temperatures from the deepest instrument on mooring are dashed. Sea-level difference between Duck and Beaufort is dashed on the Beaufort sea-level plot. Isobath coordinates are used (Up is 040°T).

mixing. The reduction in stratification is maintained after the hurricane at A2 and A3. At A1, the mixing is strong enough in the shallower water to destroy the stratification. However, the water column quickly restratifies after about September 5, because of the upwelling circulation driven by the southerly winds that followed the hurricane. The upwelling advects cooler offshore water towards the coast. Onshore current components to the northward flow are observed at the lower levels of A2 and A1. An upwelling coastal jet develops with the strongest currents occurring at A1.

Similar responses on the outer shelf to A3 are observed at D2 and D3(Figure 6.2-7(b)). The response at D2 is much stronger with large shears because it is closer to the eye. Speeds approaching 100 $cm \cdot s^{-1}$ are observed at the 5 m level of D2. The following northward event, which is quite strong further north, is relatively weak at D2. However, there is a strong onshore flow (~20 $cm \cdot s^{-1}$) at all three depths of D2. The stronger currents and shears cause more mixing than further north but still do not completely destroy the stratification. The surface onshore flux, after September 3, restores the stratification in about 10 days. Sea-level rise caused by the hurricane winds is about 30 cm at Duck and 20 cm at the Chesapeake Bay Bridge.

On Line B (Figure 6.2-7(c)), the inner and mid shelf, B1 and B2, show similar response to A2 and A1 except that the flows are more uniform with depth and the Ekman circulation is not as clear. There is some anticlockwise turning between the 20 and 30 m levels of B2. Stratification at B1 was nonexistent before the hurricane and only weak at B2. Mixing and surface cooling during the hurricane, reduce the stratification and surface temperatures at B1 and B2. Gulf Stream currents are present at B3 for this summer period. The southward flow caused by hurricane winds is very much in evidence at D2, but only manages a small short-lived reversal at the 30 m level at B3. The mixing is complete but mid-depth to bottom stratification returns with the Gulf Stream currents on September 3.

Raleigh Bay, even though it was in the direct path of the hurricane, shows only a weak response. This is because the strongest winds were directed across shelf rather than alongshelf as farther north and the presence of Gulf Stream currents to mid-shelf (See section 5.1). Again the hurricane seems to have reduced Gulf Stream currents at C3 but not enough to cause a reversal. A reversal is caused at C2 (20 m) but only about 20 $cm \cdot s^{-1}$. At the

near-surface of C1, there is only a weak southwestward flow, compared with the southward flow at B1. This may be the result of C1 being in the lee of Cape Hatteras for Emily's strongest winds. Therefore, the major shelf response to the hurricane was north of Diamond Shoals and a noteworthy result is the relative lack of effects on Gulf Stream shelf break currents.

6.3 Analysis of Wind-Forced Currents

The above sections have discussed the current and temperature responses to three major storms that occurred during the study period. A more quantitative analysis of the general relationship between longshore wind stress fluctuations, longshore pressure gradients and shelf currents is given for typical winter and summer periods. The analysis is restricted to synoptic wind-forced periods of about 2.5 to 12 days. This overlaps with the energetic higher frequency Gulf Stream meander periods of 3-10 days as discussed in Section 5. Further discussion of the effects of fronts and the advection of colder water onshore and offshore during upwelling and downwelling is given in the following chapter. This section is primarily devoted to determining the wind-forced current response during the winter when the Gulf Stream has little effect on the shelf, the water column is well mixed, fresh water outflow from the estuaries is small, and winds are strong from the frequent passage of low pressure systems. In summer, winds are much lighter, the water column is highly stratified and the Gulf Stream often intrudes to midshelf on Lines B and C. Periods for both summers are analyzed to show that there are differences between them despite many similarities in the winds and the configuration of the Gulf Stream.

6.3.1 Winter Wind-Forced Currents

The period analyzed for the winter currents is from December 20, 1992 to February 6, 1993 (48 days). This period avoids the large storm and strong southward current event of December 10-16 and the March "storm of the century." This period has the largest number of winter current meter records and the fluctuations are relatively regular with no exceptional velocities in the records. The shelf currents for the latter half of December 1992 can be seen in Figure 6.2-2.

The current spectra were calculated and EOF analysis used to find the dominant shelf wide modes for the wind-forced frequency band

(12-2.5 days). Originally each Line (A, B and C) was analyzed separately and related to local windstress. However, the results are not much different than when the data are analyzed all together. The results for mode 1, which contains 56.7% of the total normalized variance, are given in Figure 6.3-1. All the longshore component spectra north of Diamond Shoals are highly coherent with the mode (coherence squareds of 0.7 to 0.95). The upper layer longshore component at C2(5 m) is also highly coherent (coherence squared of 0.73) but the lower layers of C2 and C3 are much less coherent with the mode (coherence squareds of 0.19 to 0.27). The second mode (14.8% of the total normalized variance) contains most of the remaining signals for the C2 and C3 lower layer records. Thus, apart from C2, at 5m, Line C lower layer is much less related to the mode than the records north of Diamond Shoals. A complete record for C1 is not available for this period. It is recalled from Figure 6.2-2(d) that mooring C2 showed much warmer water in the lower water column than at the surface during December. The water column was probably still neutrally stable with a cold-fresh layer overlying warm, salty Raleigh Bay water.

It will be shown later that the first mode is highly correlated with the longshore windstress over the Hatteras shelf and the longshore pressure gradient, which can be substantial during the winter period (e.g. Figures 6.2-2 and 6.2-4). The structure of the first mode corresponds to classical Ekman circulations on a shallow homogeneous shelf for Lines A and B. Where the mid-depth ellipses are not shown in Figure 6.3-1, they are substantially similar to the bottom ellipses that are given. The surface ellipses are directed so that northward major axes are rotated clockwise from the lower layer major axes. Therefore, northward upwelling flows under southerly winds show an offshore component at the surface and an onshore component in the lower layer. The flows are reversed for southward flowing downwelling currents. The response is substantially barotropic except on Line B where, at B2, the bottom wind-forced fluctuations are a little larger than at the near surface and, at B1, a little smaller. On Line C, the surface Ekman layer appears to be deeper than at B or A because both the 30 m response at C3 and the 5 m and 15 m response at C2 have the offshore orientation of the northward major axes typical of the surface layer (5 m) ellipses to the north. However, as pointed out above, there are more complicated dynamics in Line C than the more purely wind-forced structures to the north.

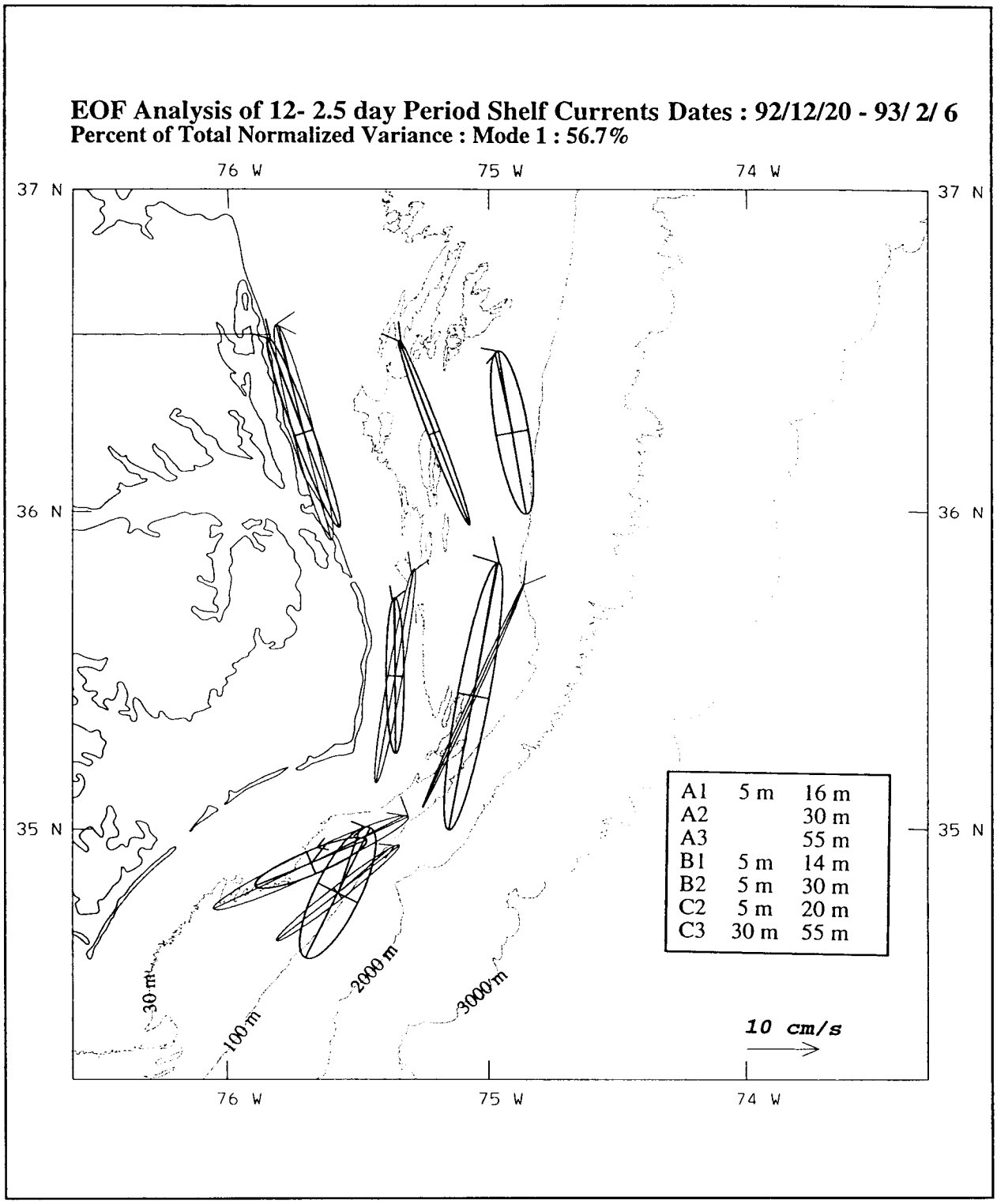

Figure 6.3-1. Current hodographs from the EOF mode 1 analysis of shelf currents for the winter of 1992-1993. Upper and lower layer ellipses are plotted with thin and thick lines, respectively.

The coherence squared and phase differences between the mode 1 spectra and the longshore windstress from the Chesapeake Light (CHLV2) and also the longshore sea-level differences between Duck and Beaufort are given in Figure 6.3-2. Coherence squareds are high (0.6 - 0.9) across the frequency band 0.1 - 0.4 cpd. The current mode lags the windstress by about five hours and the sea-level differences lag the currents by about 145°. This corresponds to a positive sea-level gradient (Duck higher than Beaufort) driving southward (or negative) currents. The importance of the pressure gradient may explain the relatively larger bottom current ellipses at B2 compared with A2 since there is an additional driving force. A rough order of magnitude of the pressure gradient force $\langle gh \cdot \Delta\acute{\eta}/\Delta y \rangle$, where g is the acceleration due to gravity, h is a mean water depth ~30 m, and the pressure difference $\Delta\acute{\eta}$ has a rms value of 0.09 m over a longshore distance of 200 km. Thus, the rms pressure gradient is about 0.13 x $10^{-3} m^2/s^2$. The rms windstress force $\langle \tau^y/\rho \rangle$ is about 0.1 x $10^{-3} m^2/s^2$. Therefore, for this period, the rms longshore pressure gradient force is approximately equal to the windstress and generally works in the same direction. This may explain the large amplitude shelf currents (see Figures 6.2-2 and 6.2-4) observed on Line B.

6.3.2 Summer 1992 Wind-Forced Currents

A very similar EOF analysis of the shelf currents to that given for the winter was performed for a 48 day period beginning June 2, 1992. Again the analysis period was chosen to avoid major events, to have similar characteristics throughout the period and maximize the number of records available for analysis. The summer 1992 regime has the Gulf Stream close to the shelf break in Raleigh Bay. The analysis of Gulf Stream in Section 5.1 showed that Gulf Stream meander fluctuations were felt at the coast on Line C but at periods longer than about 7 days. It appears that synoptic wind forcing in the 10 to 4 day band is not corrupted by Gulf Stream meander fluctuations. Winds are upwelling favorable for most of the period but there are frequent southward current reversals on Line A and at B1. At B2 and B3 and on Line C, the currents are strongly northwards with almost no reversals and clearly have the characteristics associated with Gulf Stream meanders. Sub-tidal current velocities of order 50 $cm \cdot s^{-1}$ are common at B2 and C2 on the 30 m isobath during this June-July 1992 period.

The results of the EOF analysis are given for the first mode in Figure 6.3-3. This mode is also wind-forced, as will be

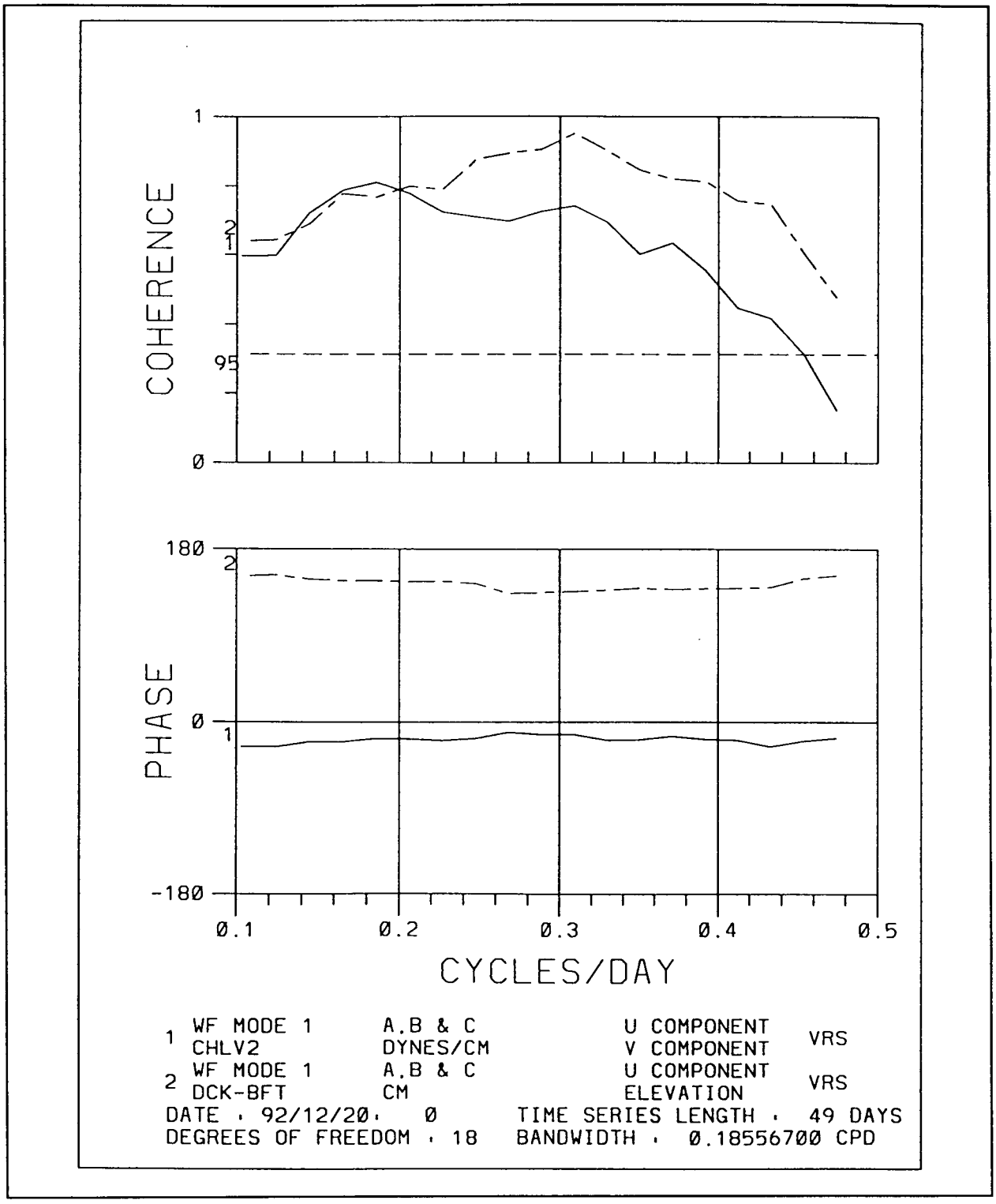

Figure 6.3-2. Coherence squared and phase differences between the winter EOF mode 1 and windstress (solid), and sea-level difference (dashed).

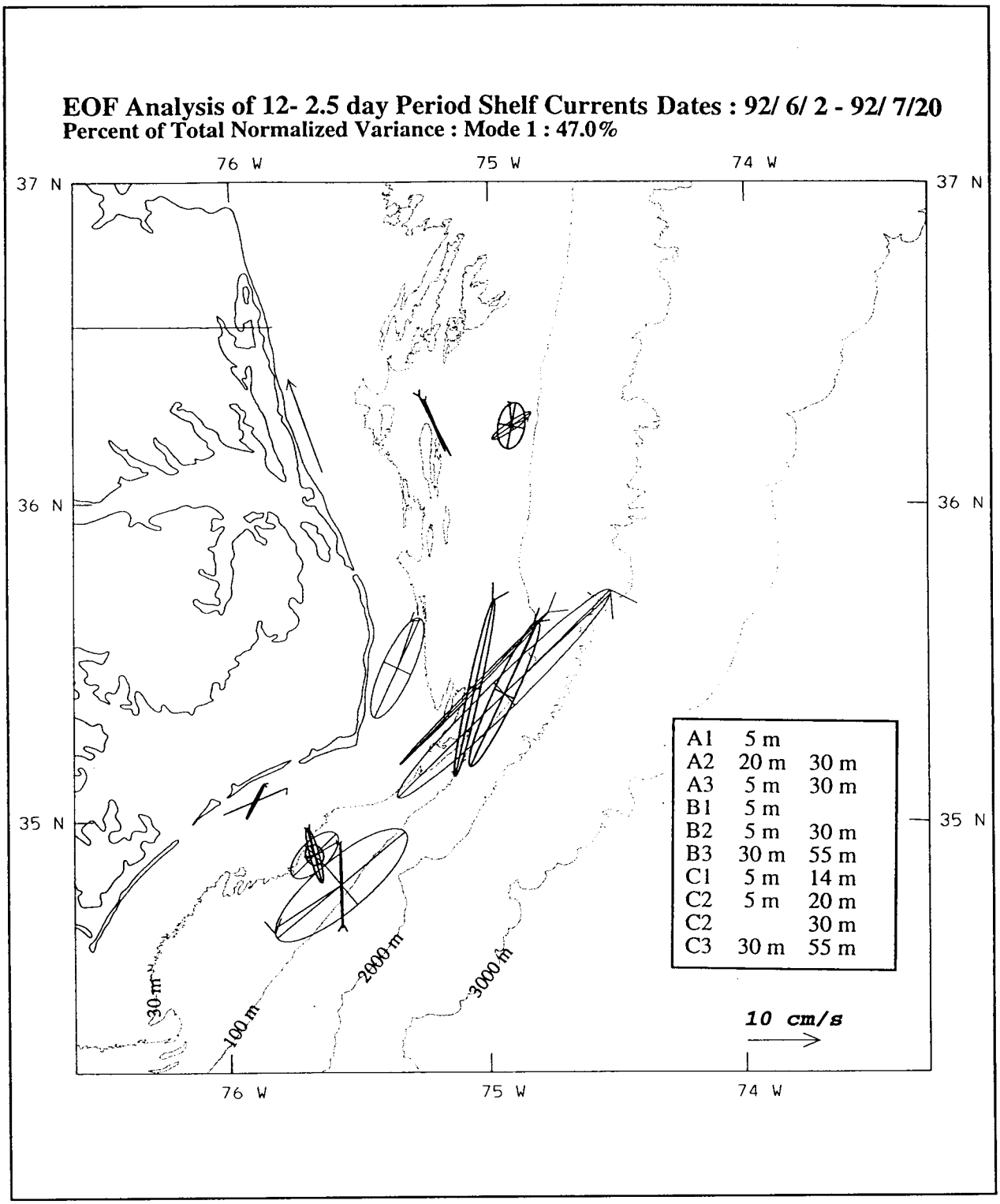

Figure 6.3-3. Current hodographs from the EOF mode 1 analysis of shelf currents for the summer of 1992. Upper and lower layer ellipses are plotted with thin and thick lines, respectively.

demonstrated below, but only accounts for 47% of the total normalized variance. Again, C2 shows little coherence with mode 1 and the remaining moorings have much more moderate (0.4-0.8) coherence squared with this mode compared to the winter analysis. The highest coherences with mode 1 are found B2. Similarly, the more important second mode (18.3% of the total normalized variance) is dominated by the C2 and C3 records. Compared to the winter, the amplitudes of the wind-forced currents are small, particularly at the inner shelf moorings. There is evidence of relatively stronger onshore-offshore flows in the surface and bottom boundary layers (e.g. at C1, B2, B3 and A3) shown by the greater offshore and onshore inclinations of the northward major axes compared to Figure 6.3-1. This is probably a result of the greater stratification of these summer months. The surprising features are the large amplitude of the response at B2 and B3 and finding a moderate response in the lower and middle water column at C3. The latter are also about 180° out of phase with the other wind-forced fluctuations. The reason for this is unclear at the present time. Therefore, on Lines B and C, wind-forced fluctuations are imposed on Gulf Stream derived flows. It is noted that the Gulf Stream flows seem to influence the mean directions of the wind forced fluctuations to be more parallel to the Gulf Stream front as can be seen by comparing the ellipses for B2 between Figures 6.3-1 and 6.3-3.

The coherence squared of the first mode with the longshore windstress from the Chesapeake Light and the sea-level difference between Duck and Beaufort are given in Figure 6.3-4. The coherences are not quite as high as for the winter but are still well above the 95% significance level for 3 to 7 day period motions. The longshore pressure gradient plays just as an important role as in winter even though the rms amplitude is about half of the winter value. This again may explain the strength of the wind-forced fluctuations at B2 and B3 where the longshore pressure gradient appears to be most effective. Mode-2 currents, as in winter, are essentially uncorrelated with wind and sea-level differences for these synoptic wind-forced frequencies.

6.3.3 Summer 1993 Wind-Forced Currents

The 48 day period analyzed in the summer of 1993 is also in June and July, beginning on June 20, and again is a period a relatively uniform fluctuations that avoids major events. Flows are predominantly southward with frequent reversals on Line A, but

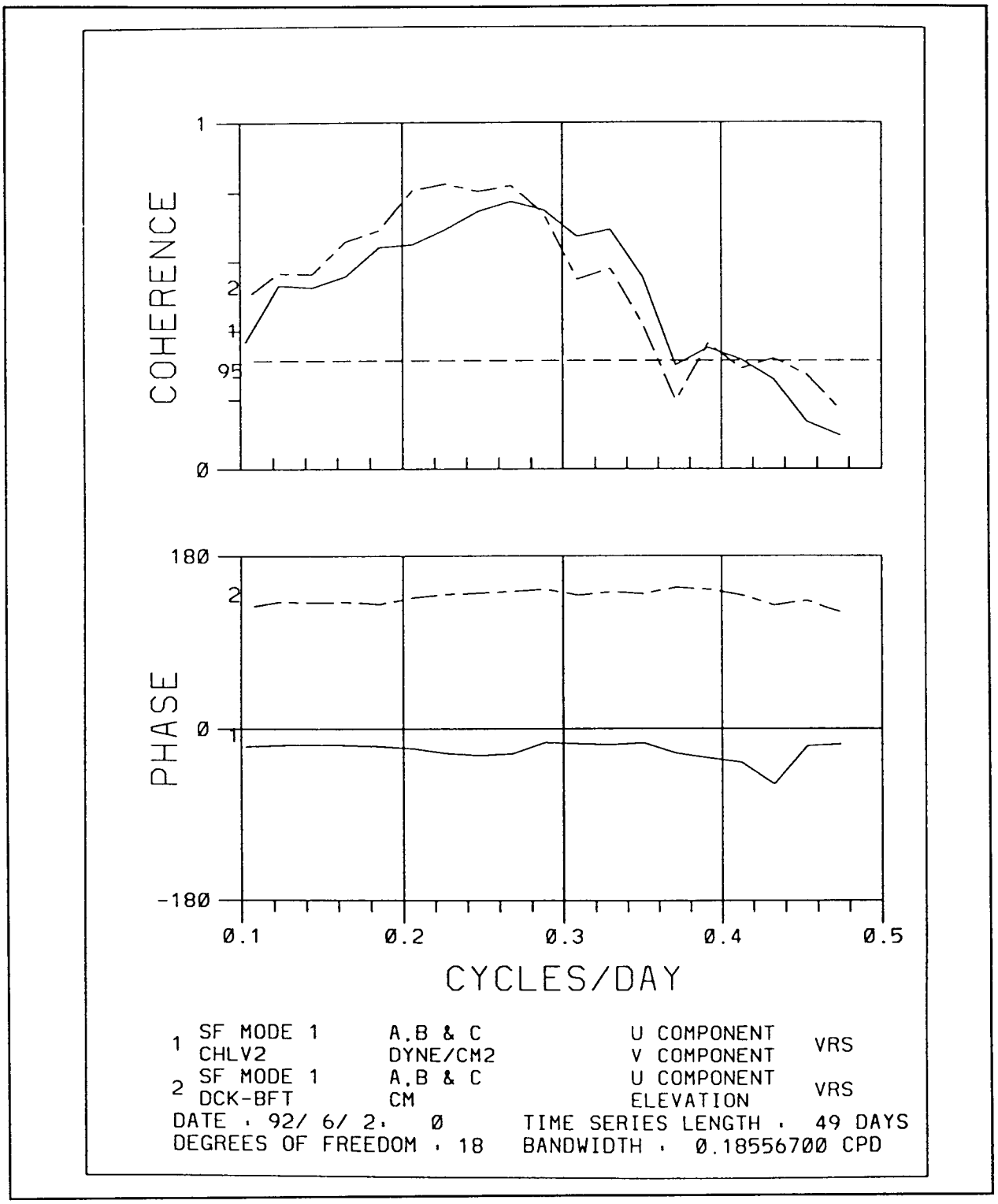

Figure 6.3-4. Coherence squared and phase differences between the summer 1992 EOF mode 1 and windstress (solid), and sea-level difference (dashed).

northwards elsewhere with few reversals. Fluctuations are quite small on Line A and at B1, in contrast to larger Gulf Stream meander type fluctuations on the outer part of Line B and C. Even C1 shows large ~40 $cm \cdot s^{-1}$ northward fluctuations which appear to coincide with the passage of meander crests. The analysis of Gulf Stream influence on shelf currents in section 5.1 showed that Gulf Stream currents were felt to mid-shelf on Line B and C and affected sea-level fluctuations at Cape Hatteras in the same 3-10 day frequency band as the synoptic windforcing. In this overlap with the wind-forcing, the summer of 1993 Gulf Stream differs from Summer 1992 as discussed above.

The first wind-forced mode (Figure 6.3-5) only accounts for 36.6% of the total normalized variance, the least of the three seasons analyzed. Moorings B2, B3, C1, C2 and C3 are least coherent with the mode whereas the remaining moorings have similar coherence squareds with the mode to those of the previous summer (0.4-0.75). The second mode is nearly as important as the first (28.3% of the total normalized variance) and primarily involves the B and C moorings in the middle and outer shelf. Compared to the 1992 summer (Figure 6.3-3), the amplitudes at B2 and B3 are much smaller though with similar characteristics (Figure 6.3-5) Amplitudes are similar on Line A, which shows the effects of very strong Ekman turning in the upper and lower boundary layers at A2 and the 5 m level of A3. Stick plots for Hurricane Emily (Figure 6.2-7(a)) show a good example of the onshore-offshore flows in highly stratified conditions at A2 during strong downwelling winds. The near-coast mooring A1 does not show a surface layer response, unlike C1 which is well mixed, implying that the surface Ekman layer must be shallower than 5 m. Therefore, the major difference with the summer 1992 is the low amplitude of the wind-forced currents on Line B that is superimposed on Gulf Stream meander derived flows.

The coherence squared of mode 1 with windstress and sea-level difference is given in Figure 6.3-6. Note that phase differences are about 180° different from the previous plot. (Figures 6.3-2 and 6.3-4), however the mode currents are also about 180° different in phase from the summer 1992 and winter modes (see Figures 6.3-1 and 6.3-3). Therefore, the windstress still leads the currents by about 6 to 12 hours. Unlike the previous periods, windstress is most coherent with the mode and sea-level difference less coherent. Sea-level difference amplitude is only about one third of the winter amplitude whereas the windstress amplitude at the Chesapeake

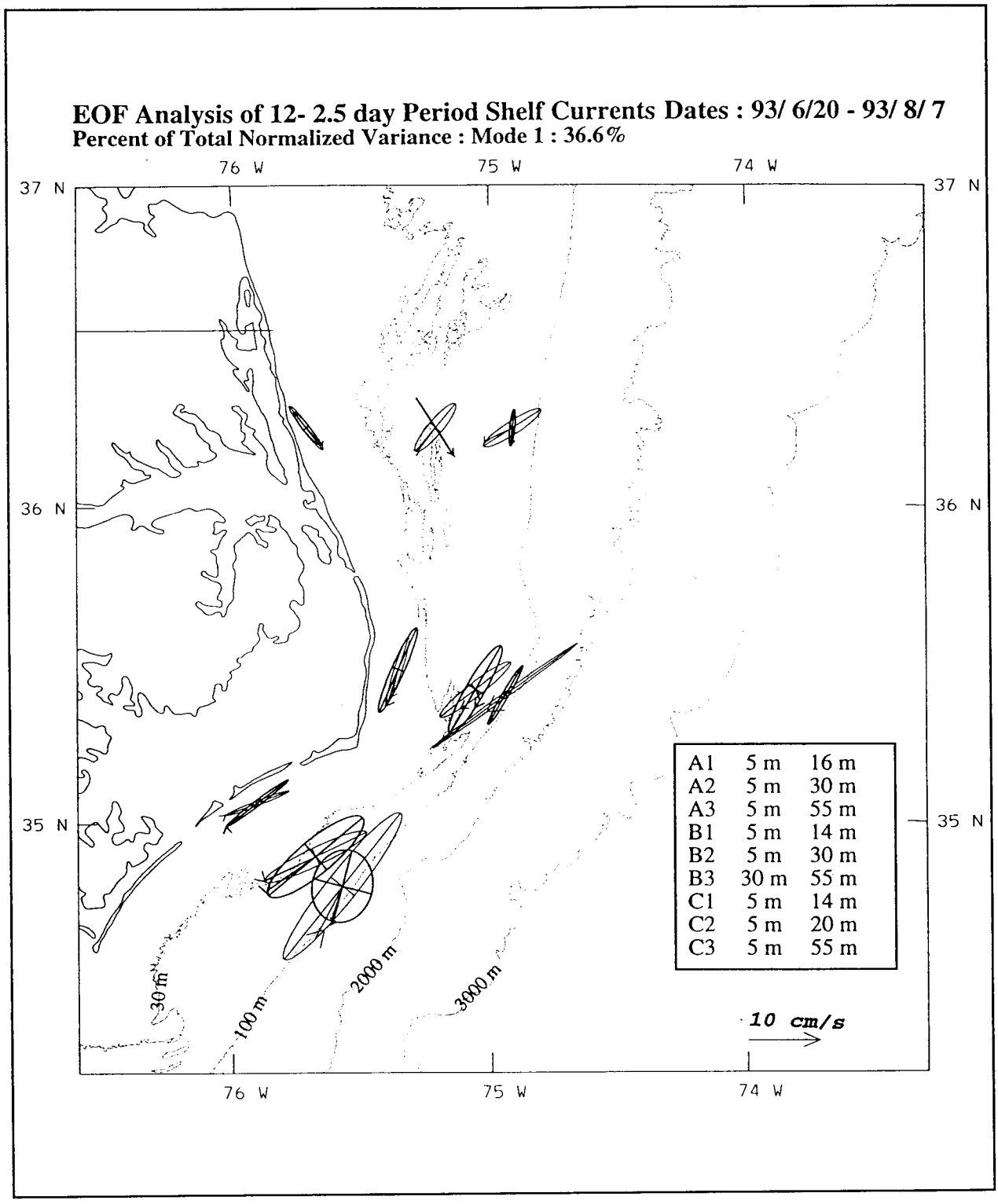

Figure 6.3-5. Current hodographs from the EOF mode 1 analysis of shelf currents for the summer of 1993. Upper and lower layer ellipses are plotted with thin and thick lines, respectively.

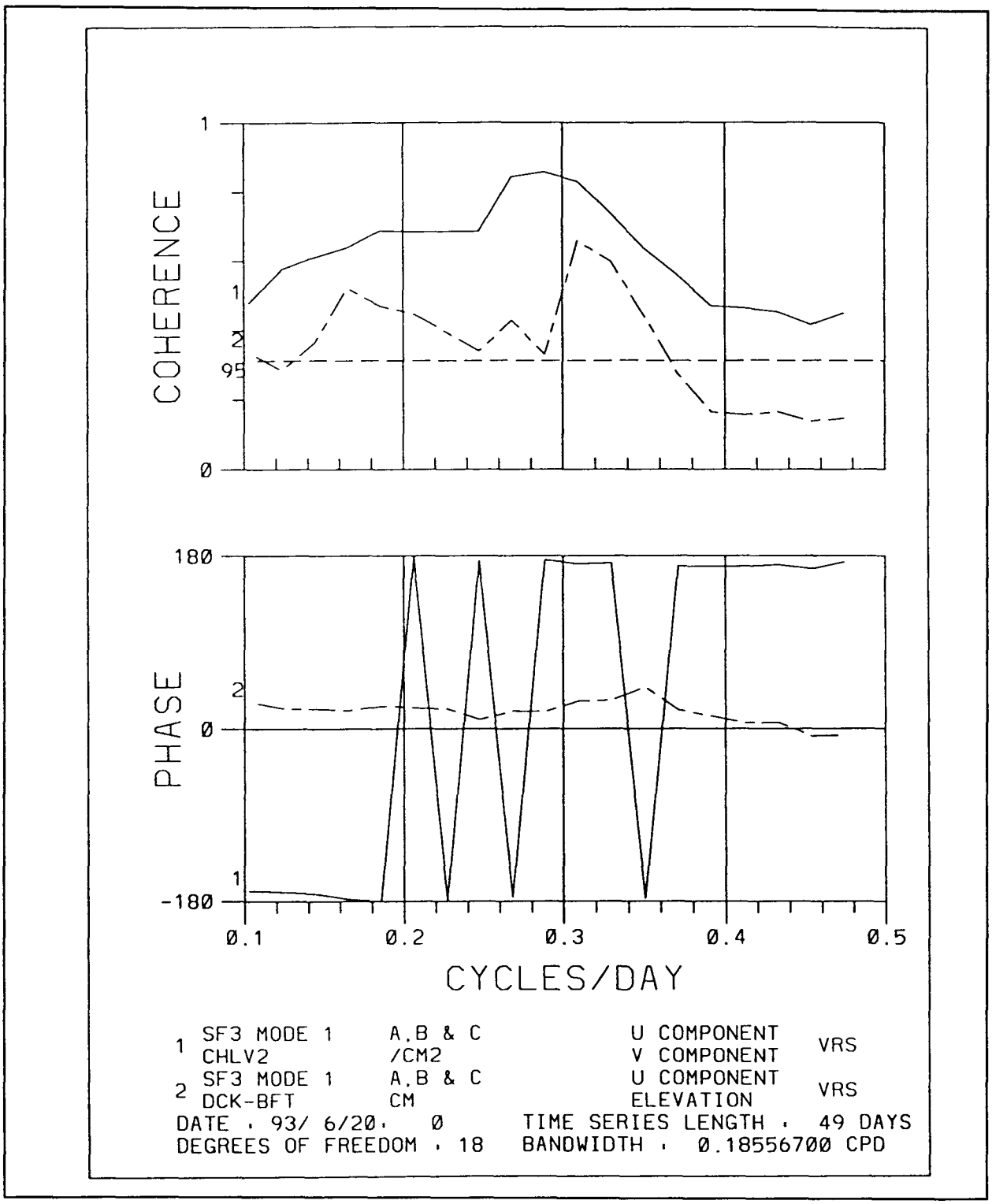

Figure 6.3-6. Coherence squared and phase differences between the summer 1993 EOF mode 1 and windstress (solid), and sea-level difference (dashed).

Light is about the same as the previous summer. Therefore longshore pressure gradients seem to be less important in the summer of 1993 and this may explain why the wind response at Line B is not amplified unlike the other two analyzed periods.

In summary, the wind response of the shelf depends on the strength of winds, the longshore pressure gradients generated around Cape Hatteras and the degree and character of the influence of the Gulf Stream on the shelf. Stratification of Line A can effect the nature of the classical wind-forced Ekman response by reducing the depths of the boundary layers. In all cases, the wind response on the Hatteras shelf is stronger and more direct than in Raleigh Bay even though the longshore components of the wind are similar on both shelves.

VII. SHELF TRANSPORT PROCESSES

Transport processes on the continental shelf on both sides of Cape Hatteras have been addressed by prior studies and recently reviewed (SAIC 1993). The 1992-1993 study data set represents the most extensive and intensive coverage in this region. Such coverage is a substantial asset in the attempt to unlock the complexities of this transition region, with many singularities: the striking water mass contrasts, the strong front separating the two shelf regions, the variety of the forcing and the rapidity and broad scale of the interactions between the shelf waters and the Gulf Stream.

7.1 Upwelling/Downwelling

7.1.1 Coastal Upwelling

Upwelling and downwelling occur along the coast in both parts of the North Carolina continental shelf during all seasons of the year. This motion is not always evident in property distributions, simply because the stratification is often so low that the upwelled water is indistinguishable from the water moving away from the coast in the upper Ekman layer. Therefore, the evidence from current velocities is not always corroborated by corresponding signals in water-mass properties. This discussion focuses on upwelling during the summer, stratified season because the property distributions aid analysis and visualization of cross-shelf wind-driven circulation. The cross-shelf response to alongshelf wind stress in winter is significantly different than in summer. Not only do the Ekman layers increase in thickness during the winter, unstratified season, but the lower-layer flow answering a divergence in the upper Ekman layer occurs at deeper layers. In the summer, the shoreward flow responding to upwelling favorable winds occurs at mid-depth, above the cold band in the Middle Atlantic Bight (Boicourt and Hacker 1976). When the alongshore motion is sufficient, a bottom Ekman layer also forms. In winter, the answering flow to upwelling winds is solely via the bottom Ekman layer.

The alongshelf structure in topography creates deeper regions in the southern Middle Atlantic Bight that allow the summer cold water in the lower layers of the outer shelf to penetrate farther into the inner shelf (Figure 7.1-1). At these alongshelf positions, the source water for upwelling is colder than at locations where the shelf cross-section is shoaler.

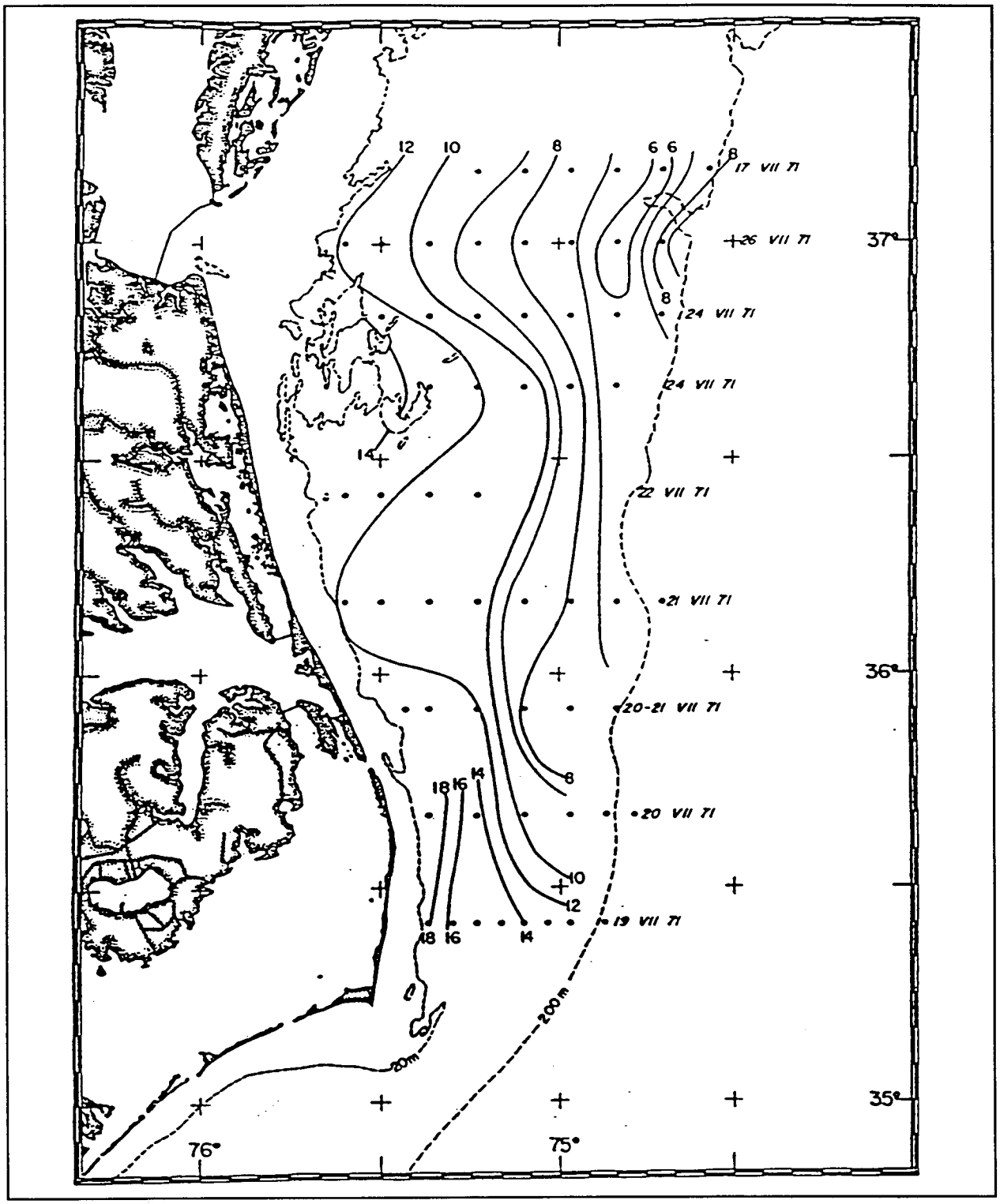

Figure 7.1-1. Map of minimum temperature in the water column below 20 m for July 1971 (from Boicourt 1973).

Winds during July and August are prevailing upwelling-favorable over the North Carolina continental shelf. The differences in the temperature and salinity signatures north (line A) and south (line B) of where the cold-band turns offshore are shown in Figures 7.1-2 and 7.1-3. Upwelling has forced the salinity minimum of the coastal current seaward while creating a temperature minimum at the shore in both sections. The temperature differences in this temperature minimum band are over 5°C. Winds during this survey were also favorable for upwelling in Raleigh Bay, but the near vertical homogeneity of the water does not supply a signal to mark this motion. A slight temperature inversion between stations 10 and 11 on line C (Figure 7.1-4) over the inner shelf may be the result of this motion.

Time-series records from moored instrumentation provide complementary information from the hydrographic distributions discussed earlier. However, though they provide continuous signals of temperature, salinity, and velocity at point, the spatial distributions of the tracers can produce geographically varying signals in the upwelled water. Furthermore, the strong stratification of the summertime southern Middle Atlantic Bight creates an upwelling signal that is not a linear function of upwelling motion, but rather a binary, on-off signal of upwelling or downwelling. An illustration of these aspects of the upwelling measures is shown in Figure 7.1-5. Northward wind stress drives offshore Ekman drift and hence upwells water from below. At mooring A1, the lower-layer water immediately offshore from this position is 14-16°C. Northward wind stress delivers this cold water to the upper instrument at mooring A1, while southward wind stress creates downwelling and a rise in temperature. The relationship between cold temperature and high salinity creates a mirror images in the two property records. Clearly, these tracer responses to wind stress are neither linear, nor are they symmetric (Figure 7.1.5). Temperature decreases appear to occur only after strong or persistent northward wind stress. Warm temperatures quickly return, often with only a slight northerly wind stress. The reason for this asymmetry is that upwelling-favorable winds work against gravitational stability of the water column in moving denser water to the surface along the coast, while downwelling works in concert with stability in returning the pycnocline to an equilibrium position after an interval of upwelling.

The temperature tracer signals at mooring B1 appear remarkably different than those at A1. The primary reason is the turning of

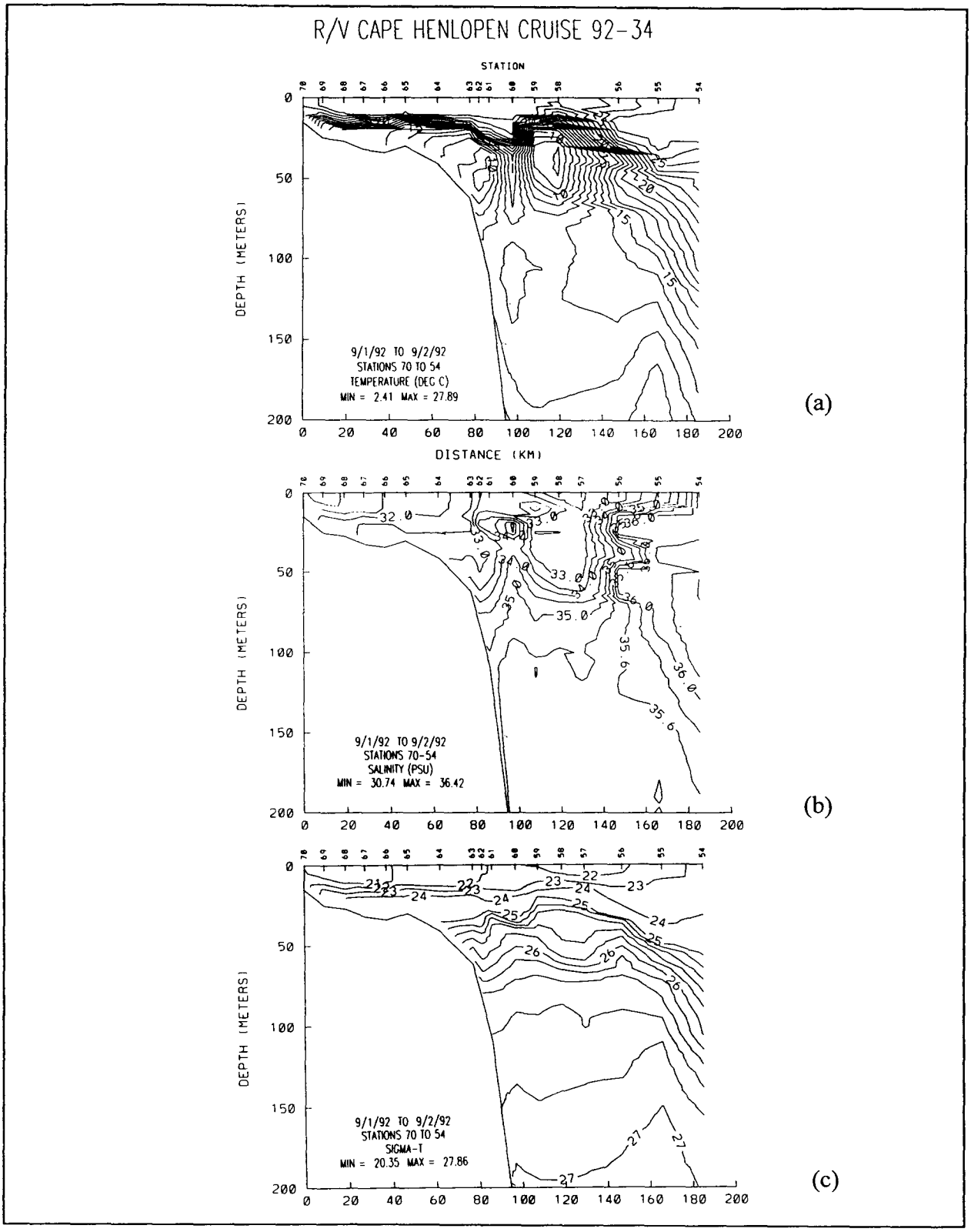

Figure 7.1-2 Cross-shelf sections along Line A of (a) temperature, (b) salinity, and (c) σ_t taken during cruise CH9234 on September 1-2, 1992.

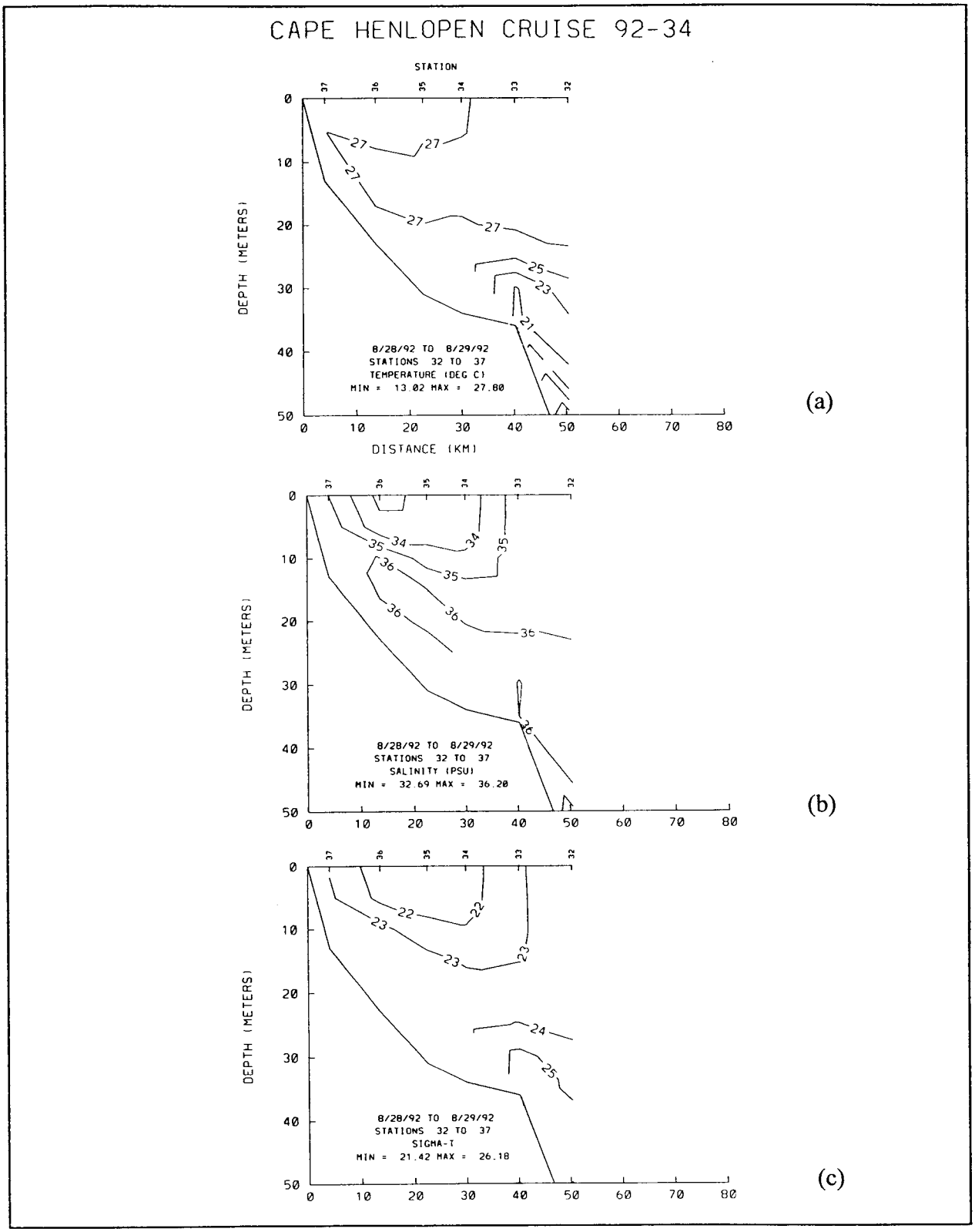

Figure 7.1-3 Cross-shelf sections along Line B of (a) temperature, (b) salinity, and (c) σ_t taken during cruise CH9234 on August 28-29, 1992.

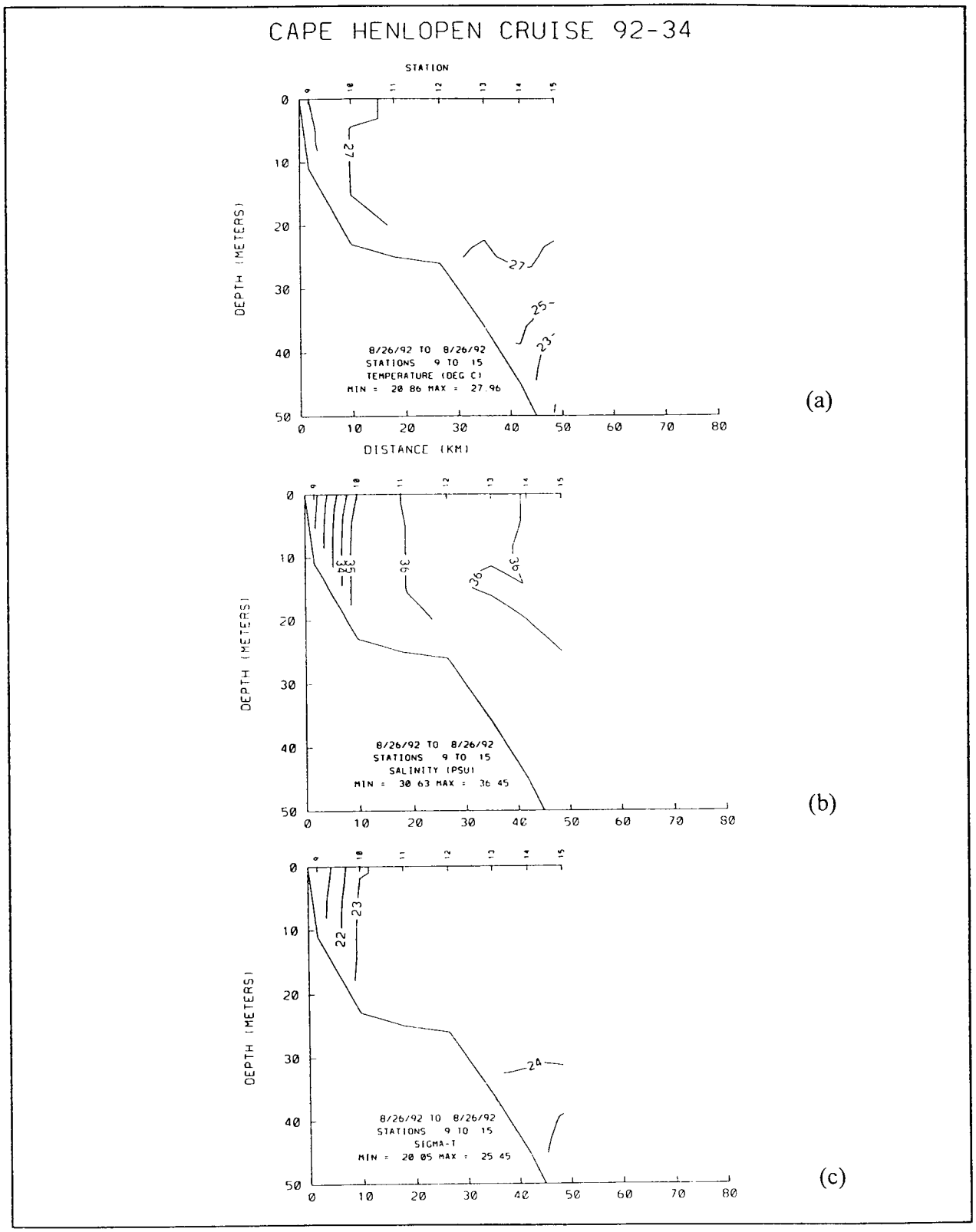

Figure 7.1-4 Cross-shelf sections along Line C of (a) temperature, (b) salinity, and (c) σ_t taken during cruise CH9234 on August 26, 1992.

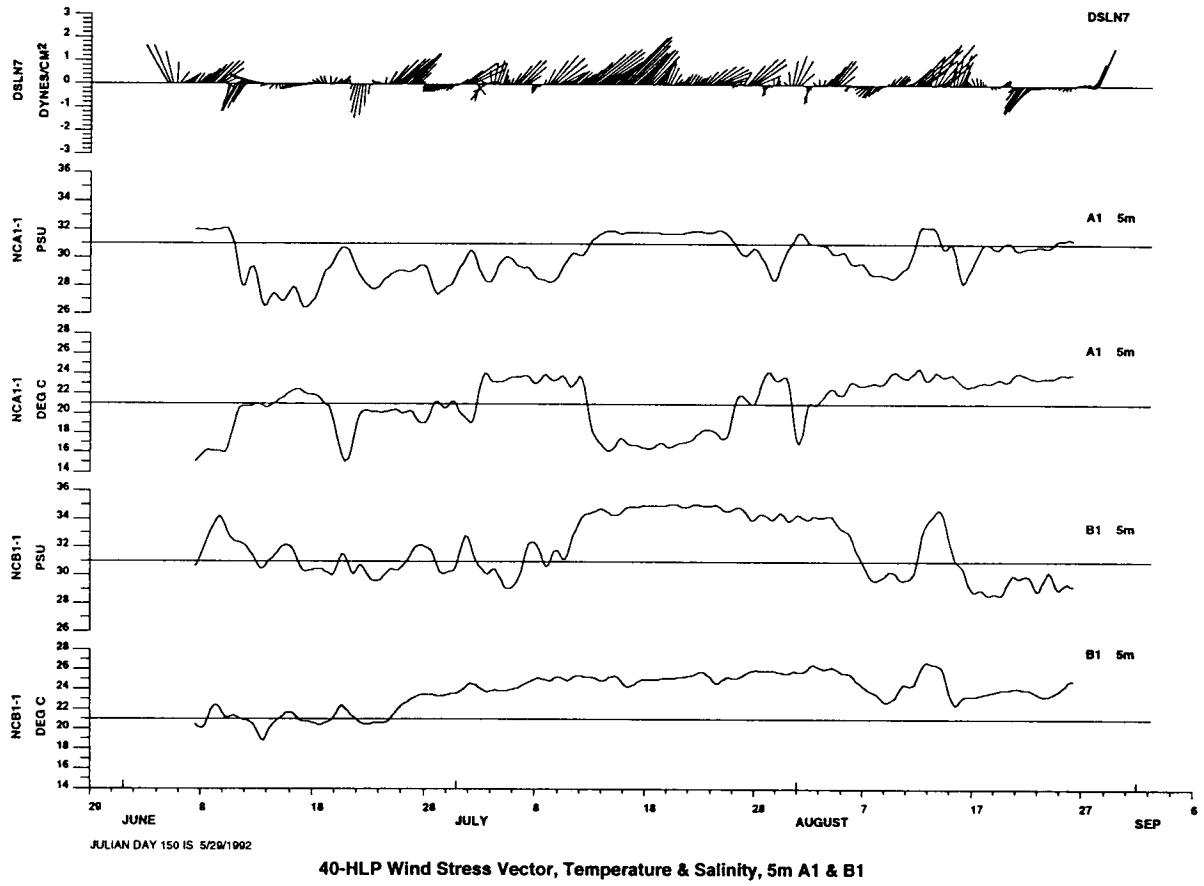

Figure 7.1-5. 40-HLP wind stress vectors (dynes•cm^{-2}) at Diamond Shoals Light, and temperature and salinity at A1 (5 m) and B1 (5 m) for summer 1992. Northward wind stress is directed positively along the ordinate.

the cold water band offshore northward of the B line, thus removing this characteristic as a signal. The minimum temperature in the shallow B1 record is 19°C. In general, the B1 temperature signal represents the summer warming of shelf waters. On closer inspection, the A1 and B1 salinity records appear more alike. The salinity at both positions decreases a short time after northerly wind events, no matter how strong or persistent. This behavior is probably the result of the rapid formation of the coastal jet of the Chesapeake Bay plume, once the opposing upwelling-favorable winds are removed. By the end of August (Figure 7.1-5), the deeper layers of the inner shelf at mooring A1 have warmed to the point where temperature is nearly lost as a tracer of upwelled water. Salinity remains a tracer at both the A1 and B1 lines until the end of the record.

Because the upwelling temperature signal at mooring A1 is more a binary (on/off) signal than a linear function of upwelling, the time rate of change of temperature might provide a better signal for upwelling activity, especially for the onset. Figure 7.1-6 shows the relationship between wind stress and the time rate of change of temperature for both 1992 and 1993. As was suspected from an inspection of the temperature records (Figure 7.1-5), the greatest rate of change of temperature occurs soon after the initiation of upwelling or downwelling favorable winds. The signals increase in amplitude during the late spring, to a maximum in July, when the largest vertical temperature differences occur. After late July, this signal diminishes.

The autospectra and coherence of the north-south wind stress and the time rate of change of temperature during summer at mooring A1 are shown for 1992 (Figure 7.1-7) and 1993 (Figure 7.1-8). The coherence in 1992 is significantly high within the double-peaked synoptic weather band, but does not extend to the low-frequency end because the time rate of change of temperature is a measure of the onset of upwelling and downwelling rather than the process itself. The phase relationship indicates that the lag of the temperature change at 5m on mooring A1 behind the driving wind stress is approximately 0.5 days. The coherence for summer 1993 (Figure 7.1-8) is not as high as 1992. The primary reason for this difference is the significantly higher buoyancy forcing during 1993. The large buoyancy flux out of Chesapeake Bay created a low-salinity current along the North Carolina coast (see section 7.3.1). As was observed during the MECCAS program (Boicourt *et al.* 1987) this buoyancy flux is often sufficient to either suppress upwelling or

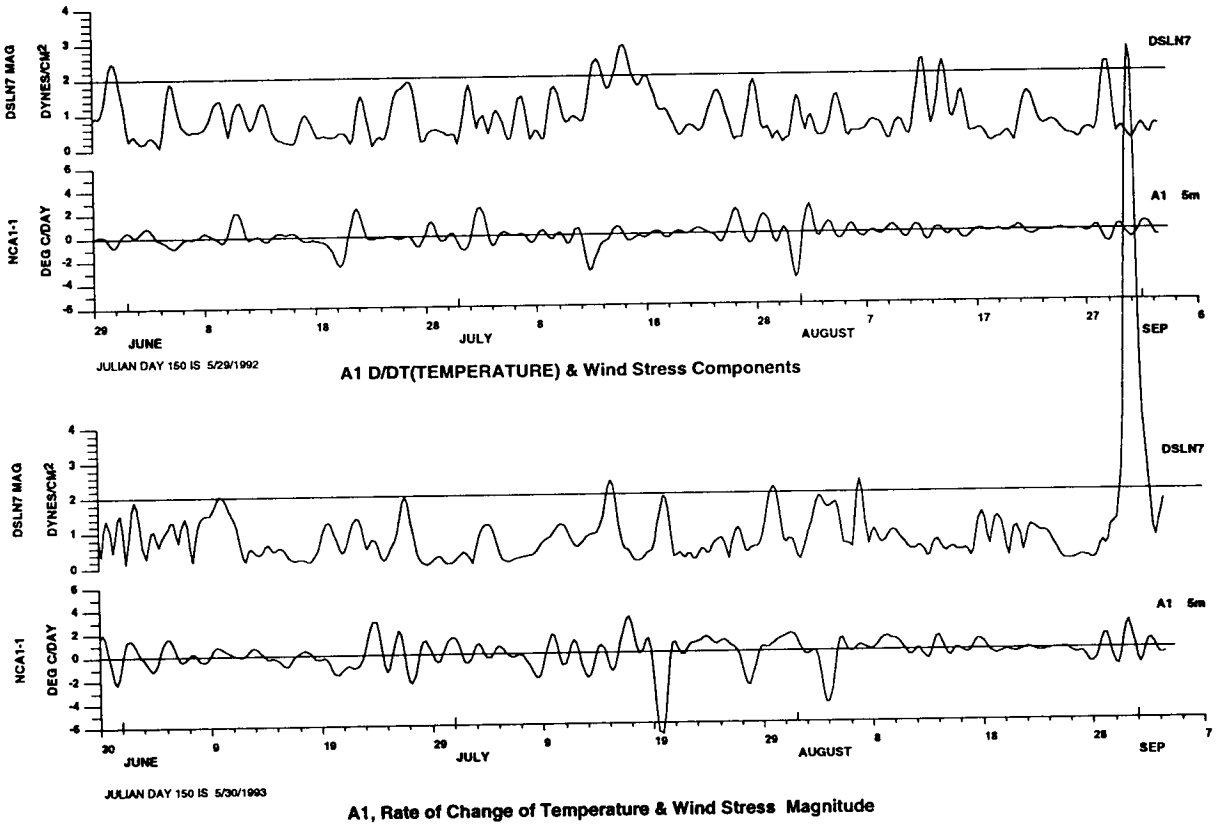

Figure 7.1-6. Diamond Shoals Light wind stress (dynes•cm^{-2}) and the time rate of change of temperature at A1 (5 m) for summer 1992 (upper pair of records) and 1993 (lower pair of records).

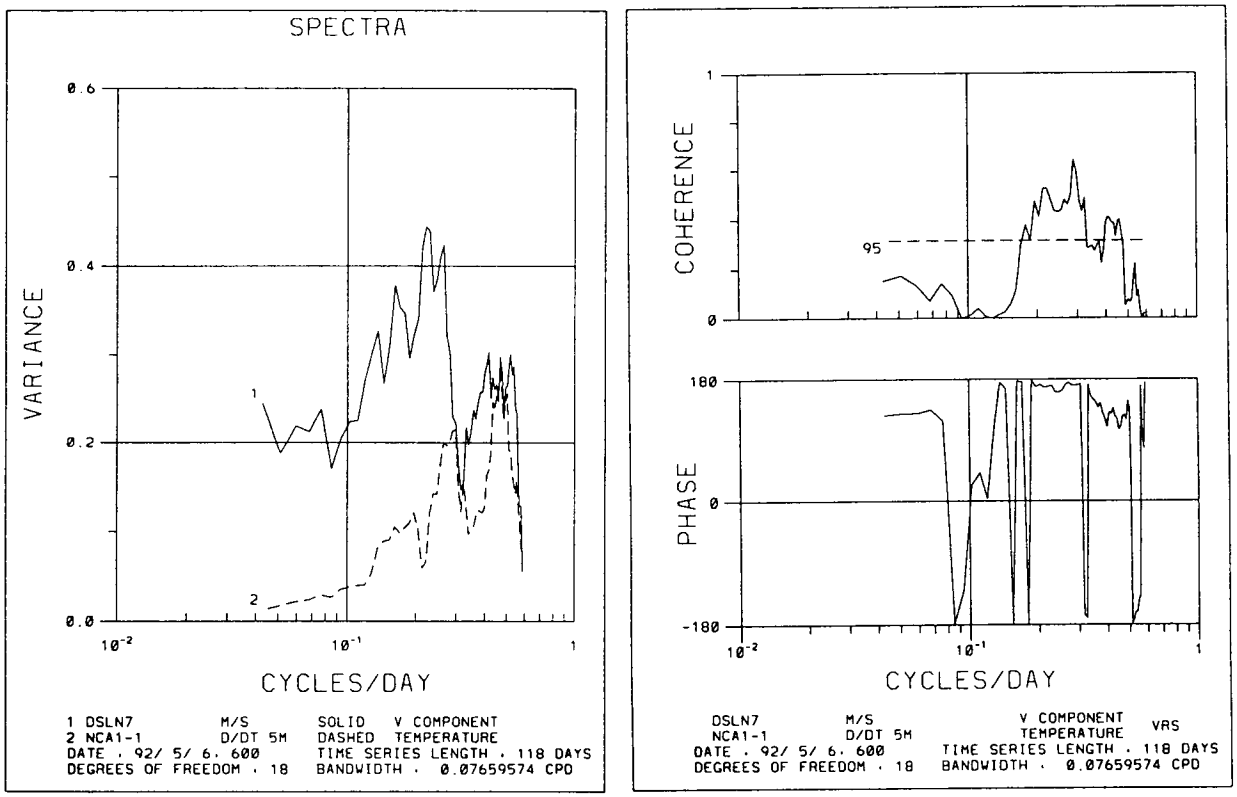

(a) (b)

Figure 7.1-7. Autospectra (a) and coherence (b) of north-south component of Diamond Shoals Light wind stress (solid line) and time rate of change of temperature at 5 m instrument on mooring A1 (dashed line) for summer 1992.

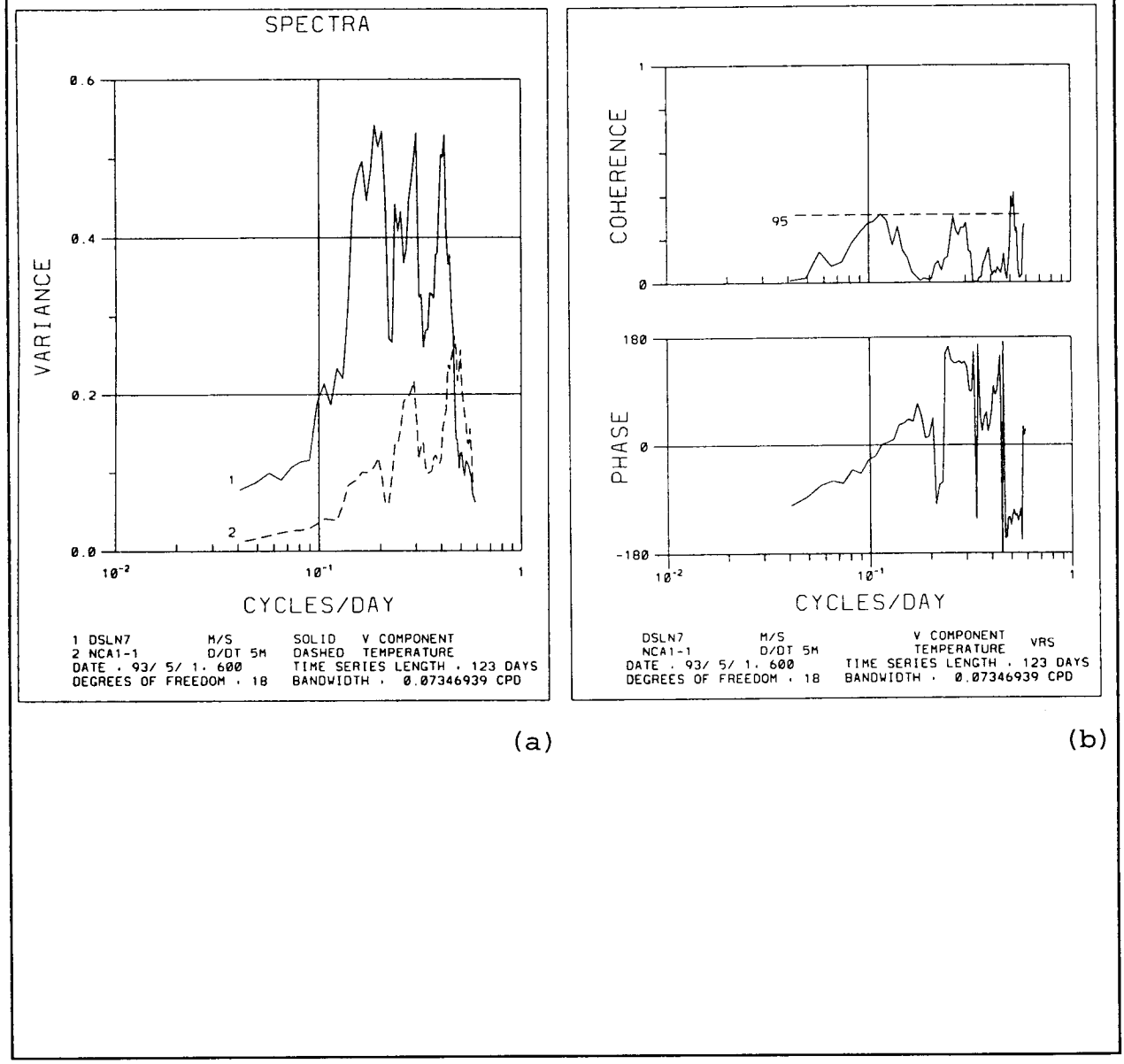

Figure 7.1-8. Autospectra (a) and coherence (b) of north-south component of Diamond Shoals Light wind stress (solid line) and time rate of change of temperature at 5 m instrument on mooring A1 (dashed line) for summer 1993.

to force upwelling to occur seaward of the front separating this low-salinity water from the ambient shelf water. A noticeable relationship between upwelling winds and temperature at the upper layer of mooring B2 during spring 1992 led to a calculation of the coherence between these two signals (Figure 7.1-9). The signals are coherent only over the 2-3 day band, with a lag of the order one day. One reason that this signal is more coherent than the record at mooring B1 (not shown) might be that during this season in 1992 the buoyancy-driven current forces the upwelling offshore. Another possible mechanism may involve advective effects from the coastal current turning offshore. Further examination of this question will be necessary to determine the answer.

The alongshelf spatial structure of source water for upwelling can be seen in satellite thermal imagery. The combination of the topographically modulated inshore penetration distance for the cold water along the bottom (Figure 7.1-1) and the offshore turning of the cold band creates an alongshelf structure that is reflected in the surface temperature signal observed in SST imagery for the 3-day interval 14-16 July 1992. The satellite SST image for July 15, 1992 (Figure 7.1-10) illustrates this. Strong upwelling-favorable winds were blowing during this interval (Figure 7.1-5), driving the upper Ekman layer flow offshore (as seen in the current vectors superimposed on the SST image). The coldest water off the North Carolina coast appears between Currituck and approximately 20 km south of Oregon Inlet. To the north, the broad ridge extending seaward from Chesapeake Bay entrance (Figure 7.1-1) prevents the coldest water from penetrating to the coast. To the south, the offshore turning of the cold band removes this cold water as a source for upwelled water.

The winter, unstratified conditions over the Middle Atlantic Bight are created when autumnal and wind mixing destroy the summer stratification. The downwelling-favorable winds of winter also contribute to these conditions, although partitioning of the roles has not been done. Upwelling-favorable winds during this season can rapidly stratify the middle and outer shelves of both the Middle and South Atlantic Bights (Boicourt and Hacker 1976; Atkinson *et al.* 1980). In the Middle Atlantic Bight, this stratification seldom lasts longer than a few days to a week. An illustration of the hydrographic structure during the latter part of the unstratified season is shown in Figures 7.1-11-13. The water column at lines A and B (Figures 7.1-11 and 7.1-12) is vertically homogeneous. Winds during these transects were

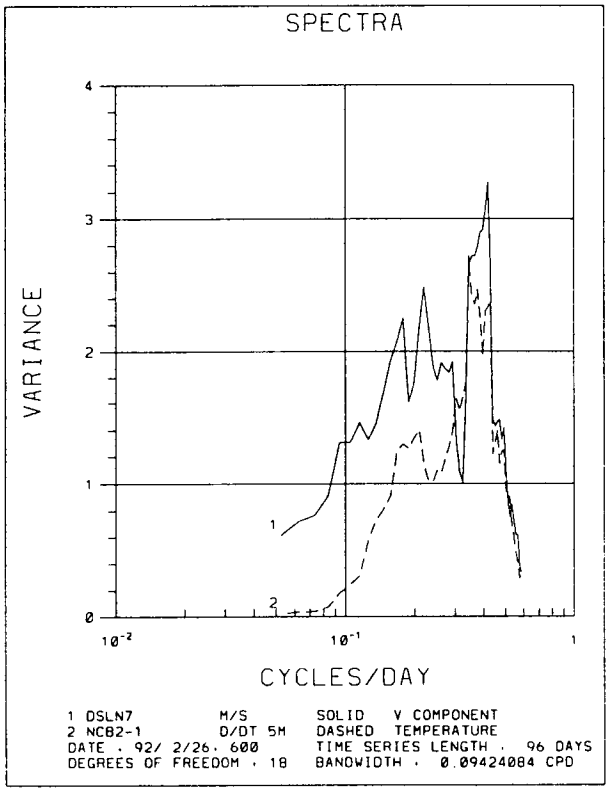

(a)

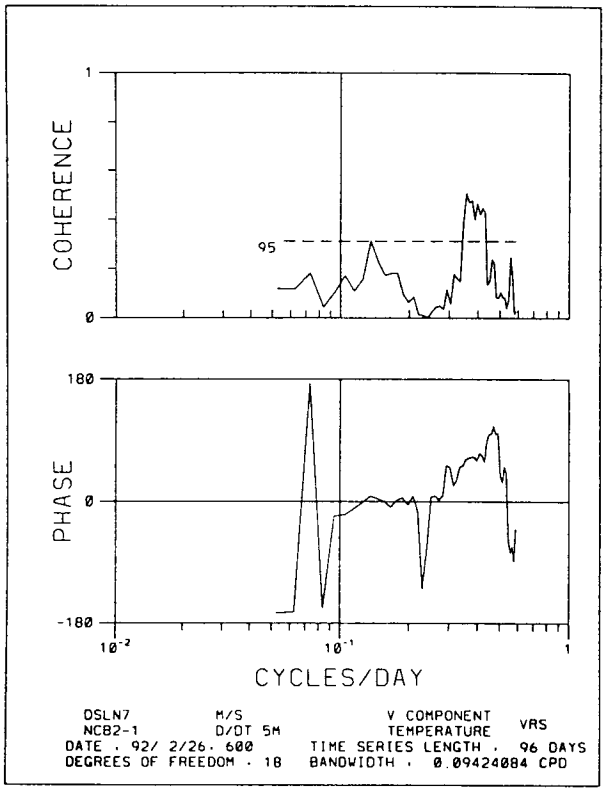

(b)

Figure 7.1-9. Autospectra (a) and coherence (b) of north-south component of Diamond Shoals Light wind stress (solid line) and time rate of change of temperature at 5 m on instrument on mooring B2 (dashed line) for spring 1992.

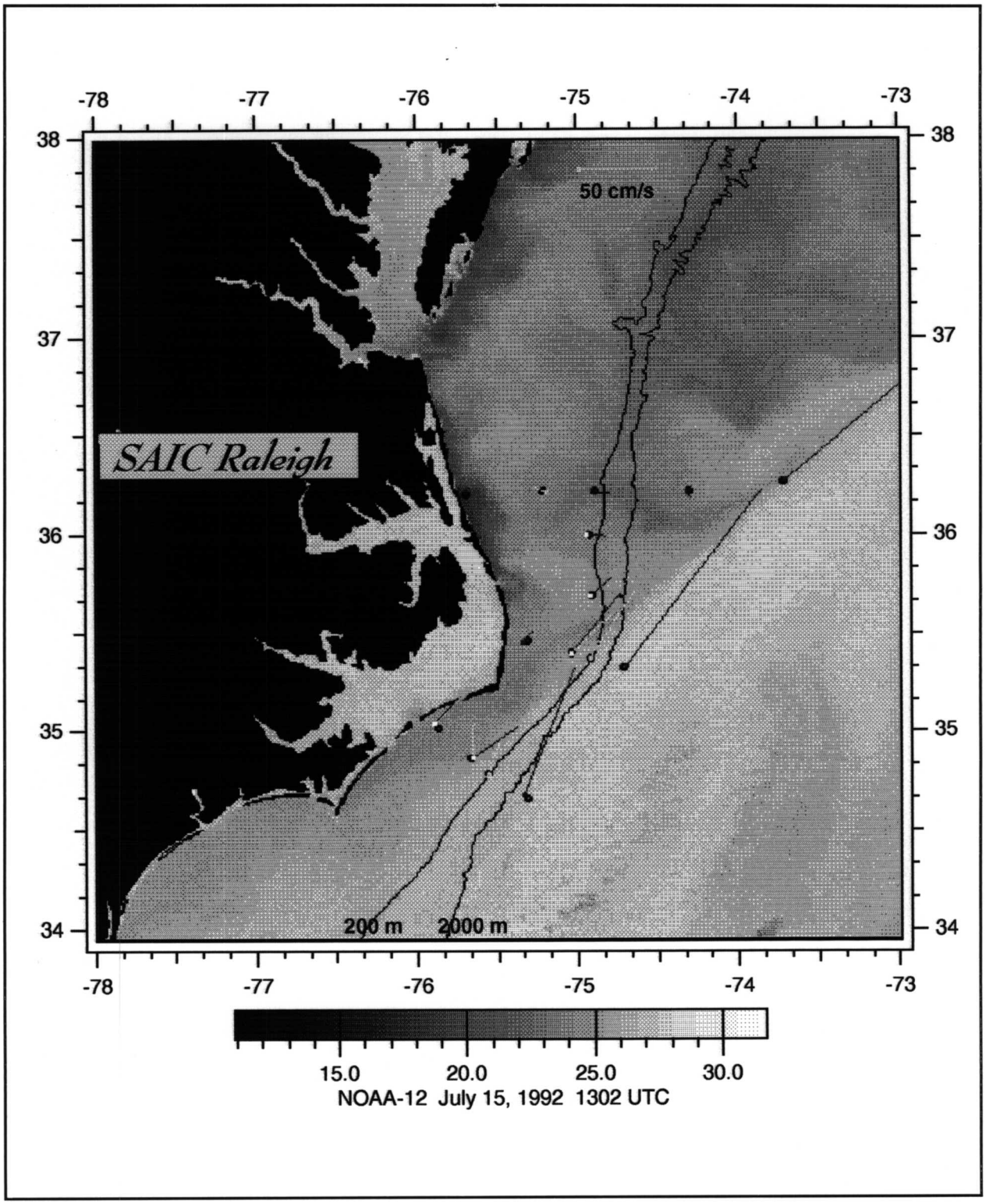

Figure 7.1-10. Satellite SST Image and Daily Average Current Vectors on July 15, 1992. Annotated as in Figure 2.2-7.

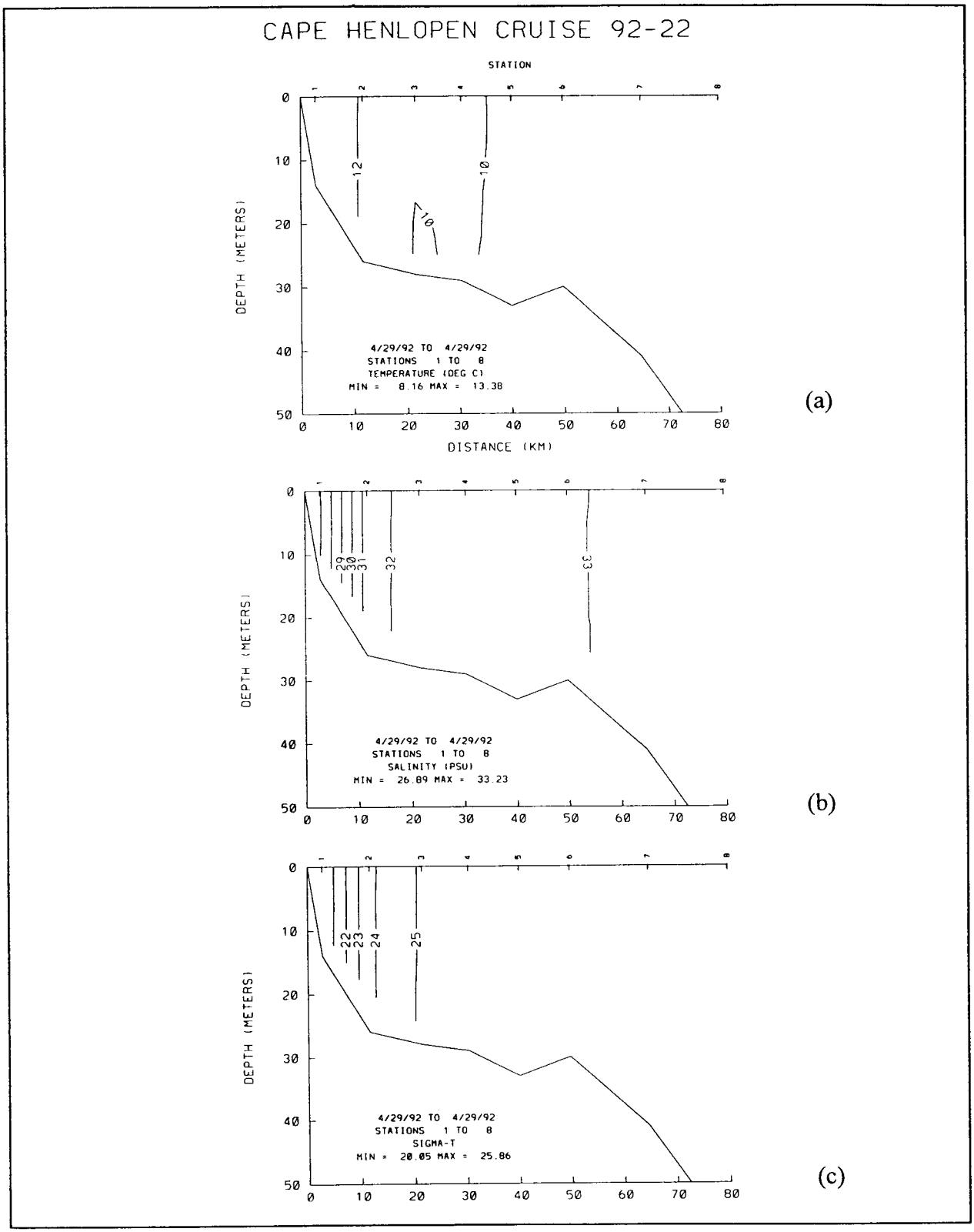

Figure 7.1-11. Cross-shelf sections along Line A of (a) temperature, (b) salinity, and (c) σ_t taken during cruise CH9222 on April 29, 1992.

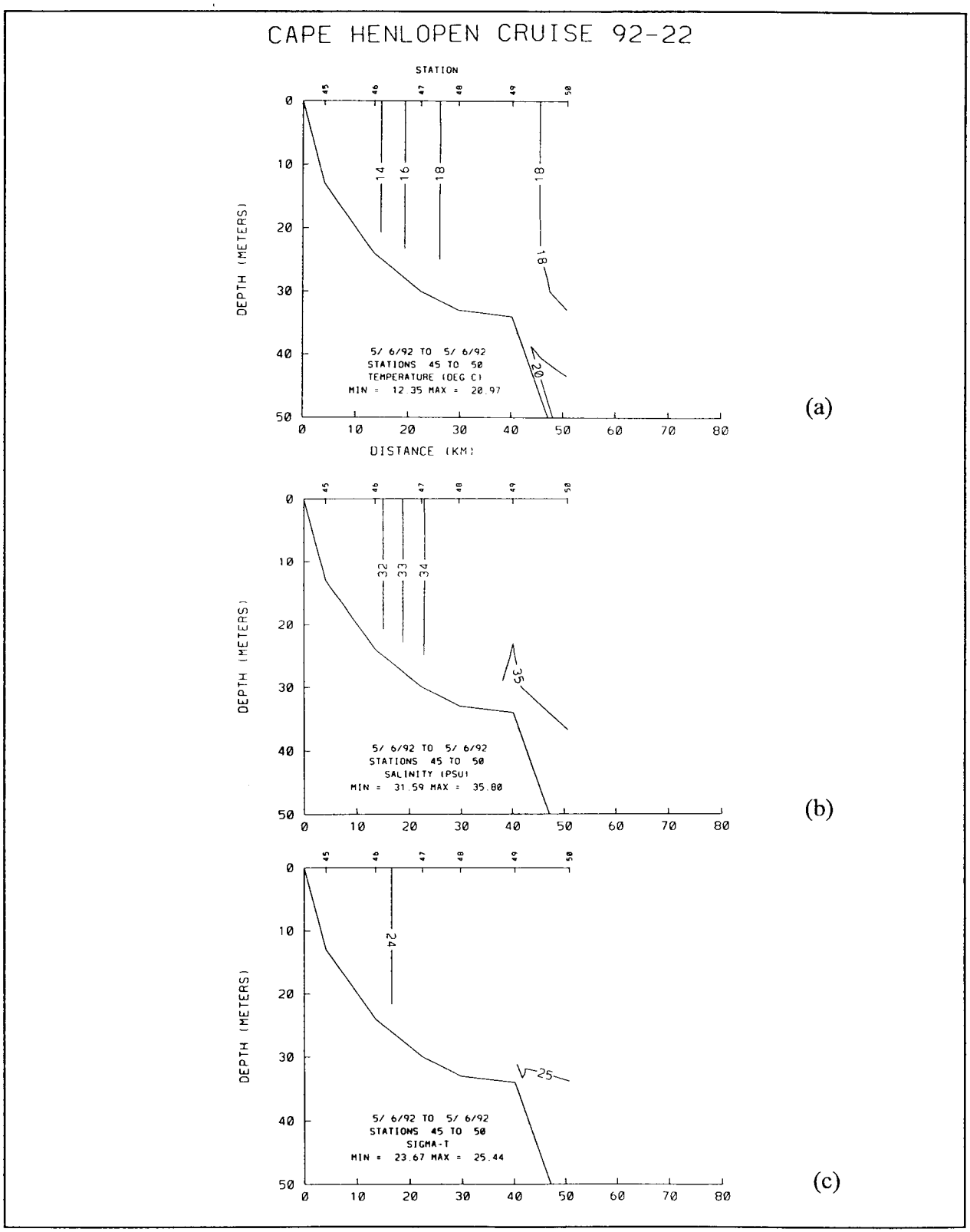

Figure 7.1-12. Cross-shelf sections along Line B of (a) temperature, (b) salinity, and (c) σ_t taken during cruise CH9222 on May 6, 1992.

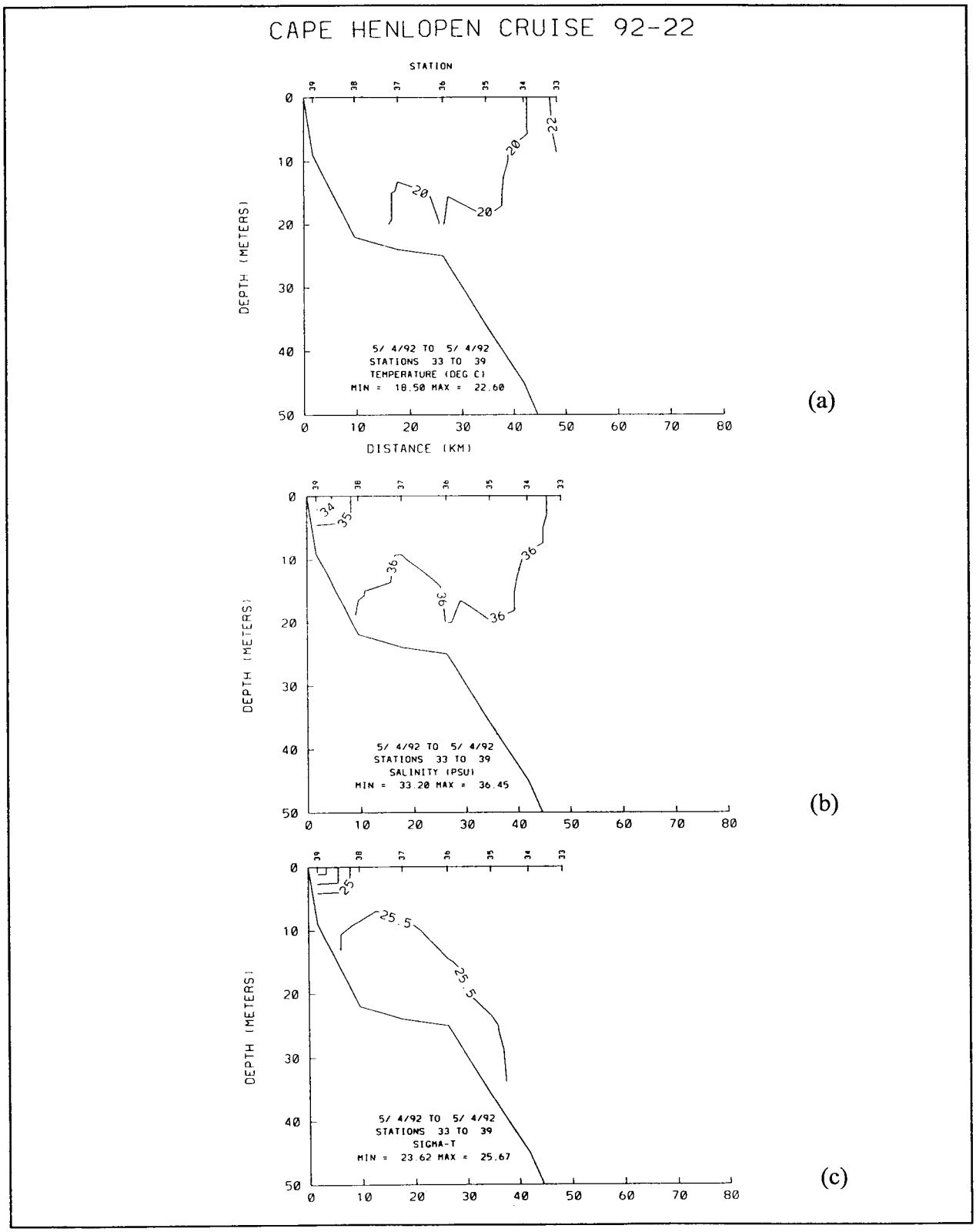

Figure 7.1-13. Cross-shelf sections along Line C of (a) temperature, (b) salinity, and (c) σ_t taken during cruise CH9222 on May 4, 1992.

downwelling favorable, but again, the quantitative contribution of vernal warming, buoyancy flux, wind mixing, and Ekman circulation has not been separated definitively. To the south, in Raleigh Bay (Figure 7.1-13), the shelf is moderately stratified, but it is not clear whether this stratification occurred as a result of a short interval of upwelling-favorable winds prior to sampling the transect, or a result of the previous northerly winds forcing buoyant, low-salinity MAB water south past Cape Hatteras.

Though buoyancy-driven and upwelling motions have been discussed separately, they are often coupled. For instance, the high spring runoff in 1993 created sufficient buoyancy flux within the coastal current in the Middle Atlantic Bight that it may have displaced upwelling along the coast. Upwelling did take place (often seaward of the stratified coastal current), but the signals were not as evident as in 1992. Another example of this coupling between processes is less dynamic (in the coupling), but nevertheless important to the dynamics of the circulation processes. The offshore turning of the cold-water band over the outer shelf in the southern Middle Atlantic Bight creates a situation where, south of this latitude, coastal upwelling no longer delivers cold water to the surface because the cold lower-layer source water is not available at that location. A third example of coupled wind and buoyancy-driven motions is the intrusions of Middle Atlantic Bight water into Raleigh Bay. Intrusions occurred during both 1992 and 1993, but the stronger Middle Atlantic Bight coastal current in 1993 not only produced a buoyancy-driven component of the flow, but also increased stratification in the southern Middle Atlantic Bight. With increased stratification, there is greater shear in the two-layer wind response. As is the case in most coastal circulation, the temperature and salinity fields are both tracers and also coupled dynamically in the circulation processes.

7.1.2 Shelf-Break Upwelling

The broad, shallow continental shelf of both the Middle Atlantic Bight and the South Atlantic Bight is prone to wind-driven upwelling, not only at the coast (see the previous discussion), but also at the shelf break. Boicourt (1973) observed these processes, which were theoretically predicted by Yoshida (1967) during both summer and winter. Although definitive description of the details of the physics is still lacking, their coincidence with the strong upwelling favorable winds suggests that the resulting calving of the cold band water in summer is related to the upwelling process.

A typical example of the summertime shelf-break upwelling and the associated apparent calving of cold, fresh water into the Slope region is shown in Figure 7.1-2. Warm, salty (S>34 psu) water has upwelled and separated a band of colder, fresher water calving off into the Slope Water from the cold band over the outer shelf. Unfortunately, the complexity of the temperature-salinity structure for these events is sufficiently high that they are seldom resolved with moored instrumentation. Occasional glimpses from fortuitously timed hydrographic surveys are the best evidence we have for these intricate motions.

7.2 Buoyancy Forcing

7.2.1 Chesapeake Bay Plume and Coastal Current

As is the case for the plume of the Columbia and Mississippi Rivers, low-salinity water emanating from the Chesapeake Bay undergoes an anticyclonic turn on the continental shelf and then forms a rotationally trapped, high-velocity current along the coast. This pattern can be disrupted by opposing wind stress, although for the Chesapeake Bay case, the plume is seldom driven far against its natural turning tendency (Chao and Boicourt 1986; Boicourt *et al.* 1987). Upwelling-favorable winds can detach the coastal current from the coast (via the Ekman drift), and if sufficiently strong, can suppress it entirely. Upon cessation of these winds, a new coastal current develops quickly and propagates as an internal bore (bore structure on a density interface rather than the sea surface) toward Cape Hatteras. Downwelling-favorable winds force the plume inshore, and accelerate and deepen the coastal current. The primary variables in the interplay here are the buoyancy flux, the wind stress, and the ambient stratification. The first two are by far the dominant influences.

Buoyancy forced motion from Chesapeake Bay was discussed briefly in section 4.3, using hydrographic measurements primarily from 1992. The interannual variability on the shelf between 1992 and 1993 resulting from the abnormally high runoff in 1993 was also discussed. The effect of Chesapeake Bay outflows on the flow of the inner shelf can be seen directly in the moored instrumentation, even during the lower runoff year 1992, when the signals were not as strong. A plot of 5-m salinity and alongshore current for moorings A1, B1, B2, and C1 is shown in Figure 7.2-1. Also plotted is the time rate of change of water level difference between Baltimore, near the head of Chesapeake Bay, and the Bay Bridge

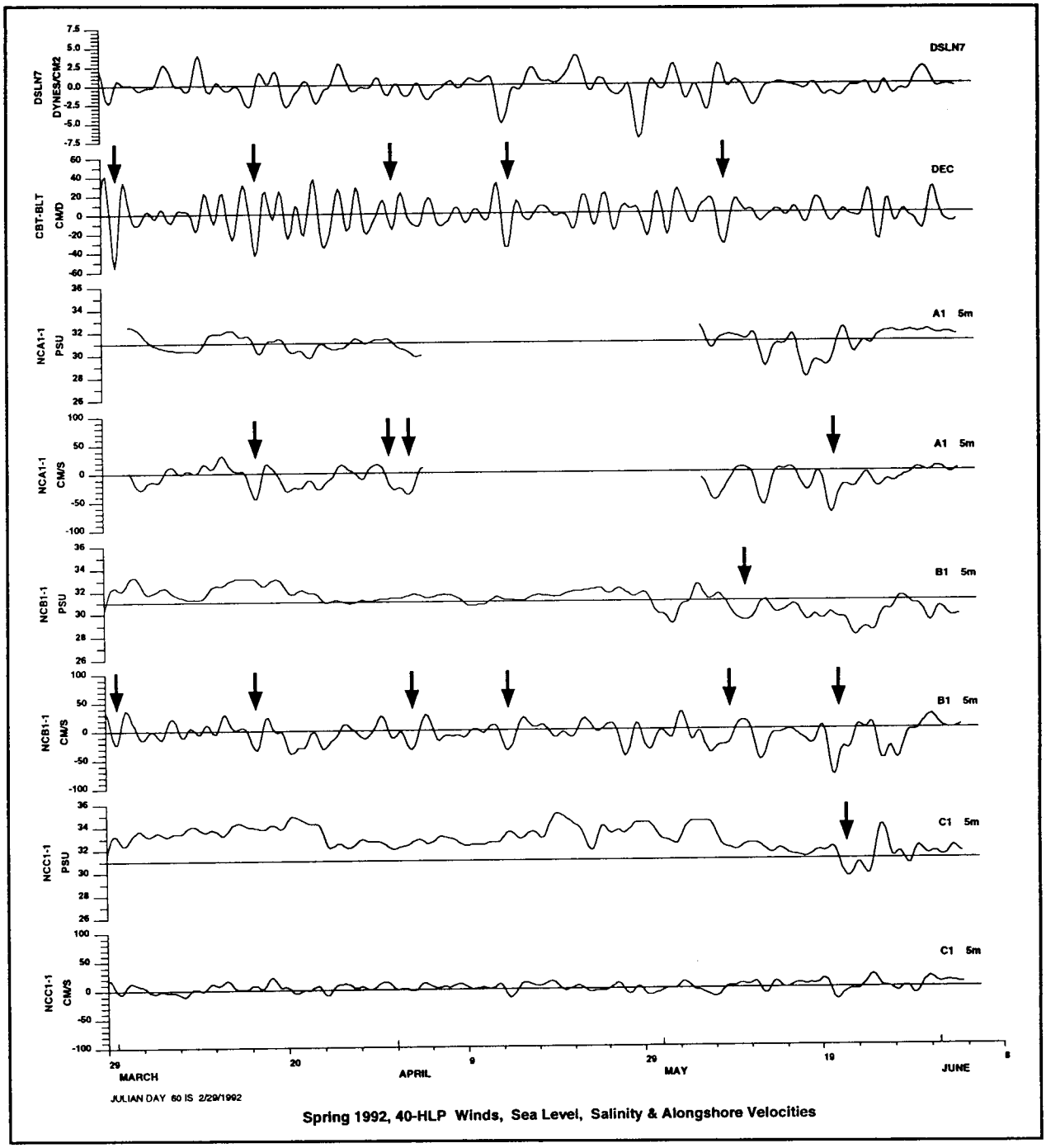

Figure 7.2-1. Diamond Shoals winds, sea level difference in Chesapeake Bay, salinity, and alongshore velocity records from 5-m instrument on moorings A1, B1, B2, and C1 for spring 1992. DEC is the low-pass filtered time rate of change of water level difference between the entrance to Chesapeake Bay (Bay Bridge Tunnel station) and Baltimore Harbor, near the head of the Bay.

Tunnel, near the entrance. This variable is proportional to the transport of water through the entrance of the Bay. Arrows indicate surge outflow events, and corresponding events recorded by instruments on A1 and B1. The apparent one-day delay between Bay surges and velocity and salinity signals at A1 and B1 does not necessarily constitute a causal relationship, with buoyancy-forced motion propagating southward over the shelf, because wind forcing driving shelf motion is obviously coupled to the surge forcing. The outflow surge of the Chesapeake Bay plume can propagate down the coast at 30-60 $cm \cdot s^{-1}$, but the apparent lack of significant phase delay between A1 and B1 suggests that the buoyancy-driven signal, if present, may be entirely masked by local wind driving at these high frequencies. Further analysis may be able to achieve a separation between these two effects under the comparatively low runoff conditions of 1992. At lower frequencies, the effect of buoyancy forcing can be seen as decreases in salinity at moorings A1, B1, and B2 (Figure 7.2-1) following outflow events. The general decline in salt over 10 days beginning March 14, for instance, follows a series of outflow surges in Chesapeake Bay. Again, caution must be used in ascribing such decreases entirely to the Chesapeake Bay outflow because the winds that drive these outflows could also be moving fresher shelf water to the south (although the alongshore gradients are typically small). Mooring C1 shows only three intervals of noticeable decrease in salinity correlated with southwestward flow along the shelf, and these decreases are modest, especially compared with spring 1993.

In 1993, buoyancy driving from the high runoff was both stronger and more clearly indicated in the measurements. Figure 7.2-2 contains the records from the inshore instruments for spring 1993. Again, the response of the coastal current to Chesapeake Bay outflows is coupled to the wind, but the individual contributions of buoyancy and wind forcing is now more apparent, especially during the stronger events. For the northerly wind events marked by arrows in Figure 7.2-2, a phase delay of 1-2 days is now evident between moorings A1 and B1, indicating southward propagation of buoyancy-driven motion. If the observed response were solely local wind driving, then significantly smaller phase delays would be observed, as in spring 1992. For 1993, the mean flows at A1 and B1 are markedly stronger and more persistent, reflecting the high buoyancy flux.

The coherence between the outflow surges from Chesapeake Bay and alongshore flow at mooring A1 is significant over the synoptic

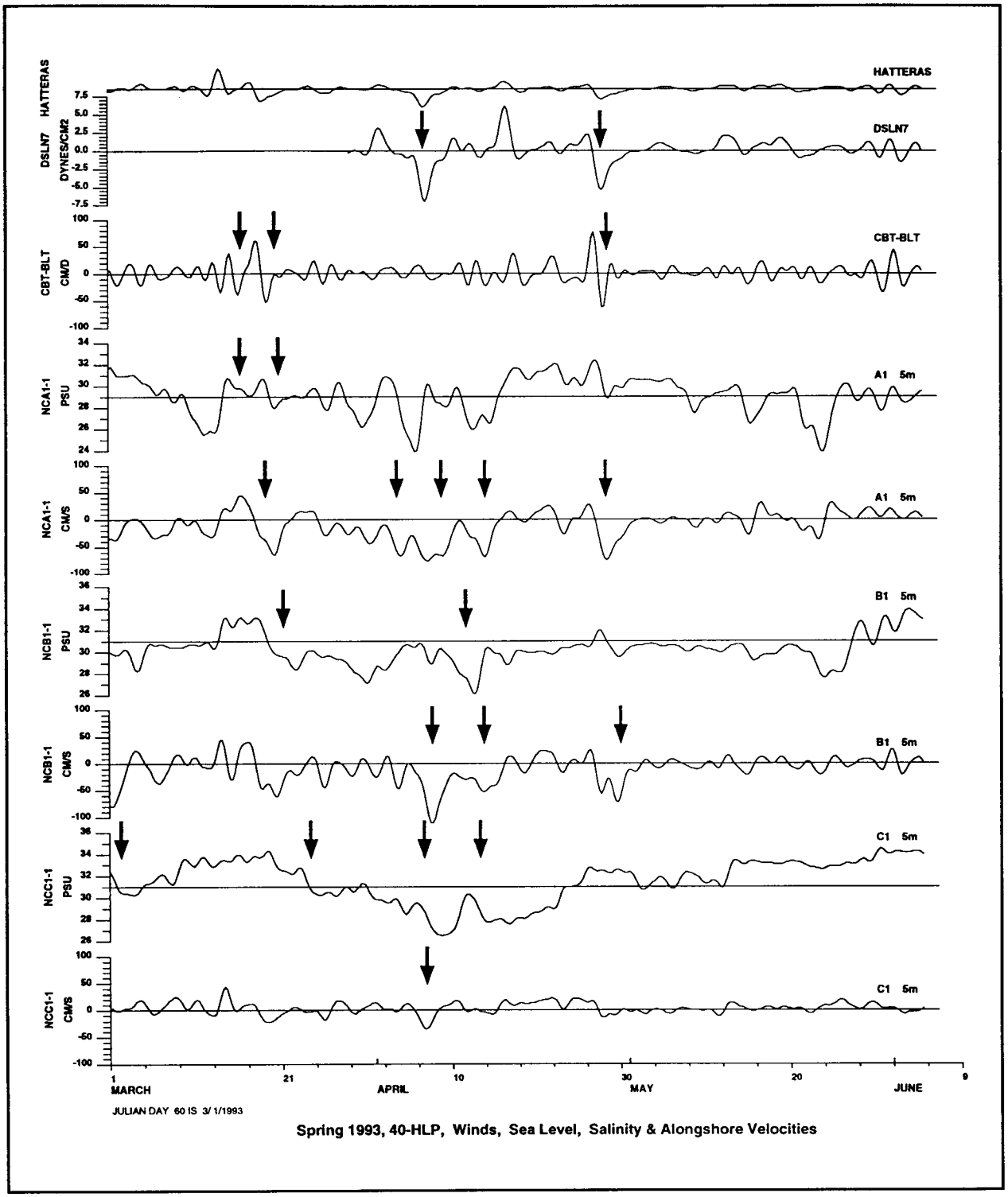

Figure 7.2-2. Diamond Shoals/Cape Hatteras winds, sea level difference in Chesapeake Bay, salinity, and alongshore velocity records from 5-m instrument on moorings A1, B1, and C1 for spring 1993. Annotated same as Figure 7.2-1.

weather band in 1992, but the coherence could be nearly entirely due to the correlation between each of these signals and the wind stress driving. The presence of two peaks in the Bay surge index, however provides specific bands in which to examine this coherence. The primary band is at approximately 0.44 cpd and corresponds to the quarter-wave seiche in Chesapeake Bay (which has a period near 2 days). A subsidiary peak is observed at 0.32 cpd, or near 3 day period. This peak is at slightly higher frequency than the previously observed 4-day subharmonic of the Chesapeake Bay seiche, and therefore its origin is somewhat uncertain. Coherence between the surge index and the alongshore flow at A1 and B1 (Figures 7.2-3 and 7.2-4) is significant at the quarter wave seiche band. The lower-frequency peak occurs in the flow variance spectrum at B1, but not at A1. However, coherence between the surge index and flow at A1 and B1, and between the flow at A1 and B1 (Figure 7.2-5) is consistently significant in this band.

At lower frequencies (below 0.2 cpd), the coherence between the surge index and flow at A1 and B1 is high, despite the characteristic low-frequency falloff in energy in the rate of change signal. As would be expected, the coherence of the alongshore flow at this band is high between moorings A1 and B1 along the inner shelf. As in the high-frequency bands, the coherence in the lower frequency weather band is a result of atmospheric forcing driving both the quarter-wave seiche in Chesapeake Bay and the flow on the continental shelf.

7.2.2 Intrusions of Middle Atlantic Bight Water into Raleigh Bay

The intrusions of Middle Atlantic Bight water around Cape Hatteras and into Raleigh Bay have been discussed in the previous section as a combination of wind-driven and buoyancy driven motion. However, such transfers have been well documented in low-runoff years, when buoyancy forcing is less likely to play a role. In these cases, this motion past Cape Hatteras is almost entirely wind driven and the salinity signals are correspondingly weaker. Temperature, however, is a good tracer during the winter season as a result of the strong thermal contrast between the Middle Atlantic Bight and the South Atlantic Bight.

The position of the Gulf Stream must play a significant role in this intrusion process. In its offshore position, the Gulf Stream may not directly affect this transport, but the circulations

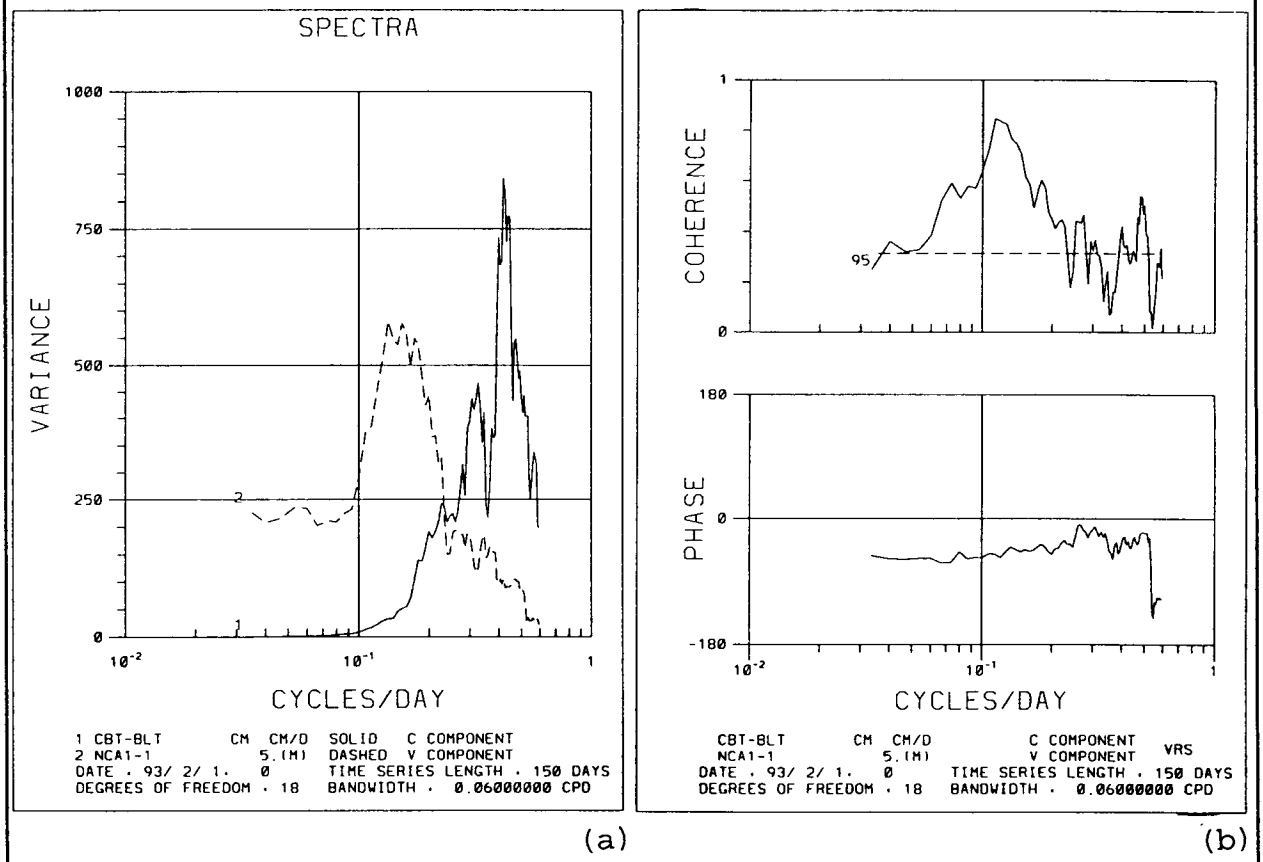

Figure 7.2-3. Autospectra (a) and coherence (b) between time rate of change of water level difference between Bay Bridge Tunnel and Baltimore (solid line) and alongshore velocity on mooring A1 (5 m) (dashed line) for spring 1992.

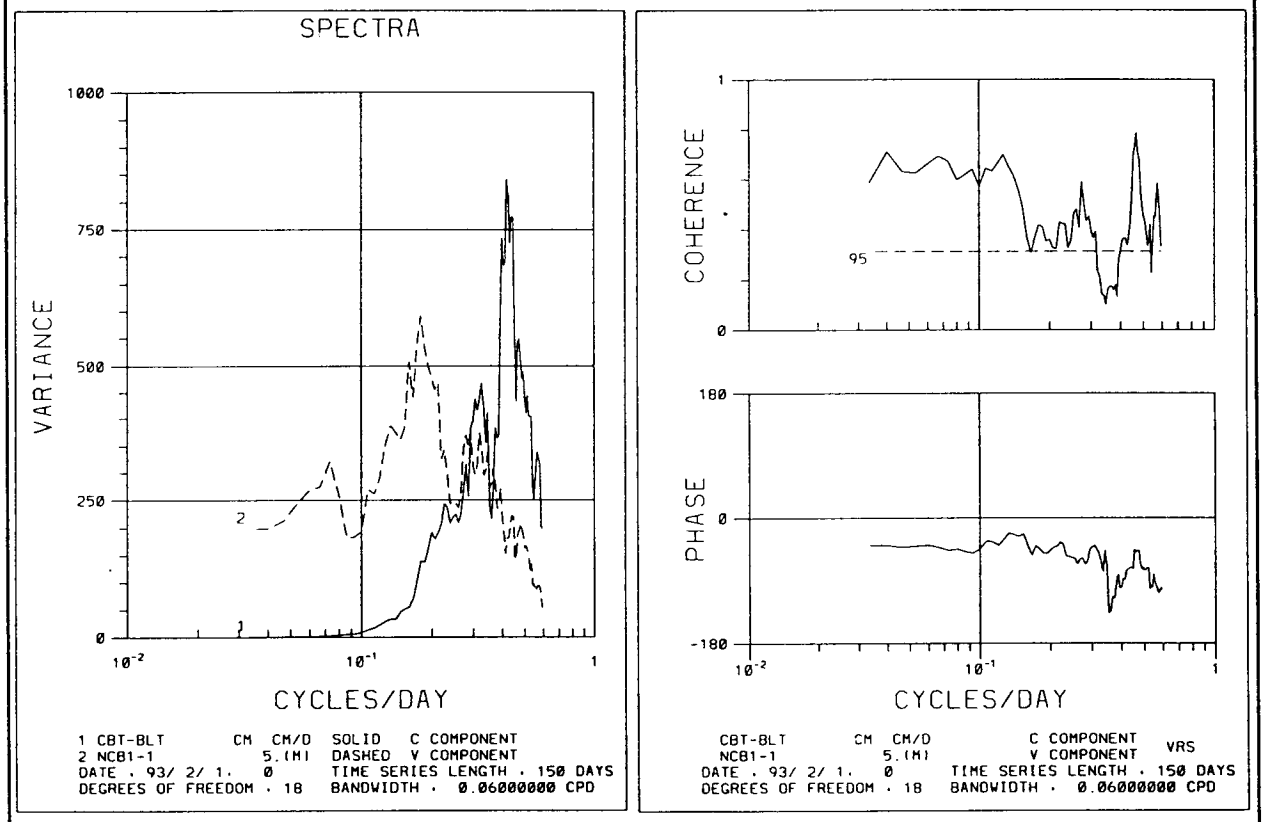

Figure 7.2-4. Autospectra (a) and coherence (b) for Bay outflow surge (solid line) and alongshore flow on mooring B1 (5 m) for spring 1993.

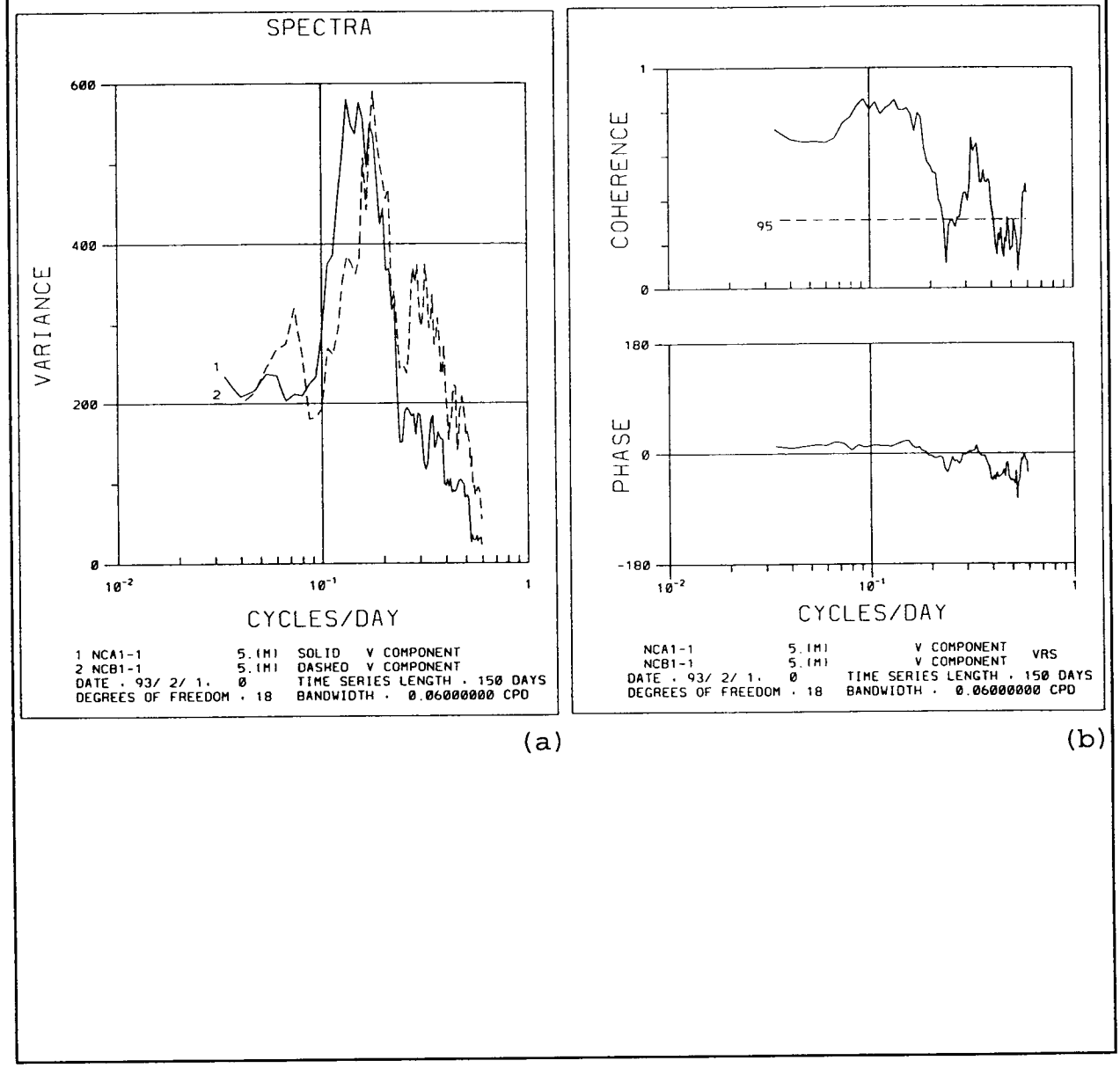

Figure 7.2-5. Autospectra (a) and coherence (b) for alongshore flow at mooring A1 (5 m) (solid line) and mooring B1 (5 m) (dashed line) for spring 1993.

associated with its large eddy mode motions are likely to influence these motions.

The strong intrusion events in spring 1993 shown in Figure 7.2-2 clearly have a buoyancy-driven component. Even without the direct buoyancy driving, the delivery of low-salinity water to near Cape Hatteras by the Chesapeake Bay plume coastal current provides a distinct tracer for these events. Coherences between alongshore flow at mooring B1 and salinity at C1 are shown in Figure 7.2-6. The coherence is significant at numerous peaks, but marginally so. Coherence between B1 flow and the time rate of change of salinity at C1 (Figure 7.2-7) is higher for this year of high runoff.

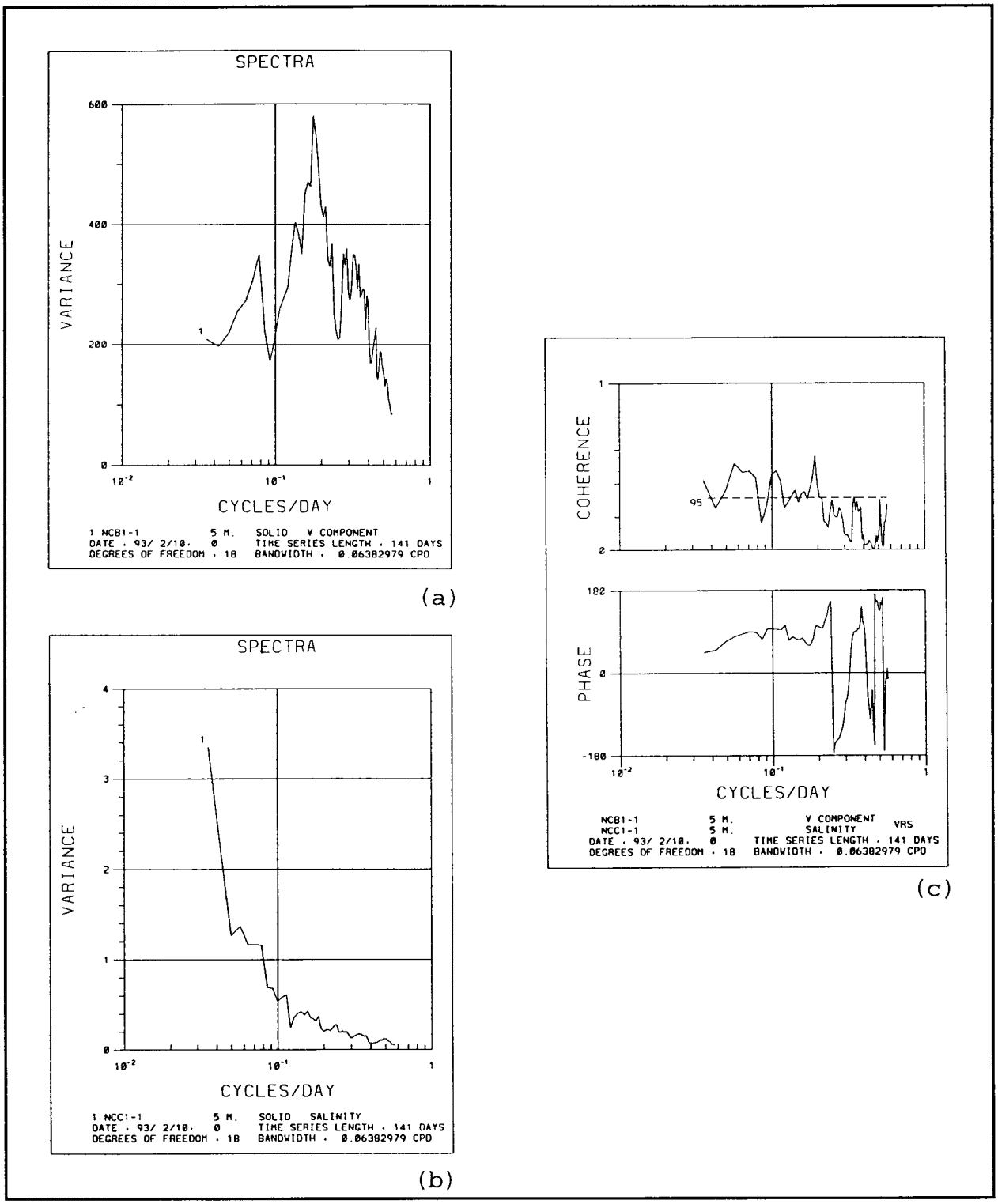

Figure 7.2-6. Autospectra of (a) alongshore flow at mooring B1 and (b) salinity at mooring C1, and coherence and phase (c) between the two in spring 1993.

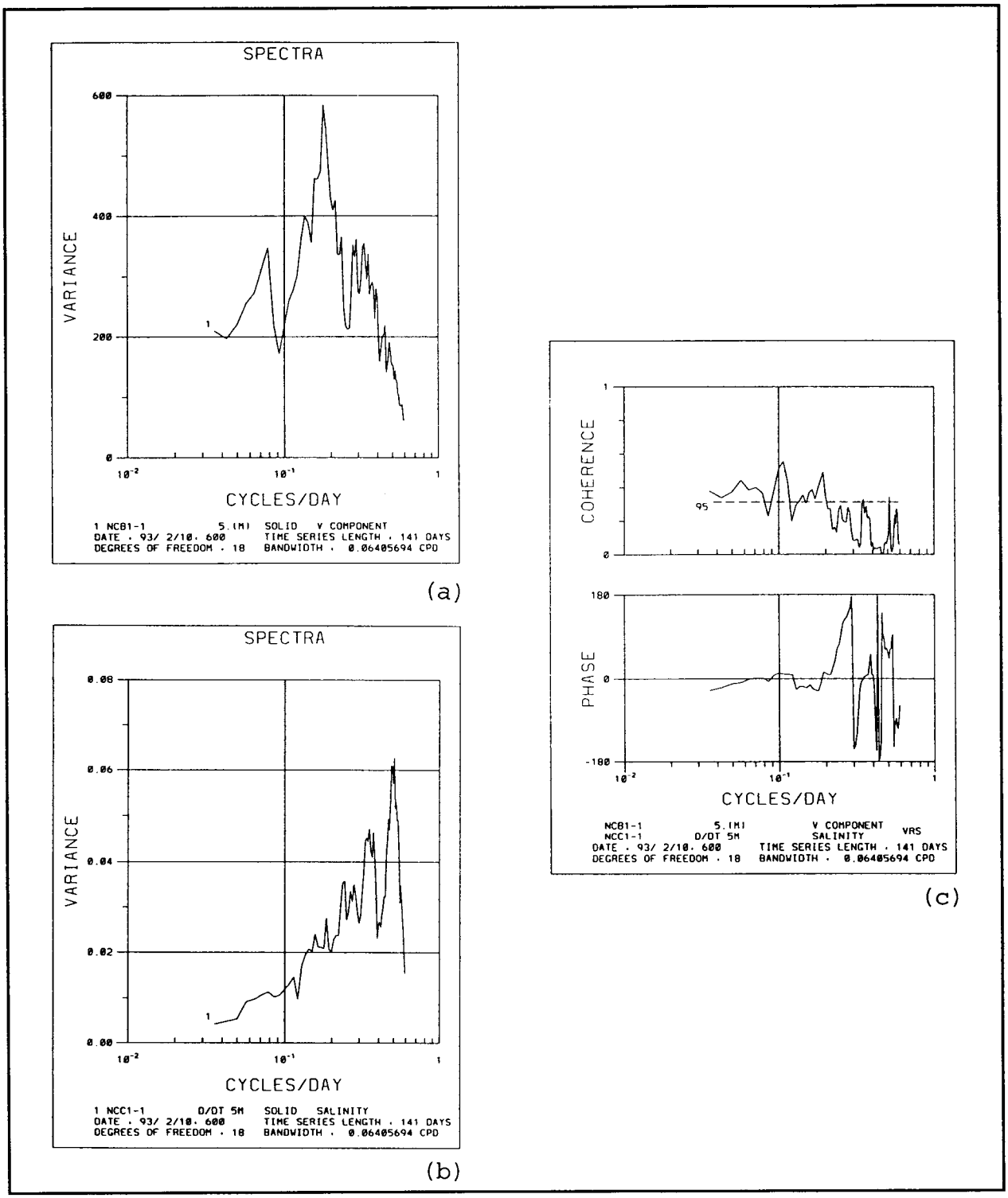

Figure 7.2-7. Autospectra of (a) alongshore flow at mooring B1 and (b) time rate of change of salinity at mooring C1, and coherence and phase (c) between the two in spring 1993.

VIII. NEARSHORE CIRCULATION

8.1 Background

This portion of the report describes the results of two special event studies which were designed to observe the configuration and strength of the Coastal Frontal Zone both north and south of Cape Hatteras. Detailed and repeated hydrographic surveys of the inner shelf region were conducted in June and September 1993. Near-surface flow measurements using Lagrangian drifters were combined with moored current meters to describe the relationship of observed ocean currents to the density structure of the coastal frontal zone both north and south of Cape Hatteras. Wind regimes were defined using data from the US Army Corps of Engineers pier at Duck, North Carolina.

Nearshore currents measured at A1, B1 and C1 were over the 22-, 21-, and 20 m isobaths respectively. Drifting buoys were deployed just north of the Line B current meters but much closer to shore than B1. At approximately 13 km offshore, B1 represents the closest current meter data to the deployment line, but it is several kilometers seaward of the deployment positions. The 20 m isobath currents are assumed to be representative of the inner shelf, defined here as depths less than 20 m. Currents at A2, B2 and C2 were outside the inner shelf as defined here.

The first Nearshore Experiment was conducted on June 11-16, 1993. Several offshore sections were repeated north of Cape Hatteras and one south of the Cape. A second experiment was conducted September 15-21, 1993. Several repeated sections were done north of Cape Hatteras. These two special experiments are referred to as First and Second Nearshore Experiments.

8.2 First Nearshore Experiment

8.2.1 Wind Regime

Wind velocity vectors (Figure 8.2-1) as this experiment began were approximately northeastward at about 6 $m \cdot s^{-1}$ which produced upcoast and offshore components north of Cape Hatteras. This regime lasted until midday June 11. On the morning of June 12, wind vectors shifted to southwestward and remained so until early on June 14. Peak wind speeds reached about 10 $m \cdot s^{-1}$ on the afternoon of June 13. A wind shift occurred again on June 14 with a northward and

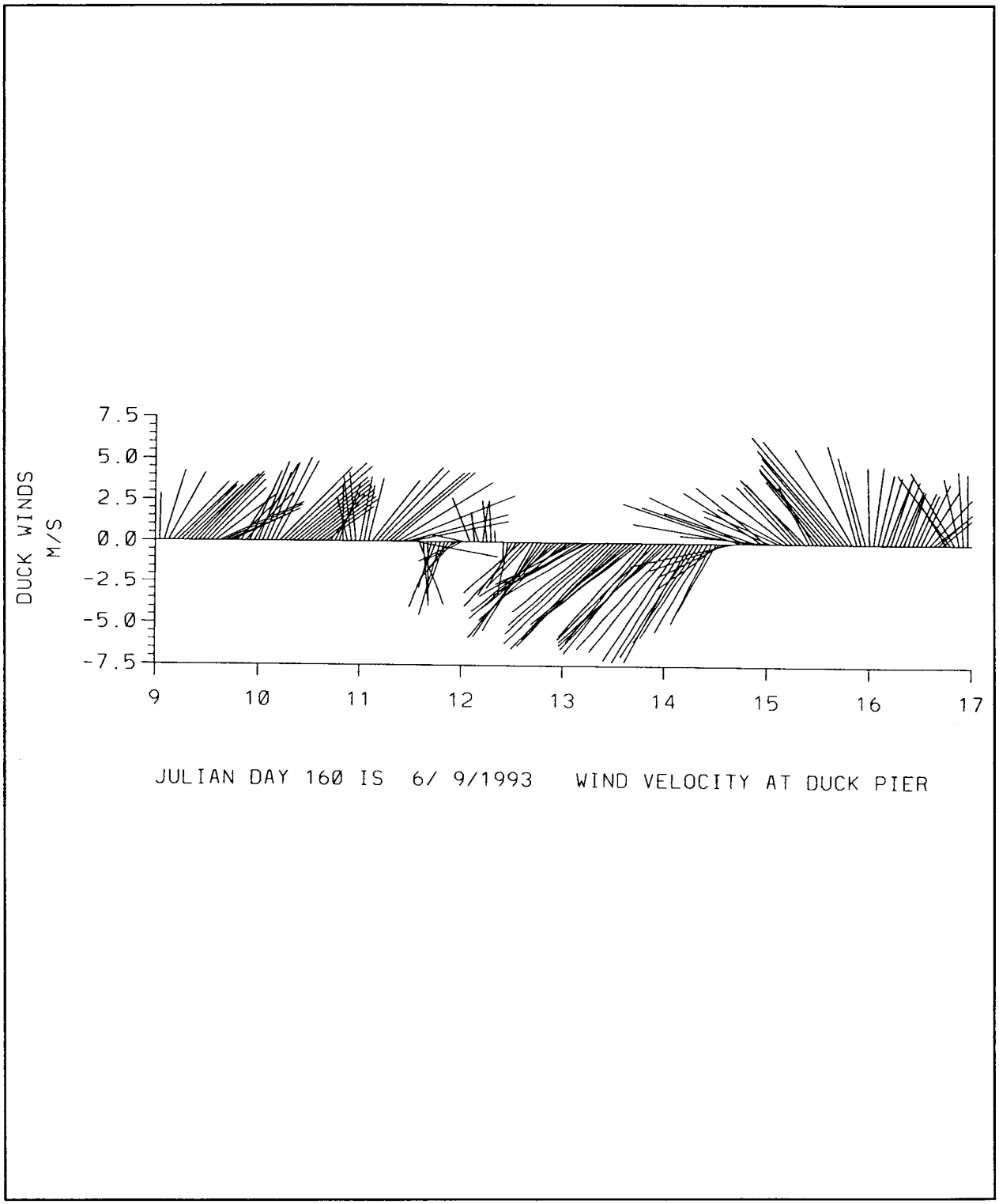

Figure 8.2-1. Wind velocity at Duck Pier from June 9-17, 1993. Data are unfiltered.

westward component. The onshore component gradually became offshore on the afternoon of June 16.

8.2.2 Hydrography and Currents

Drifter tracks during the First Nearshore Experiment are shown in Figure 8.2-2. Details of the drifter dynamics are discussed in section 8.4. Hydrographic station locations are shown in Figure 1.2-6(a).

June 11-14, 1993 (Drifter Deployment 2)

Winds switched from northeastward to southwestward over this time interval. Northward alongshelf currents decelerated throughout June 11 (Figure 8.2-3). Alongshelf currents at A1, A2, B1 and B2 became southward on June 12 and remained so throughout June 14. Currents at C1 and C2 changed similarly. Cross-shelf currents at A1 and B1 were < 5 $cm \cdot s^{-1}$, but this component was stronger at C1. Throughout the mooring region, cross-shelf currents outside the inner shelf were onshore at 5 m depth but offshore at 20 and 30 m depths. This is consistent with a downwelling circulation regime on the inner shelf that was present through June 13.

Density structure along the buoy deployment line (about 20 km north of Line B) was generally horizontal with a vertical gradient of ~$2\sigma_t$/10 m (Figure 8.2-4). A lens of low-salinity (low density) water (T>22°C; S<32 psu; σ_t<22 n; d<6 m) was located about 5-6 km offshore over the 20 m isobath. A sharp coastal front was found less than 2 km from shore with similar characteristics to the lens.

Buoys deployed near the Line B were advected southward during this period and were retrieved south of Cape Hatteras. A low-density lens (T>23.5°C; S<34.5 psu; σ_t <23.5; d<6 m) was located about 4 km offshore along the cross-section where the buoys were retrieved (Figure 8.2-4). The pycnocline underneath the lens sloped downward and offshore at a slope of 7 m/10 km with a vertical gradient of about 0.5 σ_t units/5 m. The isopycnals shoaled abruptly at a distance of 4 km offshore inside of which was a coastal frontal zone coastal frontal zone sloping upward and offshore. Water characteristics inside the coastal frontal zone were the same as those in the lens farther offshore but the coastal frontal zone was bottom-attached.

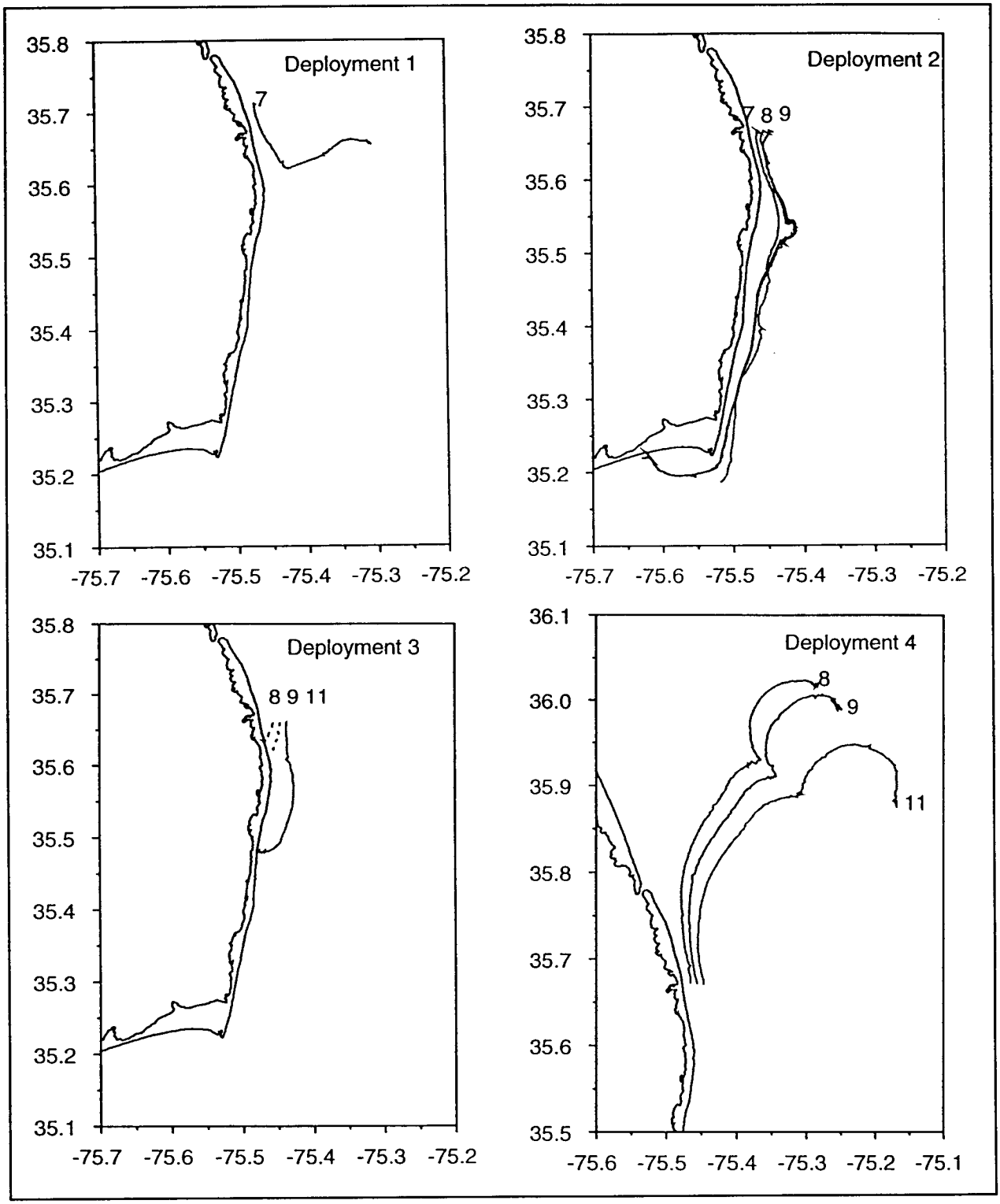

Figure 8.2-2. Drifter tracks of the first nearshore experiment - June 1993.

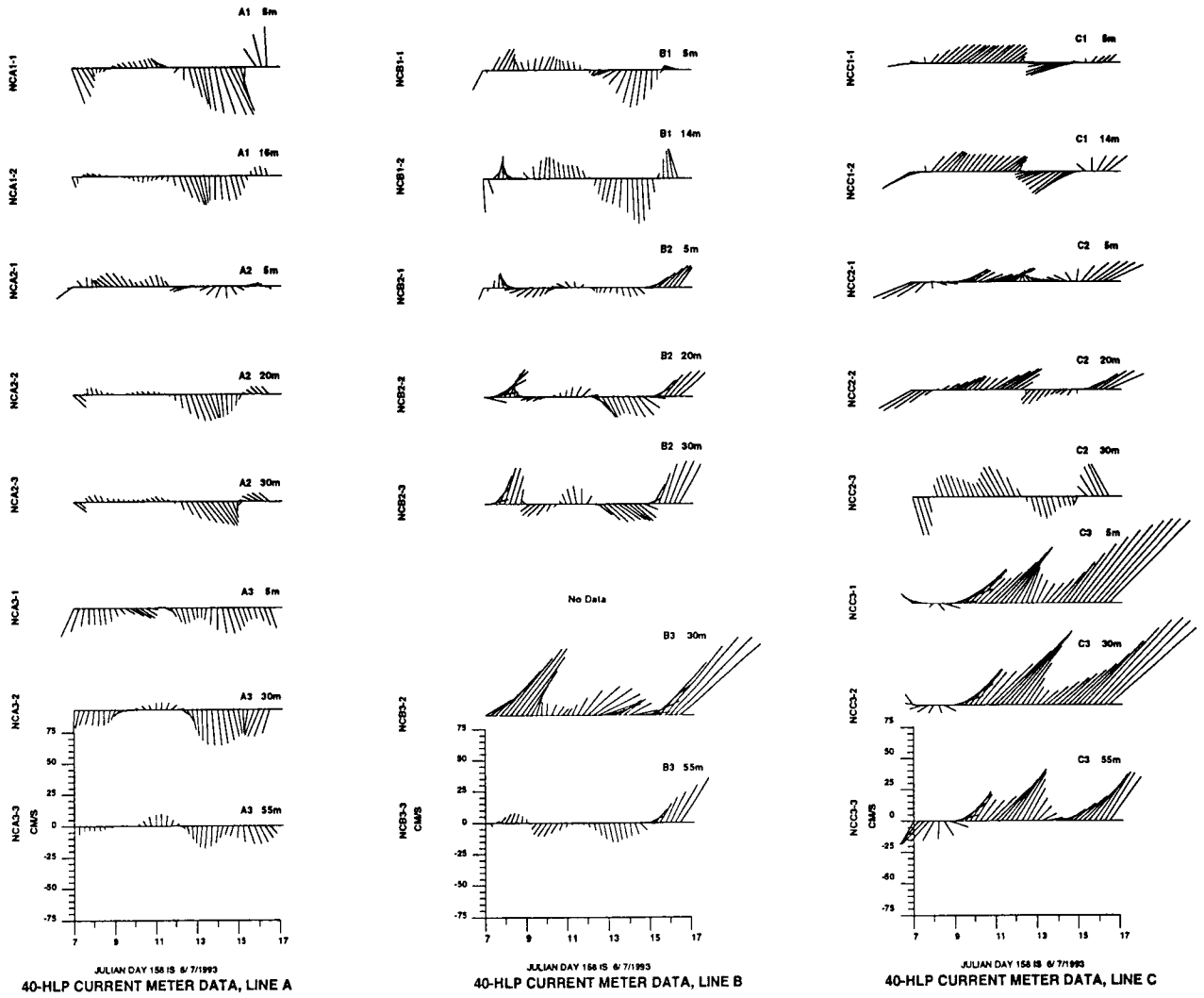

Figure 8.2-3. Current-meter data from June 7-17, 1993 (a) Line A, (b) Line B, and (c) Line C.

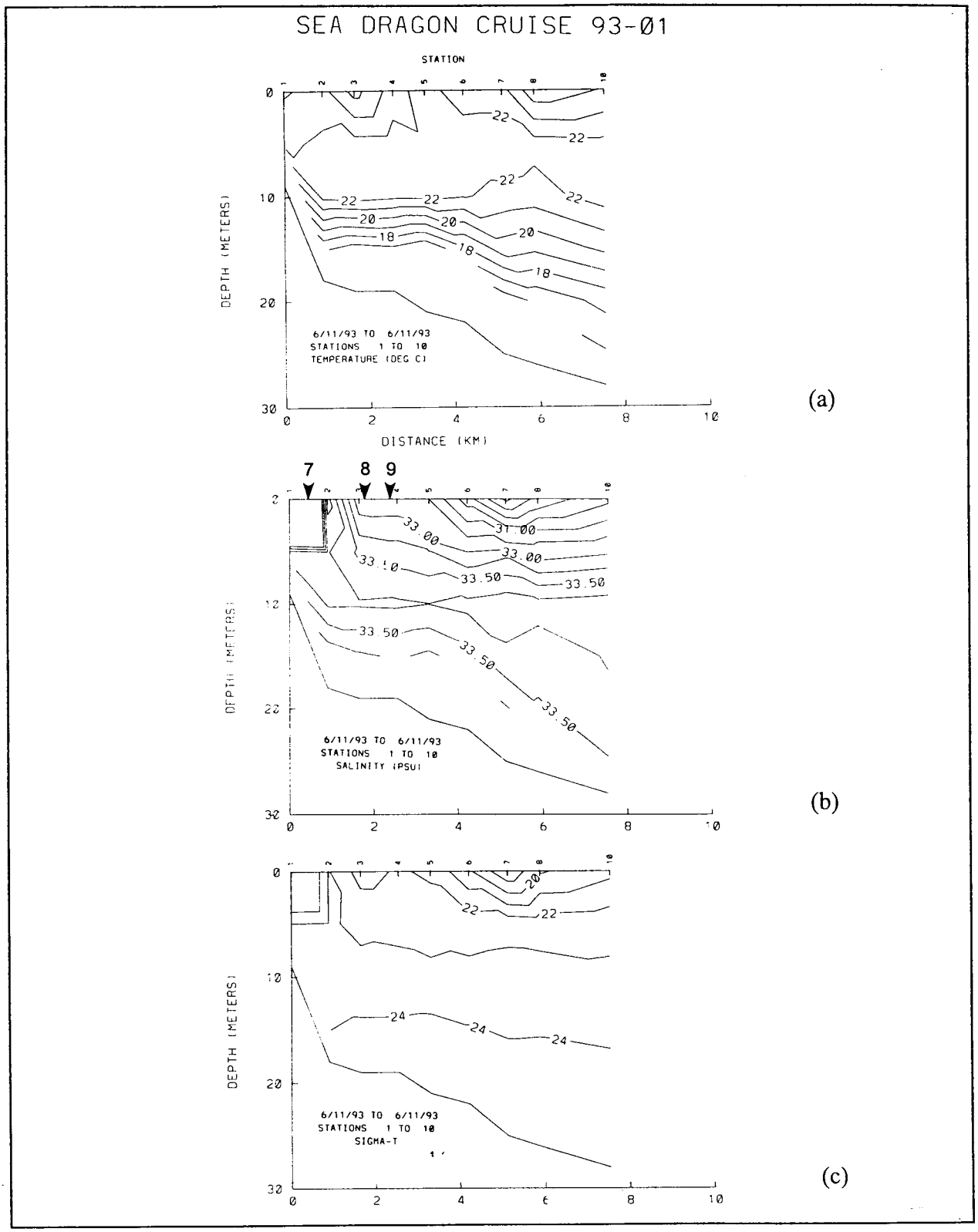

Figure 8.2-4. Cross-shelf sections of (a) temperature, (b) salinity, and (c) σ_t taken during cruise SD9301 on June 11, 1993. Arrows indicate drifter deployment sites.

Conditions south of Cape Hatteras (Figure 8.2-5) showed that vertically stratified water found 6-8 km offshore was vertically mixed in the shallower water 4 km offshore. Closer to shore, a wedge of low-salinity, low-density water was found inside the 15 m isobath). Currents at C1 (5 m) and C2 (5 m) were southward and onshore, suggesting that this low-density wedge originated from north of Cape Hatteras and was probably continuous with the low-salinity lens found on the deployment line (Figure 8.2-4). The section along the deployment line (Figure 8.2-6) was repeated after southwestward winds on June 13-14 decelerated and became northward and westward. Winds continued to change as the onshore component gradually became offshore late on June 15.

Alongshore currents on June 14 peaked southward at A1 and B1 and surface speeds exceeded 20 $cm \cdot s^{-1}$ at B1 and reached almost 40 $cm \cdot s^{-1}$ at A1. Flow was southward throughout the CTD section.

The lens of low-density water ($T>21°C$; $S<29$ psu; $\sigma_t<17$; $d<7$ m) was now trapped against the coast (Figure 8.2-6). Slightly higher salinity and density was found at the station closest to shore, evidence of enhanced vertical mixing in shallow water. Vertical density gradient through the lens was 4 σ_t units/5 m.

June 15-17, 1993 (Drifter Deployments 3 and 4)

Winds became upwelling favorable (northeastward) by June 15 and remained so when buoys were retrieved on June 17. Southward currents at B1 (5 m) began to accelerate northward by June 16. Nearbottom currents changed to northward at B1 (14 m) about 12 hours earlier. Currents evolved similarly at B2, A1 and A2. Cross-shelf currents at A2 were offshore at 5 m but onshore at 20- and 30 m meters. This pattern is consistent with an upwelling regime, and it is puzzling that the pattern at B2 remained in the downwelling mode throughout June 16.

Four CTD transects were completed at three cross-sections during this time interval. One was on the deployment line (Figure 8.2-7), two were on a line about 22 km north (about 5 km north of Oregon Inlet) (Figures 8.2-8 and 8.2-9), and another was on a line about 15 km farther north of Oregon Inlet (Figure 8.2-10). These sections indicated that the salinity and density structure within 8 km of the coast was initially horizontal on June 15 but later dipped downward in the offshore direction on June 16, consistent with the onset of upwelling.

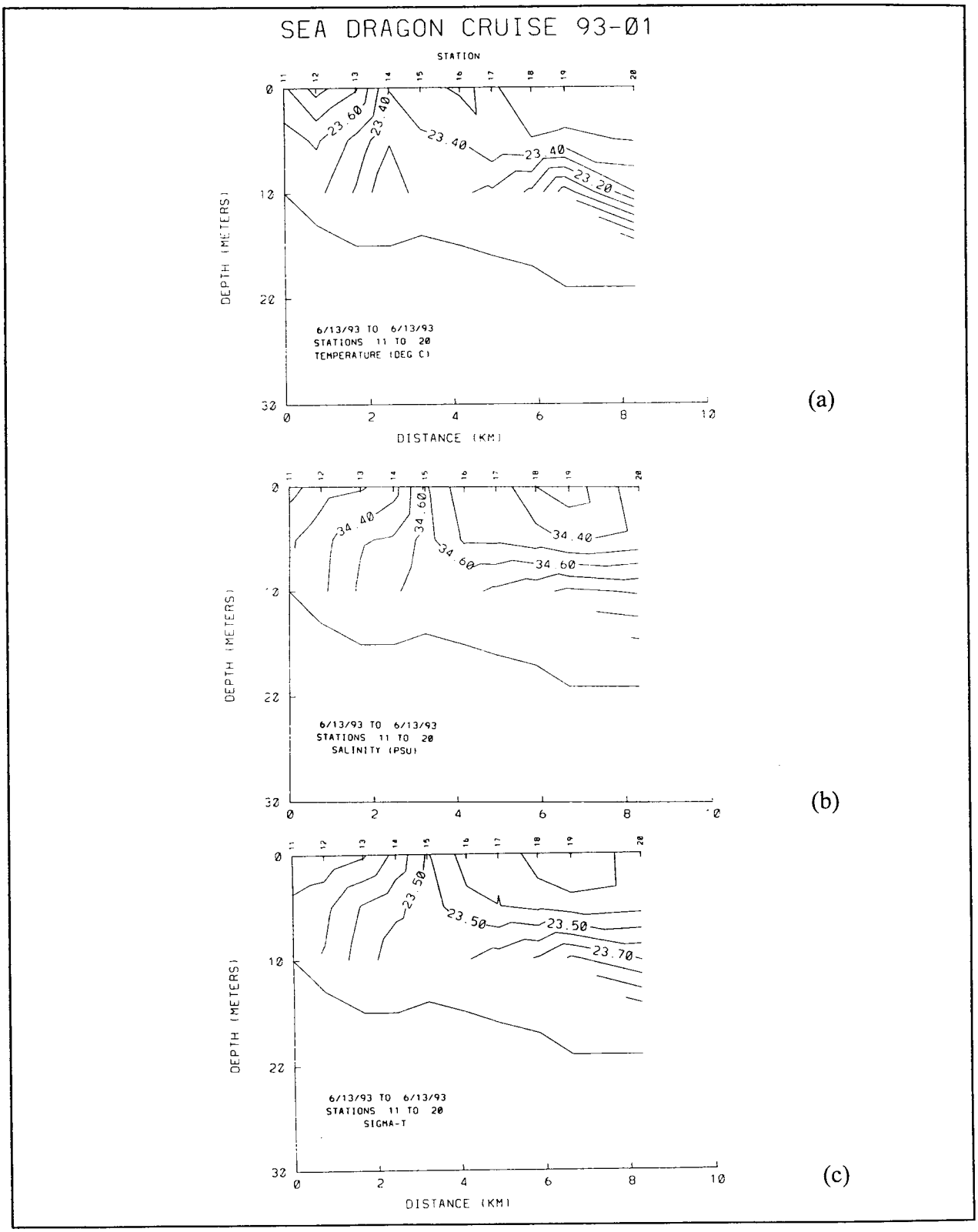

Figure 8.2-5. Cross-shelf sections of (a) temperature, (b) salinity, and (c) σ_t taken during cruise SD9301 on June 13, 1993.

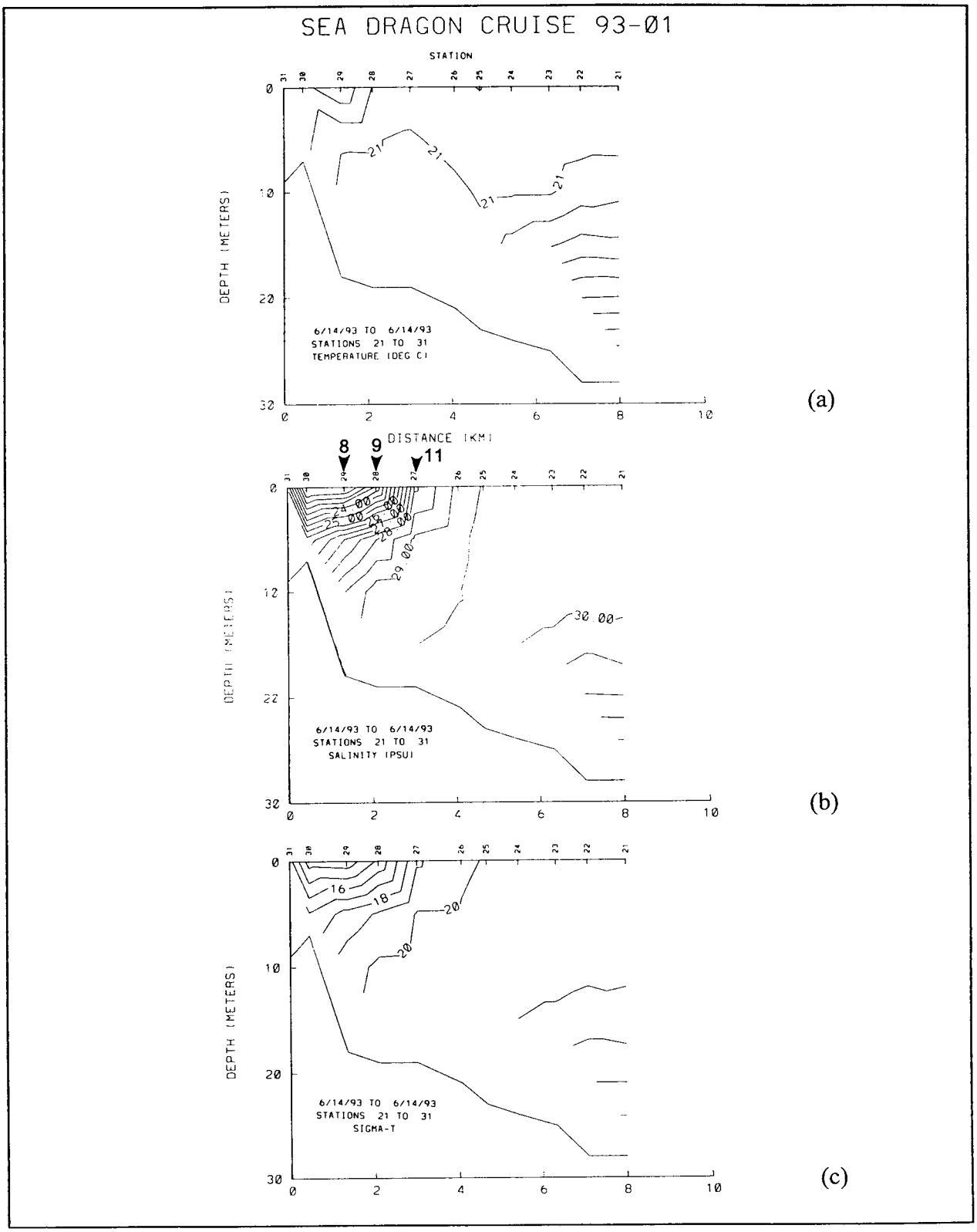

Figure 8.2-6. Cross-shelf sections of (a) temperature, (b) salinity, and (c) σ_t taken during cruise SD9301 on June 14, 1993. Arrows indicate drifter deployment sites.

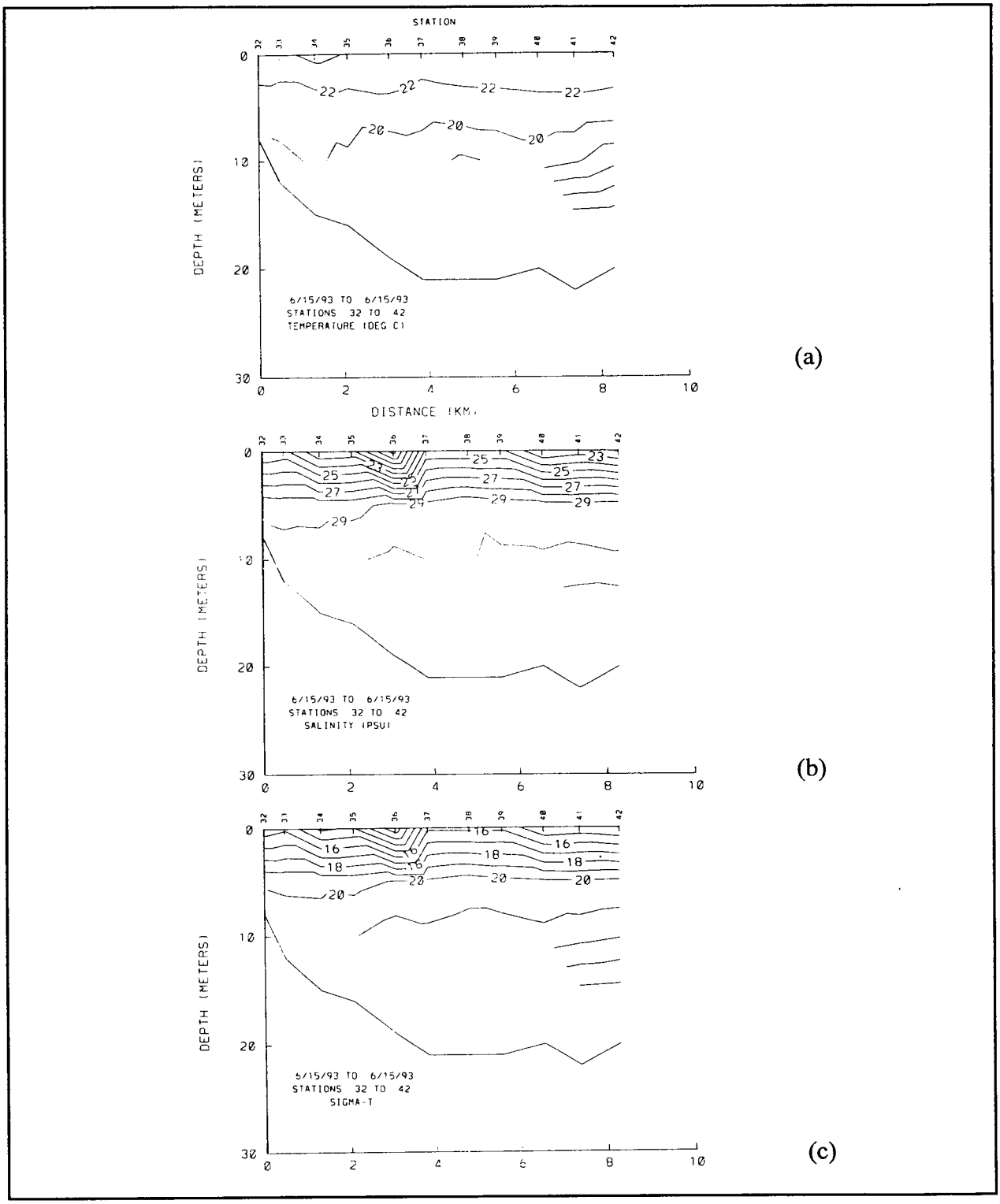

Figure 8.2-7. Cross-shelf sections of (a) temperature, (b) salinity, and (c) σ_t taken 5.6 km north of Oregon Inlet during cruise SD9301 on June 15, 1993.

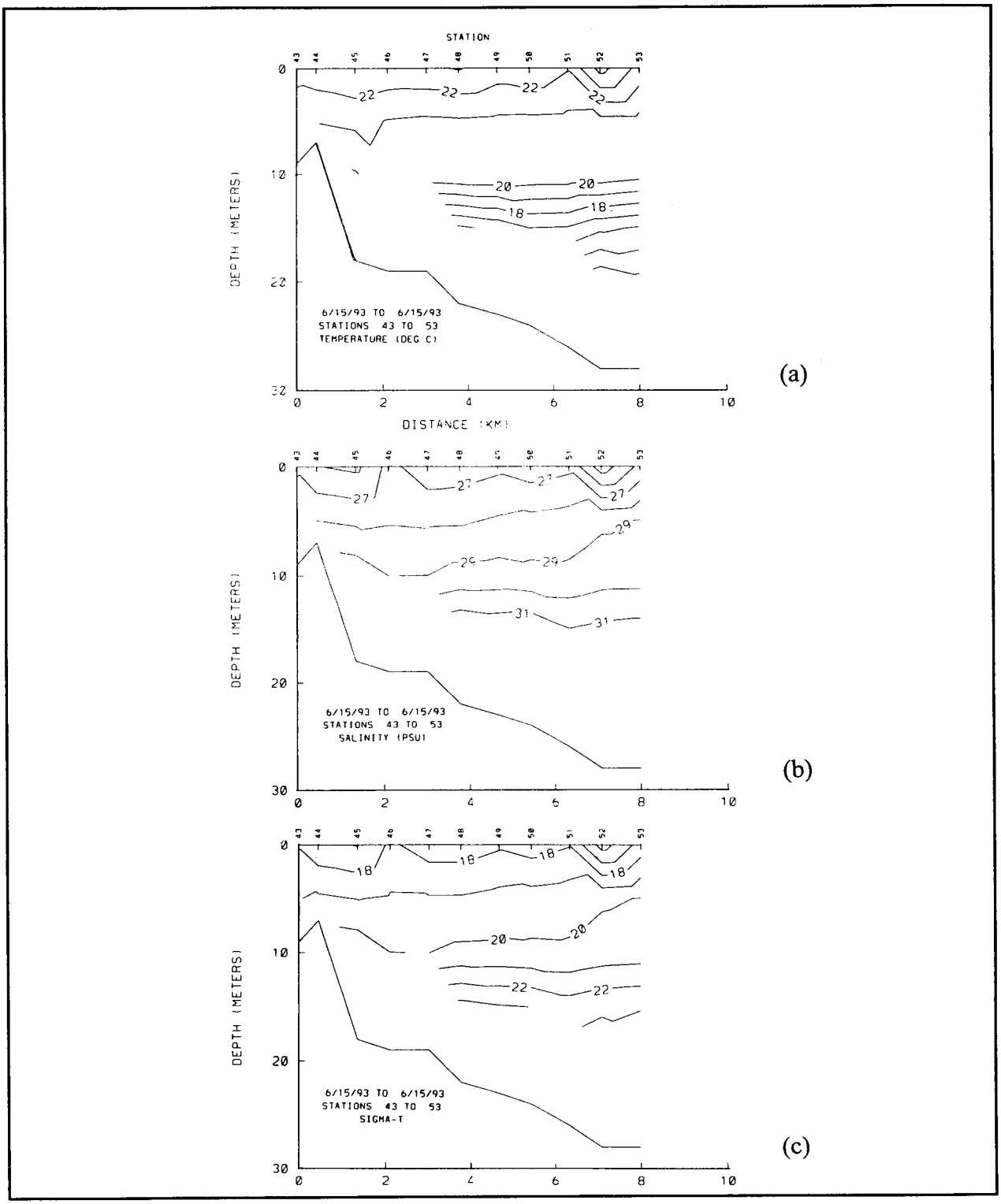

Figure 8.2-8. Cross-shelf sections of (a) temperature, (b) salinity, and (c) σ_t taken 12 km south of Oregon Inlet during cruise SD9301 on June 15, 1993.

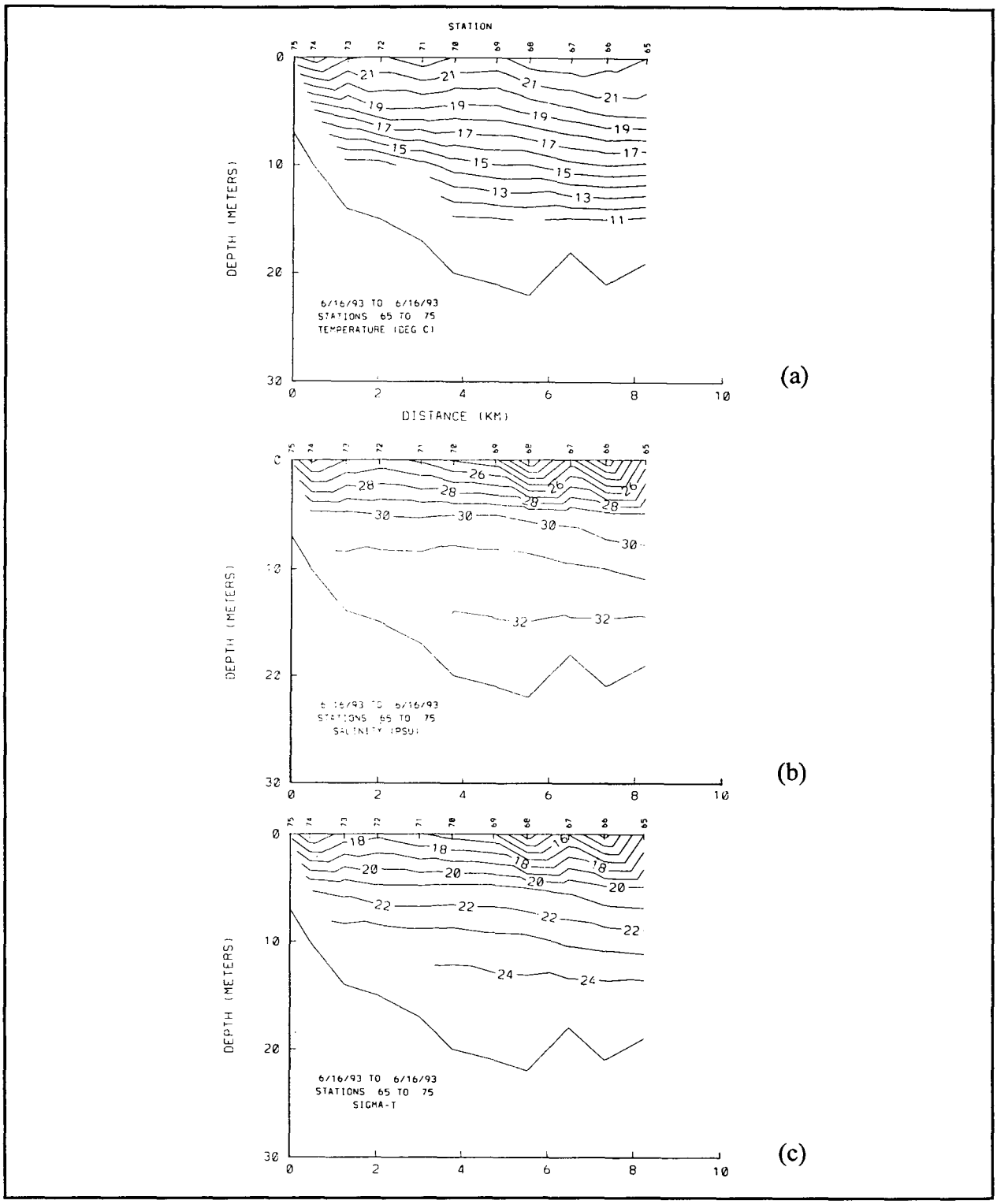

Figure 8.2-9. Cross-shelf sections of (a) temperature, (b) salinity, and (c) σ_t taken 5.6 km north of Oregon Inlet during cruise SD9301 on June 16, 1993.

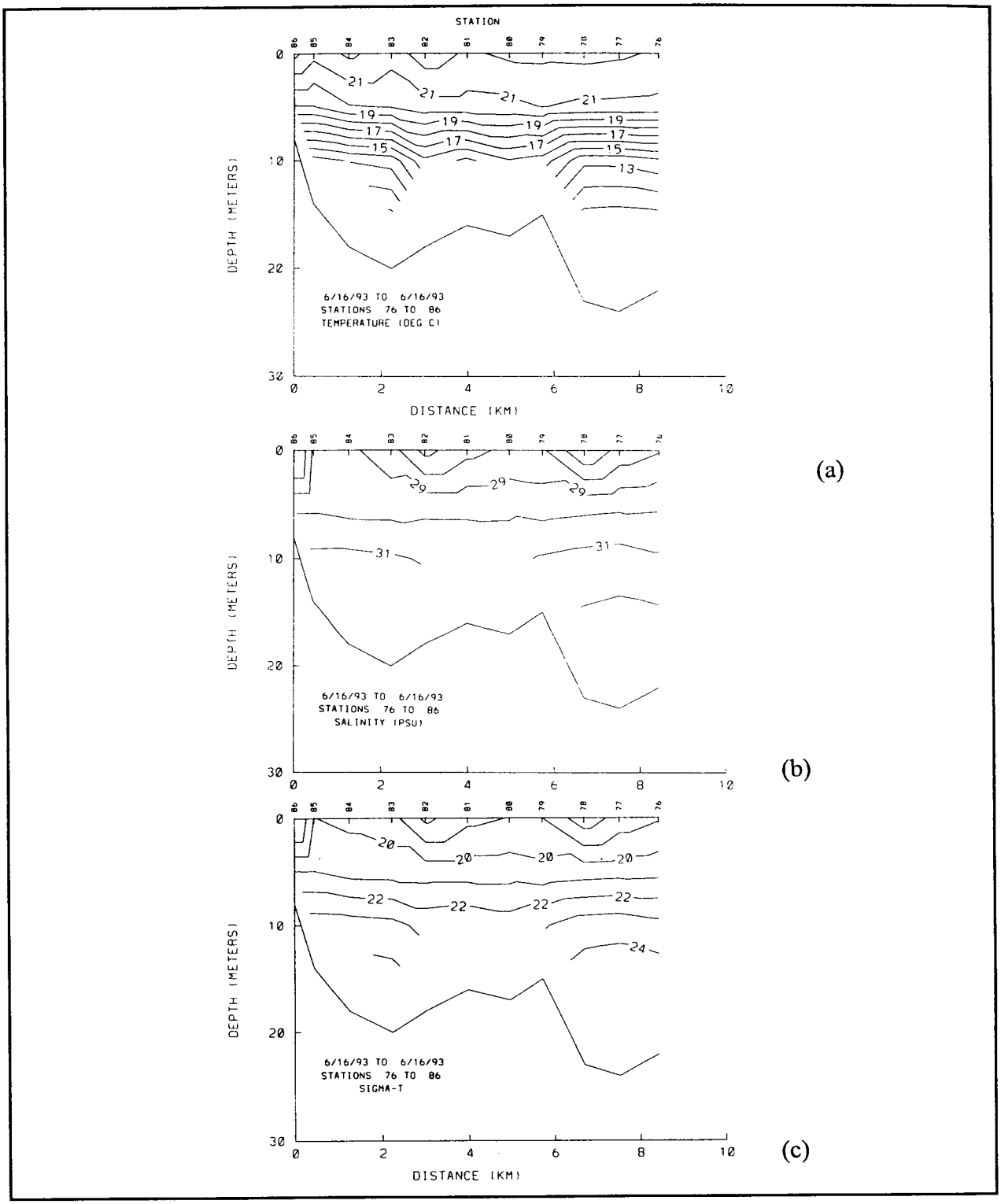

Figure 8.2-10. Cross-shelf sections of (a) temperature, (b) salinity, and (c) σ_t taken 14.8 km north of Oregon Inlet during cruise SD9301 on June 16, 1993.

Salinity on the deployment line (Figure 8.2-8) was less than 29 psu above depths of 10 m with vertical gradients of about 2 psu/10 m. Two shallow surface lens (<3 m thick) were found at 1 km and 7 km offshore. Lower salinity (<25 psu) and stronger vertical salinity gradients (6 psu/6 m) were found 5 km north of Oregon Inlet (Figure 8.2-6). A shallow surface lens of less than 21 psu was found 3 km offshore with indication of another more saline one (S<24 psu) about 7 km offshore (the seaward extent was not resolved). Within a day, salinities had increased by 1-2 psu and gradients had decreased by 50 percent along this line (Figure 8.2-9). Two surface lens (S<23 psu) were found at 5.5 and 7.5 km offshore. The presence of a lens (surface salinity < 26 psu) was indicated within 1 km of the coast. The section 15 km north of Oregon Inlet had salinities below 30 psu at depths less than 6 m (Figure 8.2-10). There were two lens (S<28 psu) at distances of 3 and 7 km from shore, and a strong coastal front within 1 km of the coast was also present.

8.3 Second Nearshore Experiment

8.3.1 Wind Regime

Winds at the Duck pier (Figure 8.3-1) generally blew northwest to northeast (upwelling favorable) for the period September 13-17. There appeared to be a seabreeze oscillation (24 hour period) in the eastward component with onshore wind components followed by offshore components. A brief calm occurred early on September 17 then winds resumed with a northward component. A reversal to strong southwestward winds (downwelling favorable) occurred on September 19 and lasted until upwelling- favorable winds resumed on September 21.

8.3.2 Hydrography and Currents

Drifter tracks during the Second Nearshore Experiment are shown in Figure 8.3-2. Details of the drifter dynamics are discussed in section 8.4. Hydrographic station locations are shown in Figure 1.2-6(b).

September 13-16, 1993 (Drifter Deployment 5)

Currents were northward at A1, A2, and B2 (Figure 8.3-3) consistent with northward wind component. The deeper meters at A2 measured onshore flow. However, the deeper flow at B2 was offshore. The alongshelf current at B1 (5 m) was very weak, while the current at

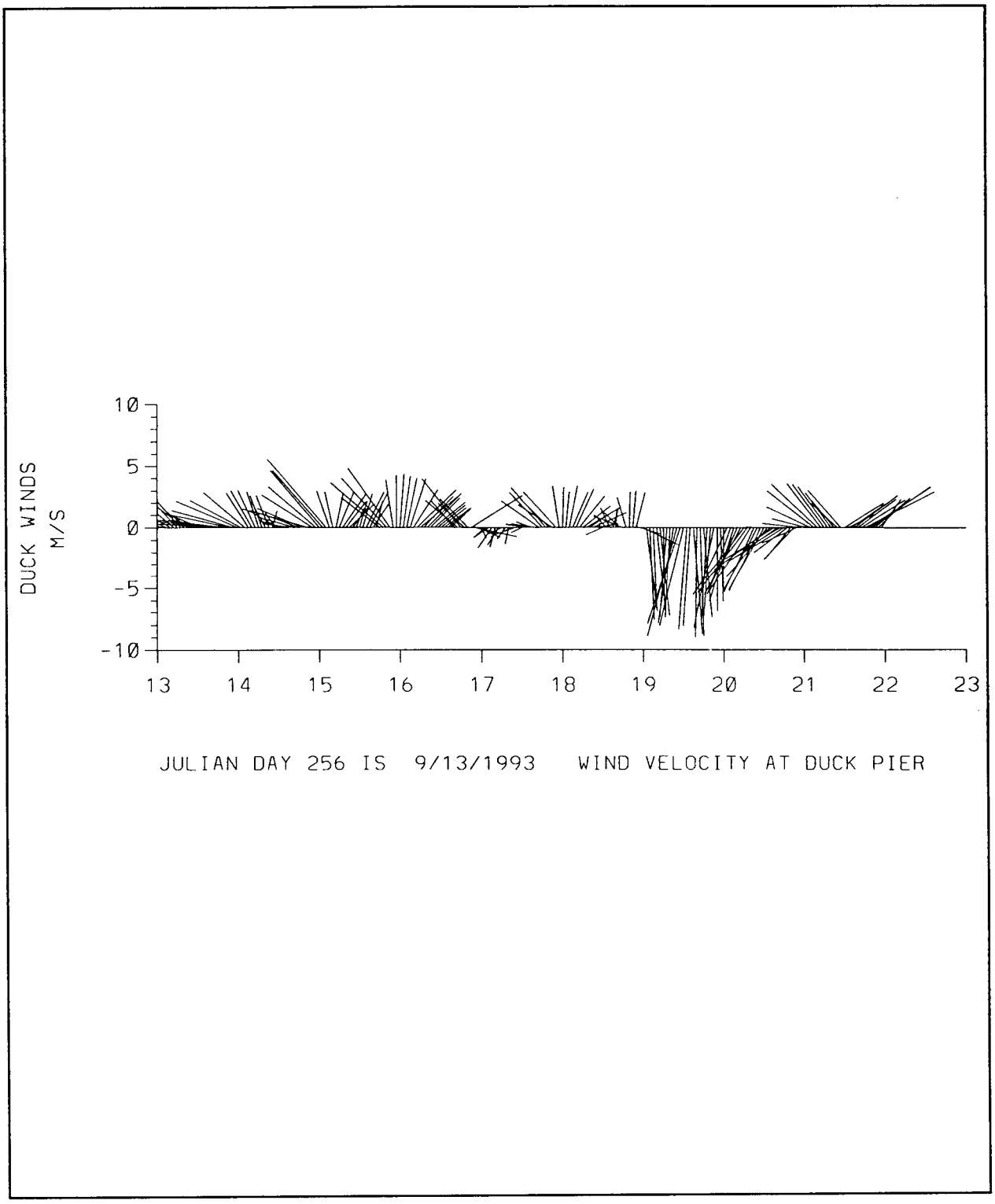

Figure 8.3-1. Wind velocity at Duck Pier from September 13-23, 1993. Data are unfiltered.

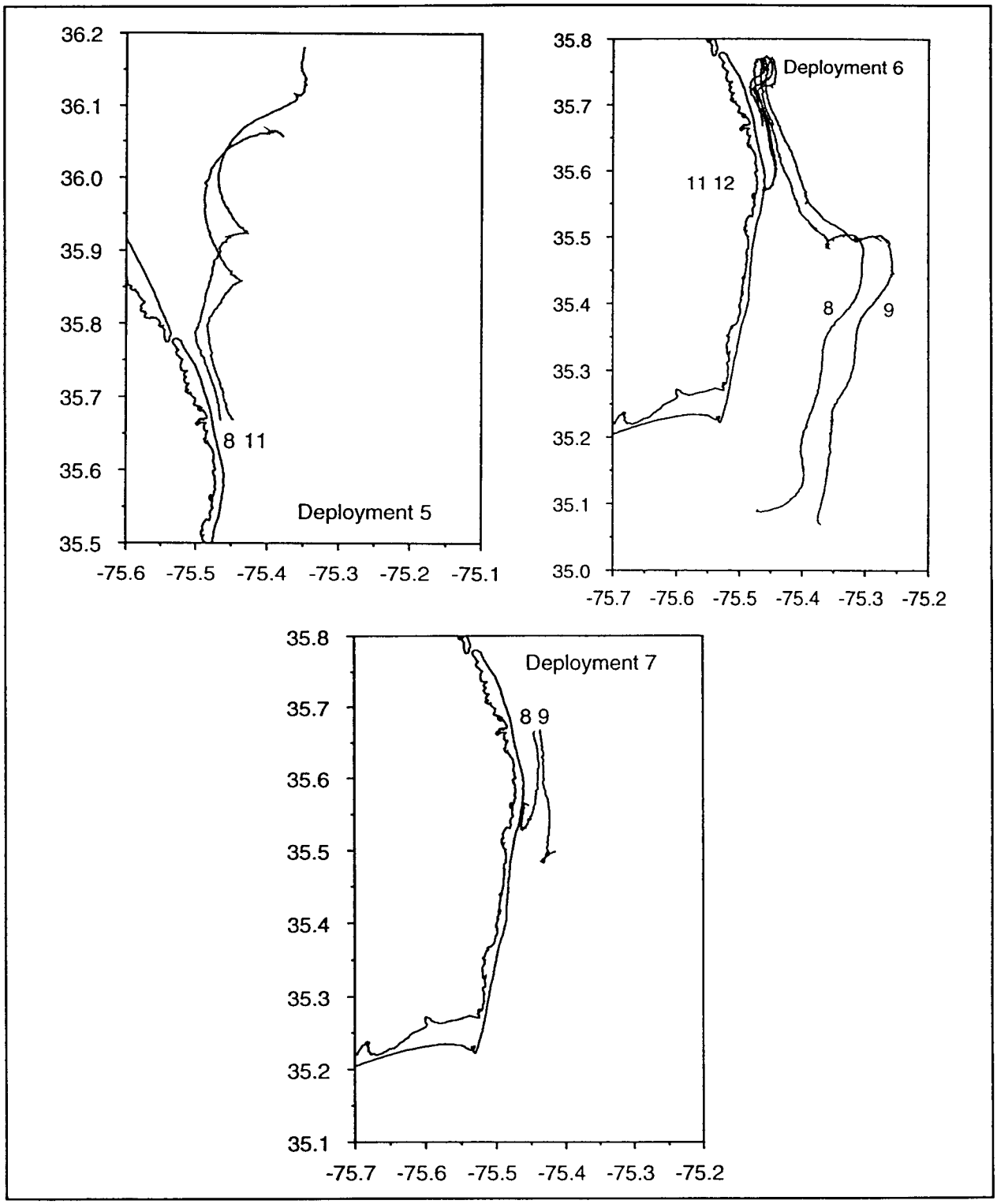

Figure 8.3-2. Drifter tracks of the second nearshore experiment - September 1993.

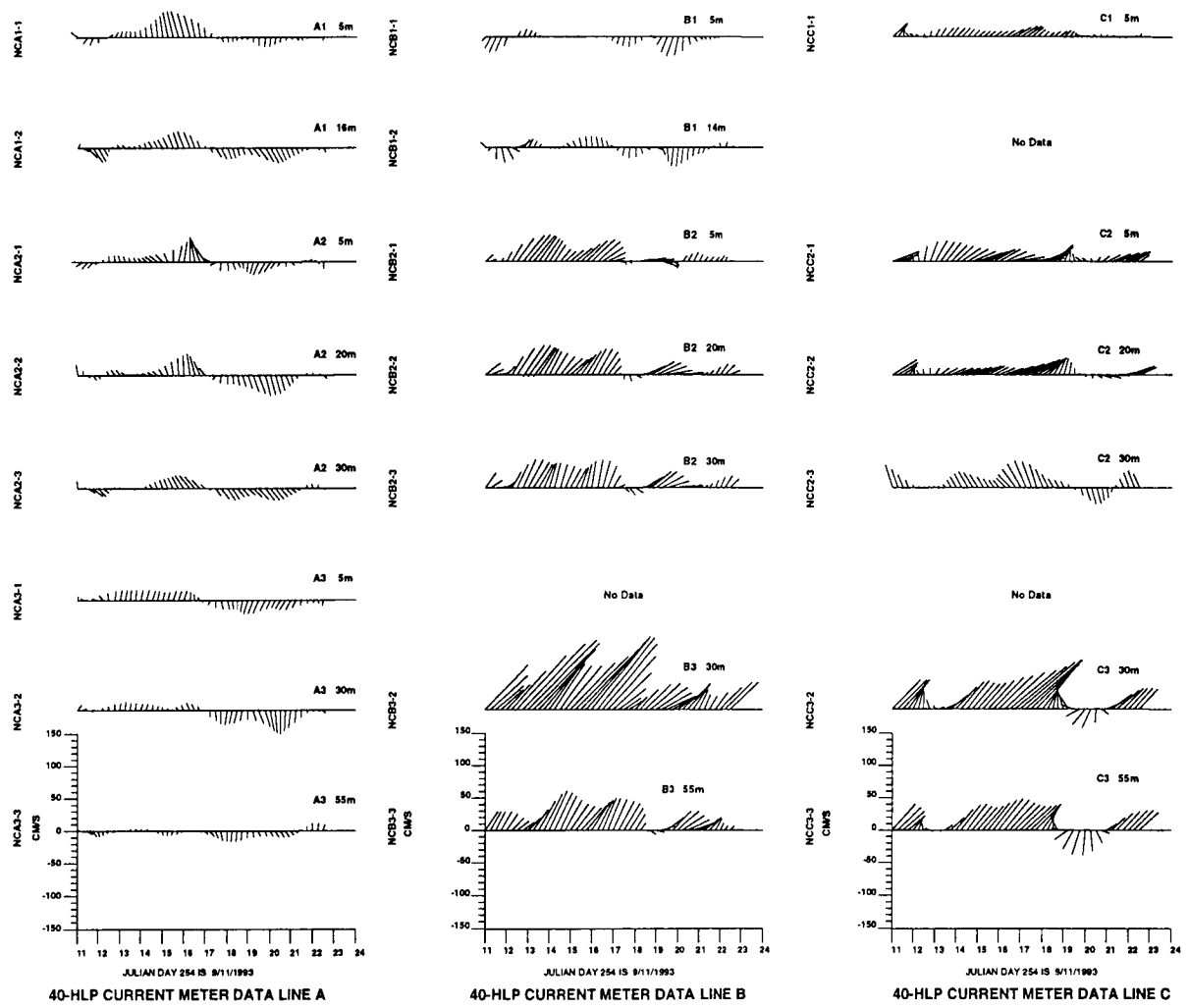

Figure 8.3-3. Current-meter data from September 11-24, 1993 (a) Line A, (b) Line B, and (c) Line C.

B1 (14 m) was stronger northward. This result is consistent with a zone of low salinity water farther to the north and trapped against the coast which would cause an alongshore pressure gradient force southward and counteract the wind stress.

A surface lens with salinities less than 31 psu was present on the CTD line about 22 km north of the buoy deployment line (Figure 8.3-4). This section was 5 km north of Oregon Inlet. Lowest salinities were confined to a region from the coast to 4 km offshore and about 5 m deep. A strong salinity gradient of 4 psu/5 m was present at the base of this portion of the lens which was further defined by two sharp salinity fronts, one at the coast and the other at 4 km offshore. Beyond the offshore front, the lens deepened to about 12 m with salinities greater than 29 psu and vertical salinity gradients significantly smaller (1.5 psu/10 m).

This coastal "lens" ranged over salinities 29-33 psu with relatively little change in temperature (Figure 8.3-4). It overlay water with salinities between 33 and 34.4 psu and a temperature range between 17.5° and 25°C. This deeper water mass was upwelled beneath the lens (Figure 8.3-4).

A section was done the following day at the buoy deployment line and extended out to a distance of 8 km from shore. The 22.5 σ_t isopycnal indicated upwelling there as well (Figure 8.3-5). A shallow lens (~5 m deep) with salinity less than 34 psu extended from the coast out to 8 km. The 34-psu isohaline broke the surface about 3 km offshore. Except for the narrow low salinity band from 0 - 4 km offshore present just north of Oregon Inlet, the scale of the lens here was quite similar to that farther north (Figure 8.3-4) and about 2 psu higher. The vertical salinity gradient below the lens was about 1.25 psu/7 m (about the same as the gradient just north of Oregon Inlet).

September 17-19, 1993 (Drifter Deployment 6)

The brief relaxation of wind during this period was accompanied by a reversal to southward currents at A1, A2 and B1. Currents at B2 stalled out and reversal was barely discernable. Currents south of Cape Hatteras (C1 and C2) continued northward. There was a brief episode of northward flow at A1, B1 and B2 as upwelling favorable winds resumed, but currents at A2 continued southward. The onset of downwelling favorable winds on September 19 was accompanied by southward flow at A1, A2, and B1 (but not at B2). As will be seen

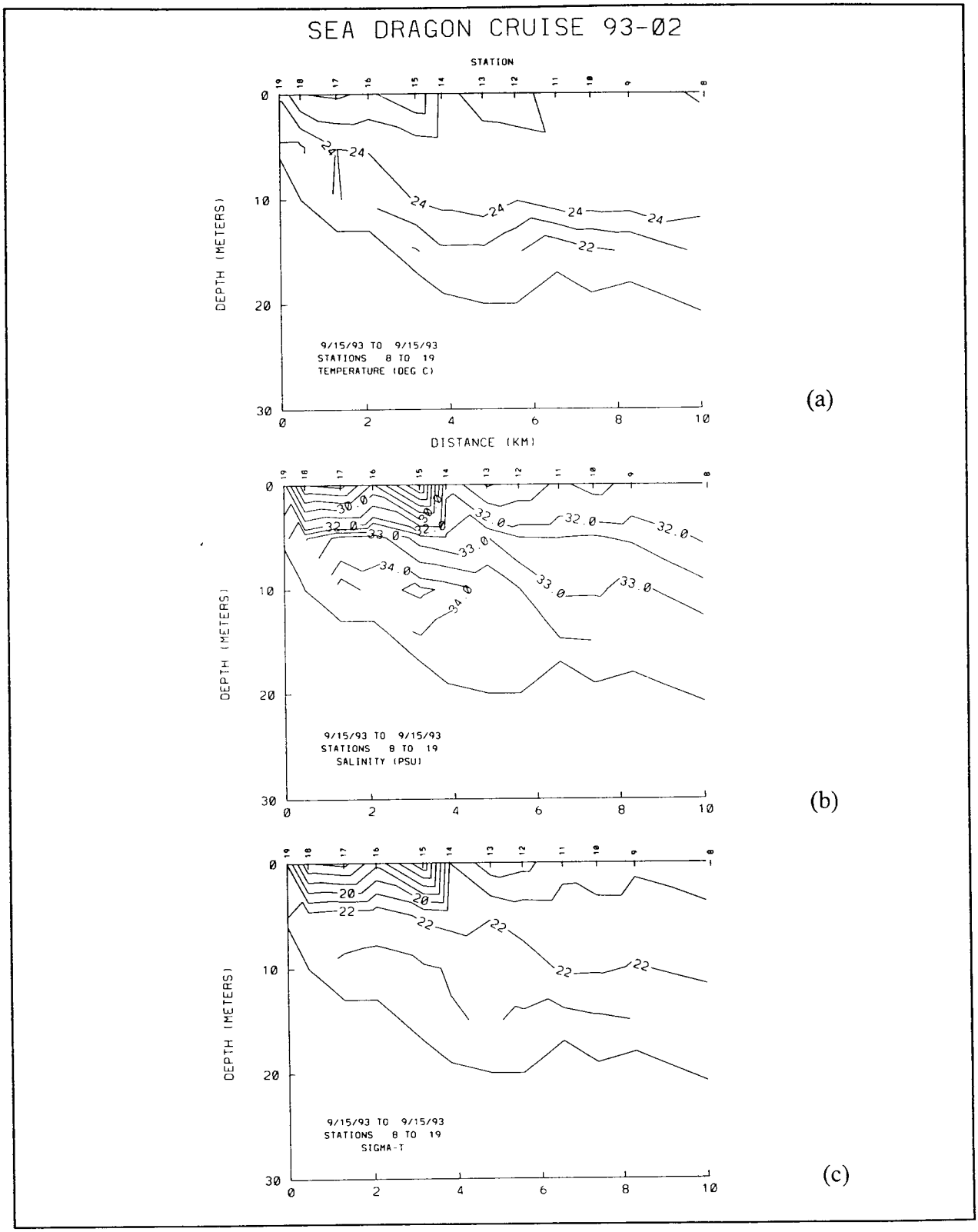

Figure 8.3-4. Cross-shelf sections of (a) temperature, (b) salinity, and (c) σ_t taken during cruise SD9302 on September 15, 1993.

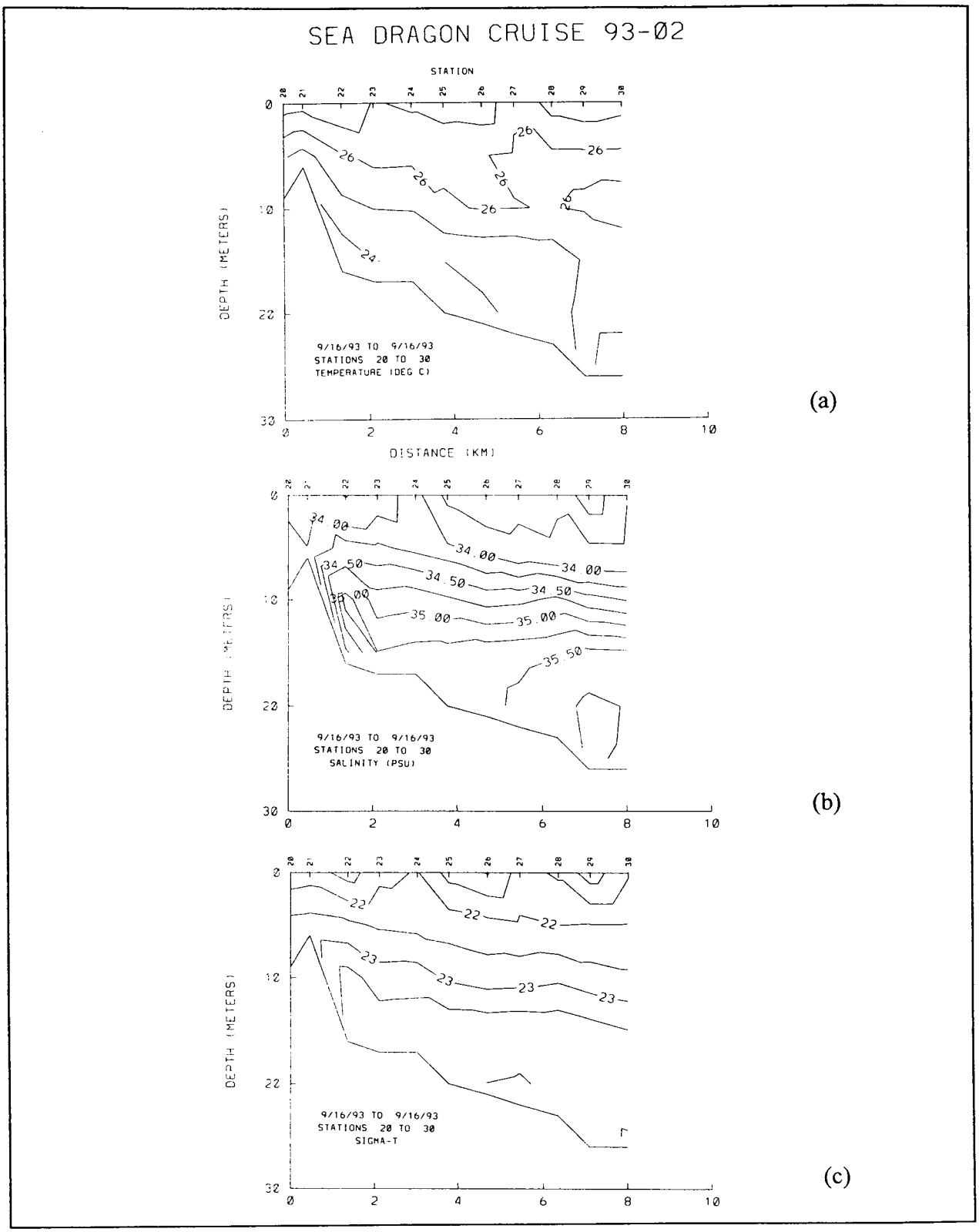

Figure 8.3-5. Cross-shelf sections of (a) temperature, (b) salinity, and (c) σ_t taken during cruise SD9302 on September 16, 1993.

below, the brief interlude of southward currents did not significantly affect the hydrography on the inner shelf.

On 17 September, the 22.5 σ_t isopycnal 10 km south of Oregon Inlet (Figure 8.3-6) remained consistent with upwelling. The low-salinity lens along the deployment line was still present, but salinities at the surface were a little higher and the vertical salinity gradient had weakened.

Two CTD sections were done on 18 September, one 10 km south of Oregon Inlet and the other near the Line B. The 22.5 σ_t isopycnal had flattened within 6-8 km from the coast (Figures 8.3-7 and 8.3-8). A wedge of low-salinity water (<34 psu) appeared along the coast out to 12 km from shore on the section near Line B (Figure 8.3-7). This wedge with lower salinities (<33 psu) was apparently present farther north (Figure 8.3-8), but its offshore extent was beyond the section limit. On both sections, the 34 psu isohaline intersected the bottom about 4 km offshore at depths between 15 and 20 m.

September 19-21, 1993 (Drifter Deployment 7)

This was a period of strong downwelling favorable winds (Figure 8.3-1). Even though the winds returned from downwelling to upwelling favorable late on September 20, currents at A1, A2 and B1 remained southward throughout September 21 (Figure 8.3-3). Currents at B2 reversed to northward. Salinities abruptedly decreased at B1 (5 and 14 m) and B2 (5 m only) on September 19 and remained low through September 23.

Circulation remained downwelling favorable on the inner shelf as confirmed by the two CTD sections conducted on September 20 (deployment line) and on September 21 (the line 20 km farther south). The 22.0 σ_t isopycnal intersected the bottom about 4 km offshore at depths between 15 and 20 m (Figures 8.3-9 and 8.3-10). Salinities were less than 33 psu inside the 20 m isobath and within 8 km offshore. A sharp salinity front was found 10 km south of Oregon Inlet less than 3 km offshore, inside of which the water was stratified by lower salinity water. Similar conditions were found farther south (Figure 8.3-10) where salinities at the coast were only slightly higher but the offshore slope of the density field was lesser. This section, conducted one day later than the one farther north may have responded to the shift in winds from downwelling to upwelling favorable.

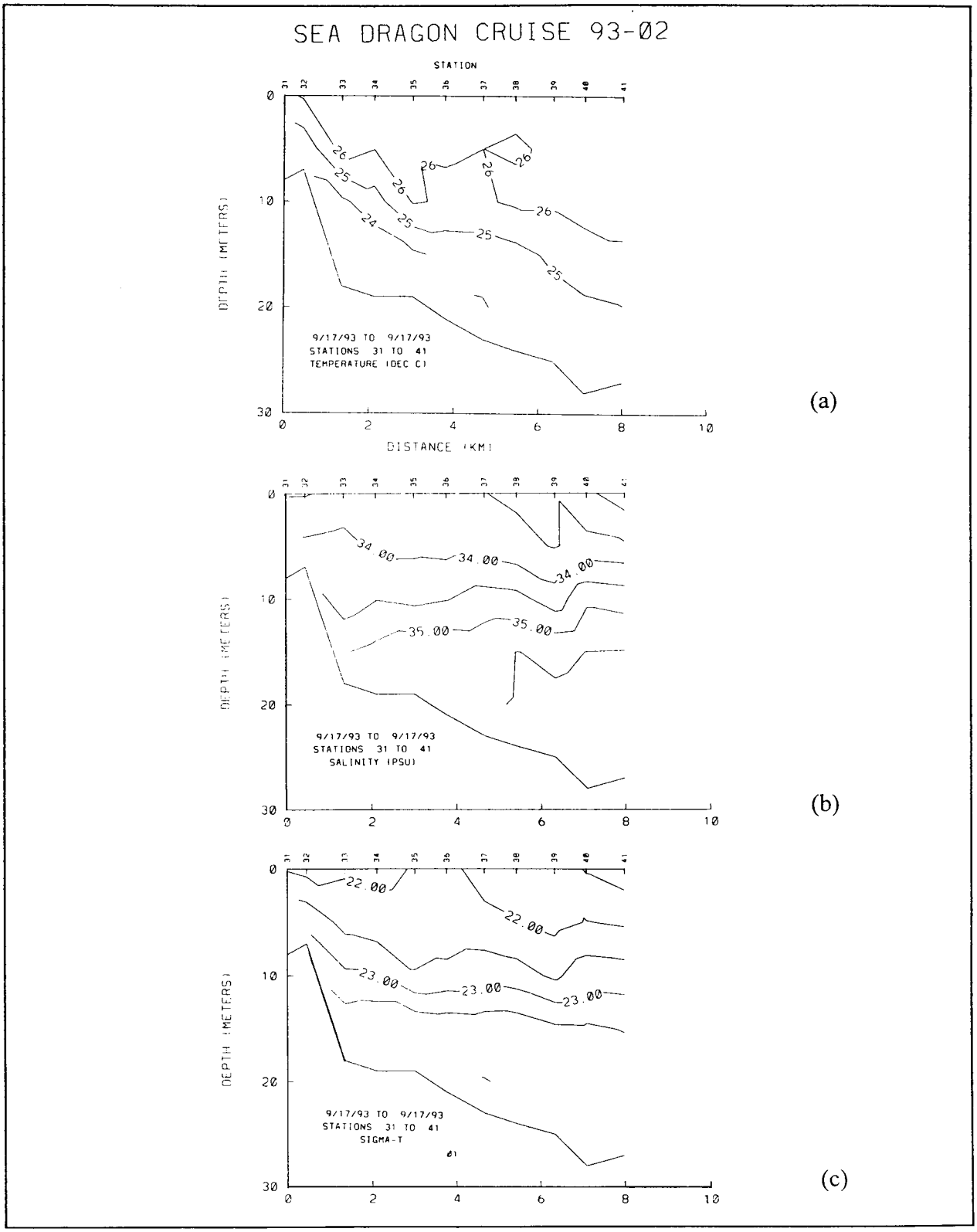

Figure 8.3-6. Cross-shelf sections of (a) temperature, (b) salinity, and (c) σ_t taken during cruise SD9302 on September 17, 1993.

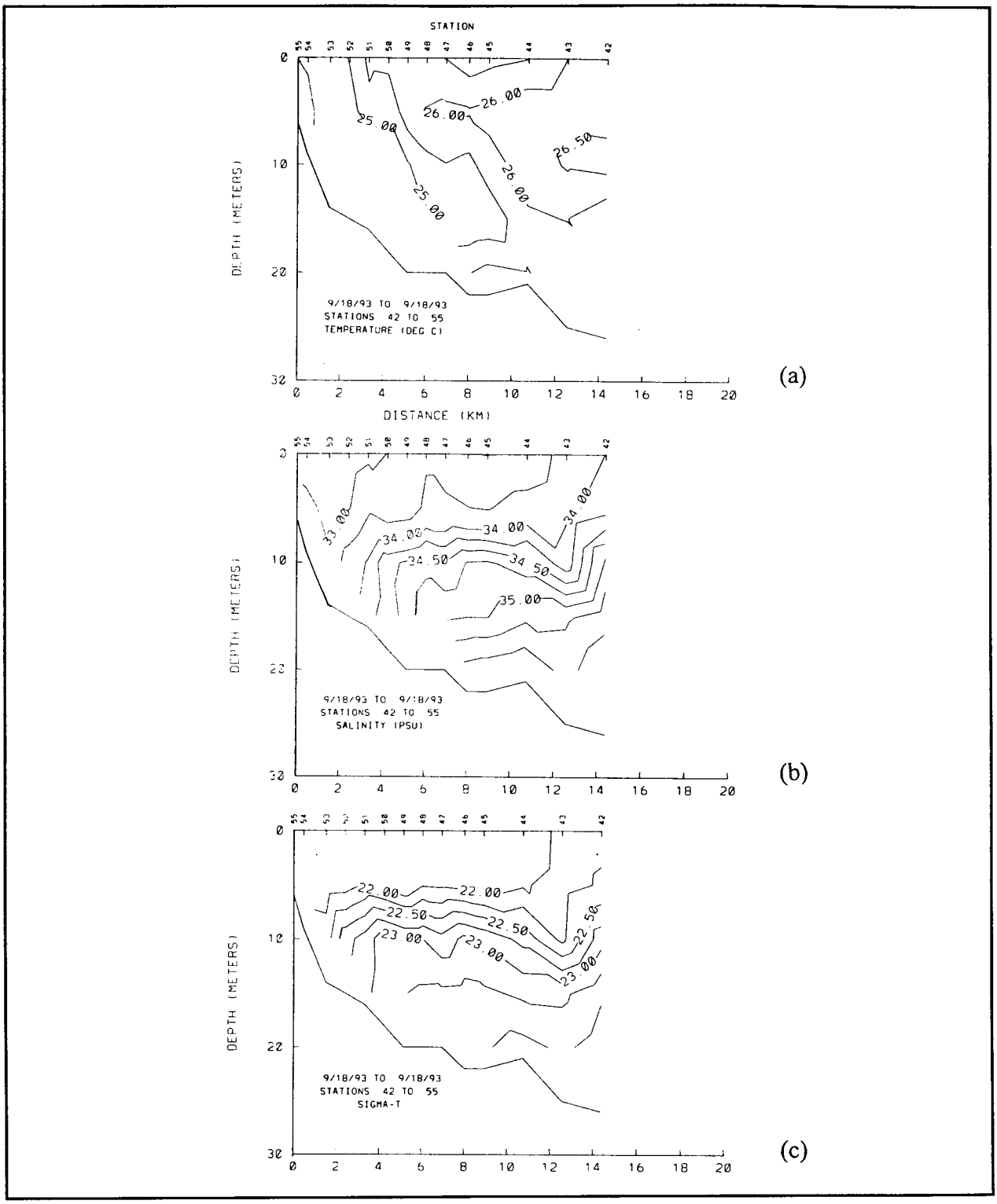

Figure 8.3-7. Cross-shelf sections of (a) temperature, (b) salinity, and (c) σ_t taken 32.4 km south of Oregon Inlet during cruise SD9302 on September 18, 1993.

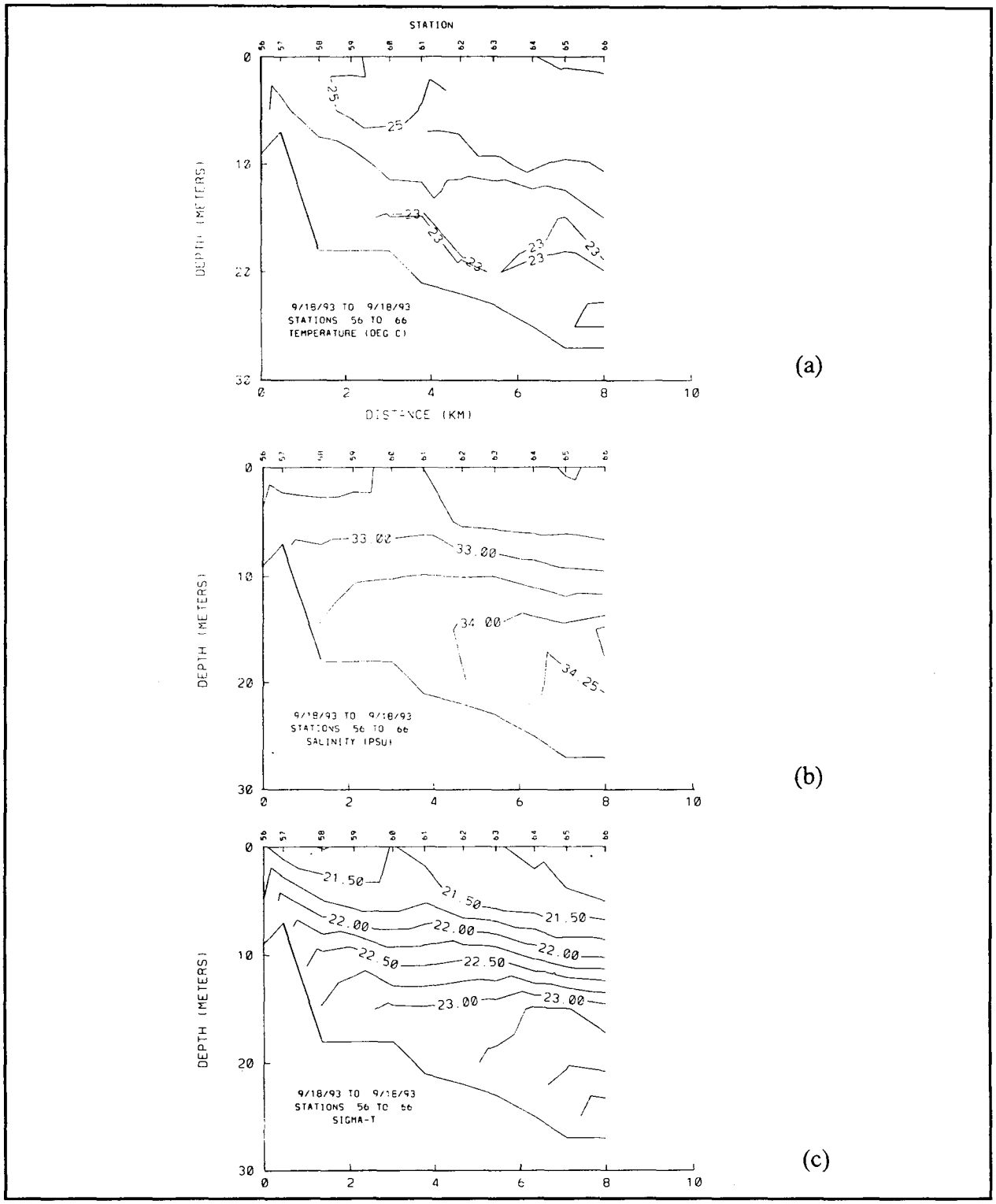

Figure 8.3-8. Cross-shelf sections of (a) temperature, (b) salinity, and (c) σ_t taken 12 km south of Oregon Inlet during cruise SD9302 on September 18, 1993.

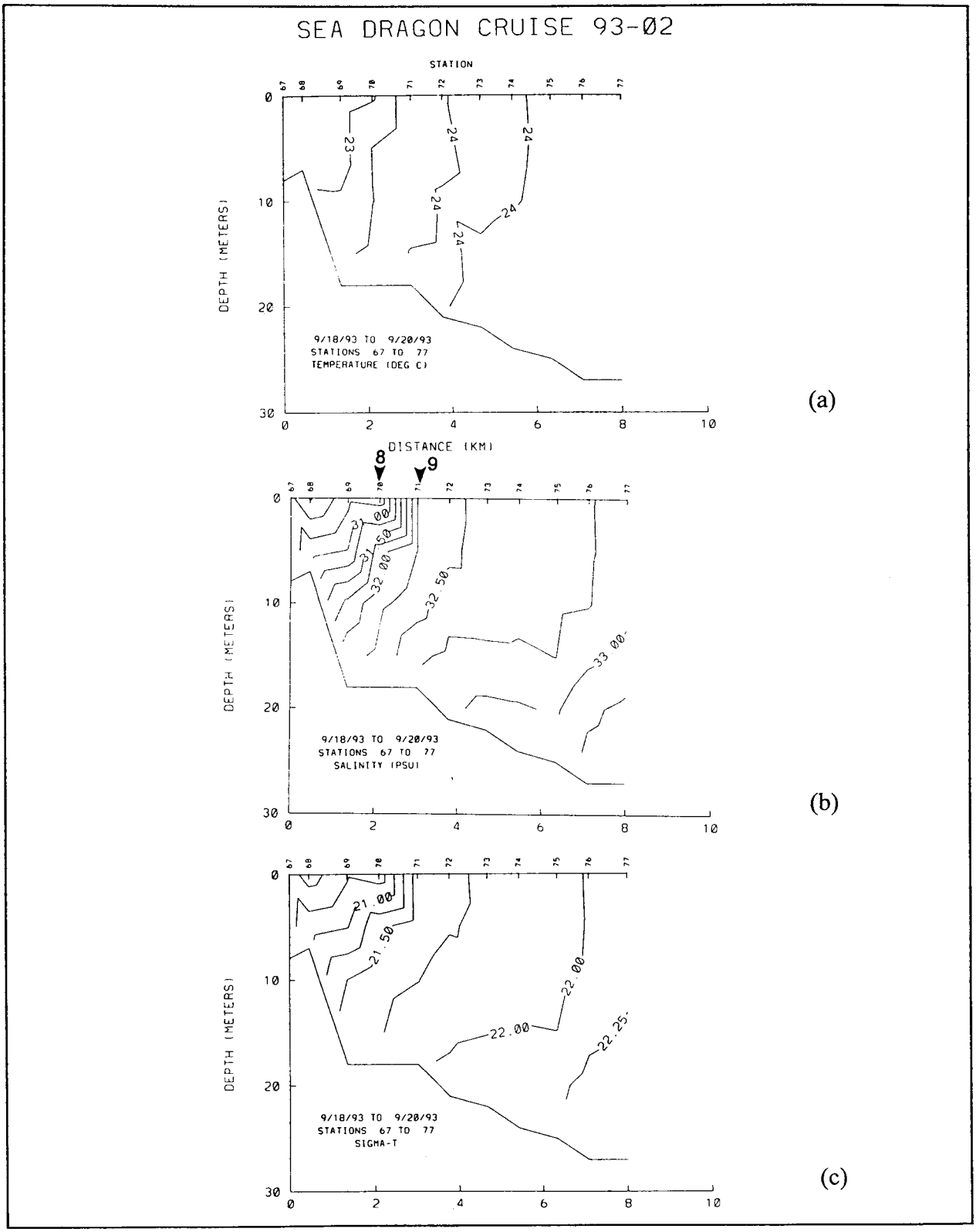

Figure 8.3-9. Cross-shelf sections of (a) temperature, (b) salinity, and (c) σ_t taken during cruise SD9302 on September 18-20, 1993. Arrows indicate drifter deployment site.

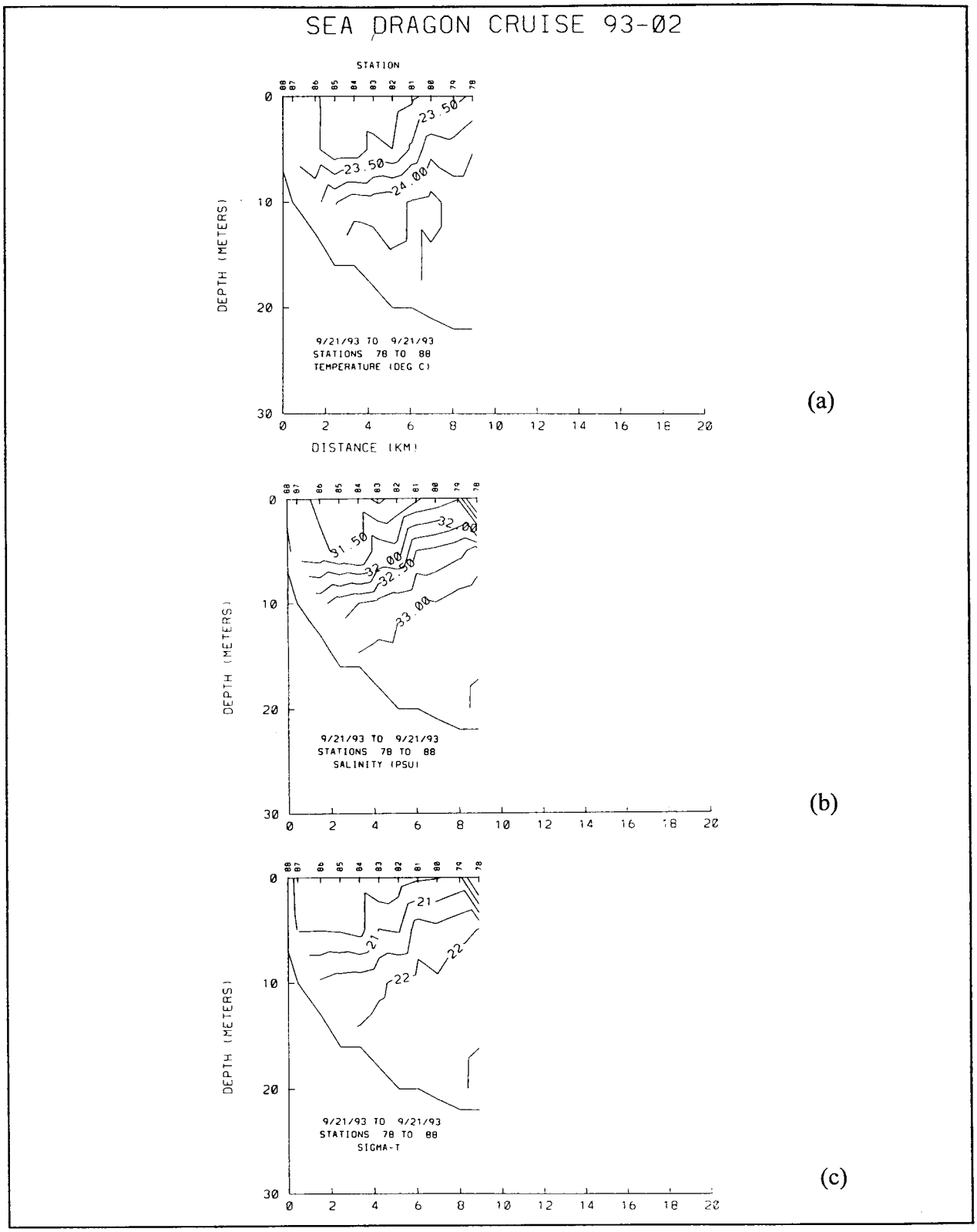

Figure 8.3-10. Cross-shelf sections of (a) temperature, (b) salinity, and (c) σ_t taken during cruise SD9302 on September 21, 1993.

8.4 Onshore/Offshore Flow

Close examination of the measurements acquired during the nearshore experiments provides considerable insight into the character of coastal circulation in the study region. Considered below are what the data of the nearshore experiments reveal regarding the influence of surface winds, convergence in the region of coastal fronts, and conditions under which transport to the beach may be expected.

The compilation of drifter tracks (Figures 8.2-2 and 8.3-2) reveals the variability of near-shore flow in the study region. Flow is seen in all directions, and both convergence and divergence is indicated. Some patterns are apparent, however. Northward drifter motion is usually accompanied by offshore (eastward) movement and divergence of drifters. All instances of drifter convergence and transport to the beach occur in conjunction with southward drifter movement. Drifter velocities (Figures 8.4-1 through 8.4-7) give evidence of strong and variable near-shore flow. North-south (roughly alongshore) velocity magnitude frequently exceeds 50 $cm \cdot s^{-1}$, while east-west velocity magnitude is often greater than 20 $cm \cdot s^{-1}$. Regular oscillations, with amplitudes of up to 10 $cm \cdot s^{-1}$, appear in many of the velocity records. They are typically strongest in the cross-shore direction. Their range of periods: 6-15 hours, falls shy of the local inertial period of 21 hours. These are most likely a manifestation of tidal motions, which tend to be polarized in the across-isobath direction over the inner shelf (Pietrafesa *et al.* 1985; Clarke 1991).

8.4.1 Relation of Near-Surface Currents and Winds

It is often useful to examine measurements of nearshore currents and winds in the context of the predicted oceanic response to winds for the simplified situation of a straight coast with no lateral buoyancy inputs. For such conditions, it is easily shown that the alongshore wind component should be much more effective in driving near-shore currents than the across-shore wind component (see Csanady 1982). Theoretical predictions also show that the alongshore flow of the idealized regime should be accelerated in the direction of the alongshore wind while the near-surface cross-shore flow should be to the right of the alongshore wind. Comparing winds measured at Duck with nearsurface currents measured at mooring B1 during the times of the near-shore experiments (Figures 8.4-8 and 8.4-9) shows a response conforming with this

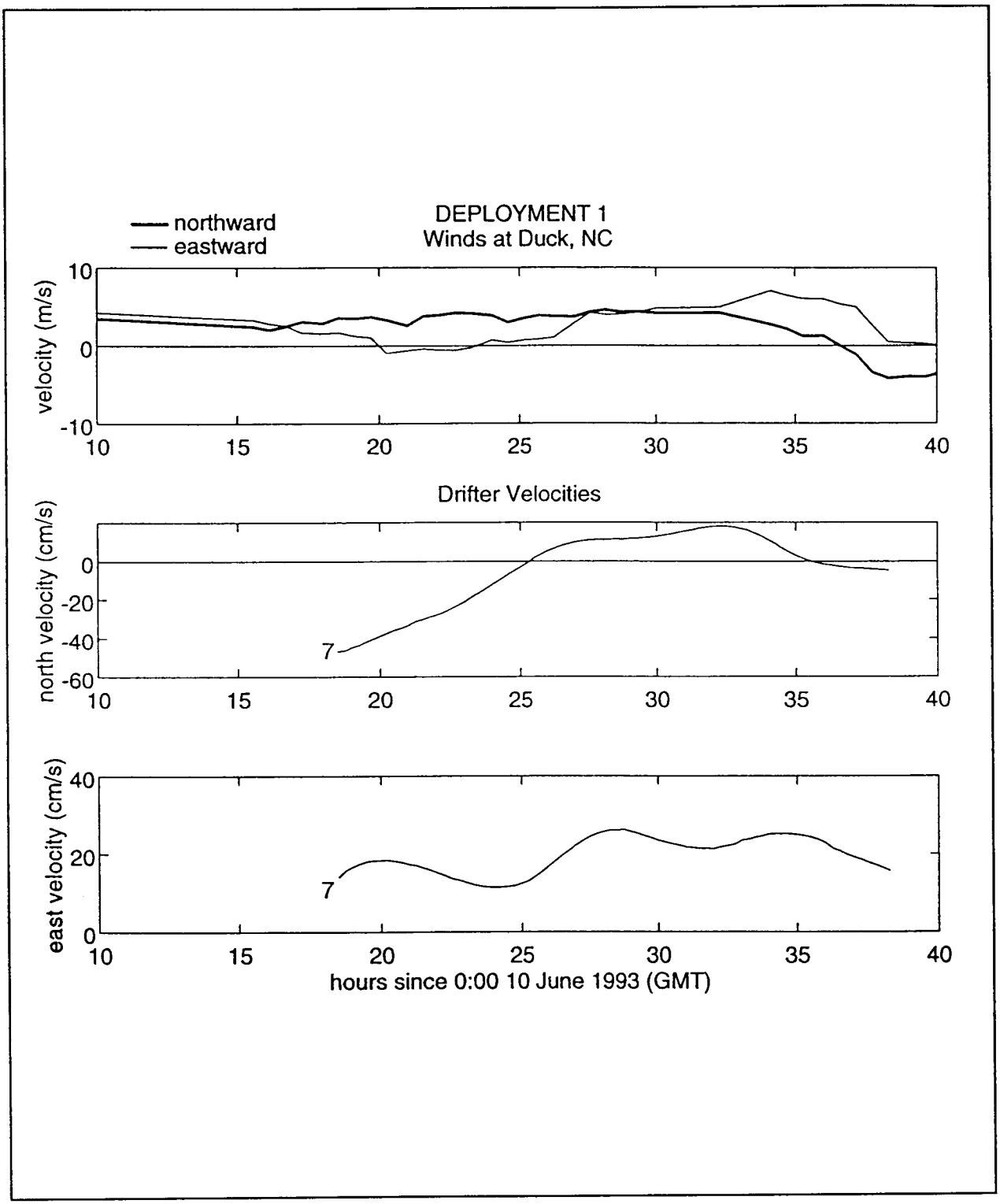

Figure 8.4-1. Northward and eastward velocity components of winds measured at Duck, NC (top panel), and northward (middle panel) and eastward (bottom panel) components of drifter velocities of deployment 1.

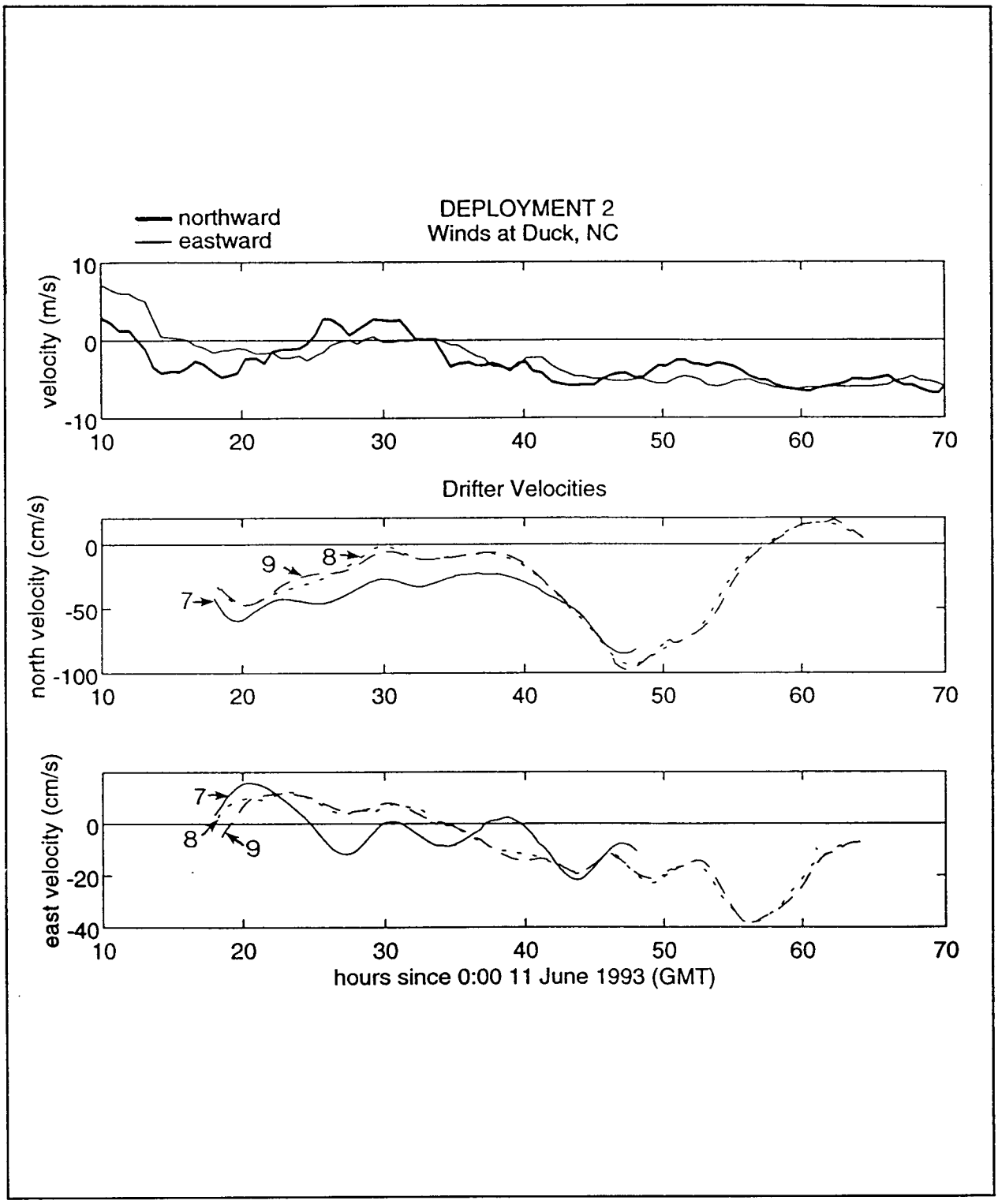

Figure 8.4-2. Same as Figure 8.4-1, except showing wind and drifter velocities of deployment 2.

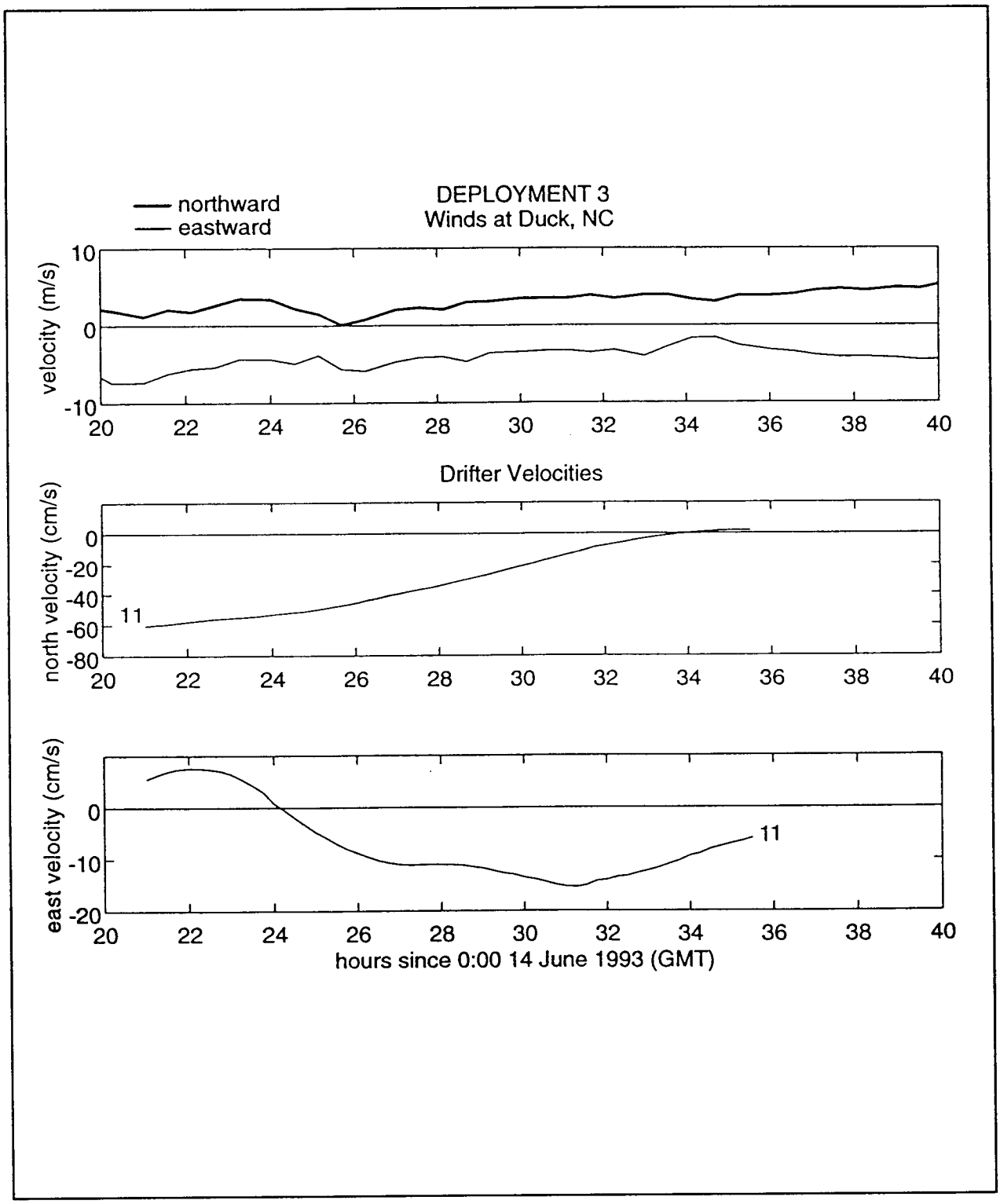

Figure 8.4-3. Same as Figure 8.4-1, except showing wind and drifter velocities of deployment 3.

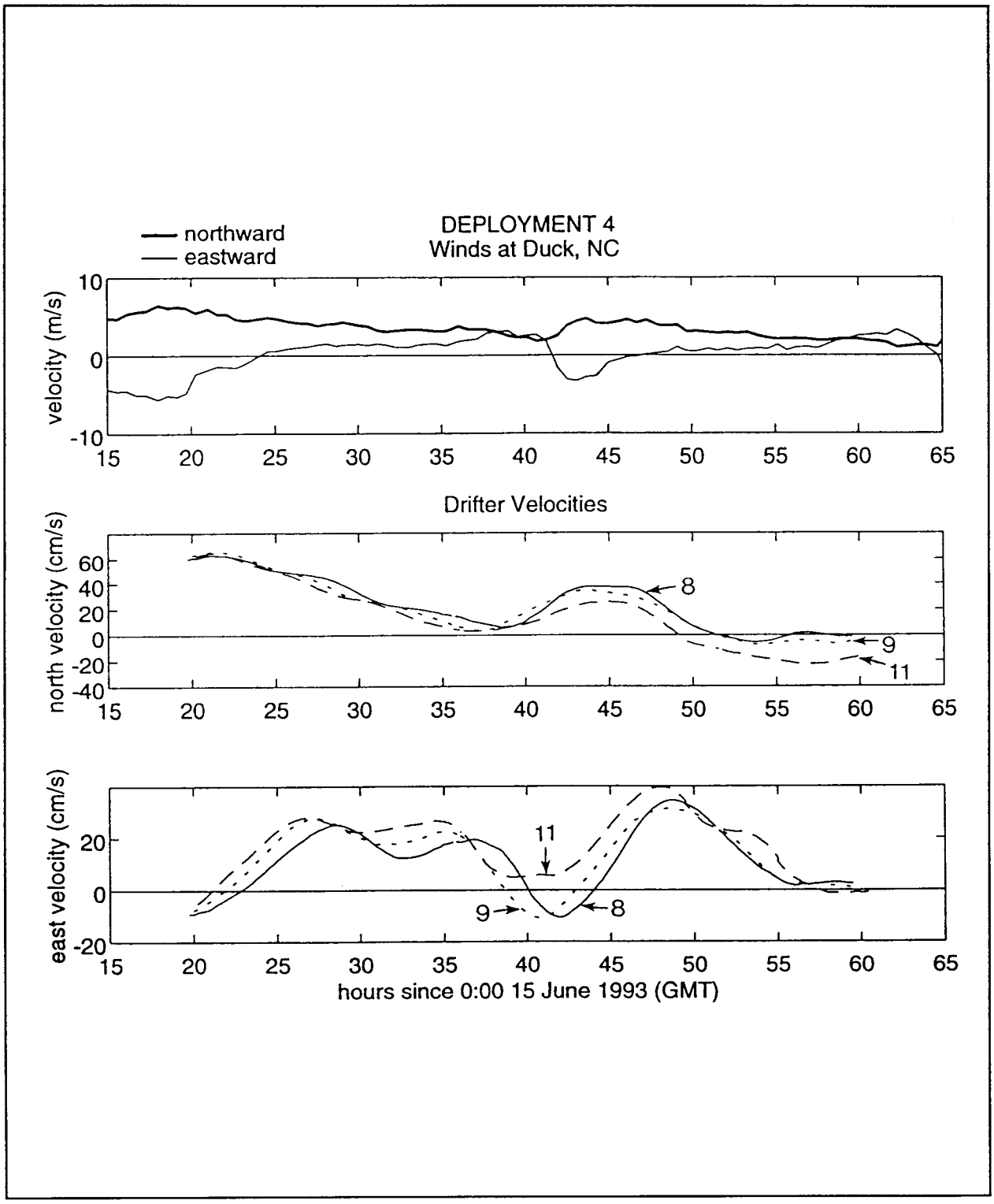

Figure 8.4-4. Same as Figure 8.4-1, except showing wind and drifter velocities of deployment 4.

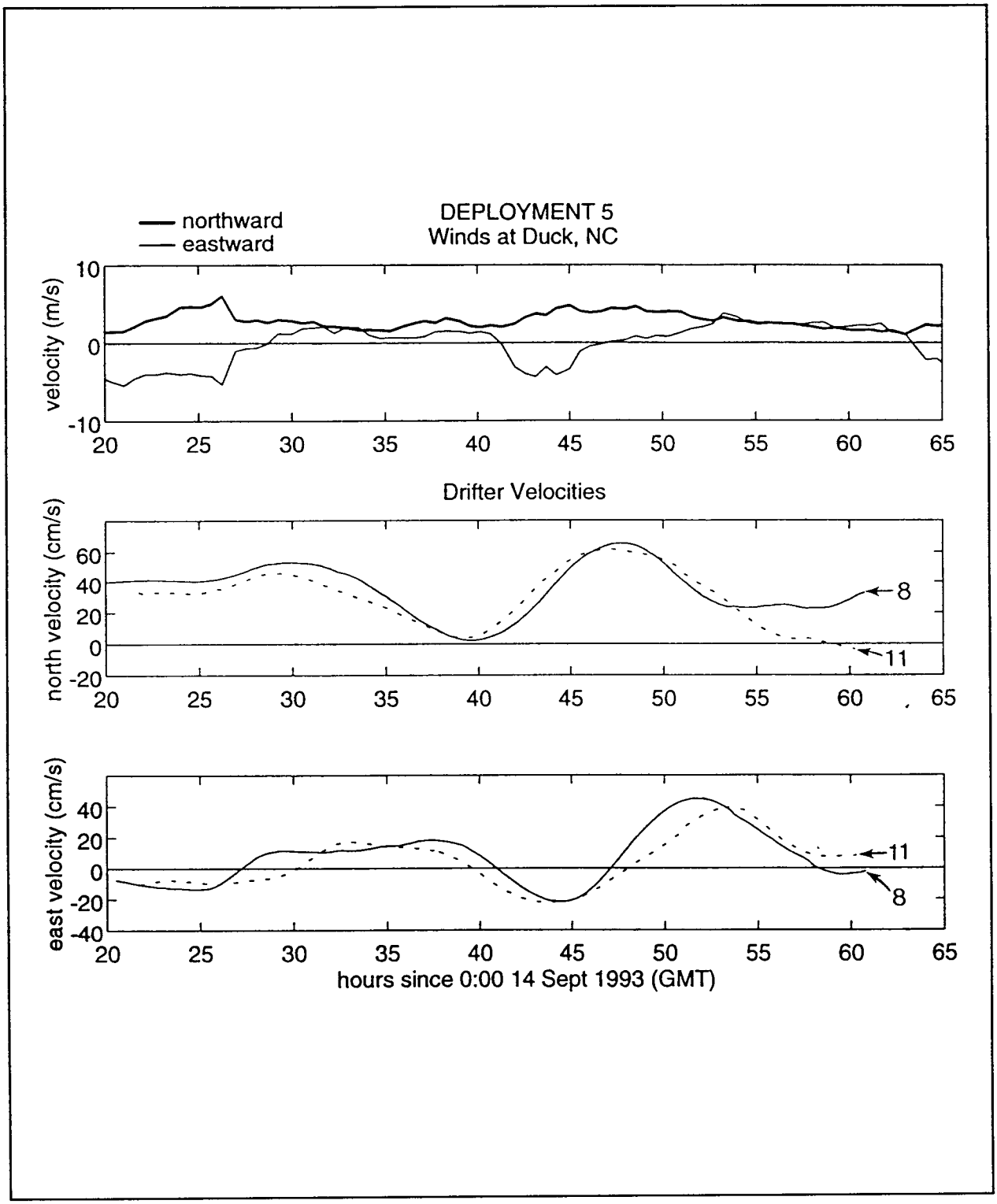

Figure 8.4-5. Same as Figure 8.4-1, except showing wind and drifter velocities of deployment 5.

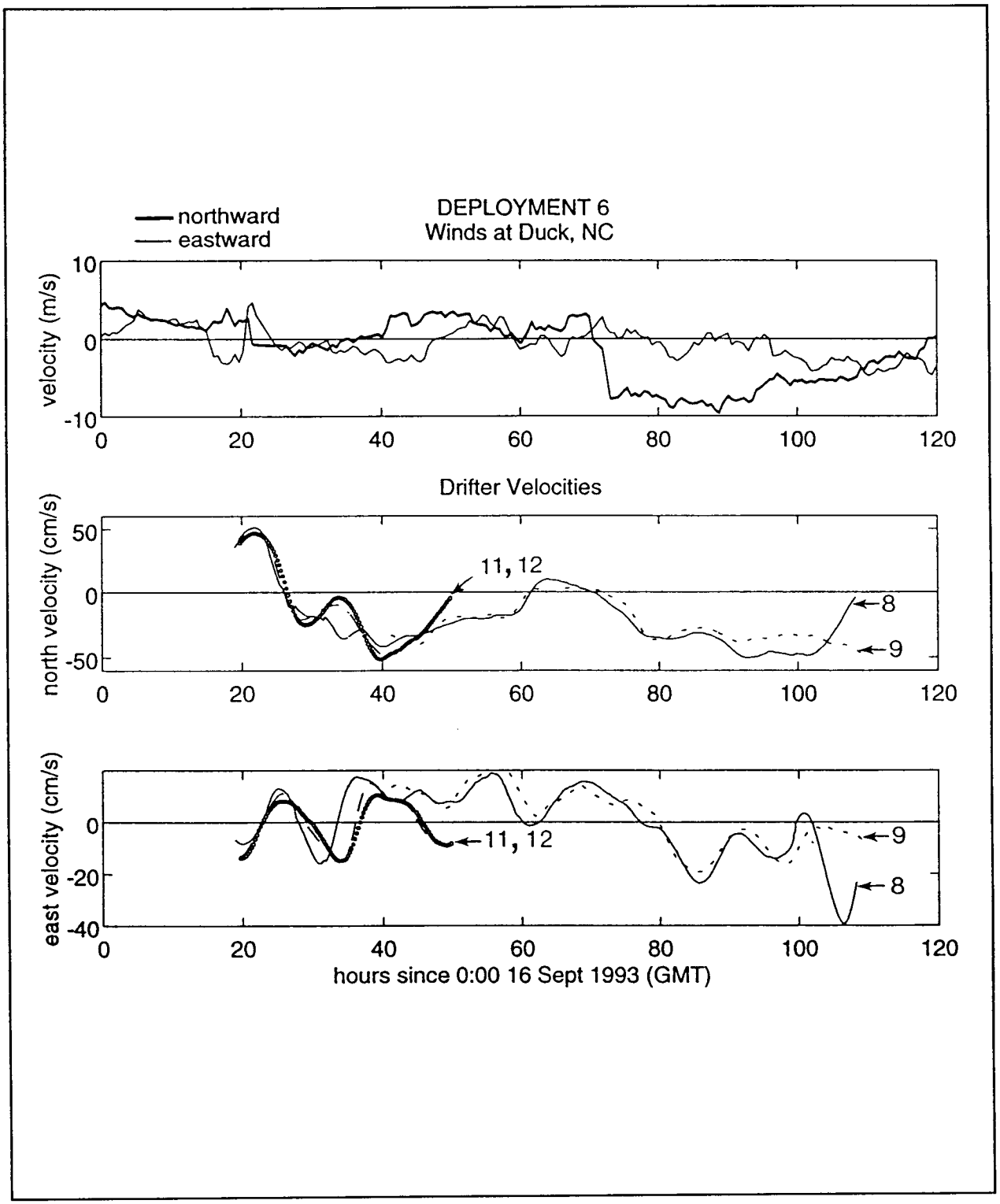

Figure 8.4-6. Same as Figure 8.4-1, except showing wind and drifter velocities of deployment 6.

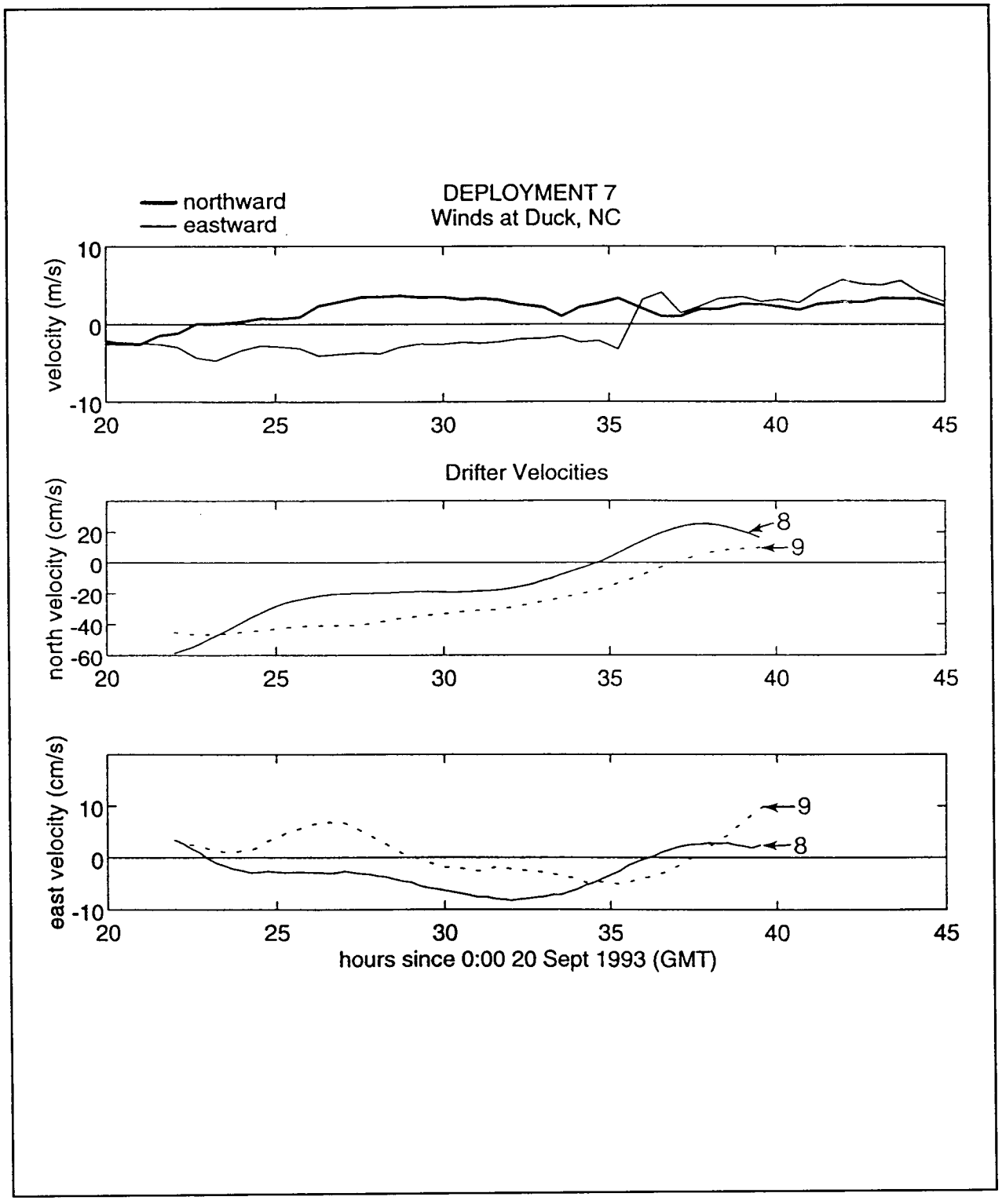

Figure 8.4-7. Same as Figure 8.4-1, except showing wind and drifter velocities of deployment 7.

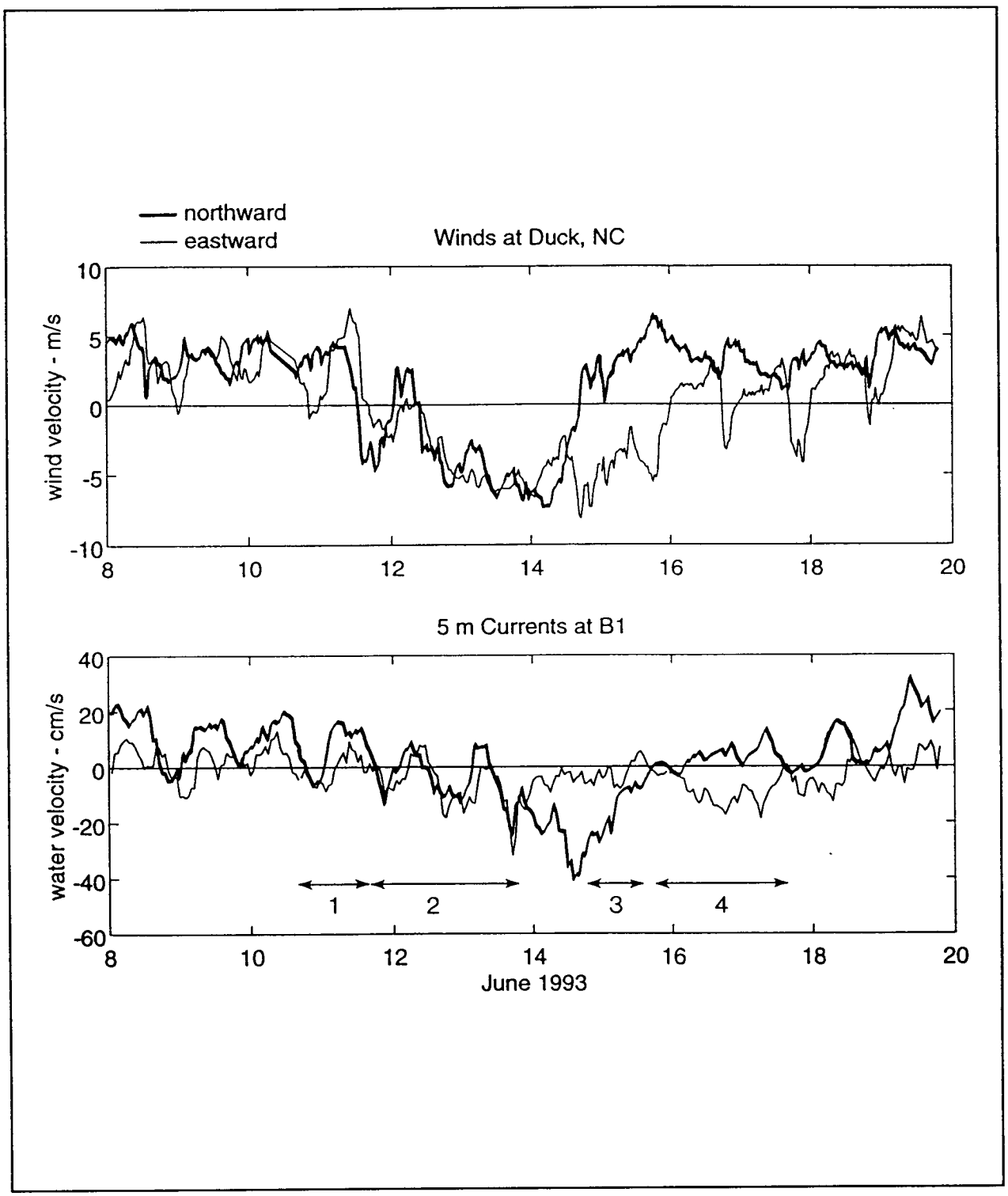

Figure 8.4-8. Northward and eastward velocity components of winds measured at Duck, NC (top panel), and currents measured 5 m beneath the surface at mooring B1 (bottom panel) during the first nearshore experiment. Times of drifter deployments 1-4 are indicated in the bottom panel.

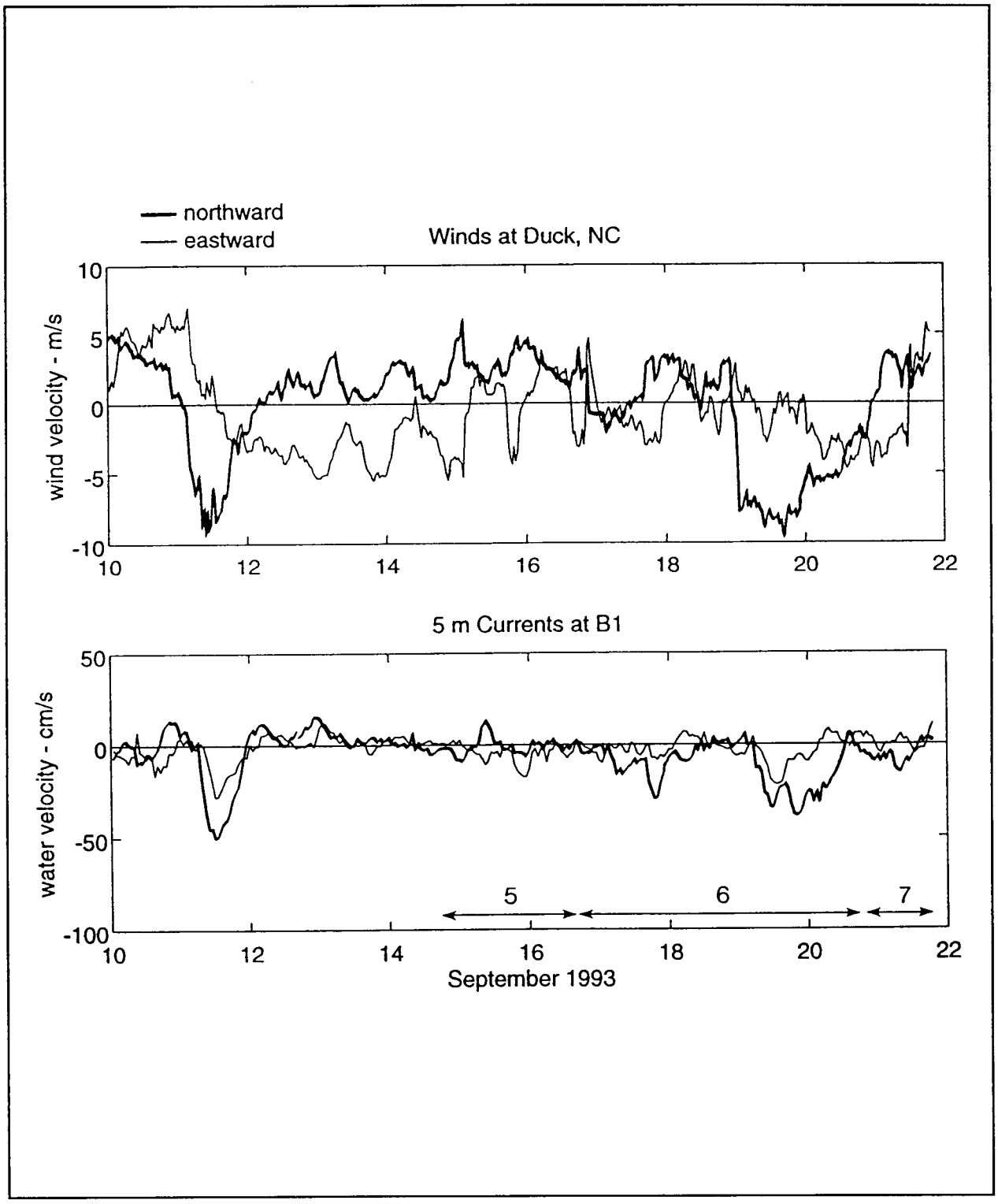

Figure 8.4-9. Same as Figure 8.4-8, except showing wind and current velocity during the second nearshore experiment. Times of drifter deployments 5-7 are indicated in the bottom panel.

theoretical "classical response" when winds are strong. For example, apparent in the Duck wind and B1 velocity records of mid-September 1993 (Figure 8.4-9) are two events of strong southward winds with coinciding strong southward and eastward currents. In agreement with the prediction that the alongshore wind should accelerate the alongshore current, the southward winds of these events lead the southward currents. An event of similar character is seen in the Duck wind and B1 velocity records of mid-June 1993 (Figure 8.4-8). However, details of the Duck winds and B1 velocities are often at odds with the classical response. Over the period June 16-18, for example, strong northward winds at Duck coincide with cross-shore flow directed westward, to the left of the alongshore wind, at the nearsurface B1 current meter (Figure 8.4-8). This on-and-off conformance with the classical response is reflected in the results of spectral analysis relating the Duck winds with the B1 near-surface currents (Figure 8.4-10). At subinertial frequencies, the coherence of north wind with east and north velocity at B1 exceeds the 80% significance level, but by very little. The phase relationships at these frequencies are in agreement with the classical response with the northward wind nearly in phase with the eastward velocity and slightly leading the northward velocity. Also conforming with the classical response are the relatively low subinertial coherences (below the 80% significance level) relating the cross-shore wind with B1 velocities.

Duck winds and velocities derived from the drifter tracks are generally in good agreement with the classical response, indicating that very near-surface and near-shore flow in the study region is strongly influenced by winds. In considering details of the drifter velocity to wind relationship below, the northward and eastward components of the drifter motion are taken as indicators alongshore and cross-shore flow, respectively. It should be realized that these components differ from the actual alongshore and cross-shore orientations. The difference is generally slight, but varies over the drifter track.

The closest match to the classical response is seen in the Duck wind and drifter velocity records of deployment 1 (Figure 8.4-1). Throughout most of this deployment, the cross-shore component of drifter velocity is to the right of the alongshore wind and the alongshore drifter velocity component increases in the direction of the alongshore wind (going from southward to northward with a northward wind). Steady increase of drifter velocity in the

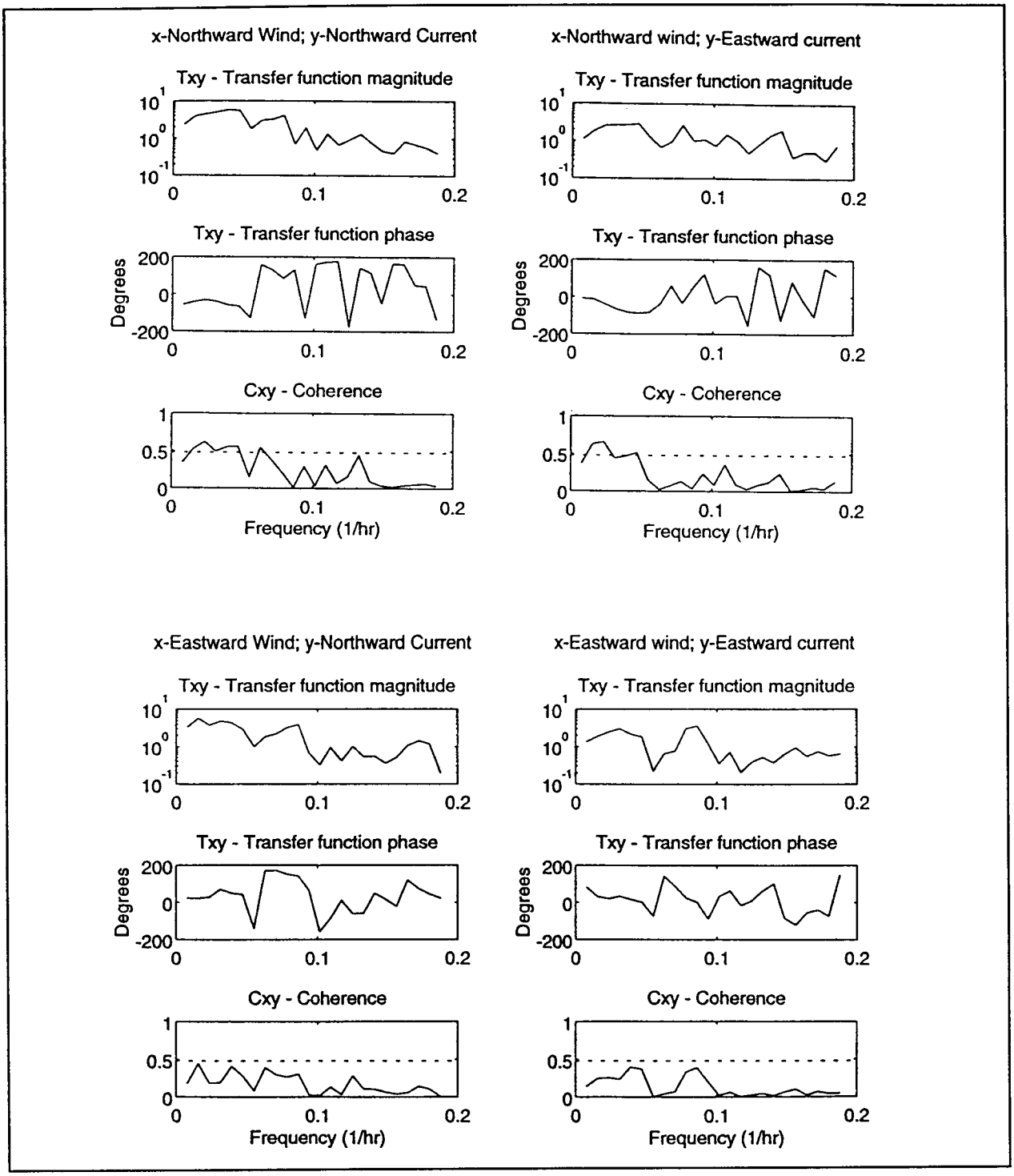

Figure 8.4-10. Results of spectral analysis relating the north and east wind velocity components measured at Duck, NC with the currents measured 5 m beneath the surface at mooring B1 during June 1993. The dashed lines in the coherence plots indicate the level at which the coherence significantly differs from zero at 95% confidence.

alongshore wind direction is also seen in the records of deployments 3 and 7 (Figures 8.4-3 and 8.4-7). However, cross-shore drifter motion of these deployments is often onshore and to the left of the alongshore wind. As discussed further below, this motion is most likely due to the strong onshore breeze apparent in the Duck wind records of these deployments. A clear "upwelling" response is evidenced by the records of deployments 4 and 5, with predominantly northward and offshore drifter motion coinciding with a northward wind (Figures 8.4-4 and 8.4-5). However, the alongshore drifter motion of deployment 4 tends to increase in a direction opposite to that of the alongshore wind. The most dramatic departure from the classical wind response is seen in the first half of the records from deployment 6 which shows strong southward drifter velocities in the face of weak northward winds (Figure 8.4-6). Records from the latter half of this deployment are, however, in good agreement with the classical wind response.

8.4.2 Transport to the Beach

Conditions under which beaching of near surface material may be expected is evidenced by the records of deployments 3, 6 and 7. Drifter tracks of all these deployments (Figures 8.2-2 and 8.3-2) suggest that nearsurface material may be subject to onbeach transport within a narrow nearshore zone, 2-4 km wide, beyond which onshore motion is unlikely. This is most clearly illustrated by the drifter tracks of deployment 6. All of these tracks are initially northward and shift in an ampersand pattern to the south. At about 35°35'N, the two most onshore tracks, at 2 km from shore, bend sharply onshore and intersect the coast. The deployment's other two drifter paths, only 0.5 and 2 km further seaward, begin to move offshore at the same latitude. A similar divergence in cross-shore flow is evidenced by the drifter paths of deployment 3. These show two drifters moving rapidly to the beach immediately after being set out at 1.8 and 2.8 km offshore. By contrast, the third drifter of this deployment, released 3.7 km from shore, is seen to move southward and roughly parallel to the coast for nearly 20 km before turning abruptly onshore and traveling to the beach. The two drifter paths of deployment 7 offer the most bizarre example of cross-shore transport seen in the nearshore experiments. Beginning at 3 and 3.5 km from shore, these tracks initially extend southward and parallel to the coast. At about 10 km from the deployment line, they diverge with the more onshore track bending to the coast. This track shows the drifter moving to within 100 m of the

shore line and then turning northward and traveling 3.5 km along the coast. An abrupt turn to offshore is seen shortly before the drifter's recovery point.

Comparing drifter velocities with Duck wind records indicates that forcing by the alongshore wind played no role in the transport of drifters to the beach. In all instances, the movement of drifters to the shore was to the left of the alongshore wind (Figures 8.4-3, 8.4-6 and 8.4-8). Currents driven by the cross-shore wind are likely to have been important in carrying drifters to shore, as drifter transport to the beach always occurred during times of strong eastward winds. Surface wave-induced transport (Stokes drift and currents due to breaking waves) is another likely contributor to onbeach drifter movement. During all deployments with drifter transport to the beach, the scientific party observed large westward swells.

8.4.3 Convergence and Influence of Fronts

Drifter tracks during deployments 2 and 6 offer clear examples of drifter convergence (Figures 8.2-2 and 8.3-2). The convergence of deployment 2 was associated with the front separating Carolina sound water, issuing from Oregon Inlet, from shelf water. This front was clearly visible to the scientific party due to the color contrast between the brown sound water and the relatively clear, greenish shelf water. Of the three drifters set out during this deployment, the two released at the most seaward points (drifters 8 and 9) were observed to rapidly converge to the front and remain on the front throughout the first 24 hours of tracking. Based on the salinity distribution measured along the deployment line (Figure 8.2-4) these drifters appear to have been deployed on the shelf water side of the front. The track of drifter 7, which was deployed in the brown sound water, suggests that convergence to the front occurred only from the shelf water side. This drifter remained shoreward of drifters 8 and 9 over the first 20 km of its track.

The convergence seen in deployment 6 involved an at-sea collision of drifters. It also appears to have been in the region of a visible surface front. As noted above, the drifters of this deployment initially moved northward. Roughly 10 hours after deployment they turned to southward, alongshore drift. During this southward drift, the drifters were visually observed in a region roughly 2 km north of the deployment line. Two drifters were seen

within a few hundred meters of each other. One, drifter 12, was on the visible surface front separating sound and shelf water. The other, drifter 11, was 100-200 m on the shoreward side of the front. The GPS-determined locations of these drifters were within 500 m over the time of their southward drift and exactly coincided for a 2 hour period before the drifters beached. They were recovered with their float and sail support rigging entangled.

Although the observations presented above suggest that the drifters which beached during deployment 6 had converged on a nearshore front, the measurements of the other deployments with onbeach drifter transport indicate that a nearshore front may often form the outer boundary of the to-the-beach surface transport region. The salinity distribution measured along the deployment line early in deployment 3 (Figure 8.2-6) indicates that the two drifters of this deployment which traveled rapidly to the beach (drifters 8 and 9) were set out inside a coastal front. The third drifter (11), which proceeded alongshore for several kilometers, was released offshore of the front. A similar set of circumstances is indicated by the deployment line salinity distribution and drifter release locations of deployment 6 (Figure 8.3-9). The nearly-beached drifter of this deployment (drifter 8) was set out inside a nearshore front. Its partner (drifter 9), which remained well offshore, was released seaward of the front.

IX. SUMMARY AND CONCLUSIONS

The dominant oceanographic feature of the study region (see Figure 1.2-2) is the Gulf Stream and its associated meanders and frontal eddies; while Slope Sea influences appear to be limited in the study area. Gulf Stream rings also appear to have little affect on regional circulation patterns except indirectly during interactions near Cape Hatteras between cold core rings and the Gulf Stream. Warm core rings were not observed during the study and are thought to be rare in the region. Cold core ring interactions were observed in April, June and December 1992 but not through at least August 1993. Cold core ring interactions reduced Gulf Stream currents to practically zero at the slope moorings: C4, during all three events; B4, in April and December and A5, only in December. There were few current reversals above 300 m at the three moorings; the strongest reversal was at B4 during the December cold core ring interaction.

The Gulf Stream path has its least variability, after leaving the confines of the Straits of Florida, in the area just southeast of Cape Hatteras. The Gulf Stream was apparently in a 'small meander' mode upstream from Cape Hatteras during most of the study period except possibly during March and June 1992. During 1992 the Gulf Stream was relatively closer to the shelf, straighter and with stronger currents than in 1993. No seasonal patterns in the Gulf Stream path were discernible but there were clear one- to four-month trends and a possible 10 km annual shift in position. The current records at deep water moorings C4, B4, and A5 (means at 100 m ≈110-125 $cm \cdot s^{-1}$ to the northeast) and C3 and B3 on the shelf edge all suggest that these moorings were in or near the edge of the Gulf Stream most of the time. In contrast, mooring A4 was in the Slope Sea all the time with weak mean (3-5 $cm \cdot s^{-1}$) currents directed to the south and southeast.

Gulf Stream currents were observable on the shelf consistently at moorings C3 and B3. Currents at these two moorings were highly coherent with currents at C4 and B4 offshore. Even during the March 1993 storm when flows on the shelf were generally southward, flow at C3 and B3 was coherent with the Gulf Stream. During Hurricane Emily in August 1993 the current at B3 reversed briefly while C3 had low or no current but no reversal.

Gulf Stream water was identifiable at mooring A3, the northernmost shelf edge mooring, about 10% of the time (12 incidents during the

first 18 months), but no comparable velocity signal was detected. These incidents varied in duration from less than a day (2 incidents) to more than five days (5 incidents). Four of the incidents penetrated to mooring A2 at mid-shelf.

While the study was not designed to provide details on the south-southwestward flowing DWBC which crosses under the Gulf Stream, data from the deep water moorings were analyzed to detect this current. The DWBC was detectable at levels below 800 m on moorings A4, B4 and C4; but at A5 the currents above 1900 m were more consistent with flow of the Slope Sea gyre curving eastward to flow along the Gulf Stream. Typical speeds were 20-30 $cm \cdot s^{-1}$ with peaks of 40-60 $cm \cdot s^{-1}$ due to TRWs superimposed on the mean flow. Variability in the deep levels was due to TRWs and coupling between upper and lower level eddies. Coupling of upper level Gulf Stream meanders with lower level eddies was most prevalent at C4 and B4. There was evidence at these moorings of growing and decaying baroclinic instabilities.

Meteorology of the region is characterized by relatively weak, northeastward winds, approximately parallel to the coast in summer and strong south-southwestward flow in winter with the synoptic wind period of 2.5 to 12 days overlapping the energetic Gulf Stream meander period of 3 to 10 days. The winter patterns are punctuated by complex cyclogenesis and cold air outbreaks which can result in severe storms with heavy snowfall along the East Coast. The summer patterns are occasionally punctuated by tropical cyclones and hurricanes. During the study period there were three major meteorological events which had varying, but generally short-lived, effects on regional circulation. A major winter storm occurred in December 1992 that forced large southward flows over the whole width of the shelf to Diamond Shoals; another storm in March 1993 ("storm of the century") caused extensive snowfall in the northeast and heavy property damage in the northern part of the Outer Banks; while Hurricane Emily in late August 1993 passed near Cape Hatteras and caused damage to the southern portion of the Outer Banks primarily through storm surge in Pamlico Sound.

Wind forced currents on the shelf in winter present a classic Ekman response. Currents at all levels north of Diamond Shoals and at C1 and C2 surface were highly coherent with winds and sea level. Large wind-forced current fluctuations on the inner shelf north and south of Cape Hatteras had important contributions from pressure gradients caused by sea level differences around Cape Hatteras.

Currents at lower levels in Raleigh Bay were less coherent with the winds and more coherent with the Gulf Stream. Gulf Stream forcing on the shelf is almost absent in winter because of the insulating affect of a strong shelf break front and stratification and stronger wind forcing. During summer the wind stress and sea level fluctuations are about half the magnitude of those in winter. Winds in summer 1993 were weaker than in 1992. In the summers of 1992 and 1993 there was evidence that Gulf Stream fluctuations were observed as far as the coast in northern Raleigh Bay (Line C).

Hydrographic surveys provided information on the various circulation processes on the North Carolina continental shelf, through brief glimpses of processes caught in the midst of their evolution, and through tracer distributions which are the integral result of processes acting over a span of time. The Gulf Stream is a source of heat, salt, and momentum to the North Carolina continental shelf. It's warm, salty waters create marked contrasts in the temperature-salinity characteristics of the shelf region. Furthermore, the combination of strong forcing (with low-frequency variability) and strong water-mass contrasts creates a situation prone to large interannual swings in the structure and circulation of these shelf waters. Two years of survey data illustrate possible interannual variability resulting from changes in Gulf Stream position, spring runoff, and changes in wind.

The seasonal progression of stratification in the Middle Atlantic Bight, primarily through vernal warming, was observed; this process was augmented in 1993 by higher and earlier than normal buoyancy flux from Chesapeake Bay. Stratification decreased spatially from north to south, not in a smooth gradient, but rather as punctuated changes at two locations. The first location is the sharp transition occurring where the cold water in the lower layers of the Middle Atlantic Bight turn offshore, 40-70 km north of Cape Hatteras. The second location is the cross shelf front separating Middle Atlantic Bight and South Atlantic Bight waters which represents what was thought to be the "oceanographic barrier" of the offshore extension of Diamond Shoals. While this front generally crossed the shelf at an angle (southwest to northeast) in the vicinity of Diamond Shoals, occasionally it was distorted along the coast by intrusions of Middle Atlantic Bight water past Diamond Shoals into Raleigh Bay. These "Virginia Coastal Water" intrusions appeared to be driven by strong and relatively long-duration southwestward wind events and occurred during all seasons of the year. Cessation of the wind events was followed closely by retreat

of the front, and the advected Middle Atlantic Bight water, back to the normal position near Cape Hatteras. Stratification in Raleigh Bay is, in general, weak and may be driven by either temperature or salinity fluctuations. Gulf Stream intrusion events, augmented by wind-driven Ekman flow, can provide transient intervals of stratification as high-salinity water moves from offshore and penetrates shoreward along the bottom.

As spring transitions into summer, the cold band water over the outer shelf in the Middle Atlantic Bight narrows, and may even decrease in temperature, reflecting the cold temperatures of the source region in the Gulf of Maine and the amount of insulation and mixing during its southward travel. The transition from spring to summer did not occur until June in 1992 but in May in 1993. Wind patterns during both summers were similar.

With the fall season comes cooling and wind mixing, and the decrease of stratification. By winter, shelf stratification on both sides of Cape Hatteras is usually transient, with intrusion and extrusion events stratifying the water column over the outer shelf. Subsequently, winter storms can quickly destratify the shelf as was observed during and following the December 1992 and March 1993 storms, in particular.

The Slope Sea portion of the study area was found to be hydrographically complex with Middle Atlantic Bight shelf water, slope water and Gulf Stream water in varying proportions. Rotary motions, coherent to at least 300 m depth, dominate near surface Slope Sea currents in the study area. The strongest of these appear to be due to the circulating flow of discharged Gulf Stream water parcels. As observed further to the north, these motions do not extend onto the continental shelf. Slope water was detected at the shelf break only once, at A3 in August 1993.

Export of water from the Middle Atlantic Bight Shelf occurs in the region just north of Diamond Shoals, generally between moorings B3 and D2 when the Gulf Stream was away from the shelf but between D2 and D1 when the Gulf Stream was closer. This shifting region is where direct export to the Gulf Stream takes place. Some Middle Atlantic Bight water may also be exported to the Gulf Stream from Raleigh Bay after first intruding into Raleigh Bay over Diamond Shoals. Another path for shelf water export is along the northern boundary of Gulf Stream water extrusions in the southern end of the Slope Sea rather than along the Gulf Stream itself. Volume

transport off the shelf along the Gulf Stream north of Diamond Shoals is estimated to be about the same magnitude as the volume transport along the continental shelf north of Cape Hatteras. Raleigh Bay shelf water also appears to be exported by entrainment along the Gulf Stream front just south of Diamond Shoals. There often are converging shelf flows in the region of Diamond Shoals from the southward flowing Middle Atlantic Bight and northward flowing Raleigh Bay water.

A series of drogued drifter deployments tracked the progression of near surface layers from the shelf to the Gulf Stream. None of the drogued drifters released outside the nearshore region were recovered ashore in the Cape Hatteras region; while seven were found beached in England (1), France (3), the Canary Islands (1), and the Bahamas (2) 14 to 35 months after deployment. Estimates of residence time on the shelf ranged from less than eight to more than 27 days. In general the drifters deployed in Raleigh Bay had the shortest residence time.

Drifter tracks during the Near Shore Experiments revealed vigorous and highly variable coastal currents near the sea surface. Although these were clearly influenced by the wind to a large degree, comparison of the drifter velocities with the wind record from the Corps of Engineers facility at Duck, North Carolina showed occasional departures from a classical nearshore wind response. Other possible contributors to the drifter motion include buoyancy-driven and surface wave-induced currents. Buoyancy-driven cross-shore motion of the drifters appeared often to have been influenced by the near-shore front common to the study area. Drifter convergence to the front was observed in two drifter deployments. On two other occasions, the front appeared to have been the outer boundary of a zone of surface transport onto the beach, i.e. drifters deployed inside the front came ashore while those deployed outside the front did not. This transport is attributed to driving by the onshore wind component with likely assistance from surface wave-induced currents. On two occasions during these experiments when ARGOS tracked drifters were left in the water rather than being redeployed, they were eventually entrained along the Gulf Stream.

Analysis of data from this program confirmed many notions about the nature of the complex circulation of the Cape Hatteras region, including the dominant role of the Gulf Stream and its meanders on Raleigh Bay and the shelf break just north of Diamond Shoals.

Export of water from the Middle Atlantic Bight shelf occurs just north of Diamond Shoals in a band whose location can shift depending on the location of the Gulf Stream.

Occasional advection of Middle Atlantic Bight water past the "oceanographic barrier" at Diamond Shoals, so-called Virginia Coastal Water instrusions, was observed. Material released on the shelf outside a near shore frontal zone, approximately 2-4 km from the beach, appears likely to be eventually entrained along the Gulf Stream. Residence times for such material ranged from eight to 27 days with generally shorter residence times being observed in Raleigh Bay. Material advected southwestward past Cape Hatteras in "Virginia Coastal Water" intrusions is advected back to the Middle Atlantic Bight when the wind forcing relaxes. It seems unlikely that materials discharged into the ocean past the mid-shelf region would find their way onto the North Carolina beaches.

X. BIBLIOGRAPHY

Aikman, F. III. 1984. Pycnocline development and its consequences in the Middle Atlantic Bight. J. Geophys. Res. 89:685-694.

Atkinson, L.P., J.J. Singer, and L.J. Pietrafesa. 1980. Volume of summer subsurface intrusions into Onslow Bay, North Carolina. Deep-Sea Res. 27A:421-434.

Bane, J.M. and W.K. Dewar. 1988. Gulf Stream bimodality and variability downstream of the Charleston Bump. J. Geophys. Res. 93:6695-6710.

Bane, J.M., D.A. Brooks, and K.R. Lorenson. 1981. Synoptic observations of the three-dimensional structure and propagation of Gulf Stream Meanders along the Carolina continental margin. J. Geophys. Res. 86:6411-6425.

Battisti, D.S. and A.J. Clark. 1982. A simple method for estimating barotropic tidal currents on continental margins with specific application to the M_2 tide off the Atlantic and Pacific coasts of the United States. J. Phys. Oceanogr. 13:8-16.

Beardsley, R.C., W.C. Boicourt, and D.V. Hansen. 1976. Physical oceanography of the Middle Atlantic Bight. pp. 20-34. In: M.G. Gross, ed. Middle Atlantic Continental Shelf and the New York Bight Special Symposium, Volume 2. American Society of Limnology and Oceanography, Gloucester Point, VA.

Bisagni, J.J. 1983. Lagrangian current measurements within the eastern margin of a warm-core Gulf Stream ring. J. Phys. Oceanogr. 13:709-715.

Blanton, J.O., J.A. Amft, D.K. Lee, and A. Riordan. 1989. Wind Stress and Heat Fluxes Observed During Winter and Spring 1986. J. Geophys. Res. 94:10686-10698.

Boicourt, W.C. 1973. The circulation of water on the continental shelf from Chesapeake Bay to Cape Hatteras. Ph.D. Thesis. The John Hopkins University. 197 pp.

Boicourt, W.C. and P.W. Hacker. 1976. Circulation on the Atlantic continental shelf of the United States, Cape May to Cape Hatteras. Mem. Soc. Roy. Sci. Liege 10:187-200.

Boicourt, W.C., S.-Y. Chao, H.W. Ducklow, P.M. Gilbert, T.C. Malone, M.R. Roman, L.P. Sanford, J.A. Fuhrman, C. Garside, and R.W. Garvine. 1987. Physics and microbial ecology of a buoyant estuarine plume on the continental shelf. EOS, Trans. AGU. 68(31):666-668.

Bumpus, D.F. 1973. A description of the circulation on the continental shelf of the east coast of the United States. Progress in Oceanography. 6:111-157.

Bumpus, D.F. and E.L. Pierce. 1955. The hydrography and the distribution of chaetognaths over the continental shelf off North Carolina. Deep-Sea Res. Suppl. 3:92-109.

Chao, S.-Y. and L.J. Pietrafesa. 1980. The subtidal response of sea level to atmospheric forcing in the Carolina Capes. J. Phys. Oceanogr. 10:1246-1255.

Chao, S.-Y. and W.C. Boicourt. 1986. Onset of Estuarine Plumes. J. Phys. Oceanogr. 16:2137-2149.

Churchill, J.H. and P.C. Cornillon. 1991a. Water discharged from the Gulf Stream north of Cape Hatteras. J. Geophys. Res. 96:22227-22243.

Churchill, J.H. and P.C. Cornillon. 1991b. Gulf Stream water on the shelf and upper slope north of Cape Hatteras. Cont. Shelf Res. 11:409-431.

Churchill, J.H., P.C. Cornillon, and G.W. Milkowski. 1986. A cyclonic eddy and shelf-slope water exchange associated with a Gulf Stream warm-core ring. J. Geophys. Res. 91:9615-9623.

Churchill, J.H., P.C. Cornillon, and P.H. Hamilton. 1989. Velocity and hydrographic structure of subsurface shelf water at the Gulf Stream's edge. J. Geophys. Res. 94:10791-10800.

Churchill, J.H., E.R. Levine, D.N. Connors, and P.C. Cornillon. 1993. Mixing of shelf, slope and Gulf Stream water over the continental slope of the Middle Atlantic Bight. Deep- Sea Res. 40:1063-1085.

Clarke, A.J. 1991. The dynamics of barotropic tides over the continental shelf and slope (Review). pp. 79-108. In B.B. Parker, ed. Tidal Hydrodynamics. John Wiley and Sons, Inc., New York.

Csanady, G.T. 1982. Circulation in the Coastal Ocean. D. Reidel Publishing Company. Dordrecht, Holland. 279 pp.

Csanady, G.T. and P.T. Shaw. 1983. The "insulating" effect of a steep continental slope. J. Geophys. Res. 88:7519-7524.

Csanady, G.T. and P. Hamilton. 1988. Circulation of Slope Water. Cont. Shelf Res. 8:565-624.

Davis, R.E., J.E. Dufour, G.J. Parks, and M.R. Perkins. 1982. Two inexpensive current following drifters Scripps Institute of Oceanography Ref. 82-28. 54 pp.

Fisher, A. 1972. Entrainment of shelf water by the Gulf Stream northeast of Cape Hatteras. J. Geophys. Res. 77:3248-3255.

Ford, W.L., J.R. Longard, and R.E. Banks. 1952. On the nature, occurrence and origin of cold low salinity water along the edge of the Gulf Stream. J. Mar. Res. 11:281-293.

Foreman, M.G.G. 1979. Manual for tidal currents analysis and prediction. Pacific Marine Science Report 78-6. Institute of Ocean Studies, Patrician Bay, Sydney, BC. 70 pp.

FRED Group. 1989. Frontal Eddy Dynamics (FRED) Experiment off North Carolina. C.C. Ebbesmeyer, ed. Prepared by Evans-Hamilton, Inc. OCS Study MMS 89-0028 Vol 2 Technical Report, March 1989. U.S. Dept. of Minerals Management Service, Herndon, VA 325 pp.

Garfield, N., III and D.L. Evans. 1987. Shelf Water Entrainment by Gulf Stream Warm-Core Rings. J. Geophys. Res. 98:13003-13012.

Garvine, R.W., K.-C. Wong, G.G. Gawarkiewicz, and R.K. McCarthy. 1988. The morphology of shelfbreak eddies. J. Geophys. Res. 93:15593-15607.

Gawarkiewicz, G., R.K. McCarthy, K. Barton, A. Masse, and T.M. Church. 1990. A Gulf Stream-derived pycnocline intrusion on the Middle Atlantic Bight shelf. J. Geophys. Res. 95:22305-22313.

Glenn, S.M. and C.C. Ebbesmeyer. 1994a. The structure and propagation of a Gulf Stream frontal eddy along the North Carolina shelf break. J. Geophys. Res. 99:5029-5046.

Glenn, S.M. and C.C. Ebbesmeyer. 1994b. Observations of Gulf Stream frontal eddies in the vicinity of Cape Hatteras. J. Geophys. Res. 99:5047-5056.

Gordon, A.L., A.F. Amos, and R.D. Gerard. 1976. New York Bight water stratification-October 1974. Am. Soc. Limnol. Oceanogr. Spec. Symp. 2:45-67.

Gordon, A.L. and F. Aikman III. 1981. Salinity maximum in the pycnocline of the Middle Atlantic Bight. Limnol. Oceanogr. 26:123-130.

Grossman, R.L. and A.K. Betts. 1990. Air-Sea Interaction During an Extreme Cold Air Outbreak From the Eastern Coast of the United States. Mon. Wea. Rev. 118:324-342.

Halkin, D. and T. Rossby. 1985. The structure and transport of the Gulf Stream at 73°W. J. Phys. Oceanogr. 15:1439-1452.

Hamilton, P. 1984. Topographic and inertial waves on the continental rise of the Mid-Atlantic Bight. J. Geophys. Res. 89:695-710.

Hamilton, P. 1987. The structure of shelf and Gulf Stream motions in the Georgia Bright. Proq. Oceanogr. 19:329-351

Hogg, N.G. 1981. Topographic waves along 70°W on the continental rise. J. Mar. Res. 39:627-649.

Houghton, R.W. and H.W. Ou. 1982. A model of the summer progression of the cold-pool temperature in the Middle Atlantic Bight. J. Phys. Oceanogr. 12:1030-1036.

Houghton, R.W. and J. Marra. 1983. Physical/biological structure and exchange across the thermohaline shelf/slope front in the New York Bight. J. Geophy. Res. 88:4467-4481.

Johns, W.E. and D.R. Watts. 1986. Time Scales and Structure of Topographic Rossby Waves and Meanders in the Deep Gulf Stream. J. Mar. Res. 44:267-290.

Johns, W.E., T. Shay, D.R. Watts, and J.M. Bane. 1994. Gulf Stream structure, transport, and recirculation near 68°W. J. Phys. Oceanogr. (submitted).

Joyce, T.M. and T.J. McDougall. 1992. Physical structure and temporal evolution of Gulf Stream warm-core ring 82B. Deep-Sea Res. 39:S19-S44.

Konrad, T.G. and S.J. Colucci. 1989. An Examination of Extreme Cold Air Outbreaks Over Eastern North America. Mon. Wea. Rev. 117:2687-2700.

Kupferman, S.L. and N. Garfield. 1977. Transport of low-salinity water at the slope water-Gulf Stream boundary. J. Geophys. Res. 82:3481-3486.

Large, W.E. and S. Pond. 1981. Open ocean flux measurements in moderate to strong winds. J. Phys. Oceanogr. 11:324-336.

Lee, T. 1994. Variability of the Gulf Stream path observed from satellite infrared images, Ph.D. thesis, University of Rhode Island, Narragansett, Rhode Island.

Lee, T.N. and P.A. Mayer. 1977. Low-frequency current variability and spin-off eddies off Southeast Florida. J. Mar. Res. 35:193-220.

Lee, T.N. and L.P. Atkinson. 1983. Low-frequency current and temperature variability from Gulf Stream frontal eddies and atmospheric forcing along the southeast U.S. Outer Continental Shelf. J. Geophys. Res. 88:4541-4568.

Lee, T.N., L.P. Atkinson, and R. Legeckis. 1981. Observations of a Gulf Stream frontal eddy on the Georgia continental shelf, April 1977. Deep-Sea Res. 28:347-378.

Lee, T.N., E. Williams, J. Wang, R. Evans, and L.P Atkinson. 1989. Response of the South Carolina Continental Shelf Waters to Wind and Gulf Stream Forcing During Winter of 1986. J. Geophys. Res. 94:10699-10714.

Lee, T.N., J.A. Yoder, and L.P. Atkinson. 1991. Gulf Stream frontal eddy influence on productivity of the Southeast U.S. Continental Shelf. J. Geophys. Res. 96:22191-22206.

Lillibridge, J.L., III, G. Hitchcock, T. Rossby, E. Lessard, M. Mork, and L. Golmen. 1990. Entrainment and mixing of shelf/slope waters in the near-surface Gulf Stream. J. Geophys. Res. 95:13065-13087.

Lyne, V.D. and G.T. Csanady. 1984. A compilation and description of hydrographic transects of the Mid-Atlantic Bight shelf-break front. Woods Hole Oceanographic Institution Technical Report, WHOI-84-19, 290 pp.

McClain, C.R., L.J. Pietrafesa, and J.A. Yoder. 1984. Observations of Gulf Stream-induced and wind-driven upwelling in the Georgia Bight using ocean color and infrared imagery. J. Geophys. Res. 89:3705-3723.

Morgan, C.W. and J.M. Bishop. 1977. An example of Gulf Stream eddy-induced water exchange in the Mid-Atlantic Bight. J. Phys. Oceanogr. 7:472-479.

NOAA. 1992. Storm Data. National Climatic Data Center, Asheville, North Carolina, vol. 35, no.12, 125 pp.

Noble, M.A. and G.R. Gelfenbaum. 1992. Seasonal Fluctuations in Sea Level on the South Carolina Shelf and Their Relationship to the Gulf Stream. J.Geophys. Res. 97(C6):9521-9529.

Norcross, J.J. and W. Harrison. 1967. Introduction. In: Circulation of Shelf Waters off the Chesapeake Bight: Surface and bottom drift of continental shelf waters between Cape Henlopen, Delaware and Cape Hatteras, North Carolina, June 1963 - December 1964. W. Harrison, J.J. Norcross, N.A. Pore, and E.M. Stanley. Environmental Sciences Services Administration Professional Paper 3. pp. 3-9.

Pickart, R.S. 1994. Gulf Stream-generated topographic Rossby waves. J. Phys. Oceanogr. (submitted).

Pickart, R.S. and D.R. Watts. 1990. Deep Western Boundary Current Variability at Cape Hatteras. J. Mar. Res. 48:765-791.

Pickart, R.S. and W.M. Smethie. 1993. How does the deep western boundary current cross the Gulf Stream? J. Phys. Oceanogr. 12:2602-2616.

Pickart, R.S. and S.S. Lindstrom. 1994. A comparison of techniques for referencing geostrophic velocities. J. Atmos. Ocean. Technol. 11:814-824.

Pietrafesa, L.J., G.S. Janowitz, and P.A. Wittman. 1985. Physical oceanographic processes in the Carolina Capes. pp. 23-32. In: L.P. Atkinson, D.W. Menzel and K.A. Bush, eds. Oceanography of the Southeastern U. S. Continental Shelf. Coastal and Estuarine Sciences 2, American Geophysical Union.

SAIC. 1993. A Review of the Physical Oceanography of the Cape Hatteras, North Carolina Region, Volume 1, Literature Synthesis. Final Report MMS 93/0031, submitted to Minerals Management Service, Atlantic OCS Office, Herndon, Virginia, 152 pp.

Shaw, P.T. and C.Y. Peng. 1987. A numerical study of the propagation of topographic Rossby waves. J. Phys. Oceanogr. 17:358-366.

Shaw, P.T. and G.T. Csanady. 1988. Topographic waves over the continental slope. J. Phys. Oceanogr. 18:813-822.

SRCC. 1993. Special Climate Summary: Hurricane Emily. Southeast Regional Climate Center, Columbia, South Carolina, August, 1993. 6 pp.

Stefansson, U., L.P. Atkinson, and D.F. Bumpus. 1971. Seasonal studies of hydrographic properties and circulation of the North Carolina shelf and slope waters. Deep-Sea Res. 18:383-420.

Thompson, E.F. 1977. Wave climate at selected locations along U.S. coasts. U.S. Army Corps of Engr., CERC. Technical Report No. 77-1:364.

Tracey K.L. and D.R. Watts. 1986. On Gulf Stream meander characteristics near Cape Hatteras. J. Geophys. Res. 91:7587-7602.

Uchupi, E. 1965. Map showing relation of land and submarine topography, Nova Scotia to Florida. U.S. Geological Survey Miscellaneous Geological Investigations, Map 1-451.

Wang, D.-P. 1979. Low-frequency sea level variability on the Middle Atlantic Bight. J. Mar. Res. 37:683-697.

Watts, D.R. 1983. Gulf Stream variability. pp. 114-144. In A.R. Robinson, ed. Eddies in Marine Science. Springer-Verlag, New York.

Watts, D.R. 1991. Equatorward currents in Temperatures 1.8-6.0°C on the Continental Slope in the Mid-Atlantic Bight. pp. 183-196. In P.C. Chu and J.C. Gascard, eds. Deep Convection and Deep Water Formation in the Oceans. Elsevier, Amsterdam.

Watts, D.R., K.L. Tracey, J.M. Bane, and T.J. Shay. 1995. Gulf Stream path and thermocline structure near 74°W and 68°W. J. Geophys. Res. 100:18,291-18,312.

Wayland, R.J. and S. Raman. 1994. Mean and Turbulent Structure of the Marine Atmospheric Boundary Layer During Two

Cold Air Outbreaks of Varying Intensities (GALE 86). Bound.-Layer Meteor. 71:43-66.

Wayland, R.J. and S. Raman. 1989. Mean and Turbulent Structure of A Baroclinic Marine Boundary Layer During the 28 January 1986 Cold Air Outbreak (GALE 86). Bound.-Layer Meteor. 48:227-254.

Worthington, L.V. 1976. On the North Atlantic circulation. John Hopkins Oceanogr. Studies No. 6. The Johns Hopkins Univ. Press. Baltimore. 110 pp.

Yoder, J.A. 1991. Role of Gulf Stream frontal eddies in forming phytoplankton patches on the outer southeastern shelf. Limnol. Oceanogr. 36:385-404.

Yoder, J.A., L.P. Atkinson, S.S. Bishop, J.O. Blanton, T.N. Lee, and L.J. Pietrafesa. 1985. Phytoplankton dynamics within Gulf Stream intrusions on the southeastern U.S. continental shelf during summer, 1981. Cont. Shelf Res. 4:611-635.

Yoshida, K. 1967. Circulation in the eastern tropical oceans with special references to upwelling and undercurrents. Jap. J. Geophys. 4:1-75.

The Department of the Interior Mission

As the Nation's principal conservation agency, the Department of the Interior has responsibility for most of our nationally owned public lands and natural resources. This includes fostering sound use of our land and water resources; protecting our fish, wildlife, and biological diversity; preserving the environmental and cultural values of our national parks and historical places; and providing for the enjoyment of life through outdoor recreation. The Department assesses our energy and mineral resources and works to ensure that their development is in the best interests of all our people by encouraging stewardship and citizen participation in their care. The Department also has a major responsibility for American Indian reservation communities and for people who live in island territories under U.S. administration.

The Minerals Management Service Mission

As a bureau of the Department of the Interior, the Minerals Management Service's (MMS) primary responsibilities are to manage the mineral resources located on the Nation's Outer Continental Shelf (OCS), collect revenue from the Federal OCS and onshore Federal and Indian lands, and distribute those revenues.

Moreover, in working to meet its responsibilities, the **Offshore Minerals Management Program** administers the OCS competitive leasing program and oversees the safe and environmentally sound exploration and production of our Nation's offshore natural gas, oil and other mineral resources. The MMS **Royalty Management Program** meets its responsibilities by ensuring the efficient, timely and accurate collection and disbursement of revenue from mineral leasing and production due to Indian tribes and allottees, States and the U.S. Treasury.

The MMS strives to fulfill its responsibilities through the general guiding principles of: (1) being responsive to the public's concerns and interests by maintaining a dialogue with all potentially affected parties and (2) carrying out its programs with an emphasis on working to enhance the quality of life for all Americans by lending MMS assistance and expertise to economic development and environmental protection.